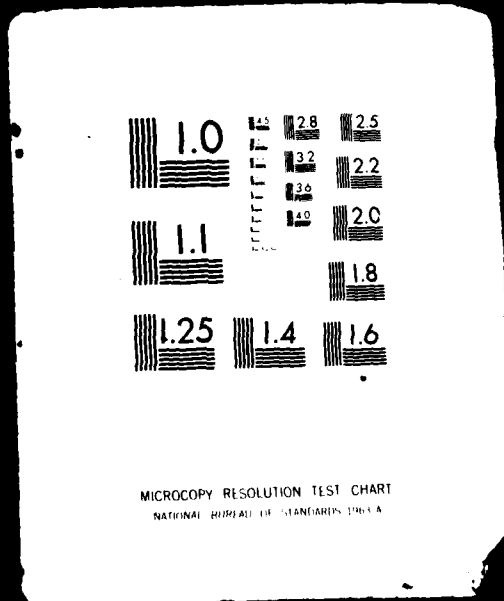


1 OF 3
AD
A111638



0

AGARD-AG-263

AG 263

AGARD-AG-263

A FURTHER COMPILATION OF COMPRESSIBLE BOUNDARY LAYER DATA
WITH A SURVEY OF TURBULENCE DATA

AD A 7 7 6 3 8

AGARD

ADVISORY GROUP FOR AEROSPACE RESEARCH & DEVELOPMENT

7 RUE ANCELLE 92200 NEUILLY SUR SEINE FRANCE

AGARDograph No. 263

A Further Compilation of Compressible Boundary Layer Data with a Survey of Turbulence Data

This document has been approved
for public release and sale; its
distribution is unlimited.

DTIC
MAR 5 1982
A



DTIC FILE COPY

FDP

NORTH ATLANTIC TREATY ORGANIZATION



DISTRIBUTION AND AVAILABILITY
ON BACK COVER

82 00 02 006

NORTH ATLANTIC TREATY ORGANIZATION
ADVISORY GROUP FOR AEROSPACE RESEARCH AND DEVELOPMENT
(ORGANISATION DU TRAITE DE L'ATLANTIQUE NORD)

AGARDograph No.263

A FURTHER COMPILATION OF COMPRESSIBLE BOUNDARY LAYER DATA
WITH A SURVEY OF TURBULENCE DATA

by

Professor Dr Ing. H.H.Fernholz
Herman Föttinger Institut für
Thermo-und-Fluiddynamik
Technische Universität Berlin
D-1000 Berlin 12
Strasse des 17 Juni 135
BRD Germany

and

P.J.Finley, M.A., Ph.D.
Department of Aeronautics
Imperial College of
Science and Technology
Prince Consort Road
London SW7 2BY
Great Britain

with a chapter by

Dr V.Mikulla
Hohenbrunner Strasse 73
D-8012 Riemerting
Germany

SELECTED
A

This document has been approved
for public release and sale, its
distribution is unlimited.

This AGARDograph was prepared at the request of the Fluid Dynamics Panel of AGARD.

THE MISSION OF AGARD

The mission of AGARD is to bring together the leading personalities of the NATO nations in the fields of science and technology relating to aerospace for the following purposes:

- Exchanging of scientific and technical information;
- Continuously stimulating advances in the aerospace sciences relevant to strengthening the common defence posture;
- Improving the co-operation among member nations in aerospace research and development;
- Providing scientific and technical advice and assistance to the North Atlantic Military Committee in the field of aerospace research and development;
- Rendering scientific and technical assistance, as requested, to other NATO bodies and to member nations in connection with research and development problems in the aerospace field;
- Providing assistance to member nations for the purpose of increasing their scientific and technical potential;
- Recommending effective ways for the member nations to use their research and development capabilities for the common benefit of the NATO community.

The highest authority within AGARD is the National Delegates Board consisting of officially appointed senior representatives from each member nation. The mission of AGARD is carried out through the Panels which are composed of experts appointed by the National Delegates, the Consultant and Exchange Programme and the Aerospace Applications Studies Programme. The results of AGARD work are reported to the member nations and the NATO Authorities through the AGARD series of publications of which this is one.

Participation in AGARD activities is by invitation only and is normally limited to citizens of the NATO nations.

The content of this publication has been reproduced directly from material supplied by AGARD or the authors.

Published November 1981

Copyright © AGARD 1981
All Rights Reserved

ISBN 92-835-1404-1



Printed by *Technical Editing and Reproduction Ltd*
Harford House, 7-9 Charlotte St, London, W1P 1HD

CONTENTS

| | | |
|-----|---|------|
| i | PREFACE - THE AGARD-EUROVISC CATALOGUE | iv |
| ii | ACKNOWLEDGEMENTS | iv |
| iii | GRAPHICAL PRESENTATION OF PROFILE DATA | v |
| iv | CLASSIFIED LIST OF SUPPLEMENTARY ENTRIES | vi |
| v | DATA ON MAGNETIC TAPE | vii |
| vi | CORRIGENDA TO AGARDographs 223, 253, 263 | viii |
| 1. | INTRODUCTION | 1 |
| 1.1 | The entries | 1 |
| 1.2 | The data collection | 3 |
| 1.3 | Background for the survey of turbulence measurements | 4 |
| 2. | HOT WIRE ANEMOMETRY IN COMPRESSIBLE TURBULENT BOUNDARY LAYERS (by V. MIKULLA) | 6 |
| 2.1 | Basis of hot wire anemometry in a compressible turbulent boundary layer | 6 |
| 2.2 | Sensors with very high overheat ratio | 9 |
| 2.3 | Special features in measurement | 14 |
| 2.4 | Conclusions | 17 |
| 3. | TURBULENCE DATA - SINGLE COMPONENTS | 18 |
| 3.1 | Normal components of the Reynolds stress - zero pressure gradient | 21 |
| 3.2 | Normal components of the Reynolds stress - various pressure gradients | 27 |
| 3.3 | Kinetic energy of the fluctuating motion | 31 |
| 3.4 | Temperature fluctuations | 32 |
| 4. | TURBULENCE DATA - TWO COMPONENT TERMS | 35 |
| 4.1 | Distribution of Reynolds shear stress ($-\overline{\rho u'v'}$) in a compressible two-dimensional boundary layer | 35 |
| 4.2 | Indirect determination of shear stress | 36 |
| 4.3 | Direct measurements of the Reynolds shear stress ($-\overline{\rho u'v'}$) - available data | 40 |
| 4.4 | Direct measurements of the Reynolds shear stress ($-\overline{\rho u'v'}$) - zero pressure gradient boundary layers | 43 |
| 4.5 | Direct measurements of Reynolds shear stress ($-\overline{\rho u'v'}$) - adverse pressure gradient boundary layers | 46 |
| 4.6 | Ratio a_1 of the Reynolds shear stress ($-\overline{\rho u'v'}$) to the kinetic energy of the fluctuating flow | 50 |
| 4.7 | Other correlation terms | 52 |
| 5. | MEAN FLOW TOPICS | |
| 5.1 | Transverse curvature effects | 54 |
| 5.2 | Validity of the Van Driest temperature - velocity transformation | 57 |
| 5.3 | Discussion of the wave structure of the shock/boundary-layer interaction (Kussoy and Horstman, 1975) | 64 |
| 6. | THE ENTRIES | 67 |
| | For pagination, see "order of sections" page 3. | |
| | A list of entries is given on page vi. | |
| 7. | REFERENCES | |

The Microfiche in the pocket part of this report may be obtained from: Advisory Group for Aerospace Research and Development, 7 Rue Ancelle 92200 Neuilly Sur Seine, France

| | |
|------------|---------|
| SEARCHED | INDEXED |
| SERIALIZED | FILED |
| A | |

R1-R9



i. PREFACE - THE AGARD-EUROVISC CATALOGUE

With the publication of this volume, the third in a series, the EUROVISC working group on compressible turbulent boundary layer data has come to the end of its programme of data collection and presentation. Throughout our aim has been to describe experiments and present data to a common standard, and to separate, so far as possible, opinion from information received by us as, in essence, factual. The data presented are of course subject to error, whether of a gross nature perhaps best described as mistakes, or, inevitably, as a result of inaccuracies both systematic and random which can not be avoided in an experimental field as taxing as this. We have been able, on occasion, to detect mistakes in published sources, and by checks on internal consistency and correspondence with the authors incorporate appropriate corrections. We hope we have not made serious mistakes ourselves. We have not made any attempt to assess the level of experimental accuracy, presenting the data available to us if we found it functionally complete and if we could make sense of it. There is a large measure of uncertainty in all high Mach number data while in most cases turbulence data are perhaps best regarded as possibly indicating trends rather than establishing values.

The three volumes, AGARDograph 223, 253 and 263 provide the data from 77 experimental studies and a commentary on the results. The experiments are described in ENTRIES of which 59 will be found in the first volume, AG 223. These are referred to in all three volumes by a reference number such as CAT 7201, while a further 18 studies described in this volume, AG 263, are distinguished by a final S, as for example CAT 7501 S. CAT I, AG 223, also contains introductory material designed to assist users of the collection which should be consulted by anyone proposing to use CAT III, AG 263. The second volume, CAT II, AG 253, contains a discussion of the mean flow data from CAT I and some, but not all, of the supplementary data collected for and presented in CAT III. In consequence, some discussion of the mean flow data in CAT III will be found in the individual entries describing the experiments. This volume also contains a presentation and discussion of the available turbulence data.

It has not been possible to print all the profile data in "hard copy" form, so the ENTRIES contain only a selection. The full profile listings are however enclosed on microfiche in pockets attached to the back cover, and on the magnetic tapes deposited with AGARD holding instructions listed below.

The very large quantity of data presented in this collection represents an enormous collective effort by the original authors who obtained it. Ours has been the secondary and less taxing task of collecting, ordering and criticising it. For the first editor this has now continued for more than ten years. Our feelings were admirably expressed 200 years ago by Edward Gibbon:

"I will not dissemble the first emotions of joy on the recovery of my freedom.....".

ii. ACKNOWLEDGEMENTS

Once more we are unable to express, in any adequate manner, our thanks to Frau C. Mohr. In a very real sense it is she who has had to put together the data collection which is the main purpose of this project. She has uncomplainingly and repeatedly rearranged all the numerical information to suit the editors' wishes, however ill advised, on occasion, our requests might be.

We also thank Frau C. King for preparing the typescript, Frau H. Berger for typing the tables and references, and Frau I. Gereke for making all our drawings.

We must again thank the DFG and TUB for funding the research work, and the Hermann-Föttinger-Institut for continued hospitality to the second author. The publication is once more funded by AGARD and we thank R.H. Rollins, executive of the Fluid Dynamics Panel, for his help and encouragement.

We are specially indebted to Dr. V. Mikulla who has at our request prepared chapter 2 of this volume. We have benefitted from the help and advice of Professor K. Gersten (Ruhr Universität Bochum) as AGARD editor. Among the many colleagues who have assisted by general discussion and detailed comments on various parts of the text, we would single out L.C. Squire (Cambridge and Professor P. Bradshaw, Imperial College).

Finally we must thank our wives and families for tolerating frequent absences of mind and body, not only in the past two years covering the preparation of this volume, but also throughout the course of the catalogue project.

iii. GRAPHICAL PRESENTATION OF PROFILE DATA

Selected profile data from the sources below may be found in the figures listed.

(a) Mean flow profiles may be found either in the main text (three number reference) or in the ENTRY (single number).

| <u>SOURCE</u> | <u>Temperature</u> | <u>Profiles</u> | |
|-------------------------|--------------------|-------------------|----------------|
| | | <u>"Inner"</u> | <u>"Outer"</u> |
| 5701s Richmond | - | 5.1.1,5.1.3,5.1.4 | 5.1.5 |
| 6801 Perry & East | - | 5.2.8 | 5.2.9 |
| 7205 Horstman & Owen | - | 4.4.1 | - |
| 7306s Rose | 2 (Entry) | 3 | 4 |
| 7405s Peterson | 5.2.1 | 5.2.7 | 5.2.9 |
| 7501s Kussoy & Horstman | 5.2.2 | 5.2.3,5.2.5 | 5.2.4,5.2.6 |
| 7703s Berg | - | 1, 3, 4 | 2 |
| 7801s Collins et al. | - | 1 | 2 |
| 7802s Kussoy et al. | - | 1, 2 and 4.4.1 | 3 |
| 7803s Laderman | - | 1 | 2 |
| 7804s Watson | - | 1, 3 | 2 |
| 7901s Voisinet | - | 2, 4, 5 | 3 |
| 7902s Chew & Squire | - | 1, 3, 5 | 2, 4 |
| 7903s Bartlett et al. | - | 1 | 2 |
| Klebanoff (1955) | - | 4.4.1 | - |
| Willmarth et al. (1976) | - | 5.1.2, 5.1.3 | - |

(b) Turbulence profiles are plotted in the main text only, for

| | |
|-------------------------|---|
| 5803 Kistler | 3.1.1-5,3.4.2-3 |
| 7101 Sturek & Danberg | 3.4.1-3 |
| 7205 Horstman & Owen | 3.1.1-5,3.1.6-9,3.4.1,4.4.2-3 |
| 7306s Rose | 3.1.6-9,3.2.6-7,3.3.3,4.4.2-3,4.5.5,4.6.1,4.6.3,4.7.1 |
| 7501s Kussoy & Horstman | 3.1.6-9,3.2.8,4.4.2-3 |
| 7802s Kussoy et al. | 3.1.1-5,3.1.6-9,3.2.1-5,3.3.1-2,4.4.2-3,4.5.1-4,4.6.1-2 |
| 8001s Mateer & Viegas | 4.5.6 |
| Klebanoff (1955) | 4.4.2-3 |
| Rose & Johnson (1975) | 4.4.4 |

iv. CLASSIFIED LIST OF SUPPLEMENTARY ENTRIES

The ENTRIES are listed in numerical order, otherwise following the conventions of § 7 of AGARDograph 223. The pressure gradient classification is given both as an abbreviation and as in AG223 § 7.1.

| | M_0 | R THETA $\times 10^{-3}$ | TW/TR | PG ² | TO | CF ³ | NX | TURB ⁴ |
|--------------------------------|---------|-----------------------------|---------|-----------------|-----|-----------------|-------|-------------------|
| 5701 RICHMOND | <1,5.8 | 1-9 | 1.0 | ZPG,IB | - | F/V | 1(3) | - |
| 5806 MORKOVIN & PHINNEY | 1.77 | 16 | 1.0 | ZPG,IB2 | - | (V) | 1 | CC HWP |
| 6002 DANBERG | 5.1 | 3-4 | 0.8,0.9 | ZPG,IA1 | P | V | 2 | - |
| 7306 ROSE | 4 | 3.4 | 1.0 | SBLI,(IIA4) | P | V | 12 | CT HWP |
| 7404 VOISINET et al. | 4.9 | 6-26 | 0.8,1.0 | ZPG,IB1 | P | - | 2 | - |
| 7405 PETERSON | 14 | 6-11 | 0.25 | FPG,IIB5 | P | V | 2 | - |
| 7501 KUSSOY & HORSTMAN | 7 | 8.5 | 0.5 | SBLI,(IIA4) | P | F | 18,19 | CT HWP |
| 7701 MABEY | 2.5-4.5 | 1-8 | 1.0 | ZPG,IA1 | P | F | 3 | - |
| 7702 LADERMAN & DEMETRIADES | 3.0 | 3-4 | 0.6-1.0 | ZPG,IB1 | P | (P) | 3 | CC HWP |
| 7703 BERG | 6 | 14-20 | 0.9 | ZPG,IB1R | P | V(F) | 17 | CC HWP |
| 7801 COLLINS et al. | 0.1-2.2 | 6,23,40 | 1.0 | ZPG,(IA1),IB2 | - | F,P,V | 4-8 | LDV |
| 7802 KUSSOY et al. | 2.3 | 30 | 1.0 | APG,IIA4 | (P) | P,surface | 13,14 | CT HWP |
| 7803 LADERMAN | 3.0 | 3-5 | 1.0 | APG,IIB2 | P | V(P) | 10,14 | - |
| 7804 WATSON | 10-12 | 3-20 | 0.4-1.1 | ZPG,IA1 | P | F | 7 | - |
| 7901 VOISINET | 2.9 | 3-60 | 1.0 | ZPG,IB1R | P | F | 1 | - |
| 7902 CHEW & SQUIRE | 2.5 | 24 | 1.0 | RELAXATION | - | P | 7 | - |
| 7903 BARTLETT et al. | 9.3 | 3-12 | 0.3 | ZPG,IA1 | P | P | 3 | (Electron) |
| 8001 MATEER & VIEGAS | 1.45 | 40-100 | 1.0 | SBLI,(IIA4) | P | surface | 7 | CT HWP |

NOTES: (1) Numerical values are nominal, not precise.

(2) SBLI: Shock boundary layer interaction.

(3) CF: F-Floating element balance, P-Preston tube, V-deduced from profile. "surface"-embedded hot wire gauge.

(4) TURB: Turbulent measurements - see tables 3.1 and 4.3.1 in the main text.

v. DATA ON MAGNETIC TAPE

For the first volume, AG 223, all the mean flow profile data and the "Kopfdaten" (Section B of each entry) were made available on magnetic tape. The format was prepared by Prof. P. Bradshaw (Imperial College) as more suitable for possible FORTRAN users than the printed format in the microfiche and hard copies. The supplementary data described in the ENTRIES of this volume have been prepared in the same tape format, with the addition of all tabular turbulence data available to us. These are added as the final files on the tape, in a different format.

Arrangements have been made with the following organizations in NATO countries to hold master copies of the data tape. These organizations will prepare copies on request; enquiries as to terms should be directed to the organization concerned.

FRANCE

O.N.E.R.A. (Direction)
29 Avenue de la Division Leclerc
92 Chatillon sous Bagneux

GERMANY

| | |
|--------------------------|----------------|
| Fachinformations-Zentrum | DFVLR |
| 7514 Eggenstein | AVA |
| Leopoldshafen 2 | 3400 Göttingen |
| | Bunsenstr. 10 |

NETHERLANDS

Netherlands Delegation to AGARD
National Aerospace Laboratory, NLR
P.O. Box 126
Delft

UNITED KINGDOM

Defence Research Information Centre
Station Square House
St Mary Cray
Orpington, Kent BR5 3 RE

UNITED STATES

COSMIC (Computer Software Management and Information Centre,
University of Georgia)
Suite 112
Barrow Hall
Athens
Georgia 30602

vi. CORRIGENDA

AGARDograph 223

For ENTRY 7305 (Watson et al.) in the tables of sections B and C the wall temperature TW was set at the recovery temperature. The proper nominal operating conditions correspond to the TW value given in section D. Thus $TW = 283 \text{ K}$ and $TW/TR = 1.05$. Other corrections include:

- page vi - Abbreviations: STP - stagnation temperature probe.
- page 13 - § 3.6, para. 2, last line: ρ' not p' .
- page 25 - eqn. 5.13: $\delta_i = -R_z [1 - (1 + 2\delta_n/R_z)^{1/2}]$.
- page 27 - 5.6, para. 2, line 4: "---, so that p_{Or} was set equal to -----".
- 5503-A-1: § DATA 55030101 - 0113.
- 7006-A-1, lines 3 & 6: Roughness values in μm .
- 7006-B-2: First profile numbered 70060406 should be 70060405.
- 7105-A-3, Table 1: Table heading; P INF at $X = 2.083 \text{ m}$.
: Last line, $X = 2.083$, $-RZ = 197.5$.
- 7209-A-1, para. 2; line 3: "--- at $X = 25 \text{ mm}$ ---".
- 7303-A-1, footnote: "--- values about 10% lower".
- 7305-A-1, Identification panel: $9 < RE/m \times 10^{-6} < 50$.
- 7401-A-1, para 2: "--- here. The plates were 0.1 m wide ---".
para 4: Reference to Smith et al. should be "1962".
- 7402-B-4, run 1702: $X = 0.623$.
- R-3 References: Fenter (1960) DRL 468 should be Fenter (1959) DRL 437.

AGARDograph 253

- page v - 7404s: Fig 2.5.20 describes inner velocity profile.
- page 13 - eqn (2.2.10): Bar on last term.
- page 39 - Fig 2.5.11, left: Ordinate should be \bar{T}/T_δ .
- page 41 - Last para, line 6: ---- and T^* , ----.
- page 117 - Fig 4.2.18 and 4.2.17 (caption): Delete.
- page 165 - para 1, last word: ---quantities.
- § 6.1, line 1: --- § 6.3, no distinction ---.
- page 171 - After eqn (6.1.16): --- at which $M = 1$.
- page 176 - line 4: --- as for a zero normal pressure ---.
- page 191 - eqn (7.1.2), RH: first term numerator should be $2\gamma(2M^2 - 1)dM$.
- eqn (7.1.3), RH: first & second term denominators should be $M^2 [2\gamma M^2 - (\gamma - 1)]$.
- page 196 - eqn (7.2.1): Integral dy .
- page 202 - eqn (7.5.5): fourth last term should be $\delta_2^2 / 2R_z$.

AGARDograph 263

- page 11 - Fig (2.1), legend: Interchange "single tungsten wire" and "ceramic supported platinum hot wire". "Commercial platinum hot wire" should be "--- hot film".
- page 55 - para 3, line 10: Add "--- equal values of Re_{δ_2} may be seen in Fig (5.1.3)."
- page 63 - Fig (5.2.7), legend: second profile, 0104, should be 0202.

1. INTRODUCTION

In preparing the first volume of this series, AGARDograph 223, we imposed certain restrictions on those flows considered as candidates for an entry. These were that the flow should be nominally two-dimensional, that the Mach number be high enough for the effects of compressibility to be significant, that the Reynolds number be high enough for at least some part of the flow to be recognisably turbulent, that there be no flow through the surface on which the boundary layer was formed, and that there be no discontinuities in the mean flow property profiles. We also required, as a general principle, that the information supplied must include profiles normal to the surface, in addition to data measured on the wall, and that the principal part of the data be presented in tabular form.

This third volume contains 18 further entries and the mean flow data presentation follows the same pattern as for AG 223. We have however included some cases in which shock waves impinge on and interact with a boundary layer, and inevitably many of the profiles in such flows incorporate what should be discontinuities in the flow properties concerned. There is also one case, Morkovin & Phinney (1958) which we include because of its historical interest in relation to the development of turbulence measuring techniques although we had to take the data from a graph.

The principal novel feature of this volume in relation to its forbears, AG 223 and AG 253, is that a great part of the main text preceding the entries is devoted to a survey of turbulence measurements. We have, inevitably, found it necessary to be slightly less strict in insisting on tabular data in discussing this area, but have, whenever possible, used tables obtained in private correspondence in addition to the sparse published data. These tabulated data have been prepared in a standard form, and samples appear in some cases as part of the entries. Tabular data for all cases considered have been gathered together and provided as part of the microfiche collection which accompanies this volume. The collection includes data for entries in AG 223, indicated by a four number serial such as CAT 7205, as well as those associated with the supplementary entries which appear below and are distinguished by a final S, such as CAT 7501S.

1.1. The entries

There is a full discussion of the planning and layout of an entry in AG 223, so that we only repeat the main points here.

An entry is composed of four sections, A - D:

Section A. This provides a description of the experiment in a standard format, and predominantly in a standard sequence. The description is keyed to a fixed set of topics indicated by numbers in the left hand margin. These may appear in any order, or be repeated if a topic recurs. The topics are

1. Description of test section
2. Flow quality
3. Observations of transition and tripping devices (trips)
4. Upstream history of the test boundary layer
5. Measures taken to test for, or ensure, two-dimensional flow
6. Measurements at the test-surface (wall measurements)
7. Probes used for boundary-layer traverses
8. Relative positions of measurement stations
9. Author's interpolation procedures and assumptions
10. Corrections to the profile data
11. Viscosity law assumed by authors
12. Editors' assumptions and interpolation procedures. Selection of data
13. Profiles presented
14. Wall data presented
- § Data summary
15. Editors' comments.

Topics 1 - 11 provide a description in which, so far as possible, we have restricted ourselves to statements which we could verify either in the published reports or by correspondence with the authors. At various

points, however, we have filled out the verifiable facts by an estimate or interpretation. Where this has happened we have inserted a marker (E). The end of the description, marked 12 - 14, describes the measures we found necessary in processing the data and is followed by (§ DATA) a brief data summary which states what was in fact measured, in contrast to data which are deduced from the measurements.

Up to this point we have tried to avoid statements of opinion, but in § 15 "Editors' comments" we have introduced much which must be considered our own interpretation and comment. In AG 223 we usually kept § 15 fairly short as the data were to be discussed at length in AG 253. Some of the entries in this volume are also discussed there, when, in the entries below, section and figure number references to AG 253 will be given. Where, however, an entry is not discussed in AG 253 or in connection with the turbulence data in chapters 3 and 4 or one of the special features of mean flow in chapter 5 of the main text of this volume, the treatment in § 15 is more extended, usually including at least a graphical treatment of the mean flow profiles.

Section B, the "Kopfdaten," contains tables of the principal boundary conditions and various derived quantities such as integral thicknesses. The table heading for a typical entry is shown here:

| | | | | | | | | |
|-----|-----|-------|-------|-----|-----|------|----|----|
| RUN | MD | TW/TR | RED2W | CF | H12 | H12K | PW | PD |
| X | POD | PW/PD | RED2D | CQ | H32 | H32K | TW | TD |
| RZ | TOD | TAUW | D2 | PI2 | H42 | D2K | UD | TR |

The list is reproduced in part at the start of this volume. There is one change: TAUW the wall shear stress replaces the simple wave indicator SW, which proved less useful than was hoped. Those quantities marked by a star (*) represent the data used as input. In many cases these data would be entered directly, but the values shown often represent the results of preliminary calculations. In particular the D-state quantities (see AG 253 § 7.1) are often derived indirectly from the profile data. The stars indicate therefore the quantities which are, functionally, the independent variables rather than those which were directly available as numbers for processing. A good example is the wall shear stress TAUW. Data are usually presented in the form of a skin friction coefficient CF. This quantity depends, in addition to the shear stress, on the reference values used in its formation, the D-state density and velocity. Many of the flows considered here have strong normal pressure gradients, so that the possible D-state properties are quite rapidly varying functions of the Y-value chosen to specify the boundary layer edge. We have adopted the practice, therefore, of reducing authors' CF input data to TAUW values for use as programme input, since we are then free to try various different D-states if we think it proper without having to consciously correct the normalisation of CF. For this reason a CF value in our tables may well differ from that given by the original author. In this, and in many other features, our selection of a D-state, however carefully considered, may be ill advised. We hope however that it is self-consistent, so that the essential data may be recovered, and, at need, represented in a form better suited to the user's prejudices.

Section C, mean profile tables, provides a selection from the available profile data. In an attempt to reduce the number of printed pages, the amount of space allotted to this section in this volume is significantly less than in AG 223. Readers will therefore need to have recourse to the full tabulation in the microfilm presentation which accompanies this volume, or the computer tape data base (see § 1.2 below and the address list at the start of this volume).

| | | | | | | | | |
|---|---|-------|------|--------|------|------|------|---------------|
| I | Y | PT2/P | P/PD | TO/TOD | M/MD | U/UD | T/TD | RHO/RHOD*U/UD |
|---|---|-------|------|--------|------|------|------|---------------|

The presentation is as in AG 223 save that for layout reasons the last column of data RHO*U/RHOD*UD has been relabelled R*U/RD*UD. At the foot of each profile is a statement of the input used to construct the profile. As for the "Kopfdaten" tables of section B, quite often the data available to us did not directly fit our scheme of presentation. The input information at the foot of a profile table is again indicative of the functional input rather than the numerical information as such. Not infrequently, a notice follows describing an averaging procedure when several sets of data were supplied for a given value of Y. The boundary layer edge state chosen or accepted by the editors is marked by the letter D. We have made clear in § 7 of AG 253 that this selection is essentially arbitrary. In using the information it is important to recognise that the scaled dimensionless information offered, while in principle more universal, is in fact critically dependent on the choice of scaling quantity used. Thus it is the pressure, velocity, or shear stress rather than the pressure ratio, velocity ratio or shear stress coefficient which represents the data entered to the catalogue. The dimensionless quantities are convenient, but coloured by the scaling process.

Section D supplies a miscellany of supplementary data. Of its very nature this does not fit the standard profile-based scheme. Typically, in AG 223, and this volume, we present such information as wall-shear stress, temperature, or pressure distributions which have not been interpolated to the profile stations. Often far more detail is available, in terms of a streamwise distribution, for these quantities than for profile-derived data. We also present, at times, a selection of turbulence data.

Turbulence data notionally form a part of section D. We have, so far, encountered tabular data for 15 distinct turbulence quantities. The greatest number presented by a single author is 10, Rose (CAT 7306S), followed by Kussoy & Horstman (CAT 7501S) and Kussoy et al. (CAT 7802S) with 6. Other authors give only a single quantity. We have not therefore attempted to adopt a standard layout for turbulence data tables. We have however adopted a standard scaling, choosing as reference quantities appropriate groupings of the local wall data, ρ_w , u_τ and T_w . The values of these may be obtained from the data in the tables of section B, and we felt it more helpful to refer the fluctuation quantities to a fixed, stated, base rather than give quantities such as local intensities $\overline{u'^2}/u^2$ etc. The scaling values ρ_w , u_τ and T_w are given with the turbulence data. In addition, for zero pressure gradient-cases we give our calculated value of the transformed outer law defect thickness Δ^* . For the reasons stated in § 7.1 of AG 253, and discussed further at various points in chapters 3 and 4 below, we consider this to be the only proper outer region scaling length. For any family of flows which have self-similar outer region velocity profiles, the ratio (Δ^*/δ) is fixed, so long as a consistent definition for δ is used, even if it does not lend itself to measurement, since

$$(\Delta^*/\delta) = \int_0^{y>\delta} \frac{u^*(\delta) - \bar{u}^*}{u_\tau} d(y/\delta).$$

We do not give a value for pressure gradient-cases since the flows are not similar to each other, and since in many cases there are strong normal pressure gradients which make Δ^* dependent on the choice of D-point.

| | | | | | | | | | | |
|---|----|----|----|----------|----------|---------|---------|---------|------------|------------|
| Y | U' | V' | W' | RHO*U'V' | RHO*U'W' | RHO*U' | RHO*V' | RHO*W' | RHO*U'T' | RHO*V'T' |
| | UT | UT | UT | RHOW*UT2 | RHOW*UT2 | RHOW*UT | RHOW*UT | RHOW*UT | RHOW*UT*TW | RHOW*UT*TW |

We then give the profiles. For 'single component' terms these are the root mean square values of the quantity in question. For two component or correlation terms they are the time means. Thus:

$$\begin{aligned} U' &= \left[\frac{\overline{u'^2}}{u_\tau^2} \right]^{1/2} & T' &= \left[\frac{\overline{T'^2}}{T_w^2} \right]^{1/2} & \text{RHO } U' &= \left[\frac{(\overline{\rho u'})^2}{\rho_w^2 u_\tau^2} \right]^{1/2} & \text{RHOW*U'V'} &= \left[\frac{\overline{\rho u'v'}}{\rho_w u_\tau^2} \right] & \text{RHO } U'T' &= \left[\frac{(\overline{\rho u'})^2 T'}{\rho_w u_\tau^2 T_w} \right] \\ UT & & TW & & \text{RHOW*UT} & & \text{RHOW*UT2} & & \text{RHOW*UT*TW} & \end{aligned}$$

The total amount of turbulence data is large, (see Tables 3.1 and 4.3.1), but the very large collections are generally either accessibly published, or of less interest than might at first seem apparent. We have therefore only given a small selection in the entries. The full listing is in the microfiche collection and the tape data base.

Order of sections. While an entry will usually consist of sections in the order A-B-C-D, we have mixed sections freely when it was possible to save space by doing so. The page numbers include an indication of the section - e.g., CAT 7204 A2/B1 which is the second page of section A for entry 7204, and also carries some or all of section B.

1.2. The data collection

The entries in this volume describe experiments which provided 420 mean flow profiles. To print these as tables would have required about 300 pages, so that only a very small proportion could actually be provided as part of the entries. The mean flow profiles for the supplementary entries are however listed in full in two forms, a set of microfiche to be found in pockets at the rear of this volume, and on magnetic tape, copies of which may be obtained from the institutions listed at the start of this volume.

Both the microfiche collection and the magnetic tape also contain a listing of all the tabular turbulence data we have processed, including a limited amount associated with the experiments described in AG 223. We have also included certain cases not described in the catalogue (Rose & Johnson, 7502S and Klebanoff, 5504S, subsonic), where we have processed graphical data in the same way as for the entries proper. In some cases we had data which we have not processed. The data collection does not include the turbulence profiles listed in AG 223 with CAT 7403. The authors have since reprocessed the data to obtain a very different answer

(Laderman & Demetriades, 1979). We have also not listed the very large amount of mass flow fluctuation data - $\overline{(\rho u)^2}$ - sent to us by Berg (CAI 1703S) as this quantity alone, in a hypersonic flow, cannot serve as more than a form of flow visualisation allowing a comparison of general turbulence levels.

Other than turbulence information, data listed as part of section D in an entry have not been reproduced in the microfiche or the data tape.

1.3 Background for the survey of turbulence measurements

Our purpose in chapters 3 and 4 of the main text of this volume is to survey the available data - experimental results - from turbulence measurements. We have not at any point in the survey considered the experimental difficulties and likely accuracy or relevance of the data, taking instead the position that these are the data reported, and that the level of uncertainty is that as given by the authors.

Measurements of the turbulence flow field are required partly for their own sake (in environmental studies at low speed, for example) but principally, as an aid to the modelling of turbulent effects for calculation methods. It is difficult to discuss possible measurements apart from the technique used to make them, but certain generalities serve to set the scene.

The aim is to provide sufficient information to 'close' the time-mean boundary layer approximation to the Navier-Stokes equations. This requires a means of predicting the various components of the Reynolds stress tensor, τ_{ij} , and in particular the shear stress ($-\bar{\rho} \overline{u'v'}$), with the normal stresses $\bar{\rho} \overline{u'^2}$, $\bar{\rho} \overline{v'^2}$ usually considered of lesser importance. The difficulty is apparent, as not only it is necessary to make measurements, usually with fragile sensors, in the hostile environment of a supersonic flow, but for the stress component of most interest it is in principle necessary to measure two components at the same time and place. There is therefore much to be gained by developing any means of relating the shear stress to the most simply measured single component, $\overline{u'^2}$. Unfortunately, while this may be done for lack of an alternative in simple models, there is no general simple inter-relationship. The development of turbulence in a flow is a complex process, and no proper description can be made unless a field equation is introduced for the significant terms of the Reynolds stress itself. This in turn requires information about the gradients of the stress terms which implies further knowledge or modelling of triple correlation terms.

It is proper then to look briefly at the possible measurements. There are three techniques of significance, here mentioned in ascending order of current success.

- a) The electron beam fluorescence technique relies on measurements of the mean and fluctuating intensity of light emitted by fluorescent gas molecules in the boundary layer which have been illuminated by a powerful electron beam. In principle the equipment can be calibrated to give values for the mean density $\bar{\rho}$ and r.m.s and spectral distribution of the density fluctuations, ρ' . The principal limitations lie in obtaining a sufficiently powerful beam without losing spatial resolution. There are very considerable problems in bringing the beam to bear on a region of interest unless the whole experiment is designed round the beam equipment. Unless the density is very low the beam spreads substantially even if the original cross section was small so that spatial resolution is lost. Despite great efforts by a number of experiments (Wallace, 1967, 1968, 1969; McRonald, 1975; Bartlett, 1981) no significant data has yet been obtained. For a general description of the technique see Bütetisch and Vennemann (1974).
- b) The laser-doppler velocimeter relies on the frequency shift of light scattered from small particles in the test gas. With modern techniques it is no longer necessary to 'seed' the flow with particles, and with a suitable arrangement of sensors it is possible to make simultaneous measurements of mean and fluctuating velocity components in any direction, given the free light paths required. The shear stress correlation may then be made electronically. Spatial resolution is good, and spectral distributions of the fluctuating terms can be obtained within certain limits of frequency. The technique is probably approaching maturity for low speed flows, and has achieved some success in compressible flow up to about $M = 3$ (see for instance Johnson & Rose, 1975; Rose & Johnson, 1975.) There remain problems of interpretation particularly near the wall, see Schairer (1980) and § 4.3 below, and it is very difficult to get accurate results (Dimotakis et al., 1979) at the high frequencies characteristic

of fluctuation in supersonic flows. A great advantage is that the technique is non-intrusive so that the life of sensors does not have to be considered, and, in comparison with the electron beam, a laser beam is relatively easily introduced into the test section. For a recent review of the technique see Durst et al. (1976).

- c) The hot-wire anemometer has provided the bulk of the available data, and all that considered at any length below. Hot wires, or analogous devices in suitable combinations can in principle provide, with the aid of modal analysis, almost any turbulent quantity desired (see for instance the ten quantities listed by Rose, 1973, CAT 7306S). The interpretation of the measurements and the extent to which the derived turbulence quantities can be said to be measured with any accuracy provide however an extensive field for controversy.

Since hot-wire anemometry has provided nearly all the useful data, and since the editors are only too conscious of their lack of expertise in this field, we have asked Dr. V. Mikulla (MBB, formerly NASA Ames) to prepare and account (chapter 2 below) of the technique and the interpretation of the results. His account of the conventional modal analysis technique is relatively brief, indicating only key features since the procedures are relatively well covered in the literature. Much of his chapter describes a technique designed to circumvent the inherent ambiguities of modal analysis, and so offer a greater measure of certainty in the determination of turbulence quantities for the future. The technique is relatively novel, and readers should not assume that it is to be regarded as an established standard one. Data obtained using it will be found in CAT 7205 (new data), 7501S 7802S and 80001S.

The electron beam can only provide one single component fluctuation quantity, $\overline{v'^2}$, and that probably not of very great importance in turbulence modelling. It is probably fair to say that the interest in the results of these investigations is mainly due to a desire by modellers to satisfy themselves that, for many purposes, they can ignore ρ' . The LDV can provide three velocity components and correlations between them. These are the most important data for an understanding of momentum transfer, but do not help directly with heat transfer problems. The hot wire can provide some form of data for all one or two component quantities, including the thermal terms, though in reducing the data it is necessary to assume various forms of linkage between the possible terms, so introducing a fundamental uncertainty.

All three techniques potentially provide spectral distributions. We do not present any of these here, as the data are essentially imprecise and so adequately assessed from graphical presentation in the original papers.

No significant triple correlation measurements have been made at supersonic mean velocities.

2. HOT WIRE ANEMOMETRY IN COMPRESSIBLE TURBULENT BOUNDARY LAYERS

by V. Mikulla

2.1 Basis of hot-wire anemometry in a compressible turbulent boundary layer

The brief summary below outlines the underlying principles of compressible hot-wire anemometry as described by Kovaszny (1950, 1953), Morkovin (1956) and Morkovin & Phinney (1958).

A hot-wire anemometer senses those changes in the kinematic and thermodynamic variables of the surrounding flow which modify the rate of heat transfer between the wire and the fluid. For instance changes in the mass flow rate per unit area flowing past the wire and changes in the temperature of this fluid affect the cooling and therefore the resistance of the wire which can be sensed as a measurable electric signal. Correct interpretation of the signal depends on understanding of the nature of the fluctuations in the fluid and an adequate knowledge of the heat transfer laws and appropriate calibration processes.

The nature of the fluctuations in compressible flow was first investigated by Kovaszny (1950, 1953) who showed that a viscous compressible heat conducting fluid can have three different kinds of small perturbation fields obeying three independent differential equations (the linearized equations for the conservation of momentum, energy and mass). The three independent modes are the vorticity mode τ' , the sound-wave mode Π' with the pressure as its principle variable and the entropy mode σ' . If the different modes are not sufficiently weak then linearisation is no longer possible and the modes are coupled in a non-linear manner.

The hot wire heated by an electric current unfortunately does not respond directly to any one of the fluctuation modes discussed above but to a linear combination of mass-flow fluctuations $m'(t)$ and stagnation temperature fluctuations θ'_T .

The equation for the change of enthalpy $E(\approx cT_w)$ of the wire reads

$$\frac{dE}{dt} = W - H \quad (2.1.1)$$

where W stands for the thermal energy $I_w^2 R_w$ generated per unit time and H for the rate of energy loss to the fluid. Since the present discussion and the suggested new measuring technique concentrate on constant temperature operation, it is this operation which is mainly described. If the wire is correctly compensated for constant temperature operation so that there is an instantaneous response to a change of T_w , then $\frac{dE}{dt} = 0$. Differentiating the equation for W logarithmically yields

$$d \ln W = 2 d \ln I_w + d \ln R_w = d \ln H \quad (2.1.2a)$$

Another form of this equation contains the wire response parameter $K^* = (d \ln R_w) / (d \ln T_w)$; (see e.g., Rose 1973) so that

$$d \ln W = 2 d \ln I_w + K d \ln T_w \quad (2.1.2b)$$

Introducing a nonlinear resistance-temperature relationship

$$R_w = R_r [1 + \{\alpha_r (T_w - T_r)\} + \gamma_r \{\alpha_r (T_w - T_r)^2\}] \quad (2.1.3)$$

and linearizing the ensuing equation Morkovin (1956, appendix) gives

$$K = \frac{1}{T + \alpha'_w} \{ \alpha_r T_r + \alpha'_w [1 + \gamma_r (\alpha'_w + 2\alpha_r T_r)] \} \quad (2.1.4)$$

where

$$\alpha'_w = \frac{I_w^2 - R_r}{R_r} \quad (\text{the overheating parameter}), \quad (2.1.5)$$

α_r = the temperature resistivity coefficient,

γ_r = the ratio of resistivity coefficients and

index r refers to 'recovery', i.e., the condition of the unheated wire.

* The perturbation in R due to T_w (averaged over the wire length) is described by this parameter.

The energy loss H to the fluid for a hot wire which has a yaw angle ϕ to the direction of the flow can be written as

$$H = Nu_t(M, Re_t, \theta, \phi) \cdot \pi \cdot l \cdot K_t (T_w - \eta T_t), \quad (2.1.6)$$

where M = Mach number,

$$Re_t = \frac{\rho u d}{\mu_t} = \text{Reynolds number},$$

$$\theta = T_w/T_t; \quad \eta = T_r/T_t,$$

l = the length of the wire; d = the diameter of the wire,

K = the thermal conductivity and

the suffix t denotes stagnation conditions.

The small sensitivity to Prandtl number in most gases is absorbed in the dependence on T_r .

Perturbations of W and H are expressed in terms of perturbations in the flow variables to be measured ρ, u, T_t , in the yaw angle ϕ and in the wire temperature which is viewed as a temporary independent variable of the perturbation process (T_w is constant for $dE/dt = 0$).

Now "the forbidding algebraic manipulations are made tractable by the use of logarithmic derivatives" (Morkovin 1956) and the logarithmic differential of H is developed as:

$$\begin{aligned} d \ln H = & \left[n_t - m_t \frac{\partial \ln Nu_t}{\partial \ln Re_t} - \left\{ \frac{\partial \ln Nu_t}{\partial \ln \theta} + \frac{\theta}{\theta - \eta} \right\} + 1 - \frac{1}{\tau_{wr}} \left\{ \frac{1}{2\alpha} \frac{\partial \ln \eta}{\partial \ln M} - m_t \frac{\partial \ln \eta}{\partial \ln Re_t} \right\} - \frac{1}{2\alpha} \frac{\partial \ln Nu_t}{\partial \ln M} \right] d \ln T_t \\ & + \left[\frac{\partial \ln Nu_t}{\partial \ln Re_t} + \frac{1}{\alpha} \frac{\partial \ln Nu_t}{\partial \ln M} - \frac{1}{\tau_{wr}} \left\{ \frac{1}{\alpha} \frac{\partial \ln \eta}{\partial \ln M} + \frac{\partial \ln \eta}{\partial \ln Re_t} \right\} \right] d \ln \eta + \left[\frac{\partial \ln Nu_t}{\partial \ln Re_t} - \frac{1}{\tau_{wr}} \frac{\partial \ln \eta}{\partial \ln Re_t} \right] d \ln \rho \\ & + \left[\frac{\partial \ln Nu_t}{\partial \ln \theta} + \frac{\theta}{\theta - \eta} \right] d \ln T_w + \left[\frac{1}{\tau_{wr}} \frac{\partial \ln \eta}{\partial \phi} - \frac{\partial \ln Nu_t}{\partial \phi} \right] d \phi, \end{aligned} \quad (2.1.7)$$

where $m_t = \partial \ln \nu_t / \partial \ln T_t$; $n_t = \partial \ln K_t / \partial \ln T_t$,

$$\tau_{wr} = \frac{T_w - T_r}{T_r}; \quad \alpha = \left(1 + \frac{\gamma - 1}{2} M^2 \right)^{-1} \quad \text{and}$$

$$d\phi = \frac{v'}{u}$$

The term in square brackets multiplied by $d \ln T_t$ is sometimes given in a slightly different form (Morkovin, 1956).

$$\left[n_t - m_t \frac{\partial \ln Nu_t}{\partial \ln Re_t} - \frac{\partial \ln Nu_t}{\partial \ln \theta} - \frac{1}{\tau_{wr}} \left\{ 1 - \frac{1}{2\alpha} \frac{\partial \ln \eta}{\partial \ln M} - m_t \frac{\partial \ln \eta}{\partial \ln Re_t} \right\} - \frac{1}{2\alpha} \frac{\partial \ln Nu_t}{\partial \ln M} \right] d \ln T_t \quad (2.1.8)$$

The plus sign in the last term of eqn.(2.1.7) is associated with a v' that increases the heat loss from the wire.

The response of the system - combining eqn.(2.1.3) and (2.1.7) - to variations in ρ, u, T_t and ϕ then consists of the coupled variations in I and R_w which are usually detected as fluctuations in voltage across the wire

$$E_w = I_w \cdot R_w \quad (2.1.9)$$

or

$$d \ln E_w = d \ln I_w + d \ln R_w = d \ln I_w + K d \ln T_w \quad (2.1.10)$$

Rose (1973) has shown that $d \ln E_w = d \ln E$ where E is the bridge voltage. This relationship holds since $E = E_w [(R_w + R_s)/R_w]$ and $d \ln R_w$ is assumed to be zero (R_s is the resistance in series with the anemometer bridge circuit including the probe cable).

Combining eqn.(2.1.2), (2.1.10) and (2.1.7) yields $d \ln H = d \ln W = 2 d \ln E - d \ln R_w$ and with $d \ln R_w = 0$

$$\frac{dE}{E} = \frac{E'}{E} = \left[\frac{1}{200} \left(100 \frac{T_t'}{T_t} \right) + \left[\frac{1}{200} \left(100 \frac{u'}{u} \right) + \left[\frac{1}{200} \left(100 \frac{\rho'}{\rho} \right) + \left[\frac{1}{200} \left(100 \frac{v'}{v} \right) \right] \right] \right] \quad (2.1.11)$$

where the contents of the square brackets are the same as for eqn(2.1.7).

Introducing the fluctuation sensitivities S for the respective variables leads to the equation which relates the fluctuation of the bridge voltage to the fluctuations of the flow variables

$$E^{*'} = S_{T_t} T_t^{*'} + S_u u^{*'} + S_\rho \rho^{*'} + S_v v^{*'} \quad (2.1.12)$$

where () * denotes fluctuations as percentages of the mean values.

The fluctuation sensitivities S apply to the entire compressible flow regime from subsonic to supersonic flow for arbitrary Reynolds numbers and for yawed and normal ($S_v = 0$) hot wires. The relationships for the fluctuation sensitivities are presented here in the form given by Rose (1973):

$$S_{T_t} = \frac{1}{2} \left[n_t + 1 - m_t \frac{\partial \ln Nu_t}{\partial \ln Re_t} - \left(\frac{\partial \ln Nu_t}{\partial \ln \theta} + \frac{\theta}{\theta - \eta} \right) + \frac{1}{\tau_{wr}} \left(\frac{1}{2\alpha} \frac{\partial \ln \eta}{\partial \ln M} + m_t \frac{\partial \ln \eta}{\partial \ln Re_t} \right) - \frac{1}{2\alpha} \frac{\partial \ln Nu_t}{\partial \ln M} \right] \quad (2.1.13)$$

$$S_u = \frac{1}{2} \left[\frac{\partial \ln Nu_t}{\partial \ln Re_t} + \frac{1}{\alpha} \frac{\partial \ln Nu_t}{\partial \ln M} - \frac{1}{\tau_{wr}} \left(\frac{1}{\alpha} \frac{\partial \ln \eta}{\partial \ln M} + \frac{\partial \ln \eta}{\partial \ln Re_t} \right) \right] \quad (2.1.14)$$

$$S_\rho = \frac{1}{2} \left[\frac{\partial \ln Nu_t}{\partial \ln Re_t} - \frac{1}{\tau_{wr}} \frac{\partial \ln \eta}{\partial \ln Re_t} \right] \quad (2.1.15)$$

$$S_v = \frac{1}{2} \left[\frac{1}{\tau_{wr}} \frac{\partial \ln \eta}{\partial \phi} - \frac{\partial \ln Nu_t}{\partial \phi} \right] \quad (2.1.16)$$

The basic practical technique for extracting quantitative information from the fluctuating signal of a hot wire in compressible flow was the original Kovaszny observation that the values of the sensitivity coefficients vary with operating conditions, especially with the temperature of the wire. When the wire is barely heated it responds mainly to stagnation temperature fluctuations whereas at high overheats the values of the sensitivity coefficients S_u , S_ρ and S_v dominate those of S_{T_t} .

In the general form above, the expressions for the sensitivities are complicated and calibration techniques designed to determine them accurately would be very difficult. Even if the three sensitivities S_{T_t} , S_u and S_ρ for a normal wire for instance could be determined, it would still not be possible to determine the fluctuating quantities $T_t^{*'}$, $u^{*'}$ and $\rho^{*'}$ using the squared RMS signal of a properly compensated anemometer at six different overheat ratios mainly because the variation of S_u and S_ρ with wire temperature is small and the resulting matrix of the six linear equations is nearly singular. A solution to this problem for supersonic flow has been given by Morkovin (1956) who showed that for $M > 1.2$ for a normal wire and $M \sin \phi > 1.2$ for a yawed wire the terms $\partial \ln Nu_t / \partial \ln M$ and $\partial \ln \eta / \partial \ln M$ are negligibly small at all wire operating temperatures yielding for the sensitivities:

$$S_u = S_\rho = S_{\rho u} = \frac{1}{2} \left[\frac{\partial \ln Nu_t}{\partial \ln Re_t} - \frac{1}{\tau_{wr}} \cdot \frac{\partial \ln \eta}{\partial \ln Re_t} \right] \quad (2.1.17)$$

$$S_{T_t} = \frac{1}{2} \left[n_t + 1 - m_t \frac{\partial \ln Nu_t}{\partial \ln Re_t} - \left(\frac{\partial \ln Nu_t}{\partial \ln \theta} + \frac{\theta}{\theta - \eta} \right) + \frac{m_t}{\tau_{wr}} \cdot \frac{\partial \ln \eta}{\partial \ln Re_t} \right] \quad (2.1.18)$$

$$S_r = \frac{1}{2} \left[\frac{1}{\tau_{wr}} \cdot \frac{\partial \ln \eta}{\partial \phi} - \frac{\partial \ln Nu_t}{\partial \phi} \right] \quad (2.1.19)$$

Under these conditions eqn.(2.1.12) reduces to

$$E^{*'} = S_{T_t} T_t^{*'} + S_{\rho_u} (\rho_u)^{*'} \pm S_v v^{*'} \quad (2.1.20)$$

For a normal wire when $S_v = 0$, this equation links the fluctuating output voltage with small fluctuations in total temperature and mass flow in the direction of the mean motion.

For a determination of $T_t^{*'}$ and $(\rho_u)^{*'}$ the Kovaszny (1953) technique is usually applied. This uses measurements of the mean square of $E^{*'}$

$$\frac{\overline{E^{*'^2}}}{(S_{T_t})^2} = F^2 \overline{(\rho_u)^{*'^2}} + \overline{T_t^{*'^2}} - 2F \overline{(\rho_u)^{*'}} \overline{T_t^{*'}} = S \quad (2.1.21)$$

where $F = -S_{\rho_u}/S_{T_t}$ is a function of the overheat ratio .

Taking three readings at three overheat ratios one obtains three different sets of corresponding values of $\overline{E^{*'^2}}$, S_{T_t} and S_{ρ_u} and can solve three linear equations for the three unknown quantities $\overline{T_t^{*'^2}}$, $\overline{(\rho_u)^{*'^2}}$ and $\overline{T_t^{*'}} \overline{(\rho_u)^{*'}}$. The sensitivities S_{T_t} , S_{ρ_u} and S_v are usually determined by direct calibration of the wire using for instance the definition given by Rose (1973)

$$S_{T_t} = \left(\frac{\partial \ln E}{\partial \ln T_t} \right)_{\rho_u, \phi} ; S_{\rho_u} = \left(\frac{\partial \ln E}{\partial \ln \rho_u} \right)_{T_t, \phi} ; S_v = \left(\frac{\partial \ln E}{\partial \ln v} \right)_{\rho_u, T_t} \quad (2.1.22)$$

Despite the fact that this now classic mode-diagram method was developed over twenty years ago, it is surprising to find that the amount of actual fluctuating data in high speed flow based on this method is rather scarce. There are several reasons for this, one of the most important ones probably being the fact that the variation of the overheat is a lengthy and difficult procedure requiring long wire life times and long tunnel running times (continuous tunnels). Nevertheless there have been extensive investigations based on the classic approach, for example those of Demetriades (1972) and Laderman (1979).

2.2. Sensors with very high overheat ratios

Since the following description is based on experience with CTA-operation the classic modal analysis is not pursued any further here. This alternate approach is suggested as it promises a more direct, faster and more accurate method of obtaining quantitative fluctuating data in compressible flows. It makes use of the advantages of hot films at high speeds and the slowly emerging significance of extreme sensor operating temperature in the easier interpretation of the sensor fluctuating signal. The time constants of hot films are not well defined and no compensating amplifiers for constant current anemometers exist that will properly restore the response of a hot film. Therefore a decision to use hot films or hot wires mounted on ceramic substrates automatically limits the experimenter to the use of constant temperature anemometry if quantitative information about fluctuating flow variables is to be obtained.

In this connection some remarks about CTA and CCA seem appropriate. It is neither useful nor possible to judge one technique as being useless and the other excellent in the high speed laboratory. The fact is that the CCA was available to the pioneers (Kovaszny, Morkovin etc.) at the time they did their work, whereas the CTA is much more common in the fluid dynamics laboratory nowadays. Which of the two instruments to use should be a question of what you want to measure with which sensor in the fastest time with the least effort (i.e., without studying the anemometer and its response for months).

If quantitative measurements of stagnation temperature fluctuations are intended, then the CCA with compensating amplifiers and single cold wires should be used.

If mass flux fluctuations are to be measured it is quicker and easier to use CTA with either wires or films at temperature loadings near the maximum possible values. The same is true for transverse velocity fluctuations and Reynolds shear stress measurements.

While Owen et al. (1975) have shown some of the problems of the standard CTA at low overheat ratios, there have also been papers that show that the CTA can have sufficient frequency response at low wire temperatures under certain conditions and with special bridge circuits (Bonnet et al. 1980).

2.2.1 Supported high temperature sensors

The approach to high speed anemometers suggested here avoids any controversy as to possible CTA frequency response problems by using the sensors at very high overheat ratios only. It is the author's opinion that this technique so simplifies the analysis of fluctuation measurements that high temperature hot-film anemometry will become a routine measurement procedure in the future. We first discuss the significance of high values of the temperature loading

$$(T_w - T_r)/T_r (= \tau_{wr}) .$$

The objective is to virtually eliminate the response of the hot film or supported hot wire to stagnation temperature fluctuations, thus avoiding any modal analysis techniques. Although this means that no information is obtained about the stagnation temperature fluctuations, it should be kept in mind that the fluctuating stagnation temperature - being a combination of u' and T' - is generally of secondary importance for turbulence research and modelling.*)

Horstman & Rose (1975) have shown for transonic flow that the ratio of stagnation temperature fluctuation sensitivity to mass-flow fluctuation sensitivity $S_{T_t}/S_{\rho u}$ approaches zero if τ_{wr} approaches the value of 1.5. Since this result is essentially independent of sensor material, sensor Reynolds number, Mach number and length to diameter ratio, it means that if a sensor can be operated at a high temperature such that $\tau_{wr} \geq 1.5$, then it will only respond to mass-flow fluctuations over the entire compressible flow region from transonic to hypersonic regardless of the magnitude of the stagnation temperature fluctuations. This observation opens new possibilities for high speed turbulence measurements with thermal sensors. While it is a consequence of the original Kovaszny observation of the variation of the sensitivities $S_{\rho u}$ and S_{T_t} with wire temperature, its potential can only now be fully exploited with the development of sputtered nickel films on quartz or pyrex and new platinum wire ceramic wedges that retain their full strength at maximum possible temperature loading.

Figure (2.1) shows the importance of the requirement $\tau_{wr} \geq 1.5$ in relation to the operating temperature of various existing hot-wire and hot-film probes. The sensitivity ratio is plotted against the sensor operating temperature for four different recovery temperatures T_r . Notice that even for non-heated flows (T_r near room temperature) with the usual operating temperature range of tungsten wires ($300K < T_w < 600K$) it is not possible to achieve a condition in which $S_{T_t}/S_{\rho u} = 0$. For these sensors it is therefore always necessary to use modal analysis techniques to separate T_t' and $(\rho u)'$. There are also commercial film probes that cannot be operated much higher than $T_w = 600K$. With these films it would also be necessary to use mode diagrams to separate the fluctuations with the additional difficulty of carefully analysing the frequency response of the CTA-operated hot films at a range of different overheat ratios.

As a typical example of the importance of the wire operating temperature we take the hot wire turbulence data obtained in a shock wave boundary layer interaction by Ardonceau et al. (1979). In this study the hot wire was only heated up to a maximum value of $\tau_{wr} = 0.7$; $a_w = (R_w - R_{T_t})/R_{T_t} = 0.8$, $T_w = 500K$ so that it was still sensitive to both T_t' and $(\rho u)'$. The required operating temperature for virtual removal of the stagnation temperature sensitivity in this particular flow would have to be about 750K. The significance of being able to increase the sensor temperature from $T_w = 600K$ to $T_w = 750K$ in a compressible flow at recovery temperatures around 300K is seen in Fig. (2.1). The ratio of sensitivities $S_{T_t}/S_{\rho u}$ decreases from 1.0 to approximately 0.2. Commercial film probes are available that can be operated at maximum temperatures around 750K and those sensors would be perfectly adequate for non-heated high speed flows being effectively sensitive to mass-flow fluctuations only. For higher recovery temperatures ($T_r \geq 400K$) there are no commercial film probes available

*) The correlation $T_t'v'$ has been mostly needed in the past to deduce the important Reynolds shear stress $\rho \overline{u'v'}$ from hot-wire measurements (equation 2.3.4). It will be shown below how an alternate assumption can replace the measurement of $T_t'v'$ in deducing $\rho \overline{u'v'}$ so that there is no major disadvantage in removing the response of the probe-anemometer system to T_t' .

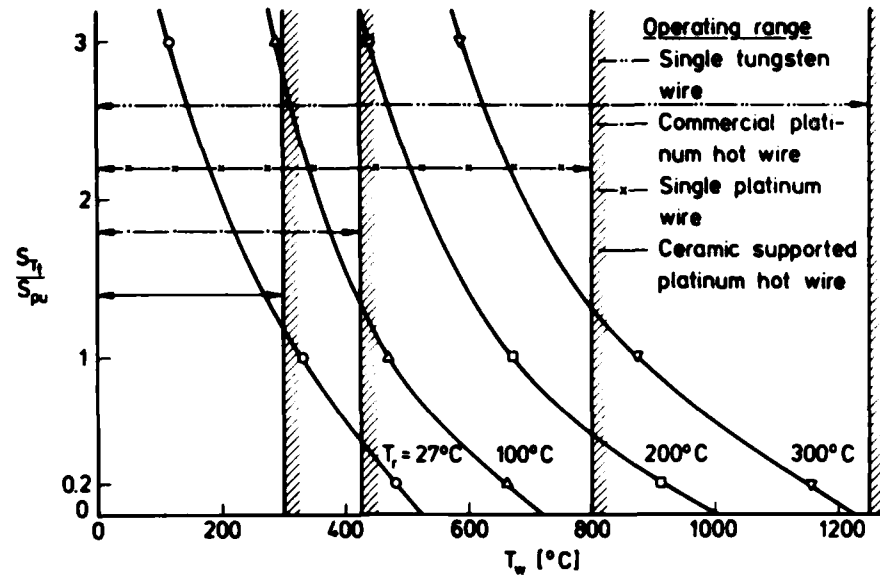


Fig. 2.1 Ratio of total temperature sensitivity to mass-flux sensitivity vs. operating sensor temperature for various recovery temperatures.

that could eliminate the response to stagnation temperature fluctuations. Only platinum and platinum-alloy wires can be operated at high enough temperatures. Figure (2.2) shows the more general diagram of the ratio of the two sensitivities S_{T_t} and $S_{\rho U}$ plotted against the temperature loading factor τ_{wr} .

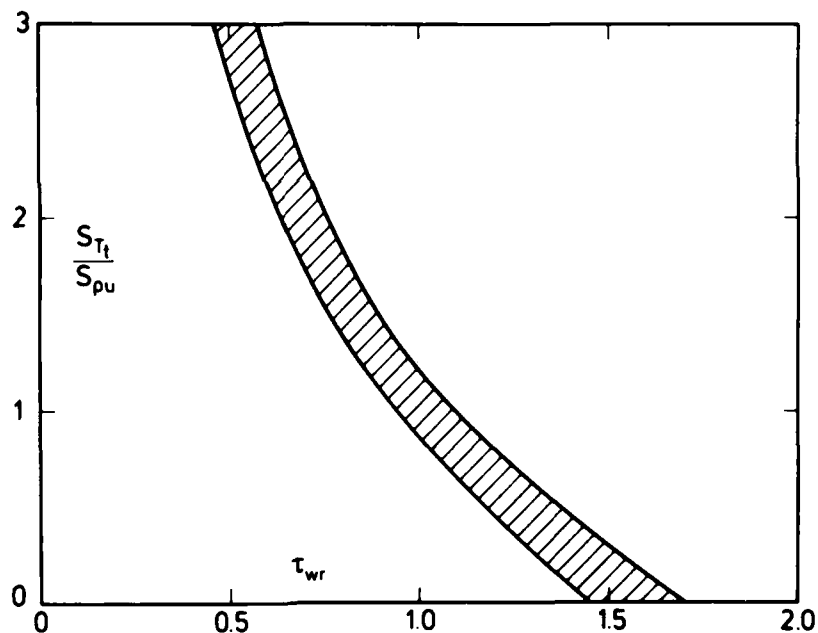


Fig. 2.2 Ratio of total temperature sensitivity to mass-flux sensitivity vs. temperature loading factor τ_{wr} .

The general problem with single wires at their maximum possible operating temperature in high speed flows is that their strength is also reduced considerably and this is particularly true for single platinum wires. One solution to this problem lies in a probe design with a platinum wire mounted on the tip edge of a high temperature very thin ceramic wedge (Mikulla & Horstman 1975). It turned out that the wires could be operated safely on such a wedge-shaped body at wire temperatures well over 1250K making them virtually solely mass flux sensitive in the whole recovery temperature range considered from $T_r = 300\text{K}$ to $T_r = 600\text{K}$ (Figure 2.1). This important characteristic was in fact the main reason for their success when used in the hypersonic boundary layer with recovery temperatures well in excess of 500K (Mikulla and Horstman 1975). The ability of wedge-shaped sensors to retain their geometry and strength while the sensing film or wire is operated just

below the oxidizing temperature has important advantages for the accuracy and interpretation of high speed turbulence measurements. In addition to eliminating the response to total temperature fluctuations the high operating temperature provides in general - just as in incompressible flow - optimum frequency response with fewer contamination problems for the probe/CTA system. It is easy to see why a ceramic hot wire wedge probe operating at $T_w = 1500K$ is less affected by dust, oil or grease particles in the flow than a tungsten wire operating at $T_w = 600K$. In the former case most of the oncoming particles are burnt away.

Figure (2.3) shows another advantage of wedge-shaped sensors compared to single hot wires. At the maximum operating temperatures considered, slanted wires and films needed for the measurement of transverse velocity

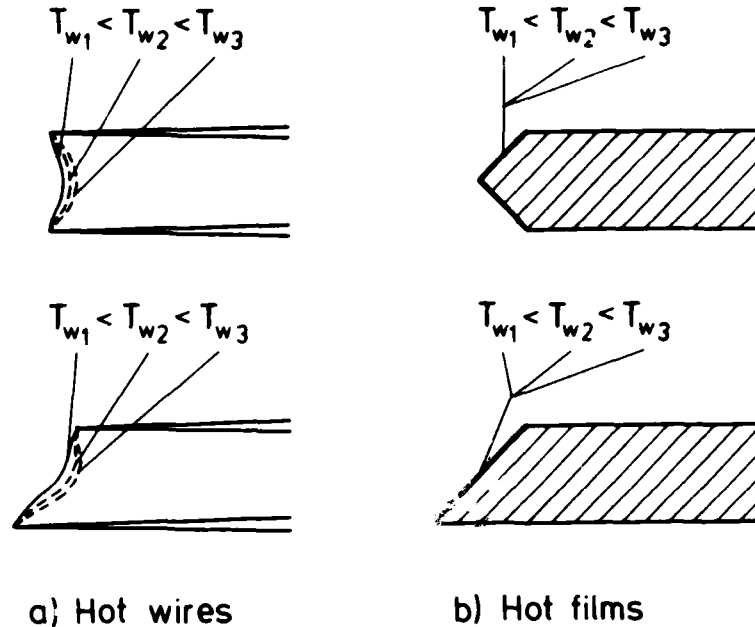


Fig. 2.3 Comparison of the geometry of single hot wires and wedge type sensors at high operating temperatures and dynamic loading.

fluctuations and Reynolds shear stresses have not only maximum sensitivity to mass flow fluctuations $(\rho u)'$ but also to the transverse velocity fluctuations v' or w' . While for the inclined single or dual films ($\phi = 45^\circ$) this increased sensitivity at high overheats is approximately the same for mass flux fluctuations and transverse velocity fluctuations, the increase of S_v or S_w with increasing wire operating temperature for the single slanted wire is significantly less than the increase of $S_{\rho u}$, firstly because of the natural slack given to most wires in high speed flow to avoid strain gauging and secondly because of the additional slack caused by elongation of the wire near the maximum operating temperatures (Figure 2.3). This elongation is particularly pronounced for platinum and platinum alloy wires. As a consequence, the single slanted wire or X-probe in compressible flow has the disadvantage that time consuming individual yaw calibration is absolutely necessary and that even with this calibration the accuracy of v' and w' measurements and consequently also of $(\rho u)'\overline{v'}$ will be less than the accuracy of $(\rho u)'$ measurements.

For the slanted single and dual hot films and supported hot wires at very high temperature loading τ_{wp} and yaw angles at 45° it can be assumed that $S_v = S_w = S_{\rho u}$ thus making separate yaw calibrations unnecessary. In addition, because of the factors discussed above, the achievable accuracy of v' , w' and $(\rho u)'\overline{v'}$ is of the same order as that for $(\rho u)'$ -measurements.

While it is difficult to assess the upper limits of the expected errors with the new sensors accurately, a comparison with the error estimates of the single tungsten wire measurements of Rose (1973) would not show an increasing error in the transverse fluctuations and cross correlation compared to $(\rho u)'$

| Rose (1973) | | Mikulla and Horstman (1975) | |
|--------------------------|------------|-----------------------------|-----------|
| $(\rho u)'$ | $\pm 8\%$ | $(\rho u)'$ | $\pm 8\%$ |
| $(\rho u)'\overline{v'}$ | $\pm 15\%$ | $(\rho u)'\overline{v'}$ | $\pm 8\%$ |
| v' | $\pm 25\%$ | v' | $\pm 8\%$ |
| w' | $\pm 25\%$ | w' | $\pm 8\%$ |

2.2.2 Calibration of highly heated sensors

The main problem with these very highly heated hot-film probes and supported hot-wire probes is the accurate determination of the sensitivity $S_{\rho u} = \frac{\partial \ln E}{\partial \ln \rho u}$ over the entire Reynolds number range encountered in the actual turbulence measurements. There have been doubts about the validity of quantitative turbulence measurements with wedge-shaped hot films in gases because of thermal feedback problems which cause the probe sensitivities to be functions of frequency (Bellhouse and Schultz 1967). This is a particularly serious problem for multiple wires or films mounted on the same substrate. It is part of the general problem area of dynamic calibration of thermal sensors which has received considerable attention among hot-wire researchers in recent years.

In order to avoid uncertainties introduced by the static calibration technique of these wedge-shaped sensors, it is suggested that a different method be used to determine $S_{\rho u}$. The wedge-shaped single or dual wire sensor is calibrated against the $(\rho u)'$ -measurement obtained with a single normal wire which might well be operated in the modal analysis method. The advantage of this method is that it is exactly the $(\rho u)'$ -measurement which is probably the most accurately measurable of all the turbulence quantities using a hot wire in high speed flow (wire slackness and elongation at high overheat are in this case the least critical). Figure (2.4) shows a typical calibration curve for a dual hot wire ceramic wedge probe. The mass flux sensitivity of this probe $S_{\rho u}$ is obtained by dividing half of the RMS-value of the instantaneous sum of the fluctuating voltages

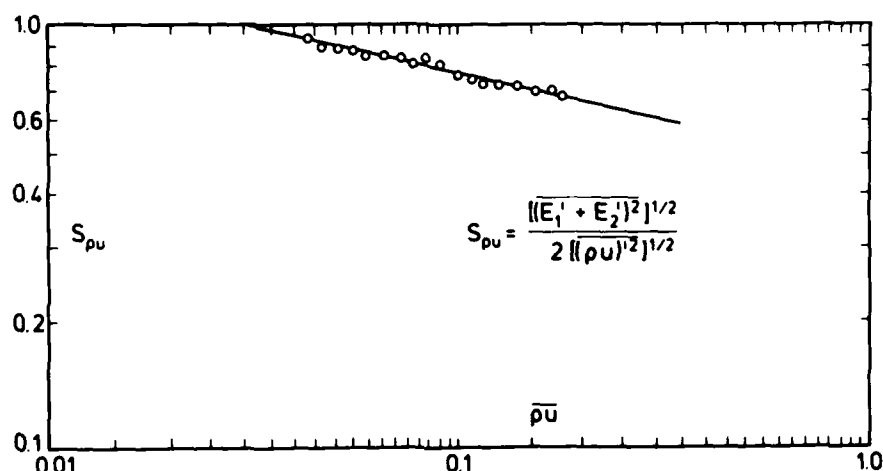


Fig. 2.4 Typical calibration curve of dual platinum wire ceramic wedge probe.

of the two supported platinum wires by the RMS-value of the measured mass-flow fluctuations obtained with the single wire. For this case:

$$S_{\rho u} = \frac{[(E_1' + E_2')^2]^{1/2}}{2[(\rho u)']^{1/2}} \quad (2.2.1a)$$

and for a single film or hot wire wedge probe correspondingly

$$S_{\rho u} = \frac{[E']^{1/2}}{[(\rho u)']^{1/2}} \quad (2.2.1b)$$

Equation (2.2.1a) in fact assumes identical or matched wires with equal sensitivities. While this is hardly ever achievable in practice it seemed a reasonable approximation in the case of the very highly heated platinum alloy wires of the ceramic dual wedge probe. Having obtained the sensitivity of a dual wedge probe in this way, it is then a straightforward matter to measure $\frac{(\rho u)'}{\rho u}$, $\frac{v'}{u}$, $\frac{(\rho u)'v'}{\rho u u}$ and by rotating the probe 90° around its axis also $\frac{w'}{u}$ and $\frac{(\rho u)'w'}{\rho u u}$.

As stated above there are already commercial hot-film probes available that can be operated near $T_w = 700K$ and for most non-heated compressible flows this sensor temperature can assure that τ_{wr} is near 1.5 thus virtually eliminating the response of the probe to T_t' . A check on the response of the sensor to $(\rho u)'$ alone can always be made by operating the sensor at two different overheat ratios near the maximum value and evaluating the mass-flux fluctuations deduced at each overheat. If the two values agree, then the assumption that

$$\frac{S_{T_t}}{S_{\rho u}} = 0 \quad \text{is correct.}$$

In practice it appears that for most compressible adiabatic flows at lower Mach numbers (subsonic to transonic) the stagnation temperature fluctuations are much smaller than the mass-flux fluctuations. In this case it may be sufficient to operate the sensors at temperatures such that τ_{wr} is about 1.0 ensuring that $S_{\rho u} (\rho u)^{1/2} \gg S_{T_t} (T_t^{1/2})$. For the platinum or platinum alloy hot-wire ceramic wedge probe the condition $\frac{S_{T_t}}{S_{\rho u}} = 0$ can be virtually ensured in most high speed wind tunnels due to their potential for very high operating temperatures ($T_w = 1250\text{K}$ to $T_w = 1500\text{K}$). The thermal sensor industry should respond to the challenge of making high temperature probes based on the combination of platinum or platinum alloy wires (diameter 5μ to 10μ) and high temperature ceramic backing material as off-the-shelf items.

2.2.3 Advantages and disadvantages of highly heated sensors

The advantages of such sensors compared to standard hot-wire probes for measurements in compressible flow are quite clear:

- (a) No mode diagram is required and therefore no variation of overheat ratios is necessary.
- (b) CTA-operation is implied with all the corresponding advantages of availability and ease of operation.
- (c) No yaw calibration for 45° -slanted sensors is necessary if the probe axis is aligned parallel to the flow.
- (d) The determination of fluctuating quantities is not dependent on squared RMS readings. (This generally results in a loss of information and of accuracy in the turbulent quantities.)
- (e) Accurate direct determination of v' and w' fluctuations at high Mach numbers may be obtained without any assumptions concerning the physics of turbulence.
- (f) Short running times (characteristic of most high speed wind tunnels) are sufficient to measure $(\rho u)'$, v' , $(\rho u)'v'$ with previously calibrated sensors.

The main disadvantage of these sensors is the general disadvantage of all wedge-shaped hot-film sensors in boundary layers near the wall. They are more affected by large mean-flux gradients and turbulence properties than single wires or fibre-film probes. In particular the dual wedge probe is not a good sensor for the wall region since the two sensors are exposed to quite different gradients. Although miniaturization of the probes would reduce this problem these sensors cannot provide accurate measurements in the very important wall region of high speed turbulent boundary layers. They have, however, one further important advantage which concerns their use in transonic flow.

2.3. Special features in measurement

2.3.1 Transonic flow

Although transonic flow is currently of major interest in aerodynamic research the use of the hot wire in this field has been hampered by the calibration difficulties described by Morkovin (1956). In a recent review and evaluation of transonic hot-wire anemometry Horstman and Rose (1977) have shown, however, that the use of thermal sensors can lead to meaningful fluctuating data in transonic turbulent boundary layers if certain conditions are met. Morkovin (1956) had observed that the terms $\partial \ln Nu_t / \partial \ln M$ and $\partial \ln \eta / \partial \ln M$ in the expressions for the sensitivities S_{T_t} and S_u (eqn. 2.1.13 and 2.1.14) were not negligible in the transonic flow regime at all wire overheats for a wide range of Reynolds numbers. Thus $S_{\rho} \neq S_u$ and since neither varies much with wire operating temperature it was not possible to use modal analysis techniques to determine the fluctuations. The significant result of the investigation of Horstman and Rose was that if the sensor operating temperature and the sensor Reynolds number were high enough, then $S_{\rho} = S_u$ just as in supersonic and hypersonic flow.

The conditions which ensure this can be summarized as follows:

$$\left. \begin{array}{l} \text{If } Re_t > 20 \\ \tau_{wr} > 0.5 \end{array} \right\} \quad \text{for } 0.4 < M < 1.2$$

then

$$S_{\rho} = S_u = S_{\rho u} = \frac{1}{2} \left[\frac{\partial \ln \text{Re}_t}{\partial \ln \text{Re}_t} - \frac{1}{\tau_{wr}} \frac{\partial \ln \tau}{\partial \ln \text{Re}_t} \right] \quad (2.3.1)$$

The first condition, $\text{Re}_t > 20$, is usually fulfilled in most transonic flows. The second condition, $\tau_{wr} > 0.5$, is automatically satisfied if the hot wire or hot film is operated at temperature loadings near $\tau_{wr} = 1.5$ or higher, as suggested for $M > 1.2$ above. This technique therefore makes possible an extension of turbulence measurements to transonic flow. For most transonic flows in unheated wind tunnels commercial hot-film wedge sensors with maximum operating temperatures up to 700K will give a high enough value of τ_{wr} . If ceramic supported platinum wires are used, however, it becomes possible to cover the entire Mach number range with a single probe. A dual wire probe which has had its sensitivity $S_{\rho u}$ measured over a sufficiently wide Reynolds number range may therefore be used straightforwardly to measure $(\rho u)'$, v' , w' and $\overline{(\rho u)'v'}$ for any Mach number. The only restriction is that Re_t must be greater than 20.

2.3.2 Shear stress measurements

The Reynolds shear stress $\bar{\rho} \overline{u'v'}$ can be obtained from the directly measured quantities $(\rho u)'$, v' , w' and $\overline{(\rho u)'v'}$ with assumptions relating to the fluctuating pressure field. Before discussing this, however, it should again be emphasized that the measurement of v' and w' is a direct measurement without requiring any assumptions concerning the magnitude of the pressure fluctuations and therefore not dependent on the Mach number. These transverse velocity fluctuations, because of the inherent properties of the measurement technique, have an accuracy which cannot be achieved for those quantities measured with single hot wires at high speeds.

If the traditional hot-wire mode diagram method is used and $(\rho u)'$, v' , T_t' and their correlations $\overline{(\rho u)'v'}$, $\overline{T_t'v'}$ and $\overline{(\rho u)'T_t'}$ are measured with X-type wire probes or single slanted wires, then in principle all the important turbulence quantities such as u' , v' and $\bar{\rho} \overline{u'v'}$ can be deduced if the assumption is made that p' is negligible. This assumption has been used and discussed extensively in the literature (see, e.g., Horstman and Rose 1977). It does seem a reasonable assumption for non-hypersonic flows. The necessary relations are given below: From the definition of stagnation temperature

$$c_p T_t = \frac{u^2}{2} + \frac{\gamma}{\gamma-1} \frac{p}{\rho}$$

it can be shown either by logarithmic differentiation or by Reynolds time averaging and neglecting all higher order terms that

$$\left(1 + \frac{\gamma-1}{2} M^2\right) \frac{T_t'}{T_t} = (\gamma-1) M^2 \frac{u'}{u} + \frac{p'}{p} - \frac{\rho'}{\rho} .$$

With $\frac{p'}{p} = 0$; $\frac{(\rho u)'}{\bar{\rho} u} = \frac{u'}{u} + \frac{\rho'}{\bar{\rho}}$ it follows that (Kistler 1954 and Rose 1973):

$$\frac{\overline{u'^2}}{\bar{u}^2} = (\alpha+\beta)^{-2} \cdot \overline{T_t'^{2\alpha}} + 2\alpha(\alpha+\beta)^{-2} \cdot \overline{(\rho u)^{2\alpha} T_t'^{2\alpha}} + \alpha^2(\alpha+\beta)^{-2} \cdot \overline{(\rho u)^{2\alpha}} , \quad (2.3.2)$$

$$\frac{\overline{\rho'^2}}{\bar{\rho}^2} = (\alpha+\beta)^{-2} \cdot \overline{T_t'^{2\beta}} - 2\beta(\alpha+\beta)^{-2} \cdot \overline{(\rho u)^{2\alpha} T_t'^{2\beta}} + \beta^2(\alpha+\beta)^{-2} \cdot \overline{(\rho u)^{2\alpha}} \quad \text{and} \quad (2.3.3)$$

$$\frac{\overline{u'v'}}{\bar{u}^2} = (\alpha+\beta)^{-1} \cdot \overline{T_t'^{\alpha} v'^{\alpha}} + \alpha(\alpha+\beta)^{-1} \cdot \overline{(\rho u)^{\alpha} v'^{\alpha}} , \quad (2.3.4)$$

where

$$\alpha = \left(1 + \frac{\gamma-1}{2} M^2\right)^{-1} , \quad \beta = \alpha(\gamma-1)M^2 .$$

Although the equation for the Reynolds shear stress (eqn. 2.3.4) is here derived with the assumption $p' = 0$ it can be shown (Mikulla and Horstman 1975) that the assumption $\overline{p'v'} = 0$ is sufficient to yield $\bar{\rho} \overline{u'v'}$ from the measured hot-wire cross-correlations $\overline{(\rho u)'v'}$ and $\overline{T_t'v'}$.

While this classical approach to the interpretation of the hot wire fluctuating signal is necessarily dependent upon the mode diagram method, it should once more be pointed out that, although it is possible in theory, in practice it is extremely difficult if not impossible to obtain accurate values of all the necessary correlation terms with single hot wires. This is especially true for all measurements involving v' and w' fluctuations. The method, using squared RMS-values of the fluctuating voltage within a 180°-rotation of a single yawed wire, gives a result which requires the difference between two large numbers. This difficulty is added to the above mentioned difficulty of reduced yaw sensitivity resulting from wire slackness and elongation at high sensor temperature.

Since with the measurement technique suggested here no information is obtained about the stagnation temperature fluctuations, it is not possible in general to deduce the velocity fluctuation u' and the density fluctuation ρ' from the measurement of $(\rho u)'$ alone. This can only be achieved for the trivial case that stagnation temperature fluctuations in the flow are so low as to be negligible. In this case equations (2.3.2) and (2.3.4) reduce to

$$\frac{\overline{u'^2}}{\bar{u}^2} = \alpha^2(\alpha+\beta)^{-2} \cdot \overline{(\rho u)'^2} \quad (2.3.5)$$

and

$$\frac{\overline{\rho'^2}}{\bar{\rho}^2} = \beta^2(\alpha+\beta)^{-2} \overline{(\rho u)'^2} \quad (2.3.6)$$

It is, however, possible to derive the very important Reynolds shear stress $\bar{\rho} \overline{u'v'}$ by an alternative route. This approach requires the assumption of a value for the turbulent Prandtl number Pr_t in addition to assuming $\overline{p'v'} = 0$. It is then possible to obtain $\bar{\rho} \overline{u'v'}$ from an accurate measurement of $\overline{(\rho u)'^2}$ alone.

If triple correlations are neglected it follows from the expression of the cross-correlation $\overline{(\rho u)'^2}$

$$\overline{(\rho u)'^2} = \bar{\rho} \overline{u'v'} + \bar{u} \overline{\rho'v'} \quad (2.3.7)$$

and from the equation of state with the assumption $\overline{p'v'} = 0$ that

$$\bar{\rho} \overline{v'v'} + \bar{v} \overline{\rho'v'} = 0 \quad (2.3.8)$$

The turbulent Prandtl number is defined as

$$Pr_t = \frac{\overline{u'v'}}{\overline{v'v'}} \frac{d\bar{T}/dy}{d\bar{u}/dy} \quad (2.3.9)$$

Expanding the energy equation

$$d\bar{T}_t/dy = d\bar{T}/dy + \frac{\bar{u}}{c_p} d\bar{u}/dy \quad (2.3.10)$$

using

$$\bar{u}^2/c_p \bar{T} = (\gamma-1)M^2 \quad ,$$

and combining equation (2.3.8-2.3.10), the following relation is obtained

$$\bar{u} \overline{\rho'v'} = \bar{\rho} \overline{u'v'} \frac{(\gamma-1)M^2}{Pr_t} \left(1 - \frac{c_p}{\bar{u}} \frac{d\bar{T}_t/dy}{d\bar{u}/dy} \right) \quad (2.3.11)$$

Substituting equation (2.3.11) into equation (2.3.7) the expression for Reynolds shear stress becomes

$$\bar{\rho} \overline{u'v'} = \left[1 + \frac{(\gamma-1)M^2}{Pr_t} \left(1 - \frac{c_p}{\bar{u}} \frac{d\bar{T}_t/dy}{d\bar{u}/dy} \right) \right]^{-1} \overline{(\rho u)'^2} \quad (2.3.12)$$

and for isoenergetic flow

$$\bar{\rho} \overline{u'v'} = \left[1 + \frac{(\gamma-1)M^2}{Pr_t} \right]^{-1} \overline{(\rho u)'^2} \quad (2.3.13)$$

It has been pointed out by Fernholz (private communication) that the expression for shear stress (equation 2.3.12) assumes that the gradient of the turbulent intensity $\frac{\partial \overline{u'^2}}{\partial y}$ is also negligible since equation (2.3.10) is more properly expanded as

$$d\overline{u'^2}/dy = d\overline{u'^2}/dy + \frac{1}{2c_p} \left[2 \bar{u} \frac{d\bar{u}}{dy} + \frac{d\overline{u'^2}}{dy} \right]$$

Since present measuring techniques and hot-wire sensors in general are not very suitable for accurate measurements very close to the viscous sublayer the assumption of a constant turbulent Prandtl number and the neglect of the gradient $\overline{u'^2}/dy$ should be quite reasonable.

It is not suggested that the new approach to the hot-wire measurement problem put forward here is the only and exclusive way of obtaining accurate measurements in high speed flows. On the contrary the author would suggest that for a problem as difficult as accurate turbulence measurements at high Mach numbers all available instruments, methods and sensors should be used, aiming at an optimal solution which combines if possible their several specific advantages. The very high temperature technique suggested here provides an addition to the available range of probes. While it is highly desirable to use as many different sensors as possible in a given flow, this coverage should be combined with the use of a chosen single sensor in as many different experiments as possible in different tunnels over the full range of Mach number. It should then, finally, become possible to distinguish the influence of Mach number on turbulent flow properties from the potentially spurious influences introduced by differing data reduction techniques.

2.4 Conclusions

This review and summary of hot-wire anemometry in compressible flow describes novel techniques for the measurement of turbulence in compressible flows with thermal sensors. While the original classical papers of Kovaszny and Morkovin remain as the basis it is shown that extreme overheating of a supported sensor leads to advantages in simplicity and accuracy of measurements of turbulent fluctuations over the full Mach number range.

The greatest amount of information about fluctuating flow variables will generally be achieved using the newly developed sensors and techniques in combination with the classical hot-wire mode diagram method.

It thus becomes apparent that the hot wire has no fundamental handicap for accurate high speed turbulence measurements in non-separated boundary layers outside the immediate wall region and that it will therefore be a complementary instrument to the LDV in this field for a long time to come.

3. TURBULENCE DATA - SINGLE COMPONENTS

When measuring fluctuating velocities in turbulent boundary layers, single component quantities such as $\overline{u'^2}$, $\overline{v'^2}$ and $\overline{w'^2}$ are measured first since the measuring technique required is straight-forward ($\overline{u'^2}$) and relatively easy ($\overline{v'^2}$, $\overline{w'^2}$), at least in subsonic flows. When multiplied by the local mean density $\bar{\rho}$ the three quantities $\bar{\rho} \overline{u'^2}$, $\bar{\rho} \overline{v'^2}$ and $\bar{\rho} \overline{w'^2}$ are the Reynolds normal stresses in a boundary layer. The ratio $(\overline{u'^2}/\bar{u}^2)^{1/2}$ is often used to characterize the local turbulence level of a flow where \bar{u} is the mean velocity, but of even much greater theoretical importance are the terms $\overline{v'^2}$ and the sum of the three components $\overline{q^2} = (\overline{u'^2} + \overline{v'^2} + \overline{w'^2})$ which is twice the specific kinetic energy of the fluctuating motion. For both $\overline{v'^2}$ and $\overline{q^2}$, so-called transport equations can be derived which play an important role in turbulence modelling. The transport equation for the kinetic energy of the fluctuating motion is part of almost every higher order turbulence model whereas a transport equation for $\overline{v'^2}$ has been used successfully for example by Wilcox and Traci (1976) and Wilcox and Rubesin (1980).

It has been interesting to find during this investigation how few measurements of all three normal stress distributions in tabular form are available both in subsonic and supersonic boundary layers and that the standard reference measurement remains the zero pressure-gradient subsonic boundary layer investigated by Klebanoff (1955).

As well as the velocity fluctuations, density, temperature and mass flux fluctuations are of interest in compressible boundary layers. Here we have even fewer data. Before we set out to discuss single component measurements it is appropriate to recall the conclusions drawn by Sandborn (1974) in his earlier study of the same topic: "Hot-wire measurements of the longitudinal component of the turbulent velocity in super- and hypersonic flow were found to agree with the incompressible data in the outer regions of the layers. Measurements of the vertical component of the turbulent velocity and the Reynolds shear stress with yawed hot wires appear questionable. Mass flux and temperature fluctuation measurements show considerable scatter from one boundary layer to another. Neither mass flux or temperature data could be correlated with the degree of similarity observed for the turbulent stress terms."

Since we still know very little about the turbulence structure of subsonic boundary layers, statements about the structure of supersonic boundary layers should be even more modest.

What we would like to investigate in the first place is whether the turbulence structure changes as a result of effects of compressibility, in boundary layers both with and without heat transfer, and secondly how pressure gradient effects and shock interactions affect the turbulence. Does similarity of the turbulence profiles exist if Reynolds number, Mach number or heat transfer change? What is the order of magnitude relationship between normal and tangential shear stresses and between the kinetic energy of the fluctuating motion? Finally, how does the shape and range of the energy spectrum compare as between the subsonic and supersonic boundary layer.

We begin our survey with Table (3.1) listing investigations in which measurements of single components of fluctuating quantities were performed. Their number is rather impressive but if one undertakes a closer inspection many data have to be excluded from our discussion, mainly because they are no longer available in tabular form. It has been our principle to compare tabulated data only and to use measurements in graphical form at most for qualitative comparisons.

Comparing the graphical presentations we find that the fluctuating velocities were made dimensionless with one of three velocities, u_δ the velocity at the outer edge of the boundary layer, u_τ the skin friction velocity $(\tau_w/\rho_w)^{1/2}$ or \bar{u} the local mean velocity, and they were invariably plotted against y/δ where δ is the boundary layer thickness. In a few cases u_∞ , the "undisturbed" upstream velocity, has been used and δ was exchanged for the momentum defect thickness δ_2 .

After our discussion of δ as a "dangerous" scaling length in compressible turbulent boundary layers in section 7 of AGARDograph 253, there is little need for a further explanation here. This rigid exclusion of δ leaves us however with the problem of determining a scaling length for the outer-region properties of a boundary layer.

Table 3.1

| Author | M_0 | Heat transfer | PG | Number of profiles | | | | $\langle \rho \rangle$ | $\langle \rho u \rangle$ | Anemometer wall geometry |
|---|------------|---------------|----------------|---------------------|---------------------|---------------------|---|------------------------|--------------------------|--------------------------------|
| | | | | $\langle u \rangle$ | $\langle v \rangle$ | $\langle w \rangle$ | $\frac{\langle T \rangle}{\langle T_0 \rangle}$ | | | |
| Morkovin & Phinney (1958) | 1.8 | AW | Z | - | - | - | - | - | 1 | CCHWA |
| Kistler (1958/59) CAT 5803 | 1.7-4.7 | AW | Z | 3 | - | - | 3 | - | 3 | CCHWA tunnel wall |
| Wallace (1968, 1969) | 8 | Cooled | Z | - | - | - | - | 5 | - | Electron beam nozzle wall |
| Waltrup & Schetz (1971), CAT 7104 | 1.9-2.4 | AW | A | 2 | - | - | - | - | - | CTHWA tunnel wall |
| Sturek & Danberg (1972a/b) CAT 7101 | 3.5 | AW | Z A | 1 1 | 1 1 | - | 1 1 | - | 1 1 | CTHWA ramp |
| Yanta & Smith (1973) | 0 | AW | Z | 1 | 1 | - | - | - | - | LDV, channel |
| Yanta & Lee (1974) | 3 | AW | Z | 8 | 8 | - | - | - | - | LDV nozzle wall |
| Yanta & Crapo (1976) | 3 | AW | Z | 4 | - | - | - | - | - | LDV nozzle wall |
| Rose (1973, 1974) CAT 7306 S | 3.9 | AW | A SBLI | 12 | 12 | 12 | 2 5 | - | - | CTHWA nozzle wall |
| Johnson & Rose (1973, 1975) | 2.9 | AW | Z | 1 | 1 | - | - | - | - | CTHWA & LDV nozzle wall |
| Johnson (1974) | 2.9 | AW | Z | 1 | - | - | - | - | - | LDV nozzle wall |
| Rose & Johnson (1975) | 2.9 | AW | A SBLI Z | 2 1 | 2 1 | - | - | - | - | LDV, CTHWA nozzle wall |
| Johnson & Rose (1976) | 0.8 | AW | Z | 2 | - | - | - | - | 2 | LDV, CTHWA flat plate |
| Rose & McDaid (1977) | 0.8 | AW | Z | 1 | - | - | - | 1 | - | CTHWA, flat plate |
| Horstman & Rose (1977) Mikulla (private com.) | 0.8 | AW | Z | 2 | 1 | 1 | - | 2 | - | CTHWA, flat plate, tunnel wall |
| Owen & Horstman (1974) | 6.7 | Cooled | Z | 1 | - | - | - 1 | 1 | 1 | CCHWA cone-ogive cylinder |
| Mikulla & Horstman (1975) | 6.9 | Cooled | Z | - | 1 | 1 | - | - | 1 | CTHWA cone-ogive cylinder |
| Owen, Horstman, Kussoy (1975) | 6.7 | Cooled | Z | 1 | - | - | - 1 | 1 | 1 | CCHWA cone-ogive cylinder |
| Mikulla & Horstman (1976) Kussoy & Horstman (1975) CAT 7501 S | 6.9 6.7 | Cooled | A SBLI Z | - | 8 | - | - | - | 8 | CTHWA cone-ogive cylinder |
| Kussoy et al. (1978) CAT 7802 S Acharya et al. (1978) CAT 7802 S | 2.3 | AW | A Z F | 25 | 25 | 25 | - | - | - | CTHWA, axisym. tunnel wall |
| Mateer et al. (1976) Mateer & Viegas (1979) Coakley & Viegas (1977) CAT 8001 | 1.4 | AW | A | - | 7 | - | - | - | - | - axisym. tunnel wall |
| Gootzait & Childs (1974, 1976, 1977) | 3.9 | AW | A Z | 8 2 | 5 2 | - | - 1 | - | - | CTHWA, axisym. nozzle wall |
| Demetriades & Laderman (1973b) and L & D (1974) CAT 7403 | 9.4 | Cooled | Z | 1 | 1 | - | 1 | - | - | CCHWA tunnel wall |

Table 3.1 cont.

| Author | M_δ | Heat transfer | PG | Number of profiles | | | | | | Anemometer wall geometry |
|---|------------|---------------|------|----------------------|----------------------|----------------------|--|-------------------------|-----------------------------|------------------------------|
| | | | | $\langle u' \rangle$ | $\langle v' \rangle$ | $\langle w' \rangle$ | $\langle T' \rangle$ $\langle T_0' \rangle$ | $\langle \rho' \rangle$ | $\langle (\rho u)' \rangle$ | |
| Laderman (1976, 1978b) Fluctuation data corrected in Laderman & Demetriades (1979) | 7.1 | AW Cooled | Z | 1 1 | 1 1 | - - | 3 4 | - - | - - | CCHWA cone |
| Laderman (1978a) Laderman & Demetriades (1979) | 3 | AW Cooled | Z | 1 | 1 | - | 1 | - | - | CCHWA flat plate |
| Dimotakis et al. (1979) | 0.1-2.2 | AW | Z | 10 | 4 | - | - | - | - | LDV, flat plate, tunnel wall |
| Ardonceanu et al. (1979) | 2.2 | AW | A | 24 | 24 | - | - | - | 23 | LDV |
| Lee (1979) | | | Ramp | | | | 4 | | | |
| Berg (1977); Kubota & Berg (1977), CAT 7703S | 6 | Cooled | Z | - | - | - | - 12 | - | 12 | CCHWA Tunnel wall |

If fluctuation measurements are available, a boundary layer edge or characteristic thickness may be defined in relation to these. Definition 'by approach to the free stream fluctuation level' cannot be very precise, as the fluctuation level measurements can never be very accurate. The availability of conditional sampling techniques however makes possible a definition in terms of the 50% intermittency point, as suggested and initially applied by Laderman & Demetriades (CAT 7403). This proposal is attractive as it provides a well conditioned intersection and should be universally applicable. It should also relate properly to the physical process of turbulent mixing in the boundary layer. The 50% intermittency point lies well within the δ -value as defined by most other criteria, but this is not of itself a disadvantage if the δ -value is defined as a suitable multiple of the y -value at 50% intermittency. Unfortunately, the 50% intermittency point is not available in most investigations yet and can thus not serve as a universal scaling length. The problems of choosing an edge criterion may be avoided by using a suitable integral thickness. If there is in fact any universal similarity in the inner and outer regions of the transformed velocity profiles of zero pressure gradient boundary layers, then the defect-integral thickness Δ^* defined in eqn. (3.3.16 of AG 253) should bear a nearly fixed proportion to the physical boundary layer thickness δ , however that may be defined. As can be seen from the definition of the defect thickness Δ^* the skin friction velocity u_τ must be available, and the van Driest transformation must hold. This may not always be the case. Another well defined integral thickness which is not restricted in this way is the momentum defect thickness δ_2 . It provides (at least in flows without normal pressure gradients) a convenient way of describing the accumulated friction effect of the boundary layer. δ_2 appears in the momentum integral equation in just this way - the integral equation itself being a convenient short-hand for a control surface momentum balance. If only because of its importance in the momentum integral equation, the momentum defect thickness is also, conventionally, the most favoured reference length for the formation of Reynolds numbers intended to correlate experimental data (for definitions and further discussion see section 7 of AG 253).

The customary use of δ_2 as a scaling length for Reynolds numbers and the fact that as an integral thickness it is precisely defined independently of a wall shear stress value, provide, with convenience, the only reasons for using it as a reference length in scaling outer region profiles. The "physical" thickness δ is ill defined, but in principle is, in any self similar flow, a fixed fraction of the outer law defect thickness Δ^* , which again, as an integral thickness is well defined though dependent on a value of the skin friction velocity u_τ . If outer region turbulence quantities are presumed to display a similar dependence on y/δ then they must be plotted using a well defined δ which is difficult to quantify, or the defect thickness Δ^* which in principle amounts to the same thing. This is very successful when done for mean flow profiles. δ_2 (or δ_1) as a fraction of Δ^* will vary with Reynolds number and so cannot serve as a proper reference length over a wide Reynolds number range.

For the inner region of a boundary layer the obvious scaling length, well known from mean flow measurements, is the ratio of the kinematic viscosity at the wall ν_w and the skin friction velocity u_τ . If we may expect any lead from mean flow behaviour, we should see similarity when data are plotted against $y^+ = (u_\tau y / \nu_w)$ for the inner region and against (y/Δ^*) for the outer region. Similarity in plots against (y/δ_2) should appear only for data covering a limited Reynolds number range.

As for the scaling velocity we find little to be gained by using the mean velocity \bar{u} since it depends on both independent variables x and y , and the outer edge velocity u_δ has definite disadvantages in all cases where an edge state - or as we usually call it a D-state - is hard to define. This is the case in all compressible boundary layers with severe pressure gradients. It may well be reasonable in many cases to use the "undisturbed" upstream velocity U_∞ when showing the development of some fluctuating quantity in the downstream direction.

3.1 Normal components of the Reynolds stress/zero pressure-gradient

Of the fluctuating velocities it is $\overline{u'^2}$ which has been measured most often. Nevertheless we know of only 8 tabulated profiles (2 in Rose 1973, 1975), all measured by hot-wire anemometry, that satisfy the boundary conditions of zero pressure-gradient and adiabatic or isothermal wall. They cover a Mach number range $1.7 \leq M_\delta \leq 7.2$ and a range of the heat transfer parameter $0.5 \leq T_w/T_r \leq 1$. We have plotted both the Reynolds normal stress $\bar{\rho} \overline{u'^2}$ and the mean square $\overline{u'^2}$ of the fluctuating velocity component u' , in order to separate out the influence of the mean density $\bar{\rho}$ on the distribution, against the inner region coordinate y^+ , and against y/Δ^* and y/δ_2 as characteristic coordinates of the outer region. We have extracted experimental data from the following investigations: Kistler (1958, CAT 5803), Horstman & Owen (1972, CAT 7205), Kussoy & Horstman (1975, CAT 7501S) and Kussoy et al. (1978, CAT 7802S). From the latter two experiments we have used the first one or two profiles of each series which were not affected by the downstream pressure rise. Unfortunately all distributions of the turbulent fluctuations had an "undocumented" upstream history which could have had an influence unknown to us, though the mean flow profiles plotted in Fig. (4.4.1) appear to conform well to the incompressible norm. Figures (3.1.1) and (3.1.2) give the inner region plots for the fluctuating velocity component u' and show no sign of profile similarity in the given Mach and Reynolds number range. When plotted against the appropriate outer region coordinate y/Δ^* in Figs. (3.1.3) and (3.1.4) there is at least a recognisable common trend. The differences in level between the various sets of data are so great, however, that it is not possible to consider any form of similarity as established. No Mach or Reynolds number effect on the normal stress $\bar{\rho} \overline{u'^2}$ can be observed but there appears to exist a Mach number effect on $\overline{u'^2}$ as can be seen from Figs. (3.1.2) and (3.1.4) where the level of the intensity decreases with increasing Mach number.

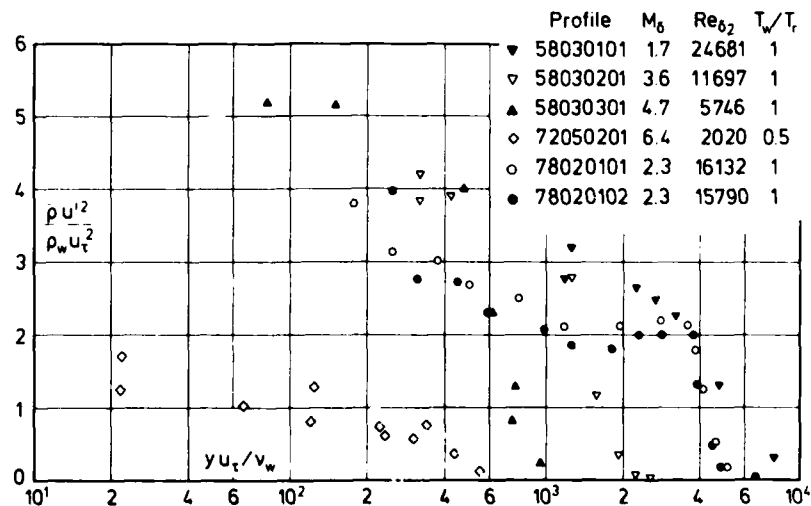


Fig. 3.1.1 Reynolds normal stress distributions in a compressible turbulent boundary layer with zero pressure-gradient (adiabatic and isothermal wall).

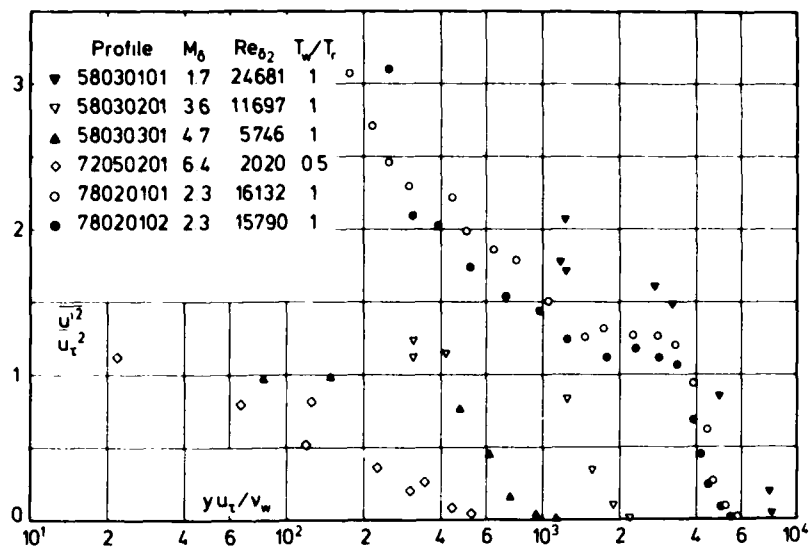


Fig. 3.1.2 Distributions of the mean square of the fluctuating velocity u' in a compressible turbulent boundary layer with zero pressure gradient (adiabatic and isothermal wall).

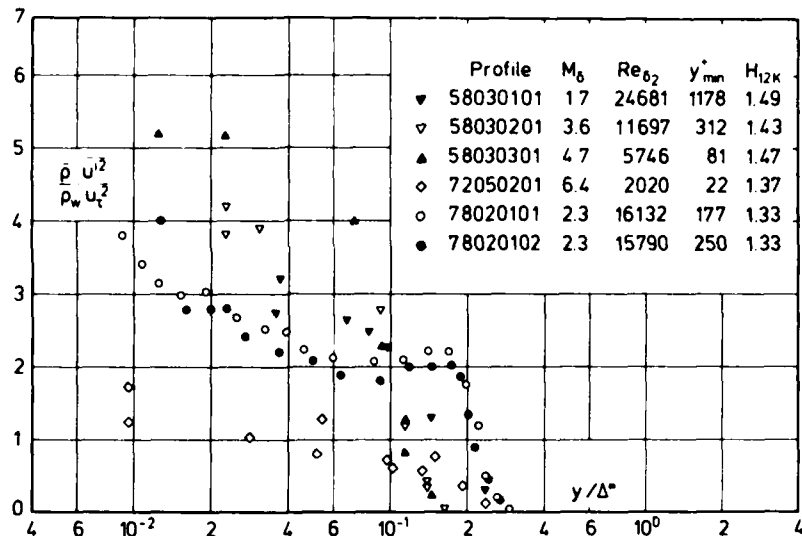


Fig. 3.1.3 Reynolds normal stress distributions in a compressible turbulent boundary layer with zero pressure gradient (adiabatic and isothermal wall).

We are well aware however that the sample of measurements available to us is very small and it is only too possible that new and systematic measurements over the whole parameter range may show a different pattern.

In the captions of Figs. (3.1.3) and (3.1.4) we have given the minimum value of y^+ as an indication of the proximity to the wall of the innermost measurements and also H_{12K} which serves as a good indicator of how far the profiles are fully developed and conform to the zero pressure gradient norm. Except for profile 72050201 the closest measurement of u' lies at the outer end of the log-law region or even beyond it. H_{12K} lies well within the range given for example by Rotta (1962, Fig. 13.6) for subsonic zero pressure-gradient boundary layers.

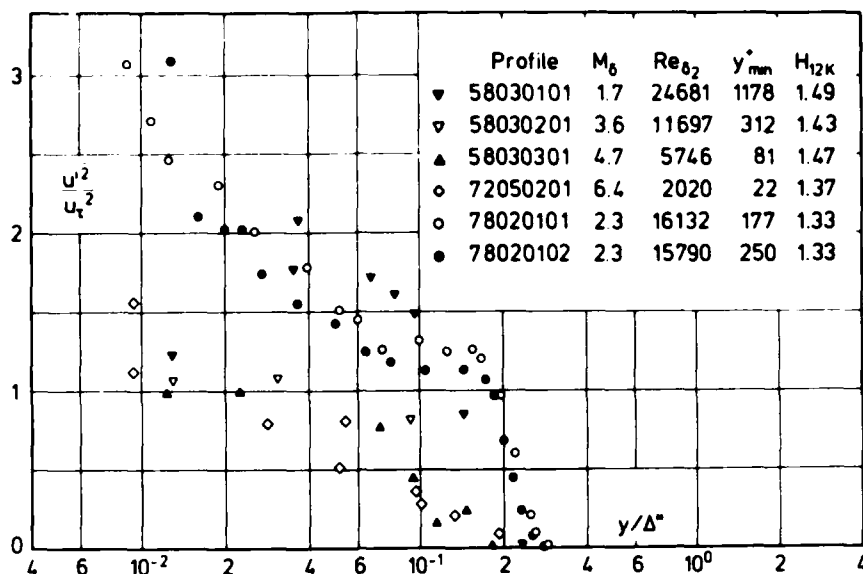


Fig. 3.1.4 Distributions of the mean square of the fluctuating velocity u' in a compressible turbulent boundary layer with zero pressure gradient (adiabatic and isothermal wall).

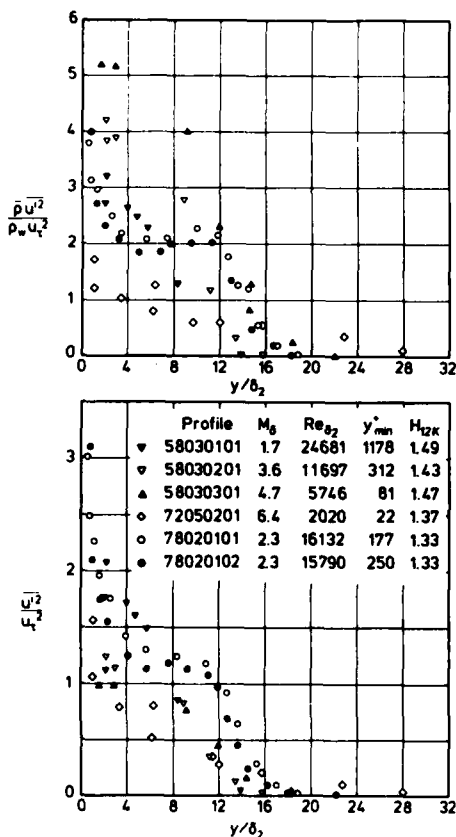


Fig. 3.1.5 a/b Reynolds normal stress and distributions in a compressible turbulent boundary layer with zero pressure gradient (adiabatic and isothermal wall).

Fig. (3.1.5 a/b) shows the normal stress $\bar{\rho} u'^2$ and the mean square \bar{u}^2 plotted against y/δ_2 in order to show the above distributions in a manner more familiar to all those who have been plotting their turbulence data against y/δ . The disadvantage of such a plot should be obvious from a comparison with the above figures. Though there exists a recognisable common trend comparable to that in Fig. (3.1.4) the distribution in the wall region is so compressed that it is almost impossible to draw any valid conclusions from such a graph.

Laser-doppler and hot-wire measurements of a single u' -distribution (Johnson & Rose 1975, graphical presentation) at $M_0 = 2.9$ show a monotonic increase towards the wall. The data agree well with each other. Closer to the wall than $y/\delta = 0.30$ their results lie up to 50% above the Kistler distributions for the most nearly matched Mach numbers (1.7 and 3.6) plotted above. The Johnson and Rose data agree well on the other hand with LDV measurements by Yanta & Crapo (1976) at a Mach number of 2.9. Yanta & Lee (1974) compared their measurements at $M_0 = 3$ with the u' -distribution of Klebanoff (1955) and found satisfactory agreement ($\pm 10\%$). All the latter measurements were plotted against y/δ in the original reports.

The picture becomes even more confusing when we look at the distributions of the other two normal stresses, $\bar{\rho} v'^2$ and $\bar{\rho} w'^2$, plotted against y^+ in Fig. (3.1.6 a and b). On the whole $\bar{\rho} w'^2$ is approximately of the same magnitude as $\bar{\rho} v'^2$. We would expect $\bar{\rho} w'^2$ to be larger than $\bar{\rho} v'^2$ from our knowledge of subsonic boundary layers, and such behaviour has been established for distributions of the normalized fluctuation velocities in transonic boundary

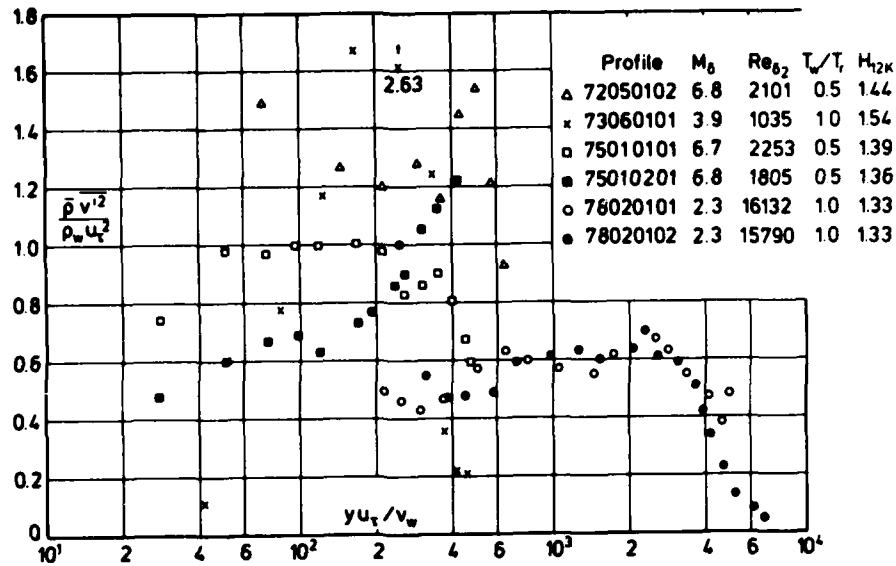


Fig. 3.1.6a Reynolds normal stress distributions in a compressible turbulent boundary layer with zero pressure gradient (adiabatic and isothermal wall).

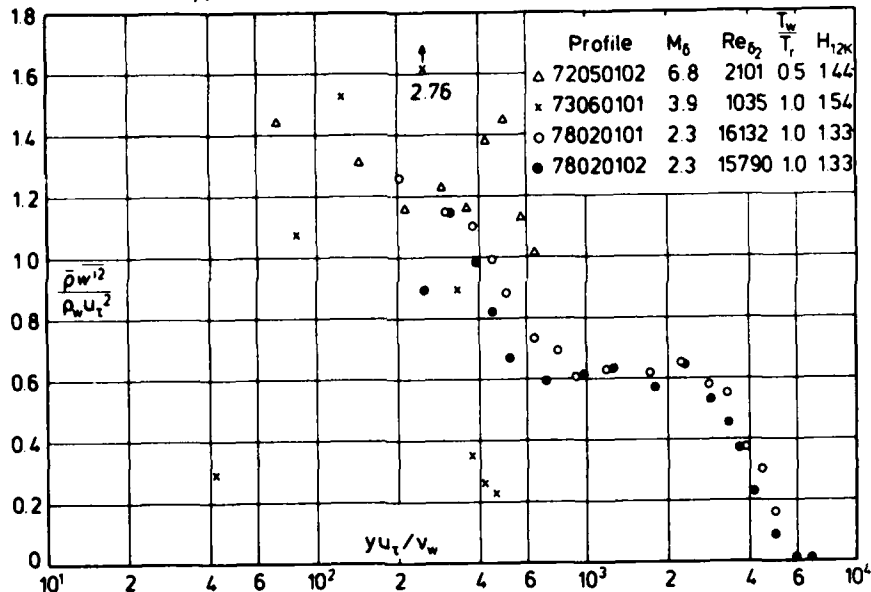


Fig. 3.1.6b Reynolds normal stress distributions in a compressible turbulent boundary layer with zero pressure gradient (adiabatic and isothermal wall).

layers (Horstman & Rose 1977), with the longitudinal velocity component u' being larger than w' and v' .

As for the distributions of $\bar{\rho} v'^2$ and $\bar{\rho} w'^2$ one finds a general pattern of behaviour in that the profiles rise from the wall, reach a peak and fall again towards the edge of the boundary layer. This is true here with two exceptions. We have no explanation for the peculiar behaviour of profile 72050102 (Horstman & Owen 1972) which shows a second peak in the outer region both in the $\bar{\rho} v'^2$ and in the $\bar{\rho} w'^2$ distribution. As can be seen in Fig. (3.1.8) this second peak is apparently due to the density distribution and not a feature of the turbulence as such.

The second exception is profile 75010201 (Kussoy & Horstman 1975) which shows an increase towards the outer edge of the boundary layer. This again is due to the influence of the density as is evident from a comparison with the respective \bar{v}^2 profile in Figs. (3.1.8) and (3.1.9a). The comparatively high peak in profile 73060101 could have been caused by the effect of the incoming shock wave (see Fig. 7306S-1). It is clearly visible also in Fig. (3.1.8) and thus apparently an effect of the turbulence structure.

Fig. (3.1.7) shows the normal stress component $\bar{\rho} \overline{v'^2}$ plotted against the outer region coordinate y/Δ^* . As in Fig. (3.1.6) where no similarity could be found for the inner region, the same absence of similarity is demonstrated here for the outer region of the boundary layer. Again, as for $\bar{\rho} \overline{u'^2}$, no influence of the Mach number can be observed on either $\bar{\rho} \overline{v'^2}$ or $\bar{\rho} \overline{w'^2}$.

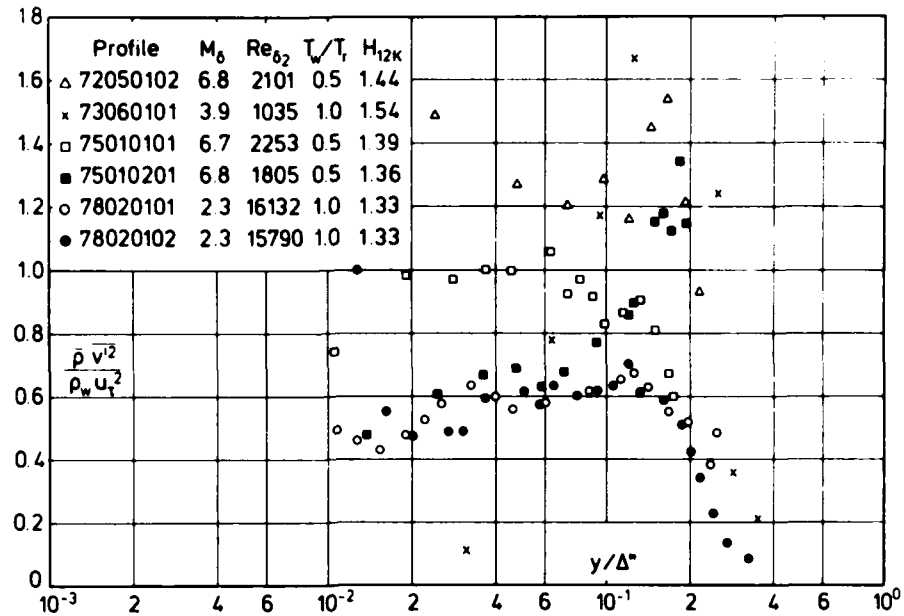


Fig. 3.1.7 Reynolds normal stress distributions in a compressible turbulent boundary layer with zero pressure gradient (adiabatic and isothermal wall).

Investigating the turbulence quantities v' and w' without the density profile, we find a common trend in all profiles in that they show a maximum and decrease both towards the wall and towards the outer edge (Figs. 3.1.8 and 3.1.9). Whereas no similarity can be established for $\overline{v'^2}$ when plotted against y^+ (Fig. 3.1.8), a similarity pattern appears to emerge in the outer region if $\overline{v'^2}$ and $\overline{w'^2}$ are plotted versus y/Δ^* (Fig. 3.1.9 a/b). The latter figure shows a Mach number effect - if such an effect can be deduced from such a small sample of data - but for $\overline{v'^2}$ and $\overline{w'^2}$ in the opposite direction to that for $\overline{u'^2}$, i.e., the fluctuation level increases with increasing Mach number.

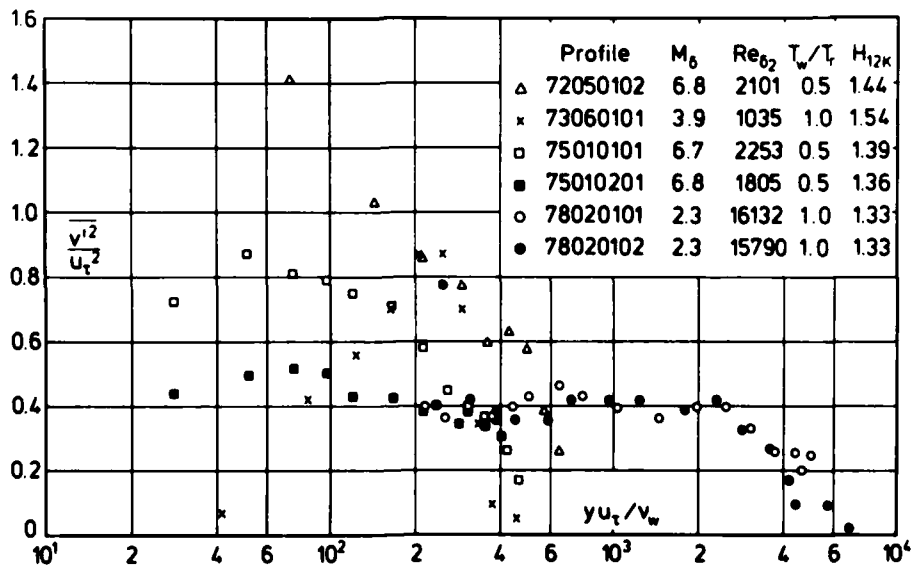


Fig. 3.1.8 Distributions of the mean square of the fluctuating velocity v' in a compressible turbulent boundary layer with zero pressure gradient (adiabatic and isothermal wall).

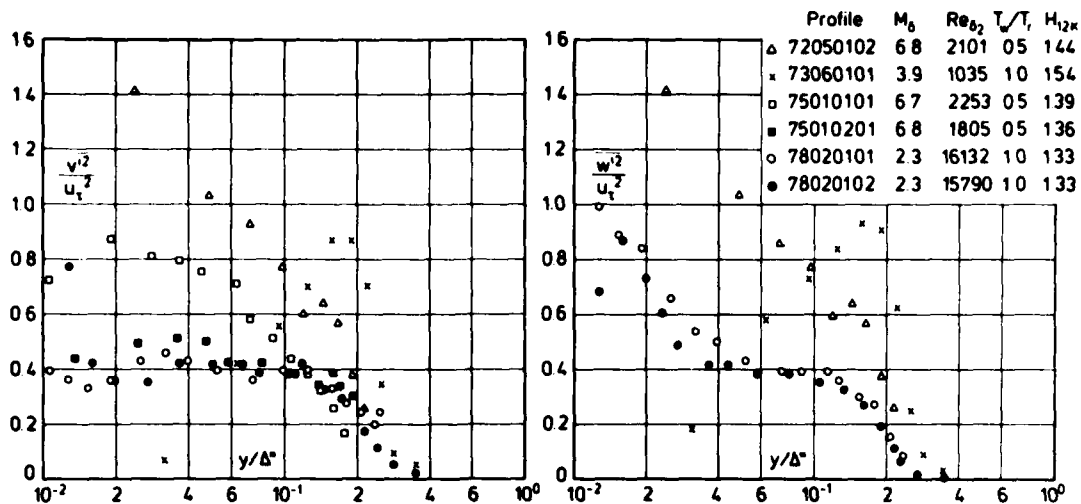


Fig. 3.1.9 a/b Distributions of the mean square of the fluctuating velocities v' and w' in a compressible turbulent boundary layer with zero pressure gradient (adiabatic and isothermal wall).

Examining the $(\overline{v'^2})^{1/2}/u_\infty$ turbulence intensity distributions presented by Yanta & Lee (1974) we find no similarity between the individual profiles even if they are plotted against " y/δ^* ". Close to the wall, profiles at the same Mach number and approximately the same Reynolds number differ by 300%. We were therefore very surprised to find a statement by the authors that "the various turbulence parameters bear a remarkable similarity to incompressible data not only in trends but also in magnitude thus indicating a Mach number independence."

Laser-doppler and hot-wire measurements performed by Johnson & Rose (1975) show a monotonic increase of $\bar{\rho} \overline{v'^2}$ towards the wall and agreement between the two measuring techniques within a band of about $\pm 20\%$. Johnson and Rose draw no conclusions from the comparison with the incompressible data which are, in any case, themselves inconsistent.

Conclusions from a small sample of measurements

After a rather exhaustive but useless attempt to find common trends or similarity in distributions of Reynolds normal stress components in compressible turbulent boundary layers with zero pressure gradient we arrive at the following conclusions:

- (1) No systematic effect of Mach number, Reynolds number or heat transfer parameter could be observed for the Reynolds normal stresses.
- (2) The Reynolds normal stress components $\bar{\rho} \overline{u'^2}$, $\bar{\rho} \overline{v'^2}$ and $\bar{\rho} \overline{w'^2}$ do not show a similar behaviour, whether in the inner or in the outer region of the boundary layer.
- (3) A trend towards similarity can be observed for the mean square fluctuating velocities $\overline{v'^2}$ and $\overline{w'^2}$ (Fig. 3.1.9).
- (4) Little can as yet be said about the behaviour of the fluctuating velocities or normal stresses in the inner region of a compressible boundary layer since no measurements have been performed close enough to the wall.
- (5) Systematic investigations of fluctuating velocities even in zero pressure-gradient compressible boundary layers are called for which cover a wide range of the above three parameters before reliable turbulence models can be established.

3.2 Normal components of the Reynolds stress - various pressure gradients

A discussion of the behaviour of normal stress components in compressible turbulent boundary layers in an adverse pressure gradient can only be a discussion of case studies at present. The two reasons for this are the scarcity of data and the lack of a suitable pressure gradient parameter which could be used to compare data from different experiments. Such a pressure gradient parameter would have to take account of boundary layer flows with both streamwise and normal pressure gradients, and of flows where both pressure gradients are present. The pressure gradient parameters which have been used most often in investigations of subsonic boundary layers are defined as

$$\Pi_1 = (\delta_1/\tau_w)dp/dx \quad \text{or} \quad \Pi_2 = (\delta_2/\tau_w)dp/dx \quad (3.2)$$

where (see also section 2.3.3 of AG 253) δ_1 is the displacement and δ_2 the momentum defect thickness. Sometimes $(v_w/\rho_w u_t^2) dp/dx$ has also been used but all three parameters have relevance only in boundary layers with no normal pressure gradient and all three tend to infinity as τ_w tends to zero at separation. When we could we have given Π_2 in all entries of AG 223 where normal pressure gradients were absent or at least small. The experimental investigations discussed below have both streamwise and normal pressure gradients and so none of the above pressure gradient parameters has any meaning.

We begin our discussion with the reflected wave case of Kussoy et al. (1978, CAT 7802S). Here the boundary layer was generated along a straight adiabatic wall and the wave structure (see figures 6.2.2 and 6.2.3 of AG 253), produced in each case by a centre body, consisted of a compression wave followed by an expansion. For series 02 the compression wave was stronger than for series 01, and was followed more rapidly by a stronger expansion wave. Figs. (3.2.1) and (3.2.2) show the distributions of the three normal stresses $\bar{\rho} \bar{u}^2$, $\bar{\rho} \bar{v}^2$ and $\bar{\rho} \bar{w}^2$ plotted against y^+ . Since no separation was observed in either of the two boundary layers this is a plausible scaling length. δ_2 is excluded as a result of the presence of the normal pressure gradient.

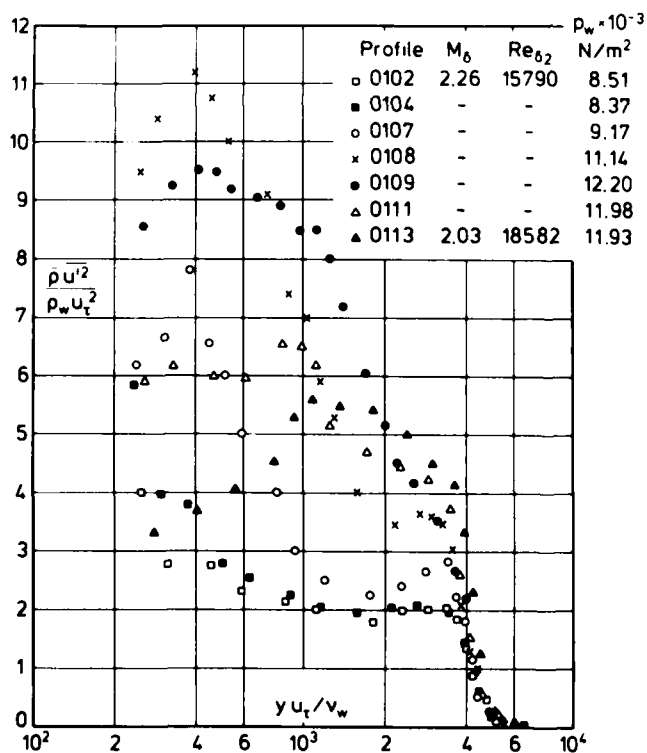


Fig. 3.2.1 Reynolds normal stress distributions in a compressible turbulent boundary layer with varied pressure gradient (adiabatic wall, origin not defined). Kussoy et al. (1978).

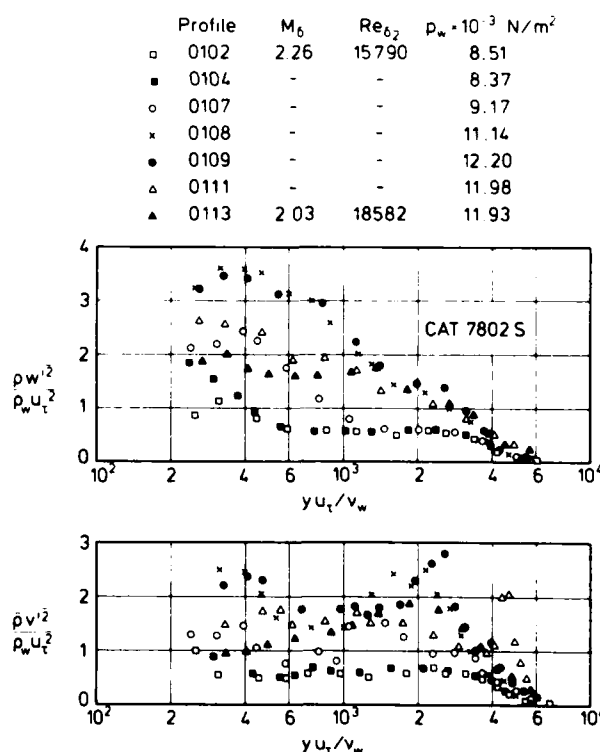


Fig. 3.2.2 Reynolds normal stress distributions in a compressible turbulent boundary layer with varied pressure gradient (adiabatic wall, origin not defined). Kussoy et al. (1978).

As can be seen from the pressure distribution (Fig. 6.2.2 of AG 253) the profiles are not affected by the incoming compression wave up to profile 0104 with the result that the turbulence structure does not change at all. We then observe a sharp increase in the level of all three normal stresses reaching a maximum for profile 0108. For the $\bar{\rho} \overline{u'^2}$ -distributions the maximum moves out into the boundary layer all the way down to profile 0113, though decreasing in relative magnitude, whereas there is only a small shift of the maximum of $\bar{\rho} \overline{w'^2}$. The $\bar{\rho} \overline{v'^2}$ distribution presents a picture in contrast to the other normal stresses in that one observes two peaks for profiles 0108 to 0111. Whether this is an effect of the outgoing expansion wave on the turbulence structure, here v' , or on the hot-wire sensor is not clear and should be investigated experimentally in more detail.

As for the differences in level of magnitude between the three normal stresses, the order is $\bar{\rho} \overline{u'^2}$, $\bar{\rho} \overline{w'^2}$ and $\bar{\rho} \overline{v'^2}$ as is observed in measurements in subsonic boundary layers. The differences are clearly more distinct than shown in the distributions of $\bar{\rho} \overline{w'^2}$ and $\bar{\rho} \overline{v'^2}$ in the zero pressure gradient flows discussed in section 3.1. above.

Fig. (3.2.3) shows the normal stress distribution ($\bar{\rho} \overline{u'^2}$) plotted versus y/Δ^* . Though the definition of the outer edge velocity u_δ , necessary for the determination of Δ^* , is problematical, the normal stress-distributions

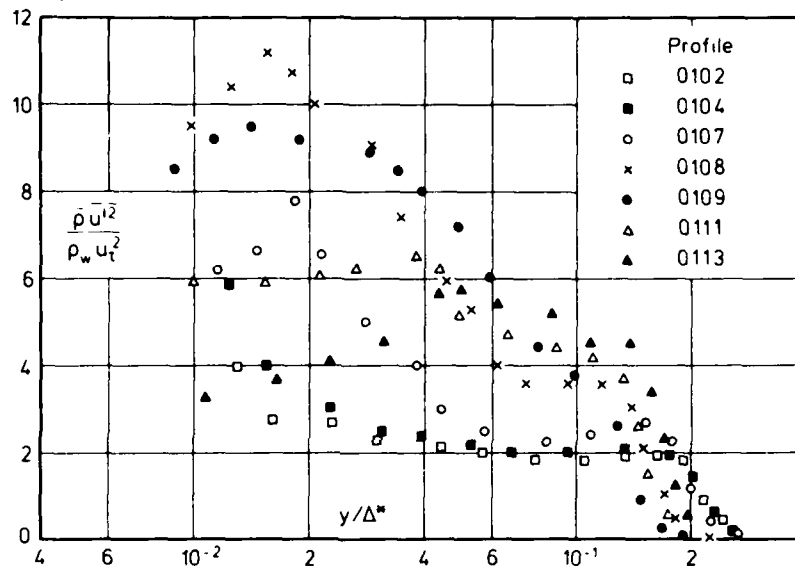


Fig. 3.2.3 Reynolds normal stress distributions in a compressible turbulent boundary layer with varied pressure gradient (adiabatic wall, origin not defined). Kussoy et al. (1978).

are qualitatively similar to those presented in Fig. (3.2.1). It is not very clear, with this reservation, why the normal stress distributions show a similar behaviour when plotted against y^+ and much less so against y/Δ^* .

The pressure distribution which generates the profiles of series 02 increases, reaches a plateau and then decreases again. The pressure rise, steeper than in series 01, leads to a higher level for the maxima of the normal stresses (Fig. 3.2.4) whereas the subsequent drop in pressure reduces the turbulence level so that it approaches the level upstream of the pressure rise in the outer region and even falls below this level in the inner region. This shows that the turbulence is more affected by pressure gradient effects in the inner region than in the outer region. Qualitatively the normal stress distributions $\bar{\rho} \overline{w'^2}$ and $\bar{\rho} \overline{v'^2}$ (Fig. 3.2.5) behave as those of series 01 (Fig. 3.2.2), and we observe again the distinct second peak of the $\bar{\rho} \overline{v'^2}$ distribution in the outer region of the boundary layer (profiles 0207 to 0211). Again the magnitude of the normal stresses follows the order $\bar{\rho} \overline{u'^2}$, $\bar{\rho} \overline{w'^2}$ and $\bar{\rho} \overline{v'^2}$.

The next two investigations were performed in boundary layers with shock interaction, and we deal with the adiabatic wall case first. The boundary layer ($M_\delta \approx 3.9$) developed on the axisymmetric nozzle and test section wall and was subjected to an adverse pressure gradient induced by the incident and reflected shock-wave system generated by a cone on the centre line (Rose 1973, CAT 7306S). The pressure distribution and the wave structure of the flow are shown in Fig. 7306S-1 of this report.

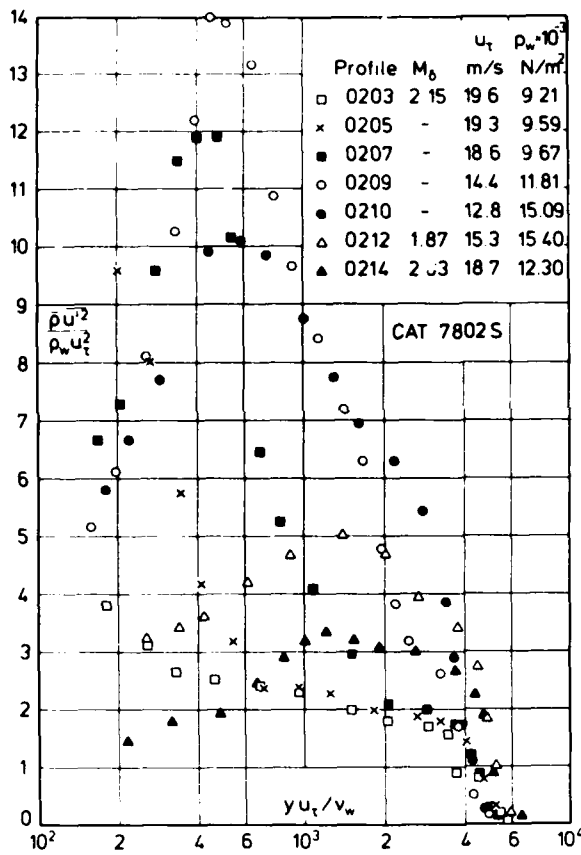


Fig. 3.2.4 Reynolds normal stress distributions in a compressible turbulent boundary layer with varied pressure gradient (adiabatic wall, origin not defined). Kussoy et al. (1978).

| Profile | M_δ | u_t m/s | $\rho_w \cdot 10^{-3}$ N/m ² |
|---------|------------|-----------|---|
| □ 0203 | 2.15 | 19.6 | 9.21 |
| ■ 0207 | - | 18.6 | 9.67 |
| ○ 0209 | - | 14.4 | 11.81 |
| ● 0210 | - | 12.8 | 15.09 |
| △ 0212 | 1.87 | 15.3 | 15.40 |
| ▲ 0214 | 2.03 | 18.7 | 12.30 |

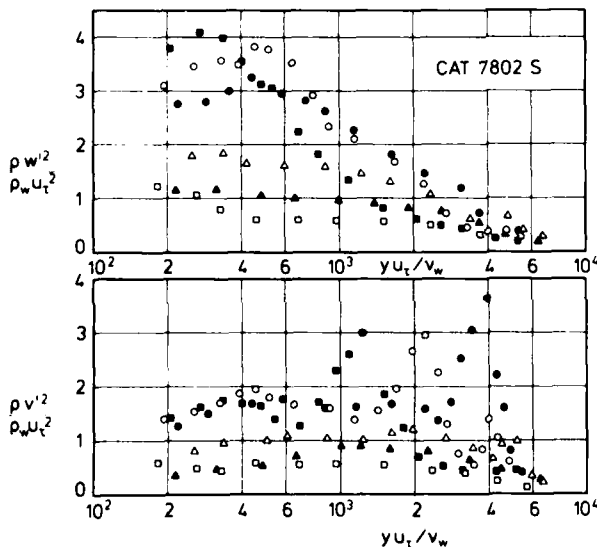


Fig. 3.2.5 Reynolds normal stress distributions in a compressible turbulent boundary layer with varied pressure gradient (adiabatic wall, origin not defined). Kussoy et al. (1978).

Again all three normal stress components were measured and are presented in Figs. (3.2.6) and (3.2.7). The turbulence levels of the three components differ greatly from those of the two previous cases. The most obvious difference lies in that $\bar{\rho} u'^2$ is smaller than both $\bar{\rho} v'^2$ and $\bar{\rho} w'^2$, reaching only about one third of the maxima of the other two normal stresses. The rise in pressure causes the turbulence structure to deviate from that of the first three profiles at profile 0104 with changes in $\bar{\rho} v'^2$ and $\bar{\rho} w'^2$ greater than in $\bar{\rho} u'^2$. Since the wall-pressure gradient increases monotonically in the region investigated in this experiment the maximum of the normal stress moves outwards into the boundary layer with the maximum decreasing only slightly in magnitude. This behaviour is observed for all three normal stresses. In contrast to the previous experiment however no double peak occurs in the $\bar{\rho} v'^2$ distributions.

The last two cases to be discussed in this section (CAT 7501S) are again boundary layers with shock interaction. Unfortunately they are less well documented than the other experiments and of the normal stresses only $\bar{\rho} v'^2$ is given. Fig. (3.2.8) shows the $\bar{\rho} v'^2$ distributions for the two boundary layer flows examined. The information about the boundary layer with pressure distribution II (series 02) is however relatively so scarce that we can only express our astonishment at the fast relaxation of profiles 0209 and 0212 to the $\bar{\rho} v'^2$ level upstream of the shock. For series 01 $\bar{\rho} v'^2$ starts at the low level upstream of the shock, increases by a factor of about 20 just downstream of the shock (profile 0105) and then decreases again in magnitude without however reaching the original level of profile 0101, even at profile 0115.

No general conclusions can be drawn from the few cases presented above and more data are needed before any useful attempt at a turbulence model for the normal stresses can be made. Beginning with Newman's (1951) early normal stress measurements in an incompressible adverse pressure gradient boundary layer one discussion has never ended (e.g., Rotta 1962). The question is whether or not at least near separation, the convection term $\partial(\bar{\rho} u'^2)/\partial x$ must be retained in a first order boundary-layer theory, since it approaches an order of magnitude which is no longer negligible. Rose (1973) and Rose & Johnson (1975) have discussed this question for compressible boundary layers. They compared the values of the average pressure gradient $\partial \bar{p} / \partial x$ (approximately $5 \times 10^5 \text{ N/m}^3$) with the maximum normal stress gradient (about $4 \times 10^4 \text{ N/m}^3$). They also found the term $\partial(\bar{\rho} u'v')/\partial y$ everywhere less than

| Profile | u_t m/s | $\rho_w \cdot 10^{-3}$ N/m ² | y_{min} mm |
|---------|--------------|--|-----------------|
| ○ 0101 | 39.1 | 2.92 | 0.5 |
| ● 0103 | 35.8 | 2.91 | 0.5 |
| ● 0104 | 27.1 | 2.98 | 0.5 |
| ○ 0105 | 24.0 | 4.89 | 0.5 |
| ● 0107 | 25.6 | 6.82 | 0.5 |
| △ 0110 | 27.1 | 8.31 | 0.5 |
| ▲ 0112 | 27.7 | 9.28 | 0.5 |

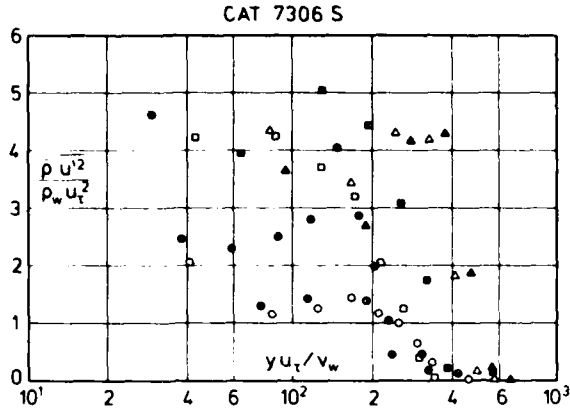


Fig. 3.2.6 Reynolds normal stress distributions in a compressible turbulent boundary layer with shock interaction (adiabatic wall, origin not defined). Rose (1973).

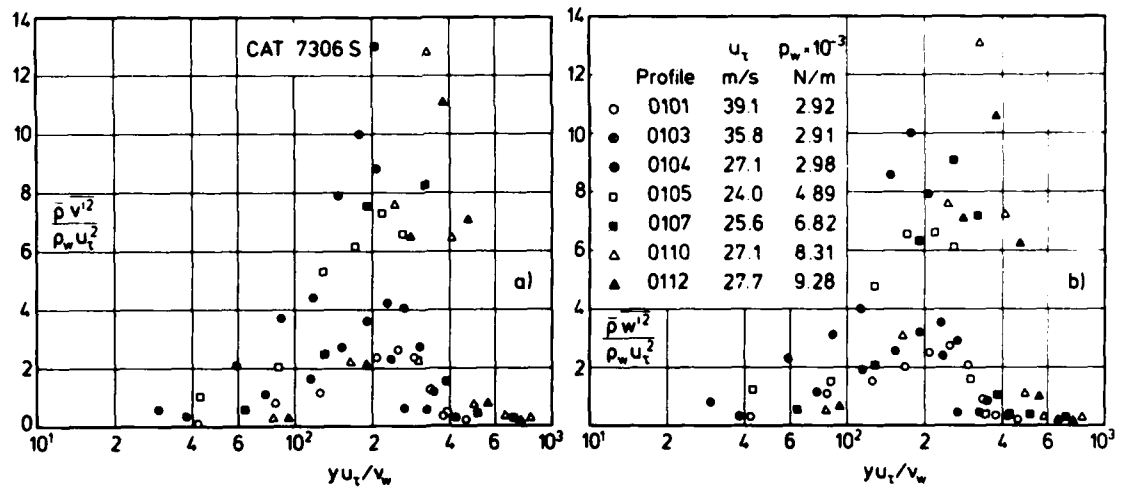


Fig. 3.2.7 a/b Reynolds normal stress distribution in a compressible turbulent boundary layer with shock interaction (adiabatic wall, origin not defined). Rose (1973).

8×10^4 N/m³ and concluded that "within engineering accuracy, the term $\partial(\bar{\rho} \overline{u'^2})/\partial x$ may be neglected throughout the entire flow upstream, within and downstream of the shock-wave interaction region. Within the interaction itself, the pressure gradient term $\partial \bar{p}/\partial x$ is an order of magnitude larger than the Reynolds stress gradient."

Rose (1973) had come to a similar but not quite the same conclusion from his evaluation of the above gradients, stating "that the flow within and just downstream of the interaction is definitely not boundary-layer-like in that $\partial(\bar{\rho} \overline{u'^2})/\partial x$ is not negligible; and, further, that the value of $\partial \bar{p}/\partial x$ varies substantially across the boundary layer" (see CAT 7306S).

The only other boundary layer flow with separation was investigated by Kussoy & Horstman (1975, CAT 7501S). Unfortunately, $\bar{\rho} \overline{u'^2}$ was not measured, and an estimate of the order of magnitude of individual terms in the momentum equation must therefore remain incomplete.

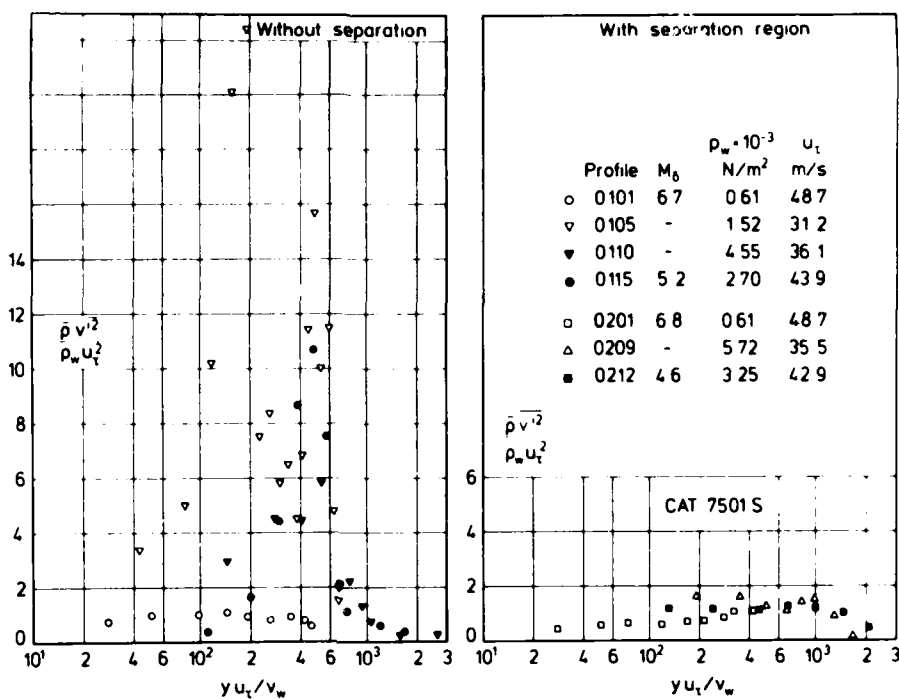


Fig. 3.2.8 Reynolds normal stress distributions in a shock/boundary-layer interaction flow (isothermal wall $T_w/T_r = 0.47$, defined origin). Kussoy & Horstman (1975).

3.3 Kinetic energy of the fluctuating motion

A discussion of the kinetic energy distribution of the fluctuating motion across compressible turbulent boundary layers is confined to three cases, two provided by Kussoy et al. (1978), CAT 7802S) and one by Rose (1973, CAT 7306S). Since there are hardly any measurements in subsonic flow which might be compared to the experiments presented here, we can only hope that more measurements will appear eventually so that a discussion about the behaviour of this important quantity gains more meaning. As is evident from the single fluctuation components discussed above, the locally scaled turbulence level increases with the increasing pressure

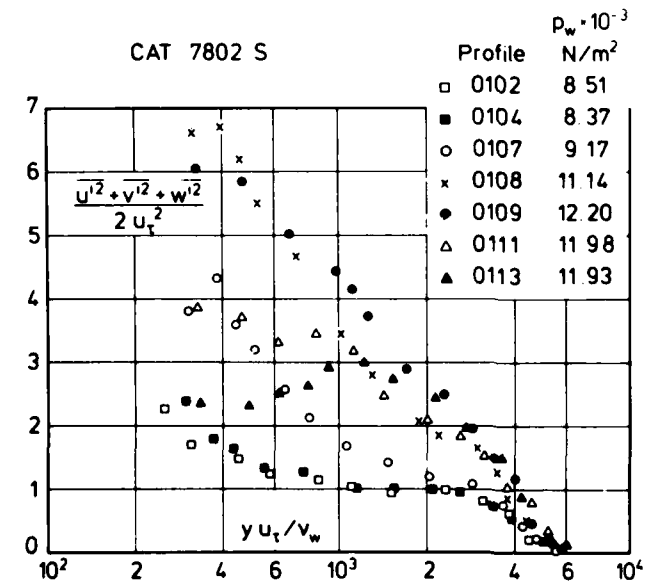


Fig. 3.3.1 Specific kinetic energy of the fluctuating motion in a compressible turbulent boundary layer with varied pressure gradient (adiabatic wall, origin not defined). Kussoy et al. (1978).

distribution where the turbulence level returns to its initial level (Fig. 3.3.2 - profiles 0203 and 0214) for series 01 the level remains higher than for the starting profile. Scaling with such a quantity as u_t (which decreases down to profile 0210 - see legend of Fig. 3.2.4) exaggerates the rise of the overall level so that in absolute terms the maxima of profiles 0207 and 0210 are about equal.

In interpreting the distributions of turbulent energy - or of any other turbulence or mean flow quantity - in flows with strong pressure gradients it is necessary to take account of the change in the scaling quantities as well as the variation of the dimensionless value. In relation to the local friction velocity the distributions of the fluctuating kinetic energy of series 02 have higher peak values than those of series 01 as a result of either the higher pressure level or the steeper pressure gradient.

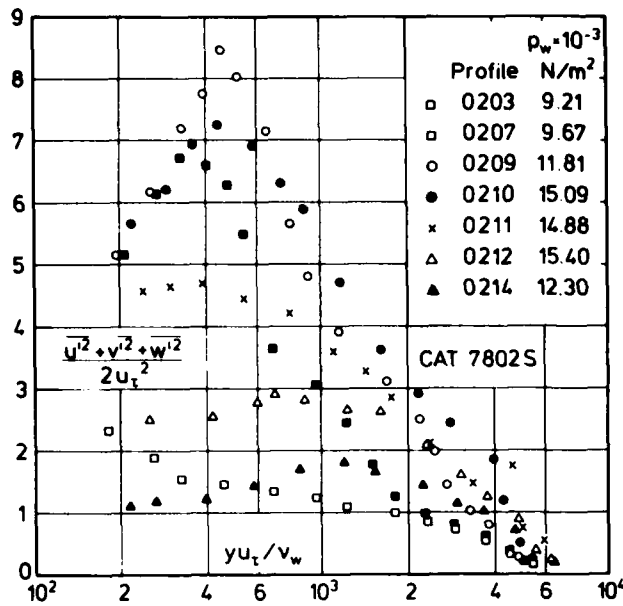


Fig. 3.3.2 Specific kinetic energy of the fluctuating motion in a compressible turbulent boundary layer with varied pressure gradient (adiabatic wall, origin not defined). Kussoy et al. (1978).

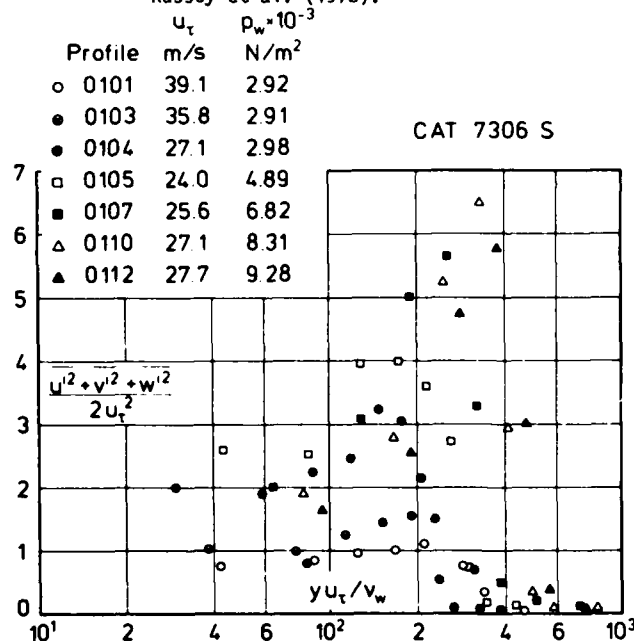


Fig. 3.3.3 Specific kinetic energy of the fluctuating motion in a compressible turbulent boundary layer with shock interaction (adiabatic wall, origin not defined). Rose (1973).

adiabatic wall, is, of course, identical to the recovery temperature T_r . The latter is again close to the total temperature.

The influence of the temperature fluctuations in comparison with other fluctuating quantities of the flow field has been investigated by Morkovin who arrived at the following equation

$$\frac{(T_0 - T)^{1/2}}{T_0} = \frac{(T - T_r)^{1/2}}{T} \left(1 + \frac{\gamma - 1}{2} M^2\right)^{-1/2} + \frac{(u'^2)^{1/2}}{\bar{u}} \frac{(\gamma - 1)^{1/2} M^2}{1 + \frac{\gamma - 1}{2} M^2} \quad (3.4.1)$$

(for details see Morkovin 1962 or section 2.4 of AG 253). Morkovin now assumed that $(T_0 - T)^{1/2} / T_0$ is an order smaller than the two remaining terms and based this assumption on measurements by Kistler (1959) who showed

Which of the two is more important calls for further investigation. It is interesting to note, however, that the scaled peak of $(u'^2 + v'^2 + w'^2)$ is reached before the maximum of the wall pressure (see the legend of Figs. 3.3.1 and 3.3.2), an observation which points to a greater importance of the pressure gradient. One may finally note that the peak of the fluctuating kinetic energy lies still in the log-law region of the boundary layer as long as the pressure is rising in the streamwise direction.

This is not the case for the profiles in the boundary layer with shock interaction presented in Fig.(3.3.3) where, in a pressure distribution which increases monotonically, the peak of the specific kinetic energy moves out almost to the edge of the boundary layer. This behaviour may be connected with the wave pattern downstream of the shock interaction but we would like to see other experiments under similar conditions confirm such a pattern before it can be discussed any further, or taken as a general rule.

If one is interested in the development of the fluctuating kinetic energy in varied pressure distributions, $(u'^2 + v'^2 + w'^2)$ would, of course, have to be referred to a fixed, upstream, scaling level such as u_t^2 for profile 01.

3.4. Temperature fluctuations

Measurements of temperature fluctuations have been reported for some investigations in compressible turbulent boundary layers but the number of data in tabular form is hardly larger than in 1974 when Sandborn reported the available results in his figure 15. He then weighted the static temperature fluctuation intensities by a representative mean static difference across the boundary layer. This coordinate was based on the concept that the temperature fluctuation level should be proportional to the mean temperature gradient across the boundary layer, which was originally proposed by Kovaszny (1953). Here we propose to nondimensionalize the static and the total temperature fluctuations by the wall temperature T_w which, in the case of an

that at a Mach number of 4.67 $(T_0^{\overline{T^2}})^{1/2} / T_0$ reached at most a value of 0.048 and about 0.02 for a Mach number 1.72.

In Fig. (3.4.1) we have plotted against y^+ and y/Δ^* the only tabulated data available to us (Sturek 1971, CAT 7101) and Owen et al. (1975, CAT 7205, Horstman & Owen 1972) and find the same order of magnitude as Kistler. If the latter data (CAT 7205) which were measured on an isothermal wall had been nondimensionalized

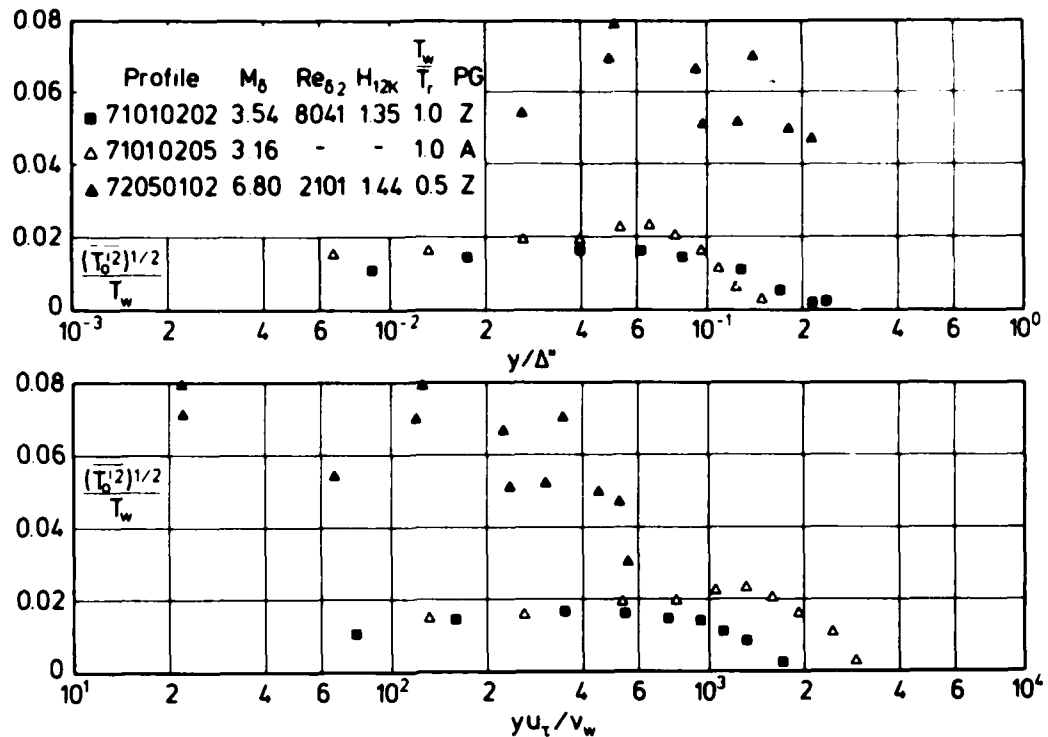


Fig. 3.4.1 Total temperature fluctuations in a compressible turbulent boundary layer with varied pressure gradient (adiabatic wall, origin not defined).

by T_0 they would have to be divided by two and would have had about the same maximum level for $(T_0^{\overline{T^2}})^{1/2}$ as Sturek's data at about half the free-stream Mach number. It is therefore at least doubtful whether Kistler's measurements above suffice to allow the conclusion that the level of the total temperature fluctuations increases with Mach number.

With the assumption that $(T_0^{\overline{T^2}})^{1/2} / T_0$ is an order smaller than the two remaining terms in eqn.(3.4.1) one can write

$$\frac{(T_0^{\overline{T^2}})^{1/2}}{T} = -(\gamma-1)\bar{M}^2 \frac{(\overline{u'^2})^{1/2}}{\bar{u}} \quad (3.4.2)$$

and, neglecting pressure fluctuations and second order terms, such as $\overline{\rho'^2 T}$, eqn.(3.4.2) yields

$$\frac{(T_0^{\overline{T^2}})^{1/2}}{T} = -\frac{(\overline{\rho'^2})^{1/2}}{\bar{\rho}} = -(\gamma-1)\bar{M}^2 \frac{(\overline{u'^2})^{1/2}}{\bar{u}} \quad (3.4.3)$$

Eqn.(3.4.3) was given by Morkovin (1960 eqn.8) and was later called Morkovin's hypothesis by Bradshaw & Ferriss (1971) who deduced from this equation that if $(\overline{\rho'^2})^{1/2} / \bar{\rho}$ is small the turbulence structure is not affected by compressibility effects.

Though the Mach number distribution reaches its maximum in the outer region of a compressible boundary layer, velocity fluctuations^{*} become small there and therefore the static temperature fluctuations also remain small.

^{*}Fig. (3.1.2) shows that the fluctuating velocity component u' becomes small if one considers that $u'_t / u_\delta = 0.035$ and 0.046 for profiles 58030101 and 58030301 respectively.

This means that nowhere in the boundary layer should the fluctuations of the static temperature become larger than about 0.1.

The static temperature-fluctuation distributions are plotted against y^+ and y/Δ^* in Fig. (3.4.2) and confirm the reasoning which we have just made, at least in the parameter range available to us. Profile 71010205 was measured in an adverse pressure gradient boundary layer but it does not show a marked difference to the zero

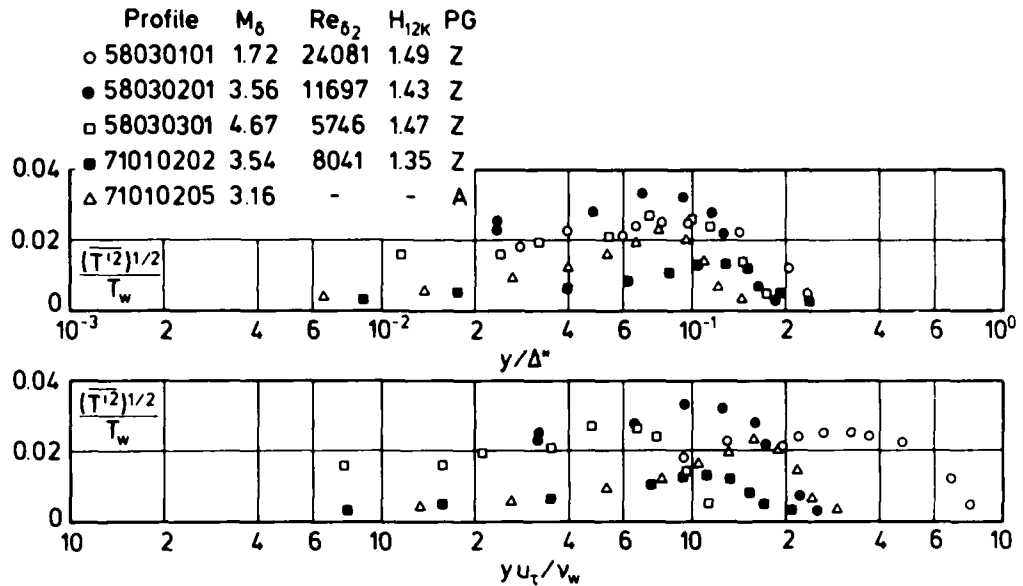


Fig. 3.4.2 Fluctuations of static temperature in a compressible turbulent boundary layer with varied pressure gradient (adiabatic wall, origin not defined).

pressure gradient cases. No Mach or Reynolds number effects can be recognized and we do not claim a similarity behaviour, not even in the y/Δ^* plot.

Fig. (3.4.3) finally gives the local "temperature turbulence level" which shows a certain influence of the Mach number on the peak level of the fluctuation distribution. Again the temperature fluctuations lie within the order of magnitude discussed above.

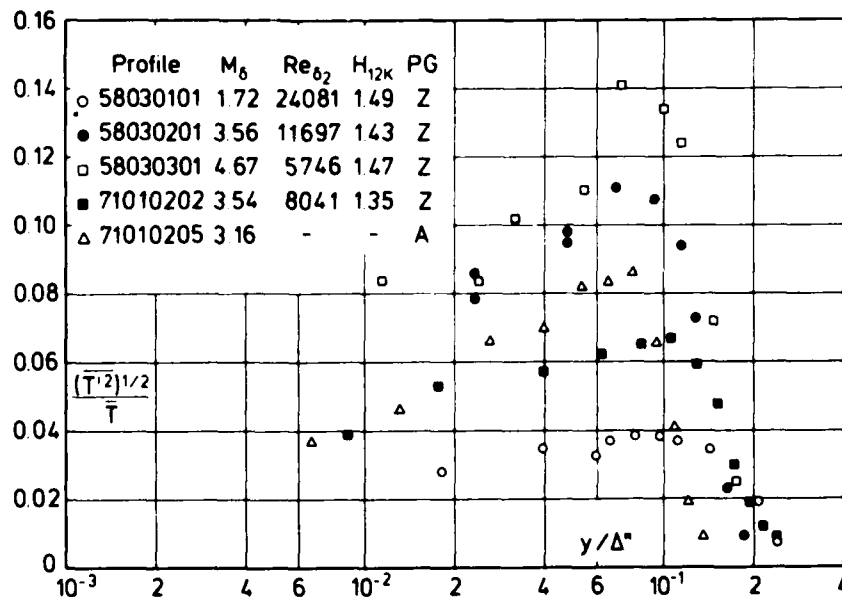


Fig. 3.4.3 Static temperature fluctuation distribution in a compressible turbulent boundary layer with varied pressure gradient (adiabatic wall, origin not defined).

4. TURBULENCE DATA - TWO COMPONENT TERMS

The system of conservation equations for compressible turbulent boundary layers can be closed if relationships for the shear-stress component $\bar{\rho} \bar{u}'v'$ and for either the heat-flux term $\bar{\rho} \bar{v}'H'$ - see eqns. (2.2.3) and (2.2.8) in AGARDograph 253 - or the turbulent Prandtl number Pr_t are known. Therefore the main aim in turbulence modelling consists of establishing such relationships, be it in the form of relatively unsophisticated Boussinesq or mixing length models or by using the transport equations for correlations of the various turbulence quantities. Comparisons with mean flow measurements have been made for various turbulence models used in numerical solution programmes by Marvin (1977), Rubesin et al. (1977), Horstman et al. (1978) and Viegas & Horstman (1979) for example.

These investigations show that our knowledge of the behaviour of the "two-component" correlations mentioned above is still incomplete and that we know little about the influence of such important parameters as Mach number, pressure gradient, heat transfer, Reynolds number, free-stream turbulence, wall roughness and wall curvature on the turbulence structure and especially on the shear stress distribution of compressible boundary layers. In this section we shall discuss the relatively few two-component correlation measurements with the main emphasis on the Reynolds shear stress component $-\bar{\rho} \bar{u}'v'$.

4.1 Distribution of Reynolds shear stress ($-\bar{\rho} \bar{u}'v'$) in a compressible two-dimensional boundary layer

Three main avenues have been explored so far so as to gain some insight into the shear stress distribution of a compressible turbulent boundary layer.

Two methods for the determination of the Reynolds shear stress distribution use the mean momentum equation for compressible boundary layers and evaluate the individual terms by either inserting semi-empirical relationships for the mean velocity and density or mean flow measurements of these two quantities. The third method attempts to measure the shear-stress distribution directly by means of hot-wire or laser-Doppler anemometry. These measurements are very difficult to perform - both as far as the design and lifetime of the probes is concerned and in consequence of uncertainties in how the probe signals should be interpreted (e.g., Laderman, 1978c). The meaning of some of these measurements is still highly controversial. We will therefore confine our discussion to those measurements which we think we understand leaving many others to a later critical review.

The qualitative behaviour of the total shear stress

$$\tau = \mu(\partial\bar{u}/\partial y) - \bar{\rho} \bar{u}'v' \quad *) \quad (4.1.1)$$

across the boundary layer can be predicted from knowledge of the shear stress and its slope at the wall and at the outer edge of the boundary layer. At the wall the shear stress is equal to the skin friction τ_w , and its slope is determined by

$$(\partial\tau/\partial y)_w = dp/dx \quad (4.1.3)$$

Equation (4.1.3) follows from the momentum equation if the boundary conditions at the wall are inserted. At the outer edge of the boundary layer both the magnitude and the slope of the shear stress are zero.

In Fig. (4.1.1) we have presented the three qualitative shear stress distributions for zero, positive and negative pressure gradients and their slope at the wall. The total shear stress τ as defined by eq. (4.1.1) contains two terms, the molecular shear stress which dominates close to the wall (viscous sublayer) and then decays rapidly, and the Reynolds shear stress τ_t which is zero at the wall, increases to a maximum value in the log-law region and then decreases to zero at the outer edge of the boundary layer.

The reader should keep this qualitative behaviour of the shear stress distribution in mind in order to make it easier to follow the subsequent discussion, which will begin with zero-pressure gradient boundary layers and continue with flows in an adverse pressure gradient.

*) The complete expression for the total shear stress containing smaller order terms was given by van Driest (1951) and reads

$$\tau = \mu(\partial\bar{u}/\partial y) - \bar{\rho} \bar{u}'v' - \bar{v} \bar{\rho}'u' - \bar{\rho}'\bar{u}'v' \quad (4.1.2)$$

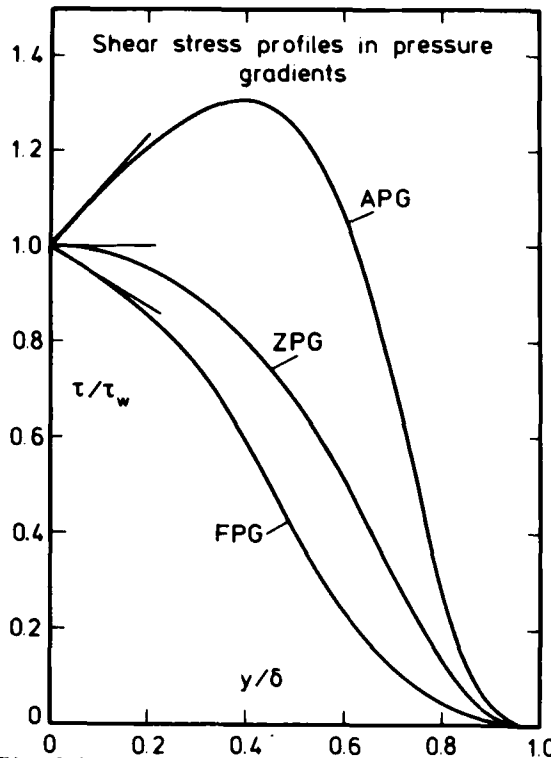


Fig. 4.1.1 Sketch to show the variation of shear stress profiles in a boundary layer in favourable (FPG), zero (ZPG) and adverse (APG) pressure gradients (shock free flow).

relatively thick and may even occupy the greater part of the boundary layer.

We first consider the influence of Mach number, Reynolds number and heat transfer on the shear-stress distribution.

Maise & McDonald (1967) calculated the shear-stress distributions for Mach and Reynolds numbers in the range $0 \leq M_\delta < 5$ and $10^3 \leq Re_\delta < 10^5$ by assuming a semi-empirical relationship for the velocity distribution and the Crocco relationship for the density-velocity distribution. The shear-stress distribution of Maise & McDonald, however, has a small disadvantage in that it approaches zero at $y/\delta = 1$ with a finite slope and thus does not fulfill the boundary layer conditions correctly. The main result of this early investigation was that it showed little effect of either the Mach or the Reynolds number on the total shear stress distribution in turbulent boundary layers along adiabatic walls. Other evaluations of eqn. (4.2.2) which include also cases with heat transfer along isothermal walls have used an assumption of similarity. This means for example that the velocity profiles \bar{u}/u_∞ collapse on to a single curve when plotted as \bar{u}/u_∞ against y/δ_2 (Squire 1971). Meier & Rotta (1970, 1971) assume that \bar{u}/u_δ and $\bar{\rho}/\rho_\delta$ are functions of the dimensionless wall distance y/δ only, i.e., that the velocity and temperature profiles are self-similar in the x direction.* They introduce $(\bar{\rho}\bar{u}/\rho_\delta u_\delta)$ as a function $F(\xi)$ with $\xi = y/\delta$ and obtain from eqn.(4.2.3)

$$\frac{\tau}{\rho_\infty u_\infty^2} = - \left[\frac{c_f}{2\delta_2} \frac{\bar{u}}{u_\infty} \int_0^y \frac{\bar{\rho}\bar{u}}{\rho_\infty u_\infty} dy - \int_0^y \frac{\bar{\rho}\bar{u}^2}{\rho_\infty u_\infty^2} dy \right] + C_1 \quad (4.2.4)$$

where C_1 is determined by the boundary conditions at the outer edge $y = \delta$ and $\tau_t = 0$. No reason is given for the choice of these unusual boundary conditions (Rotta 1964 has also used it for temperature distributions). The derivation of eqn.(4.2.4) can be understood more easily if one remembers that

$$\frac{d}{dx} \left(\frac{\delta_2}{\delta} \delta \right) = \frac{\delta_2}{\delta} \frac{d\delta}{dx} + \delta \frac{d(\delta_2/\delta)}{dx} \quad \text{and, with the second term zero for the locally selfsimilar flow } (\delta_2/\delta \text{ is}$$

assumed independent of x),

*It should be noted that, strictly, none of these forms of self-similarity can apply to even the zero pressure gradient case as such quantities as δ_2/δ are functions of Reynolds number.

4.2 Indirect determination of shear stress

4.2.1 Zero pressure gradient cases

The total shear stress distribution in a steady compressible constant pressure boundary layer can be calculated from the equation of motion (e.g., Sandborn, 1974) yielding

$$\tau = \tau_w + \int_0^y \left[\frac{\partial}{\partial x} (\bar{\rho} \bar{u}^2) - \frac{\partial}{\partial y} (\bar{\rho} \bar{u} \bar{v}) \right] dy \quad (4.2.1)$$

or, if the continuity equation is substituted into (4.2.1)

$$\tau = \tau_w + \int_0^y \frac{\partial}{\partial x} (\bar{\rho} \bar{u}^2) dy - \bar{u} \int_0^y \frac{\partial}{\partial x} (\bar{\rho} \bar{u}) dy \quad (4.2.2)$$

with the equivalent form

$$\frac{\tau}{\tau_w} = 1 + \frac{2}{c_f \rho_\delta u_\delta^2} \left[\int_0^y \frac{\partial}{\partial x} (\bar{\rho} \bar{u}^2) dy - \bar{u} \int_0^y \frac{\partial}{\partial x} (\bar{\rho} \bar{u}) dy \right]. \quad (4.2.3)$$

In eqn. (4.2.3) c_f is sometimes substituted by $2 d\delta_2/dx$ with δ_2 as the momentum defect thickness.

As mentioned above the molecular part of the shear stress, $\mu(\partial\bar{u}/\partial y)$ plays a role only in the immediate vicinity of the wall. It is therefore often neglected outside the viscous sublayer and τ is set equal to τ_t . Such a simplification may however lead to substantial errors in boundary layers at high Mach numbers and small Reynolds numbers where the viscous sublayer can become

$$\frac{d\delta_2}{dx} = \frac{\delta_2}{\delta} \frac{d\delta}{dx} = \frac{c_f}{2} \quad \text{and}$$

$$\delta^{-1} \frac{d\delta}{dx} = (c_f/2\delta_2) \quad (4.2.5)$$

The following relationship is also used

$$\int_0^y \frac{\partial F}{\partial x} dy = -\delta^{-1} \frac{d\delta}{dx} \int_0^y \frac{\partial F}{\partial y} \bar{y} dy = -\delta^{-1} \frac{d\delta}{dx} \left[F\bar{y} \Big|_0^y - \int_0^y F dy \right] \quad (*) \quad (4.2.6)$$

The evaluation of Meier's (1970) measurements along an adiabatic wall resulted in a spreading of the shear-stress profiles in the wall region - $\tau/\rho_\delta u_\delta^2$ against y/δ - i.e., showed a decrease of the shear stress maximum ($\tau_w/\rho_\delta u_\delta^2$) with increasing Mach number in the range $2.25 \leq M_\delta \leq 4.50$, and a collapse of the profiles onto each other in the outer region. Such a decrease in $c_f/2$ with Mach number is well known from theoretical considerations, and the collapse of the profiles in the outer region is probably no more than a consequence of the similarity assumption.

Bushnell & Morris (1971 a and b) have extended the above parameter range to boundary layers with heat transfer, small pressure gradients and small transverse curvature effects. For this purpose an extended evaluation equation was derived - eqn. 4 of the original paper - assuming local similarity in y/δ coordinates with δ taken at the value of y for which $\bar{\rho}/\rho_\delta = 0.995$. The shear-stress distributions which they calculated are shown in Fig. (4.2.1) from the data presented in AGARDograph 223. In no case had skin friction been measured, and in two cases at least (Jones & Feller, 1970, Lee et al., 1969) it is doubtful whether the assumption of local similarity holds. For this latter reason we have excluded the measurements by Perry (1968, see also Perry & East 1968). Additionally we may notice from table 4.2.1 that the distances between profiles - given as $\Delta x/\delta_0$ - are rather large for a calculation of derivatives and not spaced as closely together as those used by Meier & Rotta (1971). Therefore we must wonder how Bushnell & Morris arrived at such smooth curves with such small discrepancies at the outer edge (c.f. Laderman, 1979 and 1980, and the authors' own experience, which confirms Laderman's findings).

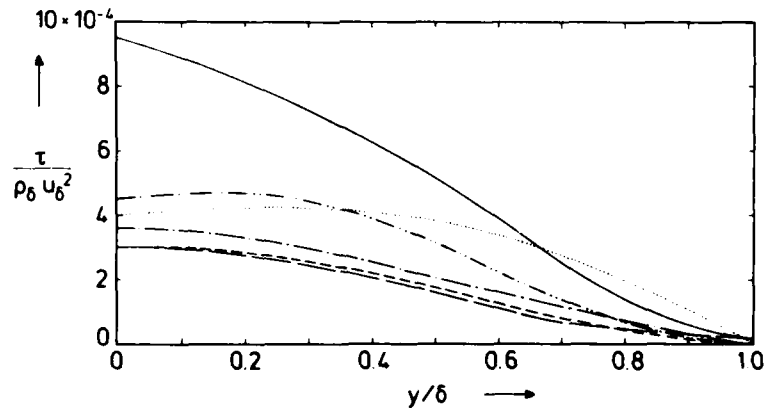


Fig. 4.2.1 Calculated shear-stress distributions in compressible turbulent boundary layers from Bushnell & Morris (1971) (zero pressure gradient, adiabatic and isothermal wall).

---- Adcock et al. (1965), — Danberg (1967), Jones & Feller (1970), -.- Lee et al. (1969), - - - Samuels (1969).

$$*) \quad \frac{\partial F}{\partial x} = \frac{dF}{d\xi} \left(\frac{\partial \xi}{\partial \delta} \right)_y \quad \frac{d\delta}{dx} = \frac{dF}{d\xi} \left(-\frac{y}{\delta^2} \right) \frac{d\delta}{dx} = \frac{dF}{d\xi} \left(-\frac{y}{\delta} \right) \frac{\partial \xi}{\partial y} \frac{d\delta}{dx} = -\frac{y}{\delta} \frac{d\delta}{dx} \frac{dF}{d\xi} \frac{d\xi}{dy} = -\delta^{-1} \frac{d\delta}{dx} \frac{\partial F}{\partial y} \quad \text{y and}$$

$$(F\bar{y})' = \frac{\partial F}{\partial y} \bar{y} + 1 \cdot F \quad \text{or} \quad F\bar{y} \Big|_{y_1}^{y_2} = \int_{y_1}^{y_2} \frac{\partial F}{\partial y} \bar{y} dy + \int_{y_1}^{y_2} F dy$$

Table 4.2.1

| Author | profile | M_δ | Re_δ | T_w/T_r | $\Delta x/\delta_0$ | C_f |
|----------------------------------|----------------------|------------|-------------|-------------|---------------------|-------|
| Adcock et al. --- (CAT 6501) | 6501-0107 | 6.02 | 13341 | ≈ 1 | 7 | NM |
| Danberg (CAT 6702) | 6702-0103 | 6.54 | 2574 | 0.52 | 3 | NM |
| Jones & Feller --- (CAT 7002) | 7702-0102 | 5.76 | 9718 | 0.81 | ≈ 20 | NM |
| | 7002-0303 | 5.75 | 46425 | 0.77 | - | NM |
| Lee et al. (1969) | - | 4.67 | 57000 | - | - | - |
| Samuels et al. --- (CAT 6701) | 6701-0103 or 0104 | 5.98 | 10863 | 0.49 | ≈ 9 | NM |

Data reconstruction for Bushnell & Morris' (1971a) shear-stress calculations.

These observations should be borne in mind if one considers Sandborn's conclusion of the existence of a "best estimate." In his survey paper on compressible turbulent boundary layers Sandborn (1974) plotted the above shear-stress distributions as τ/τ_w versus y/δ , added data at a Mach number 7.2 obtained by Horstman & Owen (1972) at intervals of $\Delta x/\delta_0 \approx 20$ and data measured and evaluated by Meier & Rotta (1971). Sandborn found only small variations between the calculated shear stress profiles and was thus able to construct a "best estimate" for the shear distribution. He states: "Between the different sets of measurements it was not possible to identify consistent Mach number or Reynolds number variations... This survey suggests that the general magnitude of the shear-stress distribution across a supersonic, adiabatic zero pressure gradient turbulent boundary layer can be estimated from mean flow data to within approximately $\pm 15\%$. The general observation of Morkovin (1962, 1964) that compressibility effects on the turbulence are 'passive' appears to be valid for the shear-stress distribution. It is possible that the incompressible, zero pressure gradient, shear-stress distribution is an adequate model for the super- and hypersonic flows, at least up to Mach number 7" (cf. Fig. 4.2.2 taken from Sandborn). Sandborn further ventures an explanation for this behaviour: "The probability exists that since all the evaluations employ a similarity approximation, the resulting distribution must be locked to a similarity shape. Obviously, the fixing of the distribution to $\tau/\tau_w = 1$ at $y/\delta = 0$ and $\tau/\tau_w = 0$ at $y/\delta = 1$, together with a zero slope at $y/\delta = 0$ makes large variations unlikely."

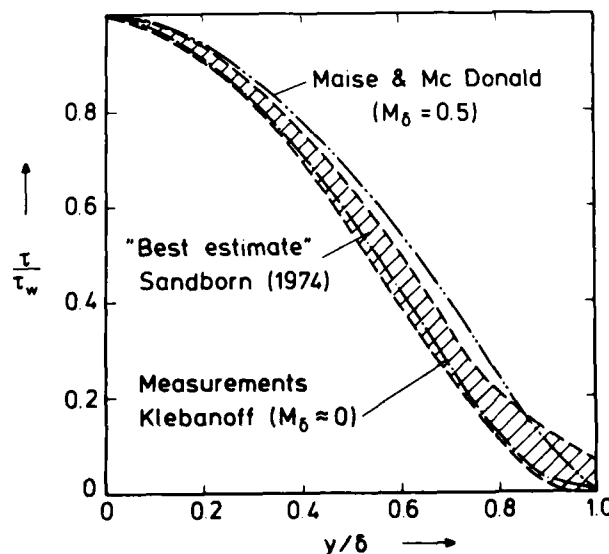


Fig. 4.2.2 Comparison of "estimated" supersonic shear stress with measurements in incompressible flow and the empirical prediction of Maise & McDonald (1967). (Figure from Sandborn 1974).

In the meantime further evaluations of shear-stress distributions from mean flow data have been published. Watson (1978) showed that shear-stress distribution at a Mach number 11, a heat transfer parameter in the range $0.38 < T_w/T_r \leq 1$, and at Reynolds numbers Re_{δ_2} below 2000 were above the subsonic flow data of Klebanoff (1955) - see the curve in Fig. (4.2.2) - but in general agreed with the body of data presented by Sandborn (1974). The boundary layer thickness used as the characteristic length scale was determined in this case as lying between the velocity and the pitot thickness and appeared to have played an important role in the calculation procedure. Other indirect shear-stress evaluations which again agree approximately with the "best estimate" or with Klebanoff's distribution are those by Mikulla & Horstman (1975) and by Collins et al. (1978), the former measurements at $M_\delta = 6.9$ along a cooled wall, the latter in a range $0.1 \leq M_\delta \leq 2.2$ along an adiabatic wall (see Dimotakis et al. 1979).

4.2.2 Adverse pressure gradient cases

In section 4.1 we described, in general terms, the constraints on the total shear-stress profile in a boundary layer. In a shock free flow these lead to shear-stress profiles similar to those found in incompressible flow, as sketched in Fig. (4.1.1). As we pointed out in section 5.1 of AG 253, there are features of compressible flows with pressure gradients which do not always have an equivalent in incompressible flow. For instance a boundary layer in a strong adverse pressure gradient becomes thinner and exerts an increased shear stress on the wall as a result of bulk compression. It is advisable to entertain some caution in comparing shear-stress distributions and we will distinguish between the three types of flows for which shear-stress distributions have become available. Of those for which mean-flow derived profiles have been published, the flows on curved ramps (Sturek & Danberg, 1971b, CAT 7101; Laderman, 1978b, CAT 7803S) are simple wave flows with pronounced streamline curvature and normal pressure gradients. The straight-wall flows of Zwartz (1970, CAT 7007), Peake et al. (1971, CAT 7102) and Lewis et al. (1972, CAT 7201) are reflected wave cases in which much of the flow should be free of pronounced curvature or normal pressure gradients. Shock-boundary layer interaction cases do not lend themselves to mean flow analysis.

The shear-stress distribution across a compressible adverse pressure-gradient boundary layer can be determined from the equation of motion and from closely spaced mean flow measurements of velocity and density. Such an evaluation is however more difficult than for a ZPG boundary layer, and it is difficult to ensure that the calculated shear-stress distributions meet the boundary conditions on both edges of the boundary layer (Sturek 1973a and Laderman 1978b).

Sturek (1973a, 1974) has derived a relationship for the turbulent shear stress τ_t in which he also considered effects of longitudinal wall curvature

$$\frac{\tau_t}{\tau_w} = \frac{1}{\tau_w} \left\{ \tau_w + \int_0^y \beta \frac{\partial}{\partial x} (\bar{\rho} \bar{u}^2) dy - \bar{u} \beta \int_0^y \frac{\partial}{\partial x} (\bar{\rho} \bar{u}) dy - 2 \int_0^y \left[\int_0^y \frac{\partial}{\partial x} (\bar{\rho} \bar{u}) dy \right] \bar{u} \beta^2 R^{-1} dy + \frac{dp}{dx} \int_0^y \beta dy \right\} \quad (4.2.7)$$

by using the equations for continuity and momentum in the form

$$\frac{\partial}{\partial x} (\bar{\rho} \bar{u}) + \frac{\partial}{\partial y} \beta^{-1} (\bar{\rho} \bar{v} + \bar{\rho}' \bar{v}') = 0 \quad (4.2.8)$$

$$\beta \bar{\rho} \bar{u} \frac{\partial \bar{u}}{\partial x} + (\bar{\rho} \bar{v} + \bar{\rho}' \bar{v}') \left(\frac{\partial \bar{u}}{\partial y} + \bar{u} \beta R^{-1} \right) = -\beta \frac{dp}{dx} + \frac{\partial}{\partial y} \left(\mu \frac{\partial \bar{u}}{\partial y} - \bar{\rho} \bar{u}' \bar{v}' \right) \quad (4.2.9)$$

where $\beta = (1+y/R)^{-1}$.

We discuss first the two simple-wave ramp-flow cases, for which no directly measured Reynolds shear stresses are available. Sturek (1973a, 1974) calculated three shear-stress distributions as shown in Fig.(4.2.3). Values of the partial derivatives have been determined along lines of constant mass flux using a least square technique which fits a parabola to the data. Since initial efforts to calculate the shear-stress distribution resulted in profiles with a large (about $6 \tau_w$) negative value in the vicinity of the boundary layer outer edge it was found that the partial derivatives at the outer edge could be in error by as much as +30%. The partial derivative of mass flux was therefore corrected in an "empirical but consistent manner." These profiles then fulfill the boundary condition at the wall, $\partial \tau / \partial y = dp/dx$, and at the outer edge with a slope tending towards zero. The trend of the three shear-stress distributions agrees qualitatively with that observed in the early stages of subsonic adverse pressure-gradient boundary layers in that the maximum of the shear stress increases and moves away from the wall into the boundary layer.

An experiment similar to that of Sturek was performed by Laderman (1978b and 1979) who investigated two adiabatic boundary layers growing over curved walls (ramps) at a nominal Mach number of 3. Laderman calculated 17 shear stress profiles using eqn.(4.2.7) but did not correct his profiles to make τ_t tend to zero for $y \rightarrow \delta$. One might agree with him that there is "no rationale for changing only one of the derivative terms, $(\partial(\bar{\rho}\bar{u})/\partial x)$, to the exclusion of others."

The effect of pressure gradient on the turbulent shear stress was summarized by Laderman as follows. "The stress distribution is extremely sensitive to dp/dx with the peak value of τ_t/τ_w rising from 60 to 300% above the wall value for the weak-to-moderate pressure gradients used in the present tests. It should be emphasized that, while τ_t/τ_w versus y is invariant with x location, the absolute magnitude of τ_w increases with x ."

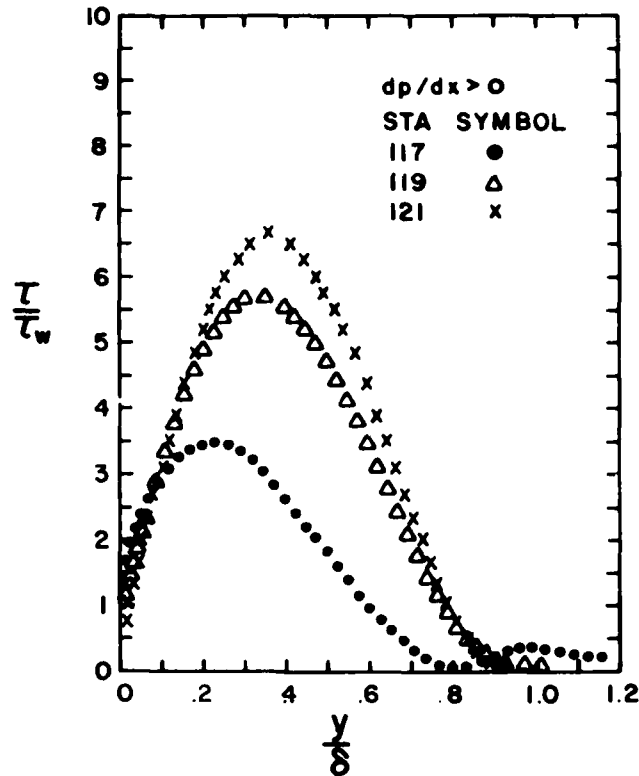


Fig. 4.2.3 Shear-stress distributions calculated from mean flow measurements (adiabatic wall, ramp flow). Taken from Sturek (1973a).

From among the reflected wave cases the experimental investigation by Lewis et al. (1972, CAT 7201) includes mean flow profiles in zero, adverse and favourable pressure gradients. Wilcox & Rubesin (1980) calculated the respective shear stress distributions from the mean flow data and found qualitative agreement with the sketched curves shown in Fig. (4.1.1) which are characteristic of the three types of pressure gradients.

The latter authors have also compared various semi-empirical relationships with the evaluated shear-stress profiles and found "no good agreement" between theory and experiment. They state that the error introduced by the evaluation methods permits assessment of the turbulence models to about $\pm 15\%$ which is fairly close to the $\pm 20\%$ estimated as the uncertainty for local shear-stress measurements by Acharya et al. (1978).

A comparison between the results of several boundary layer calculation methods and shear-stress distributions across compressible turbulent boundary layers evaluated from the mean flow measurements of Zwartz (1970, CAT 7007), Peake et al. (1971, CAT 7102), Sturek & Danberg (1971b, CAT 7101) and Lewis et al. (1972, CAT 7201) can be found in a paper by Rubesin et al. (1977).

4.3. Direct measurements of the Reynolds shear stress ($-\bar{\rho} \overline{u'v'}$) - available data

Table (4.3.1) gives a survey of measurements of Reynolds shear stress ($-\bar{\rho} \overline{u'v'}$) in compressible turbulent boundary layers by means of hot-wire anemometers and laser-Doppler velocimetry. The investigations are listed in order of date for identifiable groups of investigators. We have not separated zero and adverse pressure-gradient flows from each other since some of the important investigations contain data in both types of flow. Unfortunately few investigators have provided tabulated data so that we had to take a few essential measurements from figures in publications. This is against our stated principle (cf. AGARDograph 223) but appears to be permissible here since the experimental uncertainties in the fluctuating flow-field quantities due to the various assumptions employed and calibration errors are $\pm 20\%$ for the turbulent shear stress (Acharya et al. 1978). A closer look at some of the subsequent investigations makes this appear a conservative estimate.

A comparison of the investigations presented in Table (4.3.1) with those used by Sandborn (1974) in his earlier survey shows that the majority of measurements in the table were performed after 1974 so that a new discussion is certainly appropriate.

Table 4.3.1

| Author | M_δ | Heat transfer | Re number | No of $\overline{u'v'}$ profiles | Probe | Anemometer, wall geometry, pressure gradient |
|--|-----------------|---------------|--------------------------------------|----------------------------------|---|---|
| Demetriades & Laderman (1973b) Mean flow data in Laderman & Demetriades (1971) $\overline{u'v'}$ data corrected in Laderman & Demetriades (1979) | 9.4 | Cooled | 37×10^3 Re_θ | 1 | X-wire | CCHWA. Nozzle wall, ZPG |
| Laderman (1976) and (1978a) $\overline{u'v'}$ data corrected in Laderman & Demetriades (1979) | 7.1 | AW Cooled | $1.4 - 2 \times 10^3$ Re_θ | 2 | X-wire | CCHWA, Cone, ZPG |
| Laderman (1978a) and Laderman & Demetriades (1979) Mean flow data in Laderman (1978a) | 3 | AW Cooled | 6.57×10^6 Re/m | 2 | X-wire | CCHWA, flat plate ZPG |
| Rose (1973, 1974) CAT 7306 S | 3.9 | AW | 17×10^6 Re/m | 12 | - | CTHWA axisym. nozzle wall. APG |
| Rose & Murphy (1973) Mean flow data in Rose (1973, 1974) | 3.9 | AW | 8.7×10^4 Re_δ | 5 | No information | CTHWA, nozzle wall, shock/ boundary layer interaction. APG |
| Johnson & Rose (1973 and 1975) | 2.9 | AW | 5.7×10^7 Re/m | 1 | Yawed wire, normal wire | CTHWA, LDV nozzle wall |
| Johnson (1974) ⁺ ⁺ Measurement is superceded by Johnson & Rose (1975) Mean flow data in Reda & Murphy (1973) | 2.9 | AW | 5.7×10^7 Re/m | 1 | - | LDV (dual scatter) nozzle wall Nominally ZPG |
| Rose & Johnson (1975) | 2.9 | AW | 1.4×10^6 Re_δ | 2 | X-wire | CTHWA and LDV Nozzle wall. ZPG, APG. Shock/boundary layer interaction |
| Yanta & Lee (1974) and Yanta & Crapo (1976) Mean flow data in report (see also Lee & Smith 1974) | 3 | AW | 14×10^3 Re_θ | 8 | - | LDV (dual scatter) flat nozzle wall nominally ZPG |
| Mikulla & Horstman (1975) Mean flow data in Horstman & Owen (1972, CAT 7205). See also Owen & Horstman (1974) | 6.9 | Cooled | 2×10^5 Re_δ | 1 | Ceramic wedge probes | CTHWA, cone-ogive cylinder ZPG |
| Mikulla & Horstman (1976) | 6.9 6.7 | Cooled | 9×10^3 Re_θ | 8 | Ceramic wedge probe | CTHWA cone-ogive cylinder |
| Mikulla (private communication) Mean flow data in Marvin et al. (1975) and in Kussoy & Horstman (1975, CAT 7501 S) | " | " | " | tabulated data | " | ZPG, APG, shock boundary-layer interaction |
| Horstman & Rose (1977) | 0.78 | AW | 4×10^5 Re_δ | 1 | Dual film sensor | CTHWA. Tunnel side wall. ZPG. |
| Kussoy et al. (1978, CAT 7802 S) Acharya et al. (1978) Mean flow data in the same report | 2.3 | AW | $4 - 106 \times 10^6$ Re/m | 26 | Ceramic wedge probe (single and dual wire probes) | CTHWA, axisymmetric constant diameter tube, ZPG, APG, FPG. |
| Gootzait & Childs (1977) Mean flow data in the same report and in Gootzait (1976) | 3.9 | AW | - | 2 ZPG 6 APG | Single wire | CTHWA, axisym. wind tunnel wall APG, ZPG |
| Mateer, Brosh, Viegas (1976) and | 1. ^A | AW | 3.7×10^7 Re_x | 7 | Ceramic wedge probe | CTHWA, axisym. pipe flow. APG. Shock boundary layer interaction. |

Table 4.3.1 (cont.)

| Author and | M_δ | Heat transfer | Re number | No. of u'v' profiles | Probe | Anemometer, wall geometry, pressure gradient |
|---|------------|------------------|-------------------------------------|-------------------------|-------|--|
| Mateer & Viegas (1979) Mean flow data in (1976) report and private communication (see CAT 8001 S) | | | | | | |
| Dimotakis, Collins Lang (1979) | 0.1-2.2 | AW | 23-40 $\times 10$ Re_δ | 10 | - | LDV flat plate and ceiling boundary layer |
| Mean flow data in Collins et al. (1978, CAT 7801 S) For a critique of data see Schairer (1980) | | | | | | |

An anomaly exhibited especially by some of the earlier shear-stress measurements is that the maximum value of $-\bar{\rho} \overline{u'v'}$ occurs much further away from the wall than is expected for flows at constant pressure (as compared with Klebanoff's measurement in subsonic flow) and some authors suggest (see Sandborn 1974) that density fluctuations may contribute substantially to the turbulent shear stresses near the wall. This suggestion is based on an inspection of the complete expression for the turbulent shear stress (Hinze 1956):

$$\tau_t = -\left[\bar{\rho} \overline{u'v'} + \bar{u} \overline{\rho'v'} + \bar{v} \overline{\rho'u'} + \bar{\rho}' \overline{u'v'} \right] \quad (4.3.1)$$

As Dimotakis et al. (1979) note correctly such a conjecture is in direct opposition to the conclusion by Morkovin (1962) that effects of density fluctuations should be small compared to effects of variation in mean density for Mach numbers up to 5. The same authors have carefully analyzed their own LDV shear stress measurements and arrive at the conclusion that the departure of the Reynolds stress from the expected value near the wall is independent of Mach number ($0.1 \leq M_\delta \leq 2.2$) and is a consequence of particle depletion near the wall which is unique to boundary layers in air.

It is interesting to set against these findings recent results published by Schairer (1980), who performed measurements in a subsonic boundary layer almost identical to that of Klebanoff, using laser-Doppler velocimetry. His turbulent shear stress measurements do not decrease close to the wall, some values being even higher than those of Klebanoff. Schairer gives the scatter of the shear stress measurements near the wall as being roughly 20% of the mean shear stress at the wall and states that conclusions based on these data are highly speculative. He offers, however, an explanation for the discrepancies found with earlier LDV measurements: "Unlike the measurements of those reporting dropoff in shear stress near the wall, the measurements reported here were made with a laser velocimeter that produced moving interference fringes (Bragg cell). An argument is presented suggesting that, if $\overline{u'v'}$ is negative and the turbulence intensities are high enough, measurements of shear stress near the wall made with stationary fringes will be lower than the actual shear stress."

If Schairer's explanation proves to be correct for supersonic flows also, then the sharp decrease in $-\bar{\rho} \overline{u'v'}$ which can be noted in the shear stress measurements of Yanta & Lee (1974) is due to the same effect. In the latter experiment, in a compressible boundary layer along a straight adiabatic nozzle wall, the shear stress profiles begin to decrease from their maximum value towards the wall at y/δ values of 0.4 which is much too far out in a zero pressure-gradient boundary layer.

As for measurements of Reynolds shear stress by hot-wire anemometry, Mikulla & Horstman (1975) have emphasized two main problems which arise: "First, it is necessary to obtain accurate measurements of the cross correlations $\overline{(\rho u)'v'}$ and $\overline{T'_t v'}$. Indirect determination via the mode-diagram approach (cf. section 2) needs very accurate measurements which are difficult to obtain in part due to problems associated with wire strain gauging and vibration. These problems become more severe the higher the Mach number. Secondly, additional assumptions regarding the fluctuating flow field are required to deduce the Reynolds shear stress $-\bar{\rho} \overline{u'v'}$ from the above cross correlations." These specific problems appear to have been solved by Mikulla & Horstman, and their "post 1975" measurements should be free of these effects. It is questionable, however, whether this can be said of all other measurements. An instructive example of evaluation problems occurring in hot-wire anemometry when applied to supersonic flows may be seen by comparing Laderman & Demetriades (1973) and (1979).

We hope to have drawn the attention of those who intend to model turbulence quantities to some of the experimental problems which have to be surmounted and to the larger than usual uncertainty range for measurements of fluctuating quantities in supersonic boundary layers.

According to Morkovin (1960) the simplest conceivable statement of the supersonic - subsonic similarity for zero pressure gradient at high Reynolds numbers takes the form

$$\tau_t/\tau_w = -\bar{\rho} \overline{u'v'} / (\rho_w u_t^2) = -\bar{\rho} \overline{u'v'} / \tau_w = f(\eta) \quad (4.3.2)$$

$f(\eta)$ would represent a universal shear-stress distribution function obtainable, say, from Klebanoff's measurements (1955) at low speeds. Usually η is assumed to be y/δ but in compressible boundary layers the boundary layer thickness δ has been shown to be an ill-defined length scale (cf. section 7 of AG 253) and thus η is ill-defined. For zero pressure-gradient boundary layers any other integral thickness would be a better choice in terms of precision and Morkovin suggested for example the displacement thickness δ_{1K} at constant density. Other well defined length scales would be the momentum thickness δ_2 , the defect thickness Δ^* or the characteristic length of the inner region of the boundary layer v_w/u_t .

It is also attractive to plot the specific shear stress as $-\overline{u'v'}/u_t^2$ which gives the distribution of the correlation $-\overline{u'v'}$ itself, independent of the density which may change considerably across the boundary layer. Finally some authors make the shear stress dimensionless by $\rho_\infty u_\infty^2$ where the index ∞ denotes some undisturbed state upstream of the region of investigation. Such a form lacks connection to local flow quantities but may be useful if the development of $-\bar{\rho} \overline{u'v'}$ is to be shown in the downstream direction, for example. We have chosen to present dimensionless "shear stress" in the forms $(-\bar{\rho} \overline{u'v'} / \rho_w u_t^2)$ and $(-\overline{u'v'} / u_t^2)$ in order to show possible similarities between measurements at different Reynolds number, Mach number and heat transfer parameter. As in the case of the normal stress components discussed in the previous chapter, we will test the measurements for inner and outer layer similarity by plotting these dimensionless quantities against $y^+ = y u_t / v_w$, y/Δ^* . The full treatment will only be given to zero pressure-gradient boundary layers, since we cannot expect similarity in flows with adverse or favourable pressure gradients unless the pressure gradient in the profiles considered is constant in properly scaled dimensionless form.

Our reservations as to the use of y/δ_2 as an appropriate scaling have been adequately expressed in the previous chapter.

4.4 Direct measurements of the Reynolds shear stress $(-\bar{\rho} \overline{u'v'})$ - zero pressure gradient boundary layers

From among the 95 Reynolds shear stress profiles listed in Table (4.3.1) there were only 7 profiles in a zero pressure gradient boundary layer where data were available in tabular form. Their parameter range is as follows: $2.3 \leq M_\delta \leq 6.8$, $1000 \leq Re_{\delta_2} \leq 16100$, and $0.5 \leq T_w/T_r \leq 1$. Five of these profiles were taken as probably free from severe upstream pressure-gradients effects in the tests by Rose (1973, CAT 7306S), Kussoy & Horstman (1975, CAT 7501S) and Kussoy et al. (1978, CAT 7802S) on the wall of an axisymmetric wind tunnel and one profile from the zero pressure-gradient region on a circular cylinder aligned with the flow (Horstman & Owen 1972, CAT 7205). The shear stress profiles given in CAT 7501S were provided by V. Mikulla & C.C. Horstman as a private communication and profile 72050102 was taken from Fig.8 of Mikulla & Horstman (1975). The mean flow profiles are those of CAT 7205 so we have classified these later turbulence data with the earlier entry. Since the Reynolds shear-stress profile measured in subsonic flow by Klebanoff (1955) is used so often for a comparison with supersonic flow data we have also included this profile. Again, the data had to be taken from Fig.(5) of the Klebanoff report.

The mean flow profiles which belong to the respective shear-stress profiles are plotted in Fig. (4.4.1). The shape parameter H_{12K} is typical for velocity profiles in a zero pressure gradient boundary layer, and the wake strength $\Delta(\bar{u}^*/u_t)$ is within the range of other measurements plotted in Fig. (3.3.5) or AG 253, except for profiles 72050201 and 75010101 which are too high by about 30%. The c_f values also seem to be almost 12% low.

Fig. (4.4.2b) shows the shear stress distribution plotted against $y u_t / v_w$, and no pattern of similarity can be observed except that the data with cooling which happen to have Reynolds number of approximately 2000 and a Mach number of about 7 form a group which is different from the adiabatic wall measurements at a much higher Reynolds number but lower Mach number. Only Klebanoff's measurements approach the expected limiting value of one for $|\bar{\rho} \overline{u'v'} / \rho_w u_t^2|$ in the wall region. The "left hand side" decrease of the shear stress profiles 78020101/0102 in the outer region and that of profiles 72050102, 73060101 and 75020302 in the inner region of the boundary layer apparently has no physical explanation at a point so far out in the boundary layer and must be caused by deficiencies in the measuring techniques. The trends which we have just described are confirmed by the distributions of the correlation $-\overline{u'v'}$ shown in Fig. (4.2.2a). Fig. (4.4.3) shows the same shear stress data plotted against y/Δ^* . A trend towards a similarity pattern can be observed in the outer region for

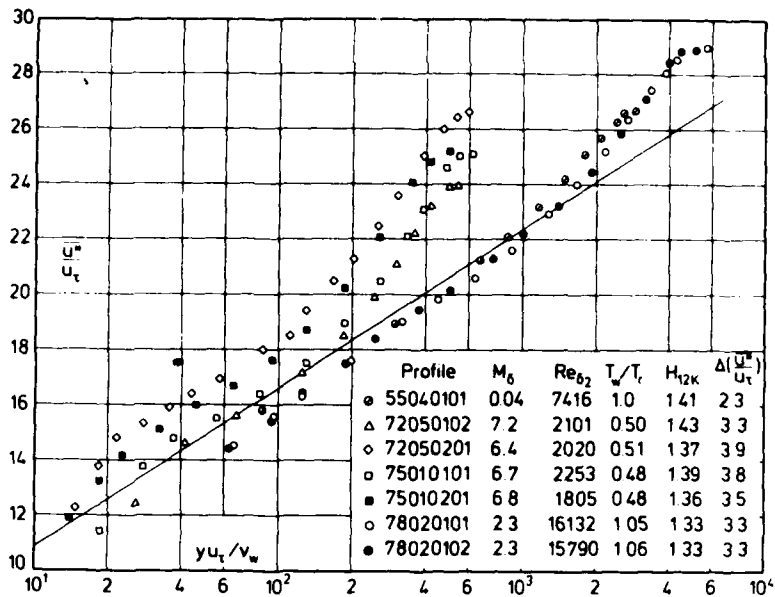


Fig. 4.4.1 Law of the wall for a compressible turbulent boundary layer with zero pressure gradient (origin not defined, adiabatic and isothermal wall).

| Profile | M ₀ | Re ₀₂ | T _w /T ₀ | H _{12K} |
|------------|----------------|------------------|--------------------------------|----------------------|
| ○ 55040101 | 0.04 | 7416 | 1.0 | 140 (Klebanoff 1955) |
| △ 72050102 | 6.8 | 2101 | 0.5 | 144 |
| x 73060101 | 3.9 | 1035 | 1.0 | 154 |
| □ 75010101 | 6.7 | 2253 | 0.5 | 139 |
| ■ 75010201 | 6.8 | 1805 | 0.5 | 136 |
| ○ 78020101 | 2.3 | 16132 | 1.0 | 133 |
| ● 78020102 | 2.3 | 15790 | 1.0 | 133 |

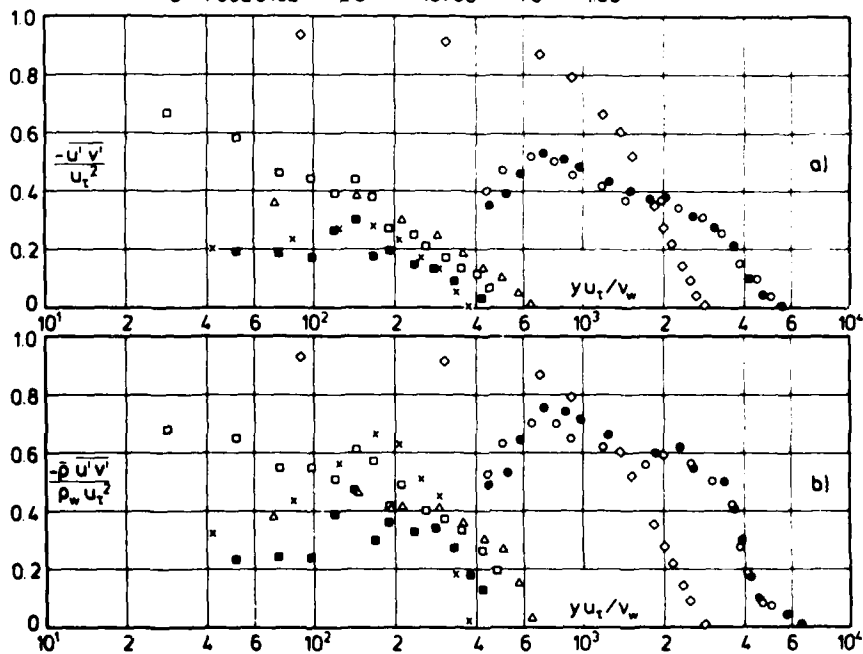


Fig. 4.4.2 a/b Reynolds shear stress distributions in a compressible turbulent boundary layer with zero pressure gradients (adiabatic and isothermal wall, origin not defined).

$-\bar{\rho} \overline{u'v'}$ (Fig. 4.4.3b) and less so for $-\overline{u'v'}$ in Fig. (4.4.3a). As in Fig. (4.4.2) we cannot discern systematic differences in the level of the individual profiles which might be caused by Mach number, Reynolds number or heat-transfer parameter effects.

| Profile | M_b | Re_{b_2} | T_w/T_t | H_{12K} |
|------------|-------|------------|-----------|-----------|
| ○ 55040101 | 0.04 | 7416 | 1.0 | 140 |
| △ 72050102 | 6.8 | 2101 | 0.5 | 144 |
| × 73060101 | 3.9 | 1035 | 1.0 | 154 |
| □ 75010101 | 6.7 | 2253 | 0.5 | 139 |
| ■ 75010201 | 6.8 | 1805 | 0.5 | 136 |
| ○ 78020101 | 2.3 | 16132 | 1.0 | 133 |
| ● 78020102 | 2.3 | 15790 | 1.0 | 133 |

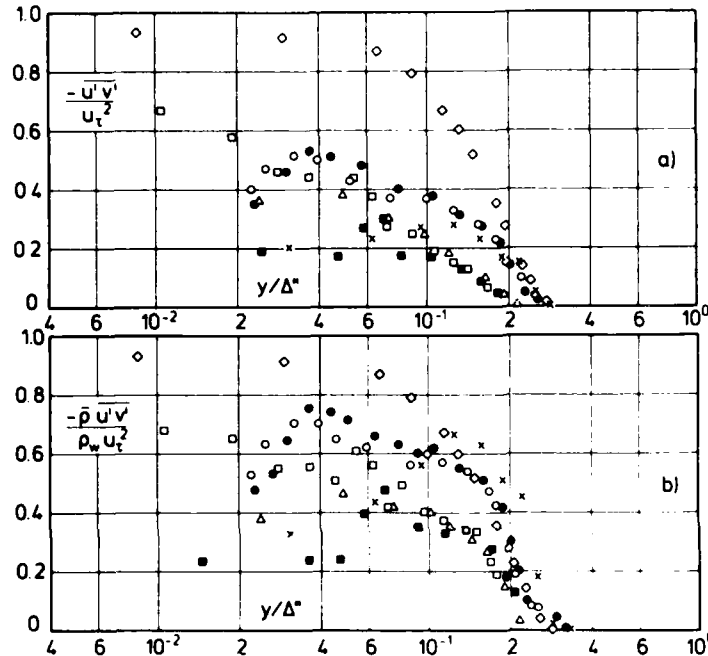


Fig. 4.4.3 a/b Reynolds shear stress distributions in a compressible turbulent boundary layer with zero pressure gradient (adiabatic and isothermal wall, origin not defined).

Demetriades (1979) - they cannot be considered here. Finally, Laderman & Demetriades (1979) have performed shear-stress measurements in an adiabatic and a cooled flat plate boundary layer at a Mach number 3. The cooled wall data in the "restored state" give fair agreement with the "best estimate" whereas the adiabatic wall data show considerable discrepancies. It is conceivable - though certainly not satisfactory - that error bands of $\pm 30\%$ are what we will have to live with using the measuring techniques at present available to us, but it seems important to make this quite clear to all those who seek to establish turbulence models based on turbulence measurements in compressible boundary layers.

We finally show a comparison between Reynolds shear-stress profiles measured by means of CT hot-wire and laser-Doppler anemometry (Fig. 4.4.4) and presented by Rose & Johnson (1975, Fig. 8). It is astonishing and encouraging at the same time to notice how small the differences are in the results obtained by both techniques. Here the turbulent boundary layer developed on the adiabatic wall of a planar wind-tunnel nozzle and test section. The incident shock wave was produced by a full-span generator set at 7° angle of incidence to the freestream flow, producing approximately a 2.5 to 1 pressure rise across the interaction. The profiles with zero pressure gradient which are of interest here were taken under conditions upstream of the incident shock wave of $M_\infty = 2.9$ and $Re_{\delta_0} = 1.4 \times 10^6$ at $x = 137$ mm.

Plotted against the outer-region coordinate y/Δ^* Klebanoff's profile taken in a subsonic boundary layer conforms well with the supersonic shear stress profiles.

We now attempt briefly to discuss those Reynolds shear stress measurements which were not available in tabulated form. A comparison with the data presented in figures (4.4.2) and (4.4.3) is difficult, however, since those data which are given in graphical form were all plotted against y/δ . Extensive measurements of fluctuating quantities were carried out by Demetriades & Laderman (1973b, CAT 7403) and by Laderman (1976, 1978a). A revised version of these data was subsequently published by Laderman (1978c) and by Laderman & Demetriades (1979). A comparison of the revised data performed by the above authors with Sandborn's "best estimate" shows fair agreement but the range of the maximum and minimum values denoted by a vertical bar lies within $\pm 30\%$ which is unacceptably large (Laderman 1976, adiabatic cone boundary layer). The shear-stress data across the cooled cone boundary layer lie however considerably below the "best estimate", with uncertainties of the same magnitude as the above measurements. Next, there are shear-stress-measurements in a Mach 9.4 tunnel-wall boundary layer (Demetriades & Laderman 1973b). Because of their uncertainty range - even after the correction reported in Laderman &

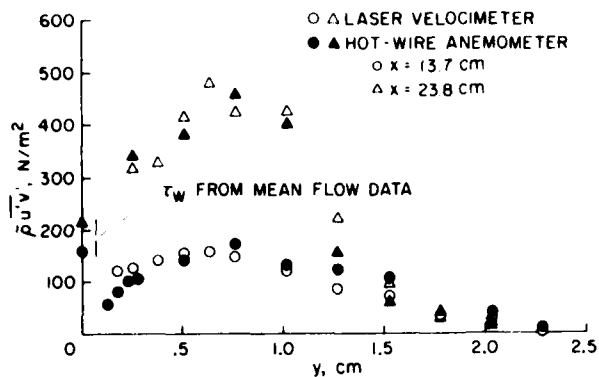


Fig. 4.4.4 Reynolds shear-stress distributions in a compressible boundary layer with varied pressure gradient (adiabatic wall, origin not defined). Taken from Rose & Johnson (1975).

4.5 Direct measurements of Reynolds shear stress ($-\bar{\rho} u'v'$) - adverse pressure gradient boundary layers

At the start of section 4.2.2 we remarked that certain features of compressible flow did not have an equivalent in low speed flow. The most marked of these is the possibility of very concentrated streamwise pressure changes in centred expansions and, as an extreme, in shock waves. The discussion of cases for which direct shear stresses have been measured will begin with adverse pressure gradient reflected wave, straight wall cases without shocks before considering shock boundary layer interactions of increasing severity. There are no measurements in curved wall flows.

Gootzait & Childs (1977) measured the Reynolds shear stress in the boundary layer on the adiabatic wall of a cylindrical extension to an axisymmetric nozzle, where the pressure gradients were induced by contoured centre bodies mounted on the wind-tunnel centreline. Though the tunnel diameter was only 53 mm (as used by Rose, CAT 7306) and the boundary layer approximately 5 mm thick, shear stress profiles were measured at 8 positions with measurements as close as 0.5 mm to the wall. Since data are not available in tabular form it is difficult to compare them with other data under similar boundary conditions. The authors found reasonably good agreement between their fluctuation measurements and shear-stress distributions calculated by means of an integration of the mean flow equations using the semi-empirical relationship of Sun & Childs (1975). Qualitatively the turbulent shear stress increases with distance downstream from the beginning of the pressure rise, and the most marked increase in $-\bar{\rho} u'v'$ occurs near the middle of the boundary layer.

The following six case studies can be discussed in more detail since mean and fluctuating flow data are available in tabular form. In five boundary layer flows with varied pressure gradients, Reynolds normal stresses were measured besides the Reynolds shear stresses. The data already presented in section 3.2 should also, therefore, be borne in mind in the following discussion.

We begin again with the reflected wave case of Kussoy et al. (1978, CAT 7802S) where two centre bodies, sting mounted on the tunnel axis, were designed to impose shock-free compressions on the boundary layer (pressure distribution I, series 01, and pressure distribution II, series 02), followed where geometry allowed, by firstly a constant pressure region and finally an expansion (series 02). Measurements of the Reynolds shear stress $-\bar{\rho} u'v'$ were performed by means of dual ceramic wedge probes operated in the constant temperature mode. A discussion of the flow field and of the mean flow data can be found in AG 253 (Figs. 6.2.2 and 6.2.3) and in section 6 (CAT 7802S) where we give a corrected version of the inner and outer law plots. The experimental data were also compared with the results of four calculation methods in an investigation by Acharya et al. (1978).

The distributions of the Reynolds shear stress $-\bar{\rho} u'v'$ and the double correlation $-\overline{u'v'}$ are plotted versus $y u_{\tau}/v_w$ in Fig. (4.5.1). The legend gives the Mach number at the beginning and the end of the pressure rise, the pressure distribution on the wall and the respective values of the skin friction velocity. The shear stress profiles react to the pressure increase downstream of 0104 by a sharp increase in level reaching a maximum value for profile 0111 (the maximum for $\bar{\rho} u'^2$ was reached at 0108 and for $\bar{\rho} v'^2$ with a double peak at 0109, Fig. 3.2.2), and with peaks of almost the same height for profiles 0108, 0109 and 0113. All shear stress distributions are typical of those in an adverse pressure gradient boundary layer in subsonic flow. What is less distinctly marked than in subsonic flow is the shift of the maxima towards the outer edge of the boundary layer.

In contrast to the distributions in zero pressure-gradient boundary layers both the $\bar{\rho} u'v'$ and $\overline{u'v'}$ profiles show a similarity behaviour in the outer region which was quite unexpected. This is partly understandable since the Reynolds number hardly changes in the region investigated but we would have expected the large

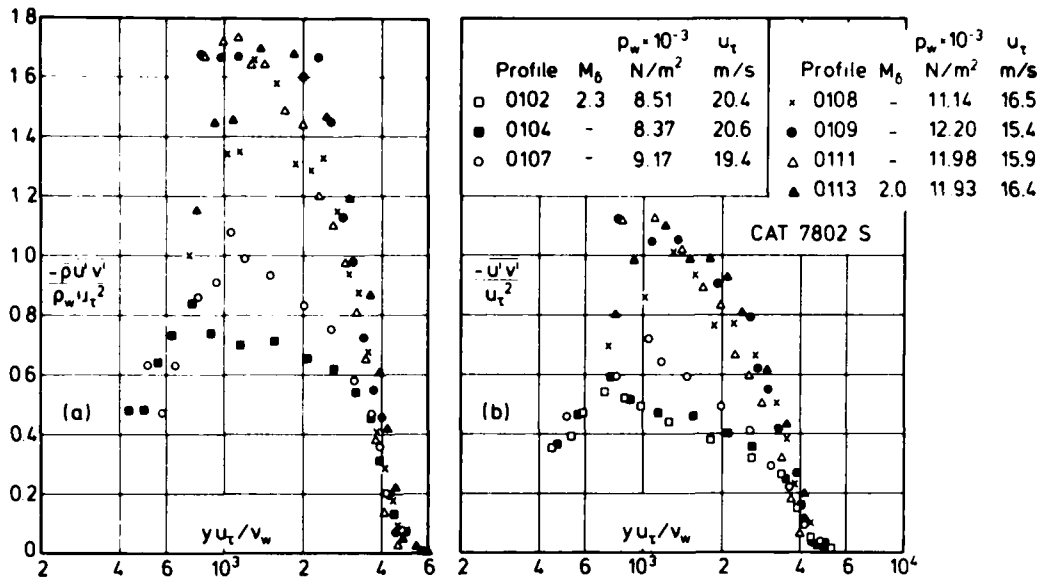


Fig. 4.5.1 Reynolds shear-stress distributions in a compressible turbulent boundary layer with varied, mainly adverse pressure gradient (adiabatic wall, origin not defined). Kussoy et al. (1978). Pressure distribution I.

eddies in the outer region and with them the Reynolds shear stress to be severely influenced by the pressure gradients and thus show no similarity at all. This behaviour might be fortuitous were it not for a similar tendency in Fig. (4.5.2a) where we have plotted the same shear-stress distributions against the outer region coordinate y/Δ^* . Here the similarity is confined to those profiles (0102, 0104, 0107) where the pressure gradient is small or even negligible but it is obvious that the "disturbed" profiles tend towards the similar ones in the downstream direction where the pressure gradient decreases again (profile 0113). The shear stress profiles of pressure distribution II (series 02) show a similar trend to those of series 01 Figs.(4.5.2b,4.5.3) but relaxation after the severe adverse pressure gradient occurs much faster (Fig.4.5.2b, profile 0214), probably due to the favourable pressure gradient further downstream. Profile 0214 lies however

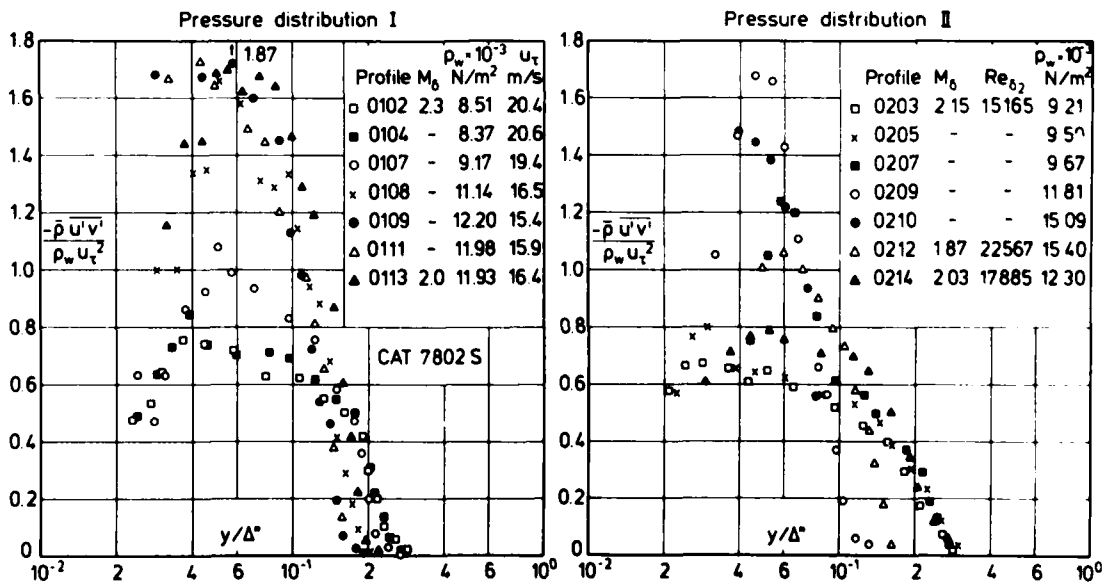


Fig. 4.5.2 Reynolds shear-stress distributions in a compressible turbulent boundary layer with varied pressure gradient (adiabatic wall, origin not defined). Kussoy et al. (1978).

| Profile | M_0 | Re_{02} | $p_w \cdot 10^{-3} \text{ N/m}^2$ |
|---------|-------|-----------|-----------------------------------|
| □ 0203 | 2.15 | 15165 | 9.21 |
| ■ 0207 | - | - | 9.67 |
| ○ 0209 | - | - | 11.81 |
| ● 0210 | - | - | 15.09 |
| △ 0212 | 1.87 | 22567 | 15.40 |
| ▲ 0214 | 2.03 | 17885 | 12.30 |

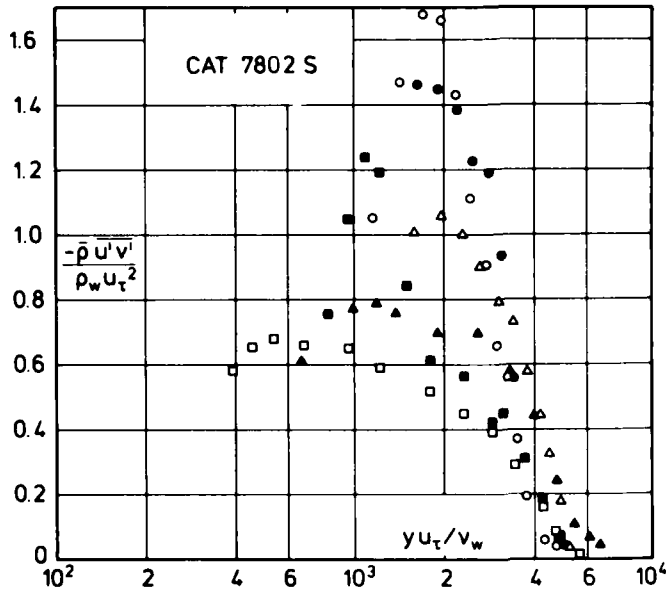


Fig. 4.5.3 Reynolds shear-stress distributions in a compressible turbulent boundary layer with zero pressure gradient (origin not defined, adiabatic wall). Kussoy et al. (1978).

stress profiles are plotted in Fig. (4.5.4), side by side for the two pressure distributions. Profiles 0101 and 0201 are, for both flows, in the region of nominally zero pressure gradient with the level of $-\bar{\rho} u'v'$ differing by roughly a factor 2. Profile 0105 was measured in the middle of the shock interaction and shows a peak value of the dimensionless shear stress which is about 20 times the value in the ZPG region upstream. The corresponding profile in series 02 is not available but is stated as being similar by Mikulla & Horstman (1976). Shear stress profiles 0110 and 0209 respectively were taken at the pressure peak or just downstream in a slightly favourable pressure-gradient region. As in Fig. (3.2.8), where we have plotted the two normal stress distributions $\bar{\rho} v'^2$, the documentation of series 01 is much more complete. For this attached flow case one can agree with the authors who state "that it displays large turbulent memory effects in that it is still typical of an adverse pressure-gradient flow although the surface pressure gradient is zero at this location." In this respect profile 0209 has reached a higher state of relaxation but its peak level is still about five times above the ZPG profile 0201. Though the last profile 0212 has a lower u_τ value than profile 0201 (see legend of Fig. 4.5.4), the overall shear-stress level is below that of the ZPG profile and must therefore be severely affected by the downstream pressure history. Kussoy & Horstman (1975) have also compared their measured shear stress distributions with those obtained from the integration of the mean momentum equation using the measured mean flow profiles. The agreement is reasonable. This experiment is remarkable in that it presents Reynolds normal and shear stresses in boundary layers with and without shock induced separation and in the flow downstream. Being well aware of the difficulty of measurements in such a complex flow we would nevertheless like to see another and more fully documented experimental investigation of this type providing all normal stresses, different devices to measure skin friction and shear-stress measurements by laser and hot-wire anemometry.

The forerunner of the above experiment (series 01) is that of Rose (1973, CAT 7306S) which is also discussed in section 3.2 (normal stresses) and section 6 of this AGARDograph. Here the adverse pressure gradient was again induced by a shock but the boundary layer was adiabatic and not cooled. The Reynolds shear stress distributions are plotted in Fig. (4.5.5), and the legend gives the distributions of the skin friction velocity

still slightly above the "undisturbed" shear-stress distribution 0203. As can be seen from the legend of Fig. (3.2.5) the values for u_τ of profiles 0203 and 0214 differ only by 5%, so our statement holds both for the scaled and unscaled profiles. There are 3 investigations with 4 test cases (cf. Table 4.2.1) where Reynolds shear stresses have been measured upstream and downstream of a shock/boundary layer interaction (Rose 1973, CAT 7306S; Mateer & Viegas 1980, CAT 8001S; Kussoy & Horstman 1975, CAT 7501S).

For the last investigation tabular data were not available other than seven profiles given by Mikulla & Horstman (1976), and mean flow data were published by Kussoy & Horstman (1975, see also chapter 5 and CAT 7501S). The test boundary layer was formed on a cone-ogive-cylinder mounted on the centre line of the wind tunnel. An annular shock generator was mounted coaxially with the model and could be traversed in the axial direction. Two deflection angles, 7.5° and 15° (series 01 and 02) were used, and the shock waves produced were followed closely by an expansion. The turbulence measurements were performed with two $10 \mu\text{m}$ diameter platinum-rhodium wires mounted on ceramic wedges which were operated using CT anemometers. Both boundary layer flows ($M_0 \approx 6.8$) were nonadiabatic, with and without separation. The shear

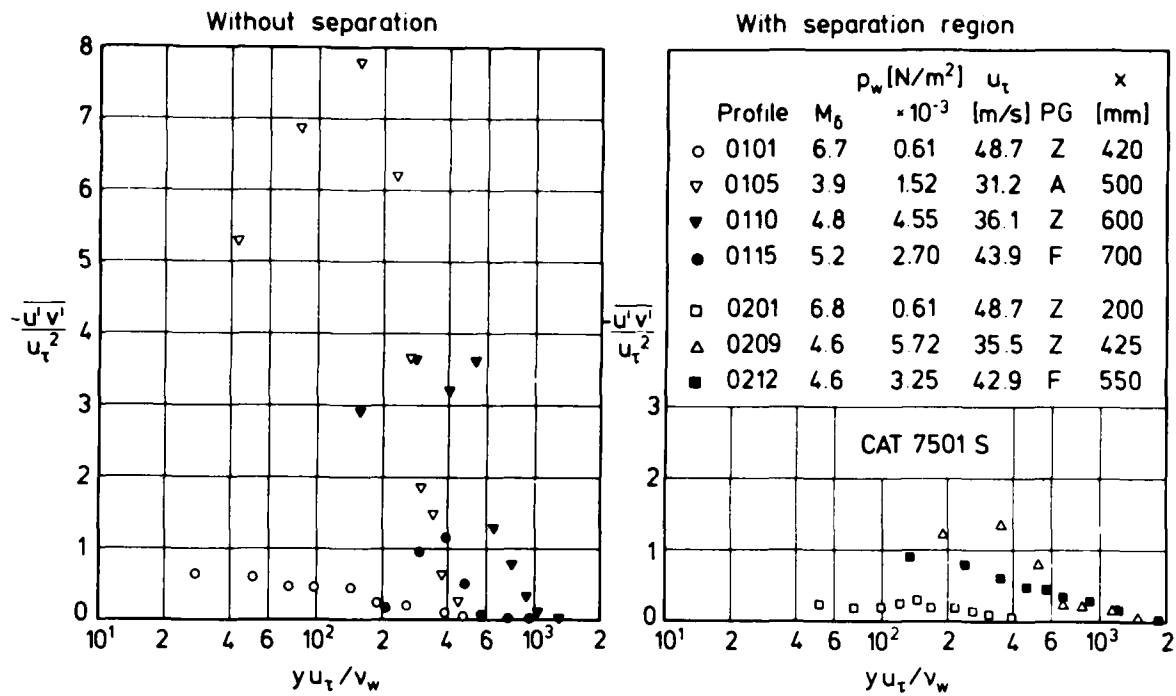


Fig. 4.5.4 Reynolds shear-stress distributions in a shock/boundary-layer interaction flow (isothermal wall, $T_w/T_r = 0.47$, defined origin). Kussoy et al. (1975).

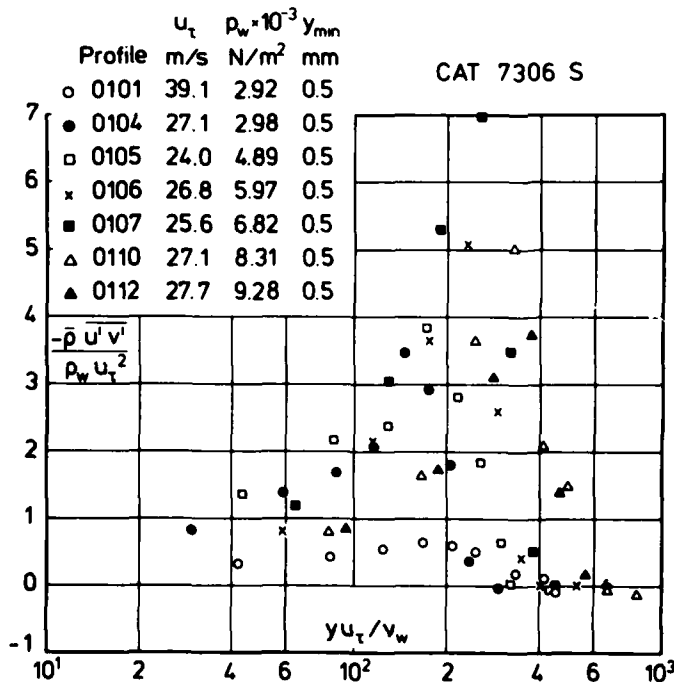


Fig. 4.5.5 Reynolds shear-stress distributions in a compressible boundary layer with shock interaction (adiabatic wall, origin not defined). Rose (1973).

u_τ - taken from Rubesin et al. (1974) - and of the wall static pressure which increases monotonically whereas u_τ has a distinct minimum at station 0105. The shear-stress distributions show the typical behaviour of those in an adverse pressure gradient, increasing in level with the increasing pressure and with the peak moving out towards the edge of the boundary layer. Profile 0112 may already be influenced by the levelling off of the pressure gradient showing a lower peak value than the upstream distributions.

Rose (1973) has also measured $\bar{\rho} \overline{v'w'}$. This turbulence term represents a circumferential shear stress which should in principle be zero. The values recorded therefore may be interpreted either as a sign of asymmetry or as an indication of the level of accuracy of the hot-wire measurements.

The experience of this first extensive investigation of the turbulence structure downstream of a shock/boundary layer interaction was apparently transferred to a similar study by Rose & Johnson (1975) who measured a shear-stress profile downstream from a shock ($x = 23.8$ cm) using an X-wire and a laser under the same flow conditions. Fig. (4.4.4) above shows both the comparison between the two undisturbed profiles and that between the two profiles downstream

from the shock. The two measuring techniques give good agreement in the zero and the adverse pressure gradient regions. Further, somewhat earlier, measurements by Rose & Murphy (1973) in a shock/boundary layer interaction region along an adiabatic wall are not available either in graphical or in tabular form. These profiles are given indirectly only as the ratio a_1 of the Reynolds shear stress $-\bar{\rho} \overline{u'v'}$ and the kinetic energy of the fluctuating flow $\bar{\rho}(\overline{u'^2} + \overline{v'^2} + \overline{w'^2})$. They are discussed in section 4.6 below.

The last series of shear-stress distributions for which tabular data are available are those performed by Mateer & Viegas (1980, CAT 8001S) in the boundary layer on the inner surface of a cylindrical duct of constant diameter. At the rear end of the duct a hollow cylindrical choke of varying cross section was inserted and its position adjusted to give a suitable position for a normal shock in the test section. The shear-stress profile 8001S 0101 (Fig.4.5.6) was measured upstream of the shock interaction and was virtually unaffected by it. The next profile for which the skin friction velocity u_τ was available, 8001S 0103, shows an increase of

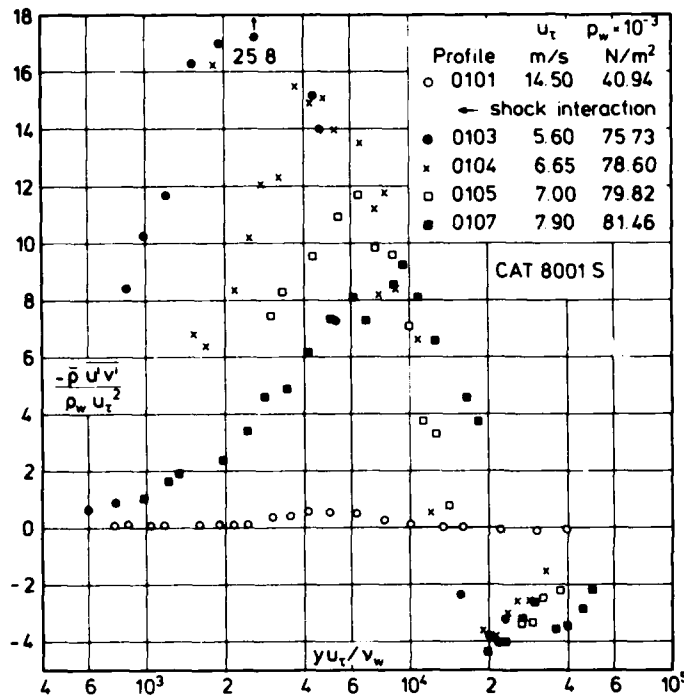


Fig. 4.5.6 Reynolds shear-stress distributions in a transonic turbulent boundary layer with shock interaction (adiabatic wall, origin not defined, $0.9 \leq M_\infty \leq 1.44$). Mateer & Viegas (1980).

the peak level of $-(\bar{\rho} \overline{u'v'})/(\rho_w u_\tau^2)$ by a factor of about 50. τ_w has fallen by a factor of two or three so that the absolute increase is also very great. The maxima in the scaled profiles fall downstream, without however recovering the upstream distribution of profile 0101. The absolute turbulence level has fallen below the upstream value at the last measuring station (0107).

The mean flow structure, discussed in the entry describing this experiment (CAT 8001S) is such that the shear stress outside the boundary layer does not fall to zero, but reverses sign as measurements continue through a high total pressure region originating in the bifurcated foot of the shock structure into a low total pressure region containing the core flow which has traversed a normal shock. An experiment of this nature is inevitably "bedevilled" by a high level of mean flow fluctuation, so that it would be unwise to build too much on the precise numerical values. The trends shown should however be valid, and the order of magnitude of the reversed stresses is much greater than any likely error range, except for profile 01 where the change in sign indicates the level of error likely to be present.

4.6 Ratio a_1 of the Reynolds shear stress $-\bar{\rho} \overline{u'v'}$ and the kinetic energy of the fluctuating flow $\bar{\rho}(\overline{u'^2} + \overline{v'^2} + \overline{w'^2})$

In his investigation of the turbulence structure of an incompressible turbulent boundary layer with zero pressure gradient Klebanoff (1955) introduced the ratio of the Reynolds shear stress $-\bar{\rho} \overline{u'v'}$ to the kinetic energy of the turbulent velocity fluctuations $\bar{q}^2 = (\bar{\rho}/2)(\overline{u'^2} + \overline{v'^2} + \overline{w'^2})$. The ratio $-\overline{u'v'}/(\overline{u'^2} + \overline{v'^2} + \overline{w'^2})$ was denoted a_1 by Bradshaw & Ferriss (1971) and used as one of the semi-empirical inputs ($a_1 = 0.15$) of their calculation method for compressible turbulent boundary layers along adiabatic walls. Rose & Murphy (1973) were apparently the first to compare this assumption with measurements in compressible boundary layers and found that the streamwise variation of this ratio is small compared with that normal to the wall and that its values range nominally from 0.08 to 0.22. The other two sets of fluctuation measurements which are complete enough for a_1 to be evaluated are those by Rose (1973, CAT 7306S) and by Kussoy et al. (1978, CAT 7802S). Since Klebanoff found a_1 to be constant in the range $0.15 \leq y/\delta \leq 0.8$ in an incompressible zero pressure-gradient boundary layer, we have plotted the available data for a compressible boundary layer in Fig. (4.6.1) and note that a_1 is by no means constant in the two boundary layers from which the measurements were taken. There appears to be a slight dependence on Reynolds number but the discrepancies between the distributions could also well be due to uncertainties of the measurements. The shape of the a_1 distribution suggests that

| | Profile | M ₆ | Re _{δ2} | H _{12K} |
|---|----------|----------------|------------------|------------------|
| x | 73060101 | 3.9 | 1035 | 154 |
| o | 78020101 | 2.3 | 16132 | 133 |
| ● | 78020102 | 2.3 | 15790 | 133 |

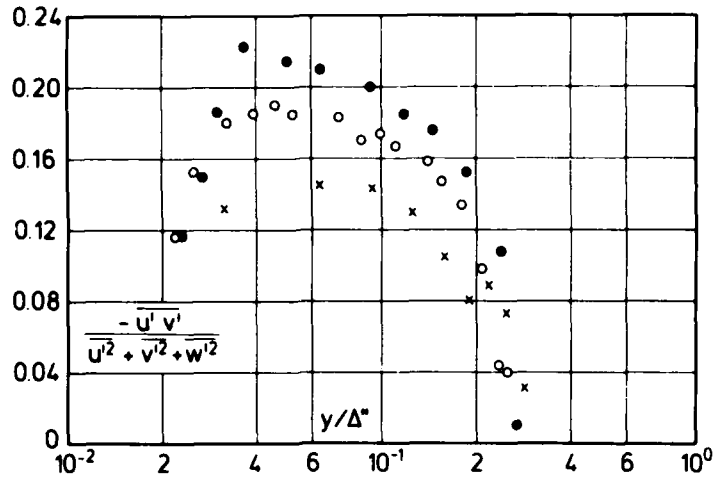


Fig. 4.6.1 Ratio of the Reynolds shear stress to turbulent energy in a compressible boundary layer with zero pressure gradient (adiabatic wall, origin not defined).

it decreases towards zero faster than the turbulent kinetic energy both towards the wall and towards the outer edge of the boundary layer.

Fig. (4.6.2) shows a_1 -distributions in the reflected wave region of an adverse pressure-gradient boundary layer for the two pressure distributions (series 01 and series 02) discussed above. The profiles show a surprisingly high degree of similarity in the outer region if plotted against yu_t/v_w . The influence of the various parameters appears to play a role only in the inner region which is however not completely covered by measurements. This similar behaviour in inner region coordinates is most probably due to the relatively small changes of Reynolds number in these two boundary layer flows, since the low and medium high Reynolds number cases in Fig. (4.6.1) do not show this similarity when plotted against y^+ .

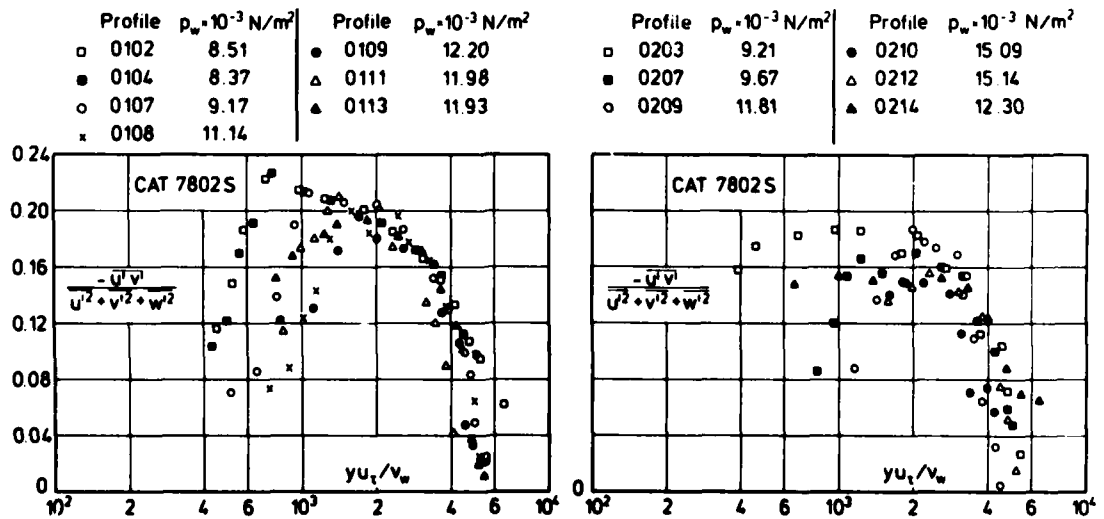


Fig. 4.6.2 Ratio of Reynolds shear stress to turbulent energy in a compressible boundary layer with varied pressure gradient (adiabatic wall, origin not defined). Kussoy et al. (1978).

In Fig. (4.6.3) we present a_1 distributions as evaluated from a shock/boundary layer experiment performed by Rose (1973). The profiles are highly disturbed by the shock, showing a wide spread in peak level and no similarity at all in the outer region.

| | Profile | u_τ m/s | $p_w \cdot 10^{-3}$ N/m ² |
|---|---------|--------------|--------------------------------------|
| ○ | 0101 | 39.1 | 2.92 |
| ● | 0104 | 27.1 | 2.98 |
| □ | 0105 | 24.0 | 4.89 |
| x | 0106 | 26.8 | 5.97 |
| ■ | 0107 | 25.6 | 6.82 |
| △ | 0110 | 27.1 | 8.31 |
| ▲ | 0112 | 27.7 | 9.28 |

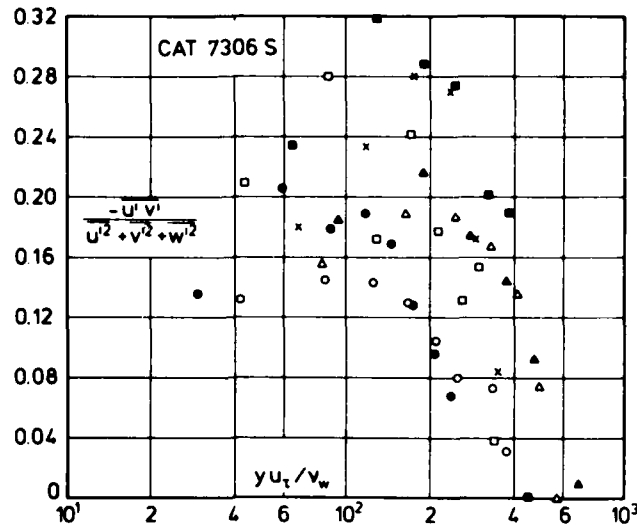


Fig. 4.6.3 Ratio of Reynolds shear stress to turbulent energy in a compressible boundary layer with shock interaction (adiabatic wall, origin not defined). Rose (1973).

It should be clear from the experiments presented here that a_1 is not a constant, not even to a first approximation. The data we have is not yet sufficient for us to suggest any general model for the variation of a_1 . Problems which occur with calculation methods of the Bradshaw type may be partly due to the assumption of a constant value for a_1 across the boundary layer.

4.7 Other correlation terms

After the Reynolds shear stress $-\overline{\rho u'v'}$ the most important quantity of the fluctuating motion is the turbulent heat flux. Sandborn (1974) gives the full expression as

$$q_t = -c_p(\overline{\rho v'T'} + \overline{v \rho'T'} + \overline{\rho'v'T'}) \quad (4.7.1)$$

which can be derived from the energy equation. In the case of a turbulent boundary layer one usually retains only the first term $-c_p \overline{\rho v'T'}$, assuming that the other two terms are at least one order of magnitude smaller. This appears plausible, certainly as long as Morkovin's hypothesis holds.

The turbulent heat flux term q_t can be obtained in much the same way as the shear stress term (Eqn. 4.1.2). Meier & Rotta (1970) have done this for the ZPG boundary layer along an adiabatic wall and Horstman & Owen (1972) for a ZPG boundary layer along an isothermal wall ($T_w/T_r = 0.5$). Sandborn (1974) compared these two evaluations in his Fig.(9) and found the heat flux to increase with increasing Mach number ($2.5 \leq M_\delta \leq 4.5$) and to decrease with increasing Reynolds number (for a constant Mach number $M_\delta = 6.8$ the Reynolds number Re_θ was varied in the range between 4900 and 9700). The only turbulence measurements from which $\overline{v'T'}$ can be deduced are those of Rose (1973) in a boundary layer with shock interaction, and they are shown in Fig.(4.7.1). We have plotted $-\overline{\rho v'T'}$ nondimensionalized with $\rho_w u_\tau T_w$ against y^+ and find a behaviour which is similar to

that of the Reynolds shear stress in Fig. (4.5.5). The maximum peak value for $-\bar{\rho} v' T'$ occurs at the same position, profile 0107, as for $-\bar{\rho} u' v'$ in Fig. (4.5.5). The turbulent heat flux is strongly increased by the adverse pressure gradient, finally decreasing towards the initial low level distribution upstream of the shock interaction.

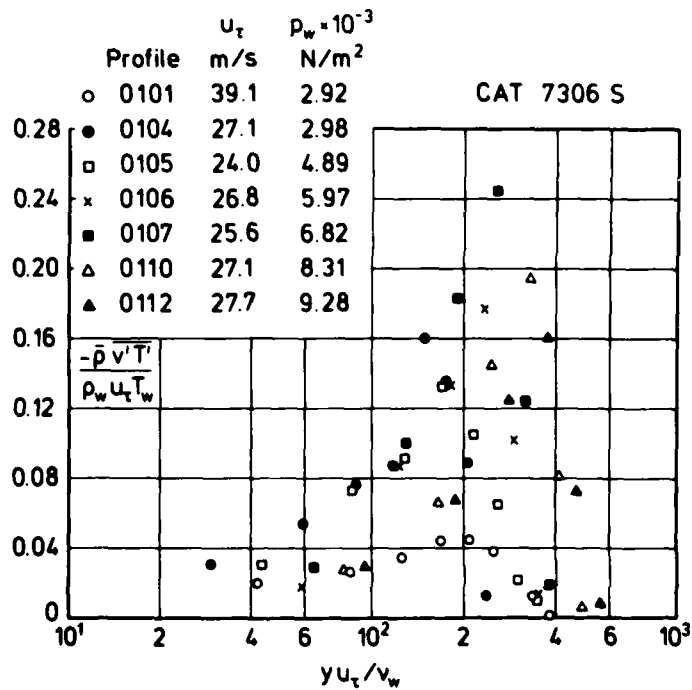


Fig. 4.7.1 Turbulent heat-transfer distributions in a compressible boundary layer with shock interaction (adiabatic wall, origin not defined). Rose (1973).

5. MEAN FLOW TOPICS

We have, in the preceding chapters, discussed turbulence data at some length. Many of the data have only become available to us since the completion of AGARDograph 223, and the new entries in this volume have also provided data which throw light on certain special features of the mean flow. In AG 223 we frequently remarked, of axisymmetric flows, that the boundary layer thickness was a substantial proportion of the transverse radius of curvature characteristic of the flow. We were not in a position to say just what the effects of large transverse curvature might be, nor at what point they might become significant. We have since obtained the data of Richmond (1957, CAT 5701S) which, with the low speed results of Willmarth et al. (1976) provide the basis of the discussion in §5.1 below.

The availability of data for strongly cooled flows with large pressure gradients at reasonably high Reynolds numbers, in particular that of Peterson (1974, CAT 7406S), Kussoy & Horstman (1975 - CAT 7501S), has made it possible to start on a proper practical assessment of the breakdown conditions for the van Driest temperature/velocity correlation and the associated transformation procedures. This is discussed in §5.2, while the flow field for one of these key cases (Kussoy & Horstman, 1975, CAT 7501S) is examined in some detail in §5.3.

5.1 Transverse curvature effects

Dealing with the effect of wall curvature on compressible turbulent boundary layers one must distinguish between curvature in the transverse (cross-sectional) and in the longitudinal (camber) direction (cf. Thomann 1968, CAT 6800). The flow along a waisted body of revolution as investigated by Winter et al. (1970, CAT 7004) contains both effects (cf. AG 253, figures 5.3.18 to 5.3.21).

If for a body of constant radius the boundary layer thickness is small compared with the body radius, then the boundary layer can be treated as if it were planar. This assumption does not hold for long slender bodies of revolution, and the boundary layer equations and turbulence models must contain terms which take into account the transverse curvature.

Very few experimental investigations are available which could serve as a basis for an order of magnitude estimate of the curvature terms in the equations or for a comparison with the results of calculation methods. We know of only three experiments, two (Richmond 1957, Willmarth et al. 1976) in a subsonic and one (Richmond 1957, CAT 5701S) in a supersonic boundary layer, and begin with a description of Richmond's investigation.

The boundary layer was formed on the outer surface of one of a number of slender cylinders aligned with the flow. For the subsonic tests two models were used. The first (series 01) consisted of an aluminium tube 3.65 m long and 25.4 mm in diameter. The front end was mounted on the tunnel settling chamber screens so that it extended along the contraction centre line into the working section. The second model (series 02) consisted of a steel wire under tension passing through the screens.

For the hypersonic test cases, results are presented for two wires ($d = 0.61, 1.63$ mm diameter, series 05 and 04) and for a composite wire-cylinder model. It consisted of a wire passing through the throat on which was mounted a 3° half-angle cone-ogive nosed cylinder to reach the 6.35 mm diameter. For the hypersonic tests, the author obtained mean velocity profiles assuming isoenergetic flow. Skin friction values were measured by means of a floating element balance for series 03 and calculated for the other series by matching the velocity profiles to the Coles' wake-and-wall profile at low speeds (Coles 1955) and by matching a transformed profile at high speeds (series 04 and 05). Fig. (5.1.1) shows 4 velocity profiles plotted in log-law coordinates with the characteristic length scale δ_1/R in the range 1.2 to 1.9. Profiles 0301 and 0302 which are denoted laminar by the author show large discrepancies from the standard log-law. Whereas profile 0301 shows a low Reynolds number, Re_{δ_2} , laminar-like velocity distribution (cf. profiles 7305/0301 and 0302 in Fig. 4.4.4 of AG 253), 0302 lies much below the log-law. This is probably a consequence of the faulty - too high - value of the skin friction. The two "turbulent" velocity profiles behave typically like velocity distributions in a moderately favourable pressure gradient (cf. profile 72010119 in Fig. 5.1.2 of AG 253), showing a "negative" wake component. The similarity between a favourable pressure gradient profile and one with large transverse curvature (suggested first by Patel 1973) is also evident from the skin-friction values which are considerably higher for the curved wall profiles than for a plane wall boundary layer at the same Mach and Reynolds number, Re_{δ_2} (for profile 0303 the values for the skin friction coefficient would be 1.94×10^3 and 1.23×10^3 respectively, with c_f (plane wall) determined according to Fernholz (1971), for example. This is a further

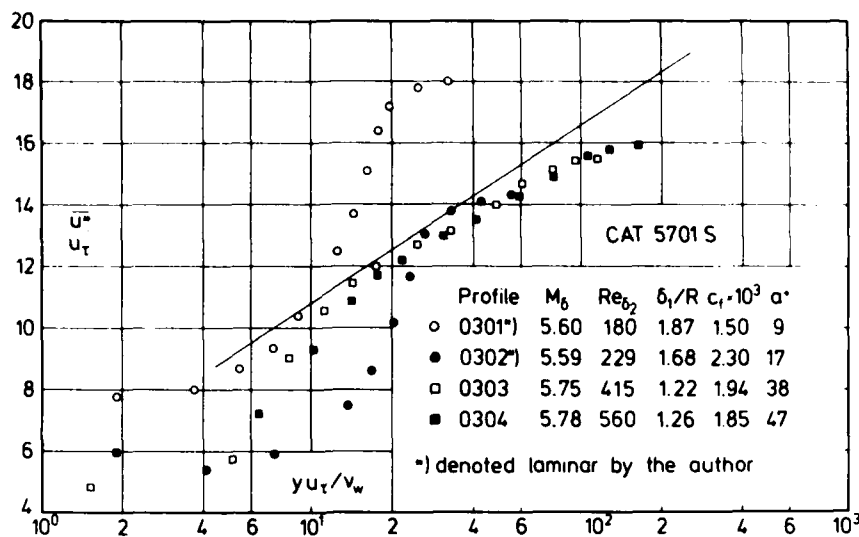


Fig. 5.1.1 Log-law for a compressible boundary layer with transverse curvature (adiabatic wall, origin not defined, ZPG, c_f from FEB). Richmond (1957).

indication that the boundary layer profiles on a cylinder are very full. The full shape is a result of the cylindrical geometry of the flow (Willmarth et al. 1976) and not of the acceleration of the stream which produces a full velocity profile on a plane wall. As for the turbulence structure, Willmarth & Yang (1970) have found in subsonic flow that the effect of transverse curvature is to reduce the spatial scale of the turbulence.

Another problem which arises in flows with transverse curvature is the choice of a suitable dimensionless length scale. Exact solutions of the equation of motion for laminar boundary layers along walls with transverse curvature have shown that $a^+ = u_\tau R / \nu_w$ may represent such a length scale besides δ_1/R . Here δ_1 denotes the displacement thickness, δ_2 the momentum loss thickness and R the body radius. We have calculated at least two of these length scales and given their values in the legends of the subsequent figures but prefer δ_1/R to a^+ since increasing values of this dimensionless length coincide with an increasing departure of the profiles from the standard log-law.

In order to compare supersonic and subsonic velocity profiles with marked transverse curvature effects we have plotted velocity profiles obtained by Willmarth et al. (1976) in subsonic flow. The test boundary layer was generated on circular cylinders, with a diameter range $0.5 \leq d \leq 51$ mm, mounted on the centre line of an octagonal vertical wind tunnel. The authors took great care to achieve flow symmetry about the cylinders and found that a cylinder must be straight to within a small fraction of its diameter for reasonably axially symmetric flow on it to be obtained. Fig. (5.1.2) shows a selection of the measured profiles, covering a range of $0.3 \leq \delta_1/R \leq 5.8$ at a considerably higher Reynolds number range than the supersonic flow profiles. The plot shows clearly that the higher δ_1/R the greater the departure from the standard log law. The shape parameter H_{12K} (ρ constant) becomes unusually small indicating that the profile is very full (with the limit of $H_{12K} = 1$ for a rectangular velocity profile). The similarity of velocity profiles with approximately equal δ_1/R where we have plotted two supersonic turbulent profiles together with equivalent subsonic ones (Willmarth et al. 1976). If the range for δ_1/R is increased further than about 6, the form of the profiles changes dramatically as can be seen in Fig. (5.1.4) where we present some of the subsonic profiles measured by Richmond. Velocity profiles with low values of δ_1/R behave like plane wall ZPG profiles whereas those with δ_1/R larger than 8 resemble profiles measured by Patel (1965) in a highly favourable pressure gradient (with profile 0502 as an exception). Following a suggestion by Rao (1967) we have plotted these latter velocity profiles against a stretched coordinate Y^+ where $Y^+ = (Ru_\tau / \nu_w) \ln[1 + (y/R)]$. They are, however, not shown here, since the pattern of the velocity profiles is not changed in such a way that the universal law is recovered. We therefore have to accept that the standard universal log-law does not hold any longer if δ_1/R exceeds, say, 0.8 (cf. Fig. 5.1.2).

Since the above velocity profiles are similar to those in favourable pressure gradient flow we do not expect agreement with the standard outer law curve which holds only for zero pressure-gradient boundary layers.

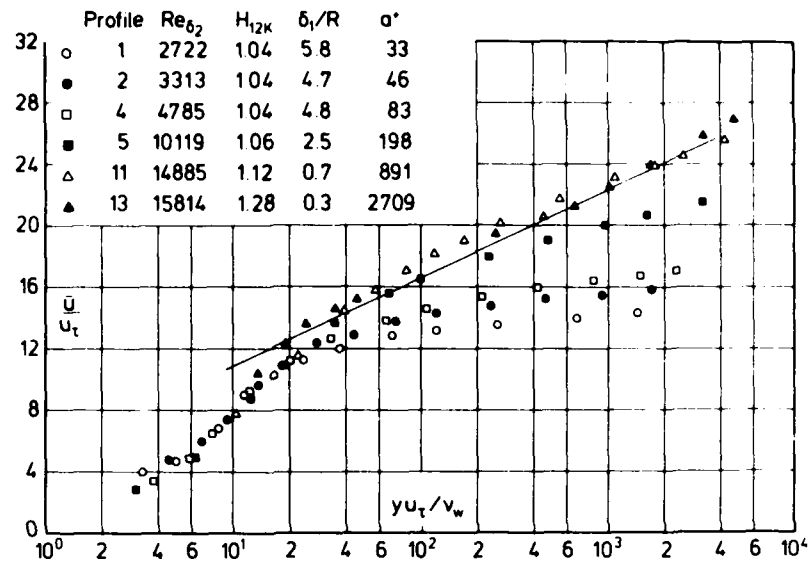


Fig. 5.1.2 Law of the wall for a subsonic turbulent boundary layer with transverse curvature (adiabatic wall, origin not defined, ZPG). Willmarth et al. (1976).

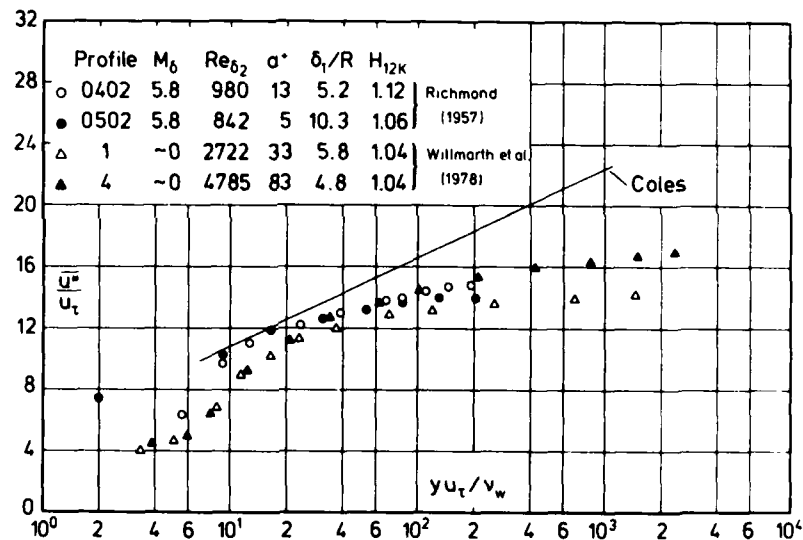


Fig. 5.1.3 Comparison of subsonic and supersonic turbulent boundary layers with strong transverse curvature effects (adiabatic wall, ZPG).

Fig. (5.1.5) shows a selection of Richmond's profiles plotted in outer law coordinates. Some systematic tendency appears to exist in that the slope of the velocity distributions becomes smaller with increasing δ_1/R which is equivalent to an increase in the pressure gradient parameter for an accelerated flow. Such a behaviour is confirmed by the FPG profiles measured by Lewis et al. (1972) - compare Figs. (5.2.1 and 5.2.2 of AG 253), for example. We should note, however, that the outer-law distribution calculated from Willmarth's data does not show such a consistent pattern as presented in Fig. (5.1.5). Finally readers should be warned not to attach too much significance to outer law plots, since the difference $u_0^* - \bar{u}^*$ will be very sensitive to small changes in the flow properties at large y -values.

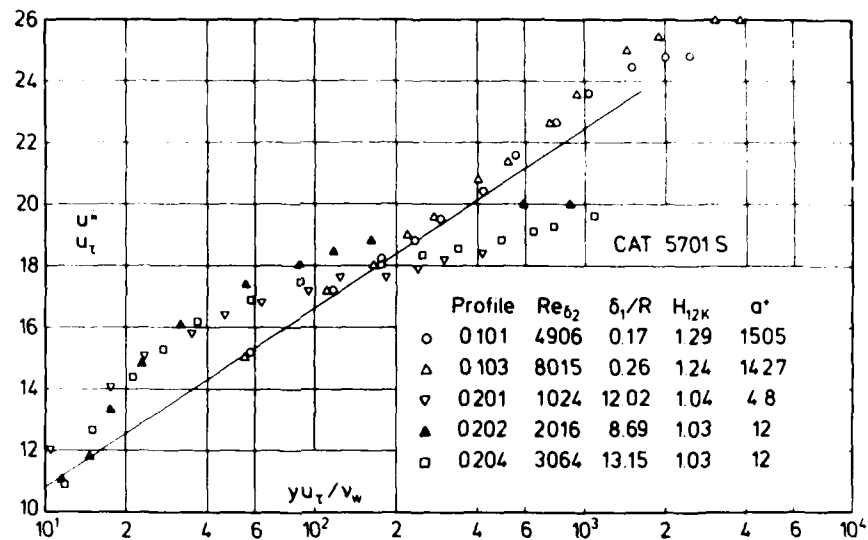


Fig. 5.1.4 Law of the wall for a subsonic turbulent boundary layer with transverse curvature (adiabatic wall, origin not defined, ZPG). Richmond (1957).

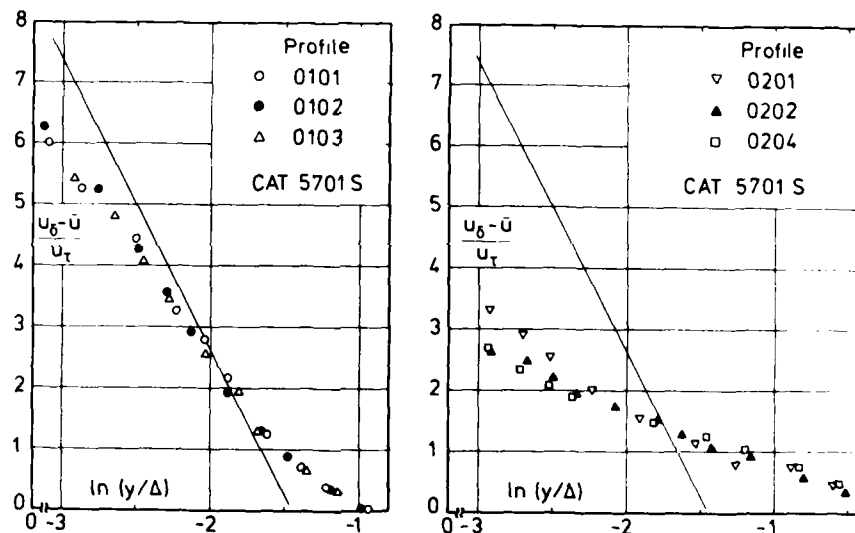


Fig. 5.1.5 Outer law for a subsonic turbulent boundary layer with transverse curvature (adiabatic wall, origin not defined, ZPG). Richmond (1957).

5.2 Validity of the van Driest temperature-velocity transformation

Throughout our discussion of mean velocity profiles in AG 253 we presumed that it was proper to make comparisons between "transformed" compressible flow profiles and the "incompressible norm" consisting of an inner region semi-logarithmic profile with an outer region wake profile. Departures from the "norm" could then be explained, at least qualitatively, in terms of the influence of the streamwise pressure gradient on the outer region and on the extent of the semi-logarithmic profile and of Reynolds number on the size of the wake component. This discussion was essentially in the same terms as for incompressible flows without heat transfer, and the vast majority of experiments studied fitted quite comfortably into this framework.

The validity of this discussion is, however, wholly dependent on the validity of the transformation used which in our specific case holds (a) for a boundary layer with a variable pressure gradient in streamwise direction dp/dx along an adiabatic wall or (b) for a boundary layer with zero pressure gradient along an isothermal wall. These restrictions enter the transformation via the temperature-velocity relationship. No other close examination of the validity of the transformation was made as for nearly all cases a sufficient justification was found in that the procedure appeared to work. In particular, no theoretical reasons were put forward for

expecting success in outer region correlations based on the transformed velocities, other than justification by good works. We therefore here summarize the assumptions which are brought together in the transformation without the details of derivation to be found in sections 3.3.1 and 2.5.4 of AG 253. The greater part of what follows is concerned with the semi-logarithmic law portion of the profile.

For incompressible flow there are many ways of deriving the semi-logarithmic velocity profile. These decline in elegance from Millikan's (1938) dimensional and functional deduction of its necessary existence to ever-increasingly complex derivations based on more and more complicated turbulence models. Since the log-law is known to exist, no turbulence model qualifies unless it can be shown to produce it. The differing models are all essentially descriptions of what happens subject to the same dimensional-constraints. There is little to be gained therefore by using a complex model when a simple one satisfying the constraints will work, even though some of the assumptions of the model are demonstrably incorrect.

In AG 253 the turbulence model used was the Prandtl mixing length model, which for those flows which display a semi-logarithmic region in incompressible flows achieves a high degree of success. This yields, assuming the sublayer thin enough, the static pressure not to vary significantly with y and the total shear stress to remain constant with y and equal to wall shear stress

$$\tau_w = \rho_w u_{\tau}^2 = -\bar{\rho} \bar{u}'v' = \ell^2 \bar{\rho} (\partial \bar{u} / \partial y)^2 \quad (5.2.1)$$

Using $\ell = \kappa y$ one obtains

$$\frac{\partial \bar{u}}{\partial y} = \frac{1}{\kappa y} u_{\tau} \left(\frac{\rho_w}{\bar{\rho}} \right)^{1/2} = \frac{1}{\kappa y} u_{\tau} \left(\frac{\bar{T}}{\bar{T}_w} \right)^{1/2} \quad (5.2.2)$$

The assumptions so far are all either reasonable in physical terms or justified by working well over a wide range in subsonic flows, with recognisable faults which would not be expected to have any particularly different effect in a compressible flow. If the density is constant, eqn.(5.2.2) integrates directly to give the semi-logarithmic law. If however the density varies, eqn.(5.2.2) is not soluble in closed form unless $(\bar{\rho}/\rho_w)$ or (\bar{T}/\bar{T}_w) can be expressed as functions of either y or \bar{u} . No mean flow profile is a universal function of (y/δ) , but, subject to various restrictions, the van Driest temperature-velocity correlation derived in section 2.5.4 of AG 253 relates (\bar{u}/u_{δ}) to $(\bar{T}/\bar{T}_{\delta})$. The relationship (eqn. 2.5.37 of AG 253) may then be inserted into eqn.(5.2.2) and integrated to give the modified velocity transformation (see section 3.3 of AG 253) which in transformed coordinates again yields the low speed semi-log law for a transformed velocity (\bar{u}^*/u_{τ}^*) , eqn.(3.3.10, AG 253) as a function of $(y u_{\tau}^*/\nu_w)$.

The transformation in the outer layer has received much less attention (e.g., Fernholz 1969, 1972) than in the inner layer. Here there are many data of importance and interest but we have no simple applicable model and so have arbitrarily extended the application of the log-law region transformation into the outer region. For the "base case", the zero pressure gradient boundary layer, the succession of profiles displayed in section 4 of AG 253 shows that the transformation correlates the data, with a few exceptions, onto the curve for incompressible flow. We have then taken this as an encouragement to apply it in other cases where there is a logarithmic law.

As mentioned above in applying the transformation we have added to the assumptions which lead to a log law those assumptions and limitations implicit in the van Driest temperature-velocity correlation. In a real flow the assumptions of the exact form that both laminar and turbulent Prandtl numbers are one, cannot be satisfied. The approximate form (Walz 1966) assumes that the mixed Prandtl number is constant and near one. The results of numerical calculations show that the velocity profile is not very sensitive to minor changes in the Prandtl number, so that this is probably not a critical assumption. The correlation can only be derived however subject to further sufficient conditions. These are that either (a) there be no heat transfer at the wall (AW) or (b) the wall temperature be constant and there be no streamwise pressure gradient (isothermal ZPG). Given these conditions the temperature-velocity correlation should be described by the various forms of eqn.(2.5.37 of AG 253). Section 2.5.6 of AG 253 was devoted to showing how well the correlation fits the experimental data and proved that for flows which, within the limits of experiment, satisfy the conditions the correlation is found to be accurate within a few percent in nearly all cases. This statement is based on the correlation of \bar{T}/\bar{T}_{δ} with \bar{u}/u_{δ} and not on the variation of the Crocco parameter which is oversensitive to small errors.

The correlation should, however, be expected to break down when both pressure gradient and heat transfer are present together. We find good agreement in strong pressure gradients on adiabatic walls (e.g., Sturek & Danberg, Fig. 5.1.5 AG 253 and Rose 7306S-2) but when pressure gradients are combined with heat transfer (e.g., Hill CAT 5901, Fig. 5.1.7; Perry & East CAT 6807, Fig. 5.1.8; Kemp & Owen CAT 7206, Fig. 5.1.10 of AG 253) the correlation breaks down and so must throw the transformation into doubt.

The interaction of the restrictions on the correlation and the application of the transformation could not, at the time of preparation for AG 253, be displayed clearly, since the Reynolds number Re_{δ_2} for the appropriate data was in most cases relatively low so that a comparison with the logarithmic law could not lead to a clear conclusion, since, for instance, transition effects in particular could not be excluded as a cause for the departure. The one exception, the data of Perry & East, then caused us some perplexity (see AG 253, p.143), but has now been joined by three other cases (Peterson 1974, CAT 7405S, and Kussoy & Horstman 1975, CAT 7501S) with pressure gradient, strong heat transfer, and relatively high Reynolds number.

The first of the new cases was reported by Peterson (1974) who performed pressure and temperature measurements in a cold wall, favourable pressure gradient turbulent boundary layer at a maximum free stream Mach number of about 13 and a heat transfer parameter $(T_w/T_r) = 0.24$. The measurements describe a simple wave expansion flow of the same general type as those studied by Fischer et al. (CAT 7001) and Beckwith et al. (CAT 7105 and Fig. 5.1.9 of AG 253). The flow at the upstream station is in the nozzle expansion field while that at the downstream station is not. Normal pressure gradients are however apparent at both stations.

The measured temperature distributions are compared with our standard, eqn.(2.5.37 of AG 253), in Fig. (5.2.1) and show large discrepancies - the measured data are much lower -, in fact larger than expected since the longitudinal pressure gradient was considered relatively modest (cf. the Mach number increase from station 01 to 02 is from 13.4 to 13.9 only). Though the "Mach number level" is much lower and the Reynolds number range

| Profile | M_∞ | T_w/T_r | Re_{δ_2} | x (m) | |
|---------|------------|-----------|-----------------|---------|------|
| --- o | 0101 | 13.4 | 0.24 | 960 | 1.92 |
| —●— | 0102 | 13.9 | 0.24 | 965 | 2.66 |
| —□— | 0202 | 14.2 | 0.24 | 1451 | 2.66 |

theory van Driest

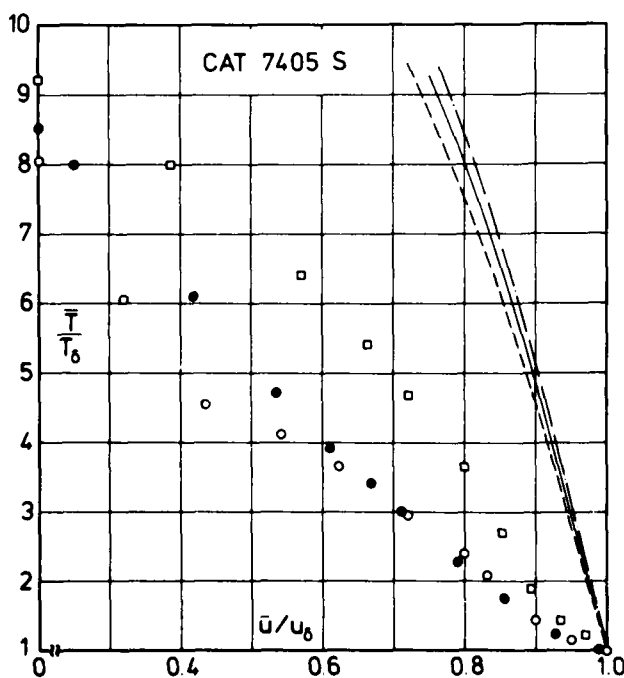


Fig. 5.2.1 Comparison between measured and theoretical temperature profiles (favourable pressure gradient, isothermal wall, origin not defined). Peterson (1974).

considerably higher than in the case investigated by Beckwith et al. (see Fig. 5.1.9 of AG 253) the discrepancies between measured and calculated temperatures are much larger in Peterson's boundary layer.

Two further sets of measurements were taken in a boundary layer with a shock boundary layer interaction and a varied pressure gradient downstream. They are remarkable in that the cooled boundary layer passes through regions of zero pressure gradient, adverse pressure gradient and finally favourable pressure gradient (for a description see Kussoy & Horstman 1975, CAT 7501S and section 5.3 below. The turbulence data is discussed in sections 3.2 and 4.5 above). This makes possible a particularly clear illustration of the influence of the combination of pressure gradient and heat transfer on the temperature/velocity correlation. Fig. (5.2.2) shows the temperature-velocity relationship for the second series (see Fig. 5.3.2 and the associated discussion). For the upstream profile 0201 agreement with theory is good. Profile 0203 is also, except in the inner region, upstream of the interaction. Agreement in the outer region is good, but the data lie high in relation to theory in the inner region. This trend becomes more marked in the downstream adverse pressure-gradient profiles shown, 0204, 0205 for which no part of the data is in agreement with theory. The data in this APG region lie up to 20% above the curves in contrast to the favourable pressure-gradient data in Fig. (5.2.1) which lie below the van Driest prediction. It is therefore

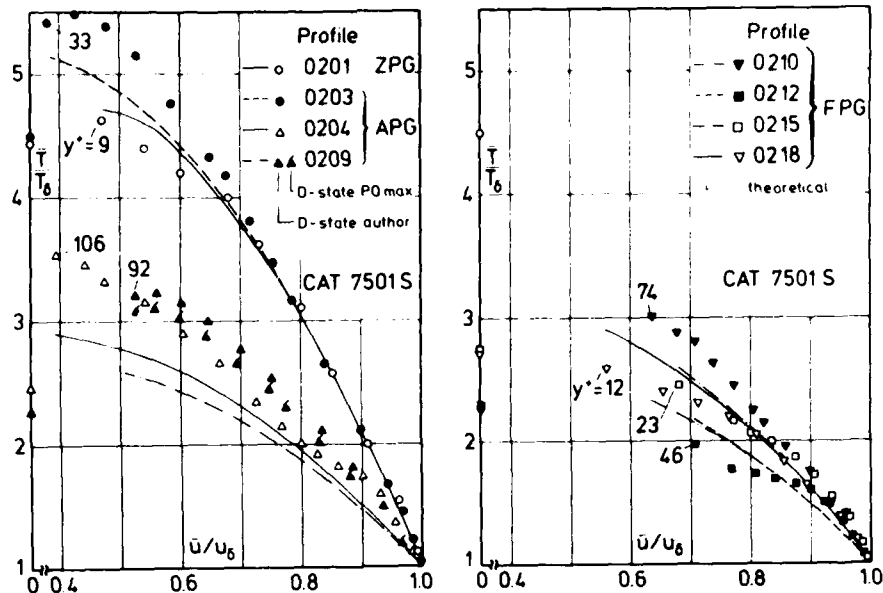


Fig. 5.2.2 Comparison between measured and theoretical temperature profiles (shock boundary-layer interaction, isothermal wall, $T_w/T_r = 0.47$, defined origin). Kussoy & Horstman (1975).

specially interesting to see the data further downstream, in a relatively modest favourable pressure-gradient region move back across the theoretical curve. In the right hand half of Fig. (5.2.2) the first profile, 0210, is locally in a favourable pressure gradient except for $15 < y < 20$, but still lies above the curve. The next profile, 0212, is entirely in a reflected wave favourable pressure gradient and lies below its curve, while as the flow relaxes (profiles 0215, 0218 - out of the field of view for Fig. 5.3.2) the data once more come into agreement with van Driest's relationship. The data for series 01 were obtained under less severe conditions (section 5.3) without shock induced boundary-layer separation and so are not discussed in detail here. They show the same general trends.

With this behaviour of the experimental temperature-velocity correlation in mind, we can now examine the velocity transformation for the semi-logarithmic law. We begin with those profiles which show only small departures from the calculated temperature distribution, that is profiles 75010201/03/15 and 18 (Fig. 5.2.3). For the ZPG profile 0201 the skin friction is apparently too low giving measurements above Coles' log-law but the wake strength is typical for a ZPG boundary layer. Profile 0203 shows the effect of the adverse pressure gradient near the wall, which shortens the log-law region. The two downstream profiles present the typical behaviour of velocity distributions in a favourable pressure gradient (e.g., Fig. 5.2.1 of AG 253). In Fig. (5.2.4) agreement with the outer law is good for the ZPG velocity distributions and the other profiles show the departures expected for the respective local pressure gradient (e.g., section 5.2 of AG 253). As for the profiles which are affected severely by the streamwise pressure gradient they show no agreement at all with the standard log-law (Fig. 5.2.5). Since we knew that the temperature-velocity correlation used so far should not hold in this case we have redefined the transformed velocity as \bar{u}_p^* where

$$\frac{\bar{u}_p^*}{u_\tau} = \frac{u_\delta}{u_\tau} \int_0^{u/u_\delta} \left(\frac{\rho}{\rho_w} \right)^{1/2} d \left(\frac{u}{u_\delta} \right) \quad (5.2.3)$$

This definition springs from the same general derivation with all the weaknesses mentioned above but does not rely on the temperature-velocity correlation (eqn. 2.5.37 of AG 253). The measured density distribution is used instead. Profiles transformed in this way are shown in Fig. (5.2.5) together with those using the conventional transformation for \bar{u}^* but neither of the two brings the profiles in and downstream of the shock interaction onto the "incompressible norm" (Coles). The effect of the change in transformation is quite large, but small compared with that which would be required to give the profiles a satisfactory log-law. No particular pattern can be seen, and were it not for the comparison with the standard outer law (Fig. 5.2.6) a

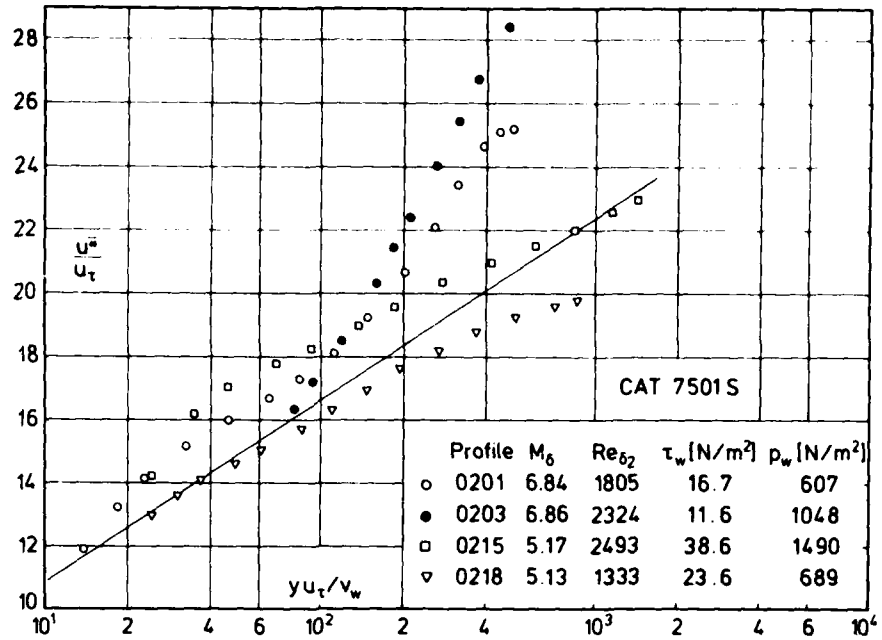


Fig. 5.2.3 Law of the wall for a compressible boundary layer with shock interaction (isothermal wall, $T_w/T_r = 0.47$, defined origin, varied pressure gradient). Kussoy & Horstman (1975).

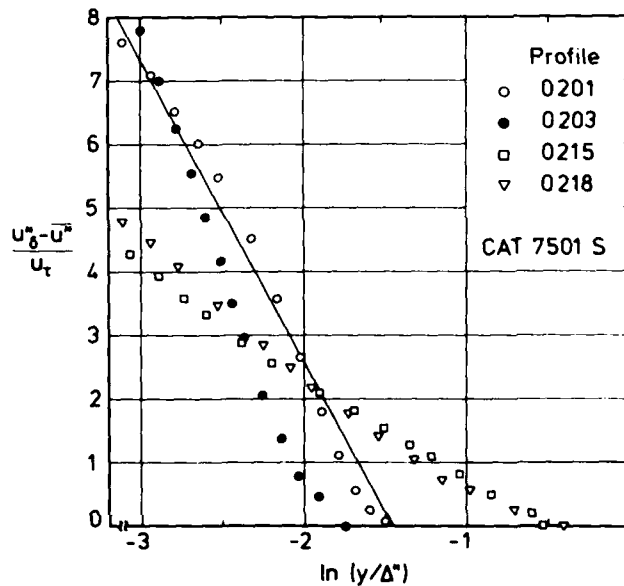


Fig. 5.2.4 Outer law for a compressible boundary layer with shock interaction (isothermal wall, $T_w/T_r = 0.47$, defined origin, varied pressure gradient). Kussoy & Horstman (1975).

physical explanation would be difficult.

Beginning with profiles 0204 and 0206, one finds the typical behaviour of a velocity distribution in a severe pressure gradient (cf. Rose CAT 7306S, Kussoy et al. CAT 7802S and in a more moderate pressure gradient Sturek & Danberg and Zwarts in Figs. 5.3.17 and 5.3.14 of AG 253) with the measurements below the outer law norm. Profiles 0208 and 0210 are already in a transitional phase and having passed through both compression and expansion waves (see Fig. 5.3.2) happen to lie quite close to the standard zero pressure gradient profile. Finally profile 0212 represents a favourable pressure gradient profile such as those in Figs. (5.2.2) and (5.2.3) of AG 253 where again the pressure gradient is much more moderate. Since we have used both transformations in Fig. (5.2.6), it is easy to observe that the differences in the outer law plot are very small. As a next step we have investigated how the transformations influence a cooled boundary layer with a favourable pressure gradient and we

find again that the measurements do not agree at all with the standard law of the wall (Fig. 5.2.7, Peterson CAT 7405S).

The figure also shows the effect of the different transformations. The profiles using measured density values are very different from those using the van Driest correlation. We also show profiles using measured temperatures as differences between these and the density based profiles show the sensitivity of the process to normal pressure gradients. Differences arising from the pressure variation seem to be relatively small. We have also plotted three profiles from Perry & East (1968, CAT 6801) in Fig. (5.2.8). They show a similar trend to those of Peterson in Fig. (5.2.7) though at a higher level in relation to the standard log law. In Fig. (5.2.6) the outer law profiles behaved on the whole in a manner explicable in terms of local, or upstream, pressure gradients. The favourable pressure-gradient profiles shown in Fig. (5.2.9) on the other hand resemble, if anything, adverse pressure-gradient profiles. We have no explanation for this behaviour,

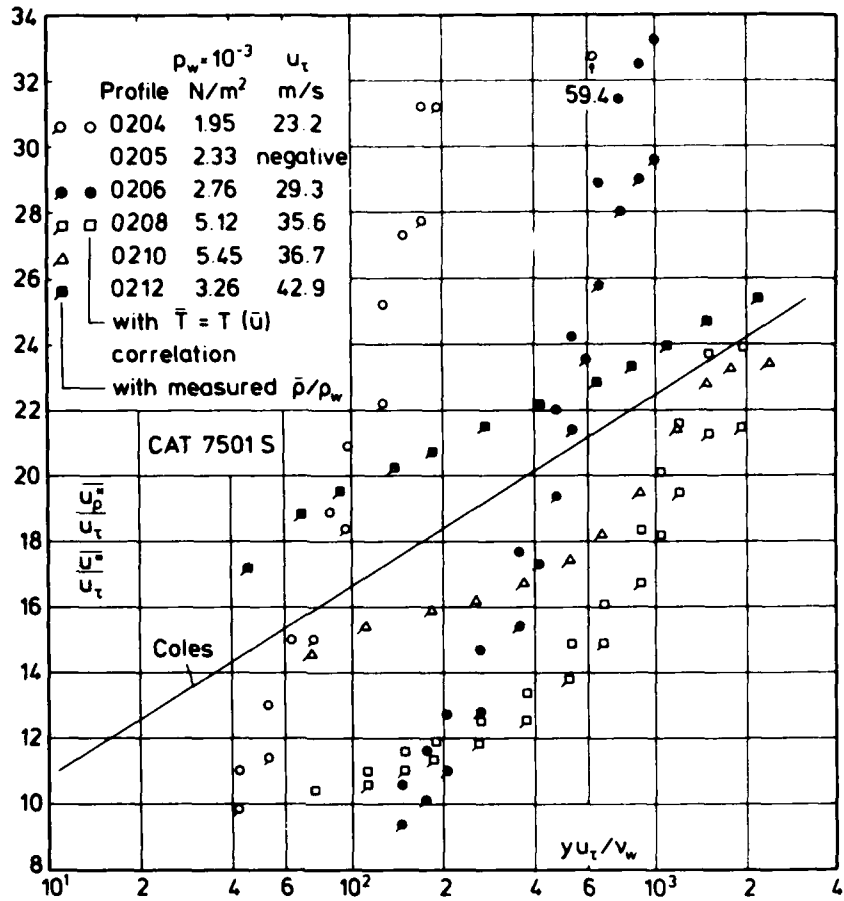


Fig. 5.2.5 Law of the wall for a compressible boundary layer with cooling and varied pressure gradient (isothermal wall, $T_w/T_r = 0.47$, defined origin). Kussoy & Horstman (1975).

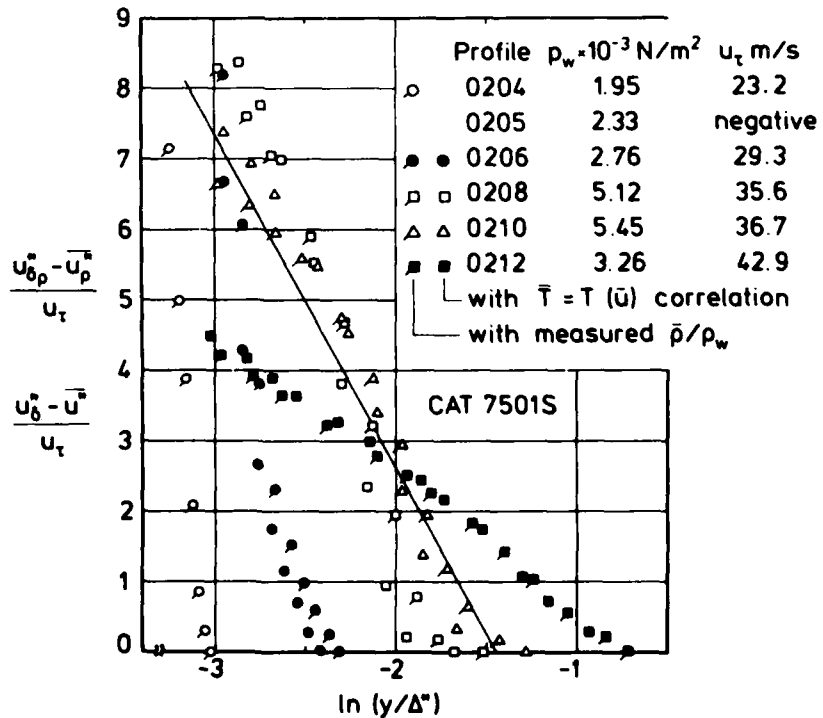


Fig. 5.2.6 Outer law for a compressible boundary layer with cooling and varied pressure gradient (isothermal wall, $T_w/T_r = 0.47$, defined origin). Kussoy & Horstman (1975).

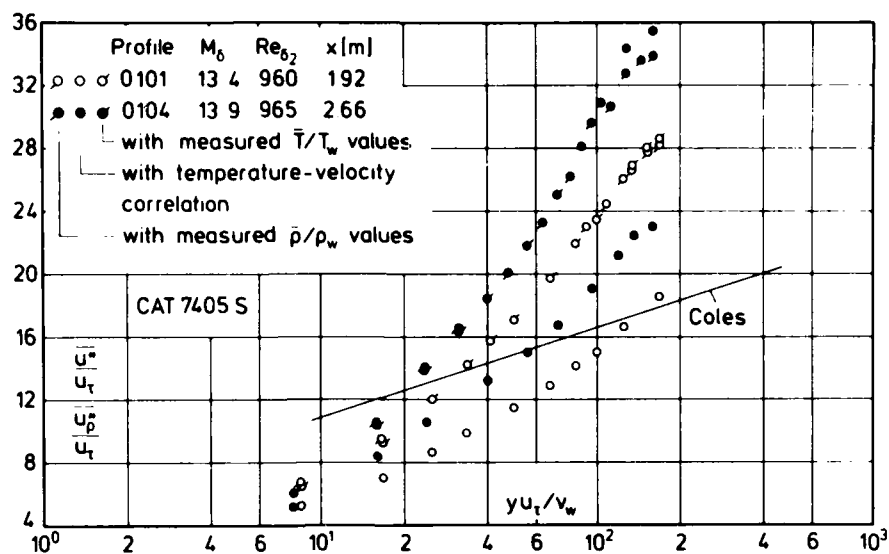


Fig. 5.2.7 Law of the wall for a compressible boundary layer with cooling and favourable pressure gradient (isothermal wall, $T_w/T_r = 0.24$, origin not defined). Peterson (1974).

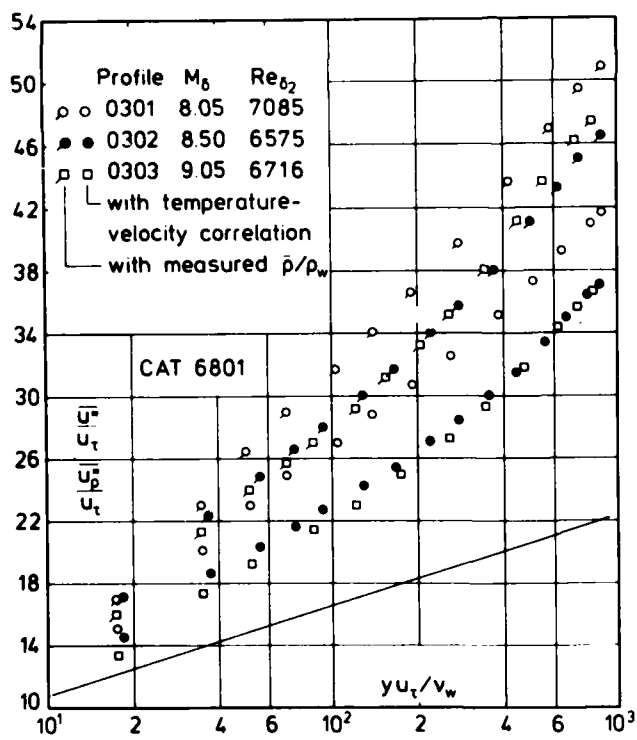


Fig. 5.2.8 Law of the wall for a compressible boundary layer with cooling and favourable pressure gradient (isothermal wall, $T_w/T_r = 0.35$, origin not defined). Perry & East (1968).

and can only refer to the similar profiles measured by Hill (CAT 5901, Fig. 5.2.12 of AG 253) and say that in certain respects they all appear to show laminar characteristics. The effect of changing to a transformation based on measured density is large for these profiles, and more marked than for CAT 7501S (Fig. 5.2.6), as would be expected because of the much greater departure of the temperature-velocity data from the van Driest relationship. As a conclusion we can only state that there are boundary conditions - such as severe wall cooling accompanied by a severe pressure gradient - which can lead to a breakdown of the standard temperature-velocity correlation (eqn. 2.5.37 of AG 253) and of the standard semi-logarithmic law. The first breakdown is to be expected since the correlation was derived under assumptions which do not cover the above boundary conditions. The departures from the law of the wall are less easy to explain, and we can only warn the reader to look out for these special boundary conditions which apparently lead to such an abrupt breakdown of the law of the wall. It is, however, comforting to note that the disturbed velocity distributions return to the semi-logarithmic law very rapidly after the pressure gradient has been relaxed (Figs. 5.2.3 and 5.2.6).

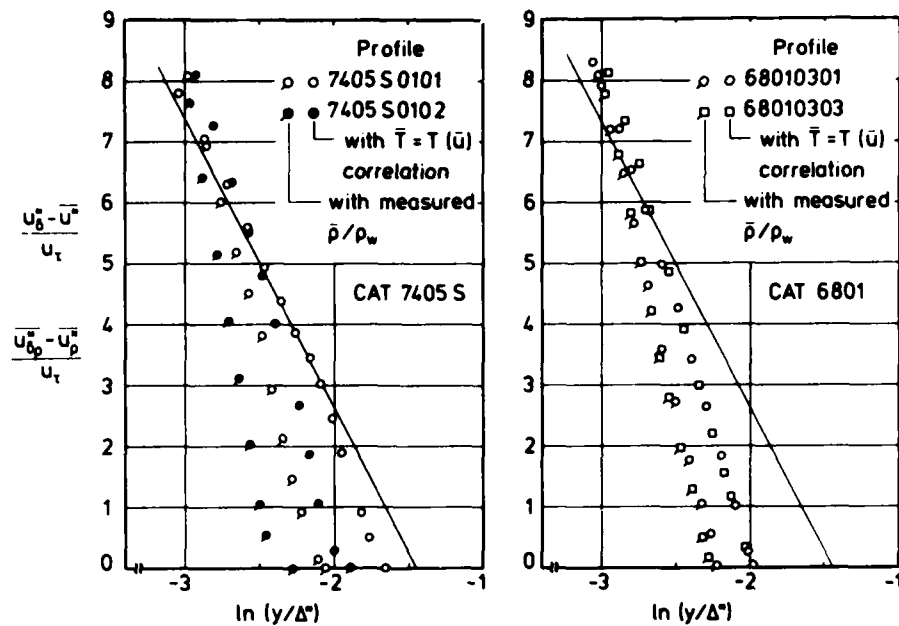


Fig. 5.2.9 Outer law for a compressible boundary layer with cooling and favourable pressure gradient (isothermal wall, origin not defined). Perry & East (1968), Peterson (1974).

5.3 Discussion of the wave structure of the shock/boundary-layer interaction (Kussoy & Horstman (1975))

Since the experiment of Kussoy & Horstman (1975, CAT 7501S) is of primary importance for the discussion of mean flow and turbulence data in this volume and one of the building blocks for turbulence modelling we thought it to be of advantage if the wave pattern of their two experimental configurations were discussed in more detail. This is a procedure in line with that followed in sections 6.1 and 6.2 of AG 253. The test boundary layer was formed on a 10° semi-apex angle cone-ogive cylinder mounted on the centre line of the tunnel. An annular shock generator was mounted coaxially with the model and could be traversed in the axial direction. Two deflection angles, 7.5° and 15° (series 01 and 02) were used, and the shock waves produced were followed closely by an expansion. Measurements were made at different stations in relation to the wave structure by traversing the shock generator, so moving the wave pattern over instruments at fixed stations in the rear part of the model.

Figure (5.3.1) shows the static pressure field for series 01, in which the boundary layer remains attached. A very small amount of upstream influence is shown by the small pressure rise in profile 0104 near the wall,

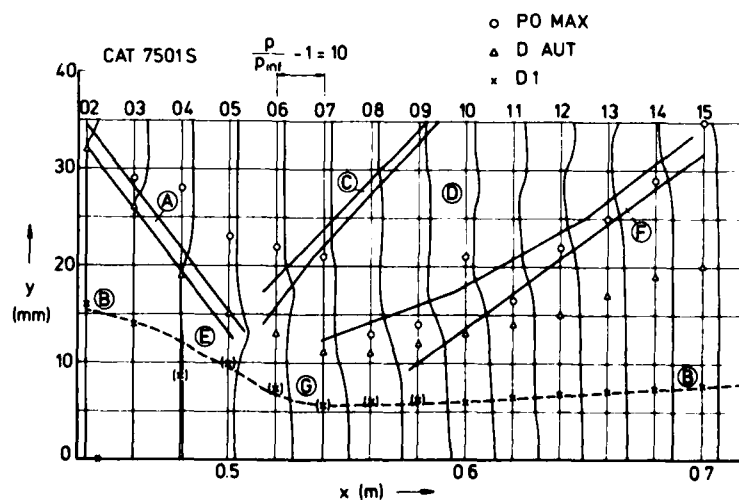


Fig. 5.3.1 Attached shock/boundary-layer interaction. Kussoy & Horstman (1975). Pressure Distribution I.

but this has negligible effect on the development of the wave structure as a whole. This is dominated by the incoming shock A and its reflection by, and deformation of, the displacement surface B - B'. For profiles 0104 to 0110 there are normal static pressure gradients large enough for the calculation of D1 to be invalid, so that in this region the form of the displacement surface as shown is speculative. There is a relatively weak reflected shock C springing from the intersection of the incoming shock and the displacement surface. Its presence implies a locally concave region - caused by the upstream influence. This is followed by a relatively weak expansion region D coming from the convex part of the displacement surface E, the incoming compression A being almost completely cancelled by the curvature of the flow. A strong compression F, initially fairly widely distributed, is then formed as the flow is turned back to the original direction by the concave portion of the displacement surface G. The whole flow field behind the incoming shock is immersed in an expansion originating from the corner at the end of the 7.5° shock generating wedge. This is relatively weak as can be seen by the slow streamwise fall in static pressure at $y = 35$ mm from profile 0103 to 0108.

In the second series (02) the pressure rise of the incoming shock A is nearly twice as large (Fig. 5.3.2). This causes the boundary layer to separate at B forming a separation bubble hatched in the figure. The bubble

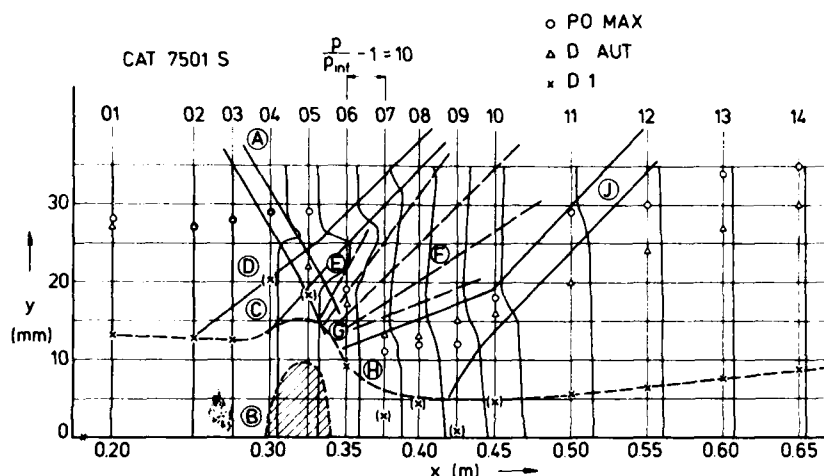


Fig. 5.3.2 Separated shock/boundary-layer interaction. Kussoy & Horstman (1975). Pressure Distribution II.

distorts the displacement surface causing a strong upstream influence. The displacement surface upstream of the bubble becomes concave C and an outgoing shock D is generated upstream of the incoming shock A. The two shocks cross, giving rise to the local pressure hump E to be seen in profile 0205 - the form and position of the hump in profile 0204 suggests that the probe was perhaps responding to an upstream influence of the shocks intersecting it downstream of the tip. The pressure rise E is then eroded by a strong expansion F springing from the convex portion of the displacement surface G. Again the exact form and position is not known as it cannot be calculated because of normal pressure gradient effects. The concave portion H of the displacement surface which follows in turn generates a compression which coalesces to form the second outgoing shock J. As in case one, the whole flow is in an expansion field spreading from the rear of the shock generator, and this is best seen in the steady fall of static pressure behind the final shock (profiles 0211 to 0214). This region is in a gentle reflected wave expansion and so shows little normal pressure gradient.

SECTION 6

THE ENTRIES

The entries are arranged in the sequence given in the table below.

Note: Boundary conditions and evaluated data are given for all profiles as section B of each entry. This data is also printed on the microfiche, which gives complete data for all profiles. The tables of section C of each entry provide only a selection of the profile data. Only selected turbulence data are given in the entry. The complete tables are printed on the microfiche.

CLASSIFIED LIST OF SUPPLEMENTARY ENTRIES

The ENTRIES are listed in numerical order, otherwise following the conventions of § 7 of AGARDograph 223. The pressure gradient classification is given both as an abbreviation and as in AG223 § 7.1.

| | M_0 | R THETA $\times 10^{-3}$ | TW/TR | PG ² | TO | CF ³ | NX | TURB ⁴ |
|--------------------------------|---------|-----------------------------|---------|-----------------|-----|-----------------|-------|-------------------|
| 5701 RICHMOND | <1,5.8 | 1-9 | 1.0 | ZPG,IB | - | F/V | 1(3) | - |
| 5806 MORKOVIN & PHINNEY | 1.77 | 16 | 1.0 | ZPG,IB2 | - | (V) | 1 | CC HWC |
| 6002 DANBERG | 5.1 | 3-4 | 0.8,0.9 | ZPG,IA1 | P | V | 2 | - |
| 7306 ROSE | 4 | 3.4 | 1.0 | SBLI,(IIA4) | P | V | 12 | CT HWP |
| 7404 VOISINET et al. | 4.9 | 6-26 | 0.8,1.0 | ZPG,IB1 | P | - | 2 | - |
| 7405 PETERSON | 14 | 6-11 | 0.25 | FPG,IIB5 | P | V | 2 | - |
| 7501 KUSSOY & HORSTMAN | 7 | 8.5 | 0.5 | SBLI,(IIA4) | P | F | 18,19 | CT HWP |
| 7701 MABEY | 2.5-4.5 | 1-8 | 1.0 | ZPG,IA1 | P | F | 3 | - |
| 7702 LADERMAN & DEMETRIADES | 3.0 | 3-4 | 0.6-1.0 | ZPG,IB1 | P | (P) | 3 | CC HWP |
| 7703 BERG | 6 | 14-20 | 0.9 | ZPG,IB1R | P | V(F) | 17 | CC HWP |
| 7801 COLLINS et al. | 0.1-2.2 | 6,23,40 | 1.0 | ZPG,(IA1),IB2 | - | F,P,V | 4-8 | LDV |
| 7802 KUSSOY et al. | 2.3 | 30 | 1.0 | APG,IIA4 | (P) | P,surface | 13,14 | CT HWP |
| 7803 LADERMAN | 3.0 | 3-5 | 1.0 | APG,IIB2 | P | V(P) | 10,14 | - |
| 7804 WATSON | 10-12 | 3-20 | 0.4-1.1 | ZPG,IA1 | P | F | 7 | - |
| 7901 VOISINET | 2.9 | 3-60 | 1.0 | ZPG,IB1R | P | F | 1 | - |
| 7902 CHEW & SQUIRE | 2.5 | 24 | 1.0 | RELAXATION | - | P | 7 | - |
| 7903 BARTLETT et al. | 9.3 | 3-12 | 0.3 | ZPG,IA1 | P | P | 3 | (Electron) |
| 8001 MATEER & VIEGAS | 1.45 | 40-100 | 1.0 | SBLI,(IIA4) | P | surface | 7 | CT HWP |

NOTES: (1) Numerical values are nominal, not precise.

(2) SBLI: Shock boundary layer interaction.

(3) CF: F-Floating element balance, P-Preston tube, V-deduced from profile. "surface"-embedded hot wire gauge.

(4) TURB: Turbulent measurements - see tables 3.1 and 4.3.1 in the main text.

| | | |
|---|--|----------|
|  | M: subsonic, 5.8 R THETA $\times 10^{-3}$: 1 - 8.5 TW/TR: 1.0 | 5701 |
| | | ZPG - AW |
| Two low speed tunnels, probably (E) $W = H = 0.60$ m and 0.90 m. $0.8 < Re/m \times 10^{-6} < 3$ Hypersonic tunnel with symmetrical nozzle. $W = H = 0.127$ m. $0.1 < P_0 < 0.6$ MN/m ² . T_0 : 380K. Air. $1.5 < Re/m \times 10^{-6} < 7.5$. | | |
| RICHMOND R.L., 1957. Experimental investigation of thick axially symmetric boundary layers on cylinders at subsonic and hypersonic speeds. GALCIT Hyp. Res. Proj. Memo 39, CALTECH, Pasadena, CA. | | |

- 1 The test boundary layer was formed on the outer surface of one of a number of slender cylinders aligned with the flow. For the subsonic tests two models were used. The first (series 01) consisted of an aluminium tube 3.65 m long and 25.4 mm in diameter. The front end of this ($X = 0$) was mounted on the tunnel settling chamber screens so that it extended along the contraction centre line into the working section ($W = H = 0.9$ m) which started at about $X = 1.8$ m. The test zone extended from $X = 2.4$ m to $X = 3.1$ m. The second model consisted of a steel wire under tension ($d = 0.61$ mm) passing through the honeycomb and screens ($X = 0$) and secured at the downstream end of the test section ($W = H = 0.6$ m, $X = 6$ m). Measurements were made at a single station ($X = 4.9$ m). The results presented here (series 02) were obtained with a "stovepipe" ($d = 0.2$ m) mounted surrounding the model in the test section. For the hypersonic tests, results are presented for two wires ($d = 0.61, 1.63$ mm, series 05, 04) and for a composite wire-cylinder model. This last (series 03) consisted of a wire ($d = 1.59$ mm) passing through the throat ($X = 0$) on which was mounted a 3° half-angle cone-ogive nosed cylinder of final diameter 6.35 mm. The change in section began at the start of the test rhombus ($X = 0.24$ m - E) and was complete by $X = 0.3$ m (E). The models continued with constant diameter to the point at which they were anchored at the rear of the test section ($X = 0.89$ m - E).
- 3 On the larger (25.4 mm - series 01) subsonic model, the boundary layer was found to be turbulent at the lowest practical tunnel speed. At the relatively high speeds used for the tests the flow was therefore presumed to be fully turbulent. For the subsonic tests on the smaller wire model, a variety of tripping devices were tried, the results being little affected by which was used. The results presented here are probably obtained (E) using a 'clay centre-body trip' of unspecified nature. For the hypersonic tests 'laminar and naturally turbulent boundary layers were found on all
- 4 models tested.' We therefore suppose that no trip was used. Since either the test model itself, or a support wire, passed upstream into a low speed region for all tests described, all the test layers had at one point passed through a favourable pressure gradient region.
- 5 No measurements of axial symmetry were made for the larger subsonic cylinder (series 01). For the subsonic tests on a wire (series 02) a strut attached to the model behind the test section could be used to displace it in any direction in the Y-Z plane. The flow at a survey station, as assessed by a "double Pitot sliding on and rotating about the wire model," "was forced to be symmetrical" by adjustment of this strut and the use of the "stovepipe" referred to above. Originally, without these precautions, "the boundary layer axial non-symmetry was found to be continually changing in an unpredictable manner."

In the hypersonic tests, the rear end of the model could be moved vertically to impose axisymmetry, but the principal source of asymmetry was the planar nature of the nozzle expansion field, which caused the side boundary layer thicknesses to be less than the top and bottom thicknesses for all models. This was most pronounced at $X = 0.25 - 0.30$ m, the axial symmetry steadily improving to

- 2 X = 0.61 m. However, due to the presence of weak waves in the free stream, measurements were taken slightly upstream of this point at X = 0.508 m. Asymmetry would seem to have been considerable as "a correction factor of from 0.842 to 0.866, depending on the free-stream Reynolds number per inch, was applied to momentum and displacement thickness as computed from the thicker boundary layer on top of the models."
- 6 No wall pressure or temperature measurements are mentioned. Skin friction measurements were made at M = 5.8 on the composite (1.59/6.35 mm - series 03) model with an FEB. The element consisted of a 12.7 mm long section of the outer surface of the cylinder, bounded by two 63 μ m gaps.
- 7 No details are given for the Pitot tubes used to give the profiles of series 01. For series 02, a HWP (d = 0.25 μ m, l = 0.38 mm) was used to give velocity profiles. The hot wire was calibrated for mean flow by observing the shedding frequency of vortices in flow normal to a standardized cylinder. The probe was mounted on a support hinged to the strut used to align the model wire so as to reduce error in the relative positioning of the model and the probe.

- In the hypersonic tests a 12-tube Pitot rake was used, with three tubes located in each of 4 planes 90° apart round the models. Since up to 26 data points are given in one profile and the values of Y for a given model do not remain constant in successive runs, it seems that there must have been
- 8 provision for altering the geometry of the rake in some way. For series 01 profiles were measured at X = 2.44, 2.74 and 3.05 m from the screens ahead of the tunnel contraction. For series 02, all measurements were made 4.88 m from the tunnel screens. In the hypersonic tests, all measurements were made 0.508 m from the tunnel throat.
- 9 For the hypersonic tests, the author obtained mean velocity profiles assuming isoenergetic flow. Wall values were calculated assuming recovery factors of 0.9 for turbulent and 0.86 for laminar flow respectively. In addition to the skin friction values measured at M = 5.8, the author gives values obtained by matching profiles to the Coles wake-and-wall profile at low speeds, using Coles' (1955) streamline hypothesis, and by matching a transformed profile at high speeds for the 'wire' results of
- 11 series 4 and 5. The Sutherland viscosity law was used.
- 12 We have presented all profiles tabulated by the author, replacing the isoenergetic total temperature assumption by the Crocco-van Driest temperature/velocity correlation with recovery factor 0.896 for all profiles, whether referred to by the author as 'laminar' (0301, 0302, 0401, 0501) or as 'turbulent'. For profile 0301 we found it necessary to interpolate a D-state point to match the author's stated edge conditions. The subsonic profiles comprise one set of measurements at three
- 13 successive situations for fixed free stream conditions (01), and one set of profiles at a single station for increasing unit Reynolds number (02). The three M = 5.8 sets consist of single station measurements for a range of unit Reynolds number on each of three models. Skin friction values are
- 14 'measured' for series 03 and as estimated by the author from the velocity profile in the other cases.
- 5 DATA: 5701 0101-0502. Pitot profiles. NX = 1(3). Skin friction from FEB (series 03) or velocity profiles.
- 15 Editors' comments. The interest of this study lies in the exceptionally large ratios of representative boundary layer thicknesses to transverse body radius (Table 1). The profiles will not be discussed in detail here as the effects of transverse curvature are considered in §5 of the main text. Some comment is justified, however, in the assessment of the experiment.

The subsonic data are useful here as they provide an indication of the effect of transverse curvature independent of the complications of high Mach number and the associated Reynolds number effects. Representative inner and outer law profiles for low and high values of δ_1/R_z are shown below. For all except series 01, marked differences from the behaviour of a normal ZPG planar boundary layer are visible. The profiles for the high Mach number cases should not be considered accurate as we do not

know whether they come from the top/bottom of the model, or from the sides where the boundary layers are thinner. As remarked in §2 above, the author applied a correction factor of about 15%, implying a substantial degree of asymmetry.

For all profiles except series 01 the measurement extended within the peak of the momentum deficit integrand, so that on this count the integral values are reliable. For all cases involving very large values of Y/R_z , however, it should be noted that the integrals will be very sensitive to small changes in the flow properties at large Y -values. We found large discrepancies between our integral values and the author's in the subsonic case. There are no comparable experiments compressible flow, but the low speed results may be compared to those of Willmarth et al. (1976). For these, δ/R_z ranged from 1.8 to 42.5, and δ_1/R_z from 0.26 to 5.8. The general tendency of the profiles is the same. The profiles are discussed further in §5.1 of the main text. The Reynolds numbers for the hypersonic measurements are relatively low, the author describing profiles 0301, 0302, 0401 and 0501 as laminar.

Table 1 Transverse curvature for profiles measured on slender cylinders

| CAT 5701 | R_z (m) | δ_1/R_z | Approx. δ/R_z | $Re_\theta \times 10^{-3}$ | $Re_{\delta_2} \times 10^{-3}$ | M_δ | |
|----------|------------------------|----------------|----------------------|----------------------------|--------------------------------|------------|----------------|
| 0101 | 1.27×10^{-2} | 0.17 | 1.7 | 4.9 | $=Re_\theta$ | 0.14 | successive |
| 0102 | " | 0.22 | 2.2 | 6.6 | " | " | stations on |
| 0103 | " | 0.26 | 2.9 | 8.0 | " | " | cylinder |
| 0201 | 3.048×10^{-4} | 12 | 76 | 1.0 | " | 0.036 | single station |
| 0202 | " | 8.7 | 89 | 2.0 | " | " | on stretched |
| 0203 | " | 12 | 90 | 2.8 | " | " | wire |
| 0204 | " | 13 | 90 | 3.1 | " | " | " |
| 0301 | 3.175×10^{-3} | 1.87 | 4.0 | 1.0 | 0.180 | 5.6 | single station |
| 0302 | " | 1.68 | 3.5 | 1.3 | 0.229 | " | on composite |
| 0303 | " | 1.22 | 3.1 | 2.4 | 0.415 | " | wire/cylinder |
| 0304 | " | 1.26 | 3.5 | 3.3 | 0.559 | " | " |
| 0401 | 8.128×10^{-4} | 4.42 | 8.7 | 1.2 | 0.214 | " | single station |
| 0402 | " | 5.22 | 10 | 5.7 | 0.978 | " | on stretched |
| 0501 | 3.048×10^{-4} | 13.2 | 27 | 2.2 | 0.398 | " | wire |
| 0502 | " | 10.3 | 42 | 5.0 | 0.842 | 5.8 | " |

CAT 57015

RICHMOND

BOUNDARY CONDITIONS AND EVALUATED DATA. SI UNITS

| RUN X * RZ * | MD POD* TOD* | TW/TR* PW/PO* TAUW | RED2W RED2D DZ | CF * CQ PIZ* | H1Z H3Z H4Z | H1ZK H3ZK DZK | PW TW UD* | PD TD TR |
|---|--------------------------------------|---------------------------------|---|----------------------------------|----------------------------|---------------------------------|---|---|
| 570150101 2.4384**+00 1.2700**-02 | 0.1354 1.0132**+05 3.0000**+02 | 1.0000 1.0000 4.1474**+00 | 4.9057**+03 4.9181**+03 1.6601**+03 | 3.2300**-03 NM 0.0000**+00 | 1.3004 1.7535 0.0007 | 1.2937 1.7534 1.6616**-03 | 1.0004**+05 2.9989**+02 4.6939**+01 | 1.0004**+05 2.9890**+02 2.9989**+02 |
| 570150102 2.7432**+00 1.2700**-02 | 0.1354 1.0132**+05 3.0000**+02 | 1.0000 1.0000 3.9162**+00 | 6.5658**+03 6.5824**+03 2.2219**-03 | 3.0500**-03 NM 0.0000**+00 | 1.2707 1.7348 0.0008 | 1.2642 1.7347 2.2238**-03 | 1.0004**+05 2.9989**+02 4.6939**+01 | 1.0004**+05 2.9890**+02 2.9989**+02 |
| 570150103 3.0480**+00 1.2700**-02 | 0.1354 1.0132**+05 3.0000**+02 | 1.0000 1.0000 3.7236**+00 | 8.0150**+03 8.0353**+03 2.7123**-03 | 2.9000**-03 NM 0.0000**+00 | 1.2388 1.7270 0.0008 | 1.2325 1.7268 2.7145**-03 | 1.0004**+05 2.9989**+02 4.6939**+01 | 1.0004**+05 2.9890**+02 2.9989**+02 |
| 570150201 4.8768**+00 3.0480**-04 | 0.0132 1.0132**+05 3.0000**+02 | 1.0000 1.0000 7.3347**-02 | 1.0248**+03 1.0249**+03 3.5156**-03 | 5.9200**-03 NM 0.0000**+00 | 1.0421 1.4242 0.0000 | 1.0421 1.4242 3.5156**-03 | 1.0131**+05 3.0000**+02 4.5900**+00 | 1.0131**+05 2.9999**+02 3.0000**+02 |
| 570150202 4.8768**+00 3.0480**-04 | 0.0357 1.0132**+05 3.0000**+02 | 1.0000 1.0000 4.4663**-01 | 2.0155**+03 2.0158**+03 2.5627**-03 | 4.9500**-03 NM 0.0000**+00 | 1.0331 1.4408 0.0003 | 1.0328 1.4408 2.5627**-03 | 1.0123**+05 2.9999**+02 1.2390**+01 | 1.0123**+05 2.9992**+02 2.9999**+02 |
| 570150203 4.8768**+00 3.0480**-04 | 0.0351 1.0132**+05 3.0000**+02 | 1.0000 1.0000 4.5242**-01 | 2.7822**+03 2.7827**+03 3.5956**-03 | 5.1800**-03 NM 0.0000**+00 | 1.0310 1.4293 0.0003 | 1.0307 1.4293 3.5956**-03 | 1.0124**+05 2.9999**+02 1.2190**+01 | 1.0124**+05 2.9993**+02 2.9999**+02 |
| 570150204 4.8768**+00 3.0480**-04 | 0.0357 1.0132**+05 3.0000**+02 | 1.0000 1.0000 4.6813**-01 | 3.0637**+03 3.0643**+03 3.8924**-03 | 5.1800**-03 NM 0.0000**+00 | 1.0297 1.4265 0.0004 | 1.0295 1.4265 3.8924**-03 | 1.0123**+05 2.9999**+02 1.2400**+01 | 1.0123**+05 2.9992**+02 2.9999**+02 |
| 570150301 5.0800**-01 3.1750**-03 | 5.6000 9.9629**+04 3.6742**+02 | 1.0000 1.0000 3.1635**+00 | 1.8024**+02 1.0025**+03 6.8609**-04 | 1.5000**-03 NM 0.0000**+00 | 8.4782 1.6628 0.1727 | 1.3770 1.5251 1.8552**-03 | 9.6072**+01 3.3446**+02 7.9809**+02 | 9.6072**+01 5.0525**+01 3.3446**+02 |
| 570150302 5.0800**-01 3.1750**-03 | 5.5900 1.6858**+05 3.8020**+02 | 1.0000 1.0000 8.2671**+00 | 2.2947**+02 1.2611**+03 5.3474**-04 | 2.3000**-03 NM 0.0000**+00 | 9.2556 1.6593 0.1672 | 1.4943 1.5106 1.5434**-03 | 1.6432**+02 3.4611**+02 8.1165**+02 | 1.6432**+02 5.2444**+01 3.4611**+02 |
| 570150303 5.0800**-01 3.1750**-03 | 5.7500 4.4437**+05 3.8020**+02 | 1.0000 1.0000 1.6392**+01 | 4.1488**+02 2.3939**+03 4.1262**-04 | 1.9400**-03 NM 0.0000**+00 | 9.3563 1.8017 0.1797 | 1.3258 1.6857 8.2801**-04 | 3.6509**+02 3.4585**+02 8.1474**+02 | 3.6509**+02 4.9944**+01 3.4585**+02 |
| 570150304 5.0800**-01 3.1750**-03 | 5.7800 5.8192**+05 3.8020**+02 | 1.0000 1.0000 2.0040**+01 | 5.5973**+02 3.2589**+03 4.3447**-04 | 1.8500**-03 NM 0.0000**+00 | 9.2223 1.8038 0.1811 | 1.2611 1.6977 8.5678**-04 | 4.6320**+02 3.4581**+02 8.1530**+02 | 4.6320**+02 4.9494**+01 3.4581**+02 |
| 570150401 5.0800**-01 8.1280**-04 | 5.7500 1.6823**+05 3.8020**+02 | 1.0000 1.0000 NM | 2.1459**+02 1.2382**+03 5.6373**-04 | NM NM 0.0000**+00 | 6.3822 1.5738 0.2052 | 1.3648 1.4326 1.2356**-03 | 1.3822**+02 3.4585**+02 8.1474**+02 | 1.3822**+02 4.9944**+01 3.4585**+02 |
| 570150402 5.0800**-01 8.1280**-04 | 5.7900 5.8192**+05 3.8020**+02 | 1.0000 1.0000 2.2910**+01 | 9.7971**+02 5.7212**+03 7.6601**-04 | 2.1300**-03 NM 0.0000**+00 | 5.5380 1.6205 0.2330 | 1.1218 1.5553 1.0967**-03 | 4.5835**+02 3.4579**+02 8.1548**+02 | 4.5835**+02 4.9346**+01 3.4579**+02 |
| 570150501 5.0800**-01 3.0480**-04 | 5.5800 1.6823**+05 3.8020**+02 | 1.0000 1.0000 NM | 3.9848**+02 2.1832**+03 9.2364**-04 | NM NM 0.0000**+00 | 4.3404 1.4717 0.2945 | 1.1081 1.4277 1.4552**-03 | 1.6576**+02 3.4613**+02 8.1145**+02 | 1.6576**+02 5.2606**+01 3.4613**+02 |
| 570150502 5.0800**-01 3.0480**-04 | 5.8300 5.8157**+05 3.8020**+02 | 1.0000 1.0000 2.4454**+01 | 8.4171**+02 4.9745**+03 6.7786**-04 | 2.3400**-03 NM 0.0000**+00 | 4.6467 1.5299 0.2846 | 1.0627 1.4969 8.7830**-04 | 4.3924**+02 3.4573**+02 8.1620**+02 | 4.3924**+02 4.8757**+01 3.4573**+02 |

| 5701S0201 | | RICHMOND | | PROFILE TABULATION | | 22 POINTS, DELTA AT POINT 21 | | | |
|-----------|-------------------------|-------------------------|------|--------------------|---------|------------------------------|---------|-----------|--|
| I | Y | PT2/P | P/PD | TO/TOD | M/MD | U/UD | T/TD | R/RD*U/UD | |
| 1 | 0.0000 ⁺ +00 | 1.0000 ⁺ +00 | NM | 1.00000 | 0.00000 | 0.00000 | 1.00003 | 0.00000 | |
| 2 | 2.2860 ⁻ -04 | 1.0000 ⁺ +00 | NM | 1.00000 | 0.32461 | 0.32462 | 1.00003 | 0.32461 | |
| 3 | 3.0480 ⁻ -04 | 1.0000 ⁺ +00 | NM | 1.00000 | 0.37472 | 0.37473 | 1.00003 | 0.37472 | |
| 4 | 3.8100 ⁻ -04 | 1.0000 ⁺ +00 | NM | 1.00000 | 0.43572 | 0.43573 | 1.00003 | 0.43572 | |
| 5 | 4.5720 ⁻ -04 | 1.0000 ⁺ +00 | NM | 1.00000 | 0.51416 | 0.51416 | 1.00002 | 0.51415 | |
| 6 | 5.3340 ⁻ -04 | 1.0000 ⁺ +00 | NM | 1.00000 | 0.57080 | 0.57081 | 1.00002 | 0.57079 | |
| 7 | 6.0960 ⁻ -04 | 1.0000 ⁺ +00 | NM | 1.00000 | 0.59912 | 0.59913 | 1.00002 | 0.59912 | |
| 8 | 6.8580 ⁻ -04 | 1.0001 ⁺ +00 | NM | 1.00000 | 0.65359 | 0.65359 | 1.00002 | 0.65358 | |
| 9 | 7.6200 ⁻ -04 | 1.0001 ⁺ +00 | NM | 1.00000 | 0.68191 | 0.68192 | 1.00002 | 0.68191 | |
| 10 | 1.1430 ⁻ -03 | 1.0001 ⁺ +00 | NM | 1.00000 | 0.76470 | 0.76471 | 1.00001 | 0.76470 | |
| 11 | 1.5240 ⁻ -03 | 1.0001 ⁺ +00 | NM | 1.00000 | 0.81917 | 0.81917 | 1.00001 | 0.81916 | |
| 12 | 1.9050 ⁻ -03 | 1.0001 ⁺ +00 | NM | 1.00000 | 0.84095 | 0.84096 | 1.00001 | 0.84095 | |
| 13 | 2.2860 ⁻ -03 | 1.0001 ⁺ +00 | NM | 1.00000 | 0.86056 | 0.86057 | 1.00001 | 0.86056 | |
| 14 | 3.0480 ⁻ -03 | 1.0001 ⁺ +00 | NM | 1.00000 | 0.89106 | 0.89107 | 1.00001 | 0.89106 | |
| 15 | 4.1910 ⁻ -03 | 1.0001 ⁺ +00 | NM | 1.00000 | 0.91503 | 0.91503 | 1.00001 | 0.91503 | |
| 16 | 6.0960 ⁻ -03 | 1.0001 ⁺ +00 | NM | 1.00000 | 0.93682 | 0.93682 | 1.00000 | 0.93682 | |
| 17 | 8.0010 ⁻ -03 | 1.0001 ⁺ +00 | NM | 1.00000 | 0.95643 | 0.95643 | 1.00000 | 0.95642 | |
| 18 | 1.1811 ⁻ -02 | 1.0001 ⁺ +00 | NM | 1.00000 | 0.95860 | 0.95861 | 1.00000 | 0.95860 | |
| 19 | 1.5621 ⁻ -02 | 1.0001 ⁺ +00 | NM | 1.00000 | 0.97603 | 0.97603 | 1.00000 | 0.97603 | |
| 20 | 1.9431 ⁻ -02 | 1.0001 ⁺ +00 | NM | 1.00000 | 0.99129 | 0.99129 | 1.00000 | 0.99128 | |
| D 21 | 2.3241 ⁻ -02 | 1.0001 ⁺ +00 | NM | 1.00000 | 1.00000 | 1.00000 | 1.00000 | 1.00000 | |
| 22 | 2.7051 ⁻ -02 | 1.0001 ⁺ +00 | NM | 1.00000 | 1.00000 | 1.00000 | 1.00000 | 1.00000 | |

INPUT VARIABLES Y,U ASSUME P=PD AND VAN DRIEST - TURBULENT

| 5701S0202 | | RICHMOND | | PROFILE TABULATION | | 21 POINTS, DELTA AT POINT 21 | | | |
|-----------|-------------------------|-------------------------|------|--------------------|---------|------------------------------|---------|-----------|--|
| I | Y | PT2/P | P/PD | TO/TOD | M/MD | U/UD | T/TD | R/RD*U/UD | |
| 1 | 0.0000 ⁺ +00 | 1.0000 ⁺ +00 | NM | 0.99997 | 0.00000 | 0.00000 | 1.00023 | 0.00000 | |
| 2 | 3.0480 ⁻ -04 | 1.0003 ⁺ +00 | NM | 0.99998 | 0.55201 | 0.55206 | 1.00016 | 0.55197 | |
| 3 | 3.8100 ⁻ -04 | 1.0003 ⁺ +00 | NM | 0.99998 | 0.58914 | 0.58918 | 1.00015 | 0.58910 | |
| 4 | 4.5720 ⁻ -04 | 1.0004 ⁺ +00 | NM | 0.99999 | 0.66340 | 0.66344 | 1.00013 | 0.66335 | |
| 5 | 5.3340 ⁻ -04 | 1.0005 ⁺ +00 | NM | 0.99999 | 0.71182 | 0.71186 | 1.00011 | 0.71178 | |
| 6 | 6.0960 ⁻ -04 | 1.0005 ⁺ +00 | NM | 0.99999 | 0.74007 | 0.74011 | 1.00010 | 0.74004 | |
| 7 | 6.8580 ⁻ -04 | 1.0005 ⁺ +00 | NM | 0.99999 | 0.77075 | 0.77078 | 1.00009 | 0.77071 | |
| 8 | 8.3820 ⁻ -04 | 1.0006 ⁺ +00 | NM | 0.99999 | 0.80223 | 0.80226 | 1.00008 | 0.80219 | |
| 9 | 1.0668 ⁻ -03 | 1.0006 ⁺ +00 | NM | 0.99999 | 0.83290 | 0.83293 | 1.00007 | 0.83287 | |
| 10 | 1.4478 ⁻ -03 | 1.0007 ⁺ +00 | NM | 0.99999 | 0.86761 | 0.86764 | 1.00006 | 0.86759 | |
| 11 | 1.8288 ⁻ -03 | 1.0007 ⁺ +00 | NM | 0.99999 | 0.88456 | 0.88458 | 1.00005 | 0.88454 | |
| 12 | 2.2098 ⁻ -03 | 1.0007 ⁺ +00 | NM | 1.00000 | 0.90151 | 0.90153 | 1.00004 | 0.90149 | |
| 13 | 2.9718 ⁻ -03 | 1.0008 ⁺ +00 | NM | 1.00000 | 0.91927 | 0.91929 | 1.00004 | 0.91926 | |
| 14 | 4.1148 ⁻ -03 | 1.0008 ⁺ +00 | NM | 1.00000 | 0.93784 | 0.93785 | 1.00003 | 0.93783 | |
| 15 | 6.0198 ⁻ -03 | 1.0008 ⁺ +00 | NM | 1.00000 | 0.95479 | 0.95480 | 1.00002 | 0.95478 | |
| 16 | 7.9248 ⁻ -03 | 1.0008 ⁺ +00 | NM | 1.00000 | 0.96932 | 0.96933 | 1.00001 | 0.96932 | |
| 17 | 1.1735 ⁻ -02 | 1.0009 ⁺ +00 | NM | 1.00000 | 0.98385 | 0.98386 | 1.00001 | 0.98385 | |
| 18 | 1.5545 ⁻ -02 | 1.0009 ⁺ +00 | NM | 1.00000 | 0.99273 | 0.99274 | 1.00000 | 0.99273 | |
| 19 | 1.9355 ⁻ -02 | 1.0009 ⁺ +00 | NM | 1.00000 | 0.99435 | 0.99435 | 1.00000 | 0.99435 | |
| 20 | 2.3165 ⁻ -02 | 1.0009 ⁺ +00 | NM | 1.00000 | 0.99919 | 0.99919 | 1.00000 | 0.99919 | |
| D 21 | 2.6975 ⁻ -02 | 1.0009 ⁺ +00 | NM | 1.00000 | 1.00000 | 1.00000 | 1.00000 | 1.00000 | |

INPUT VARIABLES Y,U ASSUME P=PD AND VAN DRIEST - TURBULENT

| 5701S0204 | | RICHMOND | | PROFILE TABULATION | | 24 POINTS, DELTA AT POINT 24 | | | |
|-----------|-------------------------|-------------------------|------|--------------------|---------|------------------------------|---------|-----------|--|
| I | Y | PT2/P | P/PD | TO/TOD | M/MD | U/UD | T/TD | R/RD*U/UD | |
| 1 | 0.0000 ⁺ +00 | 1.0000 ⁺ +00 | NM | 0.99997 | 0.00000 | 0.00000 | 1.00023 | 0.00000 | |
| 2 | 1.5240 ⁻ -04 | 1.0001 ⁺ +00 | NM | 0.99998 | 0.39512 | 0.39516 | 1.00019 | 0.39509 | |
| 3 | 2.2860 ⁻ -04 | 1.0002 ⁺ +00 | NM | 0.99998 | 0.45964 | 0.45968 | 1.00018 | 0.45959 | |
| 4 | 3.0480 ⁻ -04 | 1.0003 ⁺ +00 | NM | 0.99998 | 0.55641 | 0.55645 | 1.00016 | 0.55636 | |
| 5 | 3.8100 ⁻ -04 | 1.0004 ⁺ +00 | NM | 0.99998 | 0.64915 | 0.64919 | 1.00013 | 0.64911 | |
| 6 | 4.5720 ⁻ -04 | 1.0004 ⁺ +00 | NM | 0.99999 | 0.69673 | 0.69677 | 1.00012 | 0.69669 | |
| 7 | 5.3340 ⁻ -04 | 1.0005 ⁺ +00 | NM | 0.99999 | 0.73383 | 0.73387 | 1.00011 | 0.73379 | |
| 8 | 6.0960 ⁻ -04 | 1.0005 ⁺ +00 | NM | 0.99999 | 0.76206 | 0.76210 | 1.00010 | 0.76202 | |
| 9 | 6.8580 ⁻ -04 | 1.0005 ⁺ +00 | NM | 0.99999 | 0.78222 | 0.78226 | 1.00009 | 0.78219 | |
| 10 | 7.6200 ⁻ -04 | 1.0006 ⁺ +00 | NM | 0.99999 | 0.79674 | 0.79677 | 1.00008 | 0.79671 | |
| 11 | 9.1440 ⁻ -04 | 1.0006 ⁺ +00 | NM | 0.99999 | 0.82497 | 0.82500 | 1.00007 | 0.82494 | |
| 12 | 1.0668 ⁻ -03 | 1.0006 ⁺ +00 | NM | 0.99999 | 0.84029 | 0.84032 | 1.00007 | 0.84027 | |
| 13 | 1.4478 ⁻ -03 | 1.0007 ⁺ +00 | NM | 0.99999 | 0.86288 | 0.86290 | 1.00006 | 0.86285 | |
| 14 | 1.8288 ⁻ -03 | 1.0007 ⁺ +00 | NM | 0.99999 | 0.87982 | 0.87984 | 1.00005 | 0.87979 | |
| 15 | 2.2098 ⁻ -03 | 1.0007 ⁺ +00 | NM | 0.99999 | 0.89272 | 0.89274 | 1.00005 | 0.89270 | |
| 16 | 2.5908 ⁻ -03 | 1.0007 ⁺ +00 | NM | 1.00000 | 0.90240 | 0.90242 | 1.00004 | 0.90238 | |
| 17 | 4.4958 ⁻ -03 | 1.0008 ⁺ +00 | NM | 1.00000 | 0.92337 | 0.92339 | 1.00003 | 0.92336 | |
| 18 | 6.4008 ⁻ -03 | 1.0008 ⁺ +00 | NM | 1.00000 | 0.93547 | 0.93548 | 1.00003 | 0.93546 | |
| 19 | 8.3058 ⁻ -03 | 1.0008 ⁺ +00 | NM | 1.00000 | 0.94596 | 0.94597 | 1.00002 | 0.94595 | |
| 20 | 1.2116 ⁻ -02 | 1.0008 ⁺ +00 | NM | 1.00000 | 0.96048 | 0.96048 | 1.00002 | 0.96047 | |
| 21 | 1.5926 ⁻ -02 | 1.0008 ⁺ +00 | NM | 1.00000 | 0.97499 | 0.97500 | 1.00001 | 0.97499 | |
| 22 | 1.9736 ⁻ -02 | 1.0009 ⁺ +00 | NM | 1.00000 | 0.98387 | 0.98387 | 1.00001 | 0.98386 | |
| 23 | 2.3546 ⁻ -02 | 1.0009 ⁺ +00 | NM | 1.00000 | 0.99193 | 0.99194 | 1.00000 | 0.99193 | |
| D 24 | 2.7356 ⁻ -02 | 1.0009 ⁺ +00 | NM | 1.00000 | 1.00000 | 1.00000 | 1.00000 | 1.00000 | |

INPUT VARIABLES Y,U ASSUME P=PD AND VAN DRIEST - TURBULENT

| 5701S0402 | | RICHMOND | | PROFILE TABULATION | | 22 POINTS, DELTA AT POINT 20 | | | |
|-----------|------------------------|------------------------|------|--------------------|---------|------------------------------|---------|-----------|--|
| I | Y | PT2/P | P/PD | TO/TOD | M/MD | U/UD | T/TD | R/RD*U/UD | |
| 1 | 0.0000 ⁺ 00 | 1.0000 ⁺ 00 | NM | 0.90950 | 0.00000 | 0.00000 | 7.00752 | 0.00000 | |
| 2 | 1.2700 ⁻ 04 | 1.7287 ⁺ 00 | NM | 0.92340 | 0.15889 | 0.39195 | 6.08463 | 0.06442 | |
| 3 | 3.5560 ⁻ 04 | 2.7459 ⁺ 00 | NM | 0.93433 | 0.22625 | 0.52378 | 5.35938 | 0.09773 | |
| 4 | 5.8420 ⁻ 04 | 7.3528 ⁺ 00 | NM | 0.96110 | 0.39896 | 0.75510 | 3.58216 | 0.21080 | |
| 5 | 8.1280 ⁻ 04 | 1.1154 ⁺ 01 | NM | 0.97261 | 0.49741 | 0.83505 | 2.81839 | 0.29629 | |
| 6 | 1.0414 ⁻ 03 | 1.3574 ⁺ 01 | NM | 0.97768 | 0.55095 | 0.86795 | 2.48181 | 0.34973 | |
| 7 | 1.5240 ⁻ 03 | 1.6332 ⁺ 01 | NM | 0.98216 | 0.60622 | 0.89600 | 2.18455 | 0.41015 | |
| 8 | 1.9812 ⁻ 03 | 1.8963 ⁺ 01 | NM | 0.98553 | 0.65458 | 0.91656 | 1.96067 | 0.46748 | |
| 9 | 2.4384 ⁻ 03 | 2.1171 ⁺ 01 | NM | 0.98787 | 0.69257 | 0.93056 | 1.80534 | 0.51545 | |
| 10 | 3.3528 ⁻ 03 | 2.4942 ⁺ 01 | NM | 0.99111 | 0.75302 | 0.94960 | 1.59026 | 0.59714 | |
| 11 | 4.2926 ⁻ 03 | 2.8425 ⁺ 01 | NM | 0.99348 | 0.80484 | 0.96332 | 1.43261 | 0.67242 | |
| 12 | 5.2070 ⁻ 03 | 3.1632 ⁺ 01 | NM | 0.99529 | 0.84974 | 0.97362 | 1.31281 | 0.74163 | |
| 13 | 6.1468 ⁻ 03 | 3.4481 ⁺ 01 | NM | 0.99666 | 0.88774 | 0.98135 | 1.22202 | 0.80306 | |
| 14 | 7.0612 ⁻ 03 | 3.6905 ⁺ 01 | NM | 0.99768 | 0.91883 | 0.98709 | 1.15411 | 0.85528 | |
| 15 | 7.9692 ⁻ 03 | 3.8148 ⁺ 01 | NM | 0.99816 | 0.93437 | 0.98978 | 1.12213 | 0.88206 | |
| 16 | 8.3058 ⁻ 03 | 3.9412 ⁺ 01 | NM | 0.99862 | 0.94991 | 0.99237 | 1.09138 | 0.90928 | |
| 17 | 9.2456 ⁻ 03 | 4.1275 ⁺ 01 | NM | 0.99926 | 0.97237 | 0.99591 | 1.04902 | 0.94938 | |
| 18 | 1.0160 ⁻ 02 | 4.2885 ⁺ 01 | NM | 0.99977 | 0.99136 | 0.99875 | 1.01496 | 0.98403 | |
| 19 | 1.1074 ⁻ 02 | 4.3479 ⁺ 01 | NM | 0.99996 | 0.99827 | 0.99975 | 1.00297 | 0.99679 | |
| D 20 | 1.2014 ⁻ 02 | 4.3628 ⁺ 01 | NM | 1.00000 | 1.00000 | 1.00000 | 1.00000 | 1.00000 | |
| 21 | 1.2929 ⁻ 02 | 4.3628 ⁺ 01 | NM | 1.00000 | 1.00000 | 1.00000 | 1.00000 | 1.00000 | |
| 22 | 1.3386 ⁻ 02 | 4.3628 ⁺ 01 | NM | 1.00000 | 1.00000 | 1.00000 | 1.00000 | 1.00000 | |

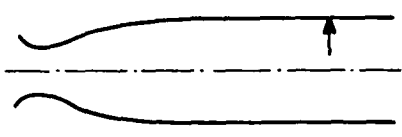
INPUT VARIABLES Y,M ASSUME P=PD AND VAN DRIEST - TURBULENT

| 5701S0501 | | RICHMOND | | PROFILE TABULATION | | 20 POINTS, DELTA AT POINT 19 | | | |
|-----------|------------------------|------------------------|------|--------------------|---------|------------------------------|---------|-----------|--|
| I | Y | PT2/P | P/PD | TO/TOD | M/MD | U/UD | T/TD | R/RD*U/UD | |
| 1 | 0.0000 ⁺ 00 | 1.0000 ⁺ 00 | NM | 0.91039 | 0.00000 | 0.00000 | 6.57964 | 0.00000 | |
| 2 | 1.2700 ⁻ 04 | 3.3382 ⁺ 00 | NM | 0.94018 | 0.26523 | 0.57654 | 4.72499 | 0.12202 | |
| 3 | 5.8420 ⁻ 04 | 4.7155 ⁺ 00 | NM | 0.94948 | 0.32437 | 0.66046 | 4.14576 | 0.15931 | |
| 4 | 1.0414 ⁻ 03 | 6.9442 ⁺ 00 | NM | 0.96042 | 0.40143 | 0.74720 | 3.46451 | 0.21567 | |
| 5 | 1.5240 ⁻ 03 | 8.6551 ⁺ 00 | NM | 0.96664 | 0.45161 | 0.79225 | 3.07749 | 0.25744 | |
| 6 | 1.9812 ⁻ 03 | 1.0283 ⁺ 01 | NM | 0.97138 | 0.49462 | 0.82500 | 2.78200 | 0.29655 | |
| 7 | 2.4384 ⁻ 03 | 1.2216 ⁺ 01 | NM | 0.97595 | 0.54122 | 0.85533 | 2.49761 | 0.34246 | |
| 8 | 2.8956 ⁻ 03 | 1.3738 ⁺ 01 | NM | 0.97894 | 0.57527 | 0.87461 | 2.31149 | 0.37838 | |
| 9 | 3.3528 ⁻ 03 | 1.6332 ⁺ 01 | NM | 0.98312 | 0.62903 | 0.90089 | 2.05116 | 0.43921 | |
| 10 | 3.8354 ⁻ 03 | 1.8865 ⁺ 01 | NM | 0.98638 | 0.67742 | 0.92088 | 1.84796 | 0.49832 | |
| 11 | 4.2926 ⁻ 03 | 2.2216 ⁺ 01 | NM | 0.98982 | 0.73656 | 0.94149 | 1.63386 | 0.57624 | |
| 12 | 4.7498 ⁻ 03 | 2.6192 ⁺ 01 | NM | 0.99299 | 0.80108 | 0.96010 | 1.43642 | 0.66839 | |
| 13 | 5.2070 ⁻ 03 | 3.0254 ⁺ 01 | NM | 0.99553 | 0.86201 | 0.97471 | 1.27860 | 0.76233 | |
| 14 | 5.6642 ⁻ 03 | 3.3954 ⁺ 01 | NM | 0.99739 | 0.91398 | 0.98535 | 1.16228 | 0.84778 | |
| 15 | 6.1468 ⁻ 03 | 3.6768 ⁺ 01 | NM | 0.99860 | 0.95161 | 0.99217 | 1.08705 | 0.91272 | |
| 16 | 6.6040 ⁻ 03 | 3.8427 ⁺ 01 | NM | 0.99924 | 0.97312 | 0.99577 | 1.04710 | 0.95098 | |
| 17 | 7.0612 ⁻ 03 | 3.9554 ⁺ 01 | NM | 0.99965 | 0.98746 | 0.99806 | 1.02160 | 0.97696 | |
| 18 | 7.5184 ⁻ 03 | 3.9981 ⁺ 01 | NM | 0.99980 | 0.99283 | 0.99890 | 1.01226 | 0.98680 | |
| D 19 | 8.1534 ⁻ 03 | 4.0554 ⁺ 01 | NM | 1.00000 | 1.00000 | 1.00000 | 1.00000 | 1.00000 | |
| 20 | 8.7630 ⁻ 03 | 3.7042 ⁺ 01 | NM | 0.99871 | 0.95520 | 0.99278 | 1.08025 | 0.91903 | |

INPUT VARIABLES Y,M ASSUME P=PD AND VAN DRIEST - LAMINAR

| 5701S0502 | | RICHMOND | | PROFILE TABULATION | | 20 POINTS, DELTA AT POINT 18 | | | |
|-----------|------------------------|------------------------|------|--------------------|---------|------------------------------|---------|-----------|--|
| I | Y | PT2/P | P/PD | TO/TOD | M/MD | U/UD | T/TD | R/RD*U/UD | |
| 1 | 0.0000 ⁺ 00 | 1.0000 ⁺ 00 | NM | 0.90934 | 0.00000 | 0.00000 | 7.09081 | 0.00000 | |
| 2 | 1.2700 ⁻ 04 | 4.3108 ⁺ 00 | NM | 0.94591 | 0.29503 | 0.63510 | 4.63408 | 0.13705 | |
| 3 | 5.8420 ⁻ 04 | 1.0498 ⁺ 01 | NM | 0.97081 | 0.47856 | 0.82345 | 2.96078 | 0.27812 | |
| 4 | 1.0414 ⁻ 03 | 1.8286 ⁺ 01 | NM | 0.98455 | 0.63808 | 0.91084 | 2.03768 | 0.44700 | |
| 5 | 1.5240 ⁻ 03 | 2.1482 ⁺ 01 | NM | 0.98799 | 0.69297 | 0.93143 | 1.80665 | 0.51556 | |
| 6 | 1.9812 ⁻ 03 | 2.3942 ⁺ 01 | NM | 0.99015 | 0.73242 | 0.94412 | 1.66165 | 0.56819 | |
| 7 | 2.4384 ⁻ 03 | 2.6423 ⁺ 01 | NM | 0.99200 | 0.77015 | 0.95488 | 1.53724 | 0.62116 | |
| 8 | 3.3528 ⁻ 03 | 3.0627 ⁺ 01 | NM | 0.99458 | 0.83019 | 0.96964 | 1.36418 | 0.71079 | |
| 9 | 4.2672 ⁻ 03 | 3.4481 ⁺ 01 | NM | 0.99648 | 0.88165 | 0.98039 | 1.23654 | 0.79285 | |
| 10 | 5.2070 ⁻ 03 | 3.8148 ⁺ 01 | NM | 0.99798 | 0.92796 | 0.98882 | 1.13547 | 0.87085 | |
| 11 | 6.1468 ⁻ 03 | 4.1130 ⁺ 01 | NM | 0.99904 | 0.96398 | 0.99467 | 1.06470 | 0.93423 | |
| 12 | 7.0612 ⁻ 03 | 4.2738 ⁺ 01 | NM | 0.99955 | 0.98285 | 0.99753 | 1.03009 | 0.96838 | |
| 13 | 8.1026 ⁻ 03 | 4.3479 ⁺ 01 | NM | 0.99978 | 0.99142 | 0.99878 | 1.01489 | 0.98412 | |
| 14 | 9.1440 ⁻ 03 | 4.3628 ⁺ 01 | NM | 0.99982 | 0.99314 | 0.99902 | 1.01189 | 0.98729 | |
| 15 | 1.0058 ⁻ 02 | 4.3777 ⁺ 01 | NM | 0.99987 | 0.99485 | 0.99927 | 1.00890 | 0.99046 | |
| 16 | 1.0998 ⁻ 02 | 4.4076 ⁺ 01 | NM | 0.99996 | 0.99828 | 0.99976 | 1.00295 | 0.99681 | |
| 17 | 1.1913 ⁻ 02 | 4.4076 ⁺ 01 | NM | 0.99996 | 0.99828 | 0.99976 | 1.00295 | 0.99681 | |
| D 18 | 1.2827 ⁻ 02 | 4.4226 ⁺ 01 | NM | 1.00000 | 1.00000 | 1.00000 | 1.00000 | 1.00000 | |
| 19 | 1.3767 ⁻ 02 | 4.4226 ⁺ 01 | NM | 1.00000 | 1.00000 | 1.00000 | 1.00000 | 1.00000 | |
| 20 | 1.4224 ⁻ 02 | 4.4226 ⁺ 01 | NM | 1.00000 | 1.00000 | 1.00000 | 1.00000 | 1.00000 | |

INPUT VARIABLES Y,M ASSUME P=PD AND VAN DRIEST - TURBULENT

| | | |
|--|--|------|
|  | M: 1.77 R THETA x 10 ⁻³ : 16 TW/TR: 1 | 5806 |
| ZPG - AW | | |
| Continuous tunnel with symmetric nozzle. W = 0.19, H = 0.28 m. PO = 93 KN/m ² . TO = 295K. Air: RE/m x 10 ⁻⁶ = 12.7 | | |
| MORKOVIN M.V., PHINNEY R.E., 1958. Extended applications of hot wire anemometry to high speed turbulent boundary layers. Dept. Aeronaut. The Johns Hopkins Univ. ASTIA AD-158-279. | | |

- 1 The test boundary layer was formed on the upper nozzle wall and flat roof of the tunnel test section.
- 3 The measuring station was 0.43 m downstream of the end of the nozzle. "Screening" was glued to the last 0.13 m of the nozzle wall so as to thicken the boundary layer. The profile station was 33 boundary layer thicknesses downstream. "It is therefore likely that the layer represents very nearly a fully developed equilibrium turbulent boundary layer." The test station is some way downstream of "the disequilibrating nozzle pressure gradient." Pressure disturbances from the screening were reflected back to the wall 0.09 m downstream of the profile station.
- 6 No wall measurements are reported, but it is suggested that since the test surface was separated from the tunnel structure by an air gap from 0.05 to 0.09 m deep, it is a "plausible hypothesis" that the flow was effectively adiabatic.
- 7 "Primary" mean flow measurements were made using an FPP ($h_1 = 0.1$, $h_2 = 0.05$, $b_1 = 0.9$ mm). Fluctuation measurements were made with a large number of HWP operating in the constant current mode. Normal wires were made from Tungsten ($d = 3.8$ μ m) with and without copper "sleeves" ($d = 13$ μ m), and of Platinum -10% Rhodium ($d = 2.5$ μ m) with and without silver "sleeves" ($d = 63$ μ m), the nominal l/d ratios of the sensing element ranging from 198 to 667. Exploratory investigations were also made using a number of X-wire probes.
- 9 The authors reduced the Pitot profile data assuming isoenergetic flow. A skin friction value was obtained by comparison with measurements by Coles (CAT 5301) and Shutts et al. (CAT 5501) and a fit to Coles' wall law (assuming $\rho_r/\rho_w = 1.1$ as did Kistler in CAT 5803).
- 12 The editors have, exceptionally, prepared this entry from the authors' graphical data, and so implicitly accepted their interpolations and smoothing procedures. We have replaced the assumption of isoenergetic
- 13 flow by the Crocco/van Driest temperature/velocity correlation. We present therefore the authors' single
- 14 profile, with their estimated CF value. The fluctuation data are presented graphically below.
- § DATA: 5806 0101. Pitot profile. CC HWP measurements, NX = 1.
- 15 Editors' comments. As remarked above, we have prepared these data from a graphical original, in contravention of our own "ground rules". We would justify this in view of the continuing relative paucity of fluctuation data, and the relative inaccessibility of the original report.

The mean flow data are completely normal, agreeing well with both inner and outer laws, using the authors' CF estimate. The importance of the study lies in the very detailed treatment of the hot-wire results. A large number of wires was used, so that the original results display both scatter and systematic differences between wires. Below, we show reproductions of Figs. 12, 13 of the source paper from which readers may make their own assessment of the authors' selection of a best fit curve.

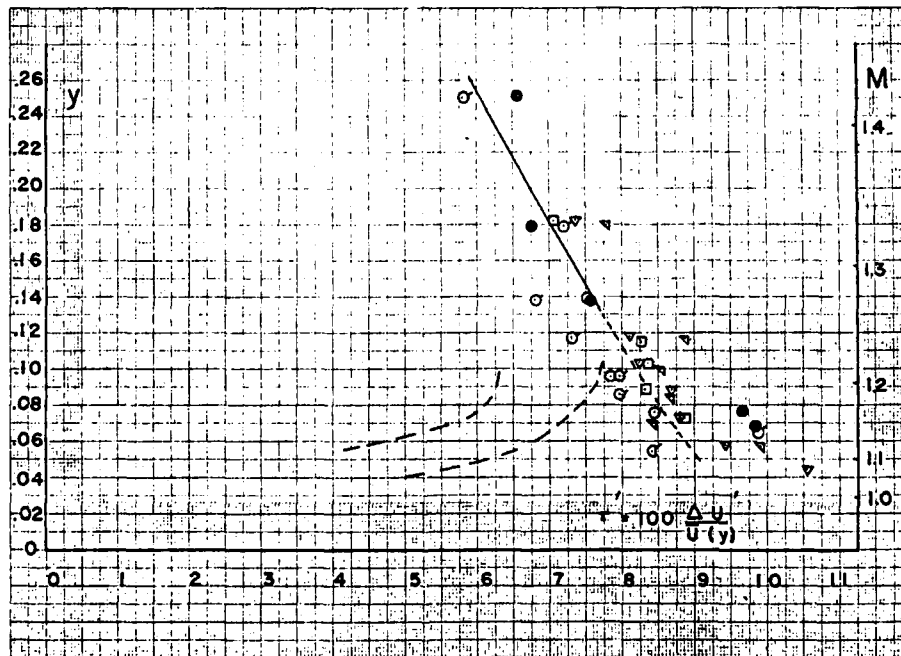
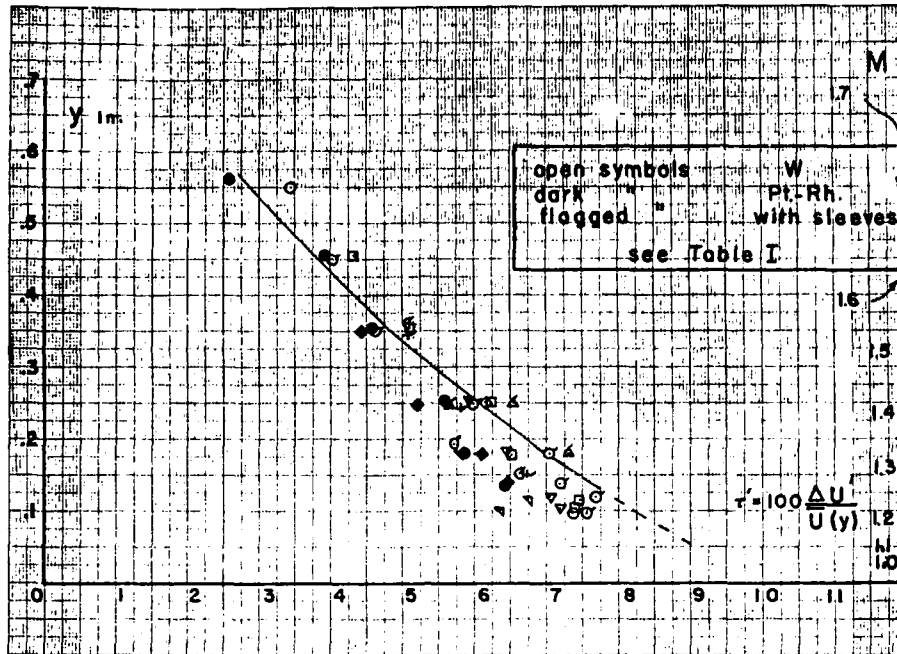


Fig. 1. (Source figure 12A/13A). Distribution of rms x-component fluctuation velocity $\Delta u'$.

Upper figure: Data for $Y > 0.1$ inch as obtained from modal analysis without correction for upstream influence in the transonic region. ("Process calibration" - Authors' APP.III).

Lower figure: Data for $Y < 0.25$ inch after correction. The two broken lines represent the envelope of the uncorrected data at low Y -values.

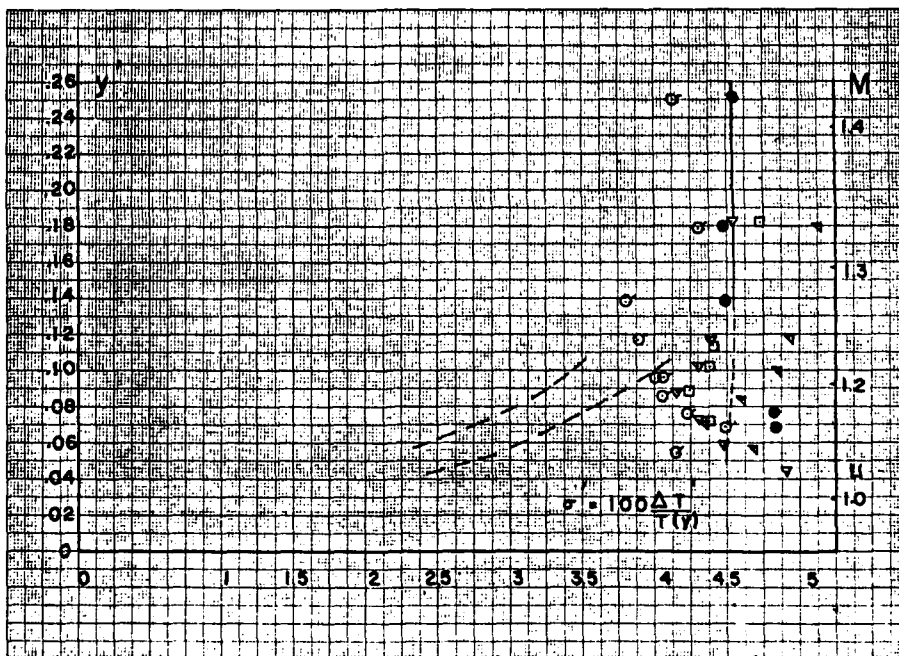
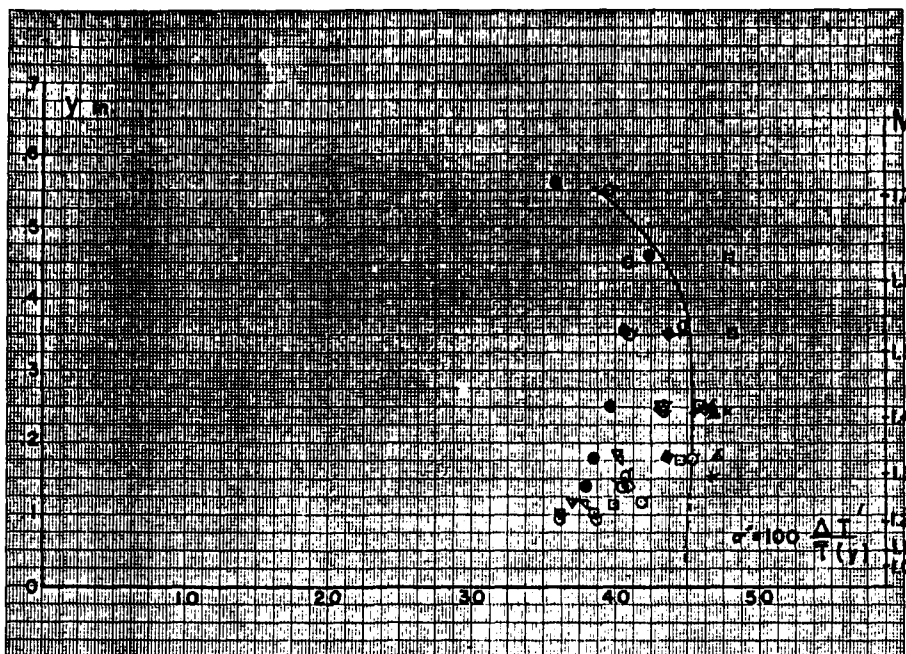


Fig. 2. (Source figures 12B/13B). Distribution of rms temperature fluctuations $\Delta T'$. Upper and lower as for Fig. 1.

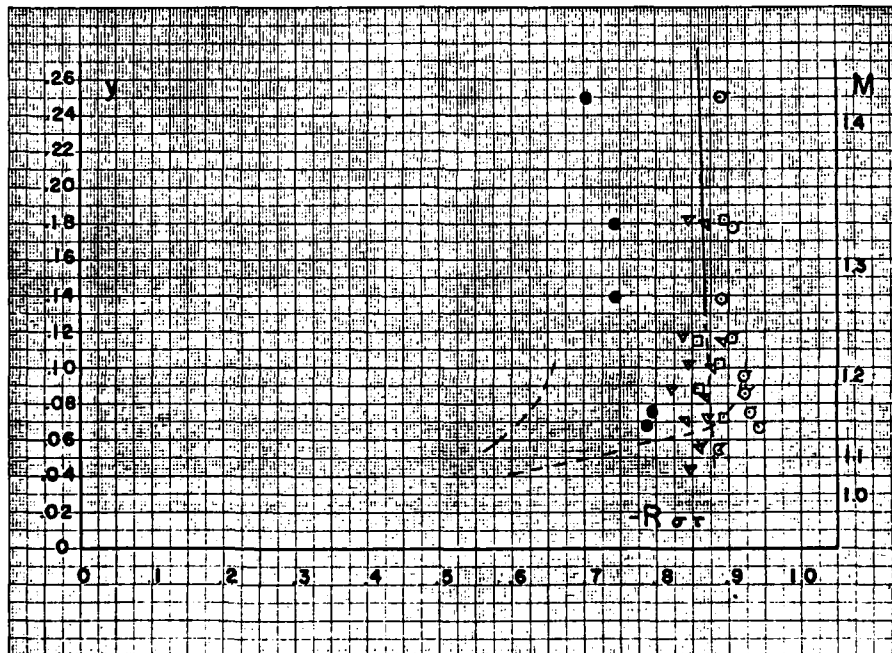
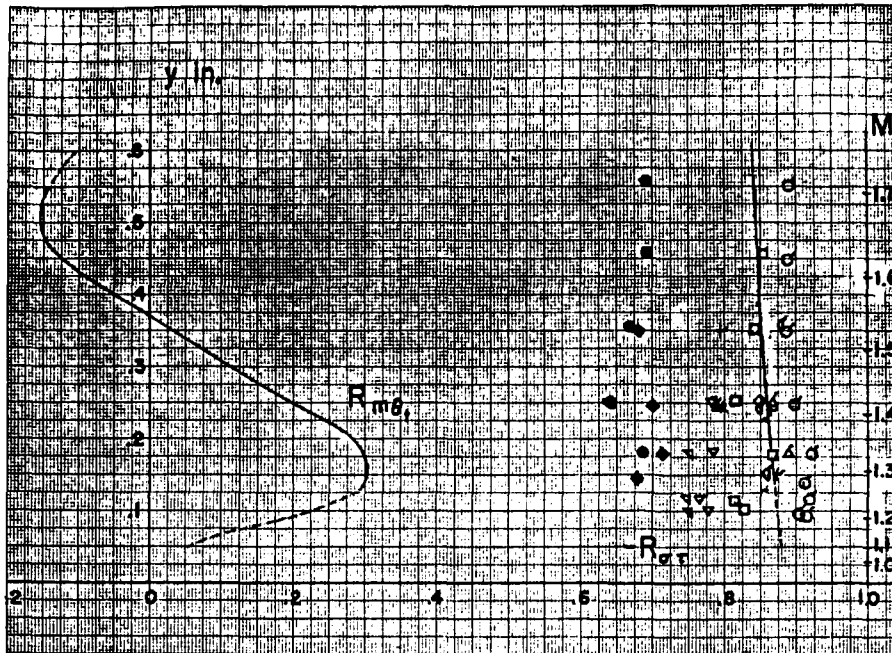
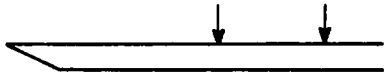


Fig. 3. (Source figure 12C/13C). Distribution of entropy-velocity fluctuation correlation function $R_{\sigma\tau}$. Upper and lower as for Fig. 1. The mass flux/total temperature correlation $R_{m\theta_t}$ is calculated from the authors' best-estimate smoothed curves as shown for the other turbulence quantities.

| CAT 5806S | | MORKOVIN | | BOUNDARY CONDITIONS AND EVALUATED DATA. SI UNITS | | | | | | |
|-----------|-----------------------|-----------------------|-----------------------|--|--------|-----------------------|-----------------------|-----------------------|--|--|
| RUN | MD * | TW/TR* | RED2W | CF | H12 | H12K | PW | PD | | |
| X | POD* | PW/POD* | RED2D | CQ | H32 | H32K | TW | TD | | |
| RZ | TOO* | TAUW * | DZ | PI2* | H42 | D2* | UD | TR | | |
| 5806S0101 | 1.7700 | 1.0000 | 1.2254 ⁺⁰⁴ | 1.8500 ⁻⁰³ | 2.5434 | 1.2884 | 1.6967 ⁺⁰⁴ | 1.6967 ⁺⁰⁴ | | |
| NM | 9.3126 ⁺⁰⁴ | 1.0000 | 1.7672 ⁺⁰⁴ | NM | 1.8132 | 1.8049 | 2.8318 ⁺⁰² | 1.8136 ⁺⁰² | | |
| INFINITE | 2.9500 ⁺⁰² | 6.8837 ⁺⁰¹ | 1.3937 ⁻⁰³ | 0.0000 ⁺⁰⁰ | 0.0726 | 1.6500 ⁻⁰³ | 4.7792 ⁺⁰² | 2.8318 ⁺⁰² | | |

| 5806S0101 | | MORKOVIN | | PROFILE TABULATION | | | 34 POINTS, DELTA AT POINT 34 | | |
|-----------|-----------------------|-----------------------|------|--------------------|---------|---------|------------------------------|-----------|--|
| I | Y | PT2/P | P/PD | TO/TOD | M/MD | U/UD | T/TD | R/RD*U/UD | |
| 1 | 0.0000 ⁺⁰⁰ | 1.0000 ⁺⁰⁰ | NM | 0.95994 | 0.00000 | 0.00000 | 1.56142 | 0.00000 | |
| 2 | 1.2497 ⁻⁰⁴ | 1.4976 ⁺⁰⁰ | NM | 0.97094 | 0.44181 | 0.52410 | 1.40721 | 0.37244 | |
| 3 | 1.5621 ⁻⁰⁴ | 1.5319 ⁺⁰⁰ | NM | 0.97153 | 0.45480 | 0.53793 | 1.39896 | 0.38452 | |
| 4 | 2.1869 ⁻⁰⁴ | 1.6224 ⁺⁰⁰ | NM | 0.97300 | 0.48644 | 0.57109 | 1.37831 | 0.41434 | |
| 5 | 2.9680 ⁻⁰⁴ | 1.6624 ⁺⁰⁰ | NM | 0.97362 | 0.49944 | 0.58449 | 1.36962 | 0.42676 | |
| 6 | 4.0615 ⁻⁰⁴ | 1.7325 ⁺⁰⁰ | NM | 0.97467 | 0.52090 | 0.60636 | 1.35500 | 0.44749 | |
| 7 | 4.6863 ⁻⁰⁴ | 1.7734 ⁺⁰⁰ | NM | 0.97525 | 0.53277 | 0.61829 | 1.34680 | 0.45908 | |
| 8 | 5.3111 ⁻⁰⁴ | 1.8078 ⁺⁰⁰ | NM | 0.97573 | 0.54237 | 0.62786 | 1.34010 | 0.46852 | |
| 9 | 6.2484 ⁻⁰⁴ | 1.8560 ⁺⁰⁰ | NM | 0.97638 | 0.55537 | 0.64071 | 1.33095 | 0.48139 | |
| 10 | 7.3419 ⁻⁰⁴ | 1.8974 ⁺⁰⁰ | NM | 0.97693 | 0.56610 | 0.65122 | 1.32333 | 0.49211 | |
| 11 | 8.1229 ⁻⁰⁴ | 1.9379 ⁺⁰⁰ | NM | 0.97745 | 0.57627 | 0.66109 | 1.31605 | 0.50233 | |
| 12 | 9.3726 ⁻⁰⁴ | 1.9939 ⁺⁰⁰ | NM | 0.97814 | 0.58983 | 0.67413 | 1.30628 | 0.51607 | |
| 13 | 1.0935 ⁻⁰³ | 2.0496 ⁺⁰⁰ | NM | 0.97882 | 0.60282 | 0.68649 | 1.29684 | 0.52936 | |
| 14 | 1.4059 ⁻⁰³ | 2.1641 ⁺⁰⁰ | NM | 0.98015 | 0.62825 | 0.71028 | 1.27818 | 0.55569 | |
| 15 | 1.7183 ⁻⁰³ | 2.2606 ⁺⁰⁰ | NM | 0.98122 | 0.64859 | 0.72894 | 1.26311 | 0.57710 | |
| 16 | 2.1869 ⁻⁰³ | 2.3901 ⁺⁰⁰ | NM | 0.98261 | 0.67458 | 0.75229 | 1.24369 | 0.60489 | |
| 17 | 2.6556 ⁻⁰³ | 2.4931 ⁺⁰⁰ | NM | 0.98367 | 0.69435 | 0.76970 | 1.22881 | 0.62638 | |
| 18 | 3.1242 ⁻⁰³ | 2.5844 ⁺⁰⁰ | NM | 0.98459 | 0.71130 | 0.78437 | 1.21601 | 0.64504 | |
| 19 | 3.7490 ⁻⁰³ | 2.7040 ⁺⁰⁰ | NM | 0.98575 | 0.73277 | 0.80262 | 1.19975 | 0.66899 | |
| 20 | 4.3739 ⁻⁰³ | 2.8047 ⁺⁰⁰ | NM | 0.98669 | 0.75028 | 0.81724 | 1.18646 | 0.68881 | |
| 21 | 4.9987 ⁻⁰³ | 2.9048 ⁺⁰⁰ | NM | 0.98761 | 0.76723 | 0.83116 | 1.17358 | 0.70822 | |
| 22 | 5.6236 ⁻⁰³ | 3.0109 ⁺⁰⁰ | NM | 0.98856 | 0.78475 | 0.84530 | 1.16027 | 0.72853 | |
| 23 | 6.2484 ⁻⁰³ | 3.1127 ⁺⁰⁰ | NM | 0.98945 | 0.80113 | 0.85830 | 1.14783 | 0.74776 | |
| 24 | 7.4981 ⁻⁰³ | 3.3271 ⁺⁰⁰ | NM | 0.99125 | 0.83446 | 0.88413 | 1.12257 | 0.78759 | |
| 25 | 8.7478 ⁻⁰³ | 3.5240 ⁺⁰⁰ | NM | 0.99283 | 0.86384 | 0.90617 | 1.10041 | 0.82349 | |
| 26 | 9.6850 ⁻⁰³ | 3.6687 ⁺⁰⁰ | NM | 0.99395 | 0.88475 | 0.92146 | 1.08472 | 0.84949 | |
| 27 | 1.0935 ⁻⁰² | 3.8416 ⁺⁰⁰ | NM | 0.99525 | 0.90904 | 0.93882 | 1.06659 | 0.88020 | |
| 28 | 1.2184 ⁻⁰² | 4.0194 ⁺⁰⁰ | NM | 0.99653 | 0.93333 | 0.95574 | 1.04859 | 0.91145 | |
| 29 | 1.3434 ⁻⁰² | 4.1893 ⁺⁰⁰ | NM | 0.99772 | 0.95593 | 0.97110 | 1.03198 | 0.94100 | |
| 30 | 1.4684 ⁻⁰² | 4.3371 ⁺⁰⁰ | NM | 0.99872 | 0.97514 | 0.98386 | 1.01797 | 0.96650 | |
| 31 | 1.5621 ⁻⁰² | 4.4211 ⁺⁰⁰ | NM | 0.99927 | 0.98588 | 0.99089 | 1.01019 | 0.98089 | |
| 32 | 1.6402 ⁻⁰² | 4.4701 ⁺⁰⁰ | NM | 0.99959 | 0.99209 | 0.99491 | 1.00570 | 0.98928 | |
| 33 | 1.7183 ⁻⁰² | 4.5060 ⁺⁰⁰ | NM | 0.99983 | 0.99661 | 0.99783 | 1.00244 | 0.99540 | |
| D 34 | 1.8745 ⁻⁰² | 4.5330 ⁺⁰⁰ | NM | 1.00000 | 1.00000 | 1.00000 | 1.00000 | 1.00000 | |

INPUT VARIABLES Y,M ASSUME P=PD AND VAN DRIEST

| | | |
|--|--|----------------------|
| rough  | M: 5.1 $R_{\theta} \times 10^{-3}$: 2.9-4.3 TW/TR: 079-0.92 | 6002 |
| | | ZPG · MHT (ROUGH) |
| Continuous tunnel with fixed contoured nozzle. $W = 0.15$; $L = 0.6$ m. $0.75 < P_0 < 1.0$ MN/m ² . T_0 : 380K. Air, $RE/m \times 10^{-6} = 15$. | | |
| DANBERG J.E., 1960. Measurements of the characteristics of the compressible turbulent boundary layer with air injection. NAVORD Rep. 6683. | | |

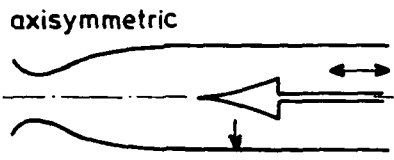
- 1 The test boundary layer was formed on a flat plate model 0.6 m long mounted with the test surface on the tunnel centreline and spanning the tunnel. Tunnel wall boundary layers were compensated for by increasing the working section and plate widths from 0.1364 m at the leading edge ($X = 0$) to 0.1545 m at the trailing edge. The leading edge was chamfered at 10° on the underside. Up to $X = 0.0698$ m the test surface was smooth. From this point to $X = 0.5334$ m the surface consisted of a "sintered woven stainless steel wire mesh insert." "The exposed surface consisted of 0.127 mm wire and was flat to within a few tenths of a millimetre." This value refers to the long-wave flatness of the surface, which had a short-wave roughness of the same order as the wire diameter. The surface was probably, however, hydrodynamically smooth. The insert, constructed to allow of tests with air injection, was 0.127 m wide. The test surface was actively cooled. There were two traverse stations at $X = 0.2925$, 0.3685 m. Transition was "expected" at $X = 0.216$ m, on the basis of the tests made by Winkler and Cha (CAT 5902). Provision was made to check the uniformity of wall temperature across the plate.
- 2 Wall temperature was measured at 6 points on the centreline and 12.7, 38.1 mm off the centreline at $X = 0.344$ m. Pitot and T_0 profiles were measured, both probes being constructed from flattened tubing with $h_2 = 0.304$ mm. The sensor for the STP was a 0.127 mm iron-constantan thermocouple bead. The general construction was as for Winkler and Cha (CAT 5902), and as described by Winkler (1954).
- 3 The author has deduced CF values from the limiting slope of the velocity profiles. A small amount of slip at the nominal surface was permitted. The static pressure was assumed constant through the layer.
- 4 We present here the four profiles measured with no wall mass transfer. They form two pairs taken at the profile station, each pair corresponding to a given nominal TW/TR value. The original report also gives data for four injection rates. The editors have accepted the author's assumptions and data reduction procedures, and present the profile-derived CF values. The D-state was assumed to be the last measured data point.
- 5 § DATA: 60020101-0202. Pitot and T_0 profiles. $NX = 2$.
- 6 Editors' comments. This experiment adds further data in the transitional range to that from its sister experiments, Winkler and Cha (CAT 5902) and Danberg (CAT 5702). The profiles are plotted as figures (2.5.21), and (4.4.8-10) in AGARDograph 253 where the skin friction data are discussed at length.

| CAT 6002S | | DANBERG | | BOUNDARY CONDITIONS AND EVALUATED DATA. SI UNITS | | | | | |
|-------------|-------------|-------------|-------------|--|---------|-------------|-------------|-------------|--|
| RUN | MD * | TW/TR | RED2W | CF * | H12 | H12K | PW | PD | |
| X * | POD* | PW/PD* | RED2D | CO | H32 | H32K | TW* | TD* | |
| RZ | TOD* | TAUW | O2 | PI2* | H42 | O2K | UD | TR | |
| 6002S0101 | 5.0500 | 0.9129 | 7.5070**+02 | 9.3600**-04 | 10.5303 | 1.6011 | 1.3371**+03 | 1.3371**+03 | |
| 2.9250**-01 | 7.4980**+05 | 1.0000 | 3.2523**+03 | NM | 1.8386 | 1.7626 | 3.1380**+02 | 6.1710**+01 | |
| INFINITE | 3.7650**+02 | 2.2342**+01 | 2.3975**-04 | 0.0000**+00 | 0.3664 | 5.0724**-04 | 7.9539**+02 | 3.4373**+02 | |
| 6002S0102 | 5.1800 | 0.8970 | 9.7485**+02 | 1.2900**-03 | 11.3930 | 1.3585 | 1.5011**+03 | 1.5011**+03 | |
| 3.6850**-01 | 9.7738**+05 | 1.0000 | 4.3394**+03 | NM | 1.8508 | 1.8123 | 3.1036**+02 | 5.9570**+01 | |
| INFINITE | 3.7900**+02 | 3.6372**+01 | 2.6341**-04 | 0.0000**+00 | 0.2324 | 5.7011**-04 | 8.0159**+02 | 3.4600**+02 | |
| 6002S0201 | 5.0860 | 0.8154 | 7.2578**+02 | 7.8300**-04 | 10.9210 | 1.6059 | 1.2999**+03 | 1.2999**+03 | |
| 2.9250**-01 | 7.5994**+05 | 1.0000 | 2.9269**+03 | NM | 1.8683 | 1.8232 | 2.7538**+02 | 5.9930**+01 | |
| INFINITE | 3.6930**+02 | 1.8430**+01 | 2.1086**-04 | 0.0000**+00 | 0.3182 | 4.2277**-04 | 7.8942**+02 | 3.3773**+02 | |
| 6002S0202 | 5.2000 | 0.7895 | 9.1559**+02 | 1.0680**-03 | 10.7583 | 1.3799 | 1.2763**+03 | 1.2763**+03 | |
| 3.6850**-01 | 8.5012**+05 | 1.0000 | 3.7066**+03 | NM | 1.8465 | 1.8051 | 2.7602**+02 | 5.9810**+01 | |
| INFINITE | 3.8314**+02 | 2.5800**+01 | 2.6521**-04 | 0.0000**+00 | 0.3308 | 5.5589**-04 | 8.0631**+02 | 3.4962**+02 | |

CF FROM VELOCITY PROFILE TABLE 20
 TRAPEZOIDAL RULE FOR 0201

| 6002S0201 | | DANBERG | | PROFILE TABULATION | | | 31 POINTS, DELTA AT POINT 31 | | |
|-----------|-------------|-------------|------|--------------------|---------|---------|------------------------------|-----------|--|
| I | Y | PT2/P | P/PD | TO/TOD | M/MD | U/UD | T/TD | R/RD*U/UD | |
| 1 | 0.0000**+00 | 1.0000**+00 | NM | 0.74431 | 0.00000 | 0.00000 | 4.59500 | 0.00000 | |
| 2 | 2.9500**-04 | 2.7454**+00 | NM | 0.92836 | 0.25754 | 0.53200 | 4.26700 | 0.12468 | |
| 3 | 3.2000**-04 | 2.7745**+00 | NM | 0.92942 | 0.25930 | 0.53500 | 4.25700 | 0.12568 | |
| 4 | 3.4500**-04 | 3.4624**+00 | NM | 0.93841 | 0.29747 | 0.59300 | 3.97400 | 0.14922 | |
| 5 | 3.9600**-04 | 4.3155**+00 | NM | 0.94588 | 0.33839 | 0.64800 | 3.66700 | 0.17671 | |
| 6 | 4.7200**-04 | 5.2431**+00 | NM | 0.95064 | 0.37765 | 0.69400 | 3.37700 | 0.20551 | |
| 7 | 5.9900**-04 | 6.9043**+00 | NM | 0.95667 | 0.43906 | 0.75500 | 2.95700 | 0.25533 | |
| 8 | 7.2600**-04 | 8.3789**+00 | NM | 0.95887 | 0.48702 | 0.79400 | 2.65800 | 0.29872 | |
| 9 | 8.5300**-04 | 9.7145**+00 | NM | 0.96083 | 0.52666 | 0.82200 | 2.43600 | 0.33744 | |
| 10 | 9.8000**-04 | 1.0471**+01 | NM | 0.96057 | 0.54785 | 0.83500 | 2.32300 | 0.35945 | |
| 11 | 1.1070**-03 | 1.1641**+01 | NM | 0.96125 | 0.57905 | 0.85300 | 2.17000 | 0.39309 | |
| 12 | 1.2340**-03 | 1.3195**+01 | NM | 0.96183 | 0.61808 | 0.87300 | 1.99500 | 0.43759 | |
| 13 | 1.3610**-03 | 1.3679**+01 | NM | 0.96091 | 0.62972 | 0.87800 | 1.94400 | 0.45165 | |
| 14 | 1.4880**-03 | 1.4182**+01 | NM | 0.96019 | 0.64161 | 0.88300 | 1.89400 | 0.46621 | |
| 15 | 1.6150**-03 | 1.4309**+01 | NM | 0.96169 | 0.64460 | 0.88500 | 1.88500 | 0.46950 | |
| 16 | 1.7420**-03 | 1.4513**+01 | NM | 0.96159 | 0.64933 | 0.88700 | 1.86600 | 0.47535 | |
| 17 | 1.8690**-03 | 1.4769**+01 | NM | 0.96265 | 0.65523 | 0.89000 | 1.84500 | 0.48238 | |
| 18 | 1.9960**-03 | 1.5153**+01 | NM | 0.96345 | 0.66395 | 0.89400 | 1.81300 | 0.49311 | |
| 19 | 2.1230**-03 | 1.5500**+01 | NM | 0.96524 | 0.67176 | 0.89800 | 1.78700 | 0.50252 | |
| 20 | 2.2500**-03 | 1.6499**+01 | NM | 0.96839 | 0.69376 | 0.90800 | 1.71300 | 0.53006 | |
| 21 | 2.3770**-03 | 1.6812**+01 | NM | 0.97158 | 0.70050 | 0.91200 | 1.69500 | 0.53805 | |
| 22 | 2.5040**-03 | 1.7629**+01 | NM | 0.96904 | 0.71781 | 0.91700 | 1.63200 | 0.56189 | |
| 23 | 2.7580**-03 | 1.9009**+01 | NM | 0.97227 | 0.74611 | 0.92800 | 1.54700 | 0.59987 | |
| 24 | 3.0120**-03 | 2.0348**+01 | NM | 0.97609 | 0.77260 | 0.93800 | 1.47400 | 0.63636 | |
| 25 | 3.2660**-03 | 2.1651**+01 | NM | 0.97787 | 0.79752 | 0.94600 | 1.40700 | 0.67235 | |
| 26 | 3.6470**-03 | 2.3658**+01 | NM | 0.98260 | 0.83446 | 0.95800 | 1.31800 | 0.72686 | |
| 27 | 4.2820**-03 | 2.6884**+01 | NM | 0.98874 | 0.89062 | 0.97400 | 1.19600 | 0.81438 | |
| 28 | 4.9170**-03 | 3.0095**+01 | NM | 0.99374 | 0.94321 | 0.98700 | 1.09500 | 0.90137 | |
| 29 | 5.5520**-03 | 3.2231**+01 | NM | 0.99780 | 0.97662 | 0.99500 | 1.03800 | 0.95857 | |
| 30 | 6.1870**-03 | 3.3309**+01 | NM | 1.00027 | 0.99306 | 0.99900 | 1.01200 | 0.98715 | |
| D 31 | 8.7270**-03 | 3.3770**+01 | NM | 1.00000 | 1.00000 | 1.00000 | 1.00000 | 1.00000 | |

INPUT VARIABLES Y,U/UD,T/TD ASSUME P=PD

| | | |
|--|---|----------------|
|  | M: 3.9 (Free stream) R THETA x 10 ⁻³ : 3.4 (Upstream) TW/TR: 1.0 | 7306 |
| | | APG-SBLI AW |
| Axially symmetric blow-down tunnel. Continuous flow. D = 53, L = 165 mm. PO: 0.37 MN/m ² . TO: 300 K. Dried and filtered air. RE/m x 10 ⁻⁶ : 17 (Free stream). | | |
| ROSE W.C., 1973. The behaviour of a compressible turbulent boundary layer in a shock-wave-induced adverse pressure gradient. NASA TN D-7092. <u>And</u> Rose, W.C. private communications. | | |

- 1 The test boundary layer was formed on the nozzle and wall of a small axisymmetric wind tunnel. The nozzle section was about 0.15 m long and fed into the cylindrical test section (D = 52.8, L = 165 mm). The adverse pressure gradient was produced by a 9° semi-apex angle cone (base diameter 33 mm) which could be traversed longitudinally. Initial measurements were made, with the cone retracted, at distances of 66, 71.1 and 76.2 mm from the start of the test section. The main body of tests was made by traversing the cone, and its associated pressure field, past a single traversing assembly mounted at the last of these three stations. It was assumed that the resulting slight changes in the state of the "undisturbed" boundary layer entering the pressure field had negligible effect. The zero for X was taken at the tip of the cone. No trips were used either on
- 2 the tunnel wall or the cone.
- 3 The Mach number in the empty test zone was 3.88 ± 0.02 . No trips were used either on the tunnel wall or the cone. The test boundary layer had passed through the predominantly simple wave favourable
- 4 pressure gradient field of the nozzle (coordinates given in table 3 of the source paper) which resulted in slight overexpansion. This was followed by a weak recompression wave, causing a static pressure rise at the wall of about 10% about 40 mm from the start of the test section. (For a comment on the role of the upstream history see §15). The axial history and transverse disposition
- 2 of non-uniformities were checked by Pitot traverses both on and off the tunnel axis. Axisymmetry
- 5 was checked by static holes at 90° intervals round the test section wall at axial intervals of 25.4 mm.
- 6 Wall pressure measurements were made at 33 positions along the test section at intervals of 2.54 mm with tappings of diameter 0.34 mm. An additional 9 tappings were used to check symmetry. Wall temperature was not measured. The values of TW given in the report were calculated by assuming $r = 0.90$. An initial series of tests designed to detect incipient separation, and so to guide the choice of cone-angle, used an orifice dam, consisting of two 0.34 mm diameter static tappings drilled at 0.75 mm centres on either side of a rectangular fence ($h = 0.13$, $\Delta X = 0.25$ mm). The dam was constructed in a plug of diameter 12.7 mm and the surface of the plug was machined to conform with the radius of the test section, with the central fence of constant height to give a width/height ratio of about 100. (A discussion of the interpretation of orifice dam results, in conjunction with observations of the behaviour of small quantities of alcohol injected as a surface flow visualisation tracer, is given in App. B of the source paper.)
- 7 The TTP used was a FWP of essentially the same construction as the normal HWP used for turbulence measurement (see below), but employed as an unheated resistance probe. A calibration of resistance against wire temperature was made in the empty tunnel for a range of total pressures and temperatures. This was used in conjunction with recovery factors suggested by Laurence and Sandborn (1962) to provide a calibration function over the range of Mach number and wire Reynolds number encountered in the test layer. Pitot pressures were measured with a FPP for which $h_1 = 0.25$, $h_2 = 0.1$, $b_2 = 0.38$ mm. The diameter of the basic tube used increased from 0.63 mm at the tip to 1.65 mm 13 mm back from the tip. The diameter then remained constant to the support approximately 40 mm back.

Two HWP were used, operated in the CT mode at five overheat ratios. All the measurements finally reported were made with two wires, one normal to the flow and the other oblique. During the 30-46 hours that the probes operated, the cold wire resistance changed by 3%. The wires were etched tungsten wires of 5 μm diameter mounted on jewellers broaches tapering from about 50 μm at the tip to about 200 μm 6.3 mm back from the tip. About 3.2 mm of the prongs extended from the end of the 1 mm diameter holder in which they were mounted. The wires were mounted fairly slackly to the prongs which were laterally separated by 0.61 and 0.66 mm for the normal and the oblique wire respectively. The effective l/d ratios were about 100. A DISA model 55D01 constant temperature system was used. Each wire was individually calibrated for each run, and the square wave response was adjusted for each experimental point (1 case for the normal wire, 4 cases for the oblique wire, two each aligned with and perpendicular to the profile normal). The signal interpretation techniques used followed those of Morkovin and Phinney (1958), Morkovin (1956) and Kovaszny (1950, 1953) and give values for the turbulent mass and heat flux, and complete Reynolds stress tensor.

8 As remarked above, the main body of data was obtained at a single station in the tunnel, but over a range of positions relative to the tip of the movable cone centre body. Mean flow and fluctuation profiles were obtained at 12 X values from X = 61.0 to 116.8 mm. For the mean flow profiles, constant Y-intervals of 0.254 mm were used, while turbulence measurements were made at Y-intervals
 9 of 0.508 mm. No interpolation was required for the Pitot and T0 data, but auxiliary assumptions were required for the third necessary state variable, here the static pressure. The pressure field was a consequence of the incident conical shock wave and its associated, distributed, reflected wave system. The author assumed that, outside the boundary layer, the total pressure loss in the incident shock, 0.4%, could be ignored, and that the distributed reflected compression waves were effectively isentropic. Thus, outside the boundary layer, P could be computed from the Rayleigh Pitot formula. The static pressures in this region, and also in the boundary layer, were additionally calculated by the two layer method of Rose (1970). Good agreement was found with the Pitot derived values, and as a cross-check, Pitot profiles within the boundary layer were also calculated and compared with those measured. A graphical comparison (Fig. 9 of the source paper) is given for the input (01) and for the downstream computed profiles 04, 05, and 07, when the wave system has left the boundary layer. Discrepancies are generally less than 5%, reaching a maximum of about 10% near the D-point for profile 07. The authors have selected the D-points on the basis of the total temperature profile which showed a marked "overshoot". No Pitot corrections are reported. Y(min) was
 11 2 h₁. Viscosity values were computed from Sutherland's relation.

12 The editors have presented all the mean flow data as tabulated by the author. Integral values for profiles with substantial discontinuities (03, 04 and to a lesser extent 05, 06) should be ignored. The author's fluctuation data are tabulated in the source paper, which is readily accessible. We therefore have not given tables here, but the data are presented with our normalisation in the
 13 microfiche tables. The single profile sequence consists of two profiles (01, 02) in which the boundary layer is undisturbed, four profiles (03-06) describing the interaction proper, and six
 14 profiles downstream of the interaction in which the boundary layer relaxes towards a linear APG condition. Values for the wall shear stress are given, taken from the graphical presentation in Rubesin et al., (1974), assuming that they used the author's D-state in defining CF.

§ DATA: 73060101-0112. Pitot and T0 profiles obtained separately. NX = 12. Hot-wire measurements with both normal and oblique wires.

15 Editors' comments. This experiment is fully and accessibly reported. We suggest that recourse should be had to the original paper, particularly for discussions of the data reduction (a great deal more calculated information is presented) and of the turbulence measurements, which are barely discussed here.

Much similar work has been performed at the University of Washington (see for instance Sun and Childs 1977) (NASA CR 2872), but this is the first of this series of experiments to become available

with tabulated data including an estimation of the static pressure. Further similar data may become available from Gootzait and Childs (1977).

The boundary layer studied develops through a shock-boundary layer interaction without separation. The shock structure induces discontinuities in the flow (e.g., 0104), and very large changes in static pressure normal to the wall. We have reduced the data following our standard scheme, using the author's estimate of the static pressure (see §9 above) so that velocity, density and temperature profiles should be accurate within the limitations of that estimate. The large static pressure variations imply that the selection of a 'free stream state' is virtually pointless save for providing scaling quantities, and that no conventional integral thickness has any meaning. The only possible boundary layer length scale to which it would be possible to give an unambiguous definition is the displacement thickness as defined in § 7.3 of AGARDograph 253. The calculated integral thicknesses in this entry should therefore be disregarded.

Since the van Driest transformation of the velocity profile is based on a temperature - velocity relationship which holds for APG flows on adiabatic walls but whose validity range for shock-boundary-layer interaction is not known, it is advisable, as the next step, to compare measurements with the theoretical relationship. For this purpose we need a free-stream state and have retained the author's values as they appear very reasonable in relation to the static pressure field (Fig. 1). The temperature profile normalized by T_δ and plotted versus \bar{u}/u_δ is then compared with eqn.(2.5.37) of AGARDograph 253. Agreement between measurements and theory is good, the values differing at most by about 4% downstream of the interaction (Fig. 2). This contradicts the author's statement that the departure of the temperature from the Crocco relationship is substantial. This latter conclusion was drawn on the basis of a plot $(T_t - T_w)/(T_{tD} - T_w)$ which we have shown to be extremely sensitive to small uncertainties in the measurements (cf. § 2.5.6 in AGARDograph 253) and which we consider therefore as an unreliable check. Nevertheless it is the temperature-distribution measurements here which are used to justify Chew & Squire's assumption (1979) of the validity of the van Driest temperature-velocity relationship in a shock-boundary-layer interaction.

Some selected velocity profiles in transformed coordinates are shown in Figs. 3 and 4. It is apparent that the upstream (0101, 0102 - the shock has not yet reached the log-law region) and downstream profiles (0110 and 0111) have a distinct log-law region. A comparison of the wake strength $\Delta(\bar{u}^*/u_t)$ with that of profiles in the same Reynolds number range (Fig. 3.3.6 of AG 253) shows that profiles 0101 to 0103 have a wake strength of approximately 3.2 against about 2. This excess wake strength may well be due to the upstream history of the flow which the author describes as "a history of the favourable pressure gradient in the expansion section and of the slight adverse gradient induced by a recompression wave." Profiles 0104 to 0108 apparently suffer severely from the normal pressure gradient and show no log-law region, with profile 0109 (not in figure) relaxing towards the more typical profile 0110. However, profiles 0110 and 0111 are still far from an "equilibrium" ZPG velocity profile.

The behaviour of the velocity profiles in the boundary layer is reflected similarly in the outer-law plot (Fig. 4) where they are compared with the "standard" ZPG profile. The deviation is largest for profile 0105 and becomes smaller as the profile moves downstream (0111). The shock strength and the subsequent disturbance is much weaker than that in series 05 of Chew & Squire's experiment (CAT 7902). We should note here that all profiles were scaled by using u_t as given in Rubesin et al. (1974), whose data reduction relies heavily on information close to the wall, when the minimum $y_{t,\nu}$ values here are from 14 to 30. These u_t values would seem to be too high by about 10%. Reynolds numbers Re_{δ_2} were rather small, 1035 for 0101 and 1759 for 0110, but little emphasis should be placed on the numerical values for profiles between 02 and 08 because of the strong normal pressure gradient effects.

The Reynolds stresses are tabulated in full in the source paper. All components of the stress tensor are assumed to become zero at the wall except T_{rx} , for which a wall shear stress value was

found by curve fitting to the law of the wall. This wall value appears, in general, not inconsistent with the hot-wire derived values in the boundary layer in the graphical presentation of the source paper.

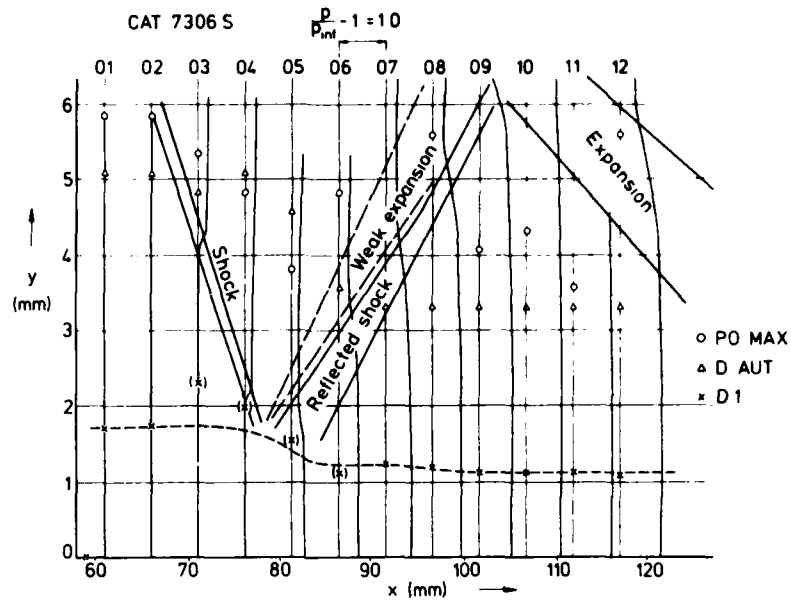


Fig. 1 Static pressure profiles and wave structure for an attached shock boundary-layer interaction. Rose (1973). PO max. Δ Authors' boundary layer edge. X values of D1 calculated without taking account of normal pressure gradient. (X) D1 values which for this reason should be discarded.

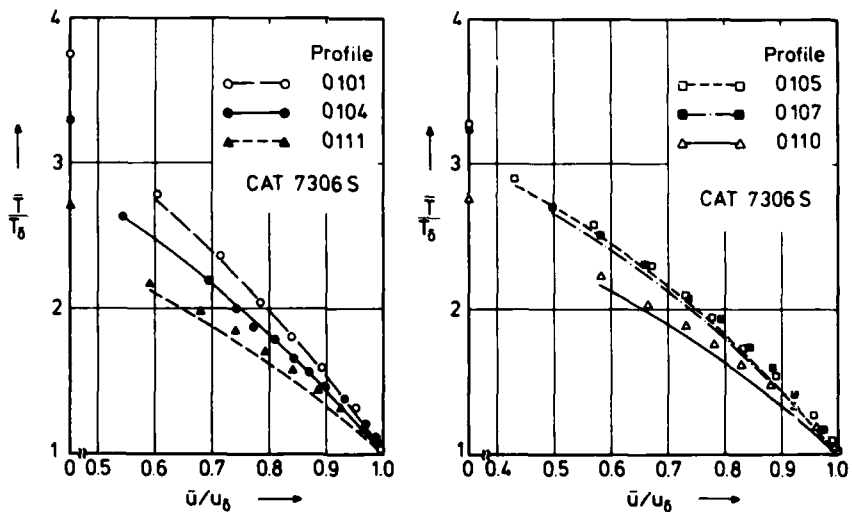


Fig. 2 Comparison between measured and theoretical temperature profiles in a compressible boundary layer with shock interaction (adiabatic wall, origin not defined). Rose (1973).

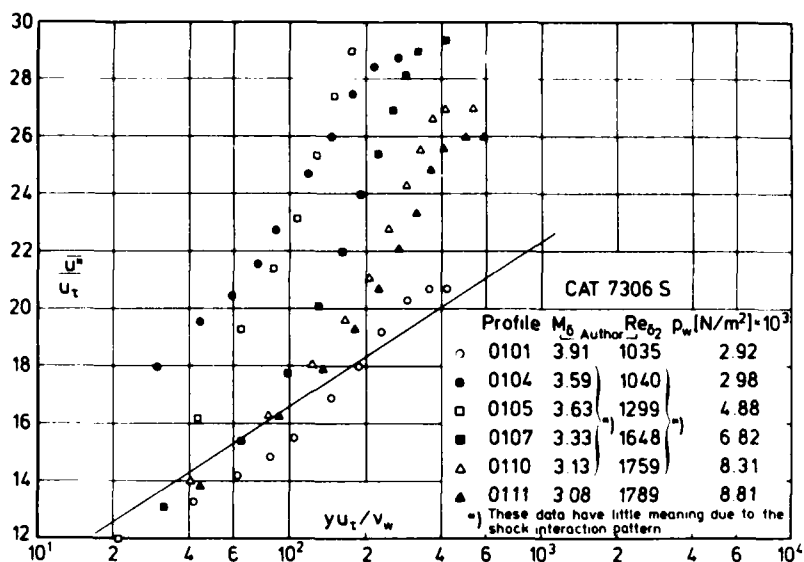


Fig. 3 Law of the wall for a compressible boundary layer with shock interaction (adiabatic wall, origin not defined, D-state author). Rose (1973).

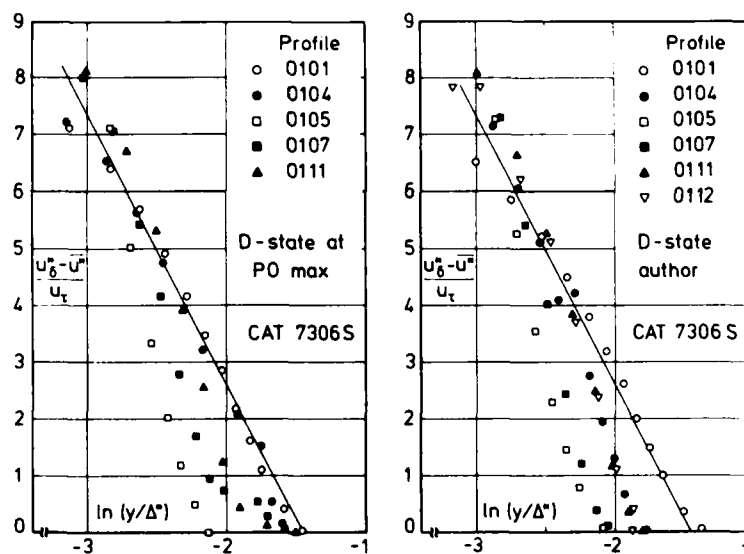


Fig. 4 Outer law for a compressible boundary layer with shock interaction (adiabatic wall, origin not defined). Rose (1973).

| CAT 73065 ROSE BOUNDARY CONDITIONS AND EVALUATED DATA. SI UNITS | | | | | | | | | |
|---|-----------------------|-----------------------|-----------------------|-----------------------|---------|-----------------------|-----------------------|-----------------------|-----------------------|
| RUN | MD * | TW/TR | REDZW | CF * | H12 | H12K | PW* | PD* | |
| X * | POD | PW/PO | REDZD | CO | H32 | H32K | TW* | TD | |
| RZ * | TOD* | TAUW | DZ | PIZ | H42 | D2K | UD | TR | |
| 7306S0101 | 3.9100 | 1.0037 | 1.0351 ⁺⁰³ | 1.7959 ⁻⁰³ | 8.8333 | 1.5396 | 2.9200 ⁺⁰³ | 2.9200 ⁺⁰³ | |
| 6.1000 ⁻⁰² | 3.9295 ⁺⁰⁵ | 1.0000 | 3.4031 ⁺⁰³ | NM | 1.8121 | 1.7923 | 2.7750 ⁺⁰² | 2.7750 ⁺⁰² | 7.3935 ⁺⁰¹ |
| -2.1567 ⁻⁰² | 3.0000 ⁺⁰² | 5.6120 ⁺⁰¹ | 1.9460 ⁻⁰⁴ | NC | -0.0007 | 3.8226 ⁻⁰⁴ | 6.7408 ⁺⁰² | 6.7408 ⁺⁰² | 2.7649 ⁺⁰² |
| 7306S0102 | 3.9100 | 1.0037 | 1.0640 ⁺⁰³ | 1.7551 ⁻⁰³ | 8.8215 | 1.5378 | 2.9200 ⁺⁰³ | 2.9200 ⁺⁰³ | |
| 6.6000 ⁻⁰² | 3.9295 ⁺⁰⁵ | 1.0000 | 3.4981 ⁺⁰³ | NM | 1.8097 | 1.7895 | 2.7750 ⁺⁰² | 2.7750 ⁺⁰² | 7.3935 ⁺⁰¹ |
| -2.2244 ⁻⁰² | 3.0000 ⁺⁰² | 5.4845 ⁺⁰¹ | 2.0003 ⁻⁰⁴ | NC | 0.0040 | 3.9556 ⁻⁰⁴ | 6.7408 ⁺⁰² | 6.7408 ⁺⁰² | 2.7649 ⁺⁰² |
| 7306S0103 | 3.6400 | 1.0016 | 9.0527 ⁺⁰² | 1.7347 ⁻⁰³ | 17.0575 | 1.5936 | 2.9130 ⁺⁰³ | 4.1947 ⁺⁰³ | |
| 7.1100 ⁻⁰² | 3.8967 ⁺⁰⁵ | 0.6944 | 2.6824 ⁺⁰³ | NM | 1.7875 | 1.7701 | 2.7780 ⁺⁰² | 8.2194 ⁺⁰¹ | |
| -2.2898 ⁻⁰² | 3.0000 ⁺⁰² | 6.7488 ⁺⁰¹ | 1.3429 ⁻⁰⁴ | NC | 0.0513 | 3.6571 ⁻⁰⁴ | 6.6165 ⁺⁰² | 2.7735 ⁺⁰² | |
| 7306S0104 | 3.5900 | 1.0010 | 1.0405 ⁺⁰³ | 1.0204 ⁻⁰³ | 13.1583 | 1.5895 | 2.9780 ⁺⁰³ | 4.3777 ⁺⁰³ | |
| 7.6200 ⁻⁰² | 3.7916 ⁺⁰⁵ | 0.6803 | 3.0229 ⁺⁰³ | NM | 1.7992 | 1.7692 | 2.7780 ⁺⁰² | 8.3855 ⁺⁰¹ | |
| -2.3390 ⁻⁰² | 3.0000 ⁺⁰² | 4.0300 ⁺⁰¹ | 1.5146 ⁻⁰⁴ | NC | 0.0045 | 3.9140 ⁻⁰⁴ | 6.5913 ⁺⁰² | 2.7752 ⁺⁰² | |
| 7306S0105 | 3.6300 | 1.0015 | 1.2989 ⁺⁰³ | 7.8571 ⁻⁰⁴ | 8.1688 | 1.8195 | 4.8880 ⁺⁰³ | 4.2526 ⁺⁰³ | |
| 8.1300 ⁻⁰² | 3.8956 ⁺⁰⁵ | 1.1494 | 3.8337 ⁺⁰³ | NM | 1.7148 | 1.6868 | 2.7780 ⁺⁰² | 8.2522 ⁺⁰¹ | |
| -2.3882 ⁻⁰² | 3.0000 ⁺⁰² | 3.0820 ⁺⁰¹ | 1.9097 ⁻⁰⁴ | NC | -0.0284 | 3.7457 ⁻⁰⁴ | 6.6115 ⁺⁰² | 2.7738 ⁺⁰² | |
| 7306S0106 | 3.5900 | 1.0010 | 1.7354 ⁺⁰³ | 1.0000 ⁻⁰³ | 4.2021 | 1.7378 | 5.9690 ⁺⁰³ | 4.3574 ⁺⁰³ | |
| 8.6400 ⁻⁰² | 3.7740 ⁺⁰⁵ | 1.3699 | 5.0418 ⁺⁰³ | NM | 1.7441 | 1.7088 | 2.7780 ⁺⁰² | 8.3855 ⁺⁰¹ | |
| -2.4313 ⁻⁰² | 3.0000 ⁺⁰² | 3.9311 ⁺⁰¹ | 2.5380 ⁻⁰⁴ | NC | -0.0494 | 3.8669 ⁻⁰⁴ | 6.5913 ⁺⁰² | 2.7752 ⁺⁰² | |
| 7306S0107 | 3.3300 | 0.9975 | 1.6485 ⁺⁰³ | 1.0612 ⁻⁰³ | 6.4939 | 1.7614 | 6.8170 ⁺⁰³ | 6.2716 ⁺⁰³ | |
| 9.1400 ⁻⁰² | 3.7482 ⁺⁰⁵ | 1.0870 | 4.3183 ⁺⁰³ | NM | 1.7282 | 1.7014 | 2.7780 ⁺⁰² | 9.3232 ⁺⁰¹ | |
| -2.4658 ⁻⁰² | 3.0000 ⁺⁰² | 5.1662 ⁺⁰¹ | 1.9041 ⁻⁰⁴ | NC | -0.0599 | 3.4750 ⁻⁰⁴ | 6.4467 ⁺⁰² | 2.7850 ⁺⁰² | |
| 7306S0108 | 3.2400 | 0.9962 | 1.7077 ⁺⁰³ | 1.1837 ⁻⁰³ | 6.5374 | 1.7356 | 7.4490 ⁺⁰³ | 7.0765 ⁺⁰³ | |
| 9.6500 ⁻⁰² | 3.7098 ⁺⁰⁵ | 1.0526 | 4.3143 ⁺⁰³ | NM | 1.7362 | 1.7128 | 2.7780 ⁺⁰² | 9.6789 ⁺⁰¹ | |
| -2.5019 ⁻⁰² | 3.0000 ⁺⁰² | 6.1552 ⁺⁰¹ | 1.8307 ⁻⁰⁴ | NC | -0.0595 | 3.3295 ⁻⁰⁴ | 6.3910 ⁺⁰² | 2.7887 ⁺⁰² | |
| 7306S0109 | 3.1800 | 0.9953 | 1.7240 ⁺⁰³ | 1.3265 ⁻⁰³ | 6.7018 | 1.7088 | 7.8800 ⁺⁰³ | 7.7224 ⁺⁰³ | |
| 1.0160 ⁻⁰¹ | 3.7070 ⁺⁰⁵ | 1.0204 | 4.2509 ⁺⁰³ | NM | 1.7462 | 1.7262 | 2.7780 ⁺⁰² | 9.9256 ⁺⁰¹ | |
| -2.5300 ⁻⁰² | 3.0000 ⁺⁰² | 7.2514 ⁺⁰¹ | 1.7473 ⁻⁰⁴ | NC | -0.0684 | 3.1809 ⁻⁰⁴ | 6.3521 ⁺⁰² | 2.7912 ⁺⁰² | |
| 7306S0110 | 3.1300 | 0.9956 | 1.7587 ⁺⁰³ | 1.3367 ⁻⁰³ | 6.7759 | 1.6866 | 8.3140 ⁺⁰³ | 8.3140 ⁺⁰³ | |
| 1.0670 ⁻⁰¹ | 3.7069 ⁺⁰⁵ | 1.0000 | 4.2531 ⁺⁰³ | NM | 1.7562 | 1.7385 | 2.7810 ⁺⁰² | 1.0137 ⁺⁰² | |
| -2.5551 ⁻⁰² | 3.0000 ⁺⁰² | 7.6215 ⁺⁰¹ | 1.7014 ⁻⁰⁴ | NC | -0.0633 | 3.0725 ⁻⁰⁴ | 6.3185 ⁺⁰² | 2.7934 ⁺⁰² | |
| 7306S0111 | 3.0800 | 0.9937 | 1.7888 ⁺⁰³ | 1.4694 ⁻⁰³ | 6.6149 | 1.6773 | 8.8130 ⁺⁰³ | 8.8130 ⁺⁰³ | |
| 1.1180 ⁻⁰¹ | 3.6483 ⁺⁰⁵ | 1.0000 | 4.2354 ⁺⁰³ | NM | 1.7638 | 1.7473 | 2.7780 ⁺⁰² | 1.0355 ⁺⁰² | |
| -2.5762 ⁻⁰² | 3.0000 ⁺⁰² | 8.5992 ⁺⁰¹ | 1.6753 ⁻⁰⁴ | NC | -0.0742 | 2.9555 ⁻⁰⁴ | 6.2839 ⁺⁰² | 2.7957 ⁺⁰² | |
| 7306S0112 | 3.0400 | 0.9930 | 1.8410 ⁺⁰³ | 1.4898 ⁻⁰³ | 6.4623 | 1.6639 | 9.2800 ⁺⁰³ | 9.2800 ⁺⁰³ | |
| 1.1680 ⁻⁰¹ | 3.6192 ⁺⁰⁵ | 1.0000 | 4.2885 ⁺⁰³ | NM | 1.7712 | 1.7558 | 2.7780 ⁺⁰² | 1.0533 ⁺⁰² | |
| -2.5928 ⁻⁰² | 3.0000 ⁺⁰² | 8.9438 ⁺⁰¹ | 1.6732 ⁻⁰⁴ | NC | -0.0784 | 2.8919 ⁻⁰⁴ | 6.2553 ⁺⁰² | 2.7975 ⁺⁰² | |

TAUW CALCULATED FROM CF (RUBESIN ET AL) WITH D-STATE DATA ROSE

| 7306S0101 ROSE PROFILE TABULATION 24 POINTS, DELTA AT POINT 21 | | | | | | | | |
|--|-----------------------|-----------------------|---------|---------|---------|---------|---------|-----------|
| I | Y | PT2/P | P/PD | TO/TOD | M/MD | U/UD | T/TD | R/RD*U/UD |
| 1 | 0.0000 ⁺⁰⁰ | 1.0000 ⁺⁰⁰ | 1.00000 | 0.92500 | 0.00000 | 0.00000 | 3.75330 | 0.00000 |
| 2 | 2.5000 ⁻⁰⁴ | 3.1198 ⁺⁰⁰ | 1.00000 | 0.96200 | 0.36317 | 0.66571 | 2.78165 | 0.21775 |
| 3 | 5.1000 ⁻⁰⁴ | 4.7618 ⁺⁰⁰ | 1.00000 | 0.97000 | 0.46547 | 0.71621 | 2.36748 | 0.30252 |
| 4 | 7.6000 ⁻⁰⁴ | 5.6918 ⁺⁰⁰ | 1.00000 | 0.96700 | 0.51407 | 0.75730 | 2.17017 | 0.34896 |
| 5 | 1.0200 ⁻⁰³ | 6.4377 ⁺⁰⁰ | 1.00000 | 0.96800 | 0.54987 | 0.78555 | 2.04093 | 0.38490 |
| 6 | 1.2700 ⁻⁰³ | 7.2348 ⁺⁰⁰ | 1.00000 | 0.97200 | 0.58568 | 0.81260 | 1.92501 | 0.42213 |
| 7 | 1.5200 ⁻⁰³ | 8.2083 ⁺⁰⁰ | 1.00000 | 0.97800 | 0.62660 | 0.84146 | 1.80339 | 0.46660 |
| 8 | 1.7800 ⁻⁰³ | 9.2483 ⁺⁰⁰ | 1.00000 | 0.98600 | 0.66752 | 0.86868 | 1.69352 | 0.51294 |
| 9 | 2.0300 ⁻⁰³ | 1.0355 ⁺⁰¹ | 1.00000 | 0.99200 | 0.70844 | 0.89277 | 1.58810 | 0.56217 |
| 10 | 2.2900 ⁻⁰³ | 1.1452 ⁺⁰¹ | 1.00000 | 0.99800 | 0.74680 | 0.91369 | 1.49689 | 0.61040 |
| 11 | 2.5400 ⁻⁰³ | 1.2766 ⁺⁰¹ | 1.00000 | 1.00500 | 0.79028 | 0.93558 | 1.40153 | 0.66755 |
| 12 | 2.7900 ⁻⁰³ | 1.3987 ⁺⁰¹ | 1.00000 | 1.01000 | 0.82864 | 0.95283 | 1.32220 | 0.72064 |
| 13 | 3.0500 ⁻⁰³ | 1.5180 ⁺⁰¹ | 1.00000 | 1.01500 | 0.86445 | 0.96794 | 1.25377 | 0.77202 |
| 14 | 3.3000 ⁻⁰³ | 1.6513 ⁺⁰¹ | 1.00000 | 1.01800 | 0.90281 | 0.98188 | 1.18283 | 0.83011 |
| 15 | 3.5600 ⁻⁰³ | 1.7435 ⁺⁰¹ | 1.00000 | 1.01700 | 0.92839 | 0.98912 | 1.13512 | 0.87138 |
| 16 | 3.8100 ⁻⁰³ | 1.8382 ⁺⁰¹ | 1.00000 | 1.01400 | 0.95396 | 0.99493 | 1.08773 | 0.91468 |
| 17 | 4.0600 ⁻⁰³ | 1.9158 ⁺⁰¹ | 1.00000 | 1.01000 | 0.97442 | 0.99847 | 1.04995 | 0.95096 |
| 18 | 4.3200 ⁻⁰³ | 1.9652 ⁺⁰¹ | 1.00000 | 1.00800 | 0.98721 | 1.00078 | 1.02768 | 0.97383 |
| 19 | 4.5700 ⁻⁰³ | 1.9951 ⁺⁰¹ | 1.00000 | 1.00500 | 0.99488 | 1.00123 | 1.01279 | 0.98858 |
| 20 | 4.8300 ⁻⁰³ | 2.0051 ⁺⁰¹ | 1.00000 | 1.00200 | 0.99744 | 1.00037 | 1.00587 | 0.99453 |
| D 21 | 5.0800 ⁻⁰³ | 2.0152 ⁺⁰¹ | 1.00000 | 1.00000 | 1.00000 | 1.00000 | 1.00000 | 1.00000 |
| 22 | 5.3300 ⁻⁰³ | 2.0152 ⁺⁰¹ | 1.00000 | 1.00000 | 1.00000 | 1.00000 | 1.00000 | 1.00000 |
| 23 | 5.5900 ⁻⁰³ | 2.0152 ⁺⁰¹ | 1.00000 | 1.00000 | 1.00000 | 1.00000 | 1.00000 | 1.00000 |
| 24 | 5.8400 ⁻⁰³ | 2.0152 ⁺⁰¹ | 1.00000 | 1.00000 | 1.00000 | 1.00000 | 1.00000 | 1.00000 |

INPUT VARIABLES Y, TO/TOD, P/PW, M

| 7306S0104 | | ROSE | PROFILE TABULATION | | | 25 POINTS, DELTA AT POINT 19 | | | |
|-----------|-----------------------|-----------------------|--------------------|---------|---------|------------------------------|---------|-----------|--|
| I | Y | PT2/P | P/PD | TO/TOD | M/MD | U/UD | T/TD | R/RD*U/UD | |
| 1 | 0.0000 ⁺⁰⁰ | 1.0000 ⁺⁰⁰ | 0.68027 | 0.92907 | 0.00000 | 0.00000 | 3.30957 | 0.00000 | |
| 2 | 2.5000 ⁻⁰⁴ | 2.4075 ⁺⁰⁰ | 0.68027 | 0.94905 | 0.33426 | 0.54271 | 2.63614 | 0.14005 | |
| 3 | 5.1000 ⁻⁰⁴ | 4.1379 ⁺⁰⁰ | 0.67347 | 0.96004 | 0.46797 | 0.69338 | 2.19540 | 0.21270 | |
| 4 | 7.6000 ⁻⁰⁴ | 5.0934 ⁺⁰⁰ | 0.67347 | 0.96204 | 0.52646 | 0.74594 | 2.00756 | 0.25024 | |
| 5 | 1.0200 ⁻⁰³ | 5.7952 ⁺⁰⁰ | 0.67347 | 0.95504 | 0.56546 | 0.77389 | 1.87305 | 0.27826 | |
| 6 | 1.2700 ⁻⁰³ | 6.6042 ⁺⁰⁰ | 0.67347 | 0.96903 | 0.60724 | 0.80958 | 1.77742 | 0.30675 | |
| 7 | 1.5200 ⁻⁰³ | 7.5920 ⁺⁰⁰ | 0.67347 | 0.97502 | 0.65460 | 0.84276 | 1.65753 | 0.34242 | |
| 8 | 1.7800 ⁻⁰³ | 8.5261 ⁺⁰⁰ | 0.67347 | 0.98202 | 0.69638 | 0.87018 | 1.56146 | 0.37532 | |
| 9 | 2.0300 ⁻⁰³ | 9.6554 ⁺⁰⁰ | 0.67347 | 0.98901 | 0.74373 | 0.89823 | 1.45863 | 0.41473 | |
| 10 | 2.2900 ⁻⁰³ | 9.1813 ⁺⁰⁰ | 0.89116 | 1.00200 | 0.72423 | 0.89411 | 1.52414 | 0.52278 | |
| 11 | 2.5400 ⁻⁰³ | 1.0933 ⁺⁰¹ | 0.90476 | 1.01399 | 0.79387 | 0.93334 | 1.38223 | 0.61093 | |
| 12 | 2.7900 ⁻⁰³ | 1.2138 ⁺⁰¹ | 0.91837 | 1.01698 | 0.83844 | 0.95371 | 1.29387 | 0.67693 | |
| 13 | 3.0500 ⁻⁰³ | 1.3329 ⁺⁰¹ | 0.93197 | 1.01698 | 0.88022 | 0.96983 | 1.21396 | 0.74455 | |
| 14 | 3.3000 ⁻⁰³ | 1.4662 ⁺⁰¹ | 0.94558 | 1.01598 | 0.92479 | 0.98493 | 1.13429 | 0.82107 | |
| 15 | 3.5600 ⁻⁰³ | 1.5884 ⁺⁰¹ | 0.95238 | 1.01199 | 0.96379 | 0.99538 | 1.06664 | 0.88876 | |
| 16 | 3.8100 ⁻⁰³ | 1.6696 ⁺⁰¹ | 0.95918 | 1.00799 | 0.98886 | 1.00082 | 1.02435 | 0.93716 | |
| 17 | 4.0600 ⁻⁰³ | 1.7156 ⁺⁰¹ | 0.97279 | 1.00500 | 1.00279 | 1.00327 | 1.00097 | 0.97503 | |
| 18 | 4.3200 ⁻⁰³ | 1.7156 ⁺⁰¹ | 0.98639 | 1.00200 | 1.00279 | 1.00178 | 0.99799 | 0.99014 | |
| D 19 | 4.5700 ⁻⁰³ | 1.7063 ⁺⁰¹ | 1.00000 | 1.00000 | 1.00000 | 1.00000 | 1.00000 | 1.00000 | |
| 20 | 4.8300 ⁻⁰³ | 1.7063 ⁺⁰¹ | 1.00680 | 1.00000 | 1.00000 | 1.00000 | 1.00000 | 1.00680 | |
| 21 | 5.0800 ⁻⁰³ | 1.6879 ⁺⁰¹ | 1.02041 | 0.99900 | 0.99443 | 0.99793 | 1.00706 | 1.01116 | |
| 22 | 5.3300 ⁻⁰³ | 1.6787 ⁺⁰¹ | 1.03401 | 0.99900 | 0.99164 | 0.99714 | 1.01113 | 1.01972 | |
| 23 | 5.5900 ⁻⁰³ | 1.6787 ⁺⁰¹ | 1.04082 | 0.99900 | 0.99164 | 0.99714 | 1.01113 | 1.02642 | |
| 24 | 5.8400 ⁻⁰³ | 1.6696 ⁺⁰¹ | 1.04762 | 0.99900 | 0.98886 | 0.99635 | 1.01521 | 1.02816 | |
| 25 | 6.1000 ⁻⁰³ | 1.6696 ⁺⁰¹ | 1.05442 | 0.99900 | 0.98886 | 0.99635 | 1.01521 | 1.03483 | |

INPUT VARIABLES Y, TO/TOD, P/PW, M

| 7306S0105 | | ROSE | PROFILE TABULATION | | | 22 POINTS, DELTA AT POINT 17 | | | |
|-----------|-----------------------|-----------------------|--------------------|---------|---------|------------------------------|---------|-----------|--|
| I | Y | PT2/P | P/PD | TO/TOD | M/MD | U/UD | T/TD | R/RD*U/UD | |
| 1 | 0.0000 ⁺⁰⁰ | 1.0000 ⁺⁰⁰ | 1.14943 | 0.92507 | 0.00000 | 0.00000 | 3.36300 | 0.00000 | |
| 2 | 2.5000 ⁻⁰⁴ | 1.6913 ⁺⁰⁰ | 1.14943 | 0.95405 | 0.24793 | 0.42834 | 2.98478 | 0.16495 | |
| 3 | 5.1000 ⁻⁰⁴ | 2.5875 ⁺⁰⁰ | 1.14943 | 0.96404 | 0.34711 | 0.56612 | 2.66003 | 0.24463 | |
| 4 | 7.6000 ⁻⁰⁴ | 3.6846 ⁺⁰⁰ | 1.14943 | 0.97003 | 0.43251 | 0.66471 | 2.36201 | 0.32347 | |
| 5 | 1.0200 ⁻⁰³ | 4.6237 ⁺⁰⁰ | 1.13793 | 0.97602 | 0.49311 | 0.72514 | 2.16247 | 0.38158 | |
| 6 | 1.2700 ⁻⁰³ | 5.5386 ⁺⁰⁰ | 1.11494 | 0.98701 | 0.54545 | 0.77355 | 2.01121 | 0.42883 | |
| 7 | 1.5200 ⁻⁰³ | 7.0597 ⁺⁰⁰ | 1.06897 | 0.99500 | 0.62259 | 0.83282 | 1.78936 | 0.49753 | |
| 8 | 1.7800 ⁻⁰³ | 8.7851 ⁺⁰⁰ | 1.02299 | 1.00500 | 0.69972 | 0.88376 | 1.59521 | 0.56675 | |
| 9 | 2.0300 ⁻⁰³ | 1.0569 ⁺⁰¹ | 0.97701 | 1.01299 | 0.77135 | 0.92370 | 1.43403 | 0.62932 | |
| 10 | 2.2900 ⁻⁰³ | 1.2216 ⁺⁰¹ | 0.93103 | 1.01698 | 0.83196 | 0.95190 | 1.30914 | 0.67698 | |
| 11 | 2.5400 ⁻⁰³ | 1.3574 ⁺⁰¹ | 0.91954 | 1.01698 | 0.87879 | 0.96989 | 1.21807 | 0.73218 | |
| 12 | 2.7900 ⁻⁰³ | 1.4920 ⁺⁰¹ | 0.93103 | 1.01499 | 0.92287 | 0.98417 | 1.13726 | 0.80570 | |
| 13 | 3.0500 ⁻⁰³ | 1.6062 ⁺⁰¹ | 0.94253 | 1.01299 | 0.95868 | 0.99450 | 1.07613 | 0.87103 | |
| 14 | 3.3000 ⁻⁰³ | 1.7156 ⁺⁰¹ | 0.95402 | 1.00799 | 0.99174 | 1.00168 | 1.02017 | 0.93674 | |
| 15 | 3.5600 ⁻⁰³ | 1.7622 ⁺⁰¹ | 0.96552 | 1.00500 | 1.00551 | 1.00400 | 0.99701 | 0.97229 | |
| 16 | 3.8100 ⁻⁰³ | 1.7716 ⁺⁰¹ | 0.97701 | 1.00200 | 1.00826 | 1.00325 | 0.99009 | 0.99001 | |
| D 17 | 4.0600 ⁻⁰³ | 1.7435 ⁺⁰¹ | 1.00000 | 1.00000 | 1.00000 | 1.00000 | 1.00000 | 1.00000 | |
| 18 | 4.3200 ⁻⁰³ | 1.7248 ⁺⁰¹ | 1.02299 | 1.00000 | 0.99449 | 0.99848 | 1.00803 | 1.01329 | |
| 19 | 4.5700 ⁻⁰³ | 1.6971 ⁺⁰¹ | 1.04598 | 0.99900 | 0.98623 | 0.99566 | 1.01921 | 1.02180 | |
| 20 | 4.8300 ⁻⁰³ | 1.6879 ⁺⁰¹ | 1.05747 | 0.99900 | 0.98347 | 0.99487 | 1.02332 | 1.02807 | |
| 21 | 5.0800 ⁻⁰³ | 1.6787 ⁺⁰¹ | 1.06897 | 0.99900 | 0.98072 | 0.99409 | 1.02745 | 1.03425 | |
| 22 | 5.3300 ⁻⁰³ | 1.6696 ⁺⁰¹ | 1.08046 | 0.99900 | 0.97796 | 0.99329 | 1.03160 | 1.04034 | |

INPUT VARIABLES Y, TO/TOD, P/PW, M

| 7306S0107 | | ROSE | PROFILE TABULATION | | | 27 POINTS, DELTA AT POINT 14 | | | |
|-----------|-----------------------|-----------------------|--------------------|---------|---------|------------------------------|---------|-----------|--|
| I | Y | PT2/P | P/PD | TO/TOD | M/MD | U/UD | T/TD | R/RD*U/UD | |
| 1 | 0.0000 ⁺⁰⁰ | 1.0000 ⁺⁰⁰ | 1.08696 | 0.92600 | 0.00000 | 0.00000 | 2.97966 | 0.00000 | |
| 2 | 2.5000 ⁻⁰⁴ | 2.0325 ⁺⁰⁰ | 1.08696 | 0.96000 | 0.31832 | 0.50554 | 2.52227 | 0.21786 | |
| 3 | 5.1000 ⁻⁰⁴ | 2.6500 ⁺⁰⁰ | 1.08696 | 0.96800 | 0.38438 | 0.58876 | 2.34606 | 0.27278 | |
| 4 | 7.6000 ⁻⁰⁴ | 3.4894 ⁺⁰⁰ | 1.08696 | 0.97800 | 0.45646 | 0.66967 | 2.15241 | 0.33818 | |
| 5 | 1.0200 ⁻⁰³ | 4.5330 ⁺⁰⁰ | 1.08696 | 0.99100 | 0.53153 | 0.74423 | 1.96044 | 0.41263 | |
| 6 | 1.2700 ⁻⁰³ | 5.6404 ⁺⁰⁰ | 1.08696 | 1.00600 | 0.60060 | 0.80543 | 1.79838 | 0.48681 | |
| 7 | 1.5200 ⁻⁰³ | 7.0018 ⁺⁰⁰ | 1.08696 | 1.01300 | 0.67568 | 0.85991 | 1.61968 | 0.57708 | |
| 8 | 1.7800 ⁻⁰³ | 8.2713 ⁺⁰⁰ | 1.08696 | 1.01800 | 0.73874 | 0.89932 | 1.48200 | 0.65960 | |
| 9 | 2.0300 ⁻⁰³ | 1.0002 ⁺⁰¹ | 1.07609 | 1.02100 | 0.81682 | 0.94019 | 1.32491 | 0.76362 | |
| 10 | 2.2900 ⁻⁰³ | 1.1754 ⁺⁰¹ | 1.06522 | 1.02100 | 0.88099 | 0.97116 | 1.19367 | 0.86665 | |
| 11 | 2.5400 ⁻⁰³ | 1.3329 ⁺⁰¹ | 1.04348 | 1.01600 | 0.94895 | 0.99110 | 1.09080 | 0.94810 | |
| 12 | 2.7900 ⁻⁰³ | 1.4155 ⁺⁰¹ | 1.03261 | 1.00700 | 0.97898 | 0.99679 | 1.03672 | 0.99284 | |
| 13 | 3.0500 ⁻⁰³ | 1.4662 ⁺⁰¹ | 1.01087 | 1.00300 | 0.99700 | 1.00056 | 1.00716 | 1.00424 | |
| D 14 | 3.3000 ⁻⁰³ | 1.4748 ⁺⁰¹ | 1.00000 | 1.00000 | 1.00000 | 1.00000 | 1.00000 | 1.00000 | |
| 15 | 3.5600 ⁻⁰³ | 1.4920 ⁺⁰¹ | 0.95652 | 1.00000 | 1.00601 | 1.00185 | 0.99176 | 0.96625 | |
| 16 | 3.8100 ⁻⁰³ | 1.5442 ⁺⁰¹ | 0.88043 | 1.00000 | 1.02402 | 1.00728 | 0.96757 | 0.91657 | |
| 17 | 4.0600 ⁻⁰³ | 1.5530 ⁺⁰¹ | 0.84783 | 1.00000 | 1.02703 | 1.00817 | 0.96361 | 0.88703 | |
| 18 | 4.3200 ⁻⁰³ | 1.6152 ⁺⁰¹ | 0.78261 | 1.00000 | 1.04805 | 1.01422 | 0.93648 | 0.84757 | |
| 19 | 4.5700 ⁻⁰³ | 1.6604 ⁺⁰¹ | 0.71739 | 1.00000 | 1.06306 | 1.01838 | 0.91771 | 0.79609 | |
| 20 | 4.8300 ⁻⁰³ | 1.6879 ⁺⁰¹ | 0.70652 | 1.00000 | 1.07207 | 1.02082 | 0.90668 | 0.79547 | |
| 21 | 5.0800 ⁻⁰³ | 1.6787 ⁺⁰¹ | 0.71739 | 1.00000 | 1.06907 | 1.02001 | 0.91034 | 0.80382 | |
| 22 | 5.3300 ⁻⁰³ | 1.6696 ⁺⁰¹ | 0.72826 | 1.00000 | 1.06607 | 1.01920 | 0.91401 | 0.81207 | |
| 23 | 5.5900 ⁻⁰³ | 1.6604 ⁺⁰¹ | 0.73913 | 1.00000 | 1.06306 | 1.01838 | 0.91771 | 0.82022 | |
| 24 | 5.8400 ⁻⁰³ | 1.6423 ⁺⁰¹ | 0.75000 | 1.00000 | 1.05706 | 1.01673 | 0.92516 | 0.82424 | |
| 25 | 6.1000 ⁻⁰³ | 1.6332 ⁺⁰¹ | 0.76087 | 1.00000 | 1.05405 | 1.01590 | 0.92891 | 0.83212 | |
| 26 | 6.3500 ⁻⁰³ | 1.6423 ⁺⁰¹ | 0.76087 | 1.00000 | 1.05706 | 1.01673 | 0.92516 | 0.83618 | |
| 27 | 6.6000 ⁻⁰³ | 1.6332 ⁺⁰¹ | 0.77174 | 1.00000 | 1.05405 | 1.01590 | 0.92891 | 0.84401 | |

INPUT VARIABLES Y, TO/TOD, P/PW, M

| 7306S0110 | | ROSE | PROFILE TABULATION | | | 27 POINTS, DELTA AT POINT 14 | | | |
|-----------|-----------|-----------|--------------------|---------|---------|------------------------------|---------|-----------|--|
| I | Y | PT2/P | P/PD | TO/TOD | M/MD | U/UD | T/TD | R/RD*U/UD | |
| 1 | 0.0000+00 | 1.0000+00 | 1.00000 | 0.92515 | 0.00000 | 0.00000 | 2.73787 | 0.00000 | |
| 2 | 2.5000-04 | 2.4663+00 | 1.00000 | 0.96806 | 0.38978 | 0.57914 | 2.20749 | 0.26733 | |
| 3 | 5.1000-04 | 3.2643+00 | 1.00000 | 0.97804 | 0.46645 | 0.66448 | 2.02928 | 0.32744 | |
| 4 | 7.6000-04 | 4.0531+00 | 1.00000 | 0.99102 | 0.53035 | 0.72926 | 1.89076 | 0.38570 | |
| 5 | 1.0200-03 | 4.8552+00 | 1.00000 | 0.99800 | 0.58786 | 0.78011 | 1.76104 | 0.44299 | |
| 6 | 1.2700-03 | 5.7952+00 | 1.00000 | 1.00599 | 0.64856 | 0.82772 | 1.62878 | 0.50818 | |
| 7 | 1.5200-03 | 7.1178+00 | 1.00000 | 1.01198 | 0.72524 | 0.88076 | 1.47486 | 0.59718 | |
| 8 | 1.7800-03 | 8.5905+00 | 1.00000 | 1.01597 | 0.80192 | 0.92494 | 1.33036 | 0.69526 | |
| 9 | 2.0300-03 | 1.0283+01 | 1.00000 | 1.01896 | 0.88179 | 0.96392 | 1.19496 | 0.80666 | |
| 10 | 2.2900-03 | 1.1678+01 | 1.00000 | 1.01896 | 0.94249 | 0.98865 | 1.10035 | 0.89849 | |
| 11 | 2.5400-03 | 1.2529+01 | 1.00000 | 1.01198 | 0.97764 | 0.99820 | 1.04250 | 0.95750 | |
| 12 | 2.7900-03 | 1.2925+01 | 1.00000 | 1.00399 | 0.99361 | 0.99982 | 1.01253 | 0.98744 | |
| 13 | 3.0500-03 | 1.3006+01 | 1.00000 | 1.00100 | 0.99681 | 0.99942 | 1.00524 | 0.99420 | |
| 14 | 3.3000-03 | 1.3086+01 | 1.00000 | 1.00000 | 1.00000 | 1.00000 | 1.00000 | 1.00000 | |
| 15 | 3.5600-03 | 1.3086+01 | 1.00000 | 1.00000 | 1.00000 | 1.00000 | 1.00000 | 1.00000 | |
| 16 | 3.8100-03 | 1.3086+01 | 1.00000 | 1.00000 | 1.00000 | 1.00000 | 1.00000 | 1.00000 | |
| 17 | 4.0600-03 | 1.3086+01 | 0.99000 | 1.00000 | 1.00000 | 1.00000 | 1.00000 | 0.99000 | |
| 18 | 4.3200-03 | 1.3247+01 | 0.98000 | 1.00000 | 1.00639 | 1.00215 | 0.99158 | 0.99044 | |
| 19 | 4.5700-03 | 1.3247+01 | 0.97000 | 1.00000 | 1.00639 | 1.00215 | 0.99158 | 0.98033 | |
| 20 | 4.8300-03 | 1.3329+01 | 0.96000 | 1.00000 | 1.00958 | 1.00321 | 0.98741 | 0.97536 | |
| 21 | 5.0800-03 | 1.3329+01 | 0.96000 | 1.00000 | 1.00958 | 1.00321 | 0.98741 | 0.97536 | |
| 22 | 5.3300-03 | 1.3329+01 | 0.95000 | 1.00000 | 1.00958 | 1.00321 | 0.98741 | 0.96520 | |
| 23 | 5.5900-03 | 1.3410+01 | 0.94000 | 1.00000 | 1.01278 | 1.00426 | 0.98325 | 0.96009 | |
| 24 | 5.8400-03 | 1.3410+01 | 0.93000 | 1.00000 | 1.01278 | 1.00426 | 0.98325 | 0.94987 | |
| 25 | 6.1000-03 | 1.3574+01 | 0.91000 | 1.00000 | 1.01917 | 1.00636 | 0.97501 | 0.93925 | |
| 26 | 6.3500-03 | 1.3821+01 | 0.89000 | 1.00000 | 1.02875 | 1.00944 | 0.96281 | 0.93310 | |
| 27 | 6.6000-03 | 1.3904+01 | 0.87000 | 1.00000 | 1.03195 | 1.01046 | 0.95879 | 0.91689 | |

INPUT VARIABLES Y, TO/TOD, P/PW, M

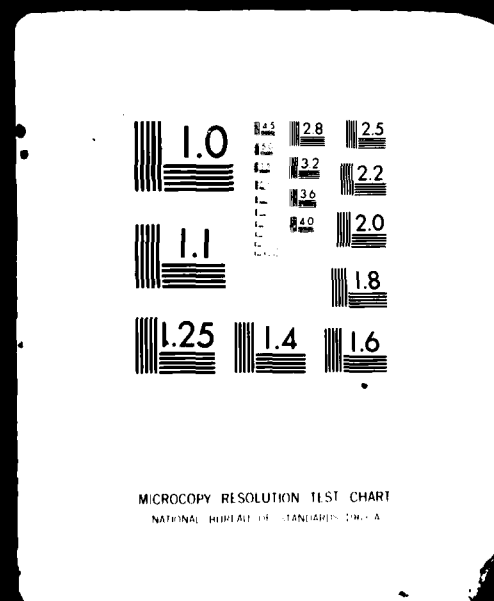
| 7306S0111 | | ROSE | PROFILE TABULATION | | | 19 POINTS, DELTA AT POINT 14 | | | |
|-----------|-----------|-----------|--------------------|---------|---------|------------------------------|---------|-----------|--|
| I | Y | PT2/P | P/PD | TO/TOD | M/MD | U/UD | T/TD | R/RD*U/UD | |
| 1 | 0.0000+00 | 1.0000+00 | 1.00000 | 0.92600 | 0.00000 | 0.00000 | 2.68288 | 0.00000 | |
| 2 | 2.5000-04 | 2.5263+00 | 1.00000 | 0.97300 | 0.40260 | 0.59115 | 2.15603 | 0.27418 | |
| 3 | 5.1000-04 | 3.4133+00 | 1.00000 | 0.98300 | 0.48701 | 0.68254 | 1.96416 | 0.34750 | |
| 4 | 7.6000-04 | 4.1807+00 | 1.00000 | 0.99400 | 0.54870 | 0.74286 | 1.83290 | 0.40529 | |
| 5 | 1.0200-03 | 5.0452+00 | 1.00000 | 0.99700 | 0.61039 | 0.79405 | 1.69232 | 0.46921 | |
| 6 | 1.2700-03 | 6.0051+00 | 1.00000 | 1.00300 | 0.67208 | 0.84074 | 1.56489 | 0.53725 | |
| 7 | 1.5200-03 | 7.1762+00 | 1.00000 | 1.01000 | 0.74026 | 0.88666 | 1.43466 | 0.61803 | |
| 8 | 1.7800-03 | 8.5261+00 | 1.00000 | 1.01600 | 0.81169 | 0.92841 | 1.30828 | 0.70964 | |
| 9 | 2.0300-03 | 1.0142+01 | 1.00000 | 1.02100 | 0.88961 | 0.96740 | 1.18253 | 0.81808 | |
| 10 | 2.2900-03 | 1.1452+01 | 1.00000 | 1.01800 | 0.94805 | 0.98991 | 1.09025 | 0.90797 | |
| 11 | 2.5400-03 | 1.2216+01 | 1.00000 | 1.01200 | 0.98052 | 0.99909 | 1.03823 | 0.96230 | |
| 12 | 2.7900-03 | 1.2607+01 | 1.00000 | 1.00600 | 0.99675 | 1.00187 | 1.01029 | 0.99166 | |
| 13 | 3.0500-03 | 1.2687+01 | 1.00000 | 1.00300 | 1.00000 | 1.00150 | 1.00300 | 0.99850 | |
| 14 | 3.3000-03 | 1.2687+01 | 1.00000 | 1.00000 | 1.00000 | 1.00000 | 1.00000 | 1.00000 | |
| 15 | 3.5600-03 | 1.2846+01 | 0.99000 | 1.00000 | 1.00649 | 1.00223 | 0.99154 | 1.00067 | |
| 16 | 3.8100-03 | 1.2846+01 | 0.99000 | 1.00000 | 1.00649 | 1.00223 | 0.99154 | 1.00067 | |
| 17 | 4.0600-03 | 1.2766+01 | 0.99000 | 1.00000 | 1.00325 | 1.00112 | 0.99576 | 0.99533 | |
| 18 | 4.3200-03 | 1.2846+01 | 0.98000 | 1.00000 | 1.00649 | 1.00223 | 0.99154 | 0.99056 | |
| 19 | 4.5700-03 | 1.2925+01 | 0.97000 | 1.00000 | 1.00974 | 1.00333 | 0.98734 | 0.98571 | |

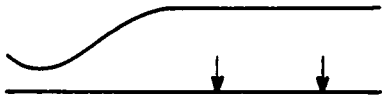
INPUT VARIABLES Y, TO/TOD, P/PW, M

| 7306S0112 | | ROSE | PROFILE TABULATION | | | 27 POINTS, DELTA AT POINT 14 | | | |
|-----------|-----------|-----------|--------------------|---------|---------|------------------------------|---------|-----------|--|
| I | Y | PT2/P | P/PD | TO/TOD | M/MD | U/UD | T/TD | R/RD*U/UD | |
| 1 | 0.0000+00 | 1.0000+00 | 1.00000 | 0.92600 | 0.00000 | 0.00000 | 2.63754 | 0.00000 | |
| 2 | 2.5000-04 | 2.6186+00 | 1.00000 | 0.97600 | 0.41776 | 0.60567 | 2.10192 | 0.28815 | |
| 3 | 5.1000-04 | 3.5279+00 | 1.00000 | 0.98700 | 0.50329 | 0.69644 | 1.91481 | 0.36371 | |
| 4 | 7.6000-04 | 4.2672+00 | 1.00000 | 0.99400 | 0.56250 | 0.75183 | 1.78647 | 0.42085 | |
| 5 | 1.0200-03 | 5.0934+00 | 1.00000 | 0.99700 | 0.62171 | 0.80015 | 1.65641 | 0.48306 | |
| 6 | 1.2700-03 | 6.0051+00 | 1.00000 | 1.00300 | 0.68092 | 0.84457 | 1.53845 | 0.54898 | |
| 7 | 1.5200-03 | 7.1762+00 | 1.00000 | 1.01100 | 0.75000 | 0.89115 | 1.41182 | 0.63121 | |
| 8 | 1.7800-03 | 8.4620+00 | 1.00000 | 1.01800 | 0.81908 | 0.93190 | 1.29445 | 0.71992 | |
| 9 | 2.0300-03 | 1.0002+01 | 1.00000 | 1.02000 | 0.89474 | 0.96848 | 1.17164 | 0.82661 | |
| 10 | 2.2900-03 | 1.1228+01 | 1.00000 | 1.01800 | 0.95066 | 0.99061 | 1.08582 | 0.91232 | |
| 11 | 2.5400-03 | 1.1984+01 | 1.00000 | 1.01200 | 0.98355 | 1.00008 | 1.03389 | 0.96730 | |
| 12 | 2.7900-03 | 1.2216+01 | 1.00000 | 1.00600 | 0.99342 | 1.00066 | 1.01463 | 0.98623 | |
| 13 | 3.0500-03 | 1.2372+01 | 1.00000 | 1.00200 | 1.00000 | 1.00100 | 1.00200 | 0.99900 | |
| 14 | 3.3000-03 | 1.2372+01 | 1.00000 | 1.00000 | 1.00000 | 1.00000 | 1.00000 | 1.00000 | |
| 15 | 3.5600-03 | 1.2450+01 | 0.99000 | 1.00000 | 1.00329 | 1.00115 | 0.99574 | 0.99538 | |
| 16 | 3.8100-03 | 1.2529+01 | 0.98000 | 1.00000 | 1.00658 | 1.00230 | 0.99151 | 0.99066 | |
| 17 | 4.0600-03 | 1.2607+01 | 0.97000 | 1.00000 | 1.00987 | 1.00343 | 0.98729 | 0.98586 | |
| 18 | 4.3200-03 | 1.2607+01 | 0.95000 | 1.00000 | 1.00987 | 1.00343 | 0.98729 | 0.96553 | |
| 19 | 4.5700-03 | 1.3167+01 | 0.89000 | 1.00000 | 1.03289 | 1.01119 | 0.95841 | 0.93901 | |
| 20 | 4.8300-03 | 1.3410+01 | 0.84000 | 1.00000 | 1.04276 | 1.01441 | 0.94635 | 0.90041 | |
| 21 | 5.0800-03 | 1.3904+01 | 0.78000 | 1.00000 | 1.06250 | 1.02067 | 0.92281 | 0.86272 | |
| 22 | 5.3300-03 | 1.4407+01 | 0.72000 | 1.00000 | 1.08224 | 1.02670 | 0.89999 | 0.82136 | |
| 23 | 5.5900-03 | 1.4834+01 | 0.67000 | 1.00000 | 1.09868 | 1.03155 | 0.88153 | 0.78402 | |
| 24 | 5.8400-03 | 1.5267+01 | 0.62000 | 1.00000 | 1.11513 | 1.03626 | 0.86354 | 0.74401 | |
| 25 | 6.1000-03 | 1.5706+01 | 0.57000 | 1.00000 | 1.13198 | 1.04082 | 0.84602 | 0.70124 | |
| 26 | 6.3500-03 | 1.4920+01 | 0.57000 | 1.00000 | 1.10197 | 1.03250 | 0.87789 | 0.67039 | |
| 27 | 6.6000-03 | 1.8095+01 | 0.45000 | 1.00000 | 1.21711 | 1.06244 | 0.76199 | 0.62743 | |

INPUT VARIABLES Y, TO/TOD, P/PW, M

2 OF 3
AD
A111638



| | | |
|---|--|-------------------------|
|  | M: 4.9 R THETA x 10 ⁻³ : 6-26 TW/TR: 0.8, 1.0 | 7404 ZPG AW - MHT |
| Boundary layer channel. Effectively continuous. W = 0.33, H = 0.272 m. 0.1 < P0 < 1. MN/m ² . T0: 340, 420K. Air, dewpoint 215-233K. 2 < RE/m x 10 ⁻⁶ < 23. | | |
| VOISINET R.L.P., LEE R.E., MEIER H.U., 1974. Comparative measurements of total temperature in a supersonic turbulent boundary layer using a conical equilibrium and combined temperature-pressure probe. NOLTR 74-10. | | |

1 The general arrangement of this experiment is as for Voisinet and Lee, CAT 7202, and only differences
will be described here. The purpose was to compare the temperature distributions obtained using the
7 ECP (Danberg 1961), for which the cone semi-angle was 5°, the support diameter 1.5 mm and the length
before increase in support diameter about 25 mm (E) with those using a combined Pitot-temperature
probe. The combined probe was as designed by Meier (1967, 1970, CAT 7003), consisting of a Pitot tube
with a circular front-face (d = 0.5 mm), followed by a conical section with half angle about 6° (E),
and containing a thermocouple bead just behind the opening. The tube can be vented in a controlled
8 as a STP when vented. The probes were mounted on a common holder, the tip of the ECP 0.75 mm higher
than the centre of the combined probe. There are two values of X, 1.702 and 2.057 m.

12 The editors have presented all the tabulated profile data, incorporating the authors' assumptions and
13 reduction procedures. The profiles are divided into an 'A' set, using the ECP, and a 'B' set using the
combined probe. Profiles 0101-0301 are for a near adiabatic wall case, 0401-0602 for TW/TR=0.8. There
are three unit Reynolds numbers in each group.

§ DATA: 74040101-0602 A and B. Pitot profiles and two T0 profiles obtained simultaneously.

15 Editors' comments. These data are among the most carefully considered total temperature surveys in
published form. Agreement between the two probe types was good. For the AW case, the combined probe
gave values up to about 2% lower near the wall, and within 1% further out. For TW/TR = 0.8, the
combined probe read up to 2.5% higher near the wall, within 1% further out. A discussion of possible
error sources in the combined probe may be found in Mabey and Sawyer (1976). Sample profiles are
shown as figures (2.5.19) and (2.5.20) in AGARDograph 253. The skin friction value was not measured,
so that the Fernholz (1971) correlation was used in order to compare the velocity profiles with the
standard logarithmic and outer law. Agreement of the measured velocity distribution with the
"standard" logarithmic laws was good (AG 253, Fig. 2.5.20), whereas for the outer law data points fell
slightly above and below the standard curve in the middle of the boundary layer and towards the edge
respectively. This behaviour was found also in Voisinet's experiment CAT 7901S, and the earlier
NOL studies such as CAT 7202. A comparison between the measured temperature and the standard
temperature-velocity relationship, eqn.(2.5.37) of AGARDograph 253 (Fig. 2.5.19), showed that the
measured profiles were between 5 and 15% lower for profiles 0401A to 0602A and 0402B to 0602B. Most of
the velocity profiles extended into the viscous sublayer.

| CAT 7404S | | VOISINET | | BOUNDARY CONDITIONS AND EVALUATED DATA, SI UNITS | | | | | | | |
|-----------------------|-----------------------|----------|-----------------------|--|---------|-----------------------|-----------------------|-----------------------|--|--|--|
| RUN | MD * | TW/TR | RED2W | CF | H12 | H12K | PW | PD* | | | |
| X * | POD | PW/PD* | RED2O | CQ | H32 | H32K | TW* | TD* | | | |
| RZ | TOD | TAUW | OZ | P12* | H42 | O2K | UD | TR | | | |
| 7404S0101A | 4.7852 | 0.9641 | 1.4570 ⁺⁰³ | NM | 10.0602 | 1.4530 | 2.4410 ⁺⁰² | 2.4410 ⁺⁰² | | | |
| 1.7020 ⁺⁰⁰ | 1.0016 ⁺⁰⁵ | 1.0000 | 6.1810 ⁺⁰³ | NM | 1.8200 | 1.7652 | 2.9820 ⁺⁰² | 6.0610 ⁺⁰¹ | | | |
| INFINITE | 3.3818 ⁺⁰² | NM | 2.5636 ⁻⁰³ | 0.0000 ⁺⁰⁰ | 0.2654 | 5.6573 ⁻⁰³ | 7.4693 ⁺⁰² | 3.0931 ⁺⁰² | | | |
| 7404S0102A | 4.7557 | 0.9749 | 1.5103 ⁺⁰³ | NM | 10.6881 | 1.4692 | 2.4670 ⁺⁰² | 2.4670 ⁺⁰² | | | |
| 2.0570 ⁺⁰⁰ | 9.7695 ⁺⁰⁴ | 1.0000 | 6.3943 ⁺⁰³ | NM | 1.8028 | 1.7510 | 3.0230 ⁺⁰² | 6.1370 ⁺⁰¹ | | | |
| INFINITE | 3.3897 ⁺⁰² | NM | 2.6905 ⁻⁰³ | 0.0000 ⁺⁰⁰ | 0.1637 | 6.2951 ⁻⁰³ | 7.4697 ⁺⁰² | 3.1010 ⁺⁰² | | | |
| 7404S0201A | 4.8305 | 0.9556 | 5.9667 ⁺⁰³ | NM | 10.0512 | 1.4020 | 1.1950 ⁺⁰³ | 1.1950 ⁺⁰³ | | | |
| 1.7020 ⁺⁰⁰ | 5.1765 ⁺⁰⁵ | 1.0000 | 2.5531 ⁺⁰⁴ | NM | 1.8301 | 1.7794 | 2.9540 ⁺⁰² | 5.9660 ⁺⁰¹ | | | |
| INFINITE | 3.3808 ⁺⁰² | NM | 2.0924 ⁻⁰³ | 0.0000 ⁺⁰⁰ | 0.2652 | 4.4970 ⁻⁰³ | 7.4697 ⁺⁰² | 3.0912 ⁺⁰² | | | |
| 7404S0202A | 4.9071 | 0.9677 | 5.7754 ⁺⁰³ | NM | 10.8266 | 1.3893 | 1.1320 ⁺⁰³ | 1.1320 ⁺⁰³ | | | |
| 2.0570 ⁺⁰⁰ | 5.3705 ⁺⁰⁵ | 1.0000 | 2.5593 ⁺⁰⁴ | NM | 1.8216 | 1.7748 | 2.9960 ⁺⁰² | 5.8250 ⁺⁰¹ | | | |
| INFINITE | 3.3878 ⁺⁰² | NM | 2.1024 ⁻⁰³ | 0.0000 ⁺⁰⁰ | 0.1912 | 4.7907 ⁻⁰³ | 7.5090 ⁺⁰² | 3.0960 ⁺⁰² | | | |
| 7404S0301A | 4.7883 | 0.9569 | 9.7003 ⁺⁰³ | NM | 10.0437 | 1.4185 | 2.3630 ⁺⁰³ | 2.3630 ⁺⁰³ | | | |
| 1.7020 ⁺⁰⁰ | 9.7319 ⁺⁰⁵ | 1.0000 | 4.0960 ⁺⁰⁴ | NM | 1.8269 | 1.7746 | 2.9590 ⁺⁰² | 6.0530 ⁺⁰¹ | | | |
| INFINITE | 3.3809 ⁺⁰² | NM | 1.7503 ⁻⁰³ | 0.0000 ⁺⁰⁰ | 0.2443 | 3.7396 ⁻⁰³ | 7.4692 ⁺⁰² | 3.0923 ⁺⁰² | | | |
| 7404S0401A | 4.7871 | 0.7765 | 2.0524 ⁺⁰³ | NM | 6.0282 | 1.4418 | 2.4320 ⁺⁰² | 2.4320 ⁺⁰² | | | |
| 1.7020 ⁺⁰⁰ | 1.0002 ⁺⁰⁵ | 1.0000 | 7.0129 ⁺⁰³ | NM | 1.8175 | 1.7620 | 2.9900 ⁺⁰² | 7.5400 ⁺⁰¹ | | | |
| INFINITE | 4.2098 ⁺⁰² | NM | 4.0496 ⁻⁰³ | 0.0000 ⁺⁰⁰ | 0.8712 | 7.1965 ⁻⁰³ | 8.3343 ⁺⁰² | 3.8504 ⁺⁰² | | | |
| 7404S0402A | 4.8060 | 0.7926 | 2.2245 ⁺⁰³ | NM | 6.1586 | 1.4484 | 2.4280 ⁺⁰² | 2.4280 ⁺⁰² | | | |
| 2.0570 ⁺⁰⁰ | 1.0214 ⁺⁰⁵ | 1.0000 | 7.7798 ⁺⁰³ | NM | 1.8086 | 1.7552 | 3.0350 ⁺⁰² | 7.4510 ⁺⁰¹ | | | |
| INFINITE | 4.1871 ⁺⁰² | NM | 4.4033 ⁻⁰³ | 0.0000 ⁺⁰⁰ | 0.8609 | 8.0310 ⁻⁰³ | 8.3177 ⁺⁰² | 3.8291 ⁺⁰² | | | |
| 7404S0501A | 4.8754 | 0.7769 | 6.6365 ⁺⁰³ | NM | 7.1800 | 1.3709 | 1.1350 ⁺⁰³ | 1.1350 ⁺⁰³ | | | |
| 1.7020 ⁺⁰⁰ | 5.1864 ⁺⁰⁵ | 1.0000 | 2.3336 ⁺⁰⁴ | NM | 1.8322 | 1.7849 | 3.0040 ⁺⁰² | 7.3520 ⁺⁰¹ | | | |
| INFINITE | 4.2303 ⁺⁰² | NM | 2.7302 ⁻⁰³ | 0.0000 ⁺⁰⁰ | 0.7072 | 5.0556 ⁻⁰³ | 8.3815 ⁺⁰² | 3.8668 ⁺⁰² | | | |
| 7404S0502A | 4.8637 | 0.7829 | 7.4641 ⁺⁰³ | NM | 7.0417 | 1.3730 | 1.1560 ⁺⁰³ | 1.1560 ⁺⁰³ | | | |
| 2.0570 ⁺⁰⁰ | 5.2095 ⁺⁰⁵ | 1.0000 | 2.6315 ⁺⁰⁴ | NM | 1.9228 | 1.7766 | 3.0200 ⁺⁰² | 7.3630 ⁺⁰¹ | | | |
| INFINITE | 4.2198 ⁺⁰² | NM | 3.0368 ⁻⁰³ | 0.0000 ⁺⁰⁰ | 0.7251 | 5.6913 ⁻⁰³ | 8.3677 ⁺⁰² | 3.8575 ⁺⁰² | | | |
| 7404S0601A | 4.9139 | 0.7793 | 1.2138 ⁺⁰⁴ | NM | 7.5119 | 1.3590 | 2.2960 ⁺⁰³ | 2.2960 ⁺⁰³ | | | |
| 1.7020 ⁺⁰⁰ | 1.0981 ⁺⁰⁶ | 1.0000 | 4.3274 ⁺⁰⁴ | NM | 1.8486 | 1.8041 | 3.0300 ⁺⁰² | 7.2990 ⁺⁰¹ | | | |
| INFINITE | 4.2548 ⁺⁰² | NM | 2.4564 ⁻⁰³ | 0.0000 ⁺⁰⁰ | 0.6645 | 4.4425 ⁻⁰³ | 8.4425 ⁺⁰² | 3.8882 ⁺⁰² | | | |
| 7404S0602A | 4.9719 | 0.7841 | 1.3007 ⁺⁰⁴ | NM | 7.6763 | 1.3460 | 2.2450 ⁺⁰³ | 2.2450 ⁺⁰³ | | | |
| 2.0570 ⁺⁰⁰ | 1.1494 ⁺⁰⁶ | 1.0000 | 4.7545 ⁺⁰⁴ | NM | 1.8393 | 1.7945 | 3.0340 ⁺⁰² | 7.1260 ⁺⁰¹ | | | |
| INFINITE | 4.2357 ⁺⁰² | NM | 2.6318 ⁻⁰³ | 0.0000 ⁺⁰⁰ | 0.6637 | 4.9426 ⁻⁰³ | 8.4150 ⁺⁰² | 3.8693 ⁺⁰² | | | |
| 7404S0101B | 4.7852 | 0.9582 | 1.4967 ⁺⁰³ | NM | 9.7628 | 1.4361 | 2.4410 ⁺⁰² | 2.4410 ⁺⁰² | | | |
| 1.7020 ⁺⁰⁰ | 1.0016 ⁺⁰⁵ | 1.0000 | 6.3131 ⁺⁰³ | NM | 1.8144 | 1.7578 | 2.9760 ⁺⁰² | 6.0860 ⁺⁰¹ | | | |
| INFINITE | 3.3958 ⁺⁰² | NM | 2.6347 ⁻⁰³ | 0.0000 ⁺⁰⁰ | 0.3044 | 5.7833 ⁻⁰³ | 7.4847 ⁺⁰² | 3.1059 ⁺⁰² | | | |
| 7404S0102B | 4.7557 | 0.9736 | 1.5345 ⁺⁰³ | NM | 10.4966 | 1.4629 | 2.4670 ⁺⁰² | 2.4670 ⁺⁰² | | | |
| 2.0570 ⁺⁰⁰ | 9.7695 ⁺⁰⁴ | 1.0000 | 6.4880 ⁺⁰³ | NM | 1.7996 | 1.7478 | 3.0230 ⁺⁰² | 6.1450 ⁺⁰¹ | | | |
| INFINITE | 3.3941 ⁺⁰² | NM | 2.7353 ⁻⁰³ | 0.0000 ⁺⁰⁰ | 0.1901 | 6.3693 ⁻⁰³ | 7.4746 ⁺⁰² | 3.1050 ⁺⁰² | | | |
| 7404S0201B | 4.8305 | 0.9551 | 5.9457 ⁺⁰³ | NM | 10.0636 | 1.3919 | 1.1950 ⁺⁰³ | 1.1950 ⁺⁰³ | | | |
| 1.7020 ⁺⁰⁰ | 5.1765 ⁺⁰⁵ | 1.0000 | 2.5417 ⁺⁰⁴ | NM | 1.8241 | 1.7699 | 2.9600 ⁺⁰² | 5.9810 ⁺⁰¹ | | | |
| INFINITE | 3.3893 ⁺⁰² | NM | 2.0909 ⁻⁰³ | 0.0000 ⁺⁰⁰ | 0.2588 | 4.5325 ⁻⁰³ | 7.4901 ⁺⁰² | 3.0990 ⁺⁰² | | | |
| 7404S0202B | 4.9071 | 0.9668 | 6.0385 ⁺⁰³ | NM | 10.3873 | 1.3671 | 1.1320 ⁺⁰³ | 1.1320 ⁺⁰³ | | | |
| 2.0570 ⁺⁰⁰ | 5.3705 ⁺⁰⁵ | 1.0000 | 2.6771 ⁺⁰⁴ | NM | 1.8210 | 1.7717 | 2.9790 ⁺⁰² | 5.7970 ⁺⁰¹ | | | |
| INFINITE | 3.3715 ⁺⁰² | NM | 2.1833 ⁻⁰³ | 0.0000 ⁺⁰⁰ | 0.2520 | 4.9236 ⁻⁰³ | 7.4909 ⁺⁰² | 3.0811 ⁺⁰² | | | |
| 7404S0301B | 4.7883 | 0.9562 | 9.9743 ⁺⁰³ | NM | 9.7644 | 1.3841 | 2.3630 ⁺⁰³ | 2.3630 ⁺⁰³ | | | |
| 1.7020 ⁺⁰⁰ | 9.7319 ⁺⁰⁵ | 1.0000 | 4.2113 ⁺⁰⁴ | NM | 1.8252 | 1.7737 | 2.9510 ⁺⁰² | 6.0410 ⁺⁰¹ | | | |
| INFINITE | 3.3742 ⁺⁰² | NM | 1.7942 ⁻⁰³ | 0.0000 ⁺⁰⁰ | 0.2775 | 3.8175 ⁻⁰³ | 7.4618 ⁺⁰² | 3.0861 ⁺⁰² | | | |
| 7404S0401B | 4.7872 | 0.7768 | 2.0436 ⁺⁰³ | NM | 6.0538 | 1.4391 | 2.4320 ⁺⁰² | 2.4320 ⁺⁰² | | | |
| 1.7020 ⁺⁰⁰ | 1.0003 ⁺⁰⁵ | 1.0000 | 6.9844 ⁺⁰³ | NM | 1.8139 | 1.7583 | 2.9920 ⁺⁰² | 7.5420 ⁺⁰¹ | | | |
| INFINITE | 4.2110 ⁺⁰² | NM | 4.0347 ⁻⁰³ | 0.0000 ⁺⁰⁰ | 0.8646 | 7.1985 ⁻⁰³ | 8.3356 ⁺⁰² | 3.8915 ⁺⁰² | | | |
| 7404S0402B | 4.8060 | 0.7954 | 2.1987 ⁺⁰³ | NM | 6.2526 | 1.4426 | 2.4280 ⁺⁰² | 2.4280 ⁺⁰² | | | |
| 2.0570 ⁺⁰⁰ | 1.0214 ⁺⁰⁵ | 1.0000 | 7.7162 ⁺⁰³ | NM | 1.8053 | 1.7515 | 3.0360 ⁺⁰² | 7.4270 ⁺⁰¹ | | | |
| INFINITE | 4.1736 ⁺⁰² | NM | 4.3464 ⁻⁰³ | 0.0000 ⁺⁰⁰ | 0.8439 | 7.9990 ⁻⁰³ | 8.3042 ⁺⁰² | 3.8168 ⁺⁰² | | | |
| 7404S0501B | 4.8755 | 0.7797 | 6.6232 ⁺⁰³ | NM | 7.2297 | 1.3614 | 1.1350 ⁺⁰³ | 1.1350 ⁺⁰³ | | | |
| 1.7020 ⁺⁰⁰ | 5.1870 ⁺⁰⁵ | 1.0000 | 2.3383 ⁺⁰⁴ | NM | 1.8312 | 1.7806 | 3.0000 ⁺⁰² | 7.3150 ⁺⁰¹ | | | |
| INFINITE | 4.2091 ⁺⁰² | NM | 2.7150 ⁻⁰³ | 0.0000 ⁺⁰⁰ | 0.6978 | 5.0638 ⁻⁰³ | 8.3606 ⁺⁰² | 3.8475 ⁺⁰² | | | |
| 7404S0502B | 4.8638 | 0.7870 | 7.3972 ⁺⁰³ | NM | 7.1084 | 1.3633 | 1.1560 ⁺⁰³ | 1.1560 ⁺⁰³ | | | |
| 2.0570 ⁺⁰⁰ | 5.2101 ⁺⁰⁵ | 1.0000 | 2.6198 ⁺⁰⁴ | NM | 1.8215 | 1.7735 | 3.0290 ⁺⁰² | 7.3460 ⁺⁰¹ | | | |
| INFINITE | 4.2102 ⁺⁰² | NM | 3.0129 ⁻⁰³ | 0.0000 ⁺⁰⁰ | 0.7128 | 5.6931 ⁻⁰³ | 8.3582 ⁺⁰² | 3.8488 ⁺⁰² | | | |
| 7404S0601B | 4.9140 | 0.7794 | 1.2262 ⁺⁰⁴ | NM | 7.3922 | 1.3162 | 2.2960 ⁺⁰³ | 2.2960 ⁺⁰³ | | | |
| 1.7020 ⁺⁰⁰ | 1.0982 ⁺⁰⁶ | 1.0000 | 4.3700 ⁺⁰⁴ | NM | 1.8449 | 1.7980 | 3.0390 ⁺⁰² | 7.3190 ⁺⁰¹ | | | |
| INFINITE | 4.2666 ⁺⁰² | NM | 2.4907 ⁻⁰³ | 0.0000 ⁺⁰⁰ | 0.6713 | 4.5327 ⁻⁰³ | 8.4289 ⁺⁰² | 3.8990 ⁺⁰² | | | |
| 7404S0602B | 4.9718 | 0.7848 | 1.3241 ⁺⁰⁴ | NM | 7.5014 | 1.3262 | 2.2460 ⁺⁰³ | 2.2460 ⁺⁰³ | | | |
| 2.0570 ⁺⁰⁰ | 1.1498 ⁺⁰⁶ | 1.0000 | 4.8409 ⁺⁰⁴ | NM | 1.8371 | 1.7901 | 3.0420 ⁺⁰² | 7.1390 ⁺⁰¹ | | | |
| INFINITE | 4.2432 ⁺⁰² | NM | 2.6858 ⁻⁰³ | 0.0000 ⁺⁰⁰ | 0.6846 | 5.0386 ⁻⁰³ | 8.4225 ⁺⁰² | 3.8762 ⁺⁰² | | | |

| 7404S0101A | | VOISINET | | PROFILE TABULATION | | 18 POINTS, DELTA AT POINT 18 | | | |
|------------|------------------------|------------------------|------|--------------------|---------|------------------------------|---------|-----------|--|
| I | Y | PT2/P | P/PD | TO/TOD | M/MD | U/UD | T/TD | R/RD*U/UD | |
| 1 | 0.0000 ⁺ 00 | 1.0000 ⁺ 00 | NM | 0.88180 | 0.00000 | 0.00000 | 4.92012 | 0.00000 | |
| 2 | 1.3210 ⁻ 03 | 1.7458 ⁺ 00 | NM | 0.91750 | 0.19412 | 0.40561 | 4.36588 | 0.09290 | |
| 3 | 2.4890 ⁻ 03 | 2.9078 ⁺ 00 | NM | 0.94020 | 0.28398 | 0.55584 | 3.83107 | 0.14509 | |
| 4 | 3.8100 ⁻ 03 | 3.7501 ⁺ 00 | NM | 0.94480 | 0.33152 | 0.62081 | 3.50663 | 0.17704 | |
| 5 | 5.3090 ⁻ 03 | 4.3495 ⁺ 00 | NM | 0.94490 | 0.36128 | 0.65627 | 3.29976 | 0.19889 | |
| 6 | 6.8830 ⁻ 03 | 5.0697 ⁺ 00 | NM | 0.94560 | 0.39394 | 0.69183 | 3.08414 | 0.22432 | |
| 7 | 1.0719 ⁻ 02 | 6.2882 ⁺ 00 | NM | 0.94240 | 0.44360 | 0.73773 | 2.76579 | 0.26673 | |
| 8 | 1.6002 ⁻ 02 | 8.6228 ⁺ 00 | NM | 0.95620 | 0.52558 | 0.80663 | 2.35547 | 0.34245 | |
| 9 | 2.0930 ⁻ 02 | 1.1208 ⁺ 01 | NM | 0.96540 | 0.60340 | 0.85747 | 2.01940 | 0.42462 | |
| 10 | 2.6848 ⁻ 02 | 1.4748 ⁺ 01 | NM | 0.97430 | 0.69590 | 0.90451 | 1.68944 | 0.53539 | |
| 11 | 3.1928 ⁻ 02 | 1.8008 ⁺ 01 | NM | 0.98030 | 0.77129 | 0.93470 | 1.46861 | 0.63645 | |
| 12 | 3.8532 ⁻ 02 | 2.2084 ⁺ 01 | NM | 0.98830 | 0.85629 | 0.96322 | 1.26537 | 0.76122 | |
| 13 | 4.3536 ⁻ 02 | 2.4316 ⁺ 01 | NM | 0.99050 | 0.89942 | 0.97482 | 1.17470 | 0.82985 | |
| 14 | 5.0775 ⁻ 02 | 2.6528 ⁺ 01 | NM | 0.99300 | 0.94021 | 0.98498 | 1.09749 | 0.89748 | |
| 15 | 6.1595 ⁻ 02 | 2.8661 ⁺ 01 | NM | 0.99600 | 0.97793 | 0.99394 | 1.03301 | 0.96218 | |
| 16 | 7.1755 ⁻ 02 | 2.9307 ⁺ 01 | NM | 0.99840 | 0.98907 | 0.99722 | 1.01654 | 0.98099 | |
| 17 | 8.1382 ⁻ 02 | 2.9567 ⁺ 01 | NM | 0.99900 | 0.99352 | 0.99833 | 1.00970 | 0.98874 | |
| D 18 | 9.0449 ⁻ 02 | 2.9948 ⁺ 01 | NM | 1.00000 | 1.00000 | 1.00000 | 1.00000 | 1.00000 | |

INPUT VARIABLES Y,M,TO/TOD ASSUME P=PD

| 7404S0201A | | VOISINET | | PROFILE TABULATION | | 16 POINTS, DELTA AT POINT 16 | | | |
|------------|------------------------|------------------------|------|--------------------|---------|------------------------------|---------|-----------|--|
| I | Y | PT2/P | P/PD | TO/TOD | M/MD | U/UD | T/TD | R/RD*U/UD | |
| 1 | 0.0000 ⁺ 00 | 1.0000 ⁺ 00 | NM | 0.87370 | 0.00000 | 0.00000 | 4.95104 | 0.00000 | |
| 2 | 9.9100 ⁻ 04 | 2.6541 ⁺ 00 | NM | 0.92100 | 0.26525 | 0.52577 | 3.92900 | 0.13382 | |
| 3 | 2.1340 ⁻ 03 | 3.2453 ⁺ 00 | NM | 0.92120 | 0.30117 | 0.57678 | 3.66771 | 0.15726 | |
| 4 | 3.2770 ⁻ 03 | 4.1119 ⁺ 00 | NM | 0.92450 | 0.34653 | 0.63495 | 3.35744 | 0.18912 | |
| 5 | 7.2140 ⁻ 03 | 5.9586 ⁺ 00 | NM | 0.93130 | 0.42671 | 0.72076 | 2.85312 | 0.25262 | |
| 6 | 1.2802 ⁻ 02 | 9.0973 ⁺ 00 | NM | 0.95440 | 0.53564 | 0.81451 | 2.31232 | 0.35225 | |
| 7 | 1.9406 ⁻ 02 | 1.3824 ⁺ 01 | NM | 0.97260 | 0.66668 | 0.89266 | 1.79282 | 0.49791 | |
| 8 | 2.5425 ⁻ 02 | 1.8720 ⁺ 01 | NM | 0.98490 | 0.77944 | 0.94027 | 1.45525 | 0.64612 | |
| 9 | 3.1877 ⁻ 02 | 2.2846 ⁺ 01 | NM | 0.99070 | 0.86308 | 0.96656 | 1.25418 | 0.77067 | |
| 10 | 3.6957 ⁻ 02 | 2.5535 ⁺ 01 | NM | 0.99560 | 0.91347 | 0.98077 | 1.15279 | 0.85078 | |
| 11 | 4.4425 ⁻ 02 | 2.7656 ⁺ 01 | NM | 0.99690 | 0.95133 | 0.98933 | 1.08148 | 0.91479 | |
| 12 | 5.1105 ⁻ 02 | 2.8855 ⁺ 01 | NM | 0.99890 | 0.97209 | 0.99435 | 1.04632 | 0.95033 | |
| 13 | 5.6464 ⁻ 02 | 2.9462 ⁺ 01 | NM | 0.99750 | 0.98242 | 0.99558 | 1.02697 | 0.96944 | |
| 14 | 6.4872 ⁻ 02 | 2.9745 ⁺ 01 | NM | 0.99790 | 0.98721 | 0.99666 | 1.01924 | 0.97784 | |
| 15 | 7.6860 ⁻ 02 | 3.0049 ⁺ 01 | NM | 0.99830 | 0.99232 | 0.99778 | 1.01104 | 0.98689 | |
| D 16 | 8.8773 ⁻ 02 | 3.0508 ⁺ 01 | NM | 1.00000 | 1.00000 | 1.00000 | 1.00000 | 1.00000 | |

INPUT VARIABLES Y,M,TO/TOD ASSUME P=PD

| 7404S0501A | | VOISINET | | PROFILE TABULATION | | 26 POINTS, DELTA AT POINT 25 | | | |
|------------|------------------------|------------------------|------|--------------------|---------|------------------------------|---------|-----------|--|
| I | Y | PT2/P | P/PD | TO/TOD | M/MD | U/UD | T/TD | R/RD*U/UD | |
| 1 | 0.0000 ⁺ 00 | 1.0000 ⁺ 00 | NM | 0.71020 | 0.00000 | 0.00000 | 5.42 | 0.00000 | |
| 2 | 9.1400 ⁻ 04 | 3.0408 ⁺ 00 | NM | 0.80730 | 0.28666 | 0.52392 | 4.724 | 0.15685 | |
| 3 | 1.3720 ⁻ 03 | 3.5163 ⁺ 00 | NM | 0.81890 | 0.31321 | 0.56145 | 3.1734 | 0.17472 | |
| 4 | 2.1840 ⁻ 03 | 4.0320 ⁺ 00 | NM | 0.82330 | 0.33946 | 0.59387 | 3.06059 | 0.19404 | |
| 5 | 2.9460 ⁻ 03 | 4.4038 ⁺ 00 | NM | 0.82640 | 0.35712 | 0.61444 | 2.96026 | 0.20756 | |
| 6 | 4.3180 ⁻ 03 | 5.1156 ⁺ 00 | NM | 0.83570 | 0.38860 | 0.65015 | 2.79908 | 0.23227 | |
| 7 | 5.7660 ⁻ 03 | 5.8504 ⁺ 00 | NM | 0.84420 | 0.41855 | 0.68139 | 2.65027 | 0.25710 | |
| 8 | 7.3150 ⁻ 03 | 6.6608 ⁺ 00 | NM | 0.85460 | 0.44921 | 0.71165 | 2.50971 | 0.28356 | |
| 9 | 8.9150 ⁻ 03 | 7.5475 ⁺ 00 | NM | 0.86450 | 0.48049 | 0.73994 | 2.37145 | 0.31202 | |
| 10 | 1.0871 ⁻ 02 | 8.7623 ⁺ 00 | NM | 0.87630 | 0.52027 | 0.77254 | 2.20492 | 0.35037 | |
| 11 | 1.2675 ⁻ 02 | 9.9682 ⁺ 00 | NM | 0.88720 | 0.55692 | 0.79991 | 2.06302 | 0.38774 | |
| 12 | 1.4707 ⁻ 02 | 1.1382 ⁺ 01 | NM | 0.89830 | 0.59702 | 0.82689 | 1.91930 | 0.43105 | |
| 13 | 1.6967 ⁻ 02 | 1.3073 ⁺ 01 | NM | 0.90970 | 0.64167 | 0.85367 | 1.76992 | 0.48232 | |
| 14 | 1.8339 ⁻ 02 | 1.4097 ⁺ 01 | NM | 0.91440 | 0.66725 | 0.86696 | 1.68821 | 0.51354 | |
| 15 | 2.0879 ⁻ 02 | 1.6045 ⁺ 01 | NM | 0.92740 | 0.71340 | 0.89119 | 1.56054 | 0.57108 | |
| 16 | 2.3597 ⁻ 02 | 1.8243 ⁺ 01 | NM | 0.93670 | 0.76209 | 0.91230 | 1.43305 | 0.63661 | |
| 17 | 2.7026 ⁻ 02 | 2.0732 ⁺ 01 | NM | 0.94560 | 0.81372 | 0.93197 | 1.31177 | 0.71047 | |
| 18 | 3.1801 ⁻ 02 | 2.3722 ⁺ 01 | NM | 0.95620 | 0.87170 | 0.95206 | 1.19286 | 0.79813 | |
| 19 | 3.9624 ⁻ 02 | 2.6877 ⁺ 01 | NM | 0.96970 | 0.92897 | 0.97142 | 1.09349 | 0.88837 | |
| 20 | 4.4704 ⁻ 02 | 2.8100 ⁺ 01 | NM | 0.97420 | 0.95024 | 0.97893 | 1.06129 | 0.92239 | |
| 21 | 5.1308 ⁻ 02 | 2.9280 ⁺ 01 | NM | 0.98600 | 0.97032 | 0.98666 | 1.03396 | 0.95425 | |
| 22 | 5.7531 ⁻ 02 | 2.9886 ⁺ 01 | NM | 0.98880 | 0.98047 | 0.99093 | 1.02144 | 0.97013 | |
| 23 | 6.3957 ⁻ 02 | 3.0265 ⁺ 01 | NM | 0.99380 | 0.98677 | 0.99456 | 1.01586 | 0.97904 | |
| 24 | 6.8834 ⁻ 02 | 3.0546 ⁺ 01 | NM | 0.99610 | 0.99141 | 0.99654 | 1.01039 | 0.98630 | |
| D 25 | 8.1382 ⁻ 02 | 3.1069 ⁺ 01 | NM | 1.00000 | 1.00000 | 1.00000 | 1.00000 | 1.00000 | |
| 26 | 9.1745 ⁻ 02 | 3.1599 ⁺ 01 | NM | 1.00330 | 1.00861 | 1.00313 | 0.98916 | 1.01413 | |

INPUT VARIABLES Y,M,TO/TOD ASSUME P=PD

| 7404S01018 | | VOISINET | PROFILE TABULATION | 20 POINTS, DELTA AT POINT 20 | | | | |
|------------|-----------|-----------|--------------------|------------------------------|---------|---------|---------|-----------|
| I | Y | PT2/P | P/PD | TO/TOD | M/MD | U/UD | T/TD | R/RD*U/UD |
| 1 | 0.0000+00 | 1.0000+00 | NM | 0.87630 | 0.00000 | 0.00000 | 4.88943 | 0.00000 |
| 2 | 3.0500-04 | 1.1830+00 | NM | 0.88900 | 0.10363 | 0.22533 | 4.72776 | 0.04766 |
| 3 | 4.5700-04 | 1.1954+00 | NM | 0.89320 | 0.10689 | 0.23262 | 4.73591 | 0.04912 |
| 4 | 1.3210-03 | 1.7456+00 | NM | 0.91470 | 0.19410 | 0.40495 | 4.35270 | 0.09303 |
| 5 | 2.4890-03 | 2.9075+00 | NM | 0.92610 | 0.28396 | 0.55162 | 3.77376 | 0.14617 |
| 6 | 3.8100-03 | 3.7501+00 | NM | 0.93190 | 0.33152 | 0.61656 | 3.45875 | 0.17826 |
| 7 | 5.3090-03 | 4.3490+00 | NM | 0.92990 | 0.36126 | 0.65102 | 3.24752 | 0.20047 |
| 8 | 6.8830-03 | 5.0697+00 | NM | 0.92840 | 0.39394 | 0.68551 | 3.02804 | 0.22639 |
| 9 | 1.0791-02 | 6.2882+00 | NM | 0.93230 | 0.44360 | 0.73377 | 2.73615 | 0.26818 |
| 10 | 1.6002-02 | 8.6221+00 | NM | 0.94620 | 0.52556 | 0.80239 | 2.33094 | 0.34424 |
| 11 | 2.0930-02 | 1.1208+01 | NM | 0.95690 | 0.60340 | 0.85368 | 2.00162 | 0.42650 |
| 12 | 2.6848-02 | 1.4748+01 | NM | 0.96780 | 0.69590 | 0.90149 | 1.67816 | 0.53719 |
| 13 | 3.1928-02 | 1.8009+01 | NM | 0.97500 | 0.77132 | 0.93218 | 1.46062 | 0.63821 |
| 14 | 3.8532-02 | 2.2084+01 | NM | 0.98360 | 0.85629 | 0.96093 | 1.25935 | 0.76304 |
| 15 | 4.3536-02 | 2.4316+01 | NM | 0.98980 | 0.89942 | 0.97448 | 1.17387 | 0.83014 |
| 16 | 5.0775-02 | 2.6528+01 | NM | 0.99400 | 0.94021 | 0.98547 | 1.09860 | 0.89703 |
| 17 | 6.1595-02 | 2.8661+01 | NM | 0.99770 | 0.97793 | 0.99479 | 1.03477 | 0.96136 |
| 18 | 7.1755-02 | 2.9307+01 | NM | 0.99790 | 0.98907 | 0.99697 | 1.01603 | 0.98124 |
| 19 | 8.1382-02 | 2.9567+01 | NM | 0.99900 | 0.99352 | 0.99833 | 1.00970 | 0.98874 |
| D 20 | 9.0449-02 | 2.9948+01 | NM | 1.00000 | 1.00000 | 1.00000 | 1.00000 | 1.00000 |

INPUT VARIABLES Y,M,TO/TOD ASSUME P=PD

| 7404S02018 | | VOISINET | PROFILE TABULATION | 18 POINTS, DELTA AT POINT 18 | | | | |
|------------|-----------|-----------|--------------------|------------------------------|---------|---------|---------|-----------|
| I | Y | PT2/P | P/PD | TO/TOD | M/MD | U/UD | T/TD | R/RD*U/UD |
| 1 | 0.0000+00 | 1.0000+00 | NM | 0.87340 | 0.00000 | 0.00000 | 4.94934 | 0.00000 |
| 2 | 3.0500-04 | 1.2968+00 | NM | 0.89650 | 0.12852 | 0.27911 | 4.71668 | 0.05918 |
| 3 | 4.8300-04 | 1.7141+00 | NM | 0.91050 | 0.18886 | 0.39721 | 4.42328 | 0.08980 |
| 4 | 9.9100-04 | 2.6541+00 | NM | 0.91600 | 0.26525 | 0.52435 | 3.90767 | 0.13418 |
| 5 | 2.1340-03 | 3.2449+00 | NM | 0.91470 | 0.30115 | 0.57471 | 3.64198 | 0.15780 |
| 6 | 3.2770-03 | 4.1119+00 | NM | 0.91990 | 0.34653 | 0.63337 | 3.34073 | 0.18959 |
| 7 | 7.2140-03 | 5.9586+00 | NM | 0.93000 | 0.42671 | 0.72025 | 2.84914 | 0.25280 |
| 8 | 1.2802-02 | 9.0973+00 | NM | 0.95080 | 0.53564 | 0.81297 | 2.30359 | 0.35291 |
| 9 | 1.9406-02 | 1.3824+01 | NM | 0.97000 | 0.66668 | 0.89147 | 1.78803 | 0.49858 |
| 10 | 2.5425-02 | 1.8720+01 | NM | 0.98060 | 0.77942 | 0.93821 | 1.44896 | 0.64751 |
| 11 | 3.1877-02 | 2.2847+01 | NM | 0.99190 | 0.86310 | 0.96715 | 1.25565 | 0.77024 |
| 12 | 3.6957-02 | 2.5535+01 | NM | 0.99620 | 0.91347 | 0.98107 | 1.15349 | 0.85052 |
| 13 | 4.4425-02 | 2.7656+01 | NM | 0.99820 | 0.95133 | 0.98998 | 1.08290 | 0.91419 |
| 14 | 5.1105-02 | 2.8855+01 | NM | 0.99830 | 0.97209 | 0.99405 | 1.04569 | 0.95062 |
| 15 | 5.6464-02 | 2.9463+01 | NM | 0.99790 | 0.98244 | 0.99579 | 1.02734 | 0.96928 |
| 16 | 6.4872-02 | 2.9746+01 | NM | 0.99880 | 0.98723 | 0.99711 | 1.02012 | 0.97744 |
| 17 | 7.6860-02 | 3.0049+01 | NM | 0.99950 | 0.99232 | 0.99838 | 1.01226 | 0.98629 |
| D 18 | 8.8773-02 | 3.0508+01 | NM | 1.00000 | 1.00000 | 1.00000 | 1.00000 | 1.00000 |

INPUT VARIABLES Y,M,TO/TOD ASSUME P=PD

| 7404S05018 | | VOISINET | PROFILE TABULATION | 29 POINTS, DELTA AT POINT 28 | | | | |
|------------|-----------|-----------|--------------------|------------------------------|---------|---------|---------|-----------|
| I | Y | PT2/P | P/PD | TO/TOD | M/MD | U/UD | T/TD | R/RD*U/UD |
| 1 | 0.0000+00 | 1.0000+00 | NM | 0.71280 | 0.00000 | 0.00000 | 4.10152 | 0.00000 |
| 2 | 3.0500-04 | 1.5518+00 | NM | 0.78300 | 0.16774 | 0.33438 | 3.97391 | 0.08414 |
| 3 | 3.5600-04 | 1.8222+00 | NM | 0.79320 | 0.19834 | 0.38892 | 3.84506 | 0.10115 |
| 4 | 5.3300-04 | 2.3491+00 | NM | 0.80710 | 0.24196 | 0.46119 | 3.63295 | 0.12695 |
| 5 | 9.1400-04 | 3.0408+00 | NM | 0.81720 | 0.28666 | 0.52712 | 3.38132 | 0.15589 |
| 6 | 1.3720-03 | 3.5163+00 | NM | 0.82210 | 0.31320 | 0.56254 | 3.22601 | 0.17438 |
| 7 | 2.1840-03 | 4.0320+00 | NM | 0.82760 | 0.33945 | 0.59541 | 3.07668 | 0.19353 |
| 8 | 2.9460-03 | 4.4038+00 | NM | 0.83340 | 0.35711 | 0.61703 | 2.98544 | 0.20668 |
| 9 | 4.3180-03 | 5.1156+00 | NM | 0.84240 | 0.38860 | 0.65275 | 2.82161 | 0.23134 |
| 10 | 5.7660-03 | 5.8504+00 | NM | 0.85180 | 0.41854 | 0.68444 | 2.67422 | 0.25594 |
| 11 | 7.3150-03 | 6.6608+00 | NM | 0.86080 | 0.44921 | 0.71422 | 2.52800 | 0.28252 |
| 12 | 8.9150-03 | 7.5475+00 | NM | 0.87030 | 0.48048 | 0.74241 | 2.38744 | 0.31097 |
| 13 | 1.0871-02 | 8.7623+00 | NM | 0.88070 | 0.52025 | 0.77448 | 2.21607 | 0.34948 |
| 14 | 1.2675-02 | 9.9682+00 | NM | 0.89030 | 0.55691 | 0.80131 | 2.07030 | 0.38705 |
| 15 | 1.4707-02 | 1.1382+01 | NM | 0.89820 | 0.59701 | 0.82684 | 1.91815 | 0.43106 |
| 16 | 1.6967-02 | 1.3072+01 | NM | 0.91040 | 0.64164 | 0.85398 | 1.77142 | 0.48209 |
| 17 | 1.8339-02 | 1.4097+01 | NM | 0.91570 | 0.66723 | 0.86758 | 1.69067 | 0.51316 |
| 18 | 2.0879-02 | 1.6044+01 | NM | 0.92490 | 0.71336 | 0.88998 | 1.55645 | 0.57180 |
| 19 | 2.3597-02 | 1.8243+01 | NM | 0.93450 | 0.76208 | 0.91122 | 1.42973 | 0.63734 |
| 20 | 2.7026-02 | 2.0732+01 | NM | 0.94630 | 0.81370 | 0.93231 | 1.31279 | 0.71018 |
| 21 | 3.1801-02 | 2.3722+01 | NM | 0.95880 | 0.87168 | 0.95335 | 1.19615 | 0.79702 |
| 22 | 3.9624-02 | 2.6878+01 | NM | 0.96980 | 0.92897 | 0.97147 | 1.09360 | 0.88833 |
| 23 | 4.4704-02 | 2.8100+01 | NM | 0.97690 | 0.95022 | 0.97928 | 1.06209 | 0.92203 |
| 24 | 5.1308-02 | 2.9280+01 | NM | 0.98520 | 0.97030 | 0.98725 | 1.03525 | 0.95364 |
| 25 | 5.7531-02 | 2.9885+01 | NM | 0.99010 | 0.98043 | 0.99157 | 1.02285 | 0.96942 |
| 26 | 6.3957-02 | 3.0265+01 | NM | 0.99330 | 0.98675 | 0.99431 | 1.01538 | 0.97925 |
| 27 | 6.8834-02 | 3.0546+01 | NM | 0.99590 | 0.99139 | 0.99644 | 1.01022 | 0.98636 |
| D 28 | 8.1382-02 | 3.1071+01 | NM | 1.00000 | 1.00000 | 1.00000 | 1.00000 | 1.00000 |
| 29 | 9.1745-02 | 3.1599+01 | NM | 1.00000 | 1.00859 | 1.00148 | 0.98594 | 1.01576 |

INPUT VARIABLES Y,M,TO/TOD ASSUME P=PD

| | | |
|--|--|---------|
| <p>axisymmetric</p>  | <p>M: 14 R THETA x 10⁻³: 6-11 TW/TR: 0.25</p> | 7405 |
| | | FPG-SHT |
| <p>Blowdown tunnel with axisymmetric contoured nozzle. Running time 55 sec. D = 0.47 m. 8 < P0 < 20 MN/m². T0: 1300K. Nitrogen. 1.4 < RE/m 10⁻⁶ < 3.8.</p> | | |
| <p>PETERSON C.W. 1974. Pressure and temperature measurements in a cold-wall hypersonic turbulent boundary layer. Proc. 1974 Heat Transfer and Fluid Mechanics Institute. <u>And</u> Peterson, C.W., private communications. <u>Also</u> Peterson and George, 1974, 1975 a,b.</p> | | |

- 1 The test boundary layer was formed on the nozzle wall of an axisymmetric M = 14 wind tunnel. Wall
8 temperature and pressure measurements were made at 10 stations ranging from X = 0.74 m to 2.74 m,
where X is the axial distance from the throat (X = 0). Profiles were measured at two stations,
2 X = 1.92 and 2.66 m. The "smooth monotonic decrease in wall pressure along the nozzle indicates that
3 no imbedded shocks or boundary layer separation are present." No boundary layer trips were used, but
4 a comparison of the measured velocity profiles with a calculated laminar profile indicated that the
profiles were fully turbulent. The nozzle wall was not actively cooled downstream of the nozzle
region (X > 0.56 m), and as a result of the short running time wall temperatures in this region
"show only a weak dependence upon axial station and test conditions." "However, the estimated heat
transfer rates were high enough near the throat to cause substantial temperature rises in wall
temperature in this region." The cooling water flow rate was the same throughout, so that the throat-
wall temperature would have been significantly higher in the higher Reynolds number cases. The
boundary layer passed through a strong simple wave expansion in the throat region, but in the test
zone the longitudinal pressure gradient was considered relatively modest.
- 6 Wall pressure was measured with tappings of 3.18 mm in diameter, while the wall temperature was found
from thermocouples buried approximately 2 mm below the surface. Pitot, total temperature and static
7 pressure profiles were measured separately at two stations, one nominally in the expansion field of
the nozzle, the other nominally downstream of the nozzle wave structure, though in fact still in a
region with pressure gradients. Pitot surveys were made using a twin-probe rake which was traversed
at right angles to the wall of the nozzle. An FPP with a rectangular face 1.27 mm high and 4.06 mm
wide was used for surveys between the wall (Y = 0) and (Y = 65 mm). To generate Pitot pressure
corrections for viscous and rarefaction effects, other rectangular FPP with h₁ ranging from 0.19 to
1.04 mm and b₁/h₁ from 2.38 to 14.67 were used in a separate calibration experiment (see Peterson
and George: 1974, 1975a and ,more briefly, 1975b.) The T0 profile was measured with a singly shielded
STP for which d₁ = 2.2 mm. In the initial surveys, reported in Peterson (1974) the static pressure
profile was obtained using a 'cone-static' probe. This consisted of a 10° half angle cone-cylinder
probe with static tappings on the conical face of the probe, essentially probe 2 of the calibration
studies reported by Peterson and George cited above. The probe diameter was 3.18 mm, with the centre
of the tapping (d = 0.15 mm) 3.18 mm from the tip and 5.72 mm from the shoulder of the cone. For the
later tests reported here (private communication) a CCP was used for which α = 10° (half angle),
d = 2.13 mm, with tappings (d = 0.41 mm) 34.1 mm downstream of the shoulder.
- 9 The author has interpolated all profile data to a set of fixed y/δ values, with the D point chosen by
inspection of the total temperature profile. Pressure readings were normalised by the instantaneous
tunnel reservoir pressure values to give fixed nominal reservoir conditions. Total temperatures were
normalised to allow for reservoir and wall temperature variations using the relationship

$$T_0 = 1 + \left[\frac{1-r}{r} \frac{T_0(m) - T_W}{T_{0D} - T_W} \right] T_0(\text{measured})$$

where r is the measured probe recovery factor. The author allowed for real gas effects by using the Beattie - Bridgeman equation of state (see Kestin, 1979, Vol. II, p. 228) and allowing for the variation of specific heats. The probe correction procedure is described in the papers by Peterson and George cited above, allowing for viscous interactions and thermal transpiration effects. Viscosities were calculated from Sutherland's formula for $T > 100K$. For $T < 100K$ a linear variation was assumed (Boudreau 1969).

The editors have accepted the corrected data as interpolated by the author, incorporating his assumptions and data reduction procedures. The boundary layer edge stagnation conditions are however calculated from the author's static state values assuming perfect gas relationships, and viscosity values were calculated according to Keyes (1952). The static pressures are those measured using a CCP. These values are discussed below. The profiles form two sets, a low Reynolds number case (series 01) and a "higher" Reynolds number case (series 02). Skin friction and wall heat transfer were not measured but the author's values deduced from a linear approximation to the inner profile are given for convenience, and were used in deducing the hypothetical static pressure profiles. The wall pressure values used were taken from the table in Peterson (1974).

§ DATA: 7405 0101 - 0202. Pitot, T_0 and static pressure profiles. $NX = 2$.

Editors' comments. The measurements presented here describe a simple wave expansion flow of the same general type as those studied by Fischer et al. (CAT 7001) and Beckwith et al. (CAT 7105). The Reynolds numbers are slightly greater - $Re_0 \times 10^{-3}$ from 6 to 12 as compared to about 10 and 4 respectively. In principle, the flow at the upstream stations is in the nozzle expansion field while that at the downstream station is not - the free stream Pitot reading is stated to be constant. Normal pressure gradients are however apparent at both stations in the boundary layer. The streamwise wall pressure gradients are consistent with the pressure differences across the boundary layer if a simple wave structure is assumed, except for profile 0102 for which the streamwise wall pressure gradient is relatively low.

A special effort was made to obtain full and appropriate calibration data for the probes used (Peterson and George, 1974, 1975). The Pitot and total temperature probes presented no special problems, but some difficulty was found with the static probes (cf. Beckwith et al., CAT 7105). Initial measurements (Peterson, 1974) were made with the cone-static probe as "it is less sensitive to gradients in the flow, causes less flow field interference near solid boundaries, is free from over expansion phenomena and usually has a faster response time..." However, it was found that probe heating effects caused large errors when $M > 8$, so the measurements for $(y/\delta) > 0.5$ were not considered trustworthy. This finding prompted the use of the conventional cone-cylinder probe for the revised tests described here. Both probes probably suffer from errors due to high turbulence, with the effects likely to be greater on the CCP. The profiles show a range of values for which $P(\text{measured}) > P_W$ at low values of Y . It seems probable that these are the result of wall interference effects, and that the CCP would be the more strongly affected because of the greater length from tip to sensing hole.

In an attempt to assess the various measurements we have calculated the static pressure following the procedure of § 6.3 of AGARDograph 253. This assumes that the overall pressure difference across the boundary layer is a result of streamwise curvature, whether caused by the wall or by displacement effects, and for convenience, that the radius of curvature of the streamlines may be considered constant. The normal stress acting is then calculated by integrating the momentum flux (Fig. 1) across the layer and matching the stress to the wall pressure and the boundary layer edge pressure (Fig. 2). The Reynolds stress contribution is then subtracted, the distribution being assumed the same as that deduced (Fig. 3) from the measurements of Beckwith et al. (1971) and Fischer et al. (1979). Since the

specific momentum flux rises quite rapidly at low values of Y (Fig. 1) this distribution was applied over the full width of the layer, though, as seen below, the Reynolds stress may not rise so rapidly. Figure 4, for profile 0202, shows a typical result. With allowance for probable wall proximity effects on the pressure measurements, the profile agrees in shape and magnitude with the measurements, though it seems that the start of significant Reynolds stress effects should be taken at about $y/\delta = 0.20$ rather than 0.05 as here. Profiles 0102, 0201 are similar. Profile 0101 however shows a large disagreement between the deduced static pressure profile and that measured (Fig. 5). To obtain agreement, it would be necessary not only to shift the Reynolds stress distribution, but to substantially change its magnitude. The intensity is assumed proportional to the wall shear stress (AGARDograph 253, eqn. 6.3.3), so that this may be a consequence of an inappropriately deduced CF value. Two values are given, depending on a linear and a parabolic fit to the profile data, and the 'linear' value was chosen for all flow profiles here because it was the lower of the two. The relevant values are given in Table 1.

The temperature and velocity profiles are discussed in detail in § 5.2 of the main text and so are not presented here. The principal feature is that in this flow with strong heat transfer and pressure gradient, the conditions required for the van Driest temperature-velocity correlation are violated. The experimental values diverge widely from eqn. 2.5.37 of AG 253, so that the validity of the transformation must also be questioned. It is therefore to be expected that, although the Reynolds numbers are relatively high for a nozzle wall study, the wall law profiles do not agree with the 'standard' semilog law. The outer region profiles also depart noticeably from the 'standard' semi-empirical outer law.

Table 1 Static pressure profiles deduced from the analysis of Finley (1977).

| y/δ | $\frac{\Delta p}{\gamma M_\infty^2 P_\infty C_f}$ | P/P_δ | | | | |
|---|---|--------------|-------|-------|--------|--|
| | | 0101 | 0102 | 0201 | 0202 | |
| 0 | 0 | 1.37 | 1.34 | 1.45 | 1.35 | |
| 0.05 | 0.1 | 1.353 | 1.329 | 1.436 | 1.340 | |
| 0.10 | 0.4 | 1.300 | 1.294 | 1.396 | 1.311 | |
| 0.15 | 1.1 | 1.176 | 1.215 | 1.306 | 1.244 | |
| 0.20 | 1.7 | 1.063 | 1.144 | 1.227 | 1.185 | |
| 0.25 | 2.1 | 0.987 | 1.095 | 1.170 | 1.143 | |
| 0.30 | 2.5 | 0.909 | 1.044 | 1.112 | 1.100 | |
| 0.35 | 2.7 | 0.864 | 1.014 | 1.075 | 1.055 | |
| 0.40 | 2.9 | 0.817 | 0.981 | 1.037 | 1.045 | |
| 0.45 | 3.0 | 0.786 | 0.958 | 1.008 | 1.023 | |
| 0.50 | 2.9 | 0.786 | 0.955 | 1.001 | 1.016 | |
| 0.55 | 2.6 | 0.819 | 0.971 | 1.014 | 1.026 | |
| 0.60 | 2.3 | 0.849 | 0.984 | 1.024 | 1.033 | |
| 0.65 | 1.9 | 0.895 | 1.006 | 1.043 | 1.045 | |
| 0.70 | 1.6 | 0.920 | 1.013 | 1.047 | 1.046 | |
| 0.75 | 1.3 | 0.942 | 1.018 | 1.047 | 1.046 | |
| 0.80 | 1.0 | 0.963 | 1.021 | 1.045 | 1.042 | |
| 0.85 | 0.7 | 0.983 | 1.022 | 1.041 | 1.038 | |
| 0.90 | 0.4 | 1.001 | 1.022 | 1.035 | 1.032 | |
| 0.95 | 0.2 | 1.000 | 1.011 | 1.018 | 1.016 | |
| 1.00 | 0 | 1.000 | 1.000 | 1.000 | 1.000 | |
| CF(linear) x 10 ³ | | 0.691 | 0.420 | 0.463 | 0.326 | |
| CF(parabolic) x 10 ³ | | 0.913 | 0.492 | 0.599 | 0.411 | |
| (Author's values deduced from profile data) | | | | | | |
| δ (mm) (Author) | | 85.09 | 127.0 | 71.12 | 111.76 | |

7405-A-4

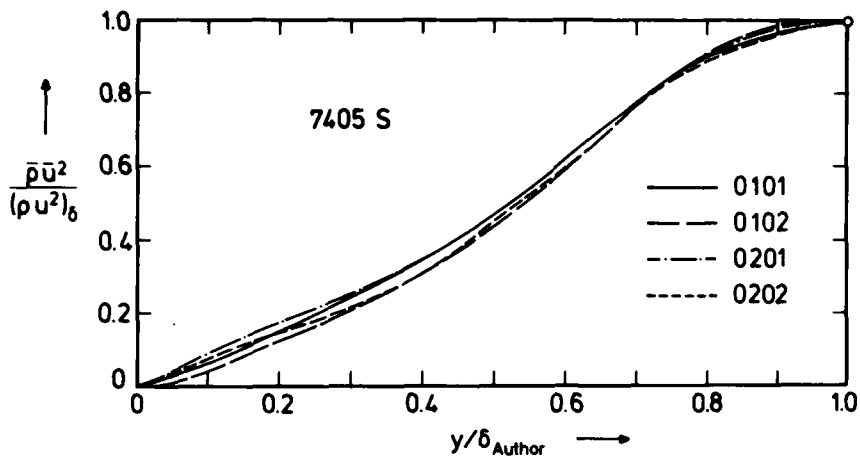


Fig. 1 Profiles of specific momentum flux through the boundary layer.

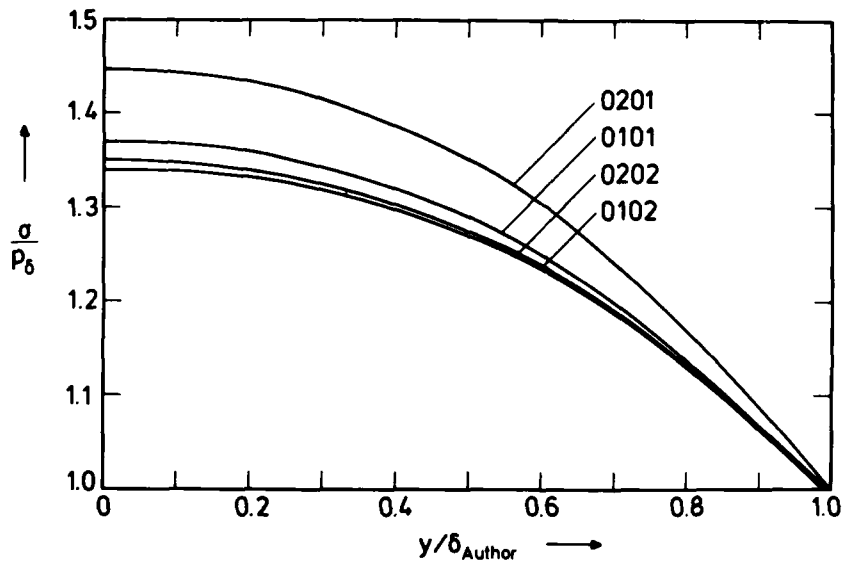


Fig. 2 Total normal stress profiles.

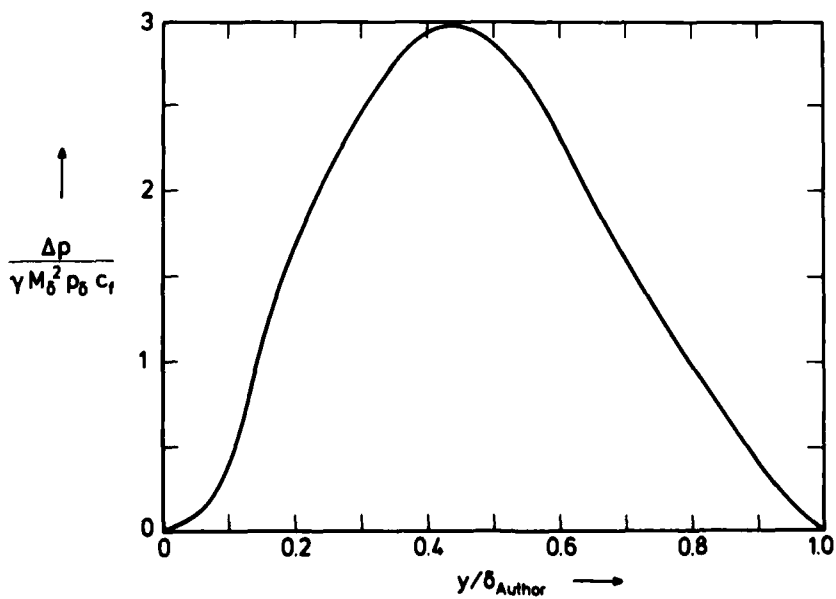


Fig. 3 Contribution of Reynolds normal stress to total normal stress.

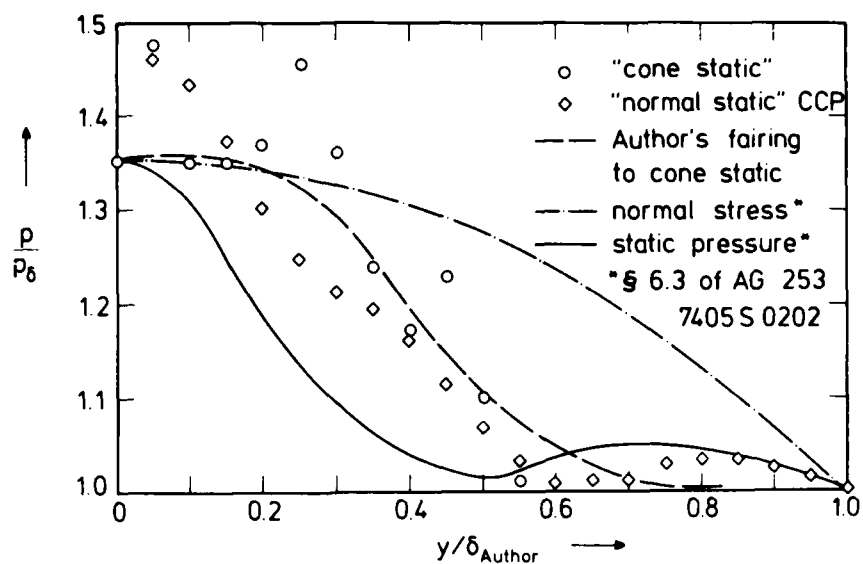


Fig. 4 Normal stress and static pressure profile 7405 S 0202. Experimental results from a "cone-static" probe (static holes on conical nose) and "normal" static probe (static holes on cylindrical surface behind nose).

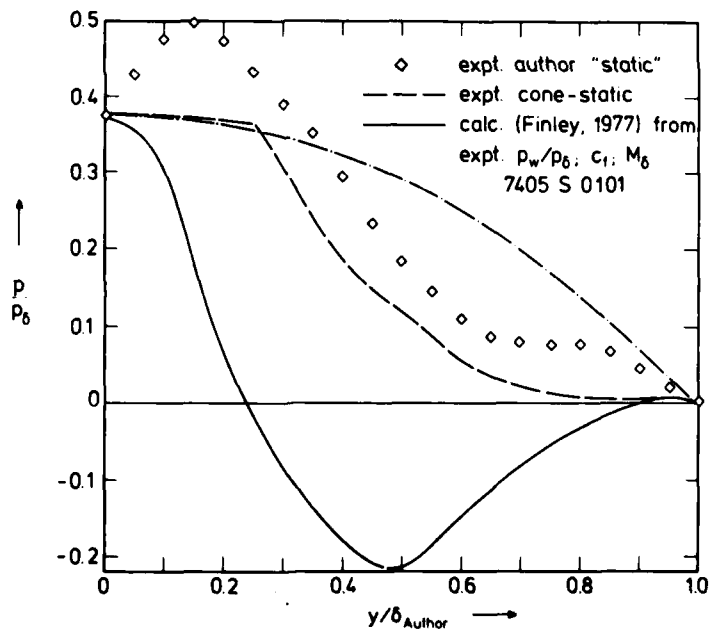


Fig. 5 Normal stress and static pressure profiles for profile 7405 S 0101.

CAT 7405S PETERSON BOUNDARY CONDITIONS AND EVALUATED DATA, SI UNITS

| RUN X * | MO * POD | TW/TR PW/PD | REDZW REDZO | CF * CQ | H12 H32 | H12K H32K | PW TW* | PD* TD* |
|------------------------|-----------------------|-----------------------|-----------------------|-----------------------|------------|-----------------------|-----------------------|-----------------------|
| RZ * | TOD | TAUM | DZ | PI2 | H42 | D2K | UD | TR |
| 7405S0101 | 13.3160 | 0.2406 | 9.6035 ⁺⁰² | 6.9120 ⁻⁰⁴ | 8.1006 | 1.8954 | 3.5465 ⁺⁰¹ | 2.5807 ⁺⁰¹ |
| 1.9185 ⁺⁰⁰ | 7.9498 ⁺⁰⁶ | 1.3742 | 6.5038 ⁺⁰³ | NM | 1.7404 | 1.6651 | 2.9830 ⁺⁰² | 3.7277 ⁺⁰¹ |
| -2.0240 ⁻⁰¹ | 1.3792 ⁺⁰³ | 2.2475 ⁺⁰⁰ | 4.3884 ⁻⁰³ | NM | 1.5233 | 9.2537 ⁻⁰³ | 1.6689 ⁺⁰³ | 1.2396 ⁺⁰³ |
| 7405S0102 | 13.8800 | 0.2386 | 9.6514 ⁺⁰² | 4.1990 ⁻⁰⁴ | 11.0708 | 2.0593 | 2.8000 ⁺⁰¹ | 2.1078 ⁺⁰¹ |
| 2.6603 ⁺⁰⁰ | 8.1868 ⁺⁰⁶ | 1.3284 | 6.9179 ⁺⁰³ | NM | 1.7359 | 1.6698 | 2.9780 ⁺⁰² | 3.5129 ⁺⁰¹ |
| -2.3110 ⁻⁰¹ | 1.3887 ⁺⁰³ | 1.1936 ⁺⁰⁰ | 5.0603 ⁻⁰³ | NM | 1.5325 | 1.2786 ⁻⁰² | 1.6761 ⁺⁰³ | 1.2479 ⁺⁰³ |
| 7405S0201 | 13.6777 | 0.2410 | 1.4388 ⁺⁰³ | 4.6270 ⁻⁰⁴ | 10.7875 | 1.6957 | 8.2967 ⁺⁰¹ | 5.7520 ⁺⁰¹ |
| 1.9185 ⁺⁰⁰ | 2.0212 ⁺⁰⁷ | 1.4424 | 1.0125 ⁺⁰⁴ | NM | 1.7818 | 1.7344 | 2.9830 ⁺⁰² | 3.5847 ⁺⁰¹ |
| -2.0240 ⁻⁰¹ | 1.3771 ⁺⁰³ | 3.4853 ⁺⁰⁰ | 2.8375 ⁻⁰³ | NM | 1.5234 | 6.9525 ⁻⁰³ | 1.6685 ⁺⁰³ | 1.2376 ⁺⁰³ |
| 7405S0202 | 14.2247 | 0.2434 | 1.4508 ⁺⁰³ | 3.2630 ⁻⁰⁴ | 14.8048 | 1.7666 | 6.0219 ⁺⁰¹ | 4.4358 ⁺⁰¹ |
| 2.6603 ⁺⁰⁰ | 2.0370 ⁺⁰⁷ | 1.3576 | 1.1101 ⁺⁰⁴ | NM | 1.7871 | 1.7324 | 2.9780 ⁺⁰² | 3.2837 ⁺⁰¹ |
| -2.3110 ⁻⁰¹ | 1.3617 ⁺⁰³ | 2.0501 ⁺⁰⁰ | 3.4098 ⁻⁰³ | NM | 1.4739 | 1.0013 ⁻⁰² | 1.6608 ⁺⁰³ | 1.2235 ⁺⁰³ |

CF: LINEAR PROFILE SKIN FRICTION ESTIMATE

7405S0101 PETERSON PROFILE TABULATION 23 POINTS, DELTA AT POINT 21

| I | Y | PT2/P | P/PD | TO/TOD | M/MD | U/UD | T/TD | R/RD*U/UD |
|------|-----------------------|-----------------------|---------|---------|---------|---------|---------|-----------|
| 1 | 0.0000 ⁺⁰⁰ | 1.0000 ⁺⁰⁰ | 1.37423 | 0.21629 | 0.00000 | 0.00000 | 8.00220 | 0.00000 |
| 2 | 4.2545 ⁻⁰³ | 4.4495 ⁺⁰⁰ | 1.42702 | 0.26374 | 0.13054 | 0.32104 | 6.04773 | 0.07575 |
| 3 | 8.5090 ⁻⁰³ | 1.0160 ⁺⁰¹ | 1.47892 | 0.30791 | 0.20442 | 0.43600 | 4.54903 | 0.14175 |
| 4 | 1.2763 ⁻⁰² | 1.7136 ⁺⁰¹ | 1.49404 | 0.39804 | 0.26818 | 0.54324 | 4.10323 | 0.19780 |
| 5 | 1.7018 ⁻⁰² | 2.5042 ⁺⁰¹ | 1.47506 | 0.47683 | 0.32565 | 0.62317 | 3.66200 | 0.25101 |
| 6 | 2.1272 ⁻⁰² | 3.3006 ⁺⁰¹ | 1.43681 | 0.53144 | 0.37472 | 0.67527 | 3.24741 | 0.29877 |
| 7 | 2.5527 ⁻⁰² | 4.1323 ⁺⁰¹ | 1.39117 | 0.58421 | 0.41989 | 0.72021 | 2.94202 | 0.34056 |
| 8 | 2.9782 ⁻⁰² | 5.0643 ⁺⁰¹ | 1.34699 | 0.63453 | 0.46533 | 0.76026 | 2.66939 | 0.38363 |
| 9 | 3.4036 ⁻⁰² | 6.2227 ⁺⁰¹ | 1.29663 | 0.68531 | 0.51625 | 0.79866 | 2.39333 | 0.43269 |
| 10 | 3.8290 ⁻⁰² | 7.7056 ⁺⁰¹ | 1.23400 | 0.72872 | 0.57490 | 0.83120 | 2.09040 | 0.49067 |
| 11 | 4.2545 ⁻⁰² | 9.2976 ⁺⁰¹ | 1.18469 | 0.76548 | 0.63183 | 0.85765 | 1.84255 | 0.55144 |
| 12 | 4.6799 ⁻⁰² | 1.1086 ⁺⁰² | 1.14317 | 0.79697 | 0.69021 | 0.87976 | 1.62466 | 0.61903 |
| 13 | 5.1054 ⁻⁰² | 1.3081 ⁺⁰² | 1.10967 | 0.82142 | 0.74497 | 0.89694 | 1.43035 | 0.69585 |
| 14 | 5.5308 ⁻⁰² | 1.4878 ⁺⁰² | 1.08943 | 0.84777 | 0.80000 | 0.91382 | 1.30480 | 0.76299 |
| 15 | 5.9563 ⁻⁰² | 1.6542 ⁺⁰² | 1.08159 | 0.88266 | 0.84369 | 0.93440 | 1.22660 | 0.82394 |
| 16 | 6.3817 ⁻⁰² | 1.8312 ⁺⁰² | 1.07697 | 0.91460 | 0.88779 | 0.95289 | 1.15203 | 0.89081 |
| 17 | 6.8072 ⁻⁰² | 1.9303 ⁺⁰² | 1.07416 | 0.94166 | 0.91157 | 0.96774 | 1.12702 | 0.92234 |
| 18 | 7.2826 ⁻⁰² | 2.0228 ⁺⁰² | 1.06417 | 0.96444 | 0.93321 | 0.98010 | 1.10302 | 0.94558 |
| 19 | 7.6581 ⁻⁰² | 2.1529 ⁺⁰² | 1.04357 | 0.98233 | 0.96280 | 0.99007 | 1.05745 | 0.97707 |
| 20 | 8.0836 ⁻⁰² | 2.2559 ⁺⁰² | 1.02222 | 0.99439 | 0.98563 | 0.99679 | 1.02278 | 0.99624 |
| D 21 | 8.5090 ⁻⁰² | 2.3221 ⁺⁰² | 1.00000 | 1.00000 | 1.00000 | 1.00000 | 1.00000 | 1.00000 |
| 22 | 8.9344 ⁻⁰² | 2.3503 ⁺⁰² | 0.97901 | 1.00414 | 1.00608 | 1.00223 | 0.99237 | 0.98873 |
| 23 | 9.3599 ⁻⁰² | 2.3385 ⁺⁰² | 0.96482 | 1.00961 | 1.00354 | 1.00489 | 1.00268 | 0.96695 |

INPUT VARIABLES Y, T/TD, M/MD, P/PD

7405S0102 PETERSON PROFILE TABULATION 22 POINTS, DELTA AT POINT 21

| I | Y | PT2/P | P/PD | TO/TOD | M/MD | U/UD | T/TD | R/RD*U/UD |
|------|-----------------------|-----------------------|---------|---------|---------|---------|---------|-----------|
| 1 | 0.0000 ⁺⁰⁰ | 1.0000 ⁺⁰⁰ | 1.32837 | 0.21445 | 0.00000 | 0.00000 | 8.47725 | 0.00000 |
| 2 | 6.3500 ⁻⁰³ | 2.5199 ⁺⁰⁰ | 1.34112 | 0.26446 | 0.08918 | 0.25228 | 8.00189 | 0.04228 |
| 3 | 1.2700 ⁻⁰² | 7.5523 ⁺⁰⁰ | 1.39552 | 0.32482 | 0.16883 | 0.41765 | 6.11942 | 0.09524 |
| 4 | 1.9050 ⁻⁰² | 1.5465 ⁺⁰¹ | 1.36792 | 0.39788 | 0.24587 | 0.53440 | 4.72439 | 0.15473 |
| 5 | 2.5400 ⁻⁰² | 2.4013 ⁺⁰¹ | 1.30260 | 0.46387 | 0.30810 | 0.61134 | 3.93711 | 0.20226 |
| 6 | 3.1750 ⁻⁰² | 3.2871 ⁺⁰¹ | 1.23256 | 0.52032 | 0.36144 | 0.66734 | 3.40890 | 0.24129 |
| 7 | 3.8100 ⁻⁰² | 4.3237 ⁺⁰¹ | 1.18974 | 0.57416 | 0.41525 | 0.71554 | 2.96924 | 0.28671 |
| 8 | 4.4450 ⁻⁰² | 5.4608 ⁺⁰¹ | 1.16723 | 0.61764 | 0.46721 | 0.75255 | 2.59452 | 0.33856 |
| 9 | 5.0800 ⁻⁰² | 6.8455 ⁺⁰¹ | 1.13101 | 0.66510 | 0.52355 | 0.78952 | 2.27412 | 0.39266 |
| 10 | 5.7150 ⁻⁰² | 8.4505 ⁺⁰¹ | 1.09034 | 0.71427 | 0.58207 | 0.82503 | 2.00900 | 0.44777 |
| 11 | 6.3500 ⁻⁰² | 1.0437 ⁺⁰² | 1.04644 | 0.75811 | 0.64721 | 0.85581 | 1.74847 | 0.51219 |
| 12 | 6.9850 ⁻⁰² | 1.2663 ⁺⁰² | 1.00851 | 0.79659 | 0.71319 | 0.88181 | 1.52876 | 0.58173 |
| 13 | 7.6200 ⁻⁰² | 1.4975 ⁺⁰² | 0.98281 | 0.83706 | 0.77579 | 0.90735 | 1.36792 | 0.65190 |
| 14 | 8.2550 ⁻⁰² | 1.7343 ⁺⁰² | 0.96154 | 0.87170 | 0.83505 | 0.92856 | 1.23652 | 0.72207 |
| 15 | 8.8900 ⁻⁰² | 2.0504 ⁺⁰² | 0.93135 | 0.89940 | 0.90814 | 0.94583 | 1.08471 | 0.81210 |
| 16 | 9.5250 ⁻⁰² | 2.2427 ⁺⁰² | 0.93230 | 0.93417 | 0.94988 | 0.96521 | 1.03254 | 0.87151 |
| 17 | 1.0160 ⁻⁰¹ | 2.3440 ⁺⁰² | 0.96596 | 0.96674 | 0.97112 | 0.98217 | 1.02289 | 0.92847 |
| 18 | 1.0795 ⁻⁰¹ | 2.3890 ⁺⁰² | 0.96698 | 0.98779 | 0.98043 | 0.99070 | 1.02106 | 0.96734 |
| 19 | 1.1430 ⁻⁰¹ | 2.4515 ⁺⁰² | 1.01487 | 0.97732 | 0.99319 | 0.99548 | 1.00461 | 0.99276 |
| 20 | 1.2065 ⁻⁰¹ | 2.4908 ⁺⁰² | 0.96698 | 0.96674 | 1.00115 | 0.99826 | 0.99425 | 1.00137 |
| D 21 | 1.2700 ⁻⁰¹ | 2.4852 ⁺⁰² | 1.00000 | 1.00000 | 1.00000 | 1.00000 | 1.00000 | 1.00000 |
| 22 | 1.3335 ⁻⁰¹ | 2.4119 ⁺⁰² | 1.02606 | 1.00217 | 0.98513 | 1.00070 | 1.03185 | 0.99508 |

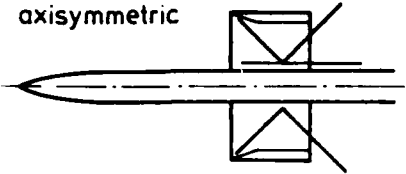
INPUT VARIABLES Y, T/TD, M/MD, P/PD

| 7405S0201 | | PETERSON | | PROFILE TABULATION | | 26 POINTS, DELTA AT POINT 21 | | | |
|-----------|------------------------|------------------------|---------|--------------------|---------|------------------------------|---------|-----------|--|
| I | Y | PT2/P | P/PD | TO/TOD | M/MD | U/UD | T/TD | R/RD*U/UD | |
| 1 | 0.0000 ⁺ 00 | 1.0000 ⁺ 00 | 1.44242 | 0.21662 | 0.00000 | 0.00000 | 8.32158 | 0.00000 | |
| 2 | 3.5560 ⁻ 03 | 6.8737 ⁺ 00 | 1.41029 | 0.33906 | 0.16287 | 0.41642 | 6.53703 | 0.08984 | |
| 3 | 7.1120 ⁻ 03 | 1.7857 ⁺ 01 | 1.35402 | 0.46104 | 0.26868 | 0.58776 | 4.78560 | 0.16630 | |
| 4 | 1.0668 ⁻ 02 | 2.6238 ⁺ 01 | 1.30621 | 0.53718 | 0.32710 | 0.66430 | 4.12452 | 0.21038 | |
| 5 | 1.4224 ⁻ 02 | 3.3804 ⁺ 01 | 1.26338 | 0.58033 | 0.37203 | 0.70669 | 3.60820 | 0.24744 | |
| 6 | 1.7780 ⁻ 02 | 4.1713 ⁺ 01 | 1.22276 | 0.62794 | 0.41382 | 0.74678 | 3.25661 | 0.28039 | |
| 7 | 2.1336 ⁻ 02 | 5.1301 ⁺ 01 | 1.18397 | 0.67066 | 0.45941 | 0.78178 | 2.89585 | 0.31963 | |
| 8 | 2.4892 ⁻ 02 | 6.1555 ⁺ 01 | 1.15267 | 0.70915 | 0.50361 | 0.81160 | 2.59712 | 0.36021 | |
| 9 | 2.6448 ⁻ 02 | 7.3645 ⁺ 01 | 1.12568 | 0.74342 | 0.55120 | 0.83760 | 2.30918 | 0.40831 | |
| 10 | 3.2004 ⁻ 02 | 8.7963 ⁺ 01 | 1.10408 | 0.77493 | 0.60271 | 0.86088 | 2.04017 | 0.46588 | |
| 11 | 3.5560 ⁻ 02 | 1.0383 ⁺ 02 | 1.08870 | 0.80577 | 0.65509 | 0.88290 | 1.81479 | 0.52942 | |
| 12 | 3.9116 ⁻ 02 | 1.2108 ⁺ 02 | 1.07597 | 0.83506 | 0.70763 | 0.90219 | 1.52546 | 0.59720 | |
| 13 | 4.2672 ⁻ 02 | 1.3955 ⁺ 02 | 1.06391 | 0.86290 | 0.75988 | 0.92020 | 1.46646 | 0.66760 | |
| 14 | 4.6228 ⁻ 02 | 1.5969 ⁺ 02 | 1.04706 | 0.89229 | 0.81305 | 0.93837 | 1.33204 | 0.73761 | |
| 15 | 4.9784 ⁻ 02 | 1.8052 ⁺ 02 | 1.02867 | 0.92290 | 0.86458 | 0.95648 | 1.22389 | 0.80391 | |
| 16 | 5.3340 ⁻ 02 | 1.9963 ⁺ 02 | 1.01856 | 0.95028 | 0.90931 | 0.97218 | 1.14305 | 0.86630 | |
| 17 | 5.6896 ⁻ 02 | 2.1402 ⁺ 02 | 1.01877 | 0.97234 | 0.94159 | 0.98443 | 1.09308 | 0.91752 | |
| 18 | 6.0452 ⁻ 02 | 2.2430 ⁺ 02 | 1.02085 | 0.98819 | 0.96399 | 0.99310 | 1.06130 | 0.95524 | |
| 19 | 6.4008 ⁻ 02 | 2.3296 ⁺ 02 | 1.01819 | 0.99637 | 0.98246 | 0.99771 | 1.03130 | 0.98503 | |
| 20 | 6.7564 ⁻ 02 | 2.3832 ⁺ 02 | 1.01001 | 0.99965 | 0.99372 | 0.99966 | 1.01199 | 0.99771 | |
| D 21 | 7.1120 ⁻ 02 | 2.4134 ⁺ 02 | 1.00000 | 1.00000 | 1.00000 | 1.00000 | 1.00000 | 1.00000 | |
| 22 | 7.4676 ⁻ 02 | 2.4231 ⁺ 02 | 0.99973 | 0.99774 | 1.00201 | 0.99892 | 0.99383 | 1.00485 | |
| 23 | 7.8232 ⁻ 02 | 2.4072 ⁺ 02 | 0.98391 | 0.99475 | 0.99872 | 0.99734 | 0.99723 | 0.98401 | |
| 24 | 8.1788 ⁻ 02 | 2.3839 ⁺ 02 | 0.97246 | 0.99197 | 0.99387 | 0.99582 | 1.00393 | 0.96460 | |
| 25 | 8.5344 ⁻ 02 | 2.3562 ⁺ 02 | 0.96069 | 0.98845 | 0.98806 | 0.99390 | 1.01186 | 0.94364 | |
| 26 | 8.8900 ⁻ 02 | 2.3286 ⁺ 02 | 0.95093 | 0.98407 | 0.98224 | 0.99153 | 1.01901 | 0.92529 | |

INPUT VARIABLES Y,T/TD,M/MD,P/PD

| 7405S0202 | | PETERSON | | PROFILE TABULATION | | 21 POINTS, DELTA AT POINT 21 | | | |
|-----------|------------------------|------------------------|---------|--------------------|---------|------------------------------|---------|-----------|--|
| I | Y | PT2/P | P/PD | TO/TOD | M/MD | U/UD | T/TD | R/RD*U/UD | |
| 1 | 0.0000 ⁺ 00 | 1.0000 ⁺ 00 | 1.35757 | 0.21869 | 0.00000 | 0.00000 | 9.06896 | 0.00000 | |
| 2 | 5.5880 ⁻ 03 | 5.3734 ⁺ 00 | 1.46134 | 0.33955 | 0.13688 | 0.38736 | 8.00838 | 0.07068 | |
| 3 | 1.1176 ⁻ 02 | 1.3761 ⁺ 01 | 1.43604 | 0.47500 | 0.22585 | 0.57262 | 6.42818 | 0.12792 | |
| 4 | 1.6764 ⁻ 02 | 2.1619 ⁺ 01 | 1.37258 | 0.56068 | 0.28494 | 0.66368 | 5.42530 | 0.16791 | |
| 5 | 2.2352 ⁻ 02 | 2.9491 ⁺ 01 | 1.30226 | 0.62129 | 0.33379 | 0.72186 | 4.67698 | 0.20099 | |
| 6 | 2.7940 ⁻ 02 | 3.6316 ⁺ 01 | 1.24487 | 0.67493 | 0.37096 | 0.76572 | 4.26062 | 0.22373 | |
| 7 | 3.3528 ⁻ 02 | 4.5996 ⁺ 01 | 1.21507 | 0.70971 | 0.41805 | 0.79822 | 3.64572 | 0.26604 | |
| 8 | 3.9116 ⁻ 02 | 5.6524 ⁺ 01 | 1.19506 | 0.74231 | 0.46388 | 0.82601 | 3.17079 | 0.31132 | |
| 9 | 4.4704 ⁻ 02 | 7.0750 ⁺ 01 | 1.16107 | 0.77526 | 0.51941 | 0.85309 | 2.69750 | 0.36719 | |
| 10 | 5.0292 ⁻ 02 | 8.9392 ⁺ 01 | 1.11353 | 0.80051 | 0.58425 | 0.87460 | 2.24090 | 0.43460 | |
| 11 | 5.5880 ⁻ 02 | 1.0982 ⁺ 02 | 1.06611 | 0.82335 | 0.64790 | 0.89263 | 1.89815 | 0.50135 | |
| 12 | 6.1468 ⁻ 02 | 1.3138 ⁺ 02 | 1.03167 | 0.85585 | 0.70889 | 0.91427 | 1.66339 | 0.56705 | |
| 13 | 6.7056 ⁻ 02 | 1.5606 ⁺ 02 | 1.00620 | 0.89030 | 0.77282 | 0.93598 | 1.46682 | 0.64206 | |
| 14 | 7.2644 ⁻ 02 | 1.7686 ⁺ 02 | 1.00601 | 0.91601 | 0.82284 | 0.95163 | 1.33752 | 0.71576 | |
| 15 | 7.8232 ⁻ 02 | 1.9766 ⁺ 02 | 1.01068 | 0.94430 | 0.87000 | 0.96801 | 1.23800 | 0.79027 | |
| 16 | 8.3820 ⁻ 02 | 2.0968 ⁺ 02 | 1.02680 | 0.96152 | 0.89614 | 0.97768 | 1.19028 | 0.84340 | |
| 17 | 8.9408 ⁻ 02 | 2.2312 ⁺ 02 | 1.03609 | 0.97228 | 0.92447 | 0.98402 | 1.13299 | 0.89986 | |
| 18 | 9.4996 ⁻ 02 | 2.3627 ⁺ 02 | 1.03380 | 0.97918 | 0.95137 | 0.98829 | 1.07911 | 0.94679 | |
| 19 | 1.0058 ⁻ 01 | 2.4796 ⁺ 02 | 1.02570 | 0.98535 | 0.97467 | 0.99202 | 1.03590 | 0.98225 | |
| 20 | 1.0617 ⁻ 01 | 2.5603 ⁺ 02 | 1.01521 | 0.99294 | 0.99043 | 0.99623 | 1.01175 | 0.99965 | |
| D 21 | 1.1176 ⁻ 01 | 2.6099 ⁺ 02 | 1.00000 | 1.00000 | 1.00000 | 1.00000 | 1.00000 | 1.00000 | |

INPUT VARIABLES Y,T/TD,M/MD,P/PD

| | | |
|--|--|-----------------|
| axisymmetric  | M: 7.2 (Free-stream) R THETA x 10 ⁻³ : 8.5 (Initially) TW/TR: 0.5 | 7501 |
| | | VPG-SBLI SHT |
| Blowdown axisymmetric wind tunnel. Useful running time 3 minutes, D = 1.07 m. PO: 3.5 MN/m ² TO: 695K. Air, dew point 205K. RE/m x 10 ⁻⁶ : 11 (Free-stream). | | |
| KUSSOY M.I., HORSTMAN C.C., 1975. An experimental documentation of a hypersonic shock-wave turbulent boundary layer interaction flow - with and without separation. NASA TMX 62,412. And: Horstman, C.C., private communications, Mikulla, V., private communications, Mikulla and Horstman (1976), Marvin et al. (1975). | | |

- 1 The test boundary layer was formed on a 10° semi-apex angle cone-ogive-cylinder 3.30 m long and 203 mm in diameter with a shoulder fairing radius of 810 mm. The model was mounted on the centreline of the tunnel, and is generally similar to that used by Horstman and Owen (CAT 7205) save that provision was made for active cooling, which would maintain a constant surface temperature of 300K ± 5K during a run. An annular shock generator, outside diameter 0.51, inside diameter 0.46 m, was mounted coaxially with the model and could be traversed in the axial direction. Two deflection angles, 7.5° and 15° (series 01 and 02) were used, and the shock waves produced were followed closely by an expansion. Measurements were made at different stations in relation to the wave structure by traversing the shock generator, so moving the wave pattern over instruments at fixed stations in the rear part of the model. The undisturbed boundary layer thickness at shock impingement point increased by about 10% as the shock structure was moved from the foremost to the rear-most position used. The X-coordinate is measured from the leading edge of the shock generator. The test region extended from X = 0.42 to 0.95 m for series 01 and X = 0.20 to 0.95 m for series 02.
- 2 The empty-tunnel inviscid flow test-core was 0.7 m in diameter and in this region small disturbances were less than ±0.05 in Mach number and ±3% in total temperature. There was an axial Mach number gradient less than 0.12/m, while free-stream turbulence fluctuations were less than 0.83% in TO and 2.7% in specific mass flow. For the stronger shock case, in which there was a small separation region, some unsteadiness of the flow was observed. Run to run variations in reservoir pressure were less than 0.5%, but TO varied by 50K during a run and from run to run. Natural transition occurred between 0.4 and 0.8 m from the model nose. The results of Horstman and Owen (CAT 7205) suggest that the initial test layer is a fully relaxed equilibrium constant pressure turbulent boundary layer. (AGARDograph 253, Figs. 4.3.5/6). Variations in surface pressure and wall shear stress around the model were measured at selected axial positions, and were less than the accuracy of measurement. Oil flow observations were also completely symmetrical.
- 6 Static pressure tappings (D = 1.6 mm) were located along the surface as well as in several instrumentation ports. TW was measured by thermocouples attached to the inside of the model skin every 50 mm. Heat transfer at the wall was determined in runs for which the cooling system was disconnected, using the thin wall transient technique with specially constructed instrumentation ports. Skin friction was measured using a Kistler FEB with the element (d = 9.5 mm) machined to the outside contour of the model. Buoyancy corrections were applied for forces induced by the longitudinal pressure gradients. Static calibrations, and electrical self-calibrations before and after each run, were repeatable to within 5%.
- 7 Pitot, static pressure and TO profiles were measured using a traverse gear with a Y-resolution of 3 μm. The Pitot probes were FPP. The first type was used for measurements outside the separation region, a full size version in the outer part of the layer and a half size version near the wall. For the full size FPP, h₁ = 0.46, h₂ = 0.26, b₁ = 2.0, b₂ = 1.8 mm. Over a length of 10 mm the section changed to a circular tube (d₁ = 1.6, d₂ = 1.3 mm). This section continued to a point about 35 mm back from the

tip, when the tube was by stages faired into a body 6 mm in diameter, mounted on a triangular strut 70 mm back from the tip. The tube was cranked about 10 mm towards the test surface. The second type had the same tip structure save that the change of section from tip to circular tube took place in 2 mm and it was attached to a 3 mm strut 5 mm back from the tip. This probe was used facing both ways in the separated zone.

Two static pressure tubes were used, both CCP with 10° half angle tips geometrically similar to those of Behrens (1963). The larger was made from 1.07 mm tube with 3 orifices ($d = 0.36$ mm) at 120° intervals 13.7 mm from the tip. The tube continued to a point 28.9 mm from the tip before increasing section to enter the same type of support as the Pitot tube, the strut being 80 mm back from the tip. A small tube was used in the separation region, facing both ways. For this the tube diameter was 0.71 mm, with 3 0.23 mm orifices 9.1 mm back from the tip. The support was of 3 mm diameter 26 mm back from the tip.

Two TTP were used, both FWP following Vas (1972). In these the sensor was a chromel-alumel thermocouple formed as a butt weld in a wire 70 μ m in diameter. An auxiliary junction is formed at one end of the wire to allow for temperature correction due to conduction along the support prongs, 10 mm long and 0.51 mm in diameter. For the longer probe, the prongs were predominantly in the stream direction and mounted on a streamwise tube 4 mm in diameter and 53 mm long. The cross section then increased gradually to a 8 mm diameter body mounted on a 20°, 6 mm wide wedge about 85 mm back from the tip. For the small probe used in the separated region, the sensor, again on prongs 10 mm long, was mounted vertically on a tube 4 mm in diameter.

8 Measurements were made at ports 1.6, 1.85, 2.1 and 2.35 m from the model tip. All other positions are stated relative to the leading edge of the shock generator.

9 The data presented are the mean of many runs, with in many cases more than one survey for each type of measurement. The data have been interpolated to chosen X and Y values by the authors, who show, graphically, the scatter in selected wall data. The reservoir total temperature variations both during a run and from run to run were eliminated by a normalisation procedure in which for every relevant datum it was assumed that $(T_0 - T_w)/(T_{0D} - T_w)$ was a function of position only. Run to run variations in
 10 normalised data were less than 5%. Wall heat transfer data errors due to longitudinal conduction were calculated to be less than 5% and no corrections were applied. The Pitot tubes were calibrated in a free jet, matching Mach number, velocity and density and the correction factors indicated were below 1% and so ignored. The static probes were also calibrated for viscous interaction effects, the correction factors agreeing with those of Behrens (1963). The greatest corrections applied were 6% in the low pressure (upstream) region and 2% downstream of the shock interaction. The total temperature probe readings were corrected following the method of Vas (1972). Radiation corrections were found to be negligible, while an independent calibration indicated a maximum corrected T_0 error of 1.5%. All data reduction procedures took account of the caloric imperfections of air.

7 Turbulence measurements were made at four X values for each wave structure by Mikulla and Horstman (1976). The probes consisted of 10 μ m wires mounted on the leading edge of slender wedges made from a refractory ceramic. The probes used correspond to two 45° inclined wires running back from a common apex with an overall width of 3.5 mm. A description is given in Mikulla and Horstman (1975). The probes are operated in the constant temperature mode and yield values for both the turbulent intensities and the Reynolds shear stress.

12 The authors note that "the choice of a boundary layer thickness for these types of interaction flows is rather arbitrary" and the editors agree (see AGARDograph 253 §7.1). The authors have set their 'D' point to the maximum PT2 reading where possible, and in the downstream region where PT2 continually increases, when the local Mach number profile no longer showed curvature. We have accepted the data as presented by the authors. There are two sets of profiles, at 19 stations for
 13 the weaker shock (01) and 18 stations for the strong shock (02). The fluctuation profiles (V. Mikulla,

- 14 private communication) are tabulated in section D, as are the complete wall measurement data. The profile tables use CF values as corrected for buoyancy effects. The uncorrected values are also given in section D. The balance was not cooled so it may be that further correction is called for. (See Voisinnet, 1977.)
- § DATA: 75010101-0213. Pitot, static pressure and TO profiles. NX = 19, 18. CQ by thin wall technique. CF from FEB. Fluctuation profiles (NX = 4).
- 15 Editors' comments. These flows are reported in great detail with exceptionally complete instrumentation, and provide obvious test cases for advanced calculation methods. Turbulence levels are very high, and further unsteadiness in the strong shock case (series 02) arises from the "large excursions" of the separation and reattachment points. The authors estimate the range of movement to have a length scale of about 15 mm, and report that the frequency of the unsteadiness was confined to a narrow band around 15 kHz (Horstman and Owen, 1974). Some question therefore arises as to whether a calculation method should lump together fluctuations from this cause and more random conventional turbulence. (The power spectra obtained by Mikulla and Horstman, 1976, show pronounced peaks at 10, 15, 25 kHz.) We must also express some reservations as to the accuracy of the static pressure profiles. While it is possible to calibrate a probe in steady flow with the appropriate mean flow conditions, the response of such probes to flows with a large fluctuating component is largely unknown. A static probe is also very likely to give dubious readings when any part of it is intersected by a shock wave. We would therefore feel that the measurements, which are very welcome, do not necessarily present a picture of the static pressure field which is accurate to the calibration accuracy of the probes, and would not be surprised if discrepancies were to be found in comparisons with calculations - the defect may lie in the measurements rather than the calculations.

The boundary layer is fairly thick compared to the body (δ/R_z up to 0.2) but such information as we have from extreme cases (Richmond, CAT 5701S) suggests that the effect of transverse curvature here will be negligible. As remarked above, the large variations of pressure in the Y direction make it very difficult to decide upon a value for δ . By the same token (see §§6,7, of AGARDograph 253) it is difficult to choose a D-state with any relevance, the D-state values here being arbitrary scaling quantities. Though it would be possible to calculate a proper displacement thickness, it would be very difficult. The conventionally defined D1, D2 etc. presented here and by the authors have no meaning, are critically dependent on the choice of D-point, and should be disregarded.

Comparisons should be made with the undisturbed flow on the same body, Horstman and Owen (CAT 7205) and with the APG and SBLI cases of Kussoy et al. (CAT 7802S) and Rose (CAT 7306S). Neither experiment is on the same large scale as this one (Rose working with a very small rig). In both cases the test layer is on the inner surface of a cylindrical test section, with the wave pattern produced by a centre-body.

| CAT 7501S | | KUSSOY/HORSTMAN BOUNDARY CONDITIONS AND EVALUATED DATA. SI UNITS | | | | | | | |
|-----------------------|-----------------------|--|-----------------------|-----------------------|---------|-----------------------|-----------------------|-----------------------|--|
| RUN | MD * | TW/TR | RE02W | CF | H12 | H12K | PW | PD* | |
| X * | POD | PW/PD | RE02D | CQ * | H32 | H32K | TW* | TD | |
| RZ * | TOD* | TAUM * | DZ | PIZ | H42 | D2K | UD | TR | |
| 7501S0101 | 6.7020 | 0.4762 | 2.2530 ⁺⁰³ | 8.7503 ⁻⁰⁴ | 13.1371 | 1.3904 | 6.0700 ⁺⁰² | 6.0700 ⁺⁰² | |
| 4.2000 ⁻⁰¹ | 1.9083 ⁺⁰⁶ | 1.0000 | 8.3567 ⁺⁰³ | 2.6241 ⁻⁰⁴ | 1.8119 | 1.7577 | 3.0000 ⁺⁰² | 6.9616 ⁺⁰¹ | |
| 1.0150 ⁻⁰¹ | 6.9500 ⁺⁰² | 1.6700 ⁺⁰¹ | 1.2256 ⁻⁰³ | NC | 0.6038 | 3.2540 ⁻⁰³ | 1.1212 ⁺⁰³ | 6.2996 ⁺⁰² | |
| 7501S0102 | 6.7150 | 0.4762 | 2.2954 ⁺⁰³ | 8.7164 ⁻⁰⁴ | 12.9841 | 1.3733 | 6.0700 ⁺⁰² | 6.0700 ⁺⁰² | |
| 4.4000 ⁻⁰¹ | 1.9318 ⁺⁰⁶ | 1.0000 | 8.5435 ⁺⁰³ | 2.6647 ⁻⁰⁴ | 1.8182 | 1.7653 | 3.0000 ⁺⁰² | 6.9373 ⁺⁰¹ | |
| 1.0150 ⁻⁰¹ | 6.9500 ⁺⁰² | 1.6700 ⁺⁰¹ | 1.2440 ⁻⁰³ | NC | 0.6145 | 3.2073 ⁻⁰³ | 1.1214 ⁺⁰³ | 6.2993 ⁺⁰² | |
| 7501S0103 | 5.7380 | 0.4769 | 1.9401 ⁺⁰³ | 1.1422 ⁻⁰³ | 11.0585 | 1.3978 | 6.2096 ⁺⁰² | 6.7620 ⁺⁰² | |
| 4.6000 ⁻⁰¹ | 8.1265 ⁺⁰⁵ | 0.9183 | 5.5139 ⁺⁰³ | 3.5701 ⁻⁰⁴ | 1.8041 | 1.7571 | 3.0000 ⁺⁰² | 9.1171 ⁺⁰¹ | |
| 1.0150 ⁻⁰¹ | 6.9153 ⁺⁰² | 1.7800 ⁺⁰¹ | 1.2663 ⁻⁰³ | NC | 0.6919 | 3.0329 ⁻⁰³ | 1.0985 ⁺⁰³ | 6.2909 ⁺⁰² | |
| 7501S0104 | 4.5590 | 0.4712 | 1.9088 ⁺⁰³ | 9.0744 ⁻⁰⁴ | 5.9104 | 1.7579 | 7.5875 ⁺⁰² | 6.9684 ⁺⁰² | |
| 4.8000 ⁻⁰¹ | 2.1702 ⁺⁰⁵ | 1.0889 | 2.9630 ⁺⁰³ | 6.8033 ⁻⁰⁴ | 1.7102 | 1.6573 | 3.0000 ⁺⁰² | 1.3477 ⁺⁰² | |
| 1.0150 ⁻⁰¹ | 6.9500 ⁺⁰² | 9.2000 ⁺⁰⁰ | 1.4623 ⁻⁰³ | NC | 0.6083 | 2.5105 ⁻⁰³ | 1.0612 ⁺⁰³ | 6.3674 ⁺⁰² | |
| 7501S0105 | 3.8980 | 0.4749 | 2.5612 ⁺⁰³ | 6.6604 ⁻⁰⁴ | 10.5079 | 2.1091 | 1.5175 ⁺⁰³ | 2.4280 ⁺⁰³ | |
| 5.0000 ⁻⁰¹ | 3.2149 ⁺⁰⁵ | 0.6250 | 4.0927 ⁺⁰³ | 4.7223 ⁻⁰⁴ | 1.6554 | 1.5639 | 3.0000 ⁺⁰² | 1.6967 ⁺⁰² | |
| 1.0150 ⁻⁰¹ | 6.8527 ⁺⁰² | 1.7200 ⁺⁰¹ | 9.3489 ⁻⁰⁴ | NC | 0.4384 | 2.5993 ⁻⁰³ | 1.0180 ⁺⁰² | 6.3165 ⁺⁰² | |
| 7501S0106 | 4.0960 | 0.4740 | 2.9117 ⁺⁰³ | 2.0187 ⁻⁰³ | 6.4282 | 2.0143 | 2.8280 ⁺⁰³ | 2.0626 ⁺⁰³ | |
| 5.2000 ⁻⁰¹ | 3.5565 ⁺⁰⁵ | 1.3711 | 4.9550 ⁺⁰³ | 8.3193 ⁻⁰⁴ | 1.6156 | 1.5777 | 3.0000 ⁺⁰² | 1.5797 ⁺⁰² | |
| 1.0150 ⁻⁰¹ | 6.8805 ⁺⁰² | 4.8900 ⁺⁰¹ | 1.1489 ⁻⁰³ | NC | 0.3663 | 2.1320 ⁻⁰³ | 1.0322 ⁺⁰³ | 6.3292 ⁺⁰² | |
| 7501S0107 | 4.8280 | 0.4721 | 3.9313 ⁺⁰³ | 1.6594 ⁻⁰³ | 5.8255 | 1.6994 | 4.0353 ⁺⁰³ | 2.4486 ⁺⁰³ | |
| 5.4000 ⁻⁰¹ | 1.0575 ⁺⁰⁶ | 1.6480 | 8.4158 ⁺⁰³ | 6.6871 ⁻⁰⁴ | 1.6711 | 1.6387 | 3.0000 ⁺⁰² | 1.2275 ⁺⁰² | |
| 1.0150 ⁻⁰¹ | 6.9500 ⁺⁰² | 6.6300 ⁺⁰¹ | 9.7716 ⁻⁰⁴ | NC | 0.2855 | 1.7997 ⁻⁰³ | 1.0725 ⁺⁰³ | 6.3549 ⁺⁰² | |
| 7501S0108 | 4.7130 | 0.4717 | 4.6423 ⁺⁰³ | 1.2373 ⁻⁰³ | 7.5157 | 1.6240 | 4.7455 ⁺⁰³ | 3.6906 ⁺⁰³ | |
| 5.6000 ⁻⁰¹ | 1.3880 ⁺⁰⁶ | 1.2859 | 9.5799 ⁺⁰³ | 5.2619 ⁻⁰⁴ | 1.6963 | 1.6638 | 3.0000 ⁺⁰² | 1.2770 ⁺⁰² | |
| 1.0150 ⁻⁰¹ | 6.9500 ⁺⁰² | 7.1000 ⁺⁰¹ | 7.9991 ⁻⁰⁴ | NC | 0.2826 | 1.7073 ⁻⁰³ | 1.0678 ⁺⁰³ | 6.3600 ⁺⁰² | |
| 7501S0109 | 4.7910 | 0.4720 | 4.8616 ⁺⁰³ | 1.1160 ⁻⁰³ | 8.1679 | 1.5883 | 4.8700 ⁺⁰³ | 3.9315 ⁺⁰³ | |
| 5.8000 ⁻⁰¹ | 1.6244 ⁺⁰⁶ | 1.2387 | 1.0286 ⁺⁰⁴ | 4.8912 ⁻⁰⁴ | 1.7162 | 1.6806 | 3.0000 ⁺⁰² | 1.2431 ⁺⁰² | |
| 1.0150 ⁻⁰¹ | 6.9500 ⁺⁰² | 7.0500 ⁺⁰¹ | 7.6323 ⁻⁰⁴ | NC | 0.2924 | 1.6952 ⁻⁰³ | 1.0710 ⁺⁰² | 6.3565 ⁺⁰² | |
| 7501S0110 | 4.8380 | 0.4721 | 4.6335 ⁺⁰³ | 1.2193 ⁻⁰³ | 7.2766 | 1.5350 | 4.5525 ⁺⁰³ | 3.4490 ⁺⁰³ | |
| 6.0000 ⁻⁰¹ | 1.5075 ⁺⁰⁶ | 1.3200 | 9.9505 ⁺⁰³ | 5.2869 ⁻⁰⁴ | 1.7384 | 1.7043 | 3.0000 ⁺⁰² | 1.2233 ⁺⁰² | |
| 1.0150 ⁻⁰¹ | 6.9500 ⁺⁰² | 6.8900 ⁺⁰¹ | 8.1458 ⁻⁰⁴ | NC | 0.3344 | 1.6626 ⁻⁰³ | 1.0729 ⁺⁰³ | 6.3544 ⁺⁰² | |
| 7501S0111 | 4.9750 | 0.4725 | 4.4209 ⁺⁰³ | 1.1882 ⁻⁰³ | 8.4340 | 1.4851 | 4.0699 ⁺⁰³ | 3.3179 ⁺⁰³ | |
| 6.2000 ⁻⁰¹ | 1.7049 ⁺⁰⁶ | 1.2267 | 9.9133 ⁺⁰³ | 4.9404 ⁻⁰⁴ | 1.7627 | 1.7282 | 3.0000 ⁺⁰² | 1.1680 ⁺⁰² | |
| 1.0150 ⁻⁰¹ | 6.9500 ⁺⁰² | 6.8300 ⁺⁰¹ | 7.6771 ⁻⁰⁴ | NC | 0.3304 | 1.6424 ⁻⁰³ | 1.0780 ⁺⁰³ | 6.3487 ⁺⁰² | |
| 7501S0112 | 5.0640 | 0.4728 | 4.1428 ⁺⁰³ | 1.1781 ⁻⁰³ | 9.3733 | 1.4159 | 3.6420 ⁺⁰³ | 3.1728 ⁺⁰³ | |
| 6.4000 ⁻⁰¹ | 1.8083 ⁺⁰⁶ | 1.1479 | 9.5518 ⁺⁰³ | 4.6476 ⁻⁰⁴ | 1.7952 | 1.7628 | 3.0000 ⁺⁰² | 1.1340 ⁺⁰² | |
| 1.0150 ⁻⁰¹ | 6.9500 ⁺⁰² | 6.7100 ⁺⁰¹ | 7.2823 ⁻⁰⁴ | NC | 0.2923 | 1.5742 ⁻⁰³ | 1.0812 ⁺⁰³ | 6.3451 ⁺⁰² | |
| 7501S0113 | 5.2890 | 0.4734 | 4.3060 ⁺⁰³ | 1.1792 ⁻⁰³ | 9.0691 | 1.3840 | 3.2766 ⁺⁰³ | 2.8280 ⁺⁰³ | |
| 6.6000 ⁻⁰¹ | 2.0829 ⁺⁰⁶ | 1.1586 | 1.0643 ⁺⁰⁴ | 4.4751 ⁻⁰⁴ | 1.8087 | 1.7768 | 3.0000 ⁺⁰² | 1.0539 ⁺⁰² | |
| 1.0150 ⁻⁰¹ | 6.9500 ⁺⁰² | 6.5300 ⁺⁰¹ | 7.8384 ⁻⁰⁴ | NC | 0.4036 | 1.6353 ⁻⁰³ | 1.0886 ⁺⁰³ | 6.3368 ⁺⁰² | |
| 7501S0114 | 5.1860 | 0.4731 | 4.1721 ⁺⁰³ | 1.1980 ⁻⁰³ | 9.1732 | 1.3399 | 2.9798 ⁺⁰³ | 2.7934 ⁺⁰³ | |
| 6.8000 ⁻⁰¹ | 1.8313 ⁺⁰⁶ | 1.0667 | 9.9905 ⁺⁰³ | 4.3582 ⁻⁰⁴ | 1.8278 | 1.8001 | 3.0000 ⁺⁰² | 1.0895 ⁺⁰² | |
| 1.0150 ⁻⁰¹ | 6.9500 ⁺⁰² | 6.3000 ⁺⁰¹ | 7.9728 ⁻⁰⁴ | NC | 0.3989 | 1.6065 ⁻⁰³ | 1.0853 ⁺⁰³ | 6.3405 ⁺⁰² | |
| 7501S0115 | 5.2400 | 0.4733 | 4.0886 ⁺⁰³ | 1.2271 ⁻⁰³ | 9.2379 | 1.3166 | 2.6969 ⁺⁰³ | 2.5524 ⁺⁰³ | |
| 7.0000 ⁻⁰¹ | 1.7790 ⁺⁰⁶ | 1.0566 | 9.9546 ⁺⁰³ | 4.3780 ⁻⁰⁴ | 1.8403 | 1.8128 | 3.0000 ⁺⁰² | 1.0706 ⁺⁰² | |
| 1.0150 ⁻⁰¹ | 6.9500 ⁺⁰² | 6.0200 ⁺⁰¹ | 8.3890 ⁻⁰⁴ | NC | 0.3917 | 1.6512 ⁻⁰³ | 1.0871 ⁺⁰³ | 6.3385 ⁺⁰² | |
| 7501S0116 | 5.3950 | 0.4737 | 4.3805 ⁺⁰³ | 1.2129 ⁻⁰³ | 8.6321 | 1.2993 | 2.3108 ⁺⁰³ | 2.1731 ⁺⁰³ | |
| 7.4000 ⁻⁰¹ | 1.8013 ⁺⁰⁶ | 1.0634 | 1.1182 ⁺⁰⁴ | 4.1310 ⁻⁰⁴ | 1.8453 | 1.8173 | 3.0000 ⁺⁰² | 1.0189 ⁺⁰² | |
| 1.0150 ⁻⁰¹ | 6.9500 ⁺⁰² | 5.3700 ⁺⁰¹ | 1.0003 ⁻⁰³ | NC | 0.5346 | 1.8720 ⁻⁰³ | 1.0919 ⁺⁰³ | 6.3332 ⁺⁰² | |
| 7501S0117 | 5.5310 | 0.4740 | 4.1840 ⁺⁰³ | 1.1752 ⁻⁰³ | 9.2110 | 1.2927 | 1.9454 ⁺⁰³ | 1.8556 ⁺⁰³ | |
| 7.8000 ⁻⁰¹ | 1.7858 ⁺⁰⁶ | 1.0484 | 1.1128 ⁺⁰⁴ | 3.9875 ⁻⁰⁴ | 1.8551 | 1.8236 | 3.0000 ⁺⁰² | 9.7634 ⁺⁰¹ | |
| 1.0150 ⁻⁰¹ | 6.9500 ⁺⁰² | 4.6700 ⁺⁰¹ | 1.0683 ⁻⁰³ | NC | 0.5359 | 1.9833 ⁻⁰³ | 1.0958 ⁺⁰³ | 6.3287 ⁺⁰² | |
| 7501S0118 | 5.6830 | 0.4744 | 3.9713 ⁺⁰³ | NM | 9.9948 | 1.2608 | 1.6626 ⁺⁰³ | 1.5794 ⁺⁰³ | |
| 8.2000 ⁻⁰¹ | 1.7904 ⁺⁰⁶ | 1.0527 | 1.1051 ⁺⁰⁴ | 3.8608 ⁻⁰⁴ | 1.8655 | 1.8371 | 3.0000 ⁺⁰² | 9.3172 ⁺⁰¹ | |
| 1.0150 ⁻⁰¹ | 6.9500 ⁺⁰² | NM | 1.1327 ⁻⁰³ | NC | 0.4630 | 2.0965 ⁻⁰³ | 1.0998 ⁺⁰³ | 6.3241 ⁺⁰² | |
| 7501S0119 | 5.8220 | 0.4747 | 3.6746 ⁺⁰³ | NM | 10.5825 | 1.2664 | 1.3864 ⁺⁰³ | 1.3451 ⁺⁰³ | |
| 8.6000 ⁻⁰¹ | 1.7661 ⁺⁰⁶ | 1.0307 | 1.0692 ⁺⁰⁴ | 3.7369 ⁻⁰⁴ | 1.8731 | 1.8382 | 3.0000 ⁺⁰² | 8.9342 ⁺⁰¹ | |
| 1.0150 ⁻⁰¹ | 6.9500 ⁺⁰² | NM | 1.1763 ⁻⁰³ | NC | 0.4898 | 2.1875 ⁻⁰³ | 1.1033 ⁺⁰³ | 6.3201 ⁺⁰² | |

| CAT 75015 KUSSOY/HORSTMAN BOUNDARY CONDITIONS AND EVALUATED DATA, SI UNITS | | | | | | | | | |
|--|---------------------|--------------------------|----------------------|-------------------|-------------------|---------------------|-----------------|-----------------|--|
| RUN X * RZ * | MD * POD TOD* | TW/TR PW/PD TAUM * | RED2W RED2D DZ | CF CQ * PIZ | H12 H32 H42 | H12K H32K D2K | PW TW* UD | PD* TD TR | |
| 750150201 | 6.8420 | 0.4764 | 1.8052**+03 | 8.3958**04 | 13.8716 | 1.3581 | 6.0700**+02 | 6.0700**+02 | |
| 2.0000**01 | 2.1743**+06 | 1.0000 | 6.9499**+03 | 2.5229**04 | 1.8228 | 1.7746 | 3.0000**+02 | 6.7068**+01 | |
| 1.0150**01 | 6.9500**+02 | 1.6700**+01 | 9.4408**04 | NC | 0.5880 | 2.5057**03 | 1.1234**+03 | 6.2970**+02 | |
| 750150202 | 6.8450 | 0.4764 | 2.0261**+03 | 8.7401**04 | 12.2146 | 1.3576 | 6.2096**+02 | 6.0700**+02 | |
| 2.5500**01 | 2.1804**+06 | 1.0230 | 7.8069**+03 | 2.8440**04 | 1.8229 | 1.7759 | 3.0000**+02 | 6.7015**+01 | |
| 1.0150**01 | 6.9500**+02 | 1.7400**+01 | 1.0588**03 | NC | 0.7306 | 2.6115**03 | 1.1235**+03 | 6.2969**+02 | |
| 750150203 | 6.8580 | 0.4764 | 2.3236**+03 | 5.8047**04 | 10.3829 | 1.6101 | 1.0483**+03 | 6.0700**+02 | |
| 2.8000**01 | 2.2067**+06 | 1.7270 | 8.9836**+03 | 3.6549**04 | 1.7571 | 1.7080 | 3.0000**+02 | 6.6786**+01 | |
| 1.0150**01 | 6.9500**+02 | 1.1600**+01 | 1.2098**03 | NC | 0.9868 | 2.6647**03 | 1.1237**+03 | 6.2967**+02 | |
| 750150204 | 4.8470 | 0.4721 | 5.6237**+03 | 2.1727**04 | 20.3135 | 2.1519 | 1.9454**+03 | 3.4144**+03 | |
| 3.0500**01 | 1.5084**+06 | 0.9698 | 1.2111**+04 | 1.7650**04 | 1.7000 | 1.6085 | 3.0000**+02 | 1.2196**+02 | |
| 1.0150**01 | 6.9500**+02 | 1.2200**+01 | 9.9529**04 | NC | 0.4018 | 4.0501**03 | 1.0732**+03 | 6.3540**+02 | |
| 750150205 | 4.0130 | 0.4689 | 3.3293**+03 | NM | 44.8998 | 4.0966 | 2.3315**+03 | 6.8979**+03 | |
| 3.3000**01 | 1.0656**+06 | 0.3380 | 5.4618**+03 | 2.3192**04 | 1.4831 | 1.4129 | 3.0000**+02 | 1.6466**+02 | |
| 1.0150**01 | 6.9500**+02 | NM | 4.0932**04 | NC | 0.5818 | 2.8673**03 | 1.0325**+03 | 6.3984**+02 | |
| 750150206 | 5.2030 | 0.4732 | 3.9812**+03 | 7.1324**04 | 8.8031 | 2.1581 | 2.7588**+03 | 2.0347**+03 | |
| 3.5500**01 | 1.3599**+06 | 1.3559 | 9.5834**+03 | 8.0442**04 | 1.6393 | 1.5612 | 3.0000**+02 | 1.0835**+02 | |
| 1.0150**01 | 6.9500**+02 | 2.7500**+01 | 1.0382**03 | NC | 0.3051 | 2.4345**03 | 1.0859**+03 | 6.3399**+02 | |
| 750150207 | 5.0990 | 0.4734 | 4.3133**+03 | 1.6753**03 | 2.3293 | 1.6541 | 3.4764**+03 | 1.9120**+03 | |
| 3.8000**01 | 1.1346**+06 | 1.8181 | 1.0063**+04 | 1.1317**03 | 1.7129 | 1.6568 | 3.0000**+02 | 1.1199**+02 | |
| 1.0150**01 | 6.9430**+02 | 5.8300**+01 | 1.2417**03 | NC | 0.6884 | 1.8119**03 | 1.0819**+03 | 6.3374**+02 | |
| 750150208 | 4.9920 | 0.4712 | 4.4114**+03 | 1.4535**03 | 5.2666 | 1.6100 | 5.1182**+03 | 2.9658**+03 | |
| 4.0000**01 | 1.5546**+06 | 1.7257 | 9.9170**+03 | 8.1071**04 | 1.7052 | 1.6731 | 3.0000**+02 | 1.1649**+02 | |
| 1.0150**01 | 6.9708**+02 | 7.5200**+01 | 8.5293**04 | NC | 0.1845 | 1.5796**03 | 1.0803**+03 | 6.3670**+02 | |
| 750150209 | 4.6410 | 0.4686 | 4.5410**+03 | 2.0611**03 | 0.7294 | 1.5711 | 5.7252**+03 | 2.6902**+03 | |
| 4.2500**01 | 9.2679**+05 | 2.1282 | 9.1066**+03 | 1.0211**03 | 1.7073 | 1.6876 | 3.0000**+02 | 1.3173**+02 | |
| 1.0150**01 | 6.9917**+02 | 8.3600**+01 | 1.1071**03 | NC | 0.1049 | 1.4984**03 | 1.0680**+03 | 6.4016**+02 | |
| 750150210 | 4.6210 | 0.4714 | 4.7591**+03 | 1.4661**03 | 5.8190 | 1.3952 | 5.4490**+03 | 3.8969**+03 | |
| 4.5000**01 | 1.3100**+06 | 1.3983 | 9.5351**+03 | 6.8904**04 | 1.7997 | 1.7756 | 3.0000**+02 | 1.3186**+02 | |
| 1.0150**01 | 6.9500**+02 | 8.5400**+01 | 8.0488**04 | NC | 0.0973 | 1.4004**03 | 1.0637**+03 | 6.3643**+02 | |
| 750150211 | 4.5570 | 0.4711 | 4.6063**+03 | 1.5014**03 | 6.7441 | 1.2741 | 4.3042**+03 | 3.7525**+03 | |
| 5.0000**01 | 1.1657**+06 | 1.1470 | 9.0402**+03 | 6.3219**04 | 1.8704 | 1.8557 | 3.0000**+02 | 1.3487**+02 | |
| 1.0150**01 | 6.9500**+02 | 8.1900**+01 | 8.2969**04 | NC | 0.2586 | 1.3064**03 | 1.0611**+03 | 6.3675**+02 | |
| 750150212 | 4.6490 | 0.4715 | 4.2820**+03 | 1.5642**03 | 6.7359 | 1.2488 | 3.2559**+03 | 2.9452**+03 | |
| 5.5000**01 | 1.0246**+06 | 1.1055 | 8.6570**+03 | 6.1774**04 | 1.8848 | 1.8719 | 3.0000**+02 | 1.3057**+02 | |
| 1.0150**01 | 6.9500**+02 | 6.9700**+01 | 9.4780**04 | NC | 0.3806 | 1.3803**03 | 1.0651**+03 | 6.3630**+02 | |
| 750150213 | 4.9040 | 0.4723 | 3.8810**+03 | 1.4843**03 | 7.1190 | 1.2411 | 2.4832**+03 | 2.1731**+03 | |
| 6.0000**01 | 1.0272**+06 | 1.1427 | 8.5104**+03 | 5.8502**04 | 1.8818 | 1.8654 | 3.0000**+02 | 1.1962**+02 | |
| 1.0150**01 | 6.9500**+02 | 5.4300**+01 | 1.0564**03 | NC | 0.2991 | 1.6012**03 | 1.0754**+03 | 6.3516**+02 | |
| 750150214 | 5.1400 | 0.4730 | 3.2202**+03 | 1.4257**03 | 8.7740 | 1.2318 | 1.8556**+03 | 1.7105**+03 | |
| 6.5000**01 | 1.0640**+06 | 1.0848 | 7.6021**+03 | 5.3711**04 | 1.8918 | 1.8725 | 3.0000**+02 | 1.1060**+02 | |
| 1.0150**01 | 6.9500**+02 | 4.5100**+01 | 1.0216**03 | NC | 0.2796 | 1.6263**03 | 1.0838**+03 | 6.3422**+02 | |
| 750150215 | 5.1700 | 0.4731 | 2.4934**+03 | 1.5032**03 | 8.8218 | 1.2306 | 1.4902**+03 | 1.3724**+03 | |
| 7.0000**01 | 8.8346**+05 | 1.0858 | 5.9412**+03 | 5.4133**04 | 1.9011 | 1.8817 | 3.0000**+02 | 1.0952**+02 | |
| 1.0150**01 | 6.9500**+02 | 3.8600**+01 | 9.7536**04 | NC | 0.2865 | 1.4882**03 | 1.0848**+03 | 6.3411**+02 | |
| 750150216 | 5.2300 | 0.4733 | 2.0822**+03 | 1.5949**03 | 8.4965 | 1.2451 | 1.2140**+03 | 1.1035**+03 | |
| 7.5000**01 | 7.6047**+05 | 1.1001 | 5.0541**+03 | 5.5597**04 | 1.9013 | 1.8755 | 3.0000**+02 | 1.0741**+02 | |
| 1.0150**01 | 6.9500**+02 | 3.3700**+01 | 9.9167**04 | NC | 0.2616 | 1.4916**03 | 1.0868**+03 | 6.3389**+02 | |
| 750150217 | 5.1420 | 0.4730 | 1.6293**+03 | 1.7597**03 | 9.2792 | 1.2580 | 8.3462**+02 | 8.4130**+02 | |
| 8.5000**01 | 5.2451**+05 | 0.9921 | 3.8489**+03 | 5.2819**04 | 1.8859 | 1.8574 | 3.0000**+02 | 1.1053**+02 | |
| 1.0150**01 | 6.9500**+02 | 2.7400**+01 | 1.0502**03 | NC | 0.4675 | 1.7054**03 | 1.0839**+03 | 6.3421**+02 | |
| 750150218 | 5.1250 | 0.4730 | 1.3330**+03 | 2.0451**03 | 7.6163 | 1.2755 | 6.8955**+02 | 6.2764**+02 | |
| 9.5000**01 | 3.8375**+05 | 1.0986 | 3.1324**+03 | 5.7188**04 | 1.8754 | 1.8464 | 3.0000**+02 | 1.1114**+02 | |
| 1.0150**01 | 6.9500**+02 | 2.3600**+01 | 1.1587**03 | NC | 0.4430 | 1.7756**03 | 1.0833**+03 | 6.3428**+02 | |

TAUM(C), TABLE 3.4 - TAUM(0205) NOT USED (NEGATIVE)

| 7501S0201 | | KUSSOY/HORSTMAN | | PROFILE TABULATION | | | 44 POINTS, DELTA AT POINT 36 | | |
|-----------|-----------|-----------------|---------|--------------------|---------|---------|------------------------------|-----------|--|
| I | Y | PT2/P | P/PD | TO/TOD | M/MD | U/UD | T/TD | R/RD*U/UD | |
| 1 | 0.0000+00 | 1.0000+00 | 1.00000 | 0.43200 | 0.00000 | 0.00000 | 4.47664 | 0.00000 | |
| 2 | 5.0000-04 | 3.4246+00 | 1.00000 | 0.64800 | 0.21967 | 0.47244 | 4.62326 | 0.10214 | |
| 3 | 7.5000-04 | 4.5646+00 | 1.00000 | 0.69300 | 0.25972 | 0.54489 | 4.40152 | 0.12380 | |
| 4 | 1.0000-03 | 5.7072+00 | 1.00000 | 0.73300 | 0.29421 | 0.60264 | 4.19556 | 0.14364 | |
| 5 | 1.2500-03 | 6.3937+00 | 1.00000 | 0.77800 | 0.31307 | 0.64192 | 4.20419 | 0.15268 | |
| 6 | 1.5000-03 | 7.0771+00 | 1.00000 | 0.79600 | 0.33075 | 0.66767 | 4.07494 | 0.16385 | |
| 7 | 1.7500-03 | 7.5319+00 | 1.00000 | 0.80700 | 0.34201 | 0.68328 | 3.99147 | 0.17119 | |
| 8 | 2.0000-03 | 8.1079+00 | 1.00000 | 0.81300 | 0.35574 | 0.69856 | 3.85597 | 0.18116 | |
| 9 | 2.5000-03 | 8.7916+00 | 1.00000 | 0.82400 | 0.37138 | 0.71693 | 3.72659 | 0.19238 | |
| 10 | 3.0000-03 | 9.3626+00 | 1.00000 | 0.83200 | 0.38395 | 0.73074 | 3.62221 | 0.20174 | |
| 11 | 3.5000-03 | 1.0044+01 | 1.00000 | 0.83800 | 0.39842 | 0.74461 | 3.49280 | 0.21318 | |
| 12 | 4.0000-03 | 1.0620+01 | 1.00000 | 0.84700 | 0.41026 | 0.75731 | 3.40746 | 0.22225 | |
| 13 | 4.5000-03 | 1.0962+01 | 1.00000 | 0.85500 | 0.41713 | 0.76575 | 3.37003 | 0.22722 | |
| 14 | 5.0000-03 | 1.1754+01 | 1.00000 | 0.86100 | 0.43262 | 0.77892 | 3.24170 | 0.24028 | |
| 15 | 6.0000-03 | 1.2782+01 | 1.00000 | 0.87500 | 0.45191 | 0.79743 | 3.11366 | 0.25611 | |
| 16 | 7.0000-03 | 1.4272+01 | 1.00000 | 0.88400 | 0.47852 | 0.81682 | 2.91383 | 0.28033 | |
| 17 | 8.0000-03 | 1.5866+01 | 1.00000 | 0.89500 | 0.50541 | 0.83577 | 2.73459 | 0.30563 | |
| 18 | 9.0000-03 | 1.7472+01 | 1.00000 | 0.90600 | 0.53113 | 0.85286 | 2.57842 | 0.33077 | |
| 19 | 1.0000-02 | 1.9178+01 | 1.00000 | 0.91600 | 0.55715 | 0.86850 | 2.42997 | 0.35741 | |
| 20 | 1.1000-02 | 2.1006+01 | 1.00000 | 0.92600 | 0.58375 | 0.88336 | 2.28994 | 0.38576 | |
| 21 | 1.2000-02 | 2.3060+01 | 1.00000 | 0.93500 | 0.61225 | 0.89743 | 2.14856 | 0.41769 | |
| 22 | 1.3000-02 | 2.5348+01 | 1.00000 | 0.94400 | 0.64250 | 0.91108 | 2.01076 | 0.45310 | |
| 23 | 1.4000-02 | 2.7746+01 | 1.00000 | 0.95500 | 0.67276 | 0.92476 | 1.88950 | 0.48942 | |
| 24 | 1.5000-02 | 3.0366+01 | 1.00000 | 0.96500 | 0.70433 | 0.93747 | 1.77160 | 0.52916 | |
| 25 | 1.6000-02 | 3.3106+01 | 1.00000 | 0.97500 | 0.73590 | 0.94940 | 1.66443 | 0.57040 | |
| 26 | 1.7000-02 | 3.6536+01 | 1.00000 | 0.98000 | 0.77360 | 0.95938 | 1.53795 | 0.62380 | |
| 27 | 1.8000-02 | 3.9497+01 | 1.00000 | 0.98600 | 0.80474 | 0.96789 | 1.44658 | 0.66909 | |
| 28 | 1.9000-02 | 4.2811+01 | 1.00000 | 0.99100 | 0.83821 | 0.97576 | 1.35514 | 0.72004 | |
| 29 | 2.0000-02 | 4.6584+01 | 1.00000 | 0.99400 | 0.87474 | 0.98255 | 1.26168 | 0.77876 | |
| 30 | 2.1000-02 | 4.9765+01 | 1.00000 | 0.99700 | 0.90441 | 0.98795 | 1.19325 | 0.82794 | |
| 31 | 2.2000-02 | 5.2511+01 | 1.00000 | 0.99900 | 0.92926 | 0.99196 | 1.13951 | 0.87052 | |
| 32 | 2.3000-02 | 5.5248+01 | 1.00000 | 1.00000 | 0.95338 | 0.99520 | 1.08966 | 0.91331 | |
| 33 | 2.4000-02 | 5.7077+01 | 1.00000 | 1.00000 | 0.96916 | 0.99689 | 1.05805 | 0.94220 | |
| 34 | 2.5000-02 | 5.8676+01 | 1.00000 | 1.00000 | 0.98275 | 0.99830 | 1.03188 | 0.96745 | |
| 35 | 2.6000-02 | 5.9807+01 | 1.00000 | 1.00000 | 0.99225 | 0.99924 | 1.01414 | 0.98531 | |
| D 36 | 2.7000-02 | 6.0737+01 | 1.00000 | 1.00000 | 1.00000 | 1.00000 | 1.00000 | 1.00000 | |
| 37 | 2.8000-02 | 6.1072+01 | 1.00000 | 1.00000 | 1.00278 | 1.00027 | 0.99500 | 1.00529 | |
| 38 | 2.9000-02 | 6.1072+01 | 1.00000 | 1.00000 | 1.00278 | 1.00027 | 0.99500 | 1.00529 | |
| 39 | 3.0000-02 | 6.1072+01 | 1.00000 | 1.00000 | 1.00278 | 1.00027 | 0.99500 | 1.00529 | |
| 40 | 3.1000-02 | 6.1072+01 | 1.00000 | 1.00000 | 1.00278 | 1.00027 | 0.99500 | 1.00529 | |
| 41 | 3.2000-02 | 6.1072+01 | 1.00000 | 1.00000 | 1.00278 | 1.00027 | 0.99500 | 1.00529 | |
| 42 | 3.3000-02 | 6.1072+01 | 1.00000 | 1.00000 | 1.00278 | 1.00027 | 0.99500 | 1.00529 | |
| 43 | 3.4000-02 | 6.1072+01 | 1.00000 | 1.00000 | 1.00278 | 1.00027 | 0.99500 | 1.00529 | |
| 44 | 3.5000-02 | 6.1072+01 | 1.00000 | 1.00000 | 1.00278 | 1.00027 | 0.99500 | 1.00529 | |

INPUT VARIABLES Y,M,P/PINF,TO/TOINF

| 7501S0203 | | KUSSOY/HDRSTMAN | | PROFILE TABULATION | | | 44 POINTS, DELTA AT POINT 37 | | |
|-----------|-----------|-----------------|---------|--------------------|---------|---------|------------------------------|-----------|--|
| I | Y | PT2/P | P/PD | TO/TOD | M/MD | U/UD | T/TD | R/RD*U/UD | |
| 1 | 0.0000+00 | 1.0000+00 | 1.72700 | 0.43200 | 0.00000 | 0.00000 | 4.49558 | 0.00000 | |
| 2 | 5.0000-04 | 1.3250+00 | 1.71600 | 0.54000 | 0.09434 | 0.21483 | 5.18535 | 0.07109 | |
| 3 | 7.5000-04 | 1.5335+00 | 1.70500 | 0.58000 | 0.11753 | 0.27163 | 5.34170 | 0.08670 | |
| 4 | 1.0000-03 | 1.8667+00 | 1.70500 | 0.61700 | 0.14407 | 0.33391 | 5.37200 | 0.10598 | |
| 5 | 1.2500-03 | 2.2145+00 | 1.69300 | 0.65400 | 0.16492 | 0.38392 | 5.41936 | 0.11994 | |
| 6 | 1.5000-03 | 2.5690+00 | 1.68200 | 0.69300 | 0.18285 | 0.42829 | 5.48622 | 0.13131 | |
| 7 | 1.7500-03 | 3.1305+00 | 1.67000 | 0.72700 | 0.20749 | 0.48149 | 5.38474 | 0.14933 | |
| 8 | 2.0000-03 | 3.7686+00 | 1.65900 | 0.74700 | 0.23199 | 0.52703 | 5.16088 | 0.16942 | |
| 9 | 2.5000-03 | 4.8271+00 | 1.64800 | 0.76700 | 0.26742 | 0.58417 | 4.77173 | 0.20175 | |
| 10 | 3.0000-03 | 5.5945+00 | 1.62500 | 0.78200 | 0.29032 | 0.61853 | 4.53913 | 0.22143 | |
| 11 | 3.5000-03 | 6.3827+00 | 1.60200 | 0.79600 | 0.31204 | 0.64884 | 4.32352 | 0.24041 | |
| 12 | 4.0000-03 | 6.9788+00 | 1.58000 | 0.80700 | 0.32750 | 0.66961 | 4.18039 | 0.25308 | |
| 13 | 4.5000-03 | 7.7376+00 | 1.55700 | 0.81800 | 0.34617 | 0.69248 | 4.00177 | 0.26943 | |
| 14 | 5.0000-03 | 8.5905+00 | 1.53400 | 0.82800 | 0.36600 | 0.71464 | 3.81259 | 0.28754 | |
| 15 | 6.0000-03 | 1.0383+01 | 1.47700 | 0.84700 | 0.40449 | 0.75365 | 3.47152 | 0.32065 | |
| 16 | 7.0000-03 | 1.2317+01 | 1.42000 | 0.86400 | 0.44226 | 0.78693 | 3.16610 | 0.35294 | |
| 17 | 8.0000-03 | 1.4416+01 | 1.36400 | 0.88000 | 0.47988 | 0.81613 | 2.89238 | 0.38487 | |
| 18 | 9.0000-03 | 1.6604+01 | 1.30700 | 0.89400 | 0.51619 | 0.84081 | 2.65331 | 0.41418 | |
| 19 | 1.0000-02 | 1.8817+01 | 1.25000 | 0.90700 | 0.55045 | 0.86186 | 2.45151 | 0.43945 | |
| 20 | 1.1000-02 | 2.1140+01 | 1.19300 | 0.92000 | 0.58428 | 0.88097 | 2.27344 | 0.46230 | |
| 21 | 1.2000-02 | 2.3603+01 | 1.13600 | 0.93200 | 0.61811 | 0.89813 | 2.11127 | 0.48325 | |
| 22 | 1.3000-02 | 2.6423+01 | 1.08000 | 0.94300 | 0.65471 | 0.91429 | 1.95016 | 0.50633 | |
| 23 | 1.4000-02 | 2.9785+01 | 1.02300 | 0.95400 | 0.69583 | 0.93027 | 1.78737 | 0.53244 | |
| 24 | 1.5000-02 | 3.2384+01 | 1.00000 | 0.96400 | 0.72601 | 0.94206 | 1.68373 | 0.55951 | |
| 25 | 1.6000-02 | 3.4653+01 | 1.00000 | 0.97400 | 0.75139 | 0.95226 | 1.60614 | 0.59288 | |
| 26 | 1.7000-02 | 3.7042+01 | 1.00000 | 0.98200 | 0.77719 | 0.96115 | 1.52940 | 0.62845 | |
| 27 | 1.8000-02 | 3.9554+01 | 1.00000 | 0.98700 | 0.80344 | 0.96826 | 1.45236 | 0.66668 | |
| 28 | 1.9000-02 | 4.2047+01 | 1.00000 | 0.99200 | 0.82867 | 0.97485 | 1.38393 | 0.70440 | |
| 29 | 2.0000-02 | 4.5116+01 | 1.00000 | 0.99400 | 0.85871 | 0.98036 | 1.30342 | 0.75215 | |
| 30 | 2.1000-02 | 4.8295+01 | 1.00000 | 0.99700 | 0.88874 | 0.98598 | 1.23078 | 0.80110 | |
| 31 | 2.2000-02 | 5.1258+01 | 1.00000 | 0.99800 | 0.91586 | 0.98990 | 1.16821 | 0.84737 | |
| 32 | 2.3000-02 | 5.3979+01 | 1.00000 | 1.00000 | 0.94007 | 0.99374 | 1.11744 | 0.88930 | |
| 33 | 2.4000-02 | 5.6481+01 | 1.00000 | 1.00000 | 0.96180 | 0.99613 | 1.07267 | 0.92865 | |
| 34 | 2.5000-02 | 5.8295+01 | 1.00000 | 1.00000 | 0.97725 | 0.99774 | 1.04238 | 0.95718 | |
| 35 | 2.6000-02 | 5.9667+01 | 1.00000 | 1.00000 | 0.98877 | 0.99890 | 1.02060 | 0.97874 | |
| 36 | 2.7000-02 | 6.0578+01 | 1.00000 | 1.00000 | 0.99635 | 0.99965 | 1.00662 | 0.99307 | |
| D 37 | 2.8000-02 | 6.1019+01 | 1.00000 | 1.00000 | 1.00000 | 1.00000 | 1.00000 | 1.00000 | |
| 38 | 2.9000-02 | 6.1019+01 | 1.00000 | 1.00000 | 1.00000 | 1.00000 | 1.00000 | 1.00000 | |
| 39 | 3.0000-02 | 6.1019+01 | 1.00000 | 1.00000 | 1.00000 | 1.00000 | 1.00000 | 1.00000 | |
| 40 | 3.1000-02 | 6.1019+01 | 1.00000 | 1.00000 | 1.00000 | 1.00000 | 1.00000 | 1.00000 | |
| 41 | 3.2000-02 | 6.1019+01 | 1.00000 | 1.00000 | 1.00000 | 1.00000 | 1.00000 | 1.00000 | |
| 42 | 3.3000-02 | 6.1019+01 | 1.00000 | 1.00000 | 1.00000 | 1.00000 | 1.00000 | 1.00000 | |
| 43 | 3.4000-02 | 6.1019+01 | 1.00000 | 1.00000 | 1.00000 | 1.00000 | 1.00000 | 1.00000 | |
| 44 | 3.5000-02 | 6.1019+01 | 1.00000 | 1.00000 | 1.00000 | 1.00000 | 1.00000 | 1.00000 | |

INPUT VARIABLES Y,M,P/PINF,TO/TOINF

| 750150206 | | KUSSOY/HORSTMAN | | PROFILE TABULATION | | 44 POINTS, DELTA AT POINT 26 | | | |
|-----------|-----------|-----------------|---------|--------------------|---------|------------------------------|---------|-----------|--|
| I | Y | PT2/P | P/PD | TO/TOD | M/MD | U/UD | T/TD | R/RD*U/UD | |
| 1 | 0.0000+00 | 1.0000+00 | 1.35591 | 0.43200 | 0.00000 | 0.00000 | 2.77095 | 0.00000 | |
| 2 | 5.0000-04 | 1.1252+00 | 1.35591 | 0.75000 | 0.07957 | 0.17161 | 4.65124 | 0.05003 | |
| 3 | 7.5000-04 | 1.1498+00 | 1.35591 | 0.76700 | 0.08668 | 0.18847 | 4.72741 | 0.05406 | |
| 4 | 1.0000-03 | 1.1753+00 | 1.35591 | 0.77800 | 0.09341 | 0.20390 | 4.76518 | 0.05802 | |
| 5 | 1.2500-03 | 1.2123+00 | 1.35591 | 0.79000 | 0.10225 | 0.22392 | 4.79579 | 0.06331 | |
| 6 | 1.5000-03 | 1.2745+00 | 1.35591 | 0.79600 | 0.11513 | 0.25128 | 4.76388 | 0.07152 | |
| 7 | 1.7500-03 | 1.3499+00 | 1.35591 | 0.80100 | 0.12858 | 0.27922 | 4.71570 | 0.08028 | |
| 8 | 2.0000-03 | 1.4619+00 | 1.35591 | 0.80700 | 0.14549 | 0.31354 | 4.64404 | 0.09154 | |
| 9 | 2.5000-03 | 1.6258+00 | 1.35591 | 0.81700 | 0.16587 | 0.35423 | 4.56105 | 0.10531 | |
| 10 | 3.0000-03 | 1.7996+00 | 1.35591 | 0.82400 | 0.18374 | 0.38841 | 4.46854 | 0.11786 | |
| 11 | 3.5000-03 | 2.0252+00 | 1.35591 | 0.83100 | 0.20315 | 0.42403 | 4.35673 | 0.13197 | |
| 12 | 4.0000-03 | 2.2497+00 | 1.35591 | 0.83800 | 0.21987 | 0.45382 | 4.26007 | 0.14444 | |
| 13 | 4.5000-03 | 2.5999+00 | 1.35591 | 0.84400 | 0.24294 | 0.49207 | 4.10266 | 0.16263 | |
| 14 | 5.0000-03 | 2.9251+00 | 1.35591 | 0.85100 | 0.26216 | 0.52288 | 3.97823 | 0.17822 | |
| 15 | 6.0000-03 | 3.8253+00 | 1.35591 | 0.86400 | 0.30848 | 0.58995 | 3.65753 | 0.21870 | |
| 16 | 7.0000-03 | 5.0260+00 | 1.35591 | 0.88100 | 0.36056 | 0.65663 | 3.31653 | 0.26845 | |
| 17 | 8.0000-03 | 6.7504+00 | 1.35591 | 0.89000 | 0.42399 | 0.72438 | 2.91898 | 0.33649 | |
| 18 | 9.0000-03 | 9.0019+00 | 1.35591 | 0.92000 | 0.49452 | 0.78800 | 2.53913 | 0.42080 | |
| 19 | 1.0000-02 | 1.2255+01 | 1.35591 | 0.94200 | 0.58140 | 0.84951 | 2.13496 | 0.53952 | |
| 20 | 1.1000-02 | 1.7146+01 | 1.30519 | 0.96600 | 0.69172 | 0.90867 | 1.72568 | 0.68726 | |
| 21 | 1.2000-02 | 2.1058+01 | 1.24761 | 0.99100 | 0.76860 | 0.94573 | 1.51403 | 0.77931 | |
| 22 | 1.3000-02 | 2.4218+01 | 1.18317 | 0.99900 | 0.82549 | 0.96495 | 1.36645 | 0.83553 | |
| 23 | 1.4000-02 | 2.7274+01 | 1.11874 | 1.00000 | 0.87699 | 0.97739 | 1.24206 | 0.88034 | |
| 24 | 1.5000-02 | 3.0093+01 | 1.06444 | 1.00000 | 0.92197 | 0.98652 | 1.14494 | 0.91716 | |
| 25 | 1.6000-02 | 3.3002+01 | 1.01700 | 1.00000 | 0.96617 | 0.99449 | 1.05948 | 0.95462 | |
| D 26 | 1.7000-02 | 3.5320+01 | 1.00000 | 1.00000 | 1.00000 | 1.00000 | 1.00000 | 1.00000 | |
| 27 | 1.8000-02 | 3.6659+01 | 1.01700 | 1.00000 | 1.01903 | 1.00290 | 0.96859 | 1.05303 | |
| 28 | 1.9000-02 | 3.6250+01 | 1.08473 | 1.00000 | 1.01326 | 1.00203 | 0.97796 | 1.11143 | |
| 29 | 2.0000-02 | 3.1949+01 | 1.30519 | 1.00000 | 0.95041 | 0.99176 | 1.08889 | 1.18876 | |
| 30 | 2.1000-02 | 2.9113+01 | 1.52566 | 1.00000 | 0.90659 | 0.98353 | 1.17692 | 1.27496 | |
| 31 | 2.2000-02 | 2.6922+01 | 1.76283 | 1.00000 | 0.87123 | 0.97614 | 1.25533 | 1.37077 | |
| 32 | 2.3000-02 | 2.4584+01 | 2.06802 | 1.00000 | 0.83183 | 0.96700 | 1.35141 | 1.47977 | |
| 33 | 2.4000-02 | 2.2942+01 | 2.30519 | 1.00000 | 0.80300 | 0.95964 | 1.42820 | 1.54891 | |
| 34 | 2.5000-02 | 2.1607+01 | 2.52566 | 1.00000 | 0.77878 | 0.95296 | 1.49735 | 1.60742 | |
| 35 | 2.6000-02 | 2.0883+01 | 2.67810 | 1.00000 | 0.76533 | 0.94904 | 1.53772 | 1.65286 | |
| 36 | 2.7000-02 | 2.0873+01 | 2.71211 | 1.00000 | 0.76514 | 0.94899 | 1.53831 | 1.67311 | |
| 37 | 2.8000-02 | 2.1399+01 | 2.67810 | 1.00000 | 0.77494 | 0.95186 | 1.50873 | 1.68961 | |
| 38 | 2.9000-02 | 2.5438+01 | 1.93228 | 1.00000 | 0.84643 | 0.97051 | 1.31465 | 1.42645 | |
| 39 | 3.0000-02 | 2.8234+01 | 1.44093 | 1.00000 | 0.89256 | 0.98068 | 1.20719 | 1.17056 | |
| 40 | 3.1000-02 | 2.8114+01 | 1.25447 | 1.00000 | 0.89064 | 0.98028 | 1.21142 | 1.01512 | |
| 41 | 3.2000-02 | 2.8738+01 | 1.20346 | 1.00000 | 0.90063 | 0.98233 | 1.18965 | 0.99374 | |
| 42 | 3.3000-02 | 2.8859+01 | 1.18646 | 1.00000 | 0.90256 | 0.98272 | 1.18552 | 0.98349 | |
| 43 | 3.4000-02 | 2.8980+01 | 1.16945 | 1.00000 | 0.90448 | 0.98310 | 1.18142 | 0.97315 | |
| 44 | 3.5000-02 | 2.9126+01 | 1.15274 | 1.00000 | 0.90678 | 0.98356 | 1.17651 | 0.96369 | |

INPUT VARIABLES Y,M,P/PINF,TO/TOINF

| 750150208 | | KUSSOY/HORSTMAN | | PROFILE TABULATION | | 44 POINTS, DELTA AT POINT 22 | | | |
|-----------|-----------|-----------------|---------|--------------------|---------|------------------------------|---------|-----------|--|
| I | Y | PT2/P | P/PD | TO/TOD | M/MD | U/UD | T/TD | R/RD*U/UD | |
| 1 | 0.0000+00 | 1.0000+00 | 1.72575 | 0.43071 | 0.00000 | 0.00000 | 2.57736 | 0.00000 | |
| 2 | 5.0000-04 | 2.4991+00 | 1.67458 | 0.82752 | 0.24659 | 0.48071 | 3.80015 | 0.21183 | |
| 3 | 7.5000-04 | 2.7459+00 | 1.65125 | 0.84945 | 0.26242 | 0.51049 | 3.78429 | 0.22275 | |
| 4 | 1.0000-03 | 3.0003+00 | 1.62812 | 0.85643 | 0.27764 | 0.53423 | 3.70242 | 0.23493 | |
| 5 | 1.2500-03 | 3.1663+00 | 1.61646 | 0.86441 | 0.28706 | 0.54968 | 3.66671 | 0.24232 | |
| 6 | 1.5000-03 | 3.3345+00 | 1.60479 | 0.87139 | 0.29627 | 0.56428 | 3.62743 | 0.24964 | |
| 7 | 1.7500-03 | 3.5048+00 | 1.59312 | 0.87537 | 0.30529 | 0.57737 | 3.57678 | 0.25717 | |
| 8 | 2.0000-03 | 3.6767+00 | 1.58146 | 0.87936 | 0.31410 | 0.58994 | 3.52754 | 0.26448 | |
| 9 | 2.5000-03 | 4.0278+00 | 1.55833 | 0.88734 | 0.33133 | 0.61381 | 3.43203 | 0.27871 | |
| 10 | 3.0000-03 | 4.5466+00 | 1.53500 | 0.89432 | 0.35517 | 0.64381 | 3.28580 | 0.30076 | |
| 11 | 3.5000-03 | 5.2689+00 | 1.52333 | 0.90030 | 0.38582 | 0.67852 | 3.09284 | 0.33419 | |
| 12 | 4.0000-03 | 5.9206+00 | 1.51167 | 0.90927 | 0.41146 | 0.70683 | 2.95105 | 0.36207 | |
| 13 | 4.5000-03 | 6.5874+00 | 1.50020 | 0.91725 | 0.43610 | 0.73206 | 2.81787 | 0.38974 | |
| 14 | 5.0000-03 | 7.5019+00 | 1.48854 | 0.92921 | 0.46775 | 0.76286 | 2.65992 | 0.42691 | |
| 15 | 6.0000-03 | 9.6828+00 | 1.46521 | 0.94915 | 0.53566 | 0.81892 | 2.33729 | 0.51337 | |
| 16 | 7.0000-03 | 1.3386+01 | 1.44187 | 0.97009 | 0.63442 | 0.88162 | 1.93116 | 0.65825 | |
| 17 | 8.0000-03 | 1.7688+01 | 1.40708 | 0.99202 | 0.73257 | 0.93110 | 1.61543 | 0.81101 | |
| 18 | 9.0000-03 | 2.3385+01 | 1.37229 | 1.01097 | 0.84515 | 0.97346 | 1.32668 | 1.00693 | |
| 19 | 1.0000-02 | 2.7368+01 | 1.32562 | 1.01994 | 0.91567 | 0.99404 | 1.17852 | 1.11812 | |
| 20 | 1.1000-02 | 2.9908+01 | 1.24437 | 1.01994 | 0.95793 | 1.00243 | 1.09506 | 1.13911 | |
| 21 | 1.2000-02 | 3.2039+01 | 1.13958 | 1.01196 | 0.99199 | 1.00460 | 1.02560 | 1.11625 | |
| D 22 | 1.3000-02 | 3.2551+01 | 1.00000 | 1.00000 | 1.00000 | 1.00000 | 1.00000 | 1.00000 | |
| 23 | 1.4000-02 | 3.3235+01 | 0.82562 | 0.99701 | 1.01062 | 1.00025 | 0.97959 | 0.84304 | |
| 24 | 1.5000-02 | 3.5817+01 | 0.65596 | 0.99701 | 1.04968 | 1.00630 | 0.91906 | 0.71822 | |
| 25 | 1.6000-02 | 3.6919+01 | 0.60479 | 0.99701 | 1.06591 | 1.00865 | 0.89546 | 0.68124 | |
| 26 | 1.7000-02 | 3.6153+01 | 0.60479 | 0.99701 | 1.05469 | 1.00704 | 0.91169 | 0.66804 | |
| 27 | 1.8000-02 | 3.6468+01 | 0.59312 | 0.99701 | 1.05929 | 1.00771 | 0.90497 | 0.66046 | |
| 28 | 1.9000-02 | 3.6659+01 | 0.59312 | 0.99701 | 1.06210 | 1.00811 | 0.90092 | 0.66369 | |
| 29 | 2.0000-02 | 3.5844+01 | 0.61625 | 0.99701 | 1.05008 | 1.00636 | 0.91847 | 0.67522 | |
| 30 | 2.1000-02 | 3.4468+01 | 0.65125 | 0.99701 | 1.02945 | 1.00324 | 0.94974 | 0.68794 | |
| 31 | 2.2000-02 | 3.3391+01 | 0.68604 | 0.99701 | 1.01302 | 1.00064 | 0.97571 | 0.70357 | |
| 32 | 2.3000-02 | 3.2422+01 | 0.72104 | 0.99701 | 0.99800 | 0.99817 | 1.00034 | 0.71947 | |
| 33 | 2.4000-02 | 3.1064+01 | 0.76750 | 0.99701 | 0.97656 | 0.99448 | 1.03702 | 0.73601 | |
| 34 | 2.5000-02 | 2.9859+01 | 0.81396 | 0.99701 | 0.95713 | 0.99095 | 1.07191 | 0.75248 | |
| 35 | 2.6000-02 | 2.9077+01 | 0.85591 | 0.99701 | 0.94431 | 0.98852 | 1.09583 | 0.77210 | |
| 36 | 2.7000-02 | 2.8365+01 | 0.89767 | 0.99701 | 0.93249 | 0.98622 | 1.11855 | 0.79147 | |
| 37 | 2.8000-02 | 2.7651+01 | 0.94187 | 0.99701 | 0.92047 | 0.98380 | 1.14232 | 0.81117 | |
| 38 | 2.9000-02 | 2.7016+01 | 0.98138 | 0.99701 | 0.90966 | 0.98155 | 1.16432 | 0.82733 | |
| 39 | 3.0000-02 | 2.6365+01 | 1.02333 | 0.99701 | 0.89844 | 0.97915 | 1.18775 | 0.84361 | |
| 40 | 3.1000-02 | 2.5814+01 | 1.06283 | 0.99701 | 0.88882 | 0.97704 | 1.20835 | 0.85938 | |
| 41 | 3.2000-02 | 2.5156+01 | 1.10479 | 0.99701 | 0.87720 | 0.97441 | 1.23391 | 0.87244 | |
| 42 | 3.3000-02 | 2.5212+01 | 1.11646 | 0.99701 | 0.87821 | 0.97464 | 1.23168 | 0.88346 | |
| 43 | 3.4000-02 | 2.5218+01 | 1.11646 | 0.99701 | 0.88361 | 0.97587 | 1.21972 | 0.89329 | |
| 44 | 3.5000-02 | 2.7274+01 | 1.02333 | 0.99701 | 0.91406 | 0.98247 | 1.15528 | 0.87026 | |

INPUT VARIABLES Y,M,P/PINF,TO/TOINF

| 7501S0215 | | KUSSOY/HORSTMAN | | PROFILE TABULATION | | 44 POINTS, DELTA AT POINT 40 | | |
|-----------|-----------|-----------------|---------|--------------------|---------|------------------------------|---------|-----------|
| I | Y | PT2/P | P/PD | TO/TOD | M/MD | U/UD | T/TO | R/RD*U/UD |
| 1 | 0.0000+00 | 1.0000+00 | 1.08580 | 0.43200 | 0.00000 | 0.00000 | 2.74138 | 0.00000 |
| 2 | 5.0000-04 | 6.9442+00 | 1.08580 | 0.77800 | 0.43327 | 0.68013 | 2.46417 | 0.29969 |
| 3 | 7.5000-04 | 9.7241+00 | 1.08580 | 0.83500 | 0.51838 | 0.76445 | 2.17475 | 0.38167 |
| 4 | 1.0000-03 | 1.1109+01 | 1.08580 | 0.86400 | 0.35590 | 0.79930 | 2.06742 | 0.41979 |
| 5 | 1.2500-03 | 1.1572+01 | 1.08580 | 0.88600 | 0.56789 | 0.81587 | 2.06399 | 0.42920 |
| 6 | 1.5000-03 | 1.2038+01 | 1.08580 | 0.89800 | 0.57969 | 0.82752 | 2.03780 | 0.44093 |
| 7 | 1.7500-03 | 1.2364+01 | 1.08580 | 0.90600 | 0.58781 | 0.83530 | 2.01934 | 0.44914 |
| 8 | 2.0000-03 | 1.2965+01 | 1.08580 | 0.91500 | 0.60251 | 0.84664 | 1.97453 | 0.46557 |
| 9 | 2.5000-03 | 1.3755+01 | 1.08580 | 0.92700 | 0.62128 | 0.86093 | 1.92027 | 0.48680 |
| 10 | 3.0000-03 | 1.4535+01 | 1.08580 | 0.93800 | 0.63926 | 0.87397 | 1.86910 | 0.50771 |
| 11 | 3.5000-03 | 1.5372+01 | 1.08580 | 0.94600 | 0.65803 | 0.88554 | 1.81104 | 0.53092 |
| 12 | 4.0000-03 | 1.6107+01 | 1.08580 | 0.95300 | 0.67408 | 0.89519 | 1.76362 | 0.55114 |
| 13 | 4.5000-03 | 1.6833+01 | 1.08050 | 0.96000 | 0.68956 | 0.90434 | 1.71999 | 0.56810 |
| 14 | 5.0000-03 | 1.7388+01 | 1.07563 | 0.96400 | 0.70116 | 0.91045 | 1.68609 | 0.58082 |
| 15 | 6.0000-03 | 1.8401+01 | 1.06546 | 0.97200 | 0.72186 | 0.92143 | 1.62937 | 0.60253 |
| 16 | 7.0000-03 | 1.9188+01 | 1.05529 | 0.97700 | 0.73752 | 0.92897 | 1.58653 | 0.61791 |
| 17 | 8.0000-03 | 1.9901+01 | 1.04556 | 0.98300 | 0.75145 | 0.93622 | 1.55224 | 0.63062 |
| 18 | 9.0000-03 | 2.0435+01 | 1.04025 | 0.98600 | 0.76170 | 0.94079 | 1.52550 | 0.64153 |
| 19 | 1.0000-02 | 2.1017+01 | 1.03538 | 0.99000 | 0.77273 | 0.94597 | 1.49864 | 0.65355 |
| 20 | 1.1000-02 | 2.1607+01 | 1.03538 | 0.99300 | 0.78375 | 0.95057 | 1.47099 | 0.66907 |
| 21 | 1.2000-02 | 2.2237+01 | 1.03538 | 0.99500 | 0.79536 | 0.95476 | 1.44100 | 0.68601 |
| 22 | 1.3000-02 | 2.2813+01 | 1.03538 | 0.99700 | 0.80880 | 0.95854 | 1.41503 | 0.70137 |
| 23 | 1.4000-02 | 2.3559+01 | 1.03052 | 0.99800 | 0.81915 | 0.96251 | 1.38065 | 0.71842 |
| 24 | 1.5000-02 | 2.4151+01 | 1.03052 | 0.99900 | 0.82959 | 0.96563 | 1.35484 | 0.73447 |
| 25 | 1.6000-02 | 2.4729+01 | 1.03052 | 0.99900 | 0.83965 | 0.96809 | 1.32934 | 0.75048 |
| 26 | 1.7000-02 | 2.5484+01 | 1.02521 | 1.00000 | 0.85261 | 0.97166 | 1.29874 | 0.76701 |
| 27 | 1.8000-02 | 2.6123+01 | 1.02521 | 1.00000 | 0.86344 | 0.97414 | 1.27286 | 0.78461 |
| 28 | 1.9000-02 | 2.6817+01 | 1.02521 | 1.00000 | 0.87505 | 0.97673 | 1.24590 | 0.80372 |
| 29 | 2.0000-02 | 2.7545+01 | 1.02034 | 1.00000 | 0.88704 | 0.97931 | 1.21887 | 0.81981 |
| 30 | 2.1000-02 | 2.8186+01 | 1.02034 | 1.00000 | 0.89749 | 0.98150 | 1.19598 | 0.83736 |
| 31 | 2.2000-02 | 2.8823+01 | 1.02034 | 1.00000 | 0.90774 | 0.98358 | 1.17409 | 0.85476 |
| 32 | 2.3000-02 | 2.9601+01 | 1.01504 | 1.00000 | 0.92012 | 0.98602 | 1.14839 | 0.87153 |
| 33 | 2.4000-02 | 3.0291+01 | 1.01504 | 1.00000 | 0.93095 | 0.98809 | 1.12654 | 0.89030 |
| 34 | 2.5000-02 | 3.0939+01 | 1.01504 | 1.00000 | 0.94101 | 0.98996 | 1.10676 | 0.90792 |
| 35 | 2.6000-02 | 3.1746+01 | 1.01017 | 1.00000 | 0.95338 | 0.99220 | 1.08308 | 0.92541 |
| 36 | 2.7000-02 | 3.2435+01 | 1.01017 | 1.00000 | 0.96383 | 0.99403 | 1.06365 | 0.94405 |
| 37 | 2.8000-02 | 3.3145+01 | 1.00531 | 1.00000 | 0.97447 | 0.99584 | 1.04435 | 0.95861 |
| 38 | 2.9000-02 | 3.3705+01 | 1.00531 | 1.00000 | 0.98279 | 0.99723 | 1.02961 | 0.97369 |
| 39 | 3.0000-02 | 3.4204+01 | 1.00531 | 1.00000 | 0.99014 | 0.99843 | 1.01682 | 0.98713 |
| D 40 | 3.1000-02 | 3.4879+01 | 1.00000 | 1.00000 | 1.00000 | 1.00000 | 1.00000 | 1.00000 |
| 41 | 3.2000-02 | 3.5320+01 | 1.00000 | 1.00000 | 1.00638 | 1.00100 | 0.98933 | 1.01180 |
| 42 | 3.3000-02 | 3.5858+01 | 0.99513 | 1.00000 | 1.01412 | 1.00219 | 0.97660 | 1.02120 |
| 43 | 3.4000-02 | 3.6305+01 | 0.99513 | 1.00000 | 1.02050 | 1.00315 | 0.96628 | 1.03311 |
| 44 | 3.5000-02 | 3.6713+01 | 0.99513 | 1.00000 | 1.02631 | 1.00401 | 0.95703 | 1.04399 |

INPUT VARIABLES Y,H,P/PINF,TO/TOINF

| 7501S0218 | | KUSSOY/HORSTMAN | | PROFILE TABULATION | | 44 POINTS, DELTA AT POINT 44 | | |
|-----------|-----------|-----------------|---------|--------------------|---------|------------------------------|---------|-----------|
| I | Y | PT2/P | P/PD | TO/TOD | M/MD | U/UD | T/TO | R/RD*U/UD |
| 1 | 0.0000+00 | 1.0000+00 | 1.09865 | 0.43200 | 0.00000 | 0.00000 | 2.70135 | 0.00000 |
| 2 | 5.0000-04 | 4.6010+00 | 1.09865 | 0.67600 | 0.34829 | 0.55964 | 2.58184 | 0.23814 |
| 3 | 7.5000-04 | 6.4984+00 | 1.09865 | 0.74400 | 0.42166 | 0.65399 | 2.40557 | 0.29868 |
| 4 | 1.0000-03 | 7.8969+00 | 1.09865 | 0.79600 | 0.46829 | 0.71220 | 2.31296 | 0.33829 |
| 5 | 1.2500-03 | 8.7005+00 | 1.09865 | 0.82400 | 0.49307 | 0.74170 | 2.26273 | 0.36012 |
| 6 | 1.5000-03 | 9.4982+00 | 1.09865 | 0.84400 | 0.51649 | 0.76569 | 2.19781 | 0.38276 |
| 7 | 1.7500-03 | 1.0002+01 | 1.09865 | 0.85800 | 0.53073 | 0.78067 | 2.16366 | 0.39640 |
| 8 | 2.0000-03 | 1.0548+01 | 1.09865 | 0.86800 | 0.54576 | 0.79395 | 2.11636 | 0.41216 |
| 9 | 2.5000-03 | 1.1340+01 | 1.08801 | 0.88300 | 0.56683 | 0.81242 | 2.05428 | 0.43028 |
| 10 | 3.0000-03 | 1.2123+01 | 1.08801 | 0.89400 | 0.58693 | 0.82790 | 1.98970 | 0.45271 |
| 11 | 3.5000-03 | 1.3062+01 | 1.07737 | 0.90400 | 0.61015 | 0.84380 | 1.91256 | 0.47532 |
| 12 | 4.0000-03 | 1.4021+01 | 1.06576 | 0.91200 | 0.63298 | 0.85787 | 1.83684 | 0.49775 |
| 13 | 4.5000-03 | 1.4894+01 | 1.05513 | 0.91900 | 0.65307 | 0.86969 | 1.77339 | 0.51745 |
| 14 | 5.0000-03 | 1.5627+01 | 1.05513 | 0.92600 | 0.66946 | 0.87958 | 1.72623 | 0.53763 |
| 15 | 6.0000-03 | 1.6980+01 | 1.05513 | 0.93800 | 0.69873 | 0.89629 | 1.64542 | 0.57475 |
| 16 | 7.0000-03 | 1.8229+01 | 1.05513 | 0.94900 | 0.72468 | 0.91056 | 1.57877 | 0.60855 |
| 17 | 8.0000-03 | 1.9375+01 | 1.05513 | 0.95900 | 0.74771 | 0.92282 | 1.52324 | 0.63922 |
| 18 | 9.0000-03 | 2.0313+01 | 1.05513 | 0.96600 | 0.76605 | 0.93179 | 1.47954 | 0.66450 |
| 19 | 1.0000-02 | 2.1047+01 | 1.05513 | 0.97200 | 0.78010 | 0.93880 | 1.44825 | 0.68396 |
| 20 | 1.1000-02 | 2.1670+01 | 1.05513 | 0.97700 | 0.79180 | 0.94452 | 1.42293 | 0.70038 |
| 21 | 1.2000-02 | 2.2599+01 | 1.05513 | 0.98200 | 0.80898 | 0.95160 | 1.38368 | 0.72564 |
| 22 | 1.3000-02 | 2.3233+01 | 1.05513 | 0.98600 | 0.82049 | 0.95654 | 1.35913 | 0.74258 |
| 23 | 1.4000-02 | 2.3953+01 | 1.05513 | 0.98900 | 0.83337 | 0.96125 | 1.33046 | 0.76232 |
| 24 | 1.5000-02 | 2.4584+01 | 1.05513 | 0.99100 | 0.84449 | 0.96494 | 1.30561 | 0.77981 |
| 25 | 1.6000-02 | 2.5235+01 | 1.04932 | 0.99300 | 0.85580 | 0.96860 | 1.28097 | 0.79344 |
| 26 | 1.7000-02 | 2.5894+01 | 1.04449 | 0.99400 | 0.86712 | 0.97169 | 1.25572 | 0.80823 |
| 27 | 1.8000-02 | 2.6319+01 | 1.04449 | 0.99600 | 0.87434 | 0.97429 | 1.24168 | 0.81956 |
| 28 | 1.9000-02 | 2.6771+01 | 1.03868 | 0.99800 | 0.88195 | 0.97694 | 1.22700 | 0.82700 |
| 29 | 2.0000-02 | 2.7450+01 | 1.03288 | 0.99900 | 0.89327 | 0.97986 | 1.20326 | 0.84111 |
| 30 | 2.1000-02 | 2.7876+01 | 1.03288 | 0.99900 | 0.90029 | 0.98133 | 1.18812 | 0.85311 |
| 31 | 2.2000-02 | 2.8341+01 | 1.02708 | 1.00000 | 0.90790 | 0.98338 | 1.17316 | 0.86092 |
| 32 | 2.3000-02 | 2.8823+01 | 1.02224 | 1.00000 | 0.91571 | 0.98495 | 1.15695 | 0.87027 |
| 33 | 2.4000-02 | 2.9247+01 | 1.02224 | 1.00000 | 0.92254 | 0.98630 | 1.14300 | 0.88209 |
| 34 | 2.5000-02 | 2.9564+01 | 1.02224 | 1.00000 | 0.92761 | 0.98728 | 1.13279 | 0.89093 |
| 35 | 2.6000-02 | 3.0056+01 | 1.01644 | 1.00000 | 0.93541 | 0.98877 | 1.11733 | 0.89949 |
| 36 | 2.7000-02 | 3.0490+01 | 1.01644 | 1.00000 | 0.94224 | 0.99005 | 1.10404 | 0.91149 |
| 37 | 2.8000-02 | 3.1089+01 | 1.01074 | 1.00000 | 0.95161 | 0.99176 | 1.08617 | 0.92279 |
| 38 | 2.9000-02 | 3.1417+01 | 1.01064 | 1.00000 | 0.95868 | 0.99268 | 1.07666 | 0.93180 |
| 39 | 3.0000-02 | 3.2026+01 | 1.00580 | 1.00000 | 0.96603 | 0.99433 | 1.05941 | 0.94402 |
| 40 | 3.1000-02 | 3.2461+01 | 1.00580 | 1.00000 | 0.97268 | 0.99548 | 1.04742 | 0.95593 |
| 41 | 3.2000-02 | 3.2795+01 | 1.00580 | 1.00000 | 0.97776 | 0.99634 | 1.03838 | 0.96509 |
| 42 | 3.3000-02 | 3.3404+01 | 1.00000 | 1.00000 | 0.98693 | 0.99787 | 1.02231 | 0.97610 |
| 43 | 3.4000-02 | 3.3849+01 | 1.00000 | 1.00000 | 0.99356 | 0.99896 | 1.01090 | 0.98819 |
| D 44 | 3.5000-02 | 3.4283+01 | 1.00000 | 1.00000 | 1.00000 | 1.00000 | 1.00000 | 1.00000 |

INPUT VARIABLES Y,H,P/PINF,TO/TOINF

SECTION D: SUPPLEMENTARY DATA
 D1 - WALL MEASUREMENTS FOR SERIES 01. FACSIMILE OF AUTHORS' TABLE 3
 AUTHORS' SYMBOLS AND UNITS

T_{wm} - wall shear stress reading from balance
 T_{wc} - wall shear stress reading corrected for buoyancy
 (pressure gradient) effects

7.5 DEGREE SHOCK WAVE GENERATOR

| IDENT CAT | x | P_w | T_{wm} | T_{wc} | ρ_w | IDENT CAT | x | P_w | T_{wm} | T_{wc} | ρ_w |
|--------------|-------|---------------------|---------------------|---------------------|---------------------|--------------|-------|---------------------|---------------------|---------------------|---------------------|
| 7501 | (cm) | (N/m ²) | (N/m ²) | (N/m ²) | (W/m ²) | 7501 | (cm) | (N/m ²) | (N/m ²) | (N/m ²) | (W/m ²) |
| 0101 | -42.0 | 607. | 16.7 | 16.7 | 6240. | | 63.0 | 3860. | 71.8 | 67.8 | 39500. |
| | -42.5 | 607. | 16.7 | 16.7 | 6240. | | 63.5 | 3740. | 71.6 | 67.6 | 34800. |
| | -43.0 | 607. | 16.7 | 16.7 | 6240. | 0112 | -64.0 | 3640. | 71.1 | 67.1 | 34200. |
| | -43.5 | 607. | 16.7 | 16.7 | 6240. | | 64.4 | 3540. | 70.6 | 66.7 | 33500. |
| 0102 | -44.0 | 607. | 16.7 | 16.7 | 6360. | | 65.0 | 3450. | 70.1 | 66.3 | 32900. |
| | -44.5 | 607. | 16.7 | 16.7 | 6470. | | 65.5 | 3360. | 69.6 | 65.9 | 32400. |
| | -45.0 | 607. | 16.7 | 17.1 | 6580. | 0113 | -66.0 | 3280. | 69.0 | 65.3 | 31800. |
| | -45.5 | 614. | 16.7 | 17.4 | 6810. | | 66.5 | 3190. | 68.4 | 64.7 | 31200. |
| 0103 | -46.0 | 621. | 16.7 | 17.8 | 7040. | | 67.0 | 3100. | 67.7 | 64.1 | 30600. |
| | -46.5 | 634. | 16.7 | 18.5 | 7380. | 0114 | -67.5 | 3050. | 67.1 | 63.6 | 30100. |
| | -47.0 | 655. | 16.7 | 19.5 | 7720. | | -68.0 | 2980. | 66.3 | 63.0 | 29500. |
| | -47.5 | 689. | 10.8 | 15.0 | 8280. | | 68.5 | 2900. | 65.7 | 62.4 | 29100. |
| 0104 | -48.0 | 759. | 4.1 | 9.2 | 9080. | | 69.0 | 2840. | 64.8 | 61.6 | 28600. |
| | -48.5 | 862. | 1.0 | 7.4 | 10800. | 0115 | -69.5 | 2760. | 64.1 | 60.9 | 28100. |
| | -49.0 | 1040. | 0.1 | 7.9 | 12500. | | -70.0 | 2700. | 63.4 | 60.2 | 27400. |
| | -49.5 | 1240. | 1.6 | 11.4 | 14400. | | 71.0 | 2610. | 61.8 | 58.7 | 26400. |
| 0105 | -50.0 | 1520. | 5.4 | 17.2 | 16500. | | 72.0 | 2490. | 59.8 | 56.9 | 25400. |
| | -50.5 | 1790. | 11.3 | 25.2 | 19300. | 0116 | -73.0 | 2410. | 58.1 | 55.5 | 24300. |
| | -51.0 | 2070. | 18.8 | 34.0 | 22100. | | -74.0 | 2310. | 56.4 | 53.7 | 23400. |
| | -51.5 | 2480. | 26.5 | 42.2 | 24400. | | 74.0 | 2210. | 54.4 | 52.0 | 22500. |
| 0106 | -52.0 | 2830. | 33.0 | 48.9 | 27000. | | 76.0 | 2100. | 52.5 | 50.1 | 21800. |
| | -52.5 | 3170. | 39.2 | 55.0 | 28900. | 0117 | -77.0 | 2030. | 50.5 | 48.2 | 21000. |
| | -53.0 | 3520. | 44.6 | 60.3 | 31200. | | 79.0 | 1900. | 48.8 | 46.7 | 20200. |
| | -53.5 | 3790. | 49.5 | 64.0 | 32900. | | 80.0 | 1810. | 47.6 | 45.5 | 19400. |
| 0107 | -54.0 | 4040. | 53.5 | 66.3 | 34800. | | 81.0 | 1720. | 45.8 | 43.8 | 18700. |
| | -54.5 | 4270. | 57.3 | 68.3 | 36500. | 0118 | -82.0 | 1660. | | | 18000. |
| | -55.0 | 4490. | 60.2 | 69.6 | 37800. | | 83.0 | 1590. | | | 17600. |
| | -55.5 | 4620. | 62.8 | 70.5 | 38800. | | 84.0 | 1520. | | | 16900. |
| 0108 | -56.0 | 4740. | 64.9 | 71.0 | 39500. | | 85.0 | 1460. | | | 16200. |
| | -56.5 | 4830. | 66.7 | 71.1 | 40100. | 0119 | -86.0 | 1390. | | | 15700. |
| | -57.0 | 4860. | 68.1 | 71.1 | 40300. | | 87.0 | 1330. | | | 15100. |
| | -57.5 | 4900. | 69.1 | 70.7 | 40300. | | 88.0 | 1270. | | | 14600. |
| 0109 | -58.0 | 4870. | 70.1 | 70.5 | 40300. | | 89.0 | 1250. | | | 14100. |
| | -58.5 | 4810. | 70.7 | 70.0 | 40200. | | 90.0 | 1210. | | | 13500. |
| | -59.0 | 4750. | 71.4 | 69.7 | 39900. | | 91.0 | 1210. | | | 13100. |
| | -59.5 | 4650. | 71.8 | 69.3 | 39500. | | 92.0 | 1180. | | | 12400. |
| 0110 | -60.0 | 4540. | 72.1 | 68.9 | 38900. | | 93.0 | 1160. | | | 11900. |
| | -60.5 | 4470. | 72.3 | 68.8 | 38500. | | 94.0 | 1130. | | | 11400. |
| | -61.0 | 4370. | 72.6 | 68.6 | 37900. | | 95.0 | 1100. | | | 11000. |
| | -61.5 | 4190. | 72.3 | 68.5 | 37300. | | 96.0 | 1100. | | | 11200. |
| 0111 | -62.0 | 4070. | 72.2 | 68.3 | 36800. | | | | | | |
| | -62.5 | 3960. | 72.1 | 68.1 | 36200. | | | | | | |

SECTION D: SUPPLEMENTARY DATA
 D2 - WALL MEASUREMENTS FOR SERIES 02. FACSIMILE OF AUTHORS' TABLE 4
 AUTHORS' SYMBOLS AND UNITS

T_{WM} - wall shear stress reading from balance
 T_{WC} - wall shear stress reading corrected for buoyancy
 (pressure gradient) effects

15 DEGREE SHOCK WAVE GENERATOR

| IDENT CAT | x (cm) | P_w (N/m ²) | T_{WM} (N/m ²) | T_{WC} (N/m ²) | ρ_w (N/m ²) |
|-----------|----------|---------------------------|------------------------------|------------------------------|------------------------------|
| 7501 | 0201 - | 20.0 | 607 | 16.7 | 6240 |
| | 0202 - | 21.0 | 607 | 16.7 | 6240 |
| | 0203 - | 22.0 | 607 | 16.7 | 6240 |
| | 0204 - | 23.0 | 607 | 16.7 | 6240 |
| | 0205 - | 24.0 | 607 | 16.7 | 6240 |
| | 0206 - | 25.0 | 607 | 16.7 | 6240 |
| | 0207 - | 26.0 | 621 | 16.3 | 7040 |
| | 0208 - | 27.5 | 689 | 15.2 | 7260 |
| | 0209 - | 27.0 | 841 | 9.3 | 7940 |
| | 0210 - | 27.5 | 911 | 5.4 | 8400 |
| 7501 | 0211 - | 28.5 | 1040 | 3.9 | 9080 |
| | 0212 - | 29.0 | 1240 | 2.9 | 9650 |
| | 0213 - | 29.5 | 1420 | 2.3 | 10200 |
| | 0214 - | 30.0 | 1610 | 1.8 | 10900 |
| | 0215 - | 30.5 | 1940 | 1.4 | 11900 |
| | 0216 - | 31.0 | 2050 | 1.2 | 12900 |
| | 0217 - | 31.5 | 2150 | 1.0 | 13900 |
| | 0218 - | 32.0 | 2210 | 0.9 | 14400 |
| | 0219 - | 32.5 | 2340 | 0.8 | 15000 |
| | 0220 - | 33.0 | 2400 | 0.7 | 15900 |
| 7501 | 0221 - | 33.5 | 2400 | 0.7 | 15900 |
| | 0222 - | 34.0 | 2400 | 0.7 | 15900 |
| | 0223 - | 34.5 | 2400 | 0.7 | 15900 |
| | 0224 - | 35.0 | 2400 | 0.7 | 15900 |
| | 0225 - | 35.5 | 2400 | 0.7 | 15900 |
| | 0226 - | 36.0 | 2400 | 0.7 | 15900 |
| | 0227 - | 36.5 | 2400 | 0.7 | 15900 |
| | 0228 - | 37.0 | 2400 | 0.7 | 15900 |
| | 0229 - | 37.5 | 2400 | 0.7 | 15900 |
| | 0230 - | 38.0 | 2400 | 0.7 | 15900 |
| 7501 | 0231 - | 38.5 | 2400 | 0.7 | 15900 |
| | 0232 - | 39.0 | 2400 | 0.7 | 15900 |
| | 0233 - | 39.5 | 2400 | 0.7 | 15900 |
| | 0234 - | 40.0 | 2400 | 0.7 | 15900 |
| | 0235 - | 40.5 | 2400 | 0.7 | 15900 |
| | 0236 - | 41.0 | 2400 | 0.7 | 15900 |
| | 0237 - | 41.5 | 2400 | 0.7 | 15900 |
| | 0238 - | 42.0 | 2400 | 0.7 | 15900 |
| | 0239 - | 42.5 | 2400 | 0.7 | 15900 |
| | 0240 - | 43.0 | 2400 | 0.7 | 15900 |
| 7501 | 0241 - | 43.5 | 2400 | 0.7 | 15900 |
| | 0242 - | 44.0 | 2400 | 0.7 | 15900 |
| | 0243 - | 44.5 | 2400 | 0.7 | 15900 |
| | 0244 - | 45.0 | 2400 | 0.7 | 15900 |
| | 0245 - | 45.5 | 2400 | 0.7 | 15900 |
| | 0246 - | 46.0 | 2400 | 0.7 | 15900 |
| | 0247 - | 46.5 | 2400 | 0.7 | 15900 |
| | 0248 - | 47.0 | 2400 | 0.7 | 15900 |
| | 0249 - | 47.5 | 2400 | 0.7 | 15900 |
| | 0250 - | 48.0 | 2400 | 0.7 | 15900 |
| 7501 | 0251 - | 48.5 | 2400 | 0.7 | 15900 |
| | 0252 - | 49.0 | 2400 | 0.7 | 15900 |
| | 0253 - | 49.5 | 2400 | 0.7 | 15900 |
| | 0254 - | 50.0 | 2400 | 0.7 | 15900 |
| | 0255 - | 50.5 | 2400 | 0.7 | 15900 |
| | 0256 - | 51.0 | 2400 | 0.7 | 15900 |
| | 0257 - | 51.5 | 2400 | 0.7 | 15900 |
| | 0258 - | 52.0 | 2400 | 0.7 | 15900 |
| | 0259 - | 52.5 | 2400 | 0.7 | 15900 |
| | 0260 - | 53.0 | 2400 | 0.7 | 15900 |
| 7501 | 0261 - | 53.5 | 2400 | 0.7 | 15900 |
| | 0262 - | 54.0 | 2400 | 0.7 | 15900 |
| | 0263 - | 54.5 | 2400 | 0.7 | 15900 |
| | 0264 - | 55.0 | 2400 | 0.7 | 15900 |
| | 0265 - | 55.5 | 2400 | 0.7 | 15900 |
| | 0266 - | 56.0 | 2400 | 0.7 | 15900 |
| | 0267 - | 56.5 | 2400 | 0.7 | 15900 |
| | 0268 - | 57.0 | 2400 | 0.7 | 15900 |
| | 0269 - | 57.5 | 2400 | 0.7 | 15900 |
| | 0270 - | 58.0 | 2400 | 0.7 | 15900 |
| 7501 | 0271 - | 58.5 | 2400 | 0.7 | 15900 |
| | 0272 - | 59.0 | 2400 | 0.7 | 15900 |
| | 0273 - | 59.5 | 2400 | 0.7 | 15900 |
| | 0274 - | 60.0 | 2400 | 0.7 | 15900 |
| | 0275 - | 60.5 | 2400 | 0.7 | 15900 |
| | 0276 - | 61.0 | 2400 | 0.7 | 15900 |
| | 0277 - | 61.5 | 2400 | 0.7 | 15900 |
| | 0278 - | 62.0 | 2400 | 0.7 | 15900 |
| | 0279 - | 62.5 | 2400 | 0.7 | 15900 |
| | 0280 - | 63.0 | 2400 | 0.7 | 15900 |
| 7501 | 0281 - | 63.5 | 2400 | 0.7 | 15900 |
| | 0282 - | 64.0 | 2400 | 0.7 | 15900 |
| | 0283 - | 64.5 | 2400 | 0.7 | 15900 |
| | 0284 - | 65.0 | 2400 | 0.7 | 15900 |
| | 0285 - | 65.5 | 2400 | 0.7 | 15900 |
| | 0286 - | 66.0 | 2400 | 0.7 | 15900 |
| | 0287 - | 66.5 | 2400 | 0.7 | 15900 |
| | 0288 - | 67.0 | 2400 | 0.7 | 15900 |
| | 0289 - | 67.5 | 2400 | 0.7 | 15900 |
| | 0290 - | 68.0 | 2400 | 0.7 | 15900 |
| 7501 | 0291 - | 68.5 | 2400 | 0.7 | 15900 |
| | 0292 - | 69.0 | 2400 | 0.7 | 15900 |
| | 0293 - | 69.5 | 2400 | 0.7 | 15900 |
| | 0294 - | 70.0 | 2400 | 0.7 | 15900 |
| | 0295 - | 70.5 | 2400 | 0.7 | 15900 |
| | 0296 - | 71.0 | 2400 | 0.7 | 15900 |
| | 0297 - | 71.5 | 2400 | 0.7 | 15900 |
| | 0298 - | 72.0 | 2400 | 0.7 | 15900 |
| | 0299 - | 72.5 | 2400 | 0.7 | 15900 |
| | 0300 - | 73.0 | 2400 | 0.7 | 15900 |
| 7501 | 0301 - | 73.5 | 2400 | 0.7 | 15900 |
| | 0302 - | 74.0 | 2400 | 0.7 | 15900 |
| | 0303 - | 74.5 | 2400 | 0.7 | 15900 |
| | 0304 - | 75.0 | 2400 | 0.7 | 15900 |
| | 0305 - | 75.5 | 2400 | 0.7 | 15900 |
| | 0306 - | 76.0 | 2400 | 0.7 | 15900 |
| | 0307 - | 76.5 | 2400 | 0.7 | 15900 |
| | 0308 - | 77.0 | 2400 | 0.7 | 15900 |
| | 0309 - | 77.5 | 2400 | 0.7 | 15900 |
| | 0310 - | 78.0 | 2400 | 0.7 | 15900 |
| 7501 | 0311 - | 78.5 | 2400 | 0.7 | 15900 |
| | 0312 - | 79.0 | 2400 | 0.7 | 15900 |
| | 0313 - | 79.5 | 2400 | 0.7 | 15900 |
| | 0314 - | 80.0 | 2400 | 0.7 | 15900 |
| | 0315 - | 80.5 | 2400 | 0.7 | 15900 |
| | 0316 - | 81.0 | 2400 | 0.7 | 15900 |
| | 0317 - | 81.5 | 2400 | 0.7 | 15900 |
| | 0318 - | 82.0 | 2400 | 0.7 | 15900 |
| | 0319 - | 82.5 | 2400 | 0.7 | 15900 |
| | 0320 - | 83.0 | 2400 | 0.7 | 15900 |
| 7501 | 0321 - | 83.5 | 2400 | 0.7 | 15900 |
| | 0322 - | 84.0 | 2400 | 0.7 | 15900 |
| | 0323 - | 84.5 | 2400 | 0.7 | 15900 |
| | 0324 - | 85.0 | 2400 | 0.7 | 15900 |
| | 0325 - | 85.5 | 2400 | 0.7 | 15900 |
| | 0326 - | 86.0 | 2400 | 0.7 | 15900 |
| | 0327 - | 86.5 | 2400 | 0.7 | 15900 |
| | 0328 - | 87.0 | 2400 | 0.7 | 15900 |
| | 0329 - | 87.5 | 2400 | 0.7 | 15900 |
| | 0330 - | 88.0 | 2400 | 0.7 | 15900 |
| 7501 | 0331 - | 88.5 | 2400 | 0.7 | 15900 |
| | 0332 - | 89.0 | 2400 | 0.7 | 15900 |
| | 0333 - | 89.5 | 2400 | 0.7 | 15900 |
| | 0334 - | 90.0 | 2400 | 0.7 | 15900 |
| | 0335 - | 90.5 | 2400 | 0.7 | 15900 |
| | 0336 - | 91.0 | 2400 | 0.7 | 15900 |
| | 0337 - | 91.5 | 2400 | 0.7 | 15900 |
| | 0338 - | 92.0 | 2400 | 0.7 | 15900 |
| | 0339 - | 92.5 | 2400 | 0.7 | 15900 |
| | 0340 - | 93.0 | 2400 | 0.7 | 15900 |
| 7501 | 0341 - | 93.5 | 2400 | 0.7 | 15900 |
| | 0342 - | 94.0 | 2400 | 0.7 | 15900 |
| | 0343 - | 94.5 | 2400 | 0.7 | 15900 |
| | 0344 - | 95.0 | 2400 | 0.7 | 15900 |
| | 0345 - | 95.5 | 2400 | 0.7 | 15900 |
| | 0346 - | 96.0 | 2400 | 0.7 | 15900 |
| | 0347 - | 96.5 | 2400 | 0.7 | 15900 |
| | 0348 - | 97.0 | 2400 | 0.7 | 15900 |
| | 0349 - | 97.5 | 2400 | 0.7 | 15900 |
| | 0350 - | 98.0 | 2400 | 0.7 | 15900 |
| 7501 | 0351 - | 98.5 | 2400 | 0.7 | 15900 |
| | 0352 - | 99.0 | 2400 | 0.7 | 15900 |
| | 0353 - | 99.5 | 2400 | 0.7 | 15900 |
| | 0354 - | 100.0 | 2400 | 0.7 | 15900 |
| | 0355 - | 100.5 | 2400 | 0.7 | 15900 |
| | 0356 - | 101.0 | 2400 | 0.7 | 15900 |
| | 0357 - | 101.5 | 2400 | 0.7 | 15900 |
| | 0358 - | 102.0 | 2400 | 0.7 | 15900 |
| | 0359 - | 102.5 | 2400 | 0.7 | 15900 |
| | 0360 - | 103.0 | 2400 | 0.7 | 15900 |
| 7501 | 0361 - | 103.5 | 2400 | 0.7 | 15900 |
| | 0362 - | 104.0 | 2400 | 0.7 | 15900 |
| | 0363 - | 104.5 | 2400 | 0.7 | 15900 |
| | 0364 - | 105.0 | 2400 | 0.7 | 15900 |
| | 0365 - | 105.5 | 2400 | 0.7 | 15900 |
| | 0366 - | 106.0 | 2400 | 0.7 | 15900 |
| | 0367 - | 106.5 | 2400 | 0.7 | 15900 |
| | 0368 - | 107.0 | 2400 | 0.7 | 15900 |
| | 0369 - | 107.5 | 2400 | 0.7 | 15900 |
| | 0370 - | 108.0 | 2400 | 0.7 | 15900 |
| 7501 | 0371 - | 108.5 | 2400 | 0.7 | 15900 |
| | 0372 - | 109.0 | 2400 | 0.7 | 15900 |
| | 0373 - | 109.5 | 2400 | 0.7 | 15900 |
| | 0374 - | 110.0 | 2400 | 0.7 | 15900 |
| | 0375 - | 110.5 | 2400 | 0.7 | 15900 |
| | 0376 - | 111.0 | 2400 | 0.7 | 15900 |
| | 0377 - | 111.5 | 2400 | 0.7 | 15900 |
| | 0378 - | 112.0 | 2400 | 0.7 | 15900 |
| | 0379 - | 112.5 | 2400 | 0.7 | 15900 |
| | 0380 - | 113.0 | 2400 | 0.7 | 15900 |
| 7501 | 0381 - | 113.5 | 2400 | 0.7 | 15900 |
| | 0382 - | 114.0 | 2400 | 0.7 | 15900 |
| | 0383 - | 114.5 | 2400 | 0.7 | 15900 |
| | 0384 - | 115.0 | 2400 | 0.7 | 15900 |
| | 0385 - | 115.5 | 2400 | 0.7 | 15900 |
| | 0386 - | 116.0 | 2400 | 0.7 | 15900 |
| | 0387 - | 116.5 | 2400 | 0.7 | 15900 |
| | 0388 - | 117.0 | 2400 | 0.7 | 15900 |
| | 0389 - | 117.5 | 2400 | 0.7 | 15900 |
| | 0390 - | 118.0 | 2400 | 0.7 | 15900 |
| 7501 | 0391 - | 118.5 | 2400 | 0.7 | 15900 |
| | 0392 - | 119.0 | 2400 | 0.7 | 15900 |
| | 0393 - | 119.5 | 2400 | 0.7 | 15900 |
| | 0394 - | 120.0 | 2400 | 0.7 | 15900 |
| | 0395 - | 120.5 | 2400 | 0.7 | 15900 |
| | 0396 - | 121.0 | 2400 | 0.7 | 15900 |
| | 0397 - | 121.5 | 2400 | 0.7 | 15900 |
| | 0398 - | 122.0 | 2400 | 0.7 | 15900 |
| | 0399 - | 122.5 | 2400 | 0.7 | 15900 |
| | 0400 - | 123.0 | 2400 | 0.7 | 15900 |
| 7501 | 0401 - | 123.5 | | | |

7501S KUSSOY/MIKULLA TURBULENCE DATA

7501S0101 UT= 4.8682E+01 RHDW= 7.0465E-03 TW= 3.0000E+02 D*= 1.4401E-01

| I | Y [M] | V' UT | RHD*U'V' RHDW*UT2 | (RHD U)' RHDW*UT |
|----|-----------|-----------|----------------------|---------------------|
| 1 | 1.5000E-3 | 8.5184E-1 | -6.8118E-1 | 2.0716E+0 |
| 2 | 2.7500E-3 | 9.3472E-1 | -6.5182E-1 | 2.5398E+0 |
| 3 | 4.0000E-3 | 9.0035E-1 | -5.5199E-1 | 2.7501E+0 |
| 4 | 5.2500E-3 | 8.9044E-1 | -5.5786E-1 | 2.9349E+0 |
| 5 | 6.5000E-3 | 8.7036E-1 | -5.1089E-1 | 3.0840E+0 |
| 6 | 7.7500E-3 | 8.7454E-1 | -6.1071E-1 | 3.2427E+0 |
| 7 | 9.0000E-3 | 8.4592E-1 | -5.6374E-1 | 3.4599E+0 |
| 8 | 1.0250E-2 | 7.6560E-1 | -4.2280E-1 | 3.6338E+0 |
| 9 | 1.1500E-2 | 7.6575E-1 | -4.9327E-1 | 3.8651E+0 |
| 10 | 1.2750E-2 | 7.1901E-1 | -4.4629E-1 | 4.0972E+0 |
| 11 | 1.4000E-2 | 6.7067E-1 | -3.9931E-1 | 4.2825E+0 |
| 12 | 1.5250E-2 | 6.6317E-1 | -3.8170E-1 | 4.6798E+0 |
| 13 | 1.6500E-2 | 6.3393E-1 | -3.7582E-1 | 5.1053E+0 |
| 14 | 1.7750E-2 | 6.2006E-1 | -3.6995E-1 | 5.5978E+0 |
| 15 | 1.9000E-2 | 6.0657E-1 | -3.3472E-1 | 5.8557E+0 |
| 16 | 2.0250E-2 | 5.7105E-1 | -3.4646E-1 | 6.3132E+0 |
| 17 | 2.1500E-2 | 5.3344E-1 | -3.3472E-1 | 6.5940E+0 |
| 18 | 2.2750E-2 | 5.1654E-1 | -2.6425E-1 | 6.8947E+0 |
| 19 | 2.4000E-2 | 4.5342E-1 | -2.3489E-1 | 6.8489E+0 |
| 20 | 2.5250E-2 | 4.1157E-1 | -1.9378E-1 | 7.0506E+0 |
| 21 | 2.6500E-2 | NM | NM | NM |
| 22 | 2.7750E-2 | NM | NM | NM |
| 23 | 2.9000E-2 | NM | NM | NM |

7501S0105 UT= 3.1247E+01 RHDW= 1.7616E-02 TW= 3.0000E+02 D*= 2.6123E-01

| I | Y [M] | V' UT | RHD*U'V' RHDW*UT2 | (RHD U)' RHDW*UT |
|----|-----------|-----------|----------------------|---------------------|
| 1 | 1.5000E-3 | 2.3167E+0 | -3.3069E+0 | 1.8130E+0 |
| 2 | 2.7500E-3 | 2.7544E+0 | -4.5042E+0 | 2.5280E+0 |
| 3 | 4.0000E-3 | 3.7958E+0 | -9.8637E+0 | 4.2042E+0 |
| 4 | 5.2500E-3 | 5.1569E+0 | -1.5508E+1 | 5.8437E+0 |
| 5 | 6.5000E-3 | 5.1392E+0 | -1.3114E+1 | 5.9694E+0 |
| 6 | 7.7500E-3 | 2.8121E+0 | -5.8726E+0 | 5.7837E+0 |
| 7 | 9.0000E-3 | 2.6366E+0 | -4.3902E+0 | 6.0677E+0 |
| 8 | 1.0250E-2 | 1.9644E+0 | -2.7938E+0 | 6.1341E+0 |
| 9 | 1.1500E-2 | 1.8385E+0 | -2.8508E+0 | 8.4610E+0 |
| 10 | 1.2750E-2 | 1.3932E+0 | -1.4824E+0 | 8.4120E+0 |
| 11 | 1.4000E-2 | 1.6228E+0 | -1.1403E+0 | 1.0039E+1 |
| 12 | 1.5250E-2 | 2.0160E+0 | -7.4120E-1 | 9.7426E+0 |
| 13 | 1.6500E-2 | 2.3150E+0 | 0. | 1.0055E+1 |
| 14 | 1.7750E-2 | 1.7760E+0 | 0. | 1.0289E+1 |
| 15 | 1.4000E-2 | 1.6288E+0 | NM | 1.1728E+1 |
| 16 | 2.0250E-2 | 1.7773E+0 | NM | 1.2189E+1 |
| 17 | 2.1500E-2 | 1.1378E+0 | NM | 8.8124E+0 |
| 18 | 2.2750E-2 | 6.4000E-1 | NM | 4.7792E+0 |
| 19 | 2.4000E-2 | NM | NM | 3.5844E+0 |

7501S0110 UT= 3.6107E+01 RHDW= 5.2849E-02 TW= 3.0000E+02 D*= 6.9378E-02

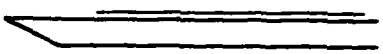
| I | Y [M] | V' UT | RHD*U'V' RHDW*UT2 | (RHD U)' RHDW*UT |
|----|-----------|-----------|----------------------|---------------------|
| 1 | 1.5000E-3 | 1.9737E+0 | -2.1919E+0 | 1.9823E+0 |
| 2 | 2.7500E-3 | 2.4233E+0 | -2.7897E+0 | 2.5302E+0 |
| 3 | 4.0000E-3 | 2.3230E+0 | -2.6474E+0 | 2.9216E+0 |
| 4 | 5.2500E-3 | 2.5254E+0 | -3.2879E+0 | 4.1191E+0 |
| 5 | 6.5000E-3 | 1.3822E+0 | -1.3379E+0 | 4.2244E+0 |
| 6 | 7.7500E-3 | 1.3626E+0 | -9.3939E-1 | 4.0550E+0 |
| 7 | 9.0000E-3 | 9.5518E-1 | -4.4123E-1 | 3.9265E+0 |
| 8 | 1.0250E-2 | 6.7236E-1 | -1.5656E-1 | 3.3641E+0 |
| 9 | 1.1500E-2 | 5.3486E-1 | -4.2699E-2 | 2.2944E+0 |
| 10 | 1.2750E-2 | 4.1848E-1 | -1.8503E-2 | 1.5339E+0 |
| 11 | 1.4000E-2 | 3.6062E-1 | -1.1387E-2 | 1.2519E+0 |
| 12 | 1.5250E-2 | 3.6214E-1 | 0. | 1.2806E+0 |
| 13 | 1.6500E-2 | 6.6653E-1 | NM | 1.5602E+0 |
| 14 | 1.7750E-2 | 1.3334E+0 | NM | 2.9358E+0 |
| 15 | 1.9000E-2 | 1.7418E+0 | NM | 2.8363E+0 |
| 16 | 2.0250E-2 | 9.4731E-1 | NM | 1.5904E+0 |
| 17 | 2.1500E-2 | 5.1949E-1 | NM | 1.1789E+0 |
| 18 | 2.2750E-2 | NM | NM | NM |

| 7501S | | KUSSOY/MIKULLA | | TURBULENCE DATA | |
|-----------|-----------|----------------|----------------------|---------------------|----------------|
| 7501S0115 | | UT= 4.3850E+01 | RHOW= 3.1308E-02 | TW= 3.0000E+02 | D*= 6.5070E-02 |
| I | Y [M] | V' UT | RHO*U*V' RHOW*UT2 | (RHO U)' RHOW*UT | |
| 1 | 1.5000E-3 | 6.0125E-1 | NM | 1.8230E+0 | |
| 2 | 2.7500E-3 | 1.2153E+0 | -1.9548E-1 | 2.3676E+0 | |
| 3 | 4.0000E-3 | 1.9385E+0 | -1.1403E+0 | 3.0536E+0 | |
| 4 | 5.2500E-3 | 2.6153E+0 | -1.4987E+0 | 3.9746E+0 | |
| 5 | 6.5000E-3 | 2.8012E+0 | -7.0047E-1 | 5.8069E+0 | |
| 6 | 7.7500E-3 | 2.2617E+0 | -1.1403E-1 | 4.2605E+0 | |
| 7 | 9.0000E-3 | 1.1599E+0 | -6.5160E-2 | 2.7344E+0 | |
| 8 | 1.0250E-2 | 8.1305E-1 | -4.8870E-2 | 2.9174E+0 | |
| 9 | 1.1500E-2 | 7.5782E-1 | 0. | 2.9494E+0 | |
| 10 | 1.2750E-2 | 6.0247E-1 | 8.1451E-2 | 2.9794E+0 | |
| 11 | 1.4000E-2 | 9.2764E-1 | 1.6290E-2 | 3.4807E+0 | |
| 12 | 1.5250E-2 | 5.1746E-1 | 6.5160E-2 | 3.2155E+0 | |
| 13 | 1.6500E-2 | 4.9560E-1 | 8.1451E-2 | 3.1164E+0 | |
| 14 | 1.7750E-2 | 4.4767E-1 | 6.5160E-2 | 3.0396E+0 | |
| 15 | 1.9000E-2 | 4.9880E-1 | 6.5160E-2 | 2.7865E+0 | |
| 16 | 2.0250E-2 | 5.4960E-1 | NM | 2.7424E+0 | |
| 17 | 2.1500E-2 | 4.2492E-1 | NM | 2.3420E+0 | |
| 18 | 2.2750E-2 | 4.0026E-1 | NM | 2.0817E+0 | |
| 19 | 2.4000E-2 | NM | NM | NM | |
| 20 | 2.5250E-2 | 0. | 0. | 0. | |

| 7501S0201 | | UT= 4.8682E+01 | RHOW= 7.0465E-03 | TW= 3.0000E+02 | D*= 1.1155E-01 |
|-----------|-----------|----------------|----------------------|---------------------|----------------|
| I | Y [M] | V' UT | RHO*U*V' RHOW*UT2 | (RHO U)' RHOW*UT | |
| 1 | 1.5000E-3 | 6.6310E-1 | NM | 2.3474E+0 | |
| 2 | 2.7500E-3 | 7.0342E-1 | -2.3489E-1 | 2.8669E+0 | |
| 3 | 4.0000E-3 | 7.1825E-1 | -2.4076E-1 | 3.1130E+0 | |
| 4 | 5.2500E-3 | 7.0812E-1 | -2.4076E-1 | 3.3518E+0 | |
| 5 | 6.5000E-3 | 6.5412E-1 | -3.9344E-1 | 3.6008E+0 | |
| 6 | 7.7500E-3 | 6.5352E-1 | -4.7565E-1 | 3.8807E+0 | |
| 7 | 9.0000E-3 | 6.5249E-1 | -2.9948E-1 | 4.1642E+0 | |
| 8 | 1.0250E-2 | 6.4614E-1 | -3.5821E-1 | 4.4694E+0 | |
| 9 | 1.1500E-2 | 6.1984E-1 | -3.5233E-1 | 4.8544E+0 | |
| 10 | 1.2750E-2 | 6.3299E-1 | -3.2885E-1 | 5.2504E+0 | |
| 11 | 1.4000E-2 | 6.2242E-1 | -3.2885E-1 | 5.7030E+0 | |
| 12 | 1.5250E-2 | 5.8828E-1 | -3.4059E-1 | 6.2224E+0 | |
| 13 | 1.6500E-2 | 6.2059E-1 | -3.1710E-1 | 6.7985E+0 | |
| 14 | 1.7750E-2 | 6.2760E-1 | -2.7012E-1 | 7.4598E+0 | |
| 15 | 1.9000E-2 | 5.8961E-1 | -2.7600E-1 | 7.3482E+0 | |
| 16 | 2.0250E-2 | 6.1702E-1 | -1.8204E-1 | 7.2607E+0 | |
| 17 | 2.1500E-2 | 5.5222E-1 | -1.8204E-1 | 6.9304E+0 | |
| 18 | 2.2750E-2 | 5.5448E-1 | -1.2919E-1 | 6.9061E+0 | |
| 19 | 2.4000E-2 | NM | NM | 6.7279E+0 | |
| 20 | 2.5250E-2 | NM | NM | 5.9509E+0 | |
| 21 | 2.6500E-2 | NM | NM | 5.0691E+0 | |

| 7501S0209 | | UT= 3.5466E+01 | RHOW= 6.6463E-02 | TW= 3.0000E+02 | D*= 4.8075E-02 |
|-----------|-----------|----------------|----------------------|---------------------|----------------|
| I | Y [M] | V' UT | RHO*U*V' RHOW*UT2 | (RHO U)' RHOW*UT | |
| 1 | 1.5000E-3 | 1.5595E+0 | -8.4459E-1 | 2.3456E+0 | |
| 2 | 2.7500E-3 | 1.5231E+0 | -9.6190E-1 | 2.4471E+0 | |
| 3 | 4.0000E-3 | 1.2935E+0 | -5.9825E-1 | 2.4781E+0 | |
| 4 | 5.2500E-3 | 1.1564E+0 | -1.9942E-1 | 2.6088E+0 | |
| 5 | 6.5000E-3 | 1.2239E+0 | -1.8769E-1 | 2.7839E+0 | |
| 6 | 7.7500E-3 | 1.1452E+0 | -2.3461E-1 | 2.8995E+0 | |
| 7 | 9.0000E-3 | 9.7617E-1 | -2.3461E-1 | 3.7032E+0 | |
| 8 | 1.0250E-2 | 7.5198E-1 | -2.2288E-1 | 3.6916E+0 | |
| 9 | 1.1500E-2 | 6.7309E-1 | -1.1730E-1 | 3.5607E+0 | |
| 10 | 1.2750E-2 | 6.1190E-1 | NM | 3.1516E+0 | |
| 11 | 1.4000E-2 | 8.8327E-1 | NM | 3.2942E+0 | |
| 12 | 1.5250E-2 | 1.3045E+0 | NM | 2.4868E+0 | |

| 7501S0212 | | UT= 4.2943E+01 | RHOW= 3.7797E-02 | TW= 3.0000E+02 | D*= 4.8830E-02 |
|-----------|-----------|----------------|----------------------|---------------------|----------------|
| I | Y [M] | V' UT | RHO*U*V' RHOW*UT2 | (RHO U)' RHOW*UT | |
| 1 | 1.5000E-3 | 9.6010E-1 | -1.1678E+0 | 2.9474E+0 | |
| 2 | 2.7500E-3 | 9.4941E-1 | -1.0693E+0 | 3.0023E+0 | |
| 3 | 4.0000E-3 | 9.0476E-1 | -8.4419E-1 | 3.0018E+0 | |
| 4 | 5.2500E-3 | 9.2105E-1 | -6.7535E-1 | 3.0451E+0 | |
| 5 | 6.5000E-3 | 9.5634E-1 | -6.6128E-1 | 3.2797E+0 | |
| 6 | 7.7500E-3 | 9.6886E-1 | -5.3465E-1 | 3.3282E+0 | |
| 7 | 9.0000E-3 | 9.3323E-1 | -5.2058E-1 | 3.5515E+0 | |
| 8 | 1.0250E-2 | 9.4061E-1 | -4.7837E-1 | 3.6166E+0 | |
| 9 | 1.1500E-2 | 9.0275E-1 | -4.0802E-1 | 3.5867E+0 | |
| 10 | 1.2750E-2 | 8.8766E-1 | -3.3768E-1 | 3.9881E+0 | |
| 11 | 1.4000E-2 | 8.2244E-1 | -3.0954E-1 | 3.5982E+0 | |
| 12 | 1.5250E-2 | 7.7906E-1 | -2.6733E-1 | 3.5561E+0 | |
| 13 | 1.6500E-2 | 7.3527E-1 | -1.9698E-1 | 3.7274E+0 | |
| 14 | 1.7750E-2 | 7.3782E-1 | -1.9698E-1 | 3.8551E+0 | |
| 15 | 1.9000E-2 | 7.1632E-1 | -2.1105E-1 | 3.9539E+0 | |
| 16 | 2.0250E-2 | 6.1929E-1 | -1.2663E-1 | 3.4592E+0 | |
| 17 | 2.1500E-2 | 5.9622E-1 | -1.4070E-1 | 3.8848E+0 | |
| 18 | 2.2750E-2 | 5.4810E-1 | -9.8489E-2 | 3.4460E+0 | |
| 19 | 2.4000E-2 | 4.9969E-1 | -9.8489E-2 | 3.7312E+0 | |
| 20 | 2.5250E-2 | NM | NM | 3.0668E+0 | |

| | | |
|---|--|----------|
|  | M: 2.5 - 4.5 R Theta x 10 ⁻³ : 1-8.2 TW/TR: 1 | 7701 |
| | | ZPG - AW |
| Continuous wind tunnel with flexible nozzle. W = 0.91, H = 1.22 m. 0.04 < P0 < 0.2 MN/m ² . T0: 315K. Air: Dew point, 243K. 3.8 < RE/m x 10 ⁻⁶ < 8.0. | | |
| MABEY D.G., 1977. Some measurements of transitional and turbulent boundary layers at low Reynolds numbers at supersonic speeds. Appendix E of: Some observations on the wake component of the velocity profiles of turbulent boundary layers at subsonic and supersonic speeds. RAE TR 77-004. <u>And:</u> Mabey et al., CAT 7402, Mabey D.G., private communication. <u>Also:</u> Mabey (1979) | | |

- 1 In all respects the equipment and procedures used were as for Mabey et al. (CAT 7402) so that the
11 description for that entry should be consulted.
- 12 The data presented here are from measurements made at three X stations on the centreline of the flat
14 plate, X = 0.368, 0.623, 0.876 m, and in principle at two unit Reynolds numbers ($4.8 \times 10^6/m$) for
Mach numbers of 2.5, 3.5, 4.0, 4.5. The 18 profiles obtained were classed as 'turbulent' (0101-0502)
and 'transitional' (0601-0901) by the author. The 'series' here divide each group up by Mach number
and for series 01/02, unit Reynolds number.
- § DATA: 70010101-0901. NX up to 3. Pitot and T0 profiles obtained with same probe. CF obtained
separately with FEB.
- 15 Editors' comments. These data extend further the very large pool of carefully observed adiabatic flat
plate data presented by Mabey et al. (CAT 7402) and Hastings and Sawyer (CAT 7006). We continue to
regard these experiments for the greater part as the basic source of such data in the range of Mach
number and Reynolds number covered. Sample profiles are plotted as Figs. 4.4.13-17 in AGARDograph 253
and are generally in excellent agreement with the "standard" wall and outer laws, with the
exception of profiles 0601/0701 shown in Fig. (4.4.16) where it appears that some gross error has
occurred. These profiles are so unrepresentative that it is probable that a less meticulous reporter
would have discarded them and possibly been right to do so.

| CAT 7701S | | MABEY BOUNDARY CONDITIONS AND EVALUATED DATA. SI UNITS | | | | | | | |
|-----------------------|-----------------------|--|-----------------------|-----------------------|--------|-----------------------|-----------------------|-----------------------|--|
| RUN | MD * | TW/TR | RED2W | CF * | H12 | H12K | Pw | PD | |
| X * | POD | PW/PD* | RED2D | CO * | H32 | H32K | TW* | TD | |
| RZ | TOD* | TAUM | DZ | P12* | H42 | D2K | UD | TR | |
| 7701S0101 | 2.5000 | 1.0132 | 9.5216 ⁺⁰² | 2.7400 ⁻⁰³ | 3.9681 | 1.5574 | 2.5445 ⁺⁰³ | 2.5445 ⁺⁰³ | |
| 6.2300 ⁻⁰¹ | 4.3476 ⁺⁰⁴ | 1.0000 | 1.8143 ⁺⁰³ | 0.0000 ⁺⁰⁰ | 1.8293 | 1.8120 | 2.9500 ⁺⁰² | 1.3733 ⁺⁰² | |
| INFINITE | 3.0900 ⁺⁰² | 3.0503 ⁺⁰¹ | 4.5922 ⁻⁰⁴ | 0.0000 ⁺⁰⁰ | 0.1655 | 6.0557 ⁻⁰⁴ | 5.8741 ⁺⁰² | 2.9115 ⁺⁰² | |
| 7701S0102 | 2.4800 | 1.0128 | 1.6961 ⁺⁰³ | 2.1900 ⁻⁰³ | 3.8226 | 1.4486 | 2.5982 ⁺⁰³ | 2.5982 ⁺⁰³ | |
| 8.7300 ⁻⁰¹ | 4.3033 ⁺⁰⁴ | 1.0000 | 3.2057 ⁺⁰³ | 0.0000 ⁺⁰⁰ | 1.8124 | 1.7970 | 2.9500 ⁺⁰² | 1.3856 ⁺⁰² | |
| INFINITE | 3.0900 ⁺⁰² | 2.4497 ⁺⁰¹ | 8.1117 ⁻⁰⁴ | 0.0000 ⁺⁰⁰ | 0.1567 | 1.0879 ⁻⁰³ | 5.8530 ⁺⁰² | 2.9127 ⁺⁰² | |
| 7701S0201 | 2.4900 | 1.0130 | 2.1924 ⁺⁰³ | 2.1200 ⁻⁰³ | 4.0263 | 1.5348 | 5.0782 ⁺⁰³ | 5.0782 ⁺⁰³ | |
| 3.6800 ⁻⁰¹ | 8.5426 ⁺⁰⁴ | 1.0000 | 4.1605 ⁺⁰³ | 0.0000 ⁺⁰⁰ | 1.8067 | 1.7930 | 2.9500 ⁺⁰² | 1.3795 ⁺⁰² | |
| INFINITE | 3.0900 ⁺⁰² | 4.6724 ⁺⁰¹ | 5.3313 ⁻⁰⁴ | 0.0000 ⁺⁰⁰ | 0.1343 | 7.2482 ⁻⁰⁴ | 5.8636 ⁺⁰² | 2.9121 ⁺⁰² | |
| 7701S0202 | 2.4900 | 1.0130 | 3.1818 ⁺⁰³ | 2.0100 ⁻⁰³ | 4.0562 | 1.4592 | 5.0782 ⁺⁰³ | 5.0782 ⁺⁰³ | |
| 6.2300 ⁻⁰¹ | 8.5426 ⁺⁰⁴ | 1.0000 | 6.0382 ⁺⁰³ | 0.0000 ⁺⁰⁰ | 1.8042 | 1.7908 | 2.9500 ⁺⁰² | 1.3795 ⁺⁰² | |
| INFINITE | 3.0900 ⁺⁰² | 4.4299 ⁺⁰¹ | 7.7373 ⁻⁰⁴ | 0.0000 ⁺⁰⁰ | 0.0837 | 1.0638 ⁻⁰³ | 5.8636 ⁺⁰² | 2.9121 ⁺⁰² | |
| 7701S0203 | 2.4900 | 1.0130 | 4.3256 ⁺⁰³ | 1.8200 ⁻⁰³ | 3.9696 | 1.4168 | 5.1424 ⁺⁰³ | 5.1424 ⁺⁰³ | |
| 8.7300 ⁻⁰¹ | 8.6507 ⁺⁰⁴ | 1.0000 | 8.2089 ⁺⁰³ | 0.0000 ⁺⁰⁰ | 1.8045 | 1.7908 | 2.9500 ⁺⁰² | 1.3795 ⁺⁰² | |
| INFINITE | 3.0900 ⁺⁰² | 4.0620 ⁺⁰¹ | 1.0387 ⁻⁰³ | 0.0000 ⁺⁰⁰ | 0.0944 | 1.4249 ⁻⁰³ | 5.8636 ⁺⁰² | 2.9121 ⁺⁰² | |
| 7701S0301 | 3.4800 | 1.0174 | 1.0042 ⁺⁰³ | 2.2000 ⁻⁰³ | 5.4647 | 1.4216 | 9.7025 ⁺⁰² | 9.7025 ⁺⁰² | |
| 8.7600 ⁻⁰¹ | 7.1928 ⁺⁰⁴ | 1.0000 | 2.8084 ⁺⁰³ | 0.0000 ⁺⁰⁰ | 1.8423 | 1.8149 | 2.9500 ⁺⁰² | 9.1465 ⁺⁰¹ | |
| INFINITE | 3.1300 ⁺⁰² | 1.8095 ⁺⁰¹ | 7.4467 ⁻⁰⁴ | 0.0000 ⁺⁰⁰ | 0.3440 | 1.1417 ⁻⁰³ | 6.6729 ⁺⁰² | 2.8996 ⁺⁰² | |
| 7701S0302 | 3.4900 | 1.0175 | 1.2688 ⁺⁰³ | 2.0700 ⁻⁰³ | 5.6016 | 1.4819 | 1.8981 ⁺⁰³ | 1.8981 ⁺⁰³ | |
| 6.2300 ⁻⁰¹ | 1.4273 ⁺⁰⁵ | 1.0000 | 3.5623 ⁺⁰³ | 0.0000 ⁺⁰⁰ | 1.8479 | 1.8253 | 2.9500 ⁺⁰² | 9.1094 ⁺⁰¹ | |
| INFINITE | 3.1300 ⁺⁰² | 3.3500 ⁺⁰¹ | 4.7857 ⁻⁰⁴ | 0.0000 ⁺⁰⁰ | 0.3373 | 7.2947 ⁻⁰⁴ | 6.6785 ⁺⁰² | 2.8992 ⁺⁰² | |
| 7701S0303 | 3.4900 | 1.0175 | 1.9373 ⁺⁰³ | 1.6900 ⁻⁰³ | 5.8767 | 1.4236 | 1.9228 ⁺⁰³ | 1.9228 ⁺⁰³ | |
| 8.7600 ⁻⁰¹ | 1.4459 ⁺⁰⁵ | 1.0000 | 5.4393 ⁺⁰³ | 0.0000 ⁺⁰⁰ | 1.8291 | 1.8056 | 2.9500 ⁺⁰² | 9.1094 ⁺⁰¹ | |
| INFINITE | 3.1300 ⁺⁰² | 2.7706 ⁺⁰¹ | 7.2136 ⁻⁰⁴ | 0.0000 ⁺⁰⁰ | 0.2515 | 1.1579 ⁻⁰³ | 6.6785 ⁺⁰² | 2.8992 ⁺⁰² | |
| 7701S0401 | 3.9600 | 1.0199 | 8.2467 ⁺⁰² | 2.0800 ⁻⁰³ | 6.3925 | 1.4082 | 6.3638 ⁺⁰² | 6.3638 ⁺⁰² | |
| 8.7600 ⁻⁰¹ | 9.1594 ⁺⁰⁴ | 1.0000 | 2.7699 ⁺⁰³ | 0.0000 ⁺⁰⁰ | 1.8560 | 1.8224 | 2.9500 ⁺⁰² | 7.5913 ⁺⁰¹ | |
| INFINITE | 3.1400 ⁺⁰² | 1.4530 ⁺⁰¹ | 7.4644 ⁻⁰⁴ | 0.0000 ⁺⁰⁰ | 0.4146 | 1.2119 ⁻⁰³ | 6.9177 ⁺⁰² | 2.8924 ⁺⁰² | |
| 7701S0402 | 3.9900 | 1.0138 | 9.2695 ⁺⁰² | 2.1000 ⁻⁰³ | 6.4020 | 1.4881 | 1.2208 ⁺⁰³ | 1.2208 ⁺⁰³ | |
| 6.2300 ⁻⁰¹ | 1.8291 ⁺⁰⁵ | 1.0000 | 3.1293 ⁺⁰³ | 0.0000 ⁺⁰⁰ | 1.8543 | 1.8274 | 2.9500 ⁺⁰² | 7.5525 ⁺⁰¹ | |
| INFINITE | 3.1600 ⁺⁰² | 2.8570 ⁺⁰¹ | 4.3296 ⁻⁰⁴ | 0.0000 ⁺⁰⁰ | 0.4586 | 7.0315 ⁻⁰⁴ | 6.9523 ⁺⁰² | 2.9099 ⁺⁰² | |
| 7701S0403 | 3.9600 | 1.0167 | 1.4886 ⁺⁰³ | 1.6400 ⁻⁰³ | 6.9959 | 1.4146 | 1.2792 ⁺⁰³ | 1.2792 ⁺⁰³ | |
| 8.7600 ⁻⁰¹ | 1.8412 ⁺⁰⁵ | 1.0000 | 4.9842 ⁺⁰³ | 0.0000 ⁺⁰⁰ | 1.8410 | 1.8133 | 2.9500 ⁺⁰² | 7.6155 ⁺⁰¹ | |
| INFINITE | 3.1500 ⁺⁰² | 2.3029 ⁺⁰¹ | 6.7136 ⁻⁰⁴ | 0.0000 ⁺⁰⁰ | 0.2900 | 1.1492 ⁻⁰³ | 6.9287 ⁺⁰² | 2.9016 ⁺⁰² | |
| 7701S0501 | 4.4600 | 1.0279 | 6.1314 ⁺⁰² | 2.0100 ⁻⁰³ | 7.6357 | 1.4512 | 4.1677 ⁺⁰² | 4.1677 ⁺⁰² | |
| 8.7600 ⁻⁰¹ | 1.1473 ⁺⁰⁵ | 1.0000 | 2.4862 ⁺⁰³ | 0.0000 ⁺⁰⁰ | 1.8645 | 1.8197 | 2.9500 ⁺⁰² | 6.2873 ⁺⁰¹ | |
| INFINITE | 3.1300 ⁺⁰² | 1.1664 ⁺⁰¹ | 6.8475 ⁻⁰⁴ | 0.0000 ⁺⁰⁰ | 0.4646 | 1.1942 ⁻⁰³ | 7.0905 ⁺⁰² | 2.8699 ⁺⁰² | |
| 7701S0502 | 4.4700 | 1.0182 | 1.0866 ⁺⁰³ | 1.4400 ⁻⁰³ | 7.3792 | 1.4083 | 7.2139 ⁺⁰² | 7.2139 ⁺⁰² | |
| 8.7600 ⁻⁰¹ | 2.0110 ⁺⁰⁵ | 1.0000 | 4.3795 ⁺⁰³ | 0.0000 ⁺⁰⁰ | 1.8559 | 1.8185 | 2.9500 ⁺⁰² | 6.3248 ⁺⁰¹ | |
| INFINITE | 3.1600 ⁺⁰² | 1.4529 ⁺⁰¹ | 7.0157 ⁻⁰⁴ | 0.0000 ⁺⁰⁰ | 0.5050 | 1.2385 ⁻⁰³ | 7.1276 ⁺⁰² | 2.8971 ⁺⁰² | |
| 7701S0601 | 2.4900 | 1.0130 | 5.3784 ⁺⁰² | 2.6800 ⁻⁰³ | 6.6174 | 2.7917 | 2.5712 ⁺⁰³ | 2.5712 ⁺⁰³ | |
| 3.6800 ⁻⁰¹ | 4.3253 ⁺⁰⁴ | 1.0000 | 1.0207 ⁺⁰³ | 0.0000 ⁺⁰⁰ | 1.6142 | 1.5692 | 2.9500 ⁺⁰² | 1.3795 ⁺⁰² | |
| INFINITE | 3.0900 ⁺⁰² | 2.9907 ⁺⁰¹ | 2.5831 ⁻⁰⁴ | 0.0000 ⁺⁰⁰ | 0.0038 | 4.2788 ⁻⁰⁴ | 5.8636 ⁺⁰² | 2.9121 ⁺⁰² | |
| 7701S0701 | 3.5100 | 1.0145 | 5.2367 ⁺⁰² | 9.9000 ⁻⁰⁴ | 9.2292 | 2.3930 | 1.8487 ⁺⁰³ | 1.8487 ⁺⁰³ | |
| 3.6800 ⁻⁰¹ | 1.4302 ⁺⁰⁵ | 1.0000 | 1.4774 ⁺⁰³ | 0.0000 ⁺⁰⁰ | 1.6804 | 1.6173 | 2.9500 ⁺⁰² | 9.0646 ⁺⁰¹ | |
| INFINITE | 3.1400 ⁺⁰² | 1.5784 ⁺⁰¹ | 2.0116 ⁻⁰⁴ | 0.0000 ⁺⁰⁰ | 0.0174 | 4.3282 ⁻⁰⁴ | 6.7003 ⁺⁰² | 2.9077 ⁺⁰² | |
| 7701S0702 | 3.5100 | 1.0178 | 5.1341 ⁺⁰² | 1.8900 ⁻⁰³ | 6.5161 | 1.6571 | 9.1978 ⁺⁰² | 9.1978 ⁺⁰² | |
| 6.2300 ⁻⁰¹ | 7.1156 ⁺⁰⁴ | 1.0000 | 1.4529 ⁺⁰³ | 0.0000 ⁺⁰⁰ | 1.8032 | 1.7597 | 2.9500 ⁺⁰² | 9.0357 ⁺⁰¹ | |
| INFINITE | 3.1300 ⁺⁰² | 1.4992 ⁺⁰¹ | 3.9576 ⁻⁰⁴ | 0.0000 ⁺⁰⁰ | 0.2312 | 6.8635 ⁻⁰⁴ | 6.6896 ⁺⁰² | 2.8985 ⁺⁰² | |
| 7701S0801 | 4.0000 | 1.0203 | 4.1032 ⁺⁰² | 1.6000 ⁻⁰³ | 8.5223 | 1.7763 | 5.9909 ⁺⁰² | 5.9909 ⁺⁰² | |
| 6.2300 ⁻⁰¹ | 9.0964 ⁺⁰⁴ | 1.0000 | 1.3992 ⁺⁰³ | 0.0000 ⁺⁰⁰ | 1.7946 | 1.7357 | 2.9500 ⁺⁰² | 7.4762 ⁺⁰¹ | |
| INFINITE | 3.1400 ⁺⁰² | 1.0736 ⁺⁰¹ | 3.8759 ⁻⁰⁴ | 0.0000 ⁺⁰⁰ | 0.1853 | 7.7628 ⁻⁰⁴ | 6.9344 ⁺⁰² | 2.8912 ⁺⁰² | |
| 7701S0901 | 4.5100 | 1.0186 | 5.7531 ⁺⁰² | 1.6300 ⁻⁰³ | 8.4900 | 1.5573 | 6.8804 ⁺⁰² | 6.8804 ⁺⁰² | |
| 6.2300 ⁻⁰¹ | 2.0163 ⁺⁰⁵ | 1.0000 | 2.3524 ⁺⁰³ | 0.0000 ⁺⁰⁰ | 1.8411 | 1.7946 | 2.9500 ⁺⁰² | 6.2352 ⁺⁰¹ | |
| INFINITE | 3.1600 ⁺⁰² | 1.9968 ⁺⁰¹ | 3.8327 ⁻⁰⁴ | 0.0000 ⁺⁰⁰ | 0.3936 | 7.3731 ⁻⁰⁴ | 7.1402 ⁺⁰² | 2.8962 ⁺⁰² | |

PD,POD CALCULATED WITH RED2,D2 (AUTHOR) WITH SUTHERLAND MUE-LAW
 TRAPEZOIDAL RULE FOR ALL INTEGRATIONS

| 7701S0301 | | MABEY | | PROFILE TABULATION | | 48 POINTS, DELTA AT POINT 48 | | |
|-----------|-----------------------|-----------------------|------|--------------------|---------|------------------------------|---------|-----------|
| I | Y | PT2/P | P/PD | TO/TOD | M/MD | U/UD | T/TD | R/RD*U/UD |
| 1 | 0.0000 ⁺⁰⁰ | 1.0000 ⁺⁰⁰ | NM | 0.94099 | 0.00000 | 0.00000 | 3.22014 | 0.00000 |
| 2 | 3.6300 ⁻⁰⁴ | 1.9287 ⁺⁰⁰ | NM | 0.95674 | 0.29194 | 0.48094 | 2.71382 | 0.17722 |
| 3 | 3.8900 ⁻⁰⁴ | 2.0370 ⁺⁰⁰ | NM | 0.95677 | 0.30513 | 0.49875 | 2.67167 | 0.18668 |
| 4 | 4.1400 ⁻⁰⁴ | 2.1964 ⁺⁰⁰ | NM | 0.95856 | 0.32306 | 0.52276 | 2.61837 | 0.19965 |
| 5 | 4.6500 ⁻⁰⁴ | 2.4613 ⁺⁰⁰ | NM | 0.95954 | 0.35010 | 0.55708 | 2.53198 | 0.22002 |
| 6 | 4.9000 ⁻⁰⁴ | 2.6403 ⁺⁰⁰ | NM | 0.95951 | 0.36693 | 0.57739 | 2.47605 | 0.23319 |
| 7 | 5.1600 ⁻⁰⁴ | 2.7702 ⁺⁰⁰ | NM | 0.95575 | 0.37859 | 0.58989 | 2.42784 | 0.24297 |
| 8 | 5.4100 ⁻⁰⁴ | 2.9069 ⁺⁰⁰ | NM | 0.96017 | 0.39041 | 0.60480 | 2.39981 | 0.25202 |
| 9 | 5.6600 ⁻⁰⁴ | 3.0398 ⁺⁰⁰ | NM | 0.96010 | 0.40153 | 0.61721 | 2.36286 | 0.26121 |
| 10 | 5.9200 ⁻⁰⁴ | 3.1747 ⁺⁰⁰ | NM | 0.95998 | 0.41246 | 0.62911 | 2.32649 | 0.27041 |
| 11 | 6.6800 ⁻⁰⁴ | 3.5340 ⁺⁰⁰ | NM | 0.95942 | 0.44011 | 0.65793 | 2.23477 | 0.29441 |
| 12 | 7.1900 ⁻⁰⁴ | 3.7414 ⁺⁰⁰ | NM | 0.95789 | 0.45524 | 0.67254 | 2.18245 | 0.30816 |
| 13 | 7.7000 ⁻⁰⁴ | 3.9298 ⁺⁰⁰ | NM | 0.95573 | 0.46853 | 0.68464 | 2.13527 | 0.32063 |
| 14 | 8.2000 ⁻⁰⁴ | 4.1183 ⁺⁰⁰ | NM | 0.95565 | 0.48144 | 0.69675 | 2.09448 | 0.33266 |
| 15 | 8.7100 ⁻⁰⁴ | 4.2525 ⁺⁰⁰ | NM | 0.95395 | 0.49040 | 0.70435 | 2.06286 | 0.34144 |
| 16 | 9.9800 ⁻⁰⁴ | 4.5623 ⁺⁰⁰ | NM | 0.94971 | 0.51048 | 0.72056 | 1.99241 | 0.36165 |
| 17 | 1.1250 ⁻⁰³ | 4.8263 ⁺⁰⁰ | NM | 0.94715 | 0.52696 | 0.73357 | 1.93784 | 0.37855 |
| 18 | 1.2520 ⁻⁰³ | 5.0369 ⁺⁰⁰ | NM | 0.94544 | 0.53973 | 0.74337 | 1.89694 | 0.39188 |
| 19 | 1.3790 ⁻⁰³ | 5.1993 ⁺⁰⁰ | NM | 0.94445 | 0.54937 | 0.75068 | 1.86712 | 0.40205 |
| 20 | 1.5060 ⁻⁰³ | 5.3787 ⁺⁰⁰ | NM | 0.94335 | 0.55982 | 0.75838 | 1.83517 | 0.41325 |
| 21 | 1.6330 ⁻⁰³ | 5.5826 ⁺⁰⁰ | NM | 0.94276 | 0.57146 | 0.76698 | 1.80137 | 0.42578 |
| 22 | 1.8890 ⁻⁰³ | 5.9111 ⁺⁰⁰ | NM | 0.94304 | 0.58971 | 0.78049 | 1.75171 | 0.44556 |
| 23 | 2.1410 ⁻⁰³ | 6.2213 ⁺⁰⁰ | NM | 0.94429 | 0.60643 | 0.79280 | 1.70910 | 0.46387 |
| 24 | 2.3950 ⁻⁰³ | 6.4861 ⁺⁰⁰ | NM | 0.94486 | 0.62034 | 0.80250 | 1.67354 | 0.47952 |
| 25 | 2.6490 ⁻⁰³ | 6.7562 ⁺⁰⁰ | NM | 0.94642 | 0.63420 | 0.81231 | 1.64052 | 0.49515 |
| 26 | 2.9030 ⁻⁰³ | 7.0262 ⁺⁰⁰ | NM | 0.94652 | 0.64776 | 0.82101 | 1.60664 | 0.51107 |
| 27 | 3.4110 ⁻⁰³ | 7.6083 ⁺⁰⁰ | NM | 0.94922 | 0.67606 | 0.83942 | 1.54165 | 0.54450 |
| 28 | 3.9190 ⁻⁰³ | 8.1379 ⁺⁰⁰ | NM | 0.95154 | 0.70080 | 0.85463 | 1.48718 | 0.57466 |
| 29 | 4.4270 ⁻⁰³ | 8.6859 ⁺⁰⁰ | NM | 0.95447 | 0.72550 | 0.86933 | 1.43581 | 0.60547 |
| 30 | 4.9350 ⁻⁰³ | 9.2001 ⁺⁰⁰ | NM | 0.95640 | 0.74794 | 0.88174 | 1.38980 | 0.63444 |
| 31 | 5.4430 ⁻⁰³ | 9.7205 ⁺⁰⁰ | NM | 0.95845 | 0.76996 | 0.89345 | 1.34647 | 0.66355 |
| 32 | 6.0780 ⁻⁰³ | 1.0377 ⁺⁰¹ | NM | 0.96137 | 0.79686 | 0.90725 | 1.29626 | 0.69990 |
| 33 | 6.7130 ⁻⁰³ | 1.1078 ⁺⁰¹ | NM | 0.96414 | 0.82466 | 0.92066 | 1.24638 | 0.73867 |
| 34 | 7.3480 ⁻⁰³ | 1.1733 ⁺⁰¹ | NM | 0.96853 | 0.84975 | 0.93307 | 1.20570 | 0.77388 |
| 35 | 7.9830 ⁻⁰³ | 1.2316 ⁺⁰¹ | NM | 0.97310 | 0.87152 | 0.94377 | 1.17268 | 0.80480 |
| 36 | 8.6180 ⁻⁰³ | 1.2881 ⁺⁰¹ | NM | 0.97625 | 0.89209 | 0.95298 | 1.14116 | 0.83510 |
| 37 | 9.2530 ⁻⁰³ | 1.3503 ⁺⁰¹ | NM | 0.97937 | 0.91419 | 0.96238 | 1.10820 | 0.86842 |
| 38 | 9.8880 ⁻⁰³ | 1.3971 ⁺⁰¹ | NM | 0.98411 | 0.93047 | 0.97029 | 1.08742 | 0.89228 |
| 39 | 1.0523 ⁻⁰² | 1.4363 ⁺⁰¹ | NM | 0.98946 | 0.94390 | 0.97739 | 1.07223 | 0.91155 |
| 40 | 1.1158 ⁻⁰² | 1.4899 ⁺⁰¹ | NM | 0.99066 | 0.96195 | 0.98379 | 1.04592 | 0.94060 |
| 41 | 1.1793 ⁻⁰² | 1.5122 ⁺⁰¹ | NM | 0.99385 | 0.96936 | 0.98769 | 1.03819 | 0.95136 |
| 42 | 1.2428 ⁻⁰² | 1.5379 ⁺⁰¹ | NM | 0.99563 | 0.97784 | 0.99120 | 1.02750 | 0.96467 |
| 43 | 1.3063 ⁻⁰² | 1.5609 ⁺⁰¹ | NM | 0.99709 | 0.98534 | 0.99420 | 1.01806 | 0.97656 |
| 44 | 1.4333 ⁻⁰² | 1.5670 ⁺⁰¹ | NM | 0.99809 | 0.98733 | 0.99530 | 1.01620 | 0.97943 |
| 45 | 1.5603 ⁻⁰² | 1.5988 ⁺⁰¹ | NM | 0.99881 | 0.99760 | 0.99870 | 1.00221 | 0.99650 |
| 46 | 1.6873 ⁻⁰² | 1.6055 ⁺⁰¹ | NM | 0.99995 | 0.99975 | 0.99990 | 1.00030 | 0.99960 |
| 47 | 1.8143 ⁻⁰² | 1.6080 ⁺⁰¹ | NM | 0.99988 | 1.00055 | 1.00010 | 0.99910 | 1.00100 |
| D 48 | 1.9413 ⁻⁰² | 1.6067 ⁺⁰¹ | NM | 1.00000 | 1.00000 | 1.00000 | 1.00000 | 1.00000 |

INPUT VARIABLES Y,U/UD,RHD/RHOD ASSUME P=PD

7701S0801

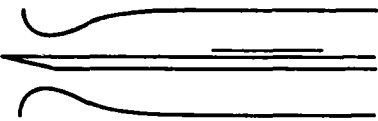
MABEY

PROFILE TABULATION

47 POINTS, DELTA AT POINT 47

| I | Y | PT2/P | P/PD | TO/TOD | M/RD | U/UD | T/TD | R/RD*U/UD |
|------|-----------------------|-----------------------|------|---------|---------|---------|---------|-----------|
| 1 | 0.0000 ⁺⁰⁰ | 1.0000 ⁺⁰⁰ | NM | 0.93904 | 0.00000 | 0.00000 | 3.94396 | 0.00000 |
| 2 | 3.6500 ⁻⁰⁴ | 1.1375 ⁺⁰⁰ | NM | 0.95025 | 0.10825 | 0.21232 | 3.84681 | 0.05519 |
| 3 | 3.8900 ⁻⁰⁴ | 1.2144 ⁺⁰⁰ | NM | 0.95277 | 0.13354 | 0.25983 | 3.78561 | 0.06864 |
| 4 | 4.1400 ⁻⁰⁴ | 1.2848 ⁺⁰⁰ | NM | 0.95521 | 0.15230 | 0.29433 | 3.73468 | 0.07881 |
| 5 | 4.3900 ⁻⁰⁴ | 1.3965 ⁺⁰⁰ | NM | 0.95783 | 0.17688 | 0.33823 | 3.65679 | 0.09249 |
| 6 | 4.6500 ⁻⁰⁴ | 1.4852 ⁺⁰⁰ | NM | 0.95940 | 0.19337 | 0.36684 | 3.59885 | 0.10193 |
| 7 | 4.9000 ⁻⁰⁴ | 1.5900 ⁺⁰⁰ | NM | 0.96199 | 0.21042 | 0.39584 | 3.53895 | 0.11185 |
| 8 | 5.1600 ⁻⁰⁴ | 1.7099 ⁺⁰⁰ | NM | 0.96408 | 0.22751 | 0.42404 | 3.47376 | 0.12207 |
| 9 | 5.4100 ⁻⁰⁴ | 1.8094 ⁺⁰⁰ | NM | 0.96568 | 0.24020 | 0.44444 | 3.42378 | 0.12981 |
| 10 | 5.6600 ⁻⁰⁴ | 1.8844 ⁺⁰⁰ | NM | 0.96702 | 0.24903 | 0.45845 | 3.38895 | 0.13528 |
| 11 | 5.9200 ⁻⁰⁴ | 1.9521 ⁺⁰⁰ | NM | 0.96764 | 0.25654 | 0.47005 | 3.35707 | 0.14002 |
| 12 | 6.1700 ⁻⁰⁴ | 2.1336 ⁺⁰⁰ | NM | 0.97034 | 0.27507 | 0.49825 | 3.28102 | 0.15186 |
| 13 | 6.6800 ⁻⁰⁴ | 2.3112 ⁺⁰⁰ | NM | 0.97170 | 0.29157 | 0.52225 | 3.20835 | 0.16278 |
| 14 | 7.1900 ⁻⁰⁴ | 2.4875 ⁺⁰⁰ | NM | 0.97149 | 0.30678 | 0.54325 | 3.13586 | 0.17324 |
| 15 | 7.7000 ⁻⁰⁴ | 2.6988 ⁺⁰⁰ | NM | 0.97638 | 0.32385 | 0.56746 | 3.07035 | 0.18482 |
| 16 | 8.2000 ⁻⁰⁴ | 2.9109 ⁺⁰⁰ | NM | 0.97825 | 0.33995 | 0.58876 | 2.99940 | 0.19629 |
| 17 | 8.7100 ⁻⁰⁴ | 3.1009 ⁺⁰⁰ | NM | 0.97969 | 0.35367 | 0.60626 | 2.93855 | 0.20631 |
| 18 | 9.9800 ⁻⁰⁴ | 3.5017 ⁺⁰⁰ | NM | 0.98021 | 0.38080 | 0.63856 | 2.81204 | 0.22708 |
| 19 | 1.1250 ⁻⁰³ | 3.9027 ⁺⁰⁰ | NM | 0.98125 | 0.40598 | 0.66687 | 2.69816 | 0.24716 |
| 20 | 1.2520 ⁻⁰³ | 4.2628 ⁺⁰⁰ | NM | 0.98138 | 0.42725 | 0.68917 | 2.60193 | 0.26487 |
| 21 | 1.3790 ⁻⁰³ | 4.5693 ⁺⁰⁰ | NM | 0.98057 | 0.44451 | 0.70607 | 2.52310 | 0.27984 |
| 22 | 1.5060 ⁻⁰³ | 4.8718 ⁺⁰⁰ | NM | 0.98060 | 0.46088 | 0.72167 | 2.45191 | 0.29433 |
| 23 | 1.6330 ⁻⁰³ | 5.1665 ⁺⁰⁰ | NM | 0.97990 | 0.47627 | 0.73547 | 2.38463 | 0.30842 |
| 24 | 1.8870 ⁻⁰³ | 5.8237 ⁺⁰⁰ | NM | 0.97980 | 0.50887 | 0.76338 | 2.25039 | 0.33922 |
| 25 | 2.1410 ⁻⁰³ | 6.4331 ⁺⁰⁰ | NM | 0.97919 | 0.53729 | 0.78558 | 2.13775 | 0.36748 |
| 26 | 2.3950 ⁻⁰³ | 7.0655 ⁺⁰⁰ | NM | 0.97853 | 0.56525 | 0.80578 | 2.03213 | 0.39652 |
| 27 | 2.6490 ⁻⁰³ | 7.7178 ⁺⁰⁰ | NM | 0.97819 | 0.59269 | 0.82428 | 1.93420 | 0.42616 |
| 28 | 2.9030 ⁻⁰³ | 8.3856 ⁺⁰⁰ | NM | 0.97856 | 0.61950 | 0.84138 | 1.84459 | 0.45614 |
| 29 | 3.4110 ⁻⁰³ | 9.8573 ⁺⁰⁰ | NM | 0.97890 | 0.67482 | 0.87289 | 1.67320 | 0.52169 |
| 30 | 3.9190 ⁻⁰³ | 1.1588 ⁺⁰¹ | NM | 0.98001 | 0.73452 | 0.90249 | 1.50967 | 0.59781 |
| 31 | 4.4270 ⁻⁰³ | 1.3405 ⁺⁰¹ | NM | 0.98124 | 0.79235 | 0.92729 | 1.36960 | 0.67705 |
| 32 | 4.9350 ⁻⁰³ | 1.5284 ⁺⁰¹ | NM | 0.98249 | 0.84799 | 0.94809 | 1.25003 | 0.75846 |
| 33 | 5.4430 ⁻⁰³ | 1.7183 ⁺⁰¹ | NM | 0.98360 | 0.90073 | 0.96540 | 1.14874 | 0.84040 |
| 34 | 6.7130 ⁻⁰³ | 1.9457 ⁺⁰¹ | NM | 0.99023 | 0.96009 | 0.98520 | 1.05300 | 0.93561 |
| 35 | 7.3480 ⁻⁰³ | 2.0057 ⁺⁰¹ | NM | 0.99455 | 0.97515 | 0.99120 | 1.03319 | 0.95936 |
| 36 | 7.9830 ⁻⁰³ | 2.0400 ⁺⁰¹ | NM | 0.99572 | 0.98365 | 0.99390 | 1.02094 | 0.97351 |
| 37 | 8.6180 ⁻⁰³ | 2.0564 ⁺⁰¹ | NM | 0.99874 | 0.98769 | 0.99640 | 1.01772 | 0.97905 |
| 38 | 9.2530 ⁻⁰³ | 2.0781 ⁺⁰¹ | NM | 0.99876 | 0.99300 | 0.99770 | 1.00949 | 0.98832 |
| 39 | 9.8880 ⁻⁰³ | 2.0807 ⁺⁰¹ | NM | 1.00025 | 0.99364 | 0.99860 | 1.01001 | 0.98871 |
| 40 | 1.0523 ⁻⁰² | 2.0885 ⁺⁰¹ | NM | 1.00053 | 0.99554 | 0.99920 | 1.00736 | 0.99190 |
| 41 | 1.1158 ⁻⁰² | 2.0957 ⁺⁰¹ | NM | 1.00029 | 0.99730 | 0.99950 | 1.00442 | 0.99510 |
| 42 | 1.1793 ⁻⁰² | 2.0871 ⁺⁰¹ | NM | 0.99810 | 0.99520 | 0.99790 | 1.00543 | 0.99251 |
| 43 | 1.2428 ⁻⁰² | 2.1035 ⁺⁰¹ | NM | 0.99539 | 0.99920 | 0.99750 | 0.99661 | 1.00089 |
| 44 | 1.3063 ⁻⁰² | 2.0959 ⁺⁰¹ | NM | 1.00167 | 0.99734 | 1.00020 | 1.00574 | 0.99450 |
| 45 | 1.4333 ⁻⁰² | 2.1000 ⁺⁰¹ | NM | 1.00119 | 0.99835 | 1.00020 | 1.00372 | 0.99650 |
| 46 | 1.5603 ⁻⁰² | 2.1076 ⁺⁰¹ | NM | 1.00091 | 1.00020 | 1.00050 | 1.00060 | 0.99990 |
| D 47 | 1.6873 ⁻⁰² | 2.1068 ⁺⁰¹ | NM | 1.00000 | 1.00000 | 1.00000 | 1.00000 | 1.00000 |

INPUT VARIABLES Y,U/UD,RHO/RHOD ASSUME P=PD

| | | |
|---|--|------|
|  | M: 3.0 R THETA x 10 ⁻³ : 3-4 TW/TR: 0.58, 0.77, 1.0 | 7702 |
| Continuous wind tunnel with fixed symmetrical nozzle. W = 0.079, H = 0.086 m. PO: 0.079 MN/m ² . TO: 318K. Air, dew point 236K. RE/m x 10 ⁻⁶ : 6.6. | | |
| LADERMAN A.J., DEMETRIADES A., 1977. Final technical report. Investigation of the structure of a cooled wall turbulent supersonic boundary layer. Aeronutronic Publication No. U-6370. Newport Beach, CA. And Laderman (1978a), Laderman A.J., private communications. | | |

- 1 The test boundary layer was formed on the upper surface of an aluminium plate (W = 76.2, L = 660.4, t = 4.75 mm) which was mounted so as to span the tunnel with the test surface on the centreline. The leading edge (X = 0), chamfered at 5° on the underside, was 100 mm upstream of the tunnel throat and measurements were made at X = 350, 388, 425 mm in the nominally constant pressure test zone. Provision was made for cooling of the plate with liquid nitrogen, the cooling system operating for X > 89 mm, and maintaining nominally constant wall temperatures for X > 200 mm. At the lowest temperatures used, a frost layer formed on the plate. Tests were made to determine the possible influence of this frost film. The wall temperature was steadily reduced with the tunnel running and with a thin-film probe mounted at Y = 0.75 mm. The temperature recorded showed no discontinuity as the frost formed. It was concluded that the frost formation had no separate effect on the flow field. Pressure tapings
- 2 were not affected, and the particle size was small enough not to cause any roughness effects. Flow
- 5 uniformity and two-dimensionality were assessed for the main part by Pitot surveys of the volume 250 < x < 480 mm, 0 < Y < 16.5 mm, -16.5 < Z < +16.5 mm. The results obtained, together with sensitive Schlieren studies, suggested that "two-dimensionality of the flow is apparent and it is noted that
- 3 there are no shocks or other wavelets in the surveyed volume." Thermocouples on and off the centreline showed that transverse variation of TW was not significant. The same surveys showed that the profiles
- 4 were "typically turbulent". The test layer has passed through the nozzle pressure gradient growing on the plate in a region without forced cooling. For the cooled wall cases therefore it also passes over a region of rapidly falling wall temperature, with profile measurements commencing about 20 boundary layer thicknesses downstream.
- 6 Wall pressure and temperature were measured by 9 static tapings (d = 0.5 mm) and 14 iron-constantan thermocouples at the positions shown in Table 1. A Preston tube was used in an attempt to determine skin friction.
- 7 Pitot and total temperature probes were carried by a traverse gear mounted in the tunnel roof. The CCP was constructed from 0.1 mm tube and tapered down over the foremost 3.1 mm to give a sharp-lipped orifice (d₁ = d₂ = 0.05 mm). The overall length of the streamwise part of the probe was 6.3 mm. The TTP consisted of an unshielded chromel-alumel thermocouple with the junction between the 0.038 mm wires formed as a 0.127 mm sphere mounted 1.5 mm ahead of the ceramic insulating support (d = 2.4, l = 25.4 mm). A calibration was made in the tunnel freestream which yielded (T(measured) - T) / (T₀(true) - T) as a function of Reynolds number based on the bead diameter. This "therefore accounts
- 8 for the effects of local Mach number". Traverses were made at X = 350, 388, 425 mm on the centreline.
- 9 The relative positions of static tapings and thermocouples may be seen in Table 1.

The authors assumed that, throughout the layer, P = PD as deduced from freestream PT₂ measurements. Differences were observed between measured PW values and PD values. The measured PW values however correspond to a very small fraction of the range of the transducer used, so that they were used for checks on two-dimensionality only. The Preston tube readings were abandoned since "they indicated C_f values considerably higher than implied by the trend of the velocity data. (This is apparently a

consequence of the large scatter inherent in existing Preston tube correlations.) This discrepancy has since been traced to a numerical error in data reduction. The values finally used were obtained from the correlation of data by Hopkins and Inouye (1971) or from one of a number of variants based on curve fittings to Coles' (1969) wall and wake law. These values and the streamwise variation of the velocity profile data have then been used to calculate the shear stress distribution through the boundary layer. The authors remark that the Pitot data are affected by wall interference at very low values of Y . Since only a very few points close to the wall were affected, no wall proximity correction was applied. "Viscous and rarefaction effects at low Re were examined and concluded to be negligible for $Y > 0.1$ mm" and no corrections made.

The editors have presented the profile data as given by the authors, incorporating therefore their assumptions and data reduction procedures. The Hopkins and Inouye (1971) CF value is given for convenience, the alternative values based on the velocity profiles being given below. The profiles form three sets taken at three successive traverse stations, the sets being distinguished by different TW/TR values.

§ DATA: 7702-0101-0303. Pitot and T_0 profiles. $NX = 3$. (CF - Preston).

Editors comments. There are relatively few experiments which describe the cooled wall boundary layer in any detail. All such data considered in AGARDograph 223 were obtained at $M = 4.9$ or above so that we have processed no strictly comparable data, the comparatively low Mach number here offering the possibility of assessing the effects of strong cooling independently of the instrumental difficulties associated with high Mach number flows. It is particularly unfortunate therefore that a mistake in data reduction resulted in the Preston tube data being discarded. A correctly processed value would have avoided the requirement for the authors' lengthy and inconclusive discussion of the Preston tube data and provided a valuable addition to the measured cooled wall data.

The profiles are given in very close detail, typically with 80 or more points in a boundary layer thickness of order 10 mm. The profiles extend down into the viscous sublayer, but, as noted by the authors, some aerodynamic interference effects are noticeable in this region. For a general discussion of the data see §§ 2.5 and 4.3 of AGARDograph 253. In Fig. 4.3.3 (AG 253) wall law plots are shown using wall shear values as assessed by the authors (Hopkins & Inouye, 1971) and from Fernholz (1971). We there concluded that the 'Fernholz' value gave the better numerical agreement while the 'Hopkins and Inouye' value have the better correlation. In both inner and outer law plots (Fig. 4.3.4, AG 253) the results conform well to the 'incompressible norm'. The measured temperature profiles also agree well with the theoretical predictions (Fig. 2.5.16, eqn. 2.5.37, AG 253), except for the data closest to the wall in the strongly cooled case (series 03).

A principal aim of the investigation was to document the flow in preparation for fluctuation measurements reported in Laderman & Demetriades (1979). The determination of shear stress from the mean flow profiles then provides an independent comparison value for the Reynolds shear stress $-\bar{\rho} \overline{u'v'}$. This procedure requires a remarkably high standard of accuracy, since it depends on the differentiation of experimentally determined quantities. It is doubtful that this can be achieved with three profiles, at least in such close succession as here, unless it is assumed a priori that the profiles are indeed self-similar. The results obtained do however agree well with the general trend of other data (Sandborn, 1974).

Of the very large number of possible comparison cases for the adiabatic flow, we might suggest Mabey (CAT 7701S) and Mabey et al. (CAT 7402) for flows with defined origin and Stalmach (CAT 5802) for a flow of similar pressure history. The nearest comparisons for the heat transfer case are Voisinnet and Lee (CAT 7202) and Gates (CAT 7301).

Note In AGARDograph 253 this experiment was mistakenly cited as a case with no upstream history. It should therefore be removed from the group listed in Table 4.3.1 and added to those listed in Table 4.3.2 of that volume.

TABLE 1
LOCATION OF PRESSURE TAPS (P) AND
THERMOCOUPLES (TC) ON PLATE SURFACE

| SENSOR | X (CM) | Z (CM) |
|--------|--------|--------|
| P1 | 8.9 | -2.03 |
| P2 | 8.9 | 0 |
| P3 | 8.9 | 2.03 |
| P4 | 20.3 | -2.03 |
| P5 | 20.3 | 2.03 |
| P6 | 34.3 | -2.03 |
| P7 | 34.3 | 2.03 |
| P8 | 45.7 | -2.03 |
| P9 | 45.7 | 2.03 |
| TC1 | 11.4 | -2.03 |
| TC2 | 11.4 | 0 |
| TC3 | 11.4 | 2.03 |
| TC4 | 17.8 | 0 |
| TC5 | 20.3 | -0.25 |
| TC6 | 27.9 | -2.03 |
| TC7 | 27.9 | 0.38 |
| TC8 | 27.9 | 2.03 |
| TC9 | 40.6 | -2.03 |
| TC10 | 40.6 | -0.38 |
| TC11 | 40.6 | 0.38 |
| TC12 | 40.6 | 2.03 |
| TC13 | 54.6 | -2.03 |
| TC14 | 54.6 | 2.03 |

SECTION D: SUPPLEMENTARY DATA

D1. PROFILE-DERIVED WALL SHEAR. FACSIMILE OF AUTHORS TABLE 5

AUTHORS SYMBOLS AND UNITS

SUMMARY OF VELOCITY CORRELATION CALCULATIONS

| IDENT CAT 7702 | x sta cm | T_w/T_{oe} | δ (1) cm | c_f (2) | c_f (3) | π (3) | δ (4) cm | c_f (4) | π (4) |
|----------------------|-------------|--------------|--------------------|-----------|-----------|-----------|--------------------|-----------|-----------|
| 0101 | 35.05 | .94 | .846 | .00199 | .00196 | .54 | .765 | .00188 | .70 |
| 0102 | 38.79 | | .899 | .00196 | .00192 | .56 | .800 | .00183 | .74 |
| 0103 | 42.52 | | .960 | .00192 | .00183 | .67 | .848 | .00176 | .84 |
| 0201 | 35.05 | .714 | .820 | .00216 | .00208 | .55 | .721 | .00201 | .70 |
| 0202 | 38.79 | | .856 | .00215 | .00204 | .58 | .757 | .00197 | .73 |
| 0203 | 42.52 | | .899 | .00210 | .00196 | .67 | .797 | .00191 | .80 |
| 0301 | 35.05 | .54 | .836 | .00233 | .00228 | .42 | .721 | .00221 | .57 |
| 0302 | 38.79 | | .861 | .00227 | .00206 | .68 | .800 | .00204 | .75 |
| 0303 | 42.52 | | .876 | .00224 | .00204 | .72 | .780 | .00199 | .84 |

(1) Determined from pitot profile

(2) Calculated from skin friction correlation (Reference 11) (Hopkins & Inouye, 1971)

(3) Calculated from velocity correlation using δ from pitot profile

(4) Calculated from velocity correlation (Reference 12) (Coles, 1968)

| CAT 77025 | | LADERMAN/D. BOUNDARY CONDITIONS AND EVALUATED DATA. SI UNITS | | | | | | | |
|-----------------------|-----------------------|--|-----------------------|-----------------------|--------|-----------------------|-----------------------|-----------------------|--|
| RUN | MD * | TW/TR | RED2W | CF * | H12 | H12K | PW | PD | |
| X * | POD* | PW/PD* | RED2D | CQ | H32 | H32K | TW* | TD | |
| RZ | TOO* | TAUM | OZ | PI2* | H42 | D2K | UD | TR | |
| 7702S0101 | 3.0411 | 1.0033 | 1.3626 ⁺⁰³ | 1.9900 ⁻⁰³ | 5.4823 | 1.4356 | 2.4912 ⁺⁰³ | 2.4912 ⁺⁰³ | |
| 3.5052 ⁻⁰¹ | 9.7309 ⁺⁰⁴ | 1.0000 | 3.1676 ⁺⁰³ | NM | 1.7865 | 1.7590 | 2.9833 ⁺⁰² | 1.1191 ⁺⁰² | |
| INFINITE | 3.1889 ⁺⁰² | 3.2093 ⁺⁰¹ | 5.0247 ⁻⁰⁴ | 0.0000 ⁺⁰⁰ | 0.0476 | 8.0975 ⁻⁰⁴ | 6.4500 ⁺⁰² | 2.9736 ⁺⁰² | |
| 7702S0102 | 3.0257 | 1.0029 | 1.4760 ⁺⁰³ | 1.9600 ⁻⁰³ | 5.4408 | 1.4237 | 2.5490 ⁺⁰³ | 2.5490 ⁺⁰³ | |
| 3.8786 ⁻⁰¹ | 9.7309 ⁺⁰⁴ | 1.0000 | 3.4108 ⁺⁰³ | NM | 1.7849 | 1.7586 | 2.9778 ⁺⁰² | 1.1245 ⁺⁰² | |
| INFINITE | 3.1833 ⁺⁰² | 3.2017 ⁺⁰¹ | 5.3516 ⁻⁰⁴ | 0.0000 ⁺⁰⁰ | 0.0431 | 8.6262 ⁻⁰⁴ | 6.4329 ⁺⁰² | 2.9692 ⁺⁰² | |
| 7702S0103 | 3.0008 | 1.0044 | 1.6364 ⁺⁰³ | 1.9200 ⁻⁰³ | 5.3797 | 1.4255 | 2.6461 ⁺⁰³ | 2.6461 ⁺⁰³ | |
| 4.2520 ⁻⁰¹ | 9.7309 ⁺⁰⁴ | 1.0000 | 3.7481 ⁺⁰³ | NM | 1.7794 | 1.7539 | 2.9889 ⁺⁰² | 1.1385 ⁺⁰² | |
| INFINITE | 3.1889 ⁺⁰² | 3.2023 ⁺⁰¹ | 5.8155 ⁻⁰⁴ | 0.0000 ⁺⁰⁰ | 0.0469 | 9.4093 ⁻⁰⁴ | 6.4197 ⁺⁰² | 2.9757 ⁺⁰² | |
| 7702S0201 | 3.0219 | 0.7657 | 1.7773 ⁺⁰³ | 2.1600 ⁻⁰³ | 4.7159 | 1.4186 | 2.5637 ⁺⁰³ | 2.5637 ⁺⁰³ | |
| 3.5052 ⁻⁰¹ | 9.7309 ⁺⁰⁴ | 1.0000 | 3.3075 ⁺⁰³ | NM | 1.7813 | 1.7601 | 2.2778 ⁺⁰² | 1.1283 ⁺⁰² | |
| INFINITE | 3.1889 ⁺⁰² | 3.5398 ⁺⁰¹ | 5.1916 ⁻⁰⁴ | 0.0000 ⁺⁰⁰ | 0.2350 | 7.7833 ⁻⁰⁴ | 6.4357 ⁺⁰² | 2.9746 ⁺⁰² | |
| 7702S0202 | 3.0263 | 0.7671 | 1.8984 ⁺⁰³ | 2.1500 ⁻⁰³ | 4.6471 | 1.3983 | 2.5469 ⁺⁰³ | 2.5469 ⁺⁰³ | |
| 3.8786 ⁻⁰¹ | 9.7309 ⁺⁰⁴ | 1.0000 | 3.5450 ⁺⁰³ | NM | 1.7810 | 1.7609 | 2.2778 ⁺⁰² | 1.1242 ⁺⁰² | |
| INFINITE | 3.1833 ⁺⁰² | 3.5105 ⁺⁰¹ | 5.5638 ⁻⁰⁴ | 0.0000 ⁺⁰⁰ | 0.2507 | 8.3349 ⁻⁰⁴ | 6.4334 ⁺⁰² | 2.9692 ⁺⁰² | |
| 7702S0203 | 2.9974 | 0.7668 | 2.0872 ⁺⁰³ | 2.1000 ⁻⁰³ | 4.6319 | 1.4191 | 2.6596 ⁺⁰³ | 2.6596 ⁺⁰³ | |
| 4.2520 ⁻⁰¹ | 9.7309 ⁺⁰⁴ | 1.0000 | 3.8521 ⁺⁰³ | NM | 1.7742 | 1.7546 | 2.2778 ⁺⁰² | 1.1382 ⁺⁰² | |
| INFINITE | 3.1833 ⁺⁰² | 3.5125 ⁺⁰¹ | 5.9508 ⁻⁰⁴ | 0.0000 ⁺⁰⁰ | 0.2460 | 8.9395 ⁻⁰⁴ | 6.4115 ⁺⁰² | 2.9706 ⁺⁰² | |
| 7702S0301 | 3.0281 | 0.5801 | 2.4791 ⁺⁰³ | 2.3300 ⁻⁰³ | 3.8007 | 1.3702 | 2.5400 ⁺⁰³ | 2.5400 ⁺⁰³ | |
| 3.5052 ⁻⁰¹ | 9.7309 ⁺⁰⁴ | 1.0000 | 3.6564 ⁺⁰³ | NM | 1.7869 | 1.7724 | 1.7222 ⁺⁰² | 1.1233 ⁺⁰² | |
| INFINITE | 3.1833 ⁺⁰² | 3.7986 ⁺⁰¹ | 5.7444 ⁻⁰⁴ | 0.0000 ⁺⁰⁰ | 0.4780 | 7.8744 ⁻⁰⁴ | 6.4347 ⁺⁰² | 2.9691 ⁺⁰² | |
| 7702S0302 | 3.0379 | 0.5801 | 2.6680 ⁺⁰³ | 2.2700 ⁻⁰³ | 4.1956 | 1.4092 | 2.5031 ⁺⁰³ | 2.5031 ⁺⁰³ | |
| 3.8786 ⁻⁰¹ | 9.7309 ⁺⁰⁴ | 1.0000 | 3.9507 ⁺⁰³ | NM | 1.7725 | 1.7563 | 1.7222 ⁺⁰² | 1.1186 ⁺⁰² | |
| INFINITE | 3.1833 ⁺⁰² | 3.6706 ⁺⁰¹ | 6.2401 ⁻⁰⁴ | 0.0000 ⁺⁰⁰ | 0.3831 | 8.9188 ⁻⁰⁴ | 6.4420 ⁺⁰² | 2.9686 ⁺⁰² | |
| 7702S0303 | 2.9856 | 0.5786 | 2.8269 ⁺⁰³ | 2.2400 ⁻⁰³ | 3.9801 | 1.3828 | 2.7071 ⁺⁰³ | 2.7071 ⁺⁰³ | |
| 4.2520 ⁻⁰¹ | 9.7309 ⁺⁰⁴ | 1.0000 | 4.0917 ⁺⁰³ | NM | 1.7695 | 1.7569 | 1.7222 ⁺⁰² | 1.1460 ⁺⁰² | |
| INFINITE | 3.1889 ⁺⁰² | 3.7836 ⁺⁰¹ | 6.2960 ⁻⁰⁴ | 0.0000 ⁺⁰⁰ | 0.4002 | 8.8295 ⁻⁰⁴ | 6.4080 ⁺⁰² | 2.9764 ⁺⁰² | |

7702S0301

LADERMAN/D.

PROFILE TABULATION

78 POINTS, DELTA AT POINT 66

| I | Y | PT2/P | P/PD | TO/TOD | M/MD | U/UD | T/TD | R/RD*U/UD |
|------|------------------------|------------------------|------|---------|---------|---------|---------|-----------|
| 1 | 0.0000 ⁺ 00 | 1.0000 ⁺ 00 | NM | 0.54101 | 0.00000 | 0.00000 | 1.53315 | 0.00000 |
| 2 | 5.0800 ⁻ 05 | 1.4906 ⁺ 00 | NM | 0.63730 | 0.25667 | 0.32581 | 1.61135 | 0.20220 |
| 3 | 5.8928 ⁻ 05 | 1.5379 ⁺ 00 | NM | 0.64831 | 0.26713 | 0.34049 | 1.62462 | 0.20958 |
| 4 | 7.9248 ⁻ 05 | 1.5971 ⁺ 00 | NM | 0.67058 | 0.27936 | 0.36020 | 1.66240 | 0.21667 |
| 5 | 9.1440 ⁻ 05 | 1.6148 ⁺ 00 | NM | 0.69197 | 0.28287 | 0.36990 | 1.71001 | 0.21632 |
| 6 | 1.0465 ⁻ 04 | 1.6621 ⁺ 00 | NM | 0.71563 | 0.29189 | 0.38656 | 1.75395 | 0.22040 |
| 7 | 1.1379 ⁻ 04 | 1.7154 ⁺ 00 | NM | 0.72141 | 0.30150 | 0.39911 | 1.75227 | 0.22776 |
| 8 | 1.3208 ⁻ 04 | 1.8810 ⁺ 00 | NM | 0.73546 | 0.32845 | 0.43325 | 1.73997 | 0.24900 |
| 9 | 1.4935 ⁻ 04 | 2.0949 ⁺ 00 | NM | 0.74496 | 0.35836 | 0.46844 | 1.70869 | 0.27415 |
| 10 | 1.5850 ⁻ 04 | 2.2017 ⁺ 00 | NM | 0.74794 | 0.37193 | 0.48360 | 1.69066 | 0.28604 |
| 11 | 1.8593 ⁻ 04 | 2.4741 ⁺ 00 | NM | 0.76001 | 0.40376 | 0.51991 | 1.65807 | 0.31356 |
| 12 | 2.1336 ⁻ 04 | 2.6986 ⁺ 00 | NM | 0.77119 | 0.42777 | 0.54720 | 1.63633 | 0.33441 |
| 13 | 2.3876 ⁻ 04 | 2.9112 ⁺ 00 | NM | 0.78080 | 0.44910 | 0.57077 | 1.61523 | 0.35337 |
| 14 | 2.6924 ⁻ 04 | 3.0884 ⁺ 00 | NM | 0.79102 | 0.46602 | 0.59005 | 1.60316 | 0.36806 |
| 15 | 3.2817 ⁻ 04 | 3.3447 ⁺ 00 | NM | 0.80262 | 0.48933 | 0.61518 | 1.58049 | 0.38923 |
| 16 | 3.8100 ⁻ 04 | 3.5054 ⁺ 00 | NM | 0.81170 | 0.50334 | 0.63080 | 1.57053 | 0.40165 |
| 17 | 4.2469 ⁻ 04 | 3.6065 ⁺ 00 | NM | 0.81605 | 0.51195 | 0.63981 | 1.56188 | 0.40964 |
| 18 | 4.7854 ⁻ 04 | 3.7492 ⁺ 00 | NM | 0.82198 | 0.52382 | 0.65207 | 1.54963 | 0.42079 |
| 19 | 5.2629 ⁻ 04 | 3.8620 ⁺ 00 | NM | 0.82562 | 0.53301 | 0.66107 | 1.53825 | 0.42976 |
| 20 | 5.8115 ⁻ 04 | 3.9806 ⁺ 00 | NM | 0.83030 | 0.54250 | 0.67063 | 1.52818 | 0.43884 |
| 21 | 6.2789 ⁻ 04 | 4.0541 ⁺ 00 | NM | 0.83329 | 0.54829 | 0.67647 | 1.52223 | 0.44439 |
| 22 | 6.9393 ⁻ 04 | 4.1280 ⁺ 00 | NM | 0.83726 | 0.55404 | 0.68264 | 1.51809 | 0.44967 |
| 23 | 7.4879 ⁻ 04 | 4.1962 ⁺ 00 | NM | 0.84153 | 0.55930 | 0.68852 | 1.51543 | 0.45434 |
| 24 | 8.8798 ⁻ 04 | 4.3950 ⁺ 00 | NM | 0.84748 | 0.57433 | 0.70257 | 1.49644 | 0.46950 |
| 25 | 1.0150 ⁻ 03 | 4.6725 ⁺ 00 | NM | 0.85459 | 0.59465 | 0.72076 | 1.46910 | 0.49061 |
| 26 | 1.1379 ⁻ 03 | 4.7964 ⁺ 00 | NM | 0.86093 | 0.60349 | 0.72990 | 1.46278 | 0.49898 |
| 27 | 1.2781 ⁻ 03 | 4.8612 ⁺ 00 | NM | 0.86529 | 0.60807 | 0.73505 | 1.46127 | 0.50302 |
| 28 | 1.3950 ⁻ 03 | 5.0321 ⁺ 00 | NM | 0.86879 | 0.61995 | 0.74502 | 1.44416 | 0.51588 |
| 29 | 1.5443 ⁻ 03 | 5.2087 ⁺ 00 | NM | 0.87777 | 0.63200 | 0.75729 | 1.43579 | 0.52743 |
| 30 | 1.6784 ⁻ 03 | 5.3793 ⁺ 00 | NM | 0.88485 | 0.64341 | 0.76817 | 1.42540 | 0.53892 |
| 31 | 1.8115 ⁻ 03 | 5.5205 ⁺ 00 | NM | 0.88922 | 0.65270 | 0.77633 | 1.41469 | 0.54876 |
| 32 | 2.0655 ⁻ 03 | 5.8257 ⁺ 00 | NM | 0.89931 | 0.67233 | 0.79364 | 1.39343 | 0.56956 |
| 33 | 2.3338 ⁻ 03 | 6.1507 ⁺ 00 | NM | 0.90970 | 0.69261 | 0.81111 | 1.37147 | 0.59142 |
| 34 | 2.5999 ⁻ 03 | 6.4815 ⁺ 00 | NM | 0.91863 | 0.71264 | 0.82737 | 1.34790 | 0.61382 |
| 35 | 2.8732 ⁻ 03 | 6.8241 ⁺ 00 | NM | 0.93378 | 0.73281 | 0.84614 | 1.33323 | 0.63466 |
| 36 | 3.1476 ⁻ 03 | 7.1668 ⁺ 00 | NM | 0.93668 | 0.75243 | 0.85866 | 1.30232 | 0.65933 |
| 37 | 3.4016 ⁻ 03 | 7.5214 ⁺ 00 | NM | 0.94559 | 0.77219 | 0.87363 | 1.28000 | 0.68253 |
| 38 | 3.6759 ⁻ 03 | 7.8761 ⁺ 00 | NM | 0.95223 | 0.79147 | 0.88695 | 1.25583 | 0.70626 |
| 39 | 3.9299 ⁻ 03 | 8.2429 ⁺ 00 | NM | 0.95836 | 0.81091 | 0.89977 | 1.23117 | 0.73082 |
| 40 | 4.2042 ⁻ 03 | 8.6219 ⁺ 00 | NM | 0.96374 | 0.83051 | 0.91199 | 1.20583 | 0.75632 |
| 41 | 4.4785 ⁻ 03 | 8.9909 ⁺ 00 | NM | 0.97114 | 0.84917 | 0.92440 | 1.18503 | 0.78006 |
| 42 | 4.7325 ⁻ 03 | 9.3768 ⁺ 00 | NM | 0.97651 | 0.86824 | 0.93574 | 1.16154 | 0.80561 |
| 43 | 4.9865 ⁻ 03 | 9.6984 ⁺ 00 | NM | 0.98125 | 0.88382 | 0.94497 | 1.14317 | 0.82662 |
| 44 | 5.2710 ⁻ 03 | 1.0083 ⁺ 01 | NM | 0.98660 | 0.90207 | 0.95544 | 1.12182 | 0.85169 |
| 45 | 5.5352 ⁻ 03 | 1.0470 ⁺ 01 | NM | 0.98664 | 0.92011 | 0.96299 | 1.09539 | 0.87913 |
| 46 | 5.6672 ⁻ 03 | 1.0637 ⁺ 01 | NM | 0.98783 | 0.92777 | 0.96669 | 1.08565 | 0.89042 |
| 47 | 5.7892 ⁻ 03 | 1.0798 ⁺ 01 | NM | 0.98882 | 0.93512 | 0.97012 | 1.07627 | 0.90137 |
| 48 | 5.9314 ⁻ 03 | 1.0977 ⁺ 01 | NM | 0.99193 | 0.94321 | 0.97485 | 1.06821 | 0.91260 |
| 49 | 6.0635 ⁻ 03 | 1.1131 ⁺ 01 | NM | 0.98987 | 0.95007 | 0.97651 | 1.05643 | 0.92434 |
| 50 | 6.1956 ⁻ 03 | 1.1285 ⁺ 01 | NM | 0.99252 | 0.95694 | 0.98046 | 1.04976 | 0.93398 |
| 51 | 6.3276 ⁻ 03 | 1.1428 ⁺ 01 | NM | 0.99060 | 0.96324 | 0.98190 | 1.03913 | 0.94493 |
| 52 | 6.4496 ⁻ 03 | 1.1552 ⁺ 01 | NM | 0.99144 | 0.96872 | 0.98438 | 1.03259 | 0.95331 |
| 53 | 6.5816 ⁻ 03 | 1.1671 ⁺ 01 | NM | 0.99091 | 0.97391 | 0.98605 | 1.02507 | 0.96193 |
| 54 | 6.7442 ⁻ 03 | 1.1808 ⁺ 01 | NM | 0.99196 | 0.97985 | 0.98875 | 1.01824 | 0.97104 |
| 55 | 6.8560 ⁻ 03 | 1.1892 ⁺ 01 | NM | 0.99145 | 0.98345 | 0.98981 | 1.01296 | 0.97714 |
| 56 | 6.9779 ⁻ 03 | 1.1969 ⁺ 01 | NM | 0.99045 | 0.98678 | 0.99051 | 1.00758 | 0.98307 |
| 57 | 7.1201 ⁻ 03 | 1.2040 ⁺ 01 | NM | 0.99293 | 0.98985 | 0.99286 | 1.00609 | 0.98885 |
| 58 | 7.2522 ⁻ 03 | 1.2094 ⁺ 01 | NM | 0.99303 | 0.99214 | 0.99372 | 1.00320 | 0.99056 |
| 59 | 7.3843 ⁻ 03 | 1.2148 ⁺ 01 | NM | 0.99111 | 0.99443 | 0.99358 | 0.99829 | 0.99528 |
| 60 | 7.5265 ⁻ 03 | 1.2165 ⁺ 01 | NM | 0.99097 | 0.99519 | 0.99378 | 0.99716 | 0.99660 |
| 61 | 7.6586 ⁻ 03 | 1.2195 ⁺ 01 | NM | 0.98993 | 0.99646 | 0.99371 | 0.99448 | 0.99922 |
| 62 | 7.7907 ⁻ 03 | 1.2237 ⁺ 01 | NM | 0.99761 | 0.99823 | 0.99818 | 0.99990 | 0.99828 |
| 63 | 7.9228 ⁻ 03 | 1.2267 ⁺ 01 | NM | 0.99527 | 0.99949 | 0.99745 | 0.99592 | 1.00154 |
| 64 | 8.0548 ⁻ 03 | 1.2267 ⁺ 01 | NM | 0.98572 | 0.99949 | 0.99266 | 0.98636 | 1.00638 |
| 65 | 8.1869 ⁻ 03 | 1.2261 ⁺ 01 | NM | 0.98817 | 0.99924 | 0.99380 | 0.98914 | 1.00471 |
| D 66 | 8.3393 ⁻ 03 | 1.2279 ⁺ 01 | NM | 1.00000 | 1.00000 | 1.00000 | 1.00000 | 1.00000 |
| 67 | 8.4714 ⁻ 03 | 1.2291 ⁺ 01 | NM | 0.98866 | 1.00051 | 0.99449 | 0.98802 | 1.00655 |
| 68 | 8.5933 ⁻ 03 | 1.2291 ⁺ 01 | NM | 0.98868 | 1.00051 | 0.99450 | 0.98803 | 1.00655 |
| 69 | 8.7152 ⁻ 03 | 1.2285 ⁺ 01 | NM | 0.98786 | 1.00025 | 0.99400 | 0.98754 | 1.00654 |
| 70 | 8.8575 ⁻ 03 | 1.2291 ⁺ 01 | NM | 0.98775 | 1.00051 | 0.99403 | 0.98710 | 1.00702 |
| 71 | 8.9794 ⁻ 03 | 1.2291 ⁺ 01 | NM | 0.98782 | 1.00051 | 0.99407 | 0.98717 | 1.00698 |
| 72 | 9.1115 ⁻ 03 | 1.2296 ⁺ 01 | NM | 0.98774 | 1.00076 | 0.99412 | 0.98677 | 1.00744 |
| 73 | 9.2334 ⁻ 03 | 1.2296 ⁺ 01 | NM | 0.98774 | 1.00076 | 0.99412 | 0.98678 | 1.00744 |
| 74 | 9.3756 ⁻ 03 | 1.2285 ⁺ 01 | NM | 0.98777 | 1.00025 | 0.99395 | 0.98744 | 1.00659 |
| 75 | 9.4976 ⁻ 03 | 1.2291 ⁺ 01 | NM | 0.98785 | 1.00051 | 0.99408 | 0.98721 | 1.00697 |
| 76 | 9.6398 ⁻ 03 | 1.2285 ⁺ 01 | NM | 0.98784 | 1.00025 | 0.99399 | 0.98752 | 1.00655 |
| 77 | 9.7719 ⁻ 03 | 1.2296 ⁺ 01 | NM | 0.98771 | 1.00076 | 0.99410 | 0.98674 | 1.00746 |
| 78 | 9.8836 ⁻ 03 | 1.2291 ⁺ 01 | NM | 0.98773 | 1.00051 | 0.99402 | 0.98708 | 1.00703 |

INPUT VARIABLES Y,M,TO/TOD ASSUME P=PD

7702S0303

LADERMAN/D.

PROFILE TABULATION

65 POINTS, DELTA AT POINT 62

| I | Y | PT2/P | P/PD | TO/TOD | M/MD | U/UD | T/TD | R/RD*U/UD |
|------|------------------------|------------------------|------|---------|---------|---------|---------|-----------|
| 1 | 0.0000 ⁺ 00 | 1.0000 ⁺ 00 | NM | 0.54007 | 0.00000 | 0.00000 | 1.50287 | 0.00000 |
| 2 | 5.0800 ⁻ 05 | 1.9482 ⁺ 00 | NM | 0.63291 | 0.34314 | 0.41400 | 1.45566 | 0.28441 |
| 3 | 6.5024 ⁻ 05 | 1.9370 ⁺ 00 | NM | 0.64160 | 0.34151 | 0.41520 | 1.47808 | 0.28090 |
| 4 | 7.8232 ⁻ 05 | 1.9537 ⁺ 00 | NM | 0.64894 | 0.34395 | 0.42002 | 1.49132 | 0.28165 |
| 5 | 8.7376 ⁻ 05 | 1.9871 ⁺ 00 | NM | 0.66055 | 0.34873 | 0.42861 | 1.51064 | 0.28373 |
| 6 | 1.0465 ⁻ 04 | 2.0651 ⁺ 00 | NM | 0.69576 | 0.35948 | 0.45095 | 1.57360 | 0.28657 |
| 7 | 1.2192 ⁻ 04 | 2.1931 ⁺ 00 | NM | 0.73356 | 0.37614 | 0.48025 | 1.63013 | 0.29461 |
| 8 | 1.7069 ⁻ 04 | 2.4320 ⁺ 00 | NM | 0.75243 | 0.40474 | 0.51524 | 1.62055 | 0.31794 |
| 9 | 2.0015 ⁻ 04 | 2.5541 ⁺ 00 | NM | 0.76223 | 0.41838 | 0.53196 | 1.61661 | 0.32906 |
| 10 | 2.2352 ⁻ 04 | 2.6594 ⁺ 00 | NM | 0.77201 | 0.42973 | 0.54631 | 1.61622 | 0.33802 |
| 11 | 2.5095 ⁻ 04 | 2.7203 ⁺ 00 | NM | 0.78165 | 0.43613 | 0.55584 | 1.62432 | 0.34220 |
| 12 | 3.0785 ⁻ 04 | 2.8422 ⁺ 00 | NM | 0.79774 | 0.44861 | 0.57340 | 1.63376 | 0.35097 |
| 13 | 3.3426 ⁻ 04 | 2.9253 ⁺ 00 | NM | 0.80139 | 0.45689 | 0.58246 | 1.62524 | 0.35838 |
| 14 | 3.8710 ⁻ 04 | 3.0195 ⁺ 00 | NM | 0.80570 | 0.46606 | 0.59251 | 1.61620 | 0.36660 |
| 15 | 4.4704 ⁻ 04 | 3.1580 ⁺ 00 | NM | 0.81373 | 0.47920 | 0.60741 | 1.60667 | 0.37806 |
| 16 | 5.1105 ⁻ 04 | 3.2744 ⁺ 00 | NM | 0.82060 | 0.48993 | 0.61957 | 1.59919 | 0.38743 |
| 17 | 5.7912 ⁻ 04 | 3.3596 ⁺ 00 | NM | 0.82521 | 0.49763 | 0.62809 | 1.59307 | 0.39427 |
| 18 | 6.4414 ⁻ 04 | 3.4712 ⁺ 00 | NM | 0.83001 | 0.50752 | 0.63852 | 1.58286 | 0.40340 |
| 19 | 7.1933 ⁻ 04 | 3.5717 ⁺ 00 | NM | 0.83413 | 0.51625 | 0.64759 | 1.57355 | 0.41154 |
| 20 | 7.8232 ⁻ 04 | 3.6665 ⁺ 00 | NM | 0.83776 | 0.52433 | 0.65583 | 1.56448 | 0.41920 |
| 21 | 8.6055 ⁻ 04 | 3.7501 ⁺ 00 | NM | 0.84142 | 0.53136 | 0.66313 | 1.55750 | 0.42577 |
| 22 | 9.1135 ⁻ 04 | 3.8281 ⁺ 00 | NM | 0.84417 | 0.53782 | 0.66955 | 1.54989 | 0.43200 |
| 23 | 1.0384 ⁻ 03 | 3.9839 ⁺ 00 | NM | 0.85067 | 0.55049 | 0.68245 | 1.53690 | 0.44404 |
| 24 | 1.1786 ⁻ 03 | 4.1438 ⁺ 00 | NM | 0.85644 | 0.56316 | 0.69487 | 1.52245 | 0.45642 |
| 25 | 1.3045 ⁻ 03 | 4.3061 ⁺ 00 | NM | 0.86324 | 0.57574 | 0.70746 | 1.50991 | 0.46855 |
| 26 | 1.4366 ⁻ 03 | 4.4281 ⁺ 00 | NM | 0.87313 | 0.58501 | 0.71864 | 1.50902 | 0.47623 |
| 27 | 1.5697 ⁻ 03 | 4.5888 ⁺ 00 | NM | 0.87222 | 0.59698 | 0.72729 | 1.48420 | 0.49002 |
| 28 | 1.7109 ⁻ 03 | 4.7493 ⁺ 00 | NM | 0.87785 | 0.60869 | 0.73828 | 1.47113 | 0.50185 |
| 29 | 1.8278 ⁻ 03 | 4.8931 ⁺ 00 | NM | 0.88245 | 0.61899 | 0.74768 | 1.45902 | 0.51245 |
| 30 | 2.1011 ⁻ 03 | 5.2025 ⁺ 00 | NM | 0.89240 | 0.64057 | 0.76713 | 1.43419 | 0.53489 |
| 31 | 2.3652 ⁻ 03 | 5.5171 ⁺ 00 | NM | 0.90309 | 0.66176 | 0.78615 | 1.41126 | 0.55706 |
| 32 | 2.6294 ⁻ 03 | 5.8203 ⁺ 00 | NM | 0.91509 | 0.68155 | 0.80439 | 1.39294 | 0.57747 |
| 33 | 2.9078 ⁻ 03 | 6.1417 ⁺ 00 | NM | 0.92370 | 0.70191 | 0.82110 | 1.36847 | 0.60002 |
| 34 | 3.1679 ⁻ 03 | 6.4576 ⁺ 00 | NM | 0.93619 | 0.72134 | 0.83859 | 1.35149 | 0.62049 |
| 35 | 3.4381 ⁻ 03 | 6.7846 ⁺ 00 | NM | 0.93808 | 0.74091 | 0.85102 | 1.31932 | 0.64504 |
| 36 | 3.7033 ⁻ 03 | 7.1060 ⁺ 00 | NM | 0.94349 | 0.75965 | 0.86418 | 1.29415 | 0.66776 |
| 37 | 3.9573 ⁻ 03 | 7.4276 ⁺ 00 | NM | 0.95405 | 0.77793 | 0.87912 | 1.27708 | 0.68839 |
| 38 | 4.1097 ⁻ 03 | 7.6216 ⁺ 00 | NM | 0.95609 | 0.78876 | 0.88589 | 1.26146 | 0.70228 |
| 39 | 4.5060 ⁻ 03 | 8.0932 ⁺ 00 | NM | 0.96908 | 0.81446 | 0.90532 | 1.23556 | 0.73272 |
| 40 | 4.7701 ⁻ 03 | 8.4319 ⁺ 00 | NM | 0.97154 | 0.83243 | 0.91547 | 1.20946 | 0.75692 |
| 41 | 5.0343 ⁻ 03 | 8.7537 ⁺ 00 | NM | 0.98113 | 0.84914 | 0.92810 | 1.19463 | 0.77690 |
| 42 | 5.3188 ⁻ 03 | 9.1236 ⁺ 00 | NM | 0.98160 | 0.86795 | 0.93716 | 1.16582 | 0.80386 |
| 43 | 5.5220 ⁻ 03 | 9.4135 ⁺ 00 | NM | 0.98823 | 0.88241 | 0.94691 | 1.15153 | 0.82231 |
| 44 | 5.8166 ⁻ 03 | 9.7993 ⁺ 00 | NM | 0.98776 | 0.90129 | 0.95501 | 1.12274 | 0.85060 |
| 45 | 6.0909 ⁻ 03 | 1.0170 ⁺ 01 | NM | 0.99619 | 0.91905 | 0.96666 | 1.10629 | 0.87379 |
| 46 | 6.3652 ⁻ 03 | 1.0516 ⁺ 01 | NM | 0.99909 | 0.93537 | 0.97482 | 1.08613 | 0.89751 |
| 47 | 6.6192 ⁻ 03 | 1.0779 ⁺ 01 | NM | 1.00011 | 0.94757 | 0.98022 | 1.07012 | 0.91600 |
| 48 | 6.7615 ⁻ 03 | 1.0953 ⁺ 01 | NM | 0.99914 | 0.95553 | 0.98289 | 1.05808 | 0.92894 |
| 49 | 6.8732 ⁻ 03 | 1.1069 ⁺ 01 | NM | 1.00326 | 0.96079 | 0.98697 | 1.05523 | 0.93531 |
| 50 | 7.0256 ⁻ 03 | 1.1219 ⁺ 01 | NM | 1.00571 | 0.96760 | 0.99080 | 1.04854 | 0.94494 |
| 51 | 7.1577 ⁻ 03 | 1.1286 ⁺ 01 | NM | 1.00511 | 0.97061 | 0.99165 | 1.04384 | 0.95001 |
| 52 | 7.2898 ⁻ 03 | 1.1403 ⁺ 01 | NM | 1.00409 | 0.97586 | 0.99315 | 1.03575 | 0.95887 |
| 53 | 7.3304 ⁻ 03 | 1.1459 ⁺ 01 | NM | 1.00362 | 0.97834 | 0.99385 | 1.03194 | 0.96308 |
| 54 | 7.5336 ⁻ 03 | 1.1604 ⁺ 01 | NM | 1.00334 | 0.98479 | 0.99611 | 1.02312 | 0.97360 |
| 55 | 7.8283 ⁻ 03 | 1.1738 ⁺ 01 | NM | 1.00294 | 0.99070 | 0.99809 | 1.01497 | 0.98337 |
| 56 | 7.9604 ⁻ 03 | 1.1794 ⁺ 01 | NM | 1.00157 | 0.99316 | 0.99831 | 1.01039 | 0.98804 |
| 57 | 8.0823 ⁻ 03 | 1.1838 ⁺ 01 | NM | 1.00104 | 0.99512 | 0.99876 | 1.00733 | 0.99149 |
| 58 | 8.2245 ⁻ 03 | 1.1861 ⁺ 01 | NM | 1.00173 | 0.99610 | 0.99946 | 1.00676 | 0.99275 |
| 59 | 8.3566 ⁻ 03 | 1.1883 ⁺ 01 | NM | 1.00117 | 0.99707 | 0.99953 | 1.00493 | 0.99462 |
| 60 | 8.4887 ⁻ 03 | 1.1928 ⁺ 01 | NM | 1.00187 | 0.99903 | 1.00058 | 1.00312 | 0.99747 |
| 61 | 8.6208 ⁻ 03 | 1.1939 ⁺ 01 | NM | 1.00189 | 0.99951 | 1.00077 | 1.00252 | 0.99826 |
| D 62 | 8.7427 ⁻ 03 | 1.1950 ⁺ 01 | NM | 1.00000 | 1.00000 | 1.00000 | 1.00000 | 1.00000 |
| 63 | 8.8748 ⁻ 03 | 1.1950 ⁺ 01 | NM | 0.99909 | 1.00000 | 0.99954 | 0.99909 | 1.00046 |
| 64 | 9.0068 ⁻ 03 | 1.1944 ⁺ 01 | NM | 1.00247 | 0.99976 | 1.00115 | 1.00278 | 0.99837 |
| 65 | 9.1389 ⁻ 03 | 1.1916 ⁺ 01 | NM | 1.00616 | 0.99854 | 1.00255 | 1.00805 | 0.99454 |

INPUT VARIABLES Y,M,TO/TOD ASSUME P=PD

| | | |
|--|---|-------------|
| <p>rough</p>  | <p>M: 6 R THETA $\times 10^{-3}$: 14 TW/TR: 0.89</p> | <p>7703</p> |
| <p>Continuous running tunnel with (here) asymmetric flexible nozzle. $H = 0.071$ m, $W = 0.139$ m increasing to 0.178 m, $L = 1.31$ m.</p> <p>PO: 1.56 MN/m². TO: 425K. Air. $RE/m \times 10^{-6}$: 15.</p> | | |
| <p>BERG D.E., 1977. Surface roughness effects on the hypersonic turbulent boundary layer. Ph.D. Thesis GALCIT Pasadena, Calif. (Also as SANDIA Laboratories, SAND 77-0587). Also: Berg (1978, 1979). And: Berg, D.E., private communications.</p> | | |

- 1 The lower flexible plate of what is normally a symmetric nozzle windtunnel was replaced by a rigid base plate. Four removable surface plates 8.9 mm thick and, in sequence, 0.222, 0.290, 0.330 and 0.330 m long could be mounted on this to give a replaceable test surface extending from $X = 0.131$ to $X = 1.307$ m, with $X = 0$ at the tunnel throat. (There would seem to be small gaps between the plates, giving $X = 0.645$ m at the start of the third plate. Any gaps are closed by the continuous mounting plate - E). The width of the test section increased from 0.139 m at the throat to 0.178 m at $X = 1.31$ m to compensate for boundary layer growth. The start of the third plate was at $X = 0.645$ m so that the replaceable test surface extended from $X = 0.061$ m to $X = 1.229$ m, with $X = 0$ at the tunnel throat.
- Measurements were made for $0.62 < X < 1.30$ m. Four sets of plates were made, one of which was smooth while the remainder had transverse square bar roughness distributions machined into them. Three roughness heights were used, 0.32, 0.64 and 1.27 mm. The wavelength of the roughness was four times the height and the top surfaces of the roughness elements were flush with the undisturbed surface of the plate, and so of the smooth surface upstream of the plate. Apart from the smooth wall case (series 01), a step change in roughness always took place at $X = 0.645$ m. For series 02, 03, 04 this was from a smooth surface to roughness heights of 0.32, 0.64, 1.27 mm respectively. For series 05, the sequence was firstly a smooth plate then a 0.292 m plate for which $K = 1.27$ mm and finally, at $X = 0.645$ m, a smooth surface again. It is stated that the earlier tests had shown that in 0.290 m, or about 10 boundary layer thicknesses, the boundary layer would reach an equilibrium state appropriate to the rough surface. Heated air was passed beneath the plate (at low speed) so as to reduce heat transfer to the plate to a minimum.
- 2 The nozzle contour was adjusted to give uniform flow with the smooth surface plates installed. Although between $X = 0.635$ and $X = 1.22$ the centre line Mach number was $6.02 \pm 1\%$, the variation was not random. The Mach number appears to rise and fall, almost periodically. The author attributes this to a pressure disturbance originating in the nozzle which is then reflected to and fro from the top to
 - 4 bottom. The "wavelength" (E) is consistent with this explanation. The test layer will also have experienced a reflected wave expansion in the nozzle, finishing just before the start of the test zone. The outermost points of the first profiles are very nearly in the last part of what would be, here, a simple wave expansion. The wall temperature rises rapidly from about 335K at $X = 0.2$ m to about 345K at
 - 5 $X = 0.65$ m. Crosstream Pitot traverses were made to check two dimensionality, showing about 5% variation in PT2 over the central 2/3 of the tunnel.
 - 6 "Direct measurements of wall temperature and pressure were made via instrumentation in the tunnel wall at 15 stations." Static tappings in the smooth surface plates were 0.36 mm in diameter. The wall shear stress could be measured at two positions ($X = 0.709, 1.217$ m), using an FEB mounted to appropriate surface plates. The balance was based on that used by Coles (CAT 5301). The rectangular element ($W = 38.0, L = 4.98$ mm) was placed with its long axis across the flow. When measurements were

being made with rough surfaces, the element was also contoured, and was of a size to accommodate a whole number of roughness element wave lengths (4,2,1 for heights of 0.32, 0.64, 1.27 mm). The element was flush with the surrounding surface to within 2.5 μm for the smooth plates and 5 μm for the rough ones. The roughness is that characterised as "D-type" (Perry et al., 1969).

- 7 Pitot, T0 and some static pressure profiles were obtained. The Pitot probe was an FPP made by flattening 1.65 mm tube and filing to give a probe face for which, approximately, $b_1 = 0.25$, $h_1 = 0.20$, $h_2 = 0.10$ mm. It was mounted pitched down at 10° . The T0 probe was a FWP after Behrens (1971) consisting of a 0.127 mm butt-welded chromel-Alumel thermocouple between supports 12.7 mm apart. To minimise conduction corrections, the lead wires within the supports were of 0.025 mm diameter. A further thermocouple on one support monitored support temperature. The static pressure probe (CCP) was of 0.81 mm diameter with a sharpened tip of half angle 8° - 10° . Four static holes ($d = 0.18$ mm) were drilled at 90° intervals 9.8 mm downstream of the probe shoulder. Hot wire probes ($d = 0.0025$, $l/d = 180$ - 200) were used with a "Shapiro-Edwards constant current set with a half power frequency of 320 kHz."
- 9 Free stream static pressure and Mach number were obtained from Pitot readings, and the static pressure assumed constant through the boundary layer in data reduction. The limited (4 profiles) static pressure data in general supported this assumption, but also indicated that a weak pressure wave is reflected from the boundary layer and affects profiles in the vicinity of $X = 1.0$ m. The maximum measured effect was a difference of 7% in static pressure across the boundary layer at $X = 0.85$ m. The authors find that the $dp/dy = 0$ assumption may cause errors in the evaluation of δ_2 of 10% while the pressure wave itself accounts for (real) anomalous behaviour of δ_2 near $X = 0.90$ m. A linear interpolation was used for T0 between the last measured value ($Y > 0.76$ mm) and the wall temperature.

The velocity profile data were reduced to an equivalent incompressible form using the van Driest transformation and an empirical quadratic temperature-velocity correlation. This gave a noticeably better fit (source, Fig. 28) than a 'Crocco' or 'Walz' correlation (e.g., eqns. 2.5.22 or 2.5.37 of AGARDograph 253). The procedure was rather complex but may be summarised (E) as follows. Skin friction was measured using the balance at $X = 0.709$ m for series 03, 04 (smooth to rough) and at $X = 1.217$ m for series 03, 04 and also series 01 (smooth). These values were used as input for a curve fit to the Coles (1968) wall and wake law so as to find values for the wake strength assuming that the small difference in X-value between balance centre and profile (12.7 mm) had negligible effect. (The value for 04, $X = 0.709$ may not have been used on grounds of internal inconsistency). The profiles were required to pass through the δ point of the Coles wall and wake law (source, p. 44). Wake strength values for all profiles of series 01 assuming no roughness effects were also found, with wall shear stress found by the fitting procedure. All other values of the wake strength were estimated following the trend of the smooth wall data and taken as input for subsequent curve fitting used to find wall shear and roughness-induced profile shift. A comparison between profile-derived shear stress values and the five measured values gives good agreement for all cases except at $X = 0.709$ m for series 04. The influence of uncertainty in the determination of the zero for Y on a rough wall was found to be small in a numerical experiment. An extended account of the curve-fitting operation is given in the source paper.

The fluctuation data were reduced by modal analysis following Kovaszny (1953), Morkovin (1956) and others. Some data were discarded as a result of serious errors, but that retained, despite a scatter of 10-20% on a "point-to-point basis", after comparison with other data is such that "the consistency of the observed magnitudes lends considerable credit to their validity."

- 10 The Pitot data were corrected for low Reynolds number effects following Ramaswamy (1971).

- 12 The editors present all the numerical data received from the author (D.E. Berg, private
 13 communication), incorporating their assumptions and data reduction procedures. We have replaced
 the author's selected δ value (based on a curve fit) with a value chosen after inspection of the
 P0 profile.

The mean flow profiles consist of five sets:

01: 14 profiles on a smooth surface starting at $X = 0.645$ m and extending to 1.306 m.

02 - 04: 17 profiles on surfaces which change from smooth to rough at $X = 0.645$ m, the profiles being
 measured from $X = 0.620$ to 1.306 m, for roughness heights of 0.32, 0.64 and 1.27 mm respectively.

05: 17 profiles on a surface which changes from rough ($k = 1.27$ mm) to smooth at $X = 0.645$, again
 extending from $X = 0.620$ to 1.306 m.

- 14 The skin friction value given with the profiles is the value deduced by the author from the curve fit
 to the profiles. These and the measured values are given in section D, taken from the author's Table III.
 The fluctuation data are not presented here, see §15 below.

§ DATA: 77030101-0517. Pitot and T0 profiles. $NX = 17$. Some CF from FEB ($NX = 2$). Fluctuation data from
 CC HWP.

- 15 Editors' comments. The interest of this study lies in the response of the boundary layer to the changes
 in roughness in series 02 - 05. The high Mach number and modest heat transfer play no significant part
 in this. Since the data reduction procedure relies critically on the wall-and-wake profile fitting we
 first consider this.

The temperature-velocity correlation between profiles is good, but lies systematically about 5% below the
 modified van Driest value of eqn. 2.5.37 in AG 253. In data reduction the author used a quadratic fit
 to his measured values. The disagreement is not sufficient to affect the transformation at a significant
 level. In Fig. 1 we show three representative profiles from the smooth wall series 01 in wall law
 coordinates. The CF value used is the curve-fit value which has been forced to agree with the balance
 value for 0112. For all three profiles there is an extended log law which agrees well with the
 'standard' value. The wake component is within the normal range for profile 0101, but noticeably large
 for the downstream profiles. In Fig. 2 we show the outer law plots and again agreement is fair for
 0101 and 0106, 0112 showing behaviour uncharacteristic of an equilibrium layer. The initial profile
 of one of the smooth-to-rough cases, 0301, is shown for comparison, measured slightly upstream of the
 change and of 0101. The increasing departure of the wake law from the standard form as we move down-
 stream is attributed to the reflecting expansion-compression referred to in §2 above. Figure 2, right,
 shows the last profiles of series 01 - 04. For 01, 03, 04 the wall shear value is constrained to
 agree with the balance value. The profiles are closely similar, and the author has assumed that
 roughness has no effect on the outer profile in the range of his experiment, so that the profile shape
 is assumed to be a function of position only. Further discussion will be confined to the inner law plots.

In Fig. 1 we show log-law plots for the final profiles of series 01 - 04. The negative shift of
 the log law at constant X is seen to increase monotonically with roughness height. In Fig. 3 we show
 representative profiles from series 04. The shift increases monotonically with X , though the rate of
 increase falls off as we move more downstream. The profiles have probably not quite reached their final
 position by station 15. Figure 4 shows the opposite change, from rough to smooth. The first profile,
 0501, is taken about 0.29 m behind the start of the roughness and so corresponds closely to profile
 0410 of the previous figure. On a wall-law plot the two show only small differences. As the flow
 develops downstream over the smooth surface, the profiles move progressively back towards the 'standard'
 wall law, with, apparently, a slight overshoot which however probably lies within the range of
 experimental uncertainty.

The position at which a change in the inner law profile becomes detectable moves upstream as the roughness
 height increases. For series 02 a change occurs at profile 07, but since it is small for 08 and absent
 for 09, the effect probably begins in earnest with profile 10. For series 03, a significant effect is

seen by profile 04, while for series 04, the effect is again seen at profile 04, though more marked.

The author has supplied us with a very great quantity of turbulence data, in the form of profiles of $(\rho u)^{1/2}$ for nearly every mean flow profile. After much deliberation we chose not to present these either here or in the microfiche and magnetic tape profiles. We reasoned that, in this form, they would not assist in the development of turbulence models. Their principal function therefore must be as a description of the spread or decay of higher turbulence levels introduced by roughness. For this purpose the author's graphical presentation of 29 $(\rho u)^{1/2}$ and $T^{1/2}$ profiles in Figs. 38, 39 of the source paper is adequate, and those wishing to pursue the topic are referred there.

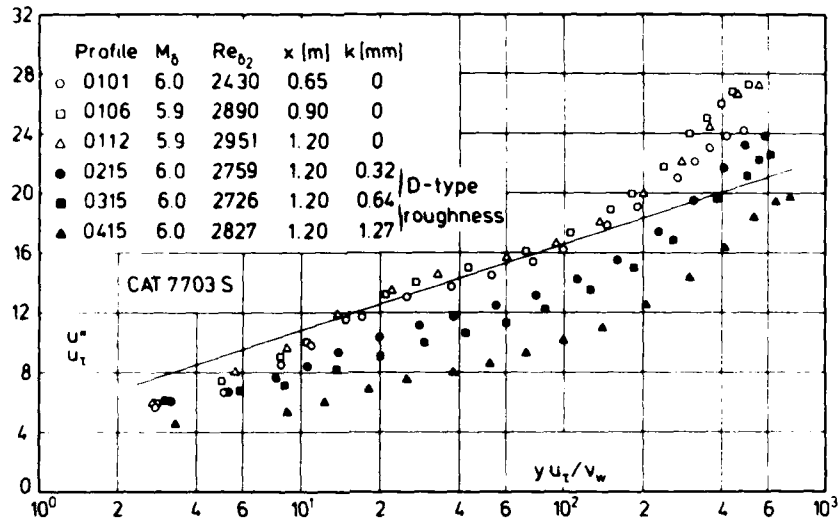


Fig. 1 Law of the wall for a compressible turbulent boundary layer along a smooth/rough wall (isothermal wall $T_w/T_r = 0.90$, origin not defined). Berg (1977).

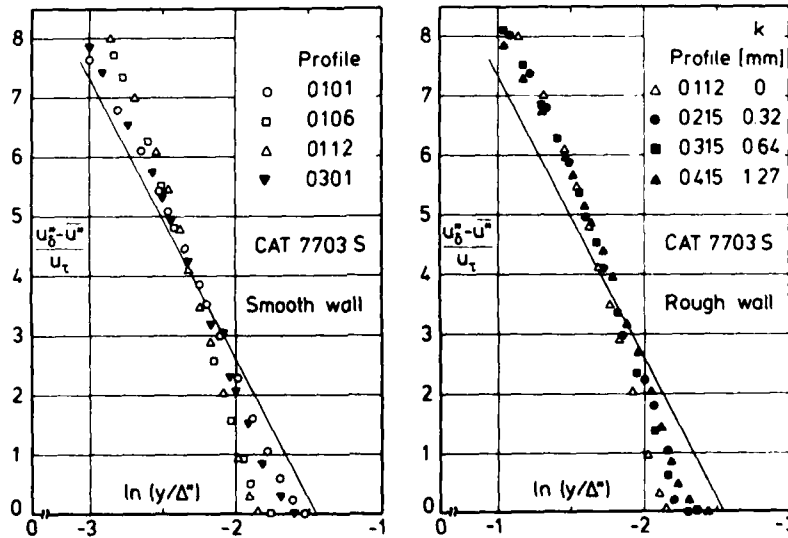


Fig. 2 Outer law for a compressible turbulent boundary layer along a smooth/rough wall (isothermal wall $T_w/T_r = 0.90$, origin not defined). Berg (1977).

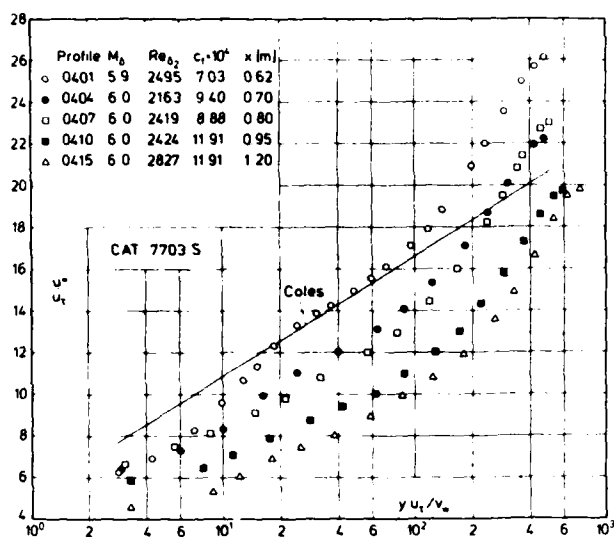


Fig. 3 Law of the wall for a compressible turbulent boundary layer along a rough wall (isothermal wall $T_w/T_\infty = 0.90$, origin not defined, $k = 1.27$ mm, D-type roughness). Berg (1977).

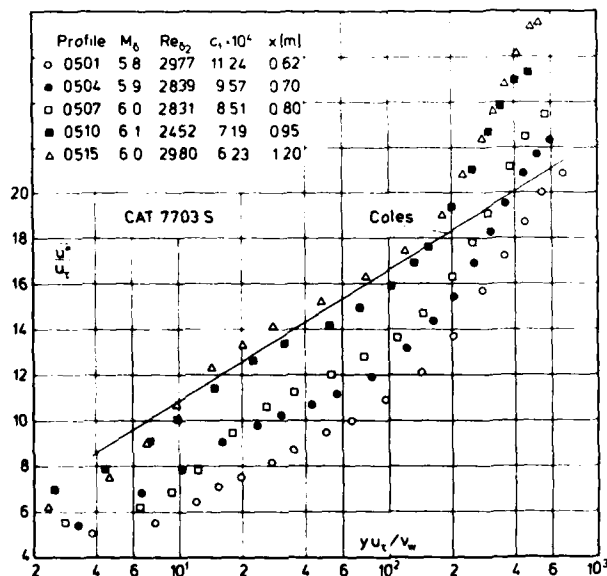


Fig. 4 Law of the wall for a compressible turbulent boundary layer along a rough wall (isothermal wall $T_w/T_\infty = 0.90$, origin not defined, $k = 1.27$ mm, D-type roughness). Berg (1977).

| CAT 7703S | | BERG | | BOUNDARY CONDITIONS AND EVALUATED DATA, SI UNITS | | | | | |
|--------------------------------------|--------------------------------------|---------------------------------|---|--|-----------------------------|---------------------------------|---|---|--|
| RUN X * RZ | MD * POO* TOD* | TW/TR PW/PO TAUW * | REDZW REDZD DZ | CF CQ PIZ* | H12 H32 H42 | H12K H32K D2K | PW TW* UD | PD TD TR | |
| 7703S0101 6.4516*-01 INFINITE | 5.9940 1.5561**+06 4.1985**+02 | 0.8983 1.0000 1.9995**+01 | 2.4304**+03 1.3559**+04 8.5920**+04 | 8.0170**+04 NM 0.0000**+00 | 11.0919 1.8261 0.6636 | 1.3873 1.7713 2.1075**+03 | 9.9168**+02 3.4271**+02 8.6070**+02 | 9.9168**+02 5.1292**+01 3.8153**+02 | |
| 7703S0102 6.9596*-01 INFINITE | 6.0411 1.5561**+06 4.1952**+02 | 0.8992 1.0000 1.9305**+01 | 2.2238**+03 1.2590**+04 8.1257**+04 | 7.9960**+04 NM 0.0000**+00 | 11.4428 1.8245 0.6450 | 1.3871 1.7675 2.0376**+03 | 9.4510**+02 3.4271**+02 8.6117**+02 | 9.4510**+02 5.0551**+01 3.8114**+02 | |
| 7703S0103 7.4676*-01 INFINITE | 6.0050 1.5561**+06 4.2054**+02 | 0.8969 1.0000 1.8616**+01 | 2.3143**+03 1.2932**+04 8.2525**+04 | 7.5209**+04 NM 0.0000**+00 | 11.8579 1.8145 0.5952 | 1.4079 1.7590 2.1451**+03 | 9.8060**+02 3.4271**+02 8.6159**+02 | 9.8060**+02 5.1211**+01 3.8213**+02 | |
| 7703S0104 7.9756*-01 INFINITE | 5.9615 1.5561**+06 4.2185**+02 | 0.8934 1.0000 1.8616**+01 | 2.5423**+03 1.3975**+04 8.7989**+04 | 7.2978**+04 NM 0.0000**+00 | 11.8691 1.8086 0.5786 | 1.4083 1.7549 2.3148**+03 | 1.0254**+03 3.4253**+02 8.6217**+02 | 1.0254**+03 5.2031**+01 3.8339**+02 | |
| 7703S0105 8.4836*-01 INFINITE | 5.8732 1.5561**+06 4.2364**+02 | 0.8884 1.0000 1.8616**+01 | 2.8770**+03 1.5327**+04 9.3589**+04 | 6.8625**+04 NM 0.0000**+00 | 11.5374 1.8061 0.5813 | 1.4150 1.7529 2.4268**+03 | 1.1234**+03 3.4219**+02 8.6238**+02 | 1.1234**+03 5.3632**+01 3.8516**+02 | |
| 7703S0106 8.9916*-01 INFINITE | 5.8996 1.5561**+06 4.2419**+02 | 0.8865 1.0000 1.7237**+01 | 2.8900**+03 1.5486**+04 9.5800**+04 | 6.4721**+04 NM 0.0000**+00 | 11.9493 1.8023 0.5467 | 1.4153 1.7508 2.5476**+03 | 1.0931**+03 3.4184**+02 8.6343**+02 | 1.0931**+03 5.3284**+01 3.8562**+02 | |
| 7703S0107 9.4996*-01 INFINITE | 6.0349 1.5561**+06 4.2309**+02 | 0.8884 1.0000 1.7926**+01 | 2.5069**+03 1.4014**+04 9.1377**+04 | 7.3933**+04 NM 0.0000**+00 | 12.1512 1.8128 0.5663 | 1.3792 1.7651 2.4104**+03 | 9.5109**+02 3.4167**+02 8.6472**+02 | 9.5109**+02 5.1073**+01 3.8440**+02 | |
| 7703S0108 1.0008**+00 INFINITE | 6.0076 1.5561**+06 4.2509**+02 | 0.8864 1.0000 1.7926**+01 | 2.5517**+03 1.4106**+04 9.1587**+04 | 7.2558**+04 NM 0.0000**+00 | 12.0456 1.8138 0.5642 | 1.3733 1.7670 2.3938**+03 | 9.7791**+02 3.4236**+02 8.6628**+02 | 9.7791**+02 5.1724**+01 3.8626**+02 | |
| 7703S0109 1.0516**+00 INFINITE | 6.0509 1.5561**+06 4.2479**+02 | 0.8880 1.0000 1.7237**+01 | 2.4415**+03 1.3689**+04 9.0396**+04 | 7.1878**+04 NM 0.0000**+00 | 12.5358 1.8088 0.5345 | 1.3842 1.7619 2.4417**+03 | 9.3567**+02 3.4271**+02 8.6673**+02 | 9.3567**+02 5.1040**+01 3.6592**+02 | |
| 7703S0110 1.1024**+00 INFINITE | 6.0089 1.5561**+06 4.2253**+02 | 0.8917 1.0000 1.7237**+01 | 2.5423**+03 1.4144**+04 9.1053**+04 | 6.9827**+04 NM 0.0000**+00 | 12.9285 1.8056 0.4781 | 1.3907 1.7591 2.5013**+03 | 9.7667**+02 3.4236**+02 8.6370**+02 | 9.7667**+02 5.1395**+01 3.8394**+02 | |
| 7703S0111 1.1532**+00 INFINITE | 6.0191 1.5561**+06 4.2207**+02 | 0.8927 1.0000 1.7237**+01 | 2.5736**+03 1.4377**+04 9.2795**+04 | 7.0323**+04 NM 0.0000**+00 | 13.3294 1.8019 0.4395 | 1.3888 1.7577 2.6039**+03 | 9.6648**+02 3.4236**+02 8.6340**+02 | 9.6648**+02 5.1184**+01 3.8350**+02 | |
| 7703S0112 1.2040**+00 INFINITE | 5.9037 1.5561**+06 4.2194**+02 | 0.8926 1.0000 1.7237**+01 | 2.9510**+03 1.5936**+04 9.7965**+04 | 6.4911**+04 NM 0.0000**+00 | 13.3414 1.7954 0.3924 | 1.4017 1.7525 2.7628**+03 | 1.0884**+03 3.4236**+02 8.6121**+02 | 1.0884**+03 5.2936**+01 3.8356**+02 | |
| 7703S0113 1.2348**+00 INFINITE | 6.0111 1.5561**+06 4.2606**+02 | 0.8843 1.0000 NM | 2.8935**+03 1.5974**+04 1.0423**+03 | 7.1878**+04 NM 0.0000**+00 | 13.0946 1.8007 0.4686 | 1.4070 1.7527 2.9160**+03 | 9.7447**+02 3.4236**+02 8.6734**+02 | 9.7447**+02 5.1790**+01 3.8714**+02 | |
| 7703S0114 1.3056**+00 INFINITE | 6.0384 1.5561**+06 4.2644**+02 | 0.8836 1.0000 NM | 2.8671**+03 1.5941**+04 1.0534**+03 | 7.1878**+04 NM 0.0000**+00 | 12.9532 1.8058 0.4907 | 1.3947 1.7570 2.9105**+03 | 9.4767**+02 3.4236**+02 8.6820**+02 | 9.4767**+02 5.1426**+01 3.8744**+02 | |
| 7703S0201 6.1976*-01 INFINITE | 5.8921 1.5837**+06 4.2236**+02 | 0.9011 1.0000 2.0684**+01 | 2.5316**+03 1.3718**+04 8.2584**+04 | 7.5917**+04 NM 0.0000**+00 | 11.8011 1.8184 0.5506 | 1.3900 1.7653 2.1088**+03 | 1.1212**+03 3.4601**+02 8.6143**+02 | 1.1212**+03 5.3172**+01 3.8397**+02 | |
| 7703S0202 6.4516*-01 INFINITE | 5.8867 1.5837**+06 4.2096**+02 | 0.9046 1.0000 1.9305**+01 | 2.5297**+03 1.3737**+04 8.2097**+04 | 7.0589**+04 NM 0.0000**+00 | 12.1326 1.8127 0.5209 | 1.4140 1.7571 2.1482**+03 | 1.1274**+03 3.4618**+02 8.5990**+02 | 1.1274**+03 5.3080**+01 3.8270**+02 | |
| 7703S0203 6.7056*-01 INFINITE | 5.9570 1.5837**+06 4.2177**+02 | 0.9036 1.0000 1.7926**+01 | 2.3232**+03 1.2863**+04 7.9405**+04 | 6.8839**+04 NM 0.0000**+00 | 12.5264 1.8118 0.5049 | 1.4042 1.7571 2.1241**+03 | 1.0483**+03 3.4636**+02 8.6200**+02 | 1.0483**+03 5.2088**+01 3.8332**+02 | |
| 7703S0204 6.9596*-01 INFINITE | 6.0006 1.5837**+06 4.2253**+02 | 0.9025 1.0000 1.7237**+01 | 2.2289**+03 1.2482**+04 7.8685**+04 | 6.8220**+04 NM 0.0000**+00 | 12.4556 1.8157 0.5238 | 1.3809 1.7632 2.0949**+03 | 1.0024**+03 3.4653**+02 8.6356**+02 | 1.0024**+03 5.1519**+01 3.8395**+02 | |
| 7703S0205 7.2136*-01 INFINITE | 6.0214 1.5837**+06 4.2275**+02 | 0.9026 1.0000 1.7926**+01 | 2.2046**+03 1.2421**+04 7.9036**+04 | 7.1976**+04 NM 0.0000**+00 | 12.4214 1.8131 0.5421 | 1.3966 1.7578 2.1202**+03 | 9.8131**+02 3.4670**+02 8.6414**+02 | 9.8131**+02 5.1233**+01 3.8411**+02 | |
| 7703S0206 7.4676*-01 INFINITE | 6.0396 1.5837**+06 4.2334**+02 | 0.9019 1.0000 1.7926**+01 | 2.1190**+03 1.1990**+04 7.7040**+04 | 7.2884**+04 NM 0.0000**+00 | 12.8680 1.8105 0.5018 | 1.3939 1.7572 2.1124**+03 | 9.6324**+02 3.4688**+02 8.6506**+02 | 9.6324**+02 5.1033**+01 3.8462**+02 | |
| 7703S0207 7.9756*-01 INFINITE | 6.0024 1.5837**+06 4.2419**+02 | 0.9008 1.0000 1.9995**+01 | 2.3326**+03 1.3038**+04 8.2736**+04 | 7.9233**+04 NM 0.0000**+00 | 13.1574 1.7981 0.4672 | 1.4178 1.7442 2.3546**+03 | 1.0006**+03 3.4722**+02 8.6528**+02 | 1.0006**+03 5.1694**+01 3.8545**+02 | |

TW FOR X > 45(IN) SET TO LAST GIVEN VALUE
 TAUW MEASURED: 0112,0304,0315,0404,0415

| CAT 77035 | | BERG | | BOUNDARY CONDITIONS AND EVALUATED DATA, SI UNITS | | | | | | |
|--------------------------------------|--------------------------------------|---------------------------------|---|--|-----------------------------|--------------------------------|---|---|--|--|
| RUN X * RZ | MM * POD* T00* | TW/TR PW/PO TAUW * | RED2W RED2D DZ | CF CQ PI7* | H12 H32 H42 | H12M H32M D2M | PW TW* LD | PD TD TR | | |
| 770350208 8.4836*-01 INFINITE | 6.0013 1.5837**+06 4.2394**+02 | 0.9014 1.0000 1.8616**+01 | 2.4088**+03 1.3468**+04 8.5348**+04 | 7.3714*-04 NM 0.0000**+00 | 12.9535 1.8030 0.4810 | 1.4015 1.7510 2.3823*-03 | 1.0017**+03 3.4722**+02 8.6500**+02 | 1.0017**+03 5.1679**+01 3.8522**+02 | | |
| 770350209 8.9915*-01 INFINITE | 5.9778 1.5837**+06 4.2360**+02 | 0.9011 1.0000 1.7926**+01 | 2.4584**+03 1.3651**+04 8.5559**+04 | 6.9837*-04 NM 0.0000**+00 | 13.4285 1.7999 0.4219 | 1.4048 1.7496 2.4371*-03 | 1.0262**+03 3.4688**+02 8.6424**+02 | 1.0262**+03 5.1996**+01 3.8495**+02 | | |
| 770350210 9.4996*-01 INFINITE | 6.0174 1.5837**+06 4.2355**+02 | 0.9004 1.0000 1.9305**+01 | 2.3658**+03 1.3282**+04 8.4621**+04 | 7.7296*-04 NM 0.0000**+00 | 13.6181 1.6015 0.4159 | 1.3965 1.7524 2.4236*-03 | 9.8539**+02 3.4653**+02 8.6489**+02 | 9.8539**+02 5.1391**+01 3.8485**+02 | | |
| 770350211 1.0008**+00 INFINITE | 5.9732 1.5837**+06 4.2394**+02 | 0.9008 1.0000 2.0684**+01 | 2.4771**+03 1.3730**+04 8.5992**+04 | 8.0324*-04 NM 0.0000**+00 | 13.7135 1.7972 0.3912 | 1.4095 1.7470 2.4641*-03 | 1.0311**+03 3.4705**+02 8.6450**+02 | 1.0311**+03 5.2108**+01 3.8527**+02 | | |
| 770350212 1.0516**+00 INFINITE | 6.0367 1.5837**+06 4.2428**+02 | 0.9003 1.0000 1.9305**+01 | 2.3227**+03 1.3107**+04 8.4394**+04 | 7.8331*-04 NM 0.0000**+00 | 14.2522 1.7928 0.3687 | 1.4208 1.7422 2.5195*-03 | 9.6615**+02 3.4705**+02 8.6597**+02 | 9.6615**+02 5.1190**+01 3.8546**+02 | | |
| 770350213 1.1024**+00 INFINITE | 6.0400 1.5837**+06 4.2415**+02 | 0.9002 1.0000 2.0684**+01 | 2.3509**+03 1.3278**+04 8.5574**+04 | 8.4118*-04 NM 0.0000**+00 | 14.1986 1.7938 0.3714 | 1.4079 1.7455 2.5479*-03 | 9.6290**+02 3.4688**+02 8.6589**+02 | 9.6290**+02 5.1125**+01 3.8536**+02 | | |
| 770350214 1.1532**+00 INFINITE | 6.0212 1.5837**+06 4.2423**+02 | 0.8990 1.0000 2.0684**+01 | 2.4451**+03 1.3721**+04 8.7768**+04 | 8.3036*-04 NM 0.0000**+00 | 14.3521 1.7871 0.3558 | 1.4250 1.7379 2.6666*-03 | 9.8155**+02 3.4653**+02 8.6565**+02 | 9.8155**+02 5.1416**+01 3.8546**+02 | | |
| 770350215 1.2040**+00 INFINITE | 5.9754 1.5837**+06 4.2389**+02 | 0.8995 1.0000 2.1374**+01 | 2.7594**+03 1.5289**+04 9.5832**+04 | 8.3128*-04 NM 0.0000**+00 | 14.4383 1.7820 0.3325 | 1.4415 1.7324 2.9386*-03 | 1.0287**+03 3.4653**+02 8.6450**+02 | 1.0287**+03 5.2069**+01 3.8523**+02 | | |
| 770350216 1.2548**+00 INFINITE | 6.1482 1.5837**+06 4.2589**+02 | 0.8959 1.0000 NM | 2.5590**+03 1.4844**+04 1.0065**+03 | NM NM 0.0000**+00 | 14.7327 1.7888 0.3763 | 1.4294 1.7371 3.1193*-03 | 8.6300**+02 3.4653**+02 8.6950**+02 | 8.6300**+02 4.9753**+01 3.8677**+02 | | |
| 770350217 1.3056**+00 INFINITE | 6.1301 1.5837**+06 4.2581**+02 | 0.8961 1.0000 NM | 2.6317**+03 1.5189**+04 1.0219**+03 | NM NM 0.0000**+00 | 14.5789 1.7938 0.3779 | 1.4180 1.7423 3.1100*-03 | 8.7887**+02 3.4653**+02 8.6911**+02 | 8.7887**+02 5.0003**+01 3.8672**+02 | | |
| 770350301 6.1976*-01 INFINITE | 5.9406 1.5865**+06 4.2190**+02 | 0.9050 1.0000 1.9995**+01 | 2.1784**+03 1.2016**+04 7.3577**+04 | 7.5778*-04 NM 0.0000**+00 | 12.0962 1.8174 0.5453 | 1.4132 1.8174 1.9070*-03 | 1.0661**+03 3.4705**+02 8.6164**+02 | 1.0661**+03 5.2357**+01 3.8347**+02 | | |
| 770350302 6.4516*-01 INFINITE | 5.8942 1.5865**+06 4.2156**+02 | 0.9060 1.0000 1.9305**+01 | 2.3193**+03 1.2633**+04 7.5765**+04 | 7.0835*-04 NM 0.0000**+00 | 12.1299 1.8097 0.5333 | 1.4400 1.7504 1.9964*-03 | 1.1207**+03 3.4722**+02 8.6065**+02 | 1.1207**+03 5.1203**+01 3.8323**+02 | | |
| 770350303 6.7056*-01 INFINITE | 5.9118 1.5865**+06 4.2300**+02 | 0.9035 1.0000 1.9995**+01 | 2.3232**+03 1.2682**+04 7.7023**+04 | 7.4274*-04 NM 0.0000**+00 | 12.3480 1.8042 0.5192 | 1.4380 1.7451 2.0911*-03 | 1.1004**+03 3.4739**+02 8.6244**+02 | 1.1004**+03 5.2942**+01 3.8452**+02 | | |
| 770350304 6.9596*-01 INFINITE | 5.9955 1.5865**+06 4.2194**+02 | 0.9065 1.0000 1.9305**+01 | 2.0880**+03 1.1719**+04 7.3433**+04 | 7.6007*-04 NM 0.0000**+00 | 12.7033 1.8051 0.5135 | 1.4292 1.7455 2.0197*-03 | 1.0094**+03 3.4757**+02 8.6286**+02 | 1.0094**+03 5.1523**+01 3.8342**+02 | | |
| 770350305 7.2136*-01 INFINITE | 5.9403 1.5865**+06 4.2058**+02 | 0.9097 1.0000 2.0684**+01 | 2.1579**+03 1.1958**+04 7.2867**+04 | 7.8377*-04 NM 0.0000**+00 | 12.7827 1.7981 0.4878 | 1.4388 1.7388 2.0374*-03 | 1.0684**+03 3.4774**+02 8.6049**+02 | 1.0684**+03 5.2197**+01 3.8227**+02 | | |
| 770350306 7.4676*-01 INFINITE | 6.0131 1.5865**+06 4.2347**+02 | 0.9042 1.0000 2.1374**+01 | 2.1012**+03 1.1820**+04 7.5017**+04 | 8.5178*-04 NM 0.0000**+00 | 12.9562 1.7960 0.5042 | 1.4494 1.7353 2.1317*-03 | 9.9142**+02 3.4792**+02 8.6473**+02 | 9.9142**+02 5.1445**+01 3.8478**+02 | | |
| 770350307 7.9756*-01 INFINITE | 5.9527 1.5865**+06 4.2355**+02 | 0.9047 1.0000 2.2753**+01 | 2.3146**+03 1.2796**+04 7.9218**+04 | 8.5958*-04 NM 0.0000**+00 | 13.1651 1.7863 0.4666 | 1.4720 1.7255 2.3029*-03 | 1.0549**+03 3.4827**+02 8.6375**+02 | 1.0549**+03 5.2375**+01 3.8495**+02 | | |
| 770350308 8.4836*-01 INFINITE | 5.9465 1.5865**+06 4.2258**+02 | 0.9050 1.0000 2.3442**+01 | 2.3976**+03 1.3242**+04 8.1483**+04 | 8.9210*-04 NM 0.0000**+00 | 13.4675 1.7816 0.4356 | 1.4811 1.7211 2.4119*-03 | 1.0616**+03 3.4757**+02 8.6264**+02 | 1.0616**+03 5.2350**+01 3.8407**+02 | | |
| 770350309 8.9916*-01 INFINITE | 5.9469 1.5865**+06 4.2292**+02 | 0.9042 1.0000 2.2063**+01 | 2.4437**+03 1.3487**+04 8.3104**+04 | 8.3983*-04 NM 0.0000**+00 | 13.5578 1.7828 0.4212 | 1.4712 1.7242 2.4564*-03 | 1.0612**+03 3.4757**+02 8.6299**+02 | 1.0612**+03 5.2386**+01 3.8438**+02 | | |
| 770350310 9.4996*-01 INFINITE | 6.0276 1.5865**+06 4.2381**+02 | 0.9013 1.0000 2.4132**+01 | 2.2466**+03 1.2658**+04 8.0919**+04 | 9.7133*-04 NM 0.0000**+00 | 13.9405 1.7856 0.4104 | 1.4538 1.7295 2.4260*-03 | 9.7686**+02 3.4705**+02 8.6533**+02 | 9.7686**+02 5.1269**+01 3.8507**+02 | | |
| 770350311 1.0008**+00 INFINITE | 6.0164 1.5865**+06 4.2377**+02 | 0.9022 1.0000 2.4132**+01 | 2.2947**+03 1.2897**+04 8.2053**+04 | 9.6386*-04 NM 0.0000**+00 | 13.8018 1.7859 0.4210 | 1.4574 1.7290 2.4444*-03 | 9.8811**+02 3.4739**+02 8.6509**+02 | 9.8811**+02 5.1432**+01 3.8504**+02 | | |

TW FOR X > 45(IN) SET TO LAST GIVEN VALUE
TAUW MEASURED: 0112,0304,0315,0404,0415

CAT 77035

BERG

BOUNDARY CONDITIONS AND EVALUATED DATA. SI UNITS

| RUN X * RZ | MD * POD* TOD* | TW/TR PW/PO TAUW * | RE02W RE02D DZ | CF CQ PI2* | H12 H32 H42 | H12K H32K D2K | PW TW* UD | PD TD TR |
|--------------------------------------|------------------------------------|--------------------------------|---|---------------------------------|-----------------------------|---------------------------------|--|--|
| 7703S0312 1.0516**00 INFINITE | 6.0000 1.5865**06 4.2368**02 | 0.9023 1.0000 2.4132**01 | 2.3258**03 1.3011**04 8.2192**04 | 9.5301**-04 NM 0.0000**00 | 13.8389 1.7849 0.4062 | 1.4444 1.7313 2.4573**-03 | 1.0048**03 3.4739**02 8.6472**02 | 1.0048**03 5.1669**01 3.8499**02 |
| 7703S0313 1.1024**00 INFINITE | 6.0028 1.5865**06 4.2355**02 | 0.9022 1.0000 2.4132**01 | 2.4288**03 1.3598**04 8.5957**-04 | 9.5485**-04 NM 0.0000**00 | 14.1037 1.7831 0.3762 | 1.4299 1.7335 2.6095**-03 | 1.0020**03 3.4722**02 8.6464**02 | 1.0020**03 5.1611**01 3.8487**02 |
| 7703S0314 1.2040**00 INFINITE | 5.9836 1.5865**06 4.2389**02 | 0.9014 1.0000 2.4132**01 | 2.5753**03 1.4325**04 8.9944**-04 | 9.4226**-04 NM 0.0000**00 | 14.1732 1.7789 0.3698 | 1.4550 1.7263 2.7527**-03 | 1.0219**03 3.4705**02 8.6465**02 | 1.0219**03 5.1944**01 3.8521**02 |
| 7703S0315 1.2040**00 INFINITE | 5.9997 1.5865**06 4.2440**02 | 0.8999 1.0000 2.3442**01 | 2.7264**03 1.9214**04 9.6342**-04 | 9.2562**-04 NM 0.0000**00 | 14.3345 1.7783 0.3632 | 1.4632 1.7242 2.9699**-03 | 1.0051**03 3.4705**02 8.6545**02 | 1.0051**03 5.1761**01 3.8565**02 |
| 7703S0316 1.2548**00 INFINITE | 6.0589 1.5865**06 4.2470**02 | 0.8995 1.0000 NM | 2.7256**03 1.5466**04 1.0048**-03 | NM NM 0.0000**00 | 14.4844 1.7830 0.3683 | 1.4487 1.7295 3.0972**-03 | 9.4616**02 3.4705**02 8.6678**02 | 9.4616**02 5.0910**01 3.8583**02 |
| 7703S0317 1.3056**00 INFINITE | 6.1157 1.5865**06 4.2559**02 | 0.8978 1.0000 NM | 2.6520**03 1.5267**04 1.0186**-03 | NM NM 0.0000**00 | 14.3116 1.7927 0.4003 | 1.4262 1.7396 3.0683**-03 | 8.9326**02 3.4705**02 8.6866**02 | 8.9326**02 5.0186**01 3.8655**02 |
| 7703S0401 6.1970**-01 INFINITE | 5.8830 1.5851**06 4.2066**02 | 0.9075 1.0000 1.9305**01 | 2.4954**03 1.3570**04 8.0818**-04 | 7.0345**-04 NM 0.0000**00 | 11.9156 1.8163 0.5395 | 1.4042 1.7600 2.0817**-03 | 1.1328**03 3.4705**02 8.5953**02 | 1.1328**03 5.3101**01 3.8244**02 |
| 7703S0402 6.4516**-01 INFINITE | 5.8812 1.5851**06 4.2117**02 | 0.9068 1.0000 1.8616**01 | 2.5828**03 1.4026**04 8.3622**-04 | 6.7747**-04 NM 0.0000**00 | 12.1118 1.8115 0.5231 | 1.4207 1.7548 2.1906**-03 | 1.1349**03 3.4722**02 8.6002**02 | 1.1349**03 5.3194**01 3.8290**02 |
| 7703S0403 6.7056**-01 INFINITE | 6.0356 1.5851**06 4.2275**02 | 0.9045 1.0000 1.6547**01 | 2.1657**03 1.2271**04 7.8475**-04 | 6.7033**-04 NM 0.0000**00 | 12.7448 1.8126 0.5181 | 1.4162 1.7552 2.1230**-03 | 9.6805**02 3.4739**02 8.6438**02 | 9.6805**02 5.1021**01 3.8409**02 |
| 7703S0404 6.9596**-01 INFINITE | 6.0212 1.5851**06 4.2202**02 | 0.9064 1.0000 2.3442**01 | 2.1627**03 1.2228**04 7.7533**-04 | 9.4024**-04 NM 0.0000**00 | 12.6082 1.8134 0.5221 | 1.4018 1.7571 2.0837**-03 | 9.8242**02 3.4757**02 8.6339**02 | 9.8242**02 5.1149**01 3.8345**02 |
| 7703S0405 7.2136**-01 INFINITE | 5.9627 1.5851**06 4.2198**02 | 0.9067 1.0000 1.7926**01 | 2.2096**03 1.2285**04 7.6011**-04 | 6.9053**-04 NM 0.0000**00 | 12.5700 1.8050 0.5160 | 1.4357 1.7447 2.0753**-03 | 1.0431**03 3.4774**02 8.6232**02 | 1.0431**03 5.2027**01 3.8351**02 |
| 7703S0406 7.4676**-01 INFINITE | 6.0478 1.5851**06 4.2168**02 | 0.9082 1.0000 1.9995**01 | 2.1113**03 1.2049**04 7.7155**-04 | 8.1679**-04 NM 0.0000**00 | 13.1950 1.7991 0.4890 | 1.4405 1.7385 2.1963**-03 | 9.5613**02 3.4792**02 8.6351**02 | 9.5613**02 5.0713**01 3.8310**02 |
| 7703S0407 7.9756**-01 INFINITE | 5.9814 1.5851**06 4.2372**02 | 0.9044 1.0000 2.2753**01 | 2.4185**03 1.3479**04 8.4578**-04 | 8.8784**-04 NM 0.0000**00 | 13.1897 1.7892 0.4695 | 1.4551 1.7298 2.4506**-03 | 1.0233**03 3.4827**02 8.6443**02 | 1.0233**03 5.1956**01 3.8508**02 |
| 7703S0408 8.4836**-01 INFINITE | 5.9335 1.5851**06 4.2283**02 | 0.9044 1.0000 2.6200**01 | 2.5192**03 1.3852**04 8.4922**-04 | 9.8894**-04 NM 0.0000**00 | 13.2547 1.7874 0.4415 | 1.4515 1.7301 2.4685**-03 | 1.0750**03 3.4757**02 8.6267**02 | 1.0750**03 5.2582**01 3.8433**02 |
| 7703S0409 8.9916**-01 INFINITE | 6.0001 1.5851**06 4.2394**02 | 0.9023 1.0000 2.7579**01 | 2.5032**03 1.4001**04 8.8608**-04 | 1.0902**-03 NM 0.0000**00 | 13.5297 1.7837 0.4482 | 1.4701 1.7242 2.6292**-03 | 1.0038**03 3.4757**02 8.6498**02 | 1.0038**03 5.1698**01 3.8522**02 |
| 7703S0410 9.4996**-01 INFINITE | 6.0246 1.5851**06 4.2406**02 | 0.9007 1.0000 2.9647**01 | 2.4240**03 1.3637**04 8.7223**-04 | 1.1919**-03 NM 0.0000**00 | 13.6506 1.7856 0.4404 | 1.4555 1.7284 2.5923**-03 | 9.7901**02 3.4705**02 8.6554**02 | 9.7901**02 5.1345**01 3.8530**02 |
| 7703S0411 1.1024**00 INFINITE | 6.0098 1.5851**06 4.2398**02 | 0.9017 1.0000 3.1026**01 | 2.4326**03 1.3639**04 8.6675**-04 | 1.2347**-03 NM 0.0000**00 | 13.9978 1.7777 0.4092 | 1.4847 1.7177 2.6399**-03 | 9.9392**02 3.4739**02 8.6519**02 | 9.9392**02 5.1557**01 3.8525**02 |
| 7703S0412 1.0516**00 INFINITE | 6.0372 1.5851**06 4.2411**02 | 0.9016 1.0000 3.2405**01 | 2.4132**03 1.3636**04 8.7687**-04 | 1.3142**-03 NM 0.0000**00 | 14.5531 1.7701 0.3756 | 1.5097 1.7091 2.7665**-03 | 9.6646**02 3.4739**02 8.6580**02 | 9.6646**02 5.1161**01 3.8532**02 |
| 7703S0413 1.1024**00 INFINITE | 6.0300 1.5851**06 4.2377**02 | 0.9018 1.0000 2.9647**01 | 2.5240**03 1.4237**04 9.1171**-04 | 1.1964**-03 NM 0.0000**00 | 14.6145 1.7642 0.3617 | 1.4960 1.7112 2.8893**-03 | 9.7362**02 3.4722**02 8.6533**02 | 9.7362**02 5.1228**01 3.8502**02 |
| 7703S0414 1.1532**00 INFINITE | 6.0279 1.5851**06 4.2385**02 | 0.9016 1.0000 2.8958**01 | 2.6473**03 1.4921**04 9.5495**-04 | 1.1669**-03 NM 0.0000**00 | 14.6347 1.7696 0.3544 | 1.4825 1.7145 3.0303**-03 | 9.7568**02 3.4722**02 8.6538**02 | 9.7568**02 5.1269**01 3.8510**02 |

TW FOR X > 45(IN) SET TO LAST GIVEN VALUE
 TAUW MEASURED: 0112,0304,0315,0404,0415

| CAT 7703S | | BERG | | BOUNDARY CONDITIONS AND EVALUATED DATA. SI UNITS | | | | | | | |
|------------------|----------------------|--------------------------|----------------------|--|-------------------|---------------------|-----------------|----------------|--|--|--|
| RUN X * RZ | MD * POD* TOD* | TW/TR PW/PO TAUM * | RED2W RED2D D2 | CF CQ PIZ* | H12 H32 H42 | H12K H32K D2K | PW TW* LD | PD TD TR | | | |
| 7703S0415 | 6.0240 | 0.9010 | 2.8270**+03 | 1.1914**-03 | 14.9504 | 1.5195 | 9.7960**+02 | 9.7960**+02 | | | |
| 1.2040**+00 | 1.5851**+06 | 1.0000 | 1.5906**+04 | NM | 1.7633 | 1.7053 | 3.4705**+02 | 5.1338**+01 | | | |
| INFINITE | 4.2394**+02 | 2.9647**+01 | 1.0167**-03 | 0.0000**+00 | 0.3342 | 3.2869**-03 | 8.6540**+02 | 3.8519**+02 | | | |
| 7703S0416 | 6.0505 | 0.9011 | 2.8463**+03 | NM | 15.1342 | 1.5215 | 9.5349**+02 | 9.5349**+02 | | | |
| 1.2548**+00 | 1.5851**+06 | 1.0000 | 1.6140**+04 | NM | 1.7622 | 1.7036 | 3.4705**+02 | 5.0944**+01 | | | |
| INFINITE | 4.2394**+02 | NM | 1.0430**-03 | 0.0000**+00 | 0.3290 | 3.4071**-03 | 6.6586**+02 | 3.8515**+02 | | | |
| 7703S0417 | 6.1258 | 0.9014 | 2.6774**+03 | NM | 15.3713 | 1.5032 | 8.8348**+02 | 8.8348**+02 | | | |
| 1.3056**+00 | 1.5851**+06 | 1.0000 | 1.5521**+04 | NM | 1.7666 | 1.7081 | 3.4705**+02 | 4.9841**+01 | | | |
| INFINITE | 4.2389**+02 | NM | 1.0345**-03 | 0.0000**+00 | 0.3314 | 3.3939**-03 | 8.6709**+02 | 3.8499**+02 | | | |
| 7703S0501 | 5.8426 | 0.8977 | 2.9772**+03 | 1.1239**-03 | 12.2700 | 1.5105 | 1.1810**+03 | 1.1810**+03 | | | |
| 6.1976**-01 | 1.5844**+06 | 1.0000 | 1.5839**+04 | NM | 1.7791 | 1.7120 | 3.4583**+02 | 5.4130**+01 | | | |
| INFINITE | 4.2368**+02 | 3.1716**+01 | 9.3778**-04 | 0.0000**+00 | 0.5274 | 2.6398**-03 | 8.6185**+02 | 1.8525**+02 | | | |
| 7703S0502 | 5.9580 | 0.8969 | 2.7725**+03 | 1.1123**-03 | 12.2833 | 1.4942 | 1.0477**+03 | 1.0477**+03 | | | |
| 6.4516**-01 | 1.5844**+06 | 1.0000 | 1.5250**+04 | NM | 1.7826 | 1.7158 | 3.4549**+02 | 5.2330**+01 | | | |
| INFINITE | 4.2385**+02 | 2.8958**+01 | 9.4841**-04 | 0.0000**+00 | 0.5667 | 2.6874**-03 | 8.6415**+02 | 3.8521**+02 | | | |
| 7703S0503 | 5.8872 | 0.9033 | 2.8875**+03 | 1.0083**-03 | 12.5799 | 1.5159 | 1.1274**+03 | 1.1274**+03 | | | |
| 6.7056**-01 | 1.5844**+06 | 1.0000 | 1.5670**+04 | NM | 1.7757 | 1.7111 | 3.4531**+02 | 5.3014**+01 | | | |
| INFINITE | 4.2050**+02 | 2.7579**+01 | 9.3472**-04 | 0.0000**+00 | 0.5165 | 2.6935**-03 | 8.5943**+02 | 3.8228**+02 | | | |
| 7703S0504 | 5.9234 | 0.8995 | 2.8393**+03 | 9.5659**-04 | 12.2142 | 1.4700 | 1.0858**+03 | 1.0858**+03 | | | |
| 6.9596**-01 | 1.5844**+06 | 1.0000 | 1.5510**+04 | NM | 1.7838 | 1.7227 | 3.4514**+02 | 5.2649**+01 | | | |
| INFINITE | 4.2211**+02 | 2.5511**+01 | 9.4483**-04 | 0.0000**+00 | 0.5552 | 2.6659**-03 | 8.6175**+02 | 3.8369**+02 | | | |
| 7703S0505 | 5.9847 | 0.9018 | 2.7368**+03 | 9.1721**-04 | 12.6035 | 1.4768 | 1.0194**+03 | 1.0194**+03 | | | |
| 7.2136**-01 | 1.5844**+06 | 1.0000 | 1.5261**+04 | NM | 1.7843 | 1.7227 | 3.4449**+02 | 5.1568**+01 | | | |
| INFINITE | 4.2096**+02 | 2.3442**+01 | 9.4986**-04 | 0.0000**+00 | 0.5394 | 2.7178**-03 | 8.6167**+02 | 3.8255**+02 | | | |
| 7703S0506 | 5.8933 | 0.8983 | 3.0034**+03 | 8.3543**-04 | 12.1061 | 1.4806 | 1.1202**+03 | 1.1202**+03 | | | |
| 7.4676**-01 | 1.5844**+06 | 1.0000 | 1.6244**+04 | NM | 1.7817 | 1.7204 | 3.4479**+02 | 5.3132**+01 | | | |
| INFINITE | 4.2219**+02 | 2.2753**+01 | 9.7740**-04 | 0.0000**+00 | 0.5582 | 2.7496**-03 | 8.6128**+02 | 3.8381**+02 | | | |
| 7703S0507 | 6.0098 | 0.8927 | 2.8309**+03 | 8.5092**-04 | 12.8713 | 1.4715 | 9.9352**+02 | 9.9352**+02 | | | |
| 7.9756**-01 | 1.5844**+06 | 1.0000 | 1.5745**+04 | NM | 1.7814 | 1.7234 | 3.4444**+02 | 5.1640**+01 | | | |
| INFINITE | 4.2466**+02 | 2.1374**+01 | 1.0035**-03 | 0.0000**+00 | 0.5211 | 2.9243**-03 | 8.6589**+02 | 3.8587**+02 | | | |
| 7703S0508 | 5.9487 | 0.8924 | 2.9835**+03 | 7.3673**-04 | 12.8668 | 1.4676 | 1.0579**+03 | 1.0579**+03 | | | |
| 8.4836**-01 | 1.5844**+06 | 1.0000 | 1.6297**+04 | NM | 1.7789 | 1.7237 | 3.4444**+02 | 5.2574**+01 | | | |
| INFINITE | 4.2466**+02 | 1.9305**+01 | 1.0125**-03 | 0.0000**+00 | 0.4959 | 2.9547**-03 | 8.6480**+02 | 3.8596**+02 | | | |
| 7703S0509 | 6.0615 | 0.8925 | 2.5696**+03 | 7.1111**-04 | 13.1376 | 1.4329 | 9.4246**+02 | 9.4246**+02 | | | |
| 8.9916**-01 | 1.5844**+06 | 1.0000 | 1.4505**+04 | NM | 1.7698 | 1.7373 | 3.4444**+02 | 5.0888**+01 | | | |
| INFINITE | 4.2483**+02 | 1.7237**+01 | 9.4504**-04 | 0.0000**+00 | 0.4995 | 2.7408**-03 | 8.6696**+02 | 3.8594**+02 | | | |
| 7703S0510 | 6.0776 | 0.8930 | 2.4519**+03 | 7.1899**-04 | 13.1104 | 1.4116 | 9.2721**+02 | 9.2721**+02 | | | |
| 9.4996**-01 | 1.5844**+06 | 1.0000 | 1.3913**+04 | NM | 1.7936 | 1.7445 | 3.4444**+02 | 5.0626**+01 | | | |
| INFINITE | 4.2462**+02 | 1.7237**+01 | 9.1182**-04 | 0.0000**+00 | 0.5015 | 2.6270**-03 | 8.6701**+02 | 3.8572**+02 | | | |
| 7703S0511 | 6.0282 | 0.8936 | 2.5503**+03 | 7.5060**-04 | 13.3313 | 1.4239 | 9.7499**+02 | 9.7499**+02 | | | |
| 1.0008**+00 | 1.5844**+06 | 1.0000 | 1.4273**+04 | NM | 1.7900 | 1.7410 | 3.4479**+02 | 5.1363**+01 | | | |
| INFINITE | 4.2466**+02 | 1.8616**+01 | 9.1660**-04 | 0.0000**+00 | 0.4619 | 2.6658**-03 | 8.6621**+02 | 3.8584**+02 | | | |
| 7703S0512 | 6.0012 | 0.8933 | 2.6720**+03 | 7.3675**-04 | 13.4512 | 1.4331 | 1.0023**+03 | 1.0023**+03 | | | |
| 1.0516**+00 | 1.5844**+06 | 1.0000 | 1.4931**+04 | NM | 1.7872 | 1.7386 | 3.4479**+02 | 5.1785**+01 | | | |
| INFINITE | 4.2479**+02 | 1.8616**+01 | 9.4227**-04 | 0.0000**+00 | 0.4409 | 2.7582**-03 | 8.6587**+02 | 3.8600**+02 | | | |
| 7703S0513 | 5.9878 | 0.8928 | 2.7925**+03 | 7.0290**-04 | 13.3946 | 1.4319 | 1.0162**+03 | 1.0162**+03 | | | |
| 1.1024**+00 | 1.5844**+06 | 1.0000 | 1.5434**+04 | NM | 1.7884 | 1.7402 | 3.4462**+02 | 5.1984**+01 | | | |
| INFINITE | 4.2475**+02 | 1.7926**+01 | 9.7496**-04 | 0.0000**+00 | 0.4402 | 2.8377**-03 | 8.6559**+02 | 3.8598**+02 | | | |
| 7703S0514 | 5.9995 | 0.8918 | 2.8268**+03 | 6.5414**-04 | 13.4103 | 1.3967 | 1.0040**+03 | 1.0040**+03 | | | |
| 1.1532**+00 | 1.5844**+06 | 1.0000 | 1.5661**+04 | NM | 1.7950 | 1.7513 | 3.4444**+02 | 5.1842**+01 | | | |
| INFINITE | 4.2504**+02 | 1.6547**+01 | 9.9519**-04 | 0.0000**+00 | 0.4304 | 2.8619**-03 | 8.6610**+02 | 3.8623**+02 | | | |
| 7703S0515 | 5.9914 | 0.8917 | 2.9801**+03 | 6.2335**-04 | 13.5043 | 1.4022 | 1.0124**+03 | 1.0124**+03 | | | |
| 1.2040**+00 | 1.5844**+06 | 1.0000 | 1.6469**+04 | NM | 1.7942 | 1.7500 | 3.4444**+02 | 5.1971**+01 | | | |
| INFINITE | 4.2509**+02 | 1.5858**+01 | 1.0431**-03 | 0.0000**+00 | 0.4186 | 3.0108**-03 | 8.6600**+02 | 3.8628**+02 | | | |
| 7703S0516 | 6.0463 | 0.8904 | 2.8531**+03 | NM | 14.4014 | 1.4124 | 9.5717**+02 | 9.5717**+02 | | | |
| 1.2548**+00 | 1.5844**+06 | 1.0000 | 1.5997**+04 | NM | 1.7971 | 1.7497 | 3.4444**+02 | 5.1231**+01 | | | |
| INFINITE | 4.2581**+02 | NM | 1.0393**-03 | 0.0000**+00 | 0.3532 | 3.0888**-03 | 8.6769**+02 | 3.8685**+02 | | | |
| 7703S0517 | 6.1466 | 0.8914 | 2.7220**+03 | NM | 14.0951 | 1.3730 | 8.6473**+02 | 8.6473**+02 | | | |
| 1.3056**+00 | 1.5844**+06 | 1.0000 | 1.5728**+04 | NM | 1.8052 | 1.7616 | 3.4444**+02 | 4.9726**+01 | | | |
| INFINITE | 4.2547**+02 | NM | 1.0636**-03 | 0.0000**+00 | 0.4121 | 3.0839**-03 | 8.6904**+02 | 3.8639**+02 | | | |

TW FOR X > 45[IN] SET TO LAST GIVEN VALUE
 TAUM MEASURED: 0112,0304,0315,0404,0415

| 7703S0401 | | BERG | | PROFILE TABULATION | | 65 POINTS, DELTA AT POINT 50 | | |
|-----------|-----------|-----------|---------|--------------------|---------|------------------------------|---------|-----------|
| I | Y | PT2/P | P/PD | TO/TOD | M/MD | U/UD | T/TD | R/RD*U/UD |
| 1 | 0.0000+00 | 1.0000+00 | 1.00000 | 0.82500 | 0.00000 | 0.00000 | 6.53562 | 0.00000 |
| 2 | 1.2700-04 | 1.4093+00 | 1.00000 | 0.82896 | 0.12198 | 0.29763 | 5.95376 | 0.04999 |
| 3 | 1.8796-04 | 1.5159+00 | 1.00000 | 0.83199 | 0.13503 | 0.32667 | 5.85230 | 0.05582 |
| 4 | 3.1242-04 | 1.8164+00 | 1.00000 | 0.84734 | 0.16390 | 0.38993 | 5.66017 | 0.06889 |
| 5 | 4.3688-04 | 2.2290+00 | 1.00000 | 0.85856 | 0.19317 | 0.44910 | 5.40534 | 0.08308 |
| 6 | 5.6388-04 | 2.6645+00 | 1.00000 | 0.86906 | 0.21836 | 0.49680 | 5.17629 | 0.09598 |
| 7 | 6.7310-04 | 2.9860+00 | 1.00000 | 0.87715 | 0.23488 | 0.52670 | 5.02846 | 0.10474 |
| 8 | 8.2042-04 | 3.5002+00 | 1.00000 | 0.88563 | 0.25885 | 0.56669 | 4.79301 | 0.11823 |
| 9 | 9.7790-04 | 3.8473+00 | 1.00000 | 0.88806 | 0.27374 | 0.58917 | 4.63241 | 0.12718 |
| 10 | 1.0820-03 | 4.1559+00 | 1.00000 | 0.88917 | 0.28628 | 0.60691 | 4.49430 | 0.13504 |
| 11 | 1.3640-03 | 4.6037+00 | 1.00000 | 0.88856 | 0.30352 | 0.62926 | 4.29826 | 0.14640 |
| 12 | 1.6027-03 | 4.9611+00 | 1.00000 | 0.88877 | 0.31657 | 0.64545 | 4.15700 | 0.15527 |
| 13 | 2.1133-03 | 5.6425+00 | 1.00000 | 0.88856 | 0.34003 | 0.67236 | 3.90994 | 0.17196 |
| 14 | 2.6111-03 | 6.3312+00 | 1.00000 | 0.88917 | 0.36216 | 0.69588 | 3.69201 | 0.18848 |
| 15 | 3.1394-03 | 6.9949+00 | 1.00000 | 0.89058 | 0.38225 | 0.71590 | 3.50755 | 0.20410 |
| 16 | 3.6551-03 | 7.8416+00 | 1.00000 | 0.89392 | 0.40643 | 0.73875 | 3.30393 | 0.22360 |
| 17 | 4.1758-03 | 8.4161+00 | 1.00000 | 0.89685 | 0.42203 | 0.75281 | 3.18192 | 0.23659 |
| 18 | 4.6761-03 | 9.0124+00 | 1.00000 | 0.89947 | 0.43763 | 0.76603 | 3.06383 | 0.25002 |
| 19 | 5.1918-03 | 9.7462+00 | 1.00000 | 0.90372 | 0.45609 | 0.78127 | 2.93420 | 0.26626 |
| 20 | 5.7379-03 | 1.0554+01 | 1.00000 | 0.90685 | 0.47557 | 0.79581 | 2.80020 | 0.28420 |
| 21 | 6.2306-03 | 1.1485+01 | 1.00000 | 0.91059 | 0.49709 | 0.81095 | 2.66144 | 0.30471 |
| 22 | 6.7488-03 | 1.2472+01 | 1.00000 | 0.91433 | 0.51892 | 0.82525 | 2.52914 | 0.32630 |
| 23 | 7.2593-03 | 1.3477+01 | 1.00000 | 0.91786 | 0.54023 | 0.83824 | 2.40755 | 0.34817 |
| 24 | 7.7800-03 | 1.4569+01 | 1.00000 | 0.92241 | 0.56247 | 0.85131 | 2.29075 | 0.37163 |
| 25 | 8.2931-03 | 1.5763+01 | 1.00000 | 0.92514 | 0.58582 | 0.86321 | 2.17117 | 0.39758 |
| 26 | 8.8163-03 | 1.7089+01 | 1.00000 | 0.92938 | 0.61071 | 0.87560 | 2.05562 | 0.42595 |
| 27 | 9.3243-03 | 1.8418+01 | 1.00000 | 0.93332 | 0.63468 | 0.88667 | 1.95174 | 0.45430 |
| 28 | 9.8459-03 | 1.9703+01 | 1.00000 | 0.93686 | 0.65701 | 0.89629 | 1.86103 | 0.48161 |
| 29 | 1.0343-02 | 2.0885+01 | 1.00000 | 0.94140 | 0.67690 | 0.90506 | 1.78775 | 0.50626 |
| 30 | 1.0876-02 | 2.2401+01 | 1.00000 | 0.94403 | 0.70158 | 0.91392 | 1.69694 | 0.53857 |
| 31 | 1.1372-02 | 2.3806+01 | 1.00000 | 0.94817 | 0.72371 | 0.92225 | 1.62393 | 0.56791 |
| 32 | 1.1895-02 | 2.5153+01 | 1.00000 | 0.95201 | 0.74431 | 0.92962 | 1.55990 | 0.59595 |
| 33 | 1.2423-02 | 2.6748+01 | 1.00000 | 0.95484 | 0.76798 | 0.93690 | 1.48829 | 0.62951 |
| 34 | 1.2931-02 | 2.8320+01 | 1.00000 | 0.95928 | 0.79062 | 0.94433 | 1.42665 | 0.66192 |
| 35 | 1.3449-02 | 2.9643+01 | 1.00000 | 0.96211 | 0.80918 | 0.94978 | 1.37770 | 0.68939 |
| 36 | 1.3960-02 | 3.1125+01 | 1.00000 | 0.96615 | 0.82947 | 0.95595 | 1.32821 | 0.71973 |
| 37 | 1.4483-02 | 3.2520+01 | 1.00000 | 0.96979 | 0.84814 | 0.96139 | 1.28489 | 0.74823 |
| 38 | 1.4981-02 | 3.4001+01 | 1.00000 | 0.97232 | 0.86752 | 0.96622 | 1.24049 | 0.77890 |
| 39 | 1.5497-02 | 3.5605+01 | 1.00000 | 0.97606 | 0.88802 | 0.97165 | 1.19723 | 0.81158 |
| 40 | 1.6022-02 | 3.6941+01 | 1.00000 | 0.97848 | 0.90474 | 0.97563 | 1.16283 | 0.83901 |
| 41 | 1.6525-02 | 3.8276+01 | 1.00000 | 0.98161 | 0.92116 | 0.97979 | 1.13133 | 0.86605 |
| 42 | 1.7059-02 | 3.9449+01 | 1.00000 | 0.98485 | 0.93534 | 0.98355 | 1.10575 | 0.88949 |
| 43 | 1.7559-02 | 4.0536+01 | 1.00000 | 0.98697 | 0.94829 | 0.98651 | 1.08223 | 0.91155 |
| 44 | 1.8090-02 | 4.1551+01 | 1.00000 | 0.98959 | 0.96022 | 0.98952 | 1.06194 | 0.93180 |
| 45 | 1.8341-02 | 4.1962+01 | 1.00000 | 0.99071 | 0.96502 | 0.99074 | 1.05401 | 0.93997 |
| 46 | 1.8598-02 | 4.2376+01 | 1.00000 | 0.99182 | 0.96981 | 0.99195 | 1.04618 | 0.94817 |
| 47 | 1.9111-02 | 4.3199+01 | 1.00000 | 0.99404 | 0.97930 | 0.99434 | 1.03095 | 0.96448 |
| 48 | 1.9619-02 | 4.3789+01 | 1.00000 | 0.99596 | 0.98603 | 0.99618 | 1.02071 | 0.97597 |
| 49 | 2.0127-02 | 4.4301+01 | 1.00000 | 0.99768 | 0.99184 | 0.99780 | 1.01205 | 0.98592 |
| D 50 | 2.0792-02 | 4.5025+01 | 1.00000 | 1.00000 | 1.00000 | 1.00000 | 1.00000 | 1.00000 |
| 51 | 2.1433-02 | 4.5591+01 | 1.00000 | 1.00131 | 1.00632 | 1.00145 | 0.99034 | 1.01122 |
| 52 | 2.2090-02 | 4.6095+01 | 1.00000 | 1.00354 | 1.01193 | 1.00325 | 0.98292 | 1.02069 |
| 53 | 2.2713-02 | 4.6417+01 | 1.00000 | 1.00495 | 1.01550 | 1.00439 | 0.97824 | 1.02673 |
| 54 | 2.3368-02 | 4.6982+01 | 1.00000 | 1.00626 | 1.02172 | 1.00580 | 0.96908 | 1.03790 |
| 55 | 2.4016-02 | 4.7466+01 | 1.00000 | 1.00738 | 1.02703 | 1.00699 | 0.96136 | 1.04747 |
| 56 | 2.4653-02 | 4.8028+01 | 1.00000 | 1.00869 | 1.03315 | 1.00836 | 0.95260 | 1.05854 |
| 57 | 2.5291-02 | 4.8480+01 | 1.00000 | 1.01020 | 1.03804 | 1.00968 | 0.94611 | 1.06720 |
| 58 | 2.5938-02 | 4.8773+01 | 1.00000 | 1.01152 | 1.04120 | 1.01070 | 0.94227 | 1.07262 |
| 59 | 2.6589-02 | 4.8953+01 | 1.00000 | 1.01253 | 1.04314 | 1.01143 | 0.94012 | 1.07585 |
| 60 | 2.7224-02 | 4.9086+01 | 1.00000 | 1.01344 | 1.04457 | 1.01204 | 0.93870 | 1.07814 |
| 61 | 2.7876-02 | 4.9342+01 | 1.00000 | 1.01404 | 1.04732 | 1.01266 | 0.93490 | 1.08317 |
| 62 | 2.8496-02 | 4.9581+01 | 1.00000 | 1.01445 | 1.04987 | 1.01315 | 0.93126 | 1.08793 |
| 63 | 2.9152-02 | 4.9886+01 | 1.00000 | 1.01475 | 1.05314 | 1.01366 | 0.92644 | 1.09415 |
| 64 | 2.9827-02 | 5.0155+01 | 1.00000 | 1.01495 | 1.05599 | 1.01408 | 0.92219 | 1.09964 |
| 65 | 3.0439-02 | 5.0203+01 | 1.00000 | 1.01505 | 1.05650 | 1.01418 | 0.92150 | 1.10059 |

INPUT VARIABLES Y, M/MD, P/PD, TO/TOD

7703S0415

BERG

PROFILE TABULATION

61 POINTS, DELTA AT POINT 59

| I | Y | PT2/P | P/PO | TO/TOD | M/MD | U/UD | T/TD | R/RD*U/UD |
|------|------------|------------|---------|---------|---------|---------|---------|-----------|
| 1 | 0.0000*-00 | 1.0000*-00 | 1.00000 | 0.81863 | 0.00000 | 0.00000 | 6.76005 | 0.00000 |
| 2 | 1.2700*-04 | 1.3800*-00 | 1.00000 | 0.82526 | 0.11524 | 0.28731 | 6.21570 | 0.04622 |
| 3 | 3.3528*-04 | 1.5433*-00 | 1.00000 | 0.83218 | 0.13486 | 0.33228 | 6.07060 | 0.05474 |
| 4 | 4.7244*-04 | 1.7561*-00 | 1.00000 | 0.84451 | 0.15508 | 0.37788 | 5.93739 | 0.06364 |
| 5 | 6.9088*-04 | 2.0789*-00 | 1.00000 | 0.85484 | 0.17908 | 0.42854 | 5.72617 | 0.07484 |
| 6 | 9.6774*-04 | 2.3660*-00 | 1.00000 | 0.85965 | 0.19681 | 0.46328 | 5.54100 | 0.08361 |
| 7 | 1.2090*-03 | 2.5233*-00 | 1.00000 | 0.86035 | 0.20568 | 0.47953 | 5.43565 | 0.08822 |
| 8 | 1.4630*-03 | 2.6969*-00 | 1.00000 | 0.86165 | 0.21494 | 0.49616 | 5.32861 | 0.09311 |
| 9 | 1.7247*-03 | 2.9367*-00 | 1.00000 | 0.86336 | 0.22699 | 0.51707 | 5.18893 | 0.09965 |
| 10 | 1.9888*-03 | 3.1184*-00 | 1.00000 | 0.86456 | 0.23566 | 0.53158 | 5.08841 | 0.10447 |
| 11 | 2.2403*-03 | 3.3256*-00 | 1.00000 | 0.86607 | 0.24512 | 0.54701 | 4.98006 | 0.10984 |
| 12 | 2.7381*-03 | 3.7405*-00 | 1.00000 | 0.86997 | 0.26295 | 0.57510 | 4.78356 | 0.12022 |
| 13 | 3.2563*-03 | 4.1405*-00 | 1.00000 | 0.87499 | 0.27898 | 0.59947 | 4.61721 | 0.12983 |
| 14 | 3.7846*-03 | 4.4335*-00 | 1.00000 | 0.87980 | 0.29014 | 0.61615 | 4.50981 | 0.13662 |
| 15 | 4.3155*-03 | 4.7665*-00 | 1.00000 | 0.88381 | 0.30229 | 0.63323 | 4.38805 | 0.14431 |
| 16 | 4.8108*-03 | 5.0963*-00 | 1.00000 | 0.88692 | 0.31384 | 0.64859 | 4.27082 | 0.15187 |
| 17 | 5.3137*-03 | 5.3968*-00 | 1.00000 | 0.89083 | 0.32400 | 0.66204 | 4.17514 | 0.15857 |
| 18 | 5.8090*-03 | 5.7537*-00 | 1.00000 | 0.89534 | 0.33566 | 0.67695 | 4.06748 | 0.16643 |
| 19 | 6.3221*-03 | 6.1557*-00 | 1.00000 | 0.89975 | 0.34831 | 0.69234 | 3.95103 | 0.17523 |
| 20 | 6.8428*-03 | 6.5228*-00 | 1.00000 | 0.90366 | 0.35946 | 0.70539 | 3.85086 | 0.18318 |
| 21 | 7.3660*-03 | 6.9638*-00 | 1.00000 | 0.90727 | 0.37241 | 0.71960 | 3.73372 | 0.19273 |
| 22 | 7.8638*-03 | 7.4099*-00 | 1.00000 | 0.90967 | 0.38506 | 0.73245 | 3.61823 | 0.20243 |
| 23 | 8.3795*-03 | 7.9191*-00 | 1.00000 | 0.91258 | 0.39900 | 0.74606 | 3.49616 | 0.21339 |
| 24 | 8.8875*-03 | 8.4275*-00 | 1.00000 | 0.91579 | 0.41245 | 0.75874 | 3.38413 | 0.22421 |
| 25 | 9.4056*-03 | 8.8938*-00 | 1.00000 | 0.91830 | 0.42440 | 0.76940 | 3.28662 | 0.23410 |
| 26 | 9.9593*-03 | 9.4629*-00 | 1.00000 | 0.92301 | 0.43855 | 0.78220 | 3.18134 | 0.24587 |
| 27 | 1.0429*-02 | 9.9961*-00 | 1.00000 | 0.92652 | 0.45139 | 0.79303 | 3.08652 | 0.25693 |
| 28 | 1.0945*-02 | 1.0662*-01 | 1.00000 | 0.93093 | 0.46693 | 0.80562 | 2.97685 | 0.27063 |
| 29 | 1.1455*-02 | 1.1314*-01 | 1.00000 | 0.93524 | 0.48167 | 0.81708 | 2.87755 | 0.28395 |
| 30 | 1.1956*-02 | 1.1987*-01 | 1.00000 | 0.93845 | 0.49641 | 0.82755 | 2.77907 | 0.29778 |
| 31 | 1.2466*-02 | 1.2814*-01 | 1.00000 | 0.94185 | 0.51394 | 0.83920 | 2.66625 | 0.31475 |
| 32 | 1.2987*-02 | 1.3531*-01 | 1.00000 | 0.94416 | 0.52869 | 0.84826 | 2.57434 | 0.32951 |
| 33 | 1.3492*-02 | 1.4385*-01 | 1.00000 | 0.94667 | 0.54572 | 0.85814 | 2.47273 | 0.34704 |
| 34 | 1.4018*-02 | 1.5330*-01 | 1.00000 | 0.94957 | 0.56394 | 0.86823 | 2.37027 | 0.36630 |
| 35 | 1.4521*-02 | 1.6165*-01 | 1.00000 | 0.95158 | 0.57958 | 0.87623 | 2.28561 | 0.38337 |
| 36 | 1.5034*-02 | 1.7206*-01 | 1.00000 | 0.95559 | 0.59851 | 0.88613 | 2.19207 | 0.40424 |
| 37 | 1.5557*-02 | 1.8321*-01 | 1.00000 | 0.95970 | 0.61813 | 0.89584 | 2.10041 | 0.42651 |
| 38 | 1.6060*-02 | 1.9465*-01 | 1.00000 | 0.96391 | 0.63765 | 0.90506 | 2.01462 | 0.44925 |
| 39 | 1.6579*-02 | 2.0683*-01 | 1.00000 | 0.96802 | 0.65777 | 0.91398 | 1.93077 | 0.47338 |
| 40 | 1.7089*-02 | 2.1799*-01 | 1.00000 | 0.97123 | 0.67570 | 0.92134 | 1.85925 | 0.49554 |
| 41 | 1.7617*-02 | 2.3296*-01 | 1.00000 | 0.97404 | 0.69900 | 0.92977 | 1.76925 | 0.52551 |
| 42 | 1.8095*-02 | 2.4649*-01 | 1.00000 | 0.97624 | 0.71942 | 0.93660 | 1.69489 | 0.55260 |
| 43 | 1.8628*-02 | 2.6061*-01 | 1.00000 | 0.97845 | 0.74014 | 0.94315 | 1.62380 | 0.58083 |
| 44 | 1.9147*-02 | 2.7670*-01 | 1.00000 | 0.98065 | 0.76305 | 0.94987 | 1.54962 | 0.61297 |
| 45 | 1.9639*-02 | 2.8927*-01 | 1.00000 | 0.98276 | 0.78048 | 0.95493 | 1.49701 | 0.63789 |
| 46 | 2.0152*-02 | 3.0629*-01 | 1.00000 | 0.98536 | 0.80349 | 0.96122 | 1.43116 | 0.67164 |
| 47 | 2.0668*-02 | 3.2304*-01 | 1.00000 | 0.98807 | 0.82550 | 0.96702 | 1.37228 | 0.70469 |
| 48 | 2.1201*-02 | 3.4009*-01 | 1.00000 | 0.99098 | 0.84731 | 0.97261 | 1.31763 | 0.73815 |
| 49 | 2.1704*-02 | 3.5896*-01 | 1.00000 | 0.99378 | 0.87062 | 0.97819 | 1.26181 | 0.77523 |
| 50 | 2.2225*-02 | 3.7618*-01 | 1.00000 | 0.99639 | 0.89173 | 0.98298 | 1.21513 | 0.80895 |
| 51 | 2.2730*-02 | 3.9271*-01 | 1.00000 | 0.99910 | 0.91135 | 0.98743 | 1.17391 | 0.84114 |
| 52 | 2.3233*-02 | 4.0942*-01 | 1.00000 | 1.00050 | 0.93078 | 0.99104 | 1.13367 | 0.87418 |
| 53 | 2.3762*-02 | 4.2235*-01 | 1.00000 | 1.00040 | 0.94552 | 0.99310 | 1.10317 | 0.90022 |
| 54 | 2.4265*-02 | 4.3547*-01 | 1.00000 | 1.00000 | 0.96026 | 0.99492 | 1.07350 | 0.92680 |
| 55 | 2.4775*-02 | 4.4563*-01 | 1.00000 | 1.00010 | 0.97151 | 0.99647 | 1.05203 | 0.94719 |
| 56 | 2.5291*-02 | 4.5317*-01 | 1.00000 | 1.00010 | 0.97978 | 0.99753 | 1.03657 | 0.96234 |
| 57 | 2.5941*-02 | 4.6031*-01 | 1.00000 | 1.00020 | 0.98755 | 0.99857 | 1.02244 | 0.97665 |
| 58 | 2.6548*-02 | 4.6547*-01 | 1.00000 | 1.00020 | 0.99313 | 0.99926 | 1.01239 | 0.98703 |
| D 59 | 2.7841*-02 | 4.7187*-01 | 1.00000 | 1.00000 | 1.00000 | 1.00000 | 1.00000 | 1.00000 |
| 60 | 2.9124*-02 | 4.7681*-01 | 1.00000 | 1.00000 | 1.00528 | 1.00063 | 0.99078 | 1.00994 |
| 61 | 3.0406*-02 | 4.7991*-01 | 1.00000 | 1.00010 | 1.00857 | 1.00108 | 0.98520 | 1.01611 |

INPUT VARIABLES Y,M/MD,P/PO,TO/TOD

7703S0501

BERG

PROFILE TABULATION

63 POINTS, DELTA AT POINT 53

| I | Y | PT2/P | P/PO | TO/TOD | M/MD | U/UD | T/TD | R/RD*U/UD |
|----|-----------------------|-----------------------|---------|---------|---------|---------|---------|-----------|
| 1 | 0.0000 ⁺⁰⁰ | 1.0000 ⁺⁰⁰ | 1.00000 | 0.81626 | 0.00000 | 0.00000 | 6.38897 | 0.00000 |
| 2 | 1.2700 ⁻⁰⁴ | 1.4248 ⁺⁰⁰ | 1.00000 | 0.82205 | 0.12486 | 0.30110 | 5.81535 | 0.05178 |
| 3 | 2.5654 ⁻⁰⁴ | 1.5268 ⁺⁰⁰ | 1.00000 | 0.82546 | 0.13720 | 0.32829 | 5.72521 | 0.05734 |
| 4 | 4.0386 ⁻⁰⁴ | 1.7696 ⁺⁰⁰ | 1.00000 | 0.83820 | 0.16107 | 0.38027 | 5.57350 | 0.06823 |
| 5 | 5.1308 ⁻⁰⁴ | 1.9944 ⁺⁰⁰ | 1.00000 | 0.84422 | 0.17872 | 0.41626 | 5.42485 | 0.07673 |
| 6 | 6.6040 ⁻⁰⁴ | 2.1675 ⁺⁰⁰ | 1.00000 | 0.85034 | 0.19055 | 0.44007 | 5.33354 | 0.08251 |
| 7 | 7.6962 ⁻⁰⁴ | 2.3249 ⁺⁰⁰ | 1.00000 | 0.85485 | 0.20045 | 0.45932 | 5.25071 | 0.08748 |
| 8 | 9.1948 ⁻⁰⁴ | 2.4912 ⁺⁰⁰ | 1.00000 | 0.85575 | 0.21024 | 0.47690 | 5.14539 | 0.09269 |
| 9 | 1.0211 ⁻⁰³ | 2.6244 ⁺⁰⁰ | 1.00000 | 0.85605 | 0.21769 | 0.48980 | 5.06259 | 0.09675 |
| 10 | 1.1735 ⁻⁰³ | 2.8004 ⁺⁰⁰ | 1.00000 | 0.85635 | 0.22707 | 0.50560 | 4.95763 | 0.10198 |
| 11 | 1.4275 ⁻⁰³ | 3.0618 ⁺⁰⁰ | 1.00000 | 0.85756 | 0.24023 | 0.52715 | 4.81508 | 0.10948 |
| 12 | 1.6891 ⁻⁰³ | 3.3244 ⁺⁰⁰ | 1.00000 | 0.85916 | 0.25268 | 0.54682 | 4.68339 | 0.11676 |
| 13 | 2.2098 ⁻⁰³ | 3.7220 ⁺⁰⁰ | 1.00000 | 0.86227 | 0.27033 | 0.57362 | 4.50274 | 0.12739 |
| 14 | 2.7330 ⁻⁰³ | 4.1206 ⁺⁰⁰ | 1.00000 | 0.86538 | 0.28685 | 0.59739 | 4.33708 | 0.13774 |
| 15 | 3.2207 ⁻⁰³ | 4.5767 ⁺⁰⁰ | 1.00000 | 0.86839 | 0.30460 | 0.62136 | 4.16120 | 0.14932 |
| 16 | 3.7643 ⁻⁰³ | 5.0614 ⁺⁰⁰ | 1.00000 | 0.87160 | 0.32235 | 0.64397 | 3.99095 | 0.16136 |
| 17 | 4.2621 ⁻⁰³ | 5.5805 ⁺⁰⁰ | 1.00000 | 0.87491 | 0.34030 | 0.66550 | 3.82439 | 0.17401 |
| 18 | 4.7752 ⁻⁰³ | 6.0585 ⁺⁰⁰ | 1.00000 | 0.87872 | 0.35601 | 0.68363 | 3.66827 | 0.18540 |
| 19 | 5.2654 ⁻⁰³ | 6.5453 ⁺⁰⁰ | 1.00000 | 0.88254 | 0.37131 | 0.70043 | 3.55833 | 0.19684 |
| 20 | 5.7785 ⁻⁰³ | 7.1535 ⁺⁰⁰ | 1.00000 | 0.88685 | 0.38957 | 0.71931 | 3.40914 | 0.21099 |
| 21 | 6.3094 ⁻⁰³ | 7.7186 ⁺⁰⁰ | 1.00000 | 0.89116 | 0.40579 | 0.73534 | 3.28369 | 0.22394 |
| 22 | 6.8224 ⁻⁰³ | 8.4779 ⁺⁰⁰ | 1.00000 | 0.89548 | 0.42660 | 0.75421 | 3.12557 | 0.24130 |
| 23 | 7.3381 ⁻⁰³ | 9.2515 ⁺⁰⁰ | 1.00000 | 0.89909 | 0.44680 | 0.77107 | 2.97822 | 0.25890 |
| 24 | 7.8588 ⁻⁰³ | 1.0212 ⁺⁰¹ | 1.00000 | 0.90270 | 0.47067 | 0.78930 | 2.81224 | 0.28067 |
| 25 | 8.3922 ⁻⁰³ | 1.1250 ⁺⁰¹ | 1.00000 | 0.90641 | 0.49515 | 0.80656 | 2.65331 | 0.30398 |
| 26 | 8.8925 ⁻⁰³ | 1.2192 ⁺⁰¹ | 1.00000 | 0.90982 | 0.51637 | 0.82052 | 2.52493 | 0.32497 |
| 27 | 9.3955 ⁻⁰³ | 1.3494 ⁺⁰¹ | 1.00000 | 0.91343 | 0.54432 | 0.83713 | 2.36521 | 0.35393 |
| 28 | 9.8146 ⁻⁰³ | 1.4655 ⁺⁰¹ | 1.00000 | 0.91674 | 0.56809 | 0.85025 | 2.24002 | 0.37957 |
| 29 | 1.0432 ⁻⁰² | 1.5691 ⁺⁰¹ | 1.00000 | 0.92136 | 0.58849 | 0.86159 | 2.14350 | 0.40196 |
| 30 | 1.0952 ⁻⁰² | 1.6737 ⁺⁰¹ | 1.00000 | 0.92557 | 0.60839 | 0.87194 | 2.05406 | 0.42449 |
| 31 | 1.1483 ⁻⁰² | 1.7857 ⁺⁰¹ | 1.00000 | 0.92998 | 0.62899 | 0.88211 | 1.96678 | 0.44850 |
| 32 | 1.1986 ⁻⁰² | 1.9248 ⁺⁰¹ | 1.00000 | 0.93420 | 0.65368 | 0.89309 | 1.86666 | 0.47844 |
| 33 | 1.2512 ⁻⁰² | 2.0590 ⁺⁰¹ | 1.00000 | 0.93831 | 0.67663 | 0.90277 | 1.78015 | 0.50713 |
| 34 | 1.3012 ⁻⁰² | 2.1946 ⁺⁰¹ | 1.00000 | 0.94212 | 0.69907 | 0.91161 | 1.70050 | 0.53608 |
| 35 | 1.3538 ⁻⁰² | 2.3528 ⁺⁰¹ | 1.00000 | 0.94583 | 0.72437 | 0.92072 | 1.61561 | 0.56989 |
| 36 | 1.4046 ⁻⁰² | 2.5013 ⁺⁰¹ | 1.00000 | 0.94904 | 0.74732 | 0.92843 | 1.54341 | 0.60154 |
| 37 | 1.4567 ⁻⁰² | 2.6433 ⁺⁰¹ | 1.00000 | 0.95235 | 0.76864 | 0.93538 | 1.48090 | 0.63163 |
| 38 | 1.5088 ⁻⁰² | 2.7865 ⁺⁰¹ | 1.00000 | 0.95566 | 0.78955 | 0.94191 | 1.42315 | 0.66184 |
| 39 | 1.5596 ⁻⁰² | 2.9379 ⁺⁰¹ | 1.00000 | 0.95927 | 0.81108 | 0.94842 | 1.36734 | 0.69362 |
| 40 | 1.6119 ⁻⁰² | 3.0926 ⁺⁰¹ | 1.00000 | 0.96379 | 0.83250 | 0.95508 | 1.31616 | 0.72565 |
| 41 | 1.6629 ⁻⁰² | 3.2491 ⁺⁰¹ | 1.00000 | 0.96850 | 0.85362 | 0.96152 | 1.26879 | 0.75782 |
| 42 | 1.7140 ⁻⁰² | 3.3875 ⁺⁰¹ | 1.00000 | 0.97282 | 0.87188 | 0.96702 | 1.23015 | 0.78610 |
| 43 | 1.7653 ⁻⁰² | 3.5417 ⁺⁰¹ | 1.00000 | 0.97613 | 0.89177 | 0.97213 | 1.18836 | 0.81805 |
| 44 | 1.8166 ⁻⁰² | 3.6855 ⁺⁰¹ | 1.00000 | 0.97883 | 0.90993 | 0.97648 | 1.15165 | 0.84790 |
| 45 | 1.8684 ⁻⁰² | 3.8097 ⁺⁰¹ | 1.00000 | 0.98144 | 0.92533 | 0.98022 | 1.12216 | 0.87351 |
| 46 | 1.9200 ⁻⁰² | 3.9015 ⁺⁰¹ | 1.00000 | 0.98385 | 0.93655 | 0.98313 | 1.10195 | 0.89217 |
| 47 | 1.9708 ⁻⁰² | 4.0106 ⁺⁰¹ | 1.00000 | 0.98616 | 0.94971 | 0.98623 | 1.07839 | 0.91454 |
| 48 | 2.0211 ⁻⁰² | 4.0876 ⁺⁰¹ | 1.00000 | 0.98866 | 0.95889 | 0.98880 | 1.06336 | 0.92989 |
| 49 | 2.0734 ⁻⁰² | 4.1723 ⁺⁰¹ | 1.00000 | 0.99127 | 0.96889 | 0.99150 | 1.04723 | 0.94679 |
| 50 | 2.1265 ⁻⁰² | 4.2561 ⁺⁰¹ | 1.00000 | 0.99398 | 0.97868 | 0.99419 | 1.03195 | 0.96341 |
| 51 | 2.1747 ⁻⁰² | 4.3195 ⁺⁰¹ | 1.00000 | 0.99649 | 0.98602 | 0.99643 | 1.02121 | 0.97573 |
| 52 | 2.2278 ⁻⁰² | 4.3870 ⁺⁰¹ | 1.00000 | 0.99870 | 0.99378 | 0.99855 | 1.00962 | 0.98903 |
| 53 | 2.2812 ⁻⁰² | 4.4415 ⁺⁰¹ | 1.00000 | 1.00000 | 1.00000 | 1.00000 | 1.00000 | 1.00000 |
| 54 | 2.3310 ⁻⁰² | 4.4847 ⁺⁰¹ | 1.00000 | 1.00090 | 1.00490 | 1.00107 | 0.99241 | 1.00873 |
| 55 | 2.3838 ⁻⁰² | 4.5298 ⁺⁰¹ | 1.00000 | 1.00130 | 1.01000 | 1.00191 | 0.98406 | 1.01815 |
| 56 | 2.4465 ⁻⁰² | 4.5898 ⁺⁰¹ | 1.00000 | 1.00171 | 1.01673 | 1.00295 | 0.97307 | 1.03070 |
| 57 | 2.5095 ⁻⁰² | 4.6318 ⁺⁰¹ | 1.00000 | 1.00251 | 1.02142 | 1.00392 | 0.96602 | 1.03923 |
| 58 | 2.5723 ⁻⁰² | 4.6658 ⁺⁰¹ | 1.00000 | 1.00391 | 1.02520 | 1.00508 | 0.96113 | 1.04572 |
| 59 | 2.6363 ⁻⁰² | 4.7072 ⁺⁰¹ | 1.00000 | 1.00572 | 1.02979 | 1.00653 | 0.95534 | 1.05358 |
| 60 | 2.7026 ⁻⁰² | 4.7248 ⁺⁰¹ | 1.00000 | 1.00772 | 1.03172 | 1.00776 | 0.95408 | 1.05626 |
| 61 | 2.7694 ⁻⁰² | 4.7582 ⁺⁰¹ | 1.00000 | 1.00963 | 1.03540 | 1.00915 | 0.94993 | 1.06233 |
| 62 | 2.8339 ⁻⁰² | 4.7860 ⁺⁰¹ | 1.00000 | 1.01103 | 1.03846 | 1.01020 | 0.94633 | 1.06750 |
| 63 | 2.8974 ⁻⁰² | 4.8150 ⁺⁰¹ | 1.00000 | 1.01174 | 1.04162 | 1.01092 | 0.94192 | 1.07325 |

INPUT VARIABLES Y, M/MD, P/PO, TO/TOD

| 7703S0515 | | BERG | | PROFILE TABULATION | | 74 POINTS, DELTA AT POINT 62 | | |
|-----------|-------------------------|-------------------------|---------|--------------------|---------|------------------------------|---------|-----------|
| I | Y | PT2/P | P/PD | TO/TOD | M/MD | U/UD | T/TD | R/RD*U/UD |
| 1 | 0.0000 ⁺ +00 | 1.0000 ⁺ +00 | 1.00000 | 0.81030 | 0.00000 | 0.00000 | 6.62765 | 0.00000 |
| 2 | 1.1938 ⁻ -04 | 1.3640 ⁺ +00 | 1.00000 | 0.81794 | 0.11365 | 0.28122 | 6.12239 | 0.04593 |
| 3 | 2.3622 ⁻ -04 | 1.5808 ⁺ +00 | 1.00000 | 0.82244 | 0.13953 | 0.33898 | 5.90199 | 0.05743 |
| 4 | 3.5560 ⁻ -04 | 1.9213 ⁺ +00 | 1.00000 | 0.83763 | 0.16902 | 0.40301 | 5.68518 | 0.07089 |
| 5 | 4.9022 ⁻ -04 | 2.4951 ⁺ +00 | 1.00000 | 0.84913 | 0.20524 | 0.47394 | 5.33266 | 0.08888 |
| 6 | 6.2484 ⁻ -04 | 2.9485 ⁺ +00 | 1.00000 | 0.85833 | 0.22881 | 0.51686 | 5.10263 | 0.10129 |
| 7 | 7.2644 ⁻ -04 | 3.2527 ⁺ +00 | 1.00000 | 0.86443 | 0.24315 | 0.54172 | 4.96355 | 0.10914 |
| 8 | 8.7122 ⁻ -04 | 3.5401 ⁺ +00 | 1.00000 | 0.86833 | 0.25589 | 0.56245 | 4.83114 | 0.11642 |
| 9 | 1.0262 ⁻ -03 | 3.8533 ⁺ +00 | 1.00000 | 0.87023 | 0.26903 | 0.58225 | 4.68392 | 0.12431 |
| 10 | 1.1455 ⁻ -03 | 4.0327 ⁺ +00 | 1.00000 | 0.87073 | 0.27626 | 0.59257 | 4.60101 | 0.12879 |
| 11 | 1.2776 ⁻ -03 | 4.2352 ⁺ +00 | 1.00000 | 0.87123 | 0.28418 | 0.60356 | 4.51073 | 0.13380 |
| 12 | 1.4249 ⁻ -03 | 4.4144 ⁺ +00 | 1.00000 | 0.87153 | 0.29100 | 0.61271 | 4.43324 | 0.13821 |
| 13 | 1.9126 ⁻ -03 | 4.9302 ⁺ +00 | 1.00000 | 0.87293 | 0.30976 | 0.63691 | 4.22765 | 0.15065 |
| 14 | 2.4232 ⁻ -03 | 5.3114 ⁺ +00 | 1.00000 | 0.87612 | 0.32290 | 0.65369 | 4.09830 | 0.15950 |
| 15 | 2.9261 ⁻ -03 | 5.6843 ⁺ +00 | 1.00000 | 0.87912 | 0.33524 | 0.66877 | 3.97965 | 0.16805 |
| 16 | 3.4366 ⁻ -03 | 5.9123 ⁺ +00 | 1.00000 | 0.88192 | 0.34256 | 0.67781 | 3.91511 | 0.17313 |
| 17 | 3.9726 ⁻ -03 | 6.3375 ⁺ +00 | 1.00000 | 0.88482 | 0.35580 | 0.69280 | 3.79137 | 0.18273 |
| 18 | 4.4679 ⁻ -03 | 6.6537 ⁺ +00 | 1.00000 | 0.88722 | 0.36533 | 0.70329 | 3.70587 | 0.18978 |
| 19 | 4.9733 ⁻ -03 | 6.9992 ⁺ +00 | 1.00000 | 0.88962 | 0.37546 | 0.71401 | 3.61638 | 0.19744 |
| 20 | 5.4991 ⁻ -03 | 7.2726 ⁺ +00 | 1.00000 | 0.89172 | 0.38329 | 0.72214 | 3.54973 | 0.20344 |
| 21 | 6.0046 ⁻ -03 | 7.6861 ⁺ +00 | 1.00000 | 0.89412 | 0.39482 | 0.73346 | 3.45104 | 0.21253 |
| 22 | 6.5049 ⁻ -03 | 8.0857 ⁺ +00 | 1.00000 | 0.89682 | 0.40566 | 0.74388 | 3.36267 | 0.22122 |
| 23 | 7.0307 ⁻ -03 | 8.5542 ⁺ +00 | 1.00000 | 0.90002 | 0.41800 | 0.75534 | 3.26545 | 0.23131 |
| 24 | 7.5311 ⁻ -03 | 8.9772 ⁺ +00 | 1.00000 | 0.90312 | 0.42883 | 0.76515 | 3.18368 | 0.24034 |
| 25 | 8.0620 ⁻ -03 | 9.3909 ⁺ +00 | 1.00000 | 0.90642 | 0.43916 | 0.77435 | 3.10904 | 0.24906 |
| 26 | 8.5750 ⁻ -03 | 9.9271 ⁺ +00 | 1.00000 | 0.90982 | 0.45220 | 0.78522 | 3.01518 | 0.26042 |
| 27 | 9.1059 ⁻ -03 | 1.0402 ⁺ +01 | 1.00000 | 0.91372 | 0.46344 | 0.79464 | 2.94012 | 0.27028 |
| 28 | 9.5987 ⁻ -03 | 1.0937 ⁺ +01 | 1.00000 | 0.91732 | 0.47577 | 0.80435 | 2.85816 | 0.28142 |
| 29 | 1.0102 ⁻ -02 | 1.1490 ⁺ +01 | 1.00000 | 0.92062 | 0.48821 | 0.81363 | 2.77736 | 0.29295 |
| 30 | 1.0625 ⁻ -02 | 1.2100 ⁺ +01 | 1.00000 | 0.92362 | 0.50155 | 0.82296 | 2.69227 | 0.30567 |
| 31 | 1.1130 ⁻ -02 | 1.2754 ⁺ +01 | 1.00000 | 0.92651 | 0.51550 | 0.83220 | 2.60616 | 0.31932 |
| 32 | 1.1636 ⁻ -02 | 1.3427 ⁺ +01 | 1.00000 | 0.92951 | 0.52944 | 0.84110 | 2.52381 | 0.33326 |
| 33 | 1.2174 ⁻ -02 | 1.4133 ⁺ +01 | 1.00000 | 0.93291 | 0.54369 | 0.84996 | 2.44401 | 0.34777 |
| 34 | 1.2654 ⁻ -02 | 1.4909 ⁺ +01 | 1.00000 | 0.93601 | 0.55893 | 0.85881 | 2.36086 | 0.36377 |
| 35 | 1.3188 ⁻ -02 | 1.5659 ⁺ +01 | 1.00000 | 0.93951 | 0.57328 | 0.86704 | 2.28744 | 0.37904 |
| 36 | 1.3693 ⁻ -02 | 1.6549 ⁺ +01 | 1.00000 | 0.94291 | 0.58983 | 0.87585 | 2.20500 | 0.39721 |
| 37 | 1.4194 ⁻ -02 | 1.7441 ⁺ +01 | 1.00000 | 0.94681 | 0.60598 | 0.88433 | 2.12970 | 0.41524 |
| 38 | 1.4719 ⁻ -02 | 1.8403 ⁺ +01 | 1.00000 | 0.95081 | 0.62293 | 0.89282 | 2.05420 | 0.43463 |
| 39 | 1.5245 ⁻ -02 | 1.9487 ⁺ +01 | 1.00000 | 0.95441 | 0.64149 | 0.90132 | 1.97414 | 0.45656 |
| 40 | 1.5738 ⁻ -02 | 2.0517 ⁺ +01 | 1.00000 | 0.95721 | 0.65864 | 0.90856 | 1.90288 | 0.47747 |
| 41 | 1.6246 ⁻ -02 | 2.1757 ⁺ +01 | 1.00000 | 0.96011 | 0.67870 | 0.91645 | 1.82329 | 0.50264 |
| 42 | 1.6782 ⁻ -02 | 2.3021 ⁺ +01 | 1.00000 | 0.96361 | 0.69857 | 0.92415 | 1.75013 | 0.52805 |
| 43 | 1.7267 ⁻ -02 | 2.4308 ⁺ +01 | 1.00000 | 0.96681 | 0.71823 | 0.93128 | 1.68128 | 0.55391 |
| 44 | 1.7795 ⁻ -02 | 2.5658 ⁺ +01 | 1.00000 | 0.97031 | 0.73829 | 0.93833 | 1.61532 | 0.58089 |
| 45 | 1.8313 ⁻ -02 | 2.7123 ⁺ +01 | 1.00000 | 0.97361 | 0.75945 | 0.94523 | 1.54906 | 0.61019 |
| 46 | 1.8824 ⁻ -02 | 2.8709 ⁺ +01 | 1.00000 | 0.97680 | 0.78172 | 0.95199 | 1.48306 | 0.64191 |
| 47 | 1.9334 ⁻ -02 | 3.0252 ⁺ +01 | 1.00000 | 0.98020 | 0.80279 | 0.95826 | 1.42485 | 0.67254 |
| 48 | 1.9842 ⁻ -02 | 3.2026 ⁺ +01 | 1.00000 | 0.98340 | 0.82636 | 0.96466 | 1.36272 | 0.70789 |
| 49 | 2.0343 ⁻ -02 | 3.3554 ⁺ +01 | 1.00000 | 0.98620 | 0.84612 | 0.96983 | 1.31379 | 0.73819 |
| 50 | 2.0861 ⁻ -02 | 3.5254 ⁺ +01 | 1.00000 | 0.98840 | 0.86759 | 0.97480 | 1.26242 | 0.77217 |
| 51 | 2.1379 ⁻ -02 | 3.6939 ⁺ +01 | 1.00000 | 0.99030 | 0.88835 | 0.97928 | 1.21517 | 0.80587 |
| 52 | 2.1885 ⁻ -02 | 3.8621 ⁺ +01 | 1.00000 | 0.99180 | 0.90862 | 0.98327 | 1.17108 | 0.83963 |
| 53 | 2.2395 ⁻ -02 | 4.0118 ⁺ +01 | 1.00000 | 0.99310 | 0.92627 | 0.98661 | 1.13453 | 0.86962 |
| 54 | 2.2857 ⁻ -02 | 4.1496 ⁺ +01 | 1.00000 | 0.99420 | 0.94222 | 0.98948 | 1.10283 | 0.89722 |
| 55 | 2.3424 ⁻ -02 | 4.2657 ⁺ +01 | 1.00000 | 0.99560 | 0.95546 | 0.99203 | 1.07801 | 0.92024 |
| 56 | 2.3937 ⁻ -02 | 4.3772 ⁺ +01 | 1.00000 | 0.99680 | 0.96800 | 0.99432 | 1.05512 | 0.94238 |
| 57 | 2.4455 ⁻ -02 | 4.4647 ⁺ +01 | 1.00000 | 0.99820 | 0.97773 | 0.99630 | 1.03834 | 0.95951 |
| 58 | 2.4938 ⁻ -02 | 4.5283 ⁺ +01 | 1.00000 | 0.99930 | 0.98475 | 0.99775 | 1.02657 | 0.97193 |
| 59 | 2.5481 ⁻ -02 | 4.5860 ⁺ +01 | 1.00000 | 1.00010 | 0.99107 | 0.99895 | 1.01595 | 0.98326 |
| 60 | 2.5982 ⁻ -02 | 4.6155 ⁺ +01 | 1.00000 | 1.00020 | 0.99428 | 0.99940 | 1.01031 | 0.98920 |
| 61 | 2.6502 ⁻ -02 | 4.6478 ⁺ +01 | 1.00000 | 1.00000 | 0.99779 | 0.99973 | 1.00388 | 0.99586 |
| 62 | 2.7005 ⁻ -02 | 4.6682 ⁺ +01 | 1.00000 | 1.00000 | 1.00000 | 1.00000 | 1.00000 | 1.00000 |
| 63 | 2.7640 ⁻ -02 | 4.6886 ⁺ +01 | 1.00000 | 0.99990 | 1.00221 | 1.00022 | 0.99604 | 1.00420 |
| 64 | 2.8296 ⁻ -02 | 4.6979 ⁺ +01 | 1.00000 | 1.00000 | 1.00321 | 1.00039 | 0.99439 | 1.00604 |
| 65 | 2.8913 ⁻ -02 | 4.6979 ⁺ +01 | 1.00000 | 1.00000 | 1.00321 | 1.00039 | 0.99439 | 1.00604 |
| 66 | 2.9591 ⁻ -02 | 4.6979 ⁺ +01 | 1.00000 | 1.00010 | 1.00321 | 1.00044 | 0.99449 | 1.00599 |
| 67 | 3.0223 ⁻ -02 | 4.6942 ⁺ +01 | 1.00000 | 1.00010 | 1.00281 | 1.00039 | 0.99519 | 1.00523 |
| 68 | 3.0866 ⁻ -02 | 4.6914 ⁺ +01 | 1.00000 | 1.00020 | 1.00251 | 1.00041 | 0.99581 | 1.00461 |
| 69 | 3.1504 ⁻ -02 | 4.6886 ⁺ +01 | 1.00000 | 1.00020 | 1.00221 | 1.00037 | 0.99634 | 1.00405 |
| 70 | 3.2139 ⁻ -02 | 4.6886 ⁺ +01 | 1.00000 | 1.00010 | 1.00221 | 1.00032 | 0.99624 | 1.00410 |
| 71 | 3.2758 ⁻ -02 | 4.6886 ⁺ +01 | 1.00000 | 1.00000 | 1.00221 | 1.00027 | 0.99614 | 1.00415 |
| 72 | 3.3431 ⁻ -02 | 4.6886 ⁺ +01 | 1.00000 | 0.99990 | 1.00221 | 1.00022 | 0.99604 | 1.00420 |
| 73 | 3.4066 ⁻ -02 | 4.6886 ⁺ +01 | 1.00000 | 0.99990 | 1.00221 | 1.00022 | 0.99604 | 1.00420 |
| 74 | 3.4709 ⁻ -02 | 4.6914 ⁺ +01 | 1.00000 | 0.99990 | 1.00251 | 1.00026 | 0.99551 | 1.00477 |

INPUT VARIABLES Y,M/MD,P/PD,TO/TOD

| | | |
|--|---|-----------|
|  | M: 0.1, 0.6 - 2.2 R THETA x 10 ⁻³ : 6, 23, 40 TW/TR: 1 | 7801 |
| | | ZPG AW |
| (M = 0.1 only). Continuous closed-return low speed tunnel, W = 1.15, H = 0.82 m. Air, RE/m x 10 ⁻⁶ : 2.2. | | |
| (Others) Continuous tunnel with symmetrical flexible nozzle. W = 0.46, H = 0.51 m. 0.067 < PO < 0.18 MN/m ² . TO: 315K. Air. 7 < RE/m x 10 ⁻⁶ < 20. | | |
| COLLINS D.J., COLES D.E., HICKS J.W., 1978. Measurements in the turbulent boundary layer at constant pressure in subsonic and supersonic flow. Part I, Mean flow. AEDC-TR-78-21. And Dimotakis, P.E., Collins, D.J., Lang, D.B., 1979. Title as above. Part II. Laser-doppler velocity measurements. AEDC-TR-79-49. | | |

- 1 Two experimental arrangements were used. For series 01 (M = 0.1), the test boundary layer was formed on a flat plate (W = 1.15, L = 2.44 m) constructed of formica -faced plywood 19 mm thick. The leading edge (X = 0) was elliptical with a transition strip immediately behind the elliptical section. The test surface was on the lower face of the plate, which completely spanned the conventional low speed tunnel, and was supported from the tunnel roof. Variation in Mach number along the plate was small, the largest excursion for given tunnel operating conditions being less than 2% at X ≈ 0.4 m. In the test zone considered here (1.524 x 2.286 m) variations were much less than this, the changes seen in the tables of section B resulting from changes in tunnel operating conditions since in a low speed tunnel M is a function of, inter alia, fan speed rather than tunnel geometry.
- 3
- 2 For series 02-11 (M = 0.6-2.2), the test boundary layer was formed on the upper nozzle wall of the wind tunnel, and a flat extension running about 1.5 m downstream from the end of the flexible nozzle. The test zone extended from X = -0.484 to X = +0.076 m, where X = 0 at the balance station which was 0.113 m downstream of the end of the flexible nozzle. A second throat was installed to ensure that the flow remained steady for the transonic cases, and Mach number variations for -1.4 < X < 0.4 were very small, in the worst case (M = 1.32, series 08, 09) being about ±2%. (Source Fig.1). There is no mean Mach number gradient. Transition was natural. The boundary layer had passed through the favourable pressure gradient in the tunnel nozzle, but had relaxed in constant pressure conditions for at least 30 boundary layer thicknesses before entering the test zone. (Source Fig.1).
- 4
- 6 The flat plate (series 01) was provided with 20 static tapings at at least 7 X-values. A Preston tube (d₁ = 2.1 mm, d₂ = 1.60 mm) was used for CF determination. The nozzle and extension (series 02-11) had 82 static tapings located throughout the test section and diffuser. At least 28 X-values were covered for -1.4 < X < 0.4. The principal method of CF measurement was by using the FEB originally used by Coles (CAT 5301). The floating element is rectangular, 6.22 mm in the X-direction, 37.85 mm in the Y-direction with gaps of 0.07 mm upstream and downstream, and 0.1 mm at each side. The element was flush with the surface to within 1 μm. No gap correction was applied. The balance is as described by Coles (1953) save for some small changes made in the method of returning the element to its null position. Additionally, three Preston tubes were used, (d₁ = 0.82, 1.62, 3.17 mm, d₂/d₁ = 0.60). CF values were calculated using the Hopkins and Keener (1966) T'correlation, and the Bradshaw and Unsworth (1974) correlation revised to take account of the revised CF values of Allen (1977) (see also Bradshaw 1977).
- 7 On the flat plate (series 01) Pitot traverses were made with an FPP (h₁ = 0.243, h₂ = 0.203 mm) at six stations. Measurements were also made at three upstream stations using a seven tube rake. Profiles on the nozzle extension (02-11) were also measured with an FPP, made by flattening 1.27 mm tube to an oval and honing the lip thickness to give an opening for which h₁ = 0.187, h₂ = 0.127 mm. The

centre of the support stem was 50.8 mm downstream of the probe tip.

Profiles of mean velocity and distributions of fluctuating velocity components were also measured using a dual forward scattering LDV operating in the single particle mode. (Dimotakis et al., 1979). These observations yield values of \bar{u} , \bar{v} , $\overline{u'^2}$, $\overline{v'^2}$ and $\overline{u'v'}$ with varying degrees of accuracy, generally good for streamwise components and poor for those in the Y-direction.

8 Measurements were made at the stations listed in table 1. All necessary interpolations were made by
 9 the authors, who assumed $P = P_w$ throughout the boundary layer and Crocco/van Driest temperature-
 10 velocity correlation, using a recovery factor of 0.885, from which T_w was also calculated. No probe
 11 corrections were applied, and viscosity was taken from the Sutherland viscosity law. In addition to
 9 CF values from the Preston tubes and FRB, values were derived from a fit to the wall and wake law. The
 mean flow data were also processed to yield the distribution of τ/τ_{wall} through the boundary layer,
 for comparison with the LDV results.

12 The editors have presented all the profiles for which tabular data was supplied. The subsonic profiles
 14 for "CIT 1-3", using the Pitot rake, are therefore omitted. The authors' assumptions and data
 reduction procedures have been accepted save that we have replaced the authors' recovery factor value
 of 0.885 by 0.896. The CF value given in the profile tables of section B is that deduced from a
 statistical fit to the law of the wall and wake. The full set of CF values obtained is given as table 1
 of section D. The LDV data are not given here as they are not in tabular form, and could not be easily
 or very appropriately so presented.

§ DATA: 78010101-1104. Pitot profiles (NX = 4-8). CF from FEB, Preston tubes and profile curve fitting.
 Mean and fluctuation data from LDV.

15 Editors' comments. The primary purpose of the mean flow measurements was to establish, as accurately as
 might be by conventional means, the flow field in which the LDV measurements were to be made. There is
 however, one special feature which makes the data set a valuable addition to the general data pool for
 ZPG/AW boundary layers, in that the results extended right through the transonic range using the same
 instruments (series 02-11, M = 0.60, 0.80, 0.98, 1.31, 2.16). (In this they may be compared to Winter
 and Gaudet - CAT 7302). The data appear to be of very good quality, and no detectable change is seen
 in the transformed velocity profiles through this range, confirming the expectation that there is no
 special feature of the transonic turbulent boundary layer (Figs. 1, 2). In Dimotakis et al. (1979)
 there is a detailed graphical presentation of the LDV data. The mean values of U agree very well with
 the Pitot-derived data at low MD values, but differ by up to 7% at M = 2.16. The turbulence intensity
 $\overline{u'^2}$ is compared to the results of Klebanoff (1954/55), and agrees, at all Mach numbers, to within a standard
 deviation, the Klebanoff values lying slightly lower. Results involving velocity components normal to
 the wall are not so satisfactory. Large discrepancies are found in the values of \bar{v} , while the authors
 state that agreement between the $\overline{v'^2}$ values and those of Klebanoff (1954/55) is fortuitous, the standard
 deviation of the LDV data being about half their absolute values. The values of the Reynolds stress
 deduced from the $\overline{u'v'}$ measurements again show quite large departures from mean flow derived results
 and the data of Klebanoff, especially in the inner region of the boundary layer ($y/\delta_2 < 3$). These data
 are further discussed by Schairer (1980).

The mean velocity profiles do not extend into the viscous sublayer, and the measurements do not reach
 further in than the momentum deficit peak in 70% of the cases. For y^+ greater than 100 the data conform
 well to the standard law of the wall ($k_1 = 0.40$ and $c = 5.10$). Typical wake strength $\Delta(\bar{u}^*/u_\tau)$ values
 given in the legend of Fig. 1 agree in general with the plot shown in Fig. 6 of Collins et al. We have
 plotted a few velocity profiles which are characteristic of the Mach and the Reynolds number range covered
 by the experiment. Fig. 2 shows the same profiles in outer law form. The profiles follow the standard
 norms fairly well, showing a slight curvature for which we have no explanation. This deviation does not
 appear in the Winter & Gaudet data (Fig. 4.2.12 of AG 253) which cover almost the same parameter range.

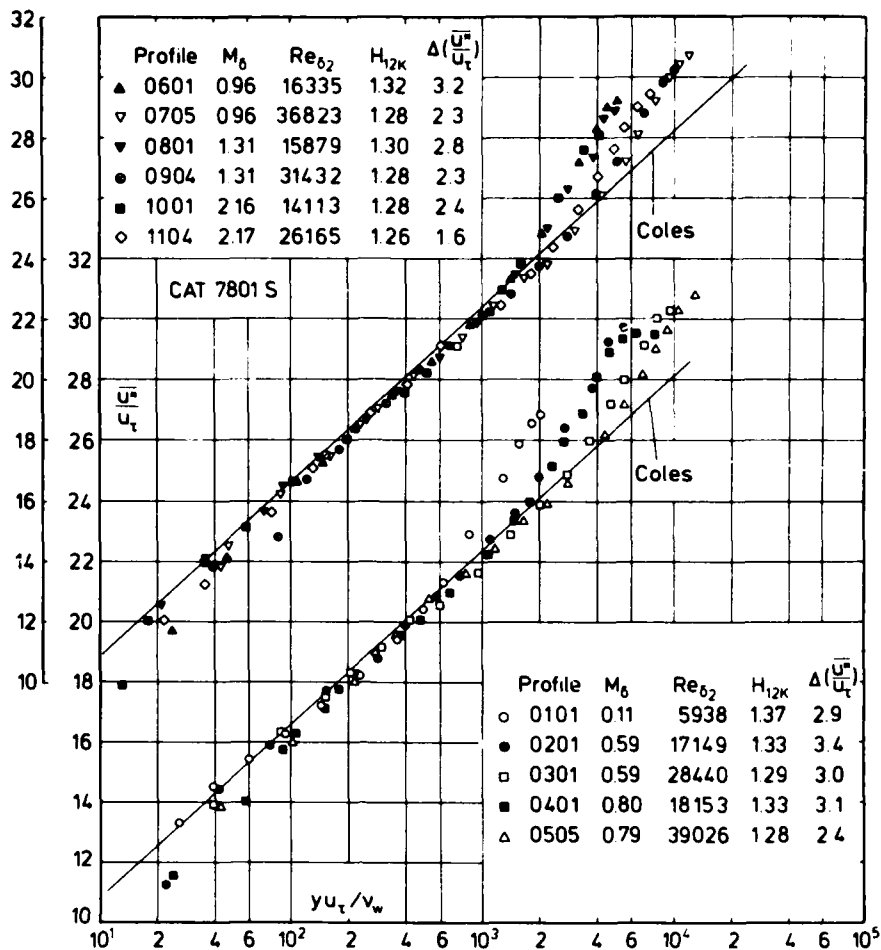


Fig. 1 Law of the wall for a compressible boundary layer (adiabatic wall, zero pressure gradient, defined origin). Collins et al. (1978).

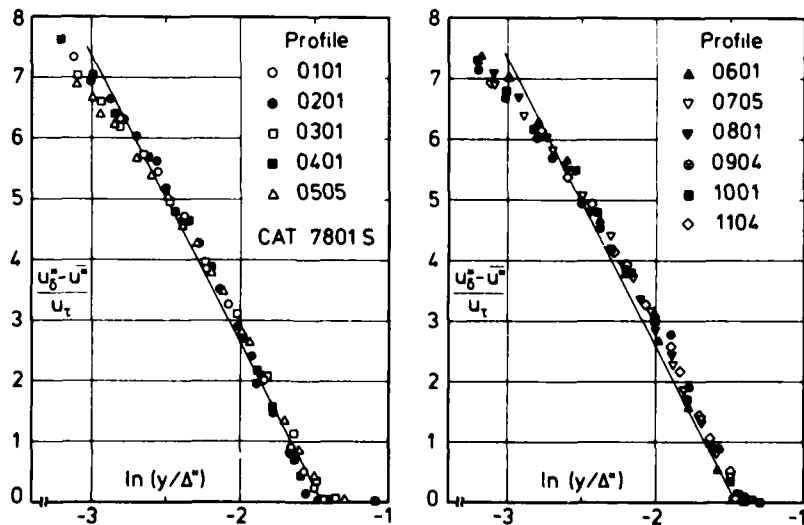


Fig. 2 Outer law for a compressible turbulent boundary layer (adiabatic wall, zero pressure gradient, defined origin). Collins et al. (1978).

Table 1 Measurement stations. (Collins et al. 1978)

| SOURCE IDENT | X (m) | Pitot | Preston | Balance | LDV | CAT IDENT |
|---|--------|----------|---------|---------|-----|-----------|
| CIT 1 | 0.304 | rake | yes | - | - | - |
| CIT 2 | 0.709 | rake | yes | - | - | - |
| CIT 3 | 0.914 | rake | yes | - | - | - |
| CIT 4 | 1.524 | traverse | yes | - | - | 0101 |
| CIT 5 | 1.676 | traverse | yes | - | - | 0102 |
| CIT 6 | 1.828 | traverse | yes | - | yes | 0103 |
| CIT 7 | 1.981 | traverse | yes | - | - | 0104 |
| CIT 8 | 2.133 | traverse | yes | - | - | 0105 |
| CIT 9 | 1.186 | traverse | yes | - | - | 0106 |
| (Series 01 - Flat plate, X = 0 at leading edge M = 0.1) | | | | | | |
| JPL 1 | -0.484 | traverse | - | - | - | 0201-0701 |
| JPL 2 | -0.262 | traverse | yes | - | yes | 0202-0702 |
| | | traverse | yes | - | yes | 0801-1101 |
| JPL 3 | -0.076 | traverse | - | - | - | 0203-0703 |
| | | traverse | - | - | - | 0802-1102 |
| JPL 4 | 0 | traverse | yes | yes | yes | 0204-0704 |
| | | traverse | yes | yes | yes | 0803-1103 |
| JPL 5 | +0.076 | traverse | - | - | - | 0205-0705 |
| | | traverse | - | - | - | 0804-1104 |

(Series 02 - 11, tunnel wall, X = 0 at balance station.)

(Series 02 - 07, sub/transonic. Series 08 - 11 supersonic.)

| CAT 78015 COLLINS/COLES/H BOUNDARY CONDITIONS AND EVALUATED DATA. SI UNITS | | | | | | | | |
|--|----------------------|--------------------------|----------------------|----------------------|-------------------|---------------------|----------------|----------------|
| RUN X * RZ | MD * POD* TOD* | TW/TR* PW/PD* TAUW | RED2W RED2D DZ | CF * CO * PIZ* | H12 H32 H42 | H12K H32K D2K | PW TW UD | PD TD TR |
| 7801S0101 | 0.1056 | 1.0000 | 5.9384*+03 | 2.7870*-03 | 1.3718 | 1.3672 | 9.9819*+04 | 9.9819*+04 |
| 1.5240*+00 | 1.0060*+05 | 1.0000 | 5.9475*+03 | 0.0000*+00 | 1.7683 | 1.7682 | 3.0698*+02 | 3.0637*+02 |
| INFINITE | 3.0705*+02 | 2.1720*+00 | 2.6617*-03 | 0.0000*+00 | 0.0004 | 2.6638*-03 | 3.7062*+01 | 3.0698*+02 |
| 7801S0102 | 0.1067 | 1.0000 | 6.0893*+03 | 2.7860*-03 | 1.3971 | 1.3923 | 9.9206*+04 | 9.9206*+04 |
| 1.6764*+00 | 1.0000*+05 | 1.0000 | 6.0987*+03 | 0.0000*+00 | 1.7641 | 1.7640 | 3.1268*+02 | 3.1204*+02 |
| INFINITE | 3.1275*+02 | 2.2047*+00 | 2.7807*-03 | 0.0000*+00 | 0.0004 | 2.7830*-03 | 3.7808*+01 | 3.1268*+02 |
| 7801S0103 | 0.1028 | 1.0000 | 6.8005*+03 | 2.7560*-03 | 1.3769 | 1.3726 | 1.0671*+05 | 1.0671*+05 |
| 1.8288*+00 | 1.0750*+05 | 1.0000 | 6.8104*+03 | 0.0000*+00 | 1.7691 | 1.7690 | 3.0368*+02 | 3.0311*+02 |
| INFINITE | 3.0375*+02 | 2.1769*+00 | 2.8887*-03 | 0.0000*+00 | 0.0004 | 2.8908*-03 | 3.5895*+01 | 3.0368*+02 |
| 7801S0104 | 0.1032 | 1.0000 | 7.1854*+03 | 2.6890*-03 | 1.3520 | 1.3476 | 9.8057*+04 | 9.8057*+04 |
| 1.9812*+00 | 9.8790*+04 | 1.0000 | 7.1960*+03 | 0.0000*+00 | 1.7755 | 1.7755 | 3.0268*+02 | 3.0211*+02 |
| INFINITE | 3.0275*+02 | 1.9664*+00 | 3.2953*-03 | 0.0000*+00 | 0.0004 | 3.2977*-03 | 3.5970*+01 | 3.0268*+02 |
| 7801S0105 | 0.1048 | 1.0000 | 7.4737*+03 | 2.6890*-03 | 1.3514 | 1.3469 | 1.0052*+05 | 1.0052*+05 |
| 1.2136*+00 | 1.0130*+05 | 1.0000 | 7.4849*+03 | 0.0000*+00 | 1.7764 | 1.7764 | 3.1078*+02 | 3.1017*+02 |
| INFINITE | 3.1085*+02 | 2.0794*+00 | 3.4036*-03 | 0.0000*+00 | 0.0004 | 3.4062*-03 | 3.7017*+01 | 3.1078*+02 |
| 7801S0106 | 0.1066 | 1.0000 | 7.8804*+03 | 2.6760*-03 | 1.3473 | 1.3426 | 9.9309*+04 | 9.9309*+04 |
| 2.2860*+00 | 1.0010*+05 | 1.0000 | 7.8926*+03 | 0.0000*+00 | 1.7767 | 1.7766 | 3.0998*+02 | 3.0935*+02 |
| INFINITE | 3.1005*+02 | 2.1119*+00 | 3.5624*-03 | 0.0000*+00 | 0.0004 | 3.5652*-03 | 3.7574*+01 | 3.0998*+02 |
| 7801S0201 | 0.5886 | 1.0000 | 1.7149*+04 | 2.1790*-03 | 1.4717 | 1.3300 | 5.2718*+04 | 5.2718*+04 |
| -4.8430*-01 | 6.6650*+04 | 1.0000 | 1.7967*+04 | 0.0000*+00 | 1.7807 | 1.7795 | 3.0369*+02 | 2.8594*+02 |
| INFINITE | 3.0575*+02 | 2.7860*+01 | 2.5019*-03 | 0.0000*+00 | 0.0120 | 2.5605*-03 | 1.9956*+02 | 3.0369*+02 |
| 7801S0202 | 0.5907 | 1.0000 | 1.9242*+04 | 2.2010*-03 | 1.4550 | 1.3132 | 5.2632*+04 | 5.2632*+04 |
| -2.6210*-01 | 6.6650*+04 | 1.0000 | 2.0164*+04 | 0.0000*+00 | 1.7886 | 1.7874 | 3.0800*+02 | 2.8987*+02 |
| INFINITE | 3.1010*+02 | 2.8299*+01 | 2.8517*-03 | 0.0000*+00 | 0.0121 | 2.9168*-03 | 2.0166*+02 | 3.0800*+02 |
| 7801S0203 | 0.5966 | 1.0000 | 2.0674*+04 | 2.1960*-03 | 1.4464 | 1.3022 | 5.2394*+04 | 5.2394*+04 |
| -7.6200*-02 | 6.6650*+04 | 1.0000 | 2.1689*+04 | 0.0000*+00 | 1.7932 | 1.7920 | 3.0121*+02 | 2.8316*+02 |
| INFINITE | 3.0331*+02 | 2.8664*+01 | 2.9610*-03 | 0.0000*+00 | 0.0124 | 3.0288*-03 | 2.0127*+02 | 3.0121*+02 |

| CAT 78015 COLLINS/COLES/H BOUNDARY CONDITIONS AND EVALUATED DATA. SI UNITS | | | | | | | | | |
|--|--------------------------------------|---------------------------------|---|---|----------------------------|---------------------------------|---|---|--|
| RUN X * RZ | MD * POD* TOD* | TW/TR* PW/PT* TAUM | RED2W RE02D D2 | CF * CQ * PIZ* | H12 H32 H42 | H12K H32K D2K | PW TW UD | PD TD TR | |
| 780150204 0.0000**+00 INFINITE | 0.5997 6.6650**+04 3.0865**+02 | 1.0000 1.0000 2.8921**+01 | 2.1420**+04 2.2479**+04 3.1266**+03 | 2.1980**+03 0.0000**+00 0.0000**+00 | 1.4389 1.7978 0.0125 | 1.2937 1.7967 3.1975**+03 | 5.2266**+04 3.0650**+02 2.0403**+02 | 5.2266**+04 2.8794**+02 3.0650**+02 | |
| 780150205 7.6200**+02 INFINITE | 0.5938 6.7710**+04 3.0889**+02 | 1.0000 1.0000 2.8896**+01 | 2.1659**+04 2.2708**+04 3.1341**+03 | 2.1950**+03 0.0000**+00 0.0000**+00 | 1.4349 1.7971 0.0123 | 1.2925 1.7960 3.2041**+03 | 5.3344**+04 3.0677**+02 2.0222**+02 | 5.3344**+04 2.8854**+02 3.0677**+02 | |
| 780150301 -4.8430**+01 INFINITE | 0.5942 1.2630**+05 3.1593**+02 | 1.0000 1.0000 5.1380**+01 | 2.8440**+04 2.9813**+04 2.2690**+03 | 2.0900**+03 0.0000**+00 0.0000**+00 | 1.4333 1.8008 0.0124 | 1.2910 1.7997 2.3189**+03 | 9.9469**+04 3.1376**+02 2.0465**+02 | 9.9469**+04 2.9509**+02 3.1376**+02 | |
| 780150302 -2.6210**+01 INFINITE | 0.5938 1.2700**+05 3.2418**+02 | 1.0000 1.0000 5.0793**+01 | 3.1650**+04 3.3166**+04 2.5952**+03 | 2.0570**+03 0.0000**+00 0.0000**+00 | 1.4304 1.8015 0.0123 | 1.2884 1.8004 2.6520**+03 | 1.0005**+05 3.2196**+02 2.0717**+02 | 1.0005**+05 3.0283**+02 3.2196**+02 | |
| 780150303 -7.6200**+02 INFINITE | 0.5934 1.2660**+05 3.1836**+02 | 1.0000 1.0000 5.0561**+01 | 3.4203**+04 3.5846**+04 2.7510**+03 | 2.0560**+03 0.0000**+00 0.0000**+00 | 1.4230 1.8052 0.0124 | 1.2816 1.8041 2.8101**+03 | 9.9766**+04 3.1618**+02 2.0519**+02 | 9.9766**+04 2.9741**+02 3.1618**+02 | |
| 780150304 0.0000**+00 INFINITE | 0.5927 1.2690**+05 3.2370**+02 | 1.0000 1.0000 5.0807**+01 | 3.5067**+04 3.6741**+04 2.8756**+03 | 2.0650**+03 0.0000**+00 0.0000**+00 | 1.4198 1.8063 0.0123 | 1.2788 1.8052 2.9369**+03 | 1.0006**+05 3.2149**+02 2.0666**+02 | 1.0006**+05 3.0245**+02 3.2149**+02 | |
| 780150305 7.6200**+02 INFINITE | 0.5917 1.2660**+05 3.2442**+02 | 1.0000 1.0000 4.9964**+01 | 3.5613**+04 3.7306**+04 2.9386**+03 | 2.0410**+03 0.0000**+00 0.0000**+00 | 1.4171 1.8057 0.0123 | 1.2766 1.8047 3.0013**+03 | 9.9902**+04 3.2221**+02 2.0656**+02 | 9.9902**+04 3.0319**+02 3.2221**+02 | |
| 780150401 -4.8430**+01 INFINITE | 0.7962 6.5710**+04 3.0889**+02 | 1.0000 1.0000 4.1014**+01 | 1.8153**+04 1.9736**+04 2.3451**+03 | 2.1360**+03 0.0000**+00 0.0000**+00 | 1.5834 1.7856 0.0209 | 1.3250 1.7834 2.4433**+03 | 4.3270**+04 3.0528**+02 2.6431**+02 | 4.3270**+04 2.7413**+02 3.0528**+02 | |
| 780150402 -2.6210**+01 INFINITE | 0.7835 6.6910**+04 3.1156**+02 | 1.0000 1.0000 4.0435**+01 | 1.9894**+04 2.1571**+04 2.5659**+03 | 2.1090**+03 0.0000**+00 0.0000**+00 | 1.5616 1.7904 0.0204 | 1.3123 1.7884 2.6682**+03 | 4.4611**+04 3.0802**+02 2.6170**+02 | 4.4611**+04 2.7749**+02 3.0802**+02 | |
| 780150403 -7.6200**+02 INFINITE | 0.8029 6.6910**+04 3.0695**+02 | 1.0000 1.0000 4.2107**+01 | 2.1588**+04 2.3505**+04 2.7094**+03 | 2.1320**+03 0.0000**+00 0.0000**+00 | 1.5533 1.7988 0.0214 | 1.2931 1.7968 2.8190**+03 | 4.3769**+04 3.0330**+02 2.6544**+02 | 4.3769**+04 2.7190**+02 3.0330**+02 | |
| 780150404 0.0000**+00 INFINITE | 0.7998 6.6650**+04 3.1205**+02 | 1.0000 1.0000 4.1517**+01 | 2.1832**+04 2.3749**+04 2.8123**+03 | 2.1200**+03 0.0000**+00 0.0000**+00 | 1.5520 1.7986 0.0212 | 1.2939 1.7966 2.9253**+03 | 4.3731**+04 3.0837**+02 2.6673**+02 | 4.3731**+04 2.7665**+02 3.0837**+02 | |
| 780150405 7.6200**+02 INFINITE | 0.7976 6.6380**+04 3.1132**+02 | 1.0000 1.0000 4.0916**+01 | 2.2763**+04 2.4751**+04 2.9382**+03 | 2.1050**+03 0.0000**+00 0.0000**+00 | 1.5518 1.7985 0.0211 | 1.2951 1.7965 3.0554**+03 | 4.3651**+04 3.0767**+02 2.6576**+02 | 4.3651**+04 2.7618**+02 3.0767**+02 | |
| 780150501 -4.8430**+01 INFINITE | 0.7947 1.3330**+05 3.2467**+02 | 1.0000 1.0000 7.9932**+01 | 3.0340**+04 3.2946**+04 2.0589**+03 | 2.0050**+03 0.0000**+00 0.0000**+00 | 1.5517 1.8012 0.0210 | 1.2970 1.7993 2.1396**+03 | 8.7905**+04 3.2088**+02 2.7053**+02 | 8.7905**+04 2.8826**+02 3.2088**+02 | |
| 780150502 -2.6210**+01 INFINITE | 0.7917 1.3340**+05 3.2831**+02 | 1.0000 1.0000 7.7153**+01 | 3.3617**+04 3.6473**+04 2.3148**+03 | 1.9930**+03 0.0000**+00 0.0000**+00 | 1.5376 1.8049 0.0209 | 1.2856 1.8032 2.4036**+03 | 8.8236**+04 3.2451**+02 2.7112**+02 | 8.8236**+04 2.9174**+02 3.2451**+02 | |
| 780150503 -7.6200**+02 INFINITE | 0.7913 1.3330**+05 3.2467**+02 | 1.0000 1.0000 7.6818**+01 | 3.6160**+04 3.9238**+04 2.4575**+03 | 1.9870**+03 0.0000**+00 0.0000**+00 | 1.5261 1.8090 0.0209 | 1.2753 1.8072 2.5497**+03 | 8.8203**+04 3.2091**+02 2.6950**+02 | 8.8203**+04 2.8854**+02 3.2091**+02 | |
| 780150504 0.0000**+00 INFINITE | 0.7888 1.3330**+05 3.2831**+02 | 1.0000 1.0000 7.6171**+01 | 3.7226**+04 4.0366**+04 2.5685**+03 | 1.9780**+03 0.0000**+00 0.0000**+00 | 1.5226 1.8101 0.0208 | 1.2736 1.8083 2.6638**+03 | 8.8423**+04 3.2453**+02 2.7023**+02 | 8.8423**+04 2.9198**+02 3.2453**+02 | |
| 780150505 7.6200**+02 INFINITE | 0.7900 1.3300**+05 3.2855**+02 | 1.0000 1.0000 7.5182**+01 | 3.9026**+04 4.2327**+04 2.6998**+03 | 1.9530**+03 0.0000**+00 0.0000**+00 | 1.5308 1.8069 0.0209 | 1.2803 1.8051 2.8018**+03 | 8.8117**+04 3.2476**+02 2.7070**+02 | 8.8117**+04 2.9209**+02 3.2476**+02 | |
| 780150601 -4.8430**+01 INFINITE | 0.9627 6.6110**+04 3.1059**+02 | 1.0000 1.0000 4.9860**+01 | 1.6335**+04 1.8418**+04 2.0264**+03 | 2.1080**+03 0.0000**+00 0.0000**+00 | 1.6986 1.7889 0.0291 | 1.3214 1.7858 2.1491**+03 | 3.6457**+04 3.0554**+02 3.1245**+02 | 3.6457**+04 2.6202**+02 3.0554**+02 | |
| 780150602 -2.6210**+01 INFINITE | 0.9617 6.6910**+04 3.1205**+02 | 1.0000 1.0000 4.9386**+01 | 1.8647**+04 2.1017**+04 2.2994**+03 | 2.0650**+03 0.0000**+00 0.0000**+00 | 1.6830 1.7925 0.0291 | 1.3079 1.7895 2.4364**+03 | 3.6942**+04 3.0698**+02 3.1290**+02 | 3.6942**+04 2.6334**+02 3.0698**+02 | |
| 780150603 -7.6200**+02 INFINITE | 0.9680 6.6380**+04 3.0938**+02 | 1.0000 1.0000 5.0049**+01 | 1.9597**+04 2.2126**+04 2.4081**+03 | 2.0970**+03 0.0000**+00 0.0000**+00 | 1.6681 1.8004 0.0296 | 1.2904 1.7976 2.5489**+03 | 3.6386**+04 3.0430**+02 3.1328**+02 | 3.6386**+04 2.6055**+02 3.0430**+02 | |
| 780150604 0.0000**+00 INFINITE | 0.9635 6.6650**+04 3.1277**+02 | 1.0000 1.0000 4.9661**+01 | 2.0075**+04 2.2635**+04 2.4919**+03 | 2.0810**+03 0.0000**+00 0.0000**+00 | 1.6731 1.7979 0.0293 | 1.2982 1.7950 2.6375**+03 | 3.6721**+04 3.0768**+02 3.1376**+02 | 3.6721**+04 2.6379**+02 3.0768**+02 | |
| 780150605 7.6200**+02 INFINITE | 0.9604 6.6650**+04 3.1205**+02 | 1.0000 1.0000 4.9180**+01 | 2.0713**+04 2.3338**+04 2.5644**+03 | 2.0670**+03 0.0000**+00 0.0000**+00 | 1.6701 1.7981 0.0291 | 1.2977 1.7952 2.7131**+03 | 3.6853**+04 3.0700**+02 3.1254**+02 | 3.6853**+04 2.6345**+02 3.0700**+02 | |

| CAT 7801S COLLINS/COLES/H BOUNDARY CONDITIONS AND EVALUATED DATA. SI UNITS | | | | | | | | | |
|--|------------------------------------|--------------------------------|--|--|----------------------------|--------------------------------|--|--|--|
| RUN X * RZ | MD * POD* TOD* | TW/TR* PW/PR* TAUM | RED2W RED2D DZ | CF * CO * PIZ* | H12 H32 H42 | H12K H32K D2K | Pw TW UD | PD TD TR | |
| 7801S0701 -4.8430*-01 INFINITE | 0.9606 1.3360*+05 3.2758*+02 | 1.0000 1.0000 9.3972*+01 | 2.8035*+04 3.1548*+04 1.8410*-03 | 1.9700*-03 0.0000*+00 0.0000*+00 | 1.6637 1.8036 0.0292 | 1.2922 1.8009 1.9455*-03 | 7.3857*+04 3.2227*+02 3.2027*+02 | 7.3857*+04 2.7655*+02 3.2227*+02 | |
| 7801S0702 -2.6210*-01 INFINITE | 0.9592 1.3270*+05 3.2976*+02 | 1.0000 1.0000 9.1802*+01 | 3.1944*+04 3.5929*+04 2.1298*-03 | 1.9400*-03 0.0000*+00 0.0000*+00 | 1.6536 1.8054 0.0292 | 1.2838 1.8028 2.2494*-03 | 7.3470*+04 3.2443*+02 3.2096*+02 | 7.3470*+04 2.7851*+02 3.2443*+02 | |
| 7801S0703 -7.6200*-02 INFINITE | 0.9577 1.3380*+05 3.2806*+02 | 1.0000 1.0000 9.3052*+01 | 3.4294*+04 3.8565*+04 2.2534*-03 | 1.9530*-03 0.0000*+00 0.0000*+00 | 1.6409 1.8106 0.0292 | 1.2736 1.8081 2.3767*-03 | 7.4204*+04 3.2277*+02 3.1971*+02 | 7.4204*+04 2.7201*+02 3.2277*+02 | |
| 7801S0704 0.0000*+00 INFINITE | 0.9608 1.3300*+05 3.3001*+02 | 1.0000 1.0000 9.1435*+01 | 3.5152*+04 3.9552*+04 2.3404*-03 | 1.9250*-03 0.0000*+00 0.0000*+00 | 1.6487 1.8092 0.0293 | 1.2787 1.8066 2.4698*-03 | 7.3504*+04 3.2466*+02 3.2153*+02 | 7.3504*+04 2.7858*+02 3.2466*+02 | |
| 7801S0705 7.6200*-02 INFINITE | 0.9577 1.3310*+05 3.3049*+02 | 1.0000 1.0000 9.0572*+01 | 3.6823*+04 4.1401*+04 2.4550*-03 | 1.9110*-03 0.0000*+00 0.0000*+00 | 1.6462 1.8082 0.0292 | 1.2785 1.8055 2.5904*-03 | 7.3818*+04 3.2516*+02 3.2089*+02 | 7.3818*+04 2.7926*+02 3.2516*+02 | |
| 7801S0801 -2.6210*-01 INFINITE | 1.3091 6.6910*+04 3.1253*+02 | 1.0000 1.0000 5.7225*+01 | 1.5679*+04 1.9631*+04 2.0800*-03 | 2.0000*-03 0.0000*+00 0.0000*+00 | 1.9952 1.7988 0.0478 | 1.3028 1.7936 2.3035*-03 | 2.3851*+04 3.0423*+02 4.0044*+02 | 2.3851*+04 2.3275*+02 3.0423*+02 | |
| 7801S0802 -7.6200*-02 INFINITE | 1.3163 6.6510*+04 3.1059*+02 | 1.0000 1.0000 5.6463*+01 | 1.6862*+04 2.0898*+04 2.2108*-03 | 1.9830*-03 0.0000*+00 0.0000*+00 | 2.0028 1.8007 0.0482 | 1.3035 1.7954 2.4486*-03 | 2.3475*+04 3.0228*+02 4.0083*+02 | 2.3475*+04 2.3675*+02 3.0228*+02 | |
| 7801S0803 0.0000*+00 INFINITE | 1.3147 6.6650*+04 3.1059*+02 | 1.0000 1.0000 5.6568*+01 | 1.7519*+04 2.1702*+04 2.2907*-03 | 1.9830*-03 0.0000*+00 0.0000*+00 | 1.9893 1.8033 0.0482 | 1.2934 1.7982 2.5341*-03 | 2.3578*+04 3.0229*+02 4.0046*+02 | 2.3578*+04 2.3081*+02 3.0229*+02 | |
| 7801S0804 7.6200*-02 INFINITE | 1.3108 6.6780*+04 3.0428*+02 | 1.0000 1.0000 5.5958*+01 | 1.8740*+04 2.3211*+04 2.3790*-03 | 1.9590*-03 0.0000*+00 0.0000*+00 | 1.9848 1.8035 0.0480 | 1.2931 1.7985 2.6301*-03 | 2.3751*+04 2.9619*+02 3.9549*+02 | 2.3751*+04 2.2646*+02 2.9619*+02 | |
| 7801S0901 -2.6210*-01 INFINITE | 1.3002 1.3330*+05 3.2467*+02 | 1.0000 1.0000 1.0495*+02 | 2.7331*+04 3.3641*+04 1.8795*-03 | 1.8440*-03 0.0000*+00 0.0000*+00 | 1.9655 1.8090 0.0475 | 1.2871 1.8042 2.0699*-03 | 4.8095*+04 3.1614*+02 4.0607*+02 | 4.8095*+04 2.4263*+02 3.1614*+02 | |
| 7801S0902 -7.6200*-02 INFINITE | 1.3128 1.3330*+05 3.2272*+02 | 1.0000 1.0000 1.0597*+02 | 2.9314*+04 3.6226*+04 2.0103*-03 | 1.8580*-03 0.0000*+00 0.0000*+00 | 1.9596 1.8156 0.0484 | 1.2714 1.8110 2.2117*-03 | 4.7276*+04 3.1412*+02 4.0777*+02 | 4.7276*+04 2.3999*+02 3.1412*+02 | |
| 7801S0903 0.0000*+00 INFINITE | 1.3069 1.3380*+05 3.2370*+02 | 1.0000 1.0000 1.0638*+02 | 2.9900*+04 3.6879*+04 2.0459*-03 | 1.8600*-03 0.0000*+00 0.0000*+00 | 1.9507 1.8163 0.0481 | 1.2691 1.8119 2.2485*-03 | 4.7841*+04 3.1513*+02 4.0701*+02 | 4.7841*+04 2.4128*+02 3.1513*+02 | |
| 7801S0904 7.6200*-02 INFINITE | 1.3076 1.3300*+05 3.1981*+02 | 1.0000 1.0000 1.0417*+02 | 3.1432*+04 3.8801*+04 2.1315*-03 | 1.8320*-03 0.0000*+00 0.0000*+00 | 1.9588 1.8141 0.0481 | 1.2754 1.8094 2.3446*-03 | 4.7506*+04 3.1133*+02 4.0473*+02 | 4.7506*+04 2.3831*+02 3.1133*+02 | |
| 7801S1001 -2.6210*-01 INFINITE | 2.1633 9.3310*+04 3.0865*+02 | 1.0000 1.0000 5.0139*+01 | 1.4113*+04 2.3400*+04 2.3219*-03 | 1.6560*-03 0.0000*+00 0.0000*+00 | 3.1555 1.8156 0.0913 | 1.2847 1.8039 2.9512*-03 | 9.2424*+03 2.9313*+02 5.4766*+02 | 9.2424*+03 1.5943*+02 2.9313*+02 | |
| 7801S1002 -7.6200*-02 INFINITE | 2.1540 9.3310*+04 3.1107*+02 | 1.0000 1.0000 5.0223*+01 | 1.4380*+04 2.3739*+04 2.3705*-03 | 1.6490*-03 0.0000*+00 0.0000*+00 | 3.1349 1.8161 0.0909 | 1.2812 1.8047 3.0064*-03 | 9.3772*+03 2.9550*+02 5.4858*+02 | 9.3772*+03 1.6135*+02 2.9550*+02 | |
| 7801S1003 0.0000*+00 INFINITE | 2.1564 9.3310*+04 3.0986*+02 | 1.0000 1.0000 4.9660*+01 | 1.5270*+04 2.5241*+04 2.5098*-03 | 1.6330*-03 0.0000*+00 0.0000*+00 | 3.1414 1.8159 0.0910 | 1.2832 1.8043 3.1846*-03 | 9.3425*+03 2.9433*+02 5.4783*+02 | 9.3425*+03 1.6055*+02 2.9433*+02 | |
| 7801S1004 7.6200*-02 INFINITE | 2.1655 9.3310*+04 3.1205*+02 | 1.0000 1.0000 4.9102*+01 | 1.5331*+04 2.5409*+04 2.5624*-03 | 1.6240*-03 0.0000*+00 0.0000*+00 | 3.1561 1.8160 0.0914 | 1.2824 1.8045 3.2571*-03 | 9.2110*+03 2.9634*+02 5.5095*+02 | 9.2110*+03 1.6103*+02 2.9634*+02 | |
| 7801S1101 -2.6210*-01 INFINITE | 2.1725 1.7990*+05 3.2418*+02 | 1.0000 1.0000 8.9019*+01 | 2.3615*+04 3.9076*+04 2.1618*-03 | 1.5340*-03 0.0000*+00 0.0000*+00 | 3.1351 1.8268 0.0923 | 1.2631 1.8158 2.7215*-03 | 1.7565*+04 3.0781*+02 5.6249*+02 | 1.7565*+04 1.6677*+02 3.0781*+02 | |
| 7801S1102 -7.6200*-02 INFINITE | 2.1626 1.8020*+05 3.2127*+02 | 1.0000 1.0000 8.9499*+01 | 2.4358*+04 4.0196*+04 2.1822*-03 | 1.5300*-03 0.0000*+00 0.0000*+00 | 3.1194 1.8264 0.0918 | 1.2638 1.8156 2.7432*-03 | 1.7868*+04 3.0512*+02 5.5865*+02 | 1.7868*+04 1.6600*+02 3.0512*+02 | |
| 7801S1103 0.0000*+00 INFINITE | 2.1752 1.7980*+05 3.2127*+02 | 1.0000 1.0000 8.8406*+01 | 2.5037*+04 4.1513*+04 2.2727*-03 | 1.5270*-03 0.0000*+00 0.0000*+00 | 3.1300 1.8288 0.0925 | 1.2563 1.8183 2.8571*-03 | 1.7480*+04 3.0502*+02 5.6033*+02 | 1.7480*+04 1.6506*+02 3.0502*+02 | |
| 7801S1104 7.6200*-02 INFINITE | 2.1736 1.8020*+05 3.2272*+02 | 1.0000 1.0000 8.7535*+01 | 2.6165*+04 4.3335*+04 2.3799*-03 | 1.5070*-03 0.0000*+00 0.0000*+00 | 3.1331 1.8268 0.0923 | 1.2598 1.8162 2.9972*-03 | 1.7563*+04 3.0641*+02 5.6137*+02 | 1.7563*+04 1.6593*+02 3.0641*+02 | |

| 7801S0301 | | COLLINS/COLES/H | | PROFILE TABULATION | | 84 POINTS, DELTA AT POINT 69 | | | |
|-----------|------------|-----------------|------|--------------------|---------|------------------------------|---------|-----------|--|
| I | Y | PT2/P | P/PD | TO/TOD | M/MD | U/UD | T/TD | R/RD*U/UD | |
| 1 | 0.0000"+00 | 1.0000"+00 | NM | 0.99314 | 0.00000 | 0.00000 | 1.06327 | 0.00000 | |
| 2 | 1.0000"-04 | 1.0515"+00 | NM | 0.99461 | 0.45225 | 0.46335 | 1.04969 | 0.44142 | |
| 3 | 2.2000"-04 | 1.0718"+00 | NM | 0.99517 | 0.53237 | 0.54409 | 1.04454 | 0.52089 | |
| 4 | 3.8000"-04 | 1.0824"+00 | NM | 0.99546 | 0.56926 | 0.58107 | 1.04191 | 0.55769 | |
| 5 | 5.2000"-04 | 1.0903"+00 | NM | 0.99567 | 0.59509 | 0.60687 | 1.03997 | 0.58355 | |
| 6 | 7.4000"-04 | 1.0995"+00 | NM | 0.99591 | 0.62384 | 0.63550 | 1.03772 | 0.61240 | |
| 7 | 9.1000"-04 | 1.1030"+00 | NM | 0.99600 | 0.63420 | 0.64579 | 1.03688 | 0.62282 | |
| 8 | 1.0200"-03 | 1.1096"+00 | NM | 0.99617 | 0.65340 | 0.66483 | 1.03530 | 0.64216 | |
| 9 | 1.3400"-03 | 1.1141"+00 | NM | 0.99629 | 0.66647 | 0.67777 | 1.03421 | 0.65535 | |
| 10 | 1.5100"-03 | 1.1157"+00 | NM | 0.99633 | 0.67079 | 0.68204 | 1.03384 | 0.65972 | |
| 11 | 1.6300"-03 | 1.1224"+00 | NM | 0.99650 | 0.68928 | 0.70031 | 1.03224 | 0.67843 | |
| 12 | 1.8100"-03 | 1.1232"+00 | NM | 0.99652 | 0.69140 | 0.70239 | 1.03206 | 0.68057 | |
| 13 | 1.9400"-03 | 1.1259"+00 | NM | 0.99659 | 0.69863 | 0.70952 | 1.03142 | 0.68791 | |
| 14 | 2.1900"-03 | 1.1307"+00 | NM | 0.99672 | 0.71130 | 0.72199 | 1.03029 | 0.70077 | |
| 15 | 2.4000"-03 | 1.1292"+00 | NM | 0.99668 | 0.70718 | 0.71794 | 1.03066 | 0.69658 | |
| 16 | 2.5500"-03 | 1.1357"+00 | NM | 0.99684 | 0.72407 | 0.73454 | 1.02913 | 0.71374 | |
| 17 | 2.8300"-03 | 1.1366"+00 | NM | 0.99686 | 0.72638 | 0.73681 | 1.02892 | 0.71610 | |
| 18 | 3.1300"-03 | 1.1407"+00 | NM | 0.99697 | 0.73683 | 0.74706 | 1.02796 | 0.72674 | |
| 19 | 3.3100"-03 | 1.1434"+00 | NM | 0.99704 | 0.74347 | 0.75356 | 1.02734 | 0.73351 | |
| 20 | 3.5900"-03 | 1.1457"+00 | NM | 0.99709 | 0.74910 | 0.75907 | 1.02681 | 0.73925 | |
| 21 | 3.9400"-03 | 1.1484"+00 | NM | 0.99716 | 0.75573 | 0.76556 | 1.02619 | 0.74602 | |
| 22 | 4.1400"-03 | 1.1507"+00 | NM | 0.99722 | 0.76136 | 0.77106 | 1.02565 | 0.75178 | |
| 23 | 4.4900"-03 | 1.1538"+00 | NM | 0.99729 | 0.76870 | 0.77823 | 1.02495 | 0.75928 | |
| 24 | 4.8100"-03 | 1.1570"+00 | NM | 0.99737 | 0.77624 | 0.78558 | 1.02422 | 0.76700 | |
| 25 | 5.0900"-03 | 1.1600"+00 | NM | 0.99745 | 0.78317 | 0.79234 | 1.02355 | 0.77411 | |
| 26 | 5.4900"-03 | 1.1628"+00 | NM | 0.99752 | 0.78981 | 0.79880 | 1.02290 | 0.78092 | |
| 27 | 5.7500"-03 | 1.1673"+00 | NM | 0.99763 | 0.79996 | 0.80867 | 1.02189 | 0.79134 | |
| 28 | 6.0500"-03 | 1.1681"+00 | NM | 0.99764 | 0.80167 | 0.81033 | 1.02172 | 0.79310 | |
| 29 | 6.4000"-03 | 1.1696"+00 | NM | 0.99768 | 0.80519 | 0.81375 | 1.02137 | 0.79672 | |
| 30 | 6.7000"-03 | 1.1718"+00 | NM | 0.99774 | 0.81001 | 0.81843 | 1.02089 | 0.80168 | |
| 31 | 7.0600"-03 | 1.1749"+00 | NM | 0.99781 | 0.81695 | 0.82515 | 1.02019 | 0.80882 | |
| 32 | 7.3000"-03 | 1.1777"+00 | NM | 0.99788 | 0.82308 | 0.83109 | 1.01957 | 0.81514 | |
| 33 | 7.6900"-03 | 1.1815"+00 | NM | 0.99797 | 0.83142 | 0.83917 | 1.01872 | 0.82375 | |
| 34 | 8.0200"-03 | 1.1839"+00 | NM | 0.99803 | 0.83645 | 0.84403 | 1.01820 | 0.82894 | |
| 35 | 8.3600"-03 | 1.1851"+00 | NM | 0.99806 | 0.83906 | 0.84655 | 1.01793 | 0.83164 | |
| 36 | 8.8200"-03 | 1.1894"+00 | NM | 0.99816 | 0.84831 | 0.85548 | 1.01697 | 0.84121 | |
| 37 | 9.3000"-03 | 1.1915"+00 | NM | 0.99821 | 0.85253 | 0.85955 | 1.01652 | 0.84558 | |
| 38 | 9.7500"-03 | 1.1973"+00 | NM | 0.99835 | 0.86470 | 0.87126 | 1.01524 | 0.85818 | |
| 39 | 1.0240"-02 | 1.2000"+00 | NM | 0.99841 | 0.87023 | 0.87658 | 1.01465 | 0.86392 | |
| 40 | 1.0650"-02 | 1.2018"+00 | NM | 0.99845 | 0.87394 | 0.88015 | 1.01426 | 0.86778 | |
| 41 | 1.1030"-02 | 1.2066"+00 | NM | 0.99857 | 0.88349 | 0.88932 | 1.01323 | 0.87771 | |
| 42 | 1.1670"-02 | 1.2096"+00 | NM | 0.99864 | 0.88963 | 0.89520 | 1.01257 | 0.88409 | |
| 43 | 1.2050"-02 | 1.2114"+00 | NM | 0.99868 | 0.89314 | 0.89857 | 1.01218 | 0.88775 | |
| 44 | 1.2400"-02 | 1.2158"+00 | NM | 0.99878 | 0.90169 | 0.90675 | 1.01125 | 0.89666 | |
| 45 | 1.2800"-02 | 1.2189"+00 | NM | 0.99885 | 0.90772 | 0.91251 | 1.01059 | 0.90295 | |
| 46 | 1.3240"-02 | 1.2208"+00 | NM | 0.99890 | 0.91144 | 0.91606 | 1.01018 | 0.90684 | |
| 47 | 1.3650"-02 | 1.2236"+00 | NM | 0.99896 | 0.91687 | 0.92125 | 1.00957 | 0.91251 | |
| 48 | 1.4100"-02 | 1.2266"+00 | NM | 0.99903 | 0.92250 | 0.92661 | 1.00895 | 0.91840 | |
| 49 | 1.4370"-02 | 1.2298"+00 | NM | 0.99910 | 0.92863 | 0.93246 | 1.00826 | 0.92482 | |
| 50 | 1.4820"-02 | 1.2301"+00 | NM | 0.99911 | 0.92913 | 0.93293 | 1.00820 | 0.92534 | |
| 51 | 1.5220"-02 | 1.2346"+00 | NM | 0.99921 | 0.93758 | 0.94097 | 1.00725 | 0.93420 | |
| 52 | 1.5810"-02 | 1.2363"+00 | NM | 0.99925 | 0.94059 | 0.94383 | 1.00691 | 0.93736 | |
| 53 | 1.6210"-02 | 1.2395"+00 | NM | 0.99932 | 0.94652 | 0.94947 | 1.00623 | 0.94359 | |
| 54 | 1.6770"-02 | 1.2431"+00 | NM | 0.99941 | 0.95316 | 0.95576 | 1.00547 | 0.95056 | |
| 55 | 1.7380"-02 | 1.2459"+00 | NM | 0.99947 | 0.95818 | 0.96053 | 1.00490 | 0.95585 | |
| 56 | 1.7830"-02 | 1.2475"+00 | NM | 0.99950 | 0.96100 | 0.96319 | 1.00457 | 0.95881 | |
| 57 | 1.8470"-02 | 1.2547"+00 | NM | 0.99967 | 0.97386 | 0.97536 | 1.00308 | 0.97237 | |
| 58 | 1.9110"-02 | 1.2582"+00 | NM | 0.99974 | 0.98000 | 0.98115 | 1.00236 | 0.97884 | |
| 59 | 1.9670"-02 | 1.2587"+00 | NM | 0.99976 | 0.98100 | 0.98210 | 1.00224 | 0.97990 | |
| 60 | 2.0150"-02 | 1.2609"+00 | NM | 0.99980 | 0.98472 | 0.98561 | 1.00181 | 0.98383 | |
| 61 | 2.0700"-02 | 1.2626"+00 | NM | 0.99984 | 0.98774 | 0.98845 | 1.00145 | 0.98702 | |
| 62 | 2.1120"-02 | 1.2639"+00 | NM | 0.99987 | 0.99005 | 0.99063 | 1.00118 | 0.98946 | |
| 63 | 2.1600"-02 | 1.2657"+00 | NM | 0.99991 | 0.99306 | 0.99347 | 1.00082 | 0.99266 | |
| 64 | 2.1950"-02 | 1.2662"+00 | NM | 0.99992 | 0.99397 | 0.99432 | 1.00072 | 0.99361 | |
| 65 | 2.2330"-02 | 1.2672"+00 | NM | 0.99994 | 0.99568 | 0.99593 | 1.00051 | 0.99542 | |
| 66 | 2.2740"-02 | 1.2683"+00 | NM | 0.99997 | 0.99759 | 0.99773 | 1.00029 | 0.99744 | |
| 67 | 2.3200"-02 | 1.2682"+00 | NM | 0.99997 | 0.99729 | 0.99745 | 1.00032 | 0.99713 | |
| 68 | 2.3680"-02 | 1.2707"+00 | NM | 1.00000 | 1.00161 | 1.00151 | 0.99981 | 1.00170 | |
| D 69 | 2.4210"-02 | 1.2697"+00 | NM | 1.00000 | 1.00000 | 1.00000 | 1.00000 | 1.00000 | |
| 70 | 2.4590"-02 | 1.2715"+00 | NM | 1.00004 | 1.00292 | 1.00274 | 0.99965 | 1.00309 | |
| 71 | 2.5550"-02 | 1.2713"+00 | NM | 1.00003 | 1.00261 | 1.00246 | 0.99969 | 1.00277 | |
| 72 | 2.6470"-02 | 1.2735"+00 | NM | 1.00008 | 1.00643 | 1.00605 | 0.99923 | 1.00682 | |
| 73 | 2.7590"-02 | 1.2739"+00 | NM | 1.00009 | 1.00714 | 1.00671 | 0.99915 | 1.00757 | |
| 74 | 2.8560"-02 | 1.2732"+00 | NM | 1.00008 | 1.00583 | 1.00548 | 0.99930 | 1.00618 | |
| 75 | 2.9540"-02 | 1.2730"+00 | NM | 1.00007 | 1.00553 | 1.00520 | 0.99934 | 1.00586 | |
| 76 | 3.0370"-02 | 1.2735"+00 | NM | 1.00008 | 1.00643 | 1.00605 | 0.99923 | 1.00682 | |
| 77 | 3.1380"-02 | 1.2728"+00 | NM | 1.00007 | 1.00523 | 1.00491 | 0.99938 | 1.00554 | |
| 78 | 3.2190"-02 | 1.2730"+00 | NM | 1.00007 | 1.00553 | 1.00520 | 0.99934 | 1.00586 | |
| 79 | 3.2980"-02 | 1.2738"+00 | NM | 1.00009 | 1.00684 | 1.00642 | 0.99918 | 1.00725 | |
| 80 | 3.3740"-02 | 1.2720"+00 | NM | 1.00005 | 1.00392 | 1.00369 | 0.99953 | 1.00416 | |
| 81 | 3.4550"-02 | 1.2732"+00 | NM | 1.00008 | 1.00583 | 1.00548 | 0.99930 | 1.00618 | |
| 82 | 3.5310"-02 | 1.2726"+00 | NM | 1.00006 | 1.00483 | 1.00454 | 0.99942 | 1.00511 | |
| 83 | 3.6180"-02 | 1.2716"+00 | NM | 1.00004 | 1.00322 | 1.00302 | 0.99962 | 1.00341 | |
| 84 | 3.7090"-02 | 1.2732"+00 | NM | 1.00008 | 1.00583 | 1.00548 | 0.99930 | 1.00618 | |

INPUT VARIABLES Y,M/MD ASSUME P=PD ASSUME VAN DRIEST

| 7801S0801 | | COLLINS/COLES/H | | PROFILE TABULATION | | 82 POINTS, DELTA AT POINT 67 | | | |
|-----------|-----------|-----------------|------|--------------------|---------|------------------------------|---------|-----------|--|
| I | Y | PT2/P | P/PD | TO/TOD | M/MD | U/UD | T/TD | R/RD*U/UD | |
| 1 | 0.0000+00 | 1.0000+00 | NM | 0.97345 | 0.00000 | 0.00000 | 1.30711 | 0.00000 | |
| 2 | 1.0000-04 | 1.2069+00 | NM | 0.97878 | 0.40133 | 0.44789 | 1.24550 | 0.35960 | |
| 3 | 1.7000-04 | 1.2725+00 | NM | 0.98024 | 0.45603 | 0.50548 | 1.22864 | 0.41142 | |
| 4 | 3.4000-04 | 1.3440+00 | NM | 0.98172 | 0.50713 | 0.55817 | 1.21143 | 0.46075 | |
| 5 | 4.3000-04 | 1.3930+00 | NM | 0.98269 | 0.53835 | 0.58980 | 1.20028 | 0.49138 | |
| 6 | 6.6000-04 | 1.4472+00 | NM | 0.98371 | 0.57007 | 0.62147 | 1.18849 | 0.52291 | |
| 7 | 1.0000-03 | 1.4940+00 | NM | 0.98455 | 0.59546 | 0.64650 | 1.17875 | 0.54846 | |
| 8 | 1.1900-03 | 1.5260+00 | NM | 0.98511 | 0.61193 | 0.66255 | 1.17230 | 0.56517 | |
| 9 | 1.4800-03 | 1.5702+00 | NM | 0.98585 | 0.63361 | 0.68349 | 1.16364 | 0.58737 | |
| 10 | 1.7100-03 | 1.5903+00 | NM | 0.98618 | 0.64304 | 0.69253 | 1.15982 | 0.59710 | |
| 11 | 2.1300-03 | 1.6266+00 | NM | 0.98677 | 0.65961 | 0.70828 | 1.15304 | 0.61427 | |
| 12 | 2.4500-03 | 1.6547+00 | NM | 0.98721 | 0.67195 | 0.71994 | 1.14793 | 0.62716 | |
| 13 | 2.8500-03 | 1.6892+00 | NM | 0.98774 | 0.68661 | 0.73368 | 1.14180 | 0.64256 | |
| 14 | 3.2300-03 | 1.7175+00 | NM | 0.98817 | 0.69825 | 0.74451 | 1.13688 | 0.65487 | |
| 15 | 3.7000-03 | 1.7464+00 | NM | 0.98859 | 0.70980 | 0.75518 | 1.13196 | 0.66714 | |
| 16 | 4.0600-03 | 1.7816+00 | NM | 0.98910 | 0.72345 | 0.76771 | 1.12610 | 0.68174 | |
| 17 | 4.3900-03 | 1.7882+00 | NM | 0.98919 | 0.72596 | 0.77000 | 1.12507 | 0.68443 | |
| 18 | 4.8600-03 | 1.8180+00 | NM | 0.98961 | 0.73710 | 0.78014 | 1.12019 | 0.69643 | |
| 19 | 5.2300-03 | 1.8502+00 | NM | 0.99005 | 0.74885 | 0.79076 | 1.11507 | 0.70915 | |
| 20 | 5.6100-03 | 1.8711+00 | NM | 0.99033 | 0.75627 | 0.79744 | 1.11182 | 0.71724 | |
| 21 | 5.9300-03 | 1.8939+00 | NM | 0.99064 | 0.76420 | 0.80453 | 1.10933 | 0.72590 | |
| 22 | 6.2200-03 | 1.9221+00 | NM | 0.99100 | 0.77384 | 0.81311 | 1.10406 | 0.73647 | |
| 23 | 6.7800-03 | 1.9509+00 | NM | 0.99137 | 0.78348 | 0.82164 | 1.09978 | 0.74709 | |
| 24 | 7.1500-03 | 1.9680+00 | NM | 0.99159 | 0.78910 | 0.82659 | 1.09728 | 0.75331 | |
| 25 | 7.5000-03 | 1.9956+00 | NM | 0.99194 | 0.79803 | 0.83442 | 1.09328 | 0.76323 | |
| 26 | 7.8800-03 | 2.0269+00 | NM | 0.99232 | 0.80797 | 0.84309 | 1.08882 | 0.77432 | |
| 27 | 8.2800-03 | 2.0413+00 | NM | 0.99250 | 0.81249 | 0.84701 | 1.08678 | 0.77937 | |
| 28 | 8.7100-03 | 2.0680+00 | NM | 0.99282 | 0.82072 | 0.85412 | 1.08306 | 0.78862 | |
| 29 | 9.0100-03 | 2.0861+00 | NM | 0.99300 | 0.82624 | 0.85888 | 1.08056 | 0.79484 | |
| 30 | 9.4100-03 | 2.1144+00 | NM | 0.99337 | 0.83477 | 0.86619 | 1.07669 | 0.80449 | |
| 31 | 9.8000-03 | 2.1390+00 | NM | 0.99366 | 0.84210 | 0.87244 | 1.07335 | 0.81282 | |
| 32 | 1.0180-02 | 2.1678+00 | NM | 0.99399 | 0.85053 | 0.87959 | 1.06950 | 0.82243 | |
| 33 | 1.0590-02 | 2.1806+00 | NM | 0.99414 | 0.85425 | 0.88273 | 1.06780 | 0.82668 | |
| 34 | 1.0890-02 | 2.1991+00 | NM | 0.99435 | 0.85957 | 0.88722 | 1.06537 | 0.83278 | |
| 35 | 1.1210-02 | 2.2192+00 | NM | 0.99458 | 0.86529 | 0.89202 | 1.06274 | 0.83936 | |
| 36 | 1.1580-02 | 2.2398+00 | NM | 0.99481 | 0.87111 | 0.89689 | 1.06007 | 0.84607 | |
| 37 | 1.2000-02 | 2.2664+00 | NM | 0.99510 | 0.87854 | 0.90308 | 1.05665 | 0.85467 | |
| 38 | 1.2290-02 | 2.2896+00 | NM | 0.99536 | 0.88496 | 0.90841 | 1.05368 | 0.86213 | |
| 39 | 1.2590-02 | 2.3031+00 | NM | 0.99551 | 0.88868 | 0.91148 | 1.05197 | 0.86645 | |
| 40 | 1.2950-02 | 2.3241+00 | NM | 0.99574 | 0.89440 | 0.91619 | 1.04932 | 0.87313 | |
| 41 | 1.3250-02 | 2.3423+00 | NM | 0.99593 | 0.89932 | 0.92023 | 1.04704 | 0.87888 | |
| 42 | 1.3630-02 | 2.3576+00 | NM | 0.99610 | 0.90343 | 0.92360 | 1.04514 | 0.88371 | |
| 43 | 1.4040-02 | 2.3833+00 | NM | 0.99637 | 0.91026 | 0.92916 | 1.04197 | 0.89174 | |
| 44 | 1.4470-02 | 2.4088+00 | NM | 0.99664 | 0.91698 | 0.93462 | 1.03884 | 0.89968 | |
| 45 | 1.4930-02 | 2.4268+00 | NM | 0.99683 | 0.92170 | 0.93844 | 1.03665 | 0.90526 | |
| 46 | 1.5260-02 | 2.4554+00 | NM | 0.99713 | 0.92913 | 0.94442 | 1.03319 | 0.91409 | |
| 47 | 1.5620-02 | 2.4714+00 | NM | 0.99730 | 0.93325 | 0.94772 | 1.03127 | 0.91899 | |
| 48 | 1.6000-02 | 2.4898+00 | NM | 0.99749 | 0.93796 | 0.95150 | 1.02907 | 0.92462 | |
| 49 | 1.6370-02 | 2.5044+00 | NM | 0.99764 | 0.94168 | 0.95446 | 1.02733 | 0.92907 | |
| 50 | 1.6680-02 | 2.5258+00 | NM | 0.99786 | 0.94710 | 0.95877 | 1.02480 | 0.93557 | |
| 51 | 1.7090-02 | 2.5502+00 | NM | 0.99810 | 0.95322 | 0.96362 | 1.02194 | 0.94294 | |
| 52 | 1.7520-02 | 2.5676+00 | NM | 0.99828 | 0.95754 | 0.96703 | 1.01992 | 0.94814 | |
| 53 | 1.7930-02 | 2.5833+00 | NM | 0.99844 | 0.96145 | 0.97011 | 1.01804 | 0.95288 | |
| 54 | 1.8330-02 | 2.6098+00 | NM | 0.99870 | 0.96798 | 0.97522 | 1.01503 | 0.96079 | |
| 55 | 1.8790-02 | 2.6238+00 | NM | 0.99884 | 0.97139 | 0.97789 | 1.01343 | 0.96493 | |
| 56 | 1.9220-02 | 2.6357+00 | NM | 0.99896 | 0.97430 | 0.98016 | 1.01206 | 0.96848 | |
| 57 | 1.9730-02 | 2.6564+00 | NM | 0.99916 | 0.97932 | 0.98406 | 1.00971 | 0.97460 | |
| 58 | 2.0100-02 | 2.6722+00 | NM | 0.99932 | 0.98314 | 0.98702 | 1.00792 | 0.97927 | |
| 59 | 2.0470-02 | 2.6914+00 | NM | 0.99950 | 0.98775 | 0.99059 | 1.00575 | 0.98492 | |
| 60 | 2.0980-02 | 2.6965+00 | NM | 0.99955 | 0.98896 | 0.99152 | 1.00519 | 0.98640 | |
| 61 | 2.1310-02 | 2.7099+00 | NM | 0.99968 | 0.99217 | 0.99399 | 1.00368 | 0.99035 | |
| 62 | 2.1690-02 | 2.7150+00 | NM | 0.99973 | 0.99337 | 0.99492 | 1.00311 | 0.99183 | |
| 63 | 2.2000-02 | 2.7234+00 | NM | 0.99981 | 0.99538 | 0.99646 | 1.00217 | 0.99430 | |
| 64 | 2.2400-02 | 2.7285+00 | NM | 0.99986 | 0.99659 | 0.99739 | 1.00160 | 0.99579 | |
| 65 | 2.2610-02 | 2.7294+00 | NM | 0.99987 | 0.99679 | 0.99754 | 1.00151 | 0.99604 | |
| 66 | 2.3020-02 | 2.7328+00 | NM | 0.99990 | 0.99759 | 0.99816 | 1.00113 | 0.99703 | |
| 67 | 2.3340-02 | 2.7430+00 | NM | 1.00000 | 1.00000 | 1.00000 | 1.00000 | 1.00000 | |
| 68 | 2.3640-02 | 2.7459+00 | NM | 1.00003 | 1.00070 | 1.00054 | 0.99967 | 1.00087 | |
| 69 | 2.4330-02 | 2.7540+00 | NM | 1.00011 | 1.00261 | 1.00199 | 0.99877 | 1.00323 | |
| 70 | 2.5130-02 | 2.7579+00 | NM | 1.00014 | 1.00351 | 1.00268 | 0.99835 | 1.00434 | |
| 71 | 2.5950-02 | 2.7540+00 | NM | 1.00011 | 1.00261 | 1.00199 | 0.99877 | 1.00323 | |
| 72 | 2.6720-02 | 2.7536+00 | NM | 1.00010 | 1.00251 | 1.00192 | 0.99882 | 1.00310 | |
| 73 | 2.7590-02 | 2.7575+00 | NM | 1.00014 | 1.00341 | 1.00261 | 0.99840 | 1.00422 | |
| 74 | 2.8540-02 | 2.7613+00 | NM | 1.00018 | 1.00432 | 1.00330 | 0.99797 | 1.00534 | |
| 75 | 2.9360-02 | 2.7575+00 | NM | 1.00014 | 1.00341 | 1.00261 | 0.99840 | 1.00422 | |
| 76 | 3.0170-02 | 2.7622+00 | NM | 1.00018 | 1.00452 | 1.00345 | 0.99788 | 1.00559 | |
| 77 | 3.1030-02 | 2.7579+00 | NM | 1.00014 | 1.00351 | 1.00268 | 0.99835 | 1.00434 | |
| 78 | 3.1830-02 | 2.7622+00 | NM | 1.00018 | 1.00452 | 1.00345 | 0.99788 | 1.00559 | |
| 79 | 3.2490-02 | 2.7566+00 | NM | 1.00013 | 1.00321 | 1.00245 | 0.99849 | 1.00397 | |
| 80 | 3.3310-02 | 2.7557+00 | NM | 1.00012 | 1.00301 | 1.00230 | 0.99858 | 1.00372 | |
| 81 | 3.4150-02 | 2.7596+00 | NM | 1.00016 | 1.00391 | 1.00299 | 0.99816 | 1.00484 | |
| 82 | 3.5030-02 | 2.7596+00 | NM | 1.00016 | 1.00391 | 1.00299 | 0.99816 | 1.00484 | |

INPUT VARIABLES Y,M/MD ASSUME P=PD ASSUME VAN DRIEST

| 7801S1104 | | COLLINS/COLES/H | | PROFILE TABULATION | | 97 POINTS, DELTA AT POINT 90 | | |
|-----------|-------------|-----------------|------|--------------------|---------|------------------------------|---------|-----------|
| I | Y | PT2/P | P/PD | TC/TOD | M/MD | U/UD | T/TD | R/RD*U/UD |
| 1 | 0.0000**+00 | 1.0000**+00 | NH | 0.94947 | 0.00000 | 0.00000 | 1.84663 | 0.00000 |
| 2 | 1.0000**+04 | 1.4431**+00 | NH | 0.95940 | 0.34196 | 0.44327 | 1.68028 | 0.26340 |
| 3 | 1.6000**+04 | 1.5518**+00 | NH | 0.96127 | 0.37625 | 0.48316 | 1.64899 | 0.29300 |
| 4 | 3.6000**+04 | 1.8612**+00 | NH | 0.96581 | 0.45337 | 0.56860 | 1.57292 | 0.36149 |
| 5 | 5.8000**+04 | 2.0947**+00 | NH | 0.96867 | 0.49920 | 0.61645 | 1.52491 | 0.40425 |
| 6 | 8.5000**+04 | 2.2926**+00 | NH | 0.97087 | 0.53349 | 0.65079 | 1.44806 | 0.43734 |
| 7 | 1.0500**+03 | 2.4035**+00 | NH | 0.97204 | 0.55144 | 0.66826 | 1.46855 | 0.45505 |
| 8 | 1.3000**+03 | 2.5337**+00 | NH | 0.97335 | 0.57160 | 0.68747 | 1.44650 | 0.47526 |
| 9 | 1.5700**+03 | 2.5912**+00 | NH | 0.97392 | 0.56022 | 0.69555 | 1.43704 | 0.46402 |
| 10 | 1.8100**+03 | 2.6919**+00 | NH | 0.97489 | 0.59497 | 0.70919 | 1.47082 | 0.49914 |
| 11 | 2.1200**+03 | 2.7671**+00 | NH | 0.97559 | 0.60570 | 0.71897 | 1.40900 | 0.51027 |
| 12 | 2.4000**+03 | 2.8388**+00 | NH | 0.97625 | 0.61572 | 0.72800 | 1.39794 | 0.52077 |
| 13 | 2.6500**+03 | 2.9201**+00 | NH | 0.97698 | 0.62686 | 0.73789 | 1.38565 | 0.53253 |
| 14 | 2.9300**+03 | 2.9812**+00 | NH | 0.97753 | 0.63508 | 0.74512 | 1.37658 | 0.54129 |
| 15 | 3.3400**+03 | 3.0447**+00 | NH | 0.97808 | 0.64350 | 0.75245 | 1.36728 | 0.55033 |
| 16 | 3.6400**+03 | 3.1232**+00 | NH | 0.97875 | 0.65373 | 0.76125 | 1.35600 | 0.56139 |
| 17 | 4.0200**+03 | 3.1762**+00 | NH | 0.97920 | 0.66055 | 0.76706 | 1.34849 | 0.56483 |
| 18 | 4.5000**+03 | 3.2538**+00 | NH | 0.97985 | 0.67038 | 0.77534 | 1.33767 | 0.57962 |
| 19 | 4.9100**+03 | 3.3144**+00 | NH | 0.98035 | 0.67800 | 0.78170 | 1.32930 | 0.58805 |
| 20 | 5.2700**+03 | 3.3660**+00 | NH | 0.98076 | 0.68432 | 0.78692 | 1.32236 | 0.59509 |
| 21 | 5.7000**+03 | 3.4358**+00 | NH | 0.98132 | 0.69284 | 0.79390 | 1.31302 | 0.60464 |
| 22 | 6.0800**+03 | 3.5083**+00 | NH | 0.98189 | 0.70156 | 0.80097 | 1.30347 | 0.61449 |
| 23 | 6.4100**+03 | 3.5442**+00 | NH | 0.98218 | 0.70608 | 0.80460 | 1.29854 | 0.61962 |
| 24 | 6.8900**+03 | 3.6048**+00 | NH | 0.98263 | 0.71300 | 0.81012 | 1.29099 | 0.62752 |
| 25 | 7.3500**+03 | 3.6821**+00 | NH | 0.98322 | 0.72202 | 0.81725 | 1.28117 | 0.63789 |
| 26 | 7.6000**+03 | 3.7021**+00 | NH | 0.98337 | 0.72433 | 0.81906 | 1.27867 | 0.64056 |
| 27 | 8.0600**+03 | 3.7834**+00 | NH | 0.98397 | 0.73365 | 0.82632 | 1.26855 | 0.65138 |
| 28 | 8.5800**+03 | 3.8471**+00 | NH | 0.98444 | 0.74087 | 0.83188 | 1.26075 | 0.65983 |
| 29 | 8.8900**+03 | 3.8855**+00 | NH | 0.98472 | 0.74519 | 0.83517 | 1.25610 | 0.66490 |
| 30 | 9.3800**+03 | 3.9512**+00 | NH | 0.98519 | 0.75251 | 0.84073 | 1.24821 | 0.67354 |
| 31 | 9.8800**+03 | 4.0276**+00 | NH | 0.98573 | 0.76093 | 0.84705 | 1.23917 | 0.68356 |
| 32 | 1.0220**+02 | 4.0643**+00 | NH | 0.98598 | 0.76494 | 0.85004 | 1.23488 | 0.68836 |
| 33 | 1.0550**+02 | 4.1003**+00 | NH | 0.98623 | 0.76885 | 0.85294 | 1.23070 | 0.69305 |
| 34 | 1.1010**+02 | 4.1468**+00 | NH | 0.98655 | 0.77387 | 0.85664 | 1.22535 | 0.69909 |
| 35 | 1.1340**+02 | 4.2029**+00 | NH | 0.98693 | 0.77988 | 0.86104 | 1.21895 | 0.70638 |
| 36 | 1.1770**+02 | 4.2661**+00 | NH | 0.98736 | 0.78660 | 0.86591 | 1.21182 | 0.71456 |
| 37 | 1.2200**+02 | 4.3338**+00 | NH | 0.98781 | 0.79372 | 0.87103 | 1.20429 | 0.72327 |
| 38 | 1.2570**+02 | 4.3808**+00 | NH | 0.98812 | 0.79864 | 0.87454 | 1.19911 | 0.72932 |
| 39 | 1.2940**+02 | 4.4311**+00 | NH | 0.98844 | 0.80385 | 0.87823 | 1.19363 | 0.73577 |
| 40 | 1.3380**+02 | 4.4690**+00 | NH | 0.98869 | 0.80776 | 0.88099 | 1.18953 | 0.74062 |
| 41 | 1.3770**+02 | 4.5346**+00 | NH | 0.98911 | 0.81448 | 0.88569 | 1.18250 | 0.74900 |
| 42 | 1.4190**+02 | 4.5988**+00 | NH | 0.98951 | 0.82100 | 0.89021 | 1.17570 | 0.75717 |
| 43 | 1.4630**+02 | 4.6465**+00 | NH | 0.98981 | 0.82581 | 0.89352 | 1.17070 | 0.76324 |
| 44 | 1.5040**+02 | 4.7146**+00 | NH | 0.99023 | 0.83263 | 0.89818 | 1.16364 | 0.77187 |
| 45 | 1.5400**+02 | 4.7661**+00 | NH | 0.99055 | 0.83775 | 0.90164 | 1.15836 | 0.77838 |
| 46 | 1.5980**+02 | 4.8373**+00 | NH | 0.99098 | 0.84477 | 0.90636 | 1.15114 | 0.78736 |
| 47 | 1.6370**+02 | 4.8701**+00 | NH | 0.99119 | 0.84797 | 0.90850 | 1.14785 | 0.79148 |
| 48 | 1.6670**+02 | 4.8803**+00 | NH | 0.99124 | 0.84898 | 0.90917 | 1.14682 | 0.79277 |
| 49 | 1.7150**+02 | 4.9670**+00 | NH | 0.99175 | 0.85740 | 0.91474 | 1.13872 | 0.80355 |
| 50 | 1.7480**+02 | 4.9961**+00 | NH | 0.99192 | 0.86021 | 0.91658 | 1.13536 | 0.80730 |
| 51 | 1.7720**+02 | 5.0525**+00 | NH | 0.99225 | 0.86562 | 0.92012 | 1.12986 | 0.81436 |
| 52 | 1.8040**+02 | 5.0882**+00 | NH | 0.99246 | 0.86903 | 0.92233 | 1.12641 | 0.81892 |
| 53 | 1.8630**+02 | 5.1462**+00 | NH | 0.99279 | 0.87455 | 0.92588 | 1.12085 | 0.82606 |
| 54 | 1.8850**+02 | 5.1887**+00 | NH | 0.99303 | 0.87856 | 0.92846 | 1.11681 | 0.83135 |
| 55 | 1.9220**+02 | 5.2100**+00 | NH | 0.99315 | 0.88057 | 0.92974 | 1.11480 | 0.83400 |
| 56 | 1.9630**+02 | 5.2817**+00 | NH | 0.99355 | 0.88728 | 0.93400 | 1.10807 | 0.84291 |
| 57 | 1.9960**+02 | 5.3367**+00 | NH | 0.99385 | 0.89240 | 0.93722 | 1.10297 | 0.84972 |
| 58 | 2.0210**+02 | 5.3497**+00 | NH | 0.99393 | 0.89360 | 0.93797 | 1.10177 | 0.85133 |
| 59 | 2.0560**+02 | 5.3865**+00 | NH | 0.99413 | 0.89701 | 0.94010 | 1.09838 | 0.85590 |
| 60 | 2.1140**+02 | 5.4585**+00 | NH | 0.99452 | 0.90363 | 0.94421 | 1.09183 | 0.86479 |
| 61 | 2.1520**+02 | 5.5200**+00 | NH | 0.99485 | 0.90925 | 0.94767 | 1.08630 | 0.87238 |
| 62 | 2.1930**+02 | 5.5510**+00 | NH | 0.99501 | 0.91205 | 0.94938 | 1.08354 | 0.87619 |
| 63 | 2.2440**+02 | 5.6465**+00 | NH | 0.99552 | 0.92068 | 0.95462 | 1.07509 | 0.88794 |
| 64 | 2.2730**+02 | 5.6700**+00 | NH | 0.99564 | 0.92278 | 0.95569 | 1.07304 | 0.89082 |
| 65 | 2.3200**+02 | 5.7193**+00 | NH | 0.99590 | 0.92720 | 0.95854 | 1.06875 | 0.89688 |
| 66 | 2.3580**+02 | 5.7768**+00 | NH | 0.99619 | 0.93231 | 0.96159 | 1.06379 | 0.90392 |
| 67 | 2.3990**+02 | 5.8131**+00 | NH | 0.99638 | 0.93552 | 0.96349 | 1.06069 | 0.90836 |
| 68 | 2.4320**+02 | 5.8665**+00 | NH | 0.99665 | 0.94023 | 0.96627 | 1.05615 | 0.91490 |
| 69 | 2.4850**+02 | 5.8962**+00 | NH | 0.99680 | 0.94284 | 0.96780 | 1.05365 | 0.91852 |
| 70 | 2.5200**+02 | 5.9341**+00 | NH | 0.99699 | 0.94615 | 0.96973 | 1.05047 | 0.92314 |
| 71 | 2.5660**+02 | 6.0136**+00 | NH | 0.99738 | 0.95307 | 0.97375 | 1.04387 | 0.93283 |
| 72 | 2.6230**+02 | 6.0541**+00 | NH | 0.99758 | 0.95658 | 0.97577 | 1.04053 | 0.93776 |
| 73 | 2.6610**+02 | 6.0993**+00 | NH | 0.99780 | 0.96039 | 0.97796 | 1.03697 | 0.94314 |
| 74 | 2.7090**+02 | 6.1661**+00 | NH | 0.99812 | 0.96621 | 0.98127 | 1.03142 | 0.95137 |
| 75 | 2.7540**+02 | 6.1861**+00 | NH | 0.99827 | 0.96791 | 0.98223 | 1.02982 | 0.95380 |
| 76 | 2.7910**+02 | 6.2190**+00 | NH | 0.99838 | 0.97072 | 0.98382 | 1.02718 | 0.95779 |
| 77 | 2.8350**+02 | 6.2769**+00 | NH | 0.99865 | 0.97563 | 0.98658 | 1.02257 | 0.96490 |
| 78 | 2.8860**+02 | 6.3137**+00 | NH | 0.99883 | 0.97874 | 0.98832 | 1.01967 | 0.96926 |
| 79 | 2.9220**+02 | 6.3423**+00 | NH | 0.99896 | 0.98115 | 0.98966 | 1.01742 | 0.97271 |
| 80 | 2.9830**+02 | 6.3876**+00 | NH | 0.99917 | 0.98496 | 0.99177 | 1.01388 | 0.97819 |
| 81 | 3.0280**+02 | 6.4080**+00 | NH | 0.99927 | 0.98866 | 0.99271 | 1.01230 | 0.98065 |
| 82 | 3.0690**+02 | 6.4332**+00 | NH | 0.99938 | 0.98877 | 0.99387 | 1.01035 | 0.98369 |
| 83 | 3.1150**+02 | 6.4548**+00 | NH | 0.99948 | 0.99057 | 0.99496 | 1.00868 | 0.98630 |
| 84 | 3.1480**+02 | 6.4861**+00 | NH | 0.99963 | 0.99318 | 0.99629 | 1.00627 | 0.99008 |
| 85 | 3.1880**+02 | 6.4994**+00 | NH | 0.99969 | 0.99428 | 0.99689 | 1.00525 | 0.99168 |
| 86 | 3.2350**+02 | 6.5127**+00 | NH | 0.99975 | 0.99539 | 0.99749 | 1.00474 | 0.99328 |
| 87 | 3.2770**+02 | 6.5333**+00 | NH | 0.99984 | 0.99709 | 0.99842 | 1.00267 | 0.99576 |
| 88 | 3.3100**+02 | 6.5478**+00 | NH | 0.99991 | 0.99830 | 0.99908 | 1.00156 | 0.99752 |
| 89 | 3.3550**+02 | 6.5624**+00 | NH | 0.99997 | 0.99950 | 0.99973 | 1.00046 | 0.99927 |
| D 90 | 3.4060**+02 | 6.5684**+00 | NH | 1.00000 | 1.00000 | 1.00000 | 1.00000 | 1.00000 |
| 91 | 3.4370**+02 | 6.5745**+00 | NH | 1.00003 | 1.00050 | 1.00027 | 0.99954 | 1.00073 |
| 92 | 3.5020**+02 | 6.5855**+00 | NH | 1.00008 | 1.00140 | 1.00076 | 0.99871 | 1.00205 |
| 93 | 3.5340**+02 | 6.5928**+00 | NH | 1.00011 | 1.00201 | 1.00108 | 0.99816 | 1.00293 |
| 94 | 3.5800**+02 | 6.6001**+00 | NH | 1.00014 | 1.00261 | 1.00141 | 0.99761 | 1.00381 |
| 95 | 3.6320**+02 | 6.6013**+00 | NH | 1.00015 | 1.00271 | 1.00146 | 0.99752 | 1.00395 |
| 96 | 3.6890**+02 | 6.6086**+00 | NH | 1.00018 | 1.00331 | 1.00179 | 0.99697 | 1.00483 |
| 97 | 3.6910**+02 | 6.6081**+00 | NH | 1.00017 | 1.00311 | 1.00168 | 0.99715 | 1.00454 |

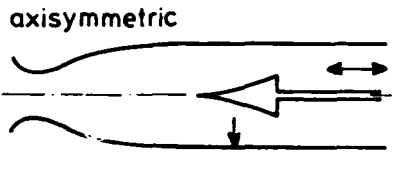
INPUT VARIABLES Y,M/MD ASSUME P=PD ASSUME VAN DRIEST

SECTION D: SUPPLEMENTARY DATA
 D.1. SKIN FRICTION DATA, FACSIMILE OF AUTHOR'S TABLE III
 AUTHOR'S SYMBOLS AND UNITS

CF FIT - curve fitting, Coles (1968).
 CF (H/K) - Preston tube, Hopkins and Keener (1966).
 CF (B/U) - Preston tube, Bradshaw and Unsworth (1974).

SKIN FRICTION SUMMARY

| IDENT CAT | STATION | ME | RE-TMETHA | CF | | | BALANCE | COMPUTED |
|--------------|---------|--------|-----------|---------|---------|------------------|---------|----------|
| | | | | 2*DTDX | FIT | PRESTON (H/K) | | |
| 7801 | CIT-1 | .1050 | 1029. | | | .004057 | .003911 | .004410 |
| | CIT-2 | .1050 | 1875. | | | .003458 | .003331 | .003703 |
| | CIT-3 | .1050 | 2798. | | | .003087 | .002982 | .003321 |
| 0101 | CIT-4 | .1058 | 5932. | | .002787 | .002630 | .002715 | .002826 |
| | CIT-5 | .1077 | 6209. | | .002786 | .002553 | .002637 | .002808 |
| | CIT-6 | .1031 | 6604. | .002768 | .002756 | .002683 | .002772 | .002782 |
| | CIT-7 | .1036 | 7270. | | .002689 | .002736 | .002825 | .002739 |
| | CIT-8 | .1052 | 7475. | | .002689 | .002611 | .002700 | .002725 |
| 0105 | CIT-9 | .1070 | 8068. | | .002676 | .002493 | .002575 | .002687 |
| 0201 | JPL-1 | .5927 | 18870. | | .002179 | | | .002249 |
| | JPL-2 | .5927 | 20180. | | .002201 | .002173 | .002169 | .002227 |
| | JPL-3 | .5986 | 22190. | | .002196 | | | .002194 |
| 0205 | JPL-4 | .4018 | 22400. | .002096 | .002198 | .002109 | .002106 | .002165 |
| | JPL-5 | .5962 | 22300. | | .002195 | | | .002192 |
| 0301 | JPL-1 | .5973 | 31460. | | .002090 | | | .002072 |
| | JPL-2 | .5964 | 34330. | | .002057 | .002012 | .002015 | .002048 |
| | JPL-3 | .5957 | 37280. | | .002056 | | | .002025 |
| 0305 | JPL-4 | .5931 | 36470. | .001992 | .002065 | .001983 | .001985 | .001994 |
| | JPL-5 | .5935 | 37930. | | .002041 | | | .002020 |
| 0401 | JPL-1 | .7958 | 19770. | | .002136 | | | .002177 |
| | JPL-2 | .7882 | 21850. | | .002109 | .002139 | .002090 | .002148 |
| | JPL-3 | .8049 | 23540. | | .002132 | | | .002117 |
| 0405 | JPL-4 | .8014 | 23710. | .002042 | .002120 | .002066 | .002027 | .002086 |
| | JPL-5 | .7995 | 24570. | | .002105 | | | .002103 |
| 0501 | JPL-1 | .7980 | 33940. | | .002005 | | | .001998 |
| | JPL-2 | .7943 | 37360. | | .001993 | .001971 | .001935 | .001974 |
| | JPL-3 | .7940 | 40190. | | .001987 | | | .001953 |
| 0505 | JPL-4 | .7921 | 41090. | .001942 | .001978 | .001920 | .001884 | .001942 |
| | JPL-5 | .7919 | 42600. | | .001953 | | | .001936 |
| 0601 | JPL-1 | .9664 | 18650. | | .002108 | | | .002144 |
| | JPL-2 | .9669 | 20890. | | .002065 | .002118 | .002024 | .002103 |
| | JPL-3 | .9719 | 22720. | | .002097 | | | .002076 |
| 0605 | JPL-4 | .9672 | 22840. | .002054 | .002081 | .002081 | .002008 | .002057 |
| | JPL-5 | .9651 | 23850. | | .002067 | | | .002062 |
| 0701 | JPL-1 | .9648 | 32330. | | .001970 | | | .001963 |
| | JPL-2 | .9626 | 36250. | | .001940 | .001932 | .001863 | .001930 |
| | JPL-3 | .9613 | 38500. | | .001953 | | | .001915 |
| 0705 | JPL-4 | .9637 | 39900. | .002014 | .001925 | .001870 | .001810 | .001947 |
| | JPL-5 | .9606 | 41550. | | .001911 | | | .001894 |
| 0801 | JPL-2 | 1.3141 | 19780. | | .002000 | .001906 | .001793 | .001994 |
| | JPL-3 | 1.3215 | 21880. | | .001983 | | | .001958 |
| | JPL-4 | 1.3197 | 21900. | .001854 | .001983 | .001913 | .001808 | .001867 |
| 0804 | JPL-5 | 1.3151 | 24190. | | .001959 | | | .001931 |
| 0901 | JPL-2 | 1.3082 | 37230. | | .001844 | .001778 | .001701 | .001802 |
| | JPL-3 | 1.3173 | 37550. | | .001858 | | | .001796 |
| | JPL-4 | 1.3125 | 37900. | .001750 | .001860 | .001802 | .001697 | .001788 |
| 0904 | JPL-5 | 1.3130 | 40210. | | .001832 | | | .001782 |
| 1001 | JPL-2 | 2.1722 | 23070. | | .001656 | .001740 | .001478 | .001607 |
| | JPL-3 | 2.1666 | 23520. | | .001649 | | | .001603 |
| | JPL-4 | 2.1642 | 24690. | .001532 | .001633 | .001683 | .001497 | .001532 |
| 1004 | JPL-5 | 2.1722 | 25060. | | .001624 | | | .001583 |
| 1101 | JPL-2 | 2.1812 | 38050. | | .001534 | .001613 | .001385 | .001476 |
| | JPL-3 | 2.1737 | 40570. | | .001530 | | | .001462 |
| | JPL-4 | 2.1820 | 41600. | .001444 | .001527 | .001573 | .001378 | .001454 |
| 1104 | JPL-5 | 2.1797 | 43060. | | .001507 | | | .001447 |

| | | |
|--|---|---------------|
|  | M: 2.3 (free stream) RE THETA $\times 10^{-3}$: 30 (upstream) TW/TR: 1 | 7802 |
| | | APG/FPG AW |
| Axisymmetric blowdown tunnel. Running time up to one hour. $D = 0.25$, $L = 2.70$ m. PO: 0.1 (0.03-0.9) MN/m ² . TO: 280K. Air. RE/m $\times 10^{-6}$: 35 (12-314). | | |
| KUSSOY M.I., HORSTMAN C.C., ACHARYA M., 1978. An experimental documentation of pressure gradient and Reynolds number effects on compressible turbulent boundary layers. NASA TM 78488. <u>And:</u> Horstman C.C., private communications. <u>Also:</u> Acharya et al. (1978) | | |

- 1 The test boundary layer was formed on the inner surface of a cylindrical test section ($D = 0.2477$, $L = 2.70$ m) attached to the exit of the axisymmetric nozzle. The surface roughness was approximately $0.4 \mu\text{m}$. One of six centre bodies could be stingmounted on the axis of the test section. These were designed to impose a shock free compression on the boundary layer, followed, where geometry allowed, by, firstly, a constant-pressure region and finally an expansion. The centre bodies could be traversed along the centre line so that their associated pressure fields moved past a single, fixed, instrumentation port in the tunnel wall about 2.90 m downstream of the tunnel throat. The position of measuring "stations" is given by their X-position relative to the nose of the centre body.
- 2 Empty-tunnel tests showed that there was an axial Mach number gradient of $-0.05/\text{m}$ as a consequence
- 4 of tunnel wall boundary layer growth. The empty tunnel boundary layer at the instrument port is a
- 3 fully developed equilibrium turbulent boundary layer (see profiles 0101, 0201). The centre bodies
- traversed by about 0.22 m, and over this distance the thickness of the boundary layer entering the
- 5 interaction varied by about 6%. Pressure variations round the test section measured at selected
- stations were within experimental error.
- 6 Wall pressure was measured at tappings 0.5 mm in diameter at 50.8 mm intervals along the cylindrical test surface. Careful wall temperature measurements were obtained as part of the shear stress instrumentation. 'Surface shear stress gauges' were made using not-wire sensors embedded in the surface of a plug made from an insulating material and contoured to match the test surface. A platinum -10% rhodium wire 25.4 μm in diameter and 6.35 mm long is heated to a predetermined temperature, which is held constant by a constant-temperature hot-wire anemometer. The power required is related to the shear stress. An accurate value for the wall temperature is required for data reduction, and each plug finally contained 6 wires at 5 mm intervals set transversely to the stream. These were, in order, a chromel-constantan thermocouple, a heated wire, two thermocouples, a second heated wire and a final thermocouple. (Note that Fig. 3 of the source paper is incorrect). A Preston tube was also used, for which $d_1 = 1.52$, $d_2 = 0.85$ mm for the first 2.1 mm, the internal diameter then falling to 0.6 mm. The length was 50.8 mm.
- 7 Mean flow Pitot, static pressure and TO profiles were measured. The Pitot was an FPP for which $h_1 = 0.127$, $h_2 = 0.076$, $b_1 = 1.0$ mm. Over a length of 13 mm this section became circular ($d_1 = 1.59$ mm) and then stayed constant to a point 22.9 mm back from the tip. The overall length to the probe support was 50.8 mm, the remainder consisting of 3.2 mm diameter tubing. Two static probes were used, one, after Behrens (1963), a CCP with cone half angle 10° , diameter 1.07 mm, and three 0.36 mm orifices 13.69 mm back from the tip, the other a "Pinckney" (1974) probe with a 10° half angle tip faired into a tube of the same diameter, with four 0.36 mm orifices on the faired portion 5.08 mm back from the tip. The total-temperature probe was an FWP of the design described by Vas (1972). The sensor is a chromel-constantan thermocouple ($d = 76 \mu\text{m}$) mounted on tapered prongs 3.8 mm long.

An auxiliary junction on one of the supports gives the wire-end temperature, required for the elimination of conduction errors. The prongs are mounted on a cylinder 4.4 mm in diameter, the overall length to the probe support being 50.8 mm.

Fluctuation quantities were measured with a single hot wire ($d = 10\mu\text{m}$, $l = 1.5\text{ mm}$, text, figure 1.27) and a similar hot wire which was supported over its whole length by an epoxy film probe ($d = 1.1\text{ mm}$). The probes were operated in the constant temperature mode. The bare hot wire was used for initial measurements in the undisturbed boundary layer, but the design was not sufficiently robust for general use. The film-backed probe was calibrated dynamically for additional thermal inertia effects against a bare wire probe. The calibration of the hot film probe followed the procedures outlined in Horstman and Rose (1977) and Acharya (1977). The authors observe that this probe cannot be used at transonic local Mach numbers so that shear stress values are only measured in positions where $M > 1.2$. Modal analysis showed that total temperature fluctuations were very small, so that - except for this initial study - probes were operated at single, very high overheat ratios so as to respond to mass flow fluctuations only.

- 9 The authors present average PW values for each station relative to the centre body tip, there being very little difference between pressure distributions plotted on this basis for values from three successive (0.1 m apart) static holes. Quite large differences were found in the CF values given by the two surface shear stress gauges, and the values presented are again an average obtained from these devices. In zero pressure gradient conditions the calibration ensured that these values agreed with the profile-fit derived values of CF (the Preston tube value was a little larger). In the regions of strong pressure gradient, the Preston tube and to a lesser degree profile-fit methods are inherently inaccurate. The surface gauge is in principle a sublayer device and so should be relatively little affected by pressure gradients. The total temperature measurements showed that the greatest variation
- 10 in T_0 was 1/2%, so that T_0 was assumed constant in data reduction. No Pitot corrections were applied,
- 11 and Sutherland's viscosity law was used.
- 12 The editors have presented all the mean flow profile data obtained by the authors, incorporating their
- 13 assumptions and data reduction procedures. These form two sets, one for each of two centre bodies, of
- 14 13 and 14 profiles. The first profile in each set is a representative "undisturbed" profile for which we have arbitrarily set $X = 0$. The skin friction values are those given by the authors, obtained as the average from two surface shear gauges. The fluctuation profiles are given in full in the source paper, and we present sample values in section D. The authors present, in addition, wall pressure and CF values for four other centre bodies, as well as the two for which profiles are available, for four unit Reynolds numbers: 12, 35, 105 and 314×10^6 . These values differ slightly from those presented in the author's profile tables, which have been used here.
- § DATA: 78010101-0214. Pitot, static pressure and (T_0) profiles obtained separately. CF from surface shear gauges (embedded hot wire) and (Preston tubes). Fluctuation data from CT HWP and dual wedge probes. $NX = 13-14$.
- 15 Editors' comments. The experiment provides detailed information for two flow fields which are sufficiently complex to test an advanced calculation method without introducing the complications of shock discontinuities and recirculation regions. The data were discussed at length in AGARDograph 253, but as a result of an unfortunate error in the original evaluation of skin friction from the surface gauges, the criticism of the profiles must be reconsidered. The revised data are used here for figures 1-3 which should be regarded as replacing Figs.(5.3.6a, b; 5.3.7) of AG 253. The presentation of the static pressure field there in Figs.(6.2.2; 6.2.3) is of course unaffected.

The wall law profiles for the milder pressure gradient, series 01, show a semi-log region which agrees with the wall law well within the limits determined by the authors' suggestion of a $\pm 15\%$ uncertainty in the wall shear stress (Fig.1). Series 02 follows the same trend (Fig.2) save that the profile for 0210 suggests that the measured wall stress value is too great by about 20%. Profiles 0101 to 0106 and 0201 to 0207 do not show significant pressure gradient effects and agree well with the

'incompressible norm' (Eqn. 3.3.17 of AG 253), shown as the solid line. The wake strength for profiles 0101-0106 is about 3 which agrees well with other data for this Reynolds number range (Fig. 3.3.4, AG 253). The wake strength in Fig. 1 however shows a marked increase for 0107, at the start of the pressure gradient at the wall but well downstream of the start in the outer region, and this develops to much higher values for profiles 0109 and 0111 respectively at the end of the pressure gradient at the wall and in the outer region. The wake in series 02 similarly increases for 0207 to a maximum around 0209/0210 before decreasing for profiles 0212, 0214 under the influence of the favourable pressure gradient in the outer region.

The outer law plots are much less affected by the change in wall shear value as may be seen by comparing Fig. 3 with Fig. 5.3.7 of AG 253. The earlier discussion therefore remains valid.

The temperature profile shows excellent agreement with the theoretical temperature - velocity relationship (eqn. 2.5.37, AG 253). No velocity profile, however, extends into the sublayer.

Though certain doubts as to the accuracy of the wall shear stress data must remain, these data are unique in providing both mean and fluctuating data at a good number of streamwise stations, so providing a good test case for calculation methods.

Comparable axisymmetric cases, in order of severity of pressure rise, are: Lewis et al. (CAT 7201); the present case; Rose (CAT 7306S), with a shock wave; Kussoy and Horstman (CAT 7501S) with two shock cases, the second of which is strong enough to cause separation.

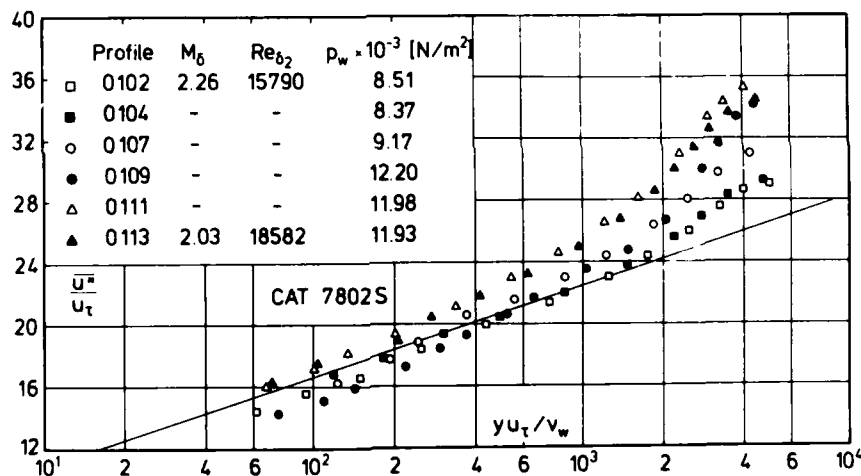


Fig. 1 Law of the wall for an axisymmetric compressible turbulent boundary layer (adiabatic wall, varied pressure gradient, origin not defined, authors' D-state). Kussoy et al. (1978).

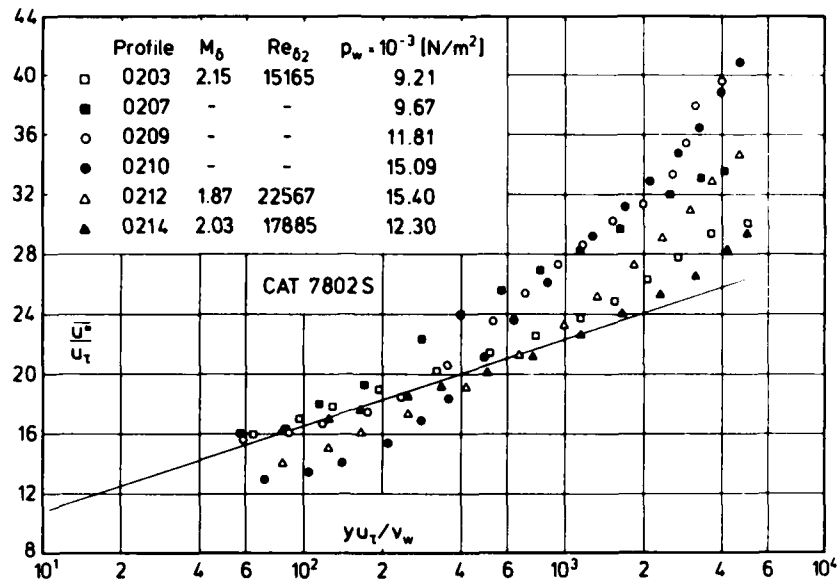


Fig. 2 Law of the wall for an axisymmetric compressible turbulent boundary layer (adiabatic wall, varied pressure gradient, origin not defined, authors' D-state). Kussoy et al. (1978).

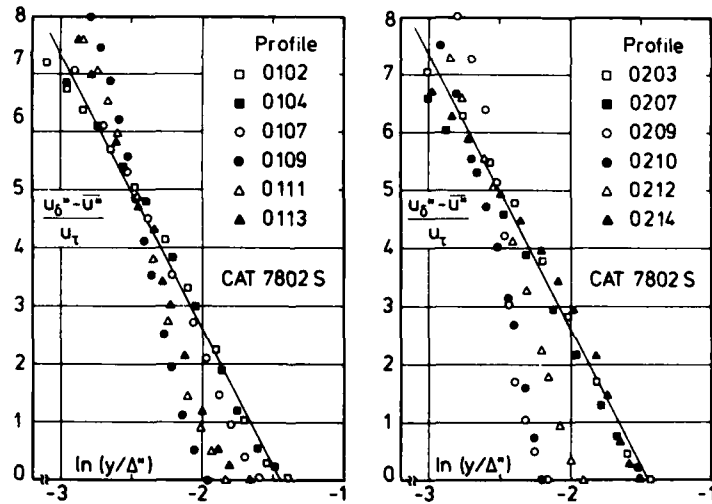


Fig. 3 Outer law for an axisymmetric compressible turbulent boundary layer (adiabatic wall, varied pressure gradient, origin not defined, authors' D-state). Kussoy et al. (1978).

| CAT 78025 KUSSDY/HORSTMAN BOUNDARY CONDITIONS AND EVALUATED DATA. SI UNITS | | | | | | | | | |
|--|--------------------------------------|---------------------------------|---|----------------------------------|----------------------------|---------------------------------|---|---|--|
| RUN X * RZ * | MD * POD* TOD* | TW/TR PW/PD TAUW * | RED2W RED2D DZ | CF CQ * PIZ | H12 H32 H42 | H12K H32K D2K | PW TW* UD | PD TD TR | |
| 7802S0101 0.0000*+00 -1.2385*-01 | 2.2550 1.0132**+05 2.7800**+02 | 1.0553 1.0000 4.4536**+01 | 1.6132**+04 2.9254**+04 2.4147**+03 | 1.4390**+03 0.0000**+00 NC | 3.7159 1.8261 0.0000 | 1.3342 1.8170 3.2368**+03 | 8.6945**+03 2.7800**+02 5.3079**+02 | 8.6945**+03 1.3783**+02 2.6342**+02 | |
| 7802S0102 1.7750*-01 -1.2385*-01 | 2.2690 1.0132**+05 2.7800**+02 | 1.0557 1.0000 4.4536**+01 | 1.5790**+04 2.8797**+04 2.3934**+03 | 1.4528**+03 0.0000**+00 NC | 3.7443 1.8255 0.0000 | 1.3323 1.8174 3.2219**+03 | 8.5060**+03 2.7800**+02 5.3242**+02 | 8.5060**+03 1.3697**+02 2.6333**+02 | |
| 7802S0103 1.9750*-01 -1.2385*-01 | 2.2550 1.0132**+05 2.7800**+02 | 1.0553 0.9794 4.4536**+01 | 1.5553**+04 2.8204**+04 2.3280**+03 | 1.4390**+03 0.0000**+00 NC | 3.9334 1.8269 0.0000 | 1.3305 1.8188 3.1776**+03 | 8.5156**+03 2.7800**+02 5.3079**+02 | 8.6945**+03 1.3783**+02 2.6342**+02 | |
| 7802S0104 2.1750*-01 -1.2385*-01 | 2.2590 1.0132**+05 2.7800**+02 | 1.0554 0.9690 4.4536**+01 | 1.5462**+04 2.8085**+04 2.3228**+03 | 1.4430**+03 0.0000**+00 NC | 4.0854 1.8262 0.0000 | 1.3299 1.8184 3.2120**+03 | 8.3723**+03 2.7800**+02 5.3126**+02 | 8.6402**+03 1.3758**+02 2.6340**+02 | |
| 7802S0105 2.3750*-01 -1.2385*-01 | 2.2000 1.0132**+05 2.7800**+02 | 1.0539 0.9047 4.4536**+01 | 1.4443**+04 2.5612**+04 2.0584**+03 | 1.3872**+03 0.0000**+00 NC | 4.8541 1.8285 0.0000 | 1.3284 1.8206 2.9906**+03 | 8.5728**+03 2.7800**+02 5.2425**+02 | 9.4761**+03 1.4126**+02 2.6378**+02 | |
| 7802S0106 2.9750*-01 -1.2385*-01 | 2.1990 1.0132**+05 2.7800**+02 | 1.0539 0.9086 4.4536**+01 | 1.4936**+04 2.6475**+04 2.1267**+03 | 1.3863**+03 0.0000**+00 NC | 4.6011 1.8270 0.0000 | 1.3374 1.8177 3.0696**+03 | 8.6235**+03 2.7800**+02 5.2413**+02 | 9.4909**+03 1.4132**+02 2.6379**+02 | |
| 7802S0107 2.7750*-01 -1.2385*-01 | 2.1790 1.0132**+05 2.7800**+02 | 1.0534 0.9366 4.3106**+01 | 1.5941**+04 2.8029**+04 2.2300**+03 | 1.3244**+03 0.0000**+00 NC | 4.1802 1.8082 0.0000 | 1.3780 1.7973 3.1704**+03 | 9.1721**+03 2.7800**+02 5.2169**+02 | 9.7927**+03 1.4259**+02 2.6392**+02 | |
| 7802S0108 2.9750*-01 -1.2385*-01 | 2.1500 1.0132**+05 2.7800**+02 | 1.0526 1.0871 3.7915**+01 | 2.0653**+04 3.5889**+04 2.8164**+03 | 1.1435**+03 0.0000**+00 NC | 2.3851 1.7737 0.0000 | 1.4500 1.7596 3.3393**+03 | 1.1139**+04 2.7800**+02 5.1810**+02 | 1.0247**+04 1.4445**+02 2.6411**+02 | |
| 7802S0109 3.1750*-01 -1.2385*-01 | 2.1480 1.0132**+05 2.7800**+02 | 1.0525 1.1872 3.6411**+01 | 2.3951**+04 4.1587**+04 3.2604**+03 | 1.0967**+03 0.0000**+00 NC | 1.7376 1.7643 0.0000 | 1.4691 1.7493 3.5697**+03 | 1.2203**+04 2.7800**+02 5.1785**+02 | 1.0279**+04 1.4458**+02 2.6412**+02 | |
| 7802S0110 3.3750*-01 -1.2385*-01 | 2.0790 1.0132**+05 2.7800**+02 | 1.0507 1.0066 3.7238**+01 | 2.0075**+04 3.3903**+04 2.5742**+03 | 1.0750**+03 0.0000**+00 NC | 2.9582 1.7700 0.0000 | 1.4646 1.7545 3.3279**+03 | 1.1525**+04 2.7800**+02 5.0899**+02 | 1.1450**+04 1.4911**+02 2.6460**+02 | |
| 7802S0111 3.5750*-01 -1.2385*-01 | 2.0280 1.0132**+05 2.7800**+02 | 1.0492 0.9663 3.8141**+01 | 1.9315**+04 3.1962**+04 2.3717**+03 | 1.0686**+03 0.0000**+00 NC | 3.4071 1.7820 0.0000 | 1.4223 1.7710 3.1857**+03 | 1.1980**+04 2.7800**+02 5.0218**+02 | 1.2397**+04 1.5253**+02 2.6495**+02 | |
| 7802S0112 3.7750*-01 -1.2385*-01 | 2.0320 1.0132**+05 2.7800**+02 | 1.0494 0.9534 3.9571**+01 | 1.8170**+04 3.0115**+04 2.2387**+03 | 1.1112**+03 0.0000**+00 NC | 3.6342 1.7861 0.0000 | 1.4088 1.7760 3.0536**+03 | 1.1747**+04 2.7800**+02 5.0272**+02 | 1.2320**+04 1.5226**+02 2.6492**+02 | |
| 7802S0113 3.9750*-01 -1.2385*-01 | 2.0280 1.0132**+05 2.7800**+02 | 1.0492 0.9621 4.0022**+01 | 1.8582**+04 3.0750**+04 2.2818**+03 | 1.1213**+03 0.0000**+00 NC | 3.5979 1.7906 0.0000 | 1.4036 1.7803 3.0857**+03 | 1.1927**+04 2.7800**+02 5.0218**+02 | 1.2397**+04 1.5253**+02 2.6495**+02 | |
| 7802S0202 1.4400*-01 -1.2385*-01 | 2.2310 1.0132**+05 2.7800**+02 | 1.0547 1.0000 4.4536**+01 | 1.5666**+04 2.8132**+04 2.2950**+03 | 1.4160**+03 0.0000**+00 NC | 3.6463 1.8275 0.0000 | 1.3248 1.8202 3.0551**+03 | 9.0273**+03 2.7800**+02 5.2797**+02 | 9.0273**+03 1.3932**+02 2.6358**+02 | |
| 7802S0203 1.8400*-01 -1.2385*-01 | 2.2030 1.0132**+05 2.7800**+02 | 1.0540 0.9766 4.4536**+01 | 1.5165**+04 2.6925**+04 2.1670**+03 | 1.3899**+03 0.0000**+00 NC | 3.9111 1.8272 0.0000 | 1.3247 1.8204 2.9339**+03 | 9.2106**+03 2.7800**+02 5.2462**+02 | 9.4317**+03 1.4107**+02 2.6376**+02 | |
| 7802S0204 2.0400*-01 -1.2385*-01 | 2.1580 1.0132**+05 2.7800**+02 | 1.0528 0.9390 4.4536**+01 | 1.4692**+04 2.5613**+04 2.0176**+03 | 1.3500**+03 0.0000**+00 NC | 4.3376 1.8266 0.0000 | 1.3377 1.8180 2.8048**+03 | 9.5021**+03 2.7800**+02 5.1910**+02 | 1.0120**+04 1.4394**+02 2.6406**+02 | |
| 7802S0205 2.2400*-01 -1.2385*-01 | 2.1240 1.0132**+05 2.7800**+02 | 1.0519 0.8985 4.4536**+01 | 1.4461**+04 2.4868**+04 1.9279**+03 | 1.3214**+03 0.0000**+00 NC | 4.6768 1.8374 0.0000 | 1.3121 1.8302 2.7347**+03 | 9.5888**+03 2.7800**+02 5.1481**+02 | 1.0672**+04 1.4614**+02 2.6429**+02 | |
| 7802S0206 2.4400*-01 -1.2385*-01 | 2.1040 1.0132**+05 2.7800**+02 | 1.0513 0.8569 4.4175**+01 | 1.4185**+04 2.4197**+04 1.8585**+03 | 1.2946**+03 0.0000**+00 NC | 5.1755 1.8308 0.0000 | 1.3390 1.8203 2.7498**+03 | 9.4355**+03 2.7800**+02 5.1225**+02 | 1.1011**+04 1.4745**+02 2.6442**+02 | |
| 7802S0207 2.6400*-01 -1.2385*-01 | 2.0360 1.0132**+05 2.7800**+02 | 1.0495 0.7900 4.1707**+01 | 1.3617**+04 2.2605**+04 1.6834**+03 | 1.1739**+03 0.0000**+00 NC | 5.9895 1.8300 0.0000 | 1.3473 1.8174 2.6304**+03 | 9.6728**+03 2.7800**+02 5.0326**+02 | 1.2244**+04 1.5199**+02 2.6490**+02 | |
| 7802S0208 2.8400*-01 -1.2385*-01 | 2.0410 1.0132**+05 2.7800**+02 | 1.0496 0.8301 3.6471**+01 | 1.9462**+04 3.2373**+04 2.4162**+03 | 1.0295**+03 0.0000**+00 NC | 4.0536 1.7860 0.0000 | 1.4342 1.7696 3.4211**+03 | 1.0085**+04 2.7800**+02 5.0394**+02 | 1.2149**+04 1.5163**+02 2.6486**+02 | |
| 7802S0209 3.0400*-01 -1.2385*-01 | 2.0120 1.0132**+05 2.7800**+02 | 1.0488 0.9298 3.0573**+01 | 2.8723**+04 4.7230**+04 3.4800**+03 | 8.4885**+04 0.0000**+00 NC | 2.3751 1.7621 0.0000 | 1.5073 1.7386 4.2228**+03 | 1.1818**+04 2.7800**+02 4.9999**+02 | 1.2710**+04 1.5362**+02 2.6506**+02 | |
| 7802S0210 3.2400*-01 -1.2385*-01 | 1.9350 1.0132**+05 2.7800**+02 | 1.0466 1.0532 3.0734**+01 | 2.9581**+04 4.7184**+04 3.3634**+03 | 8.1912**+04 0.0000**+00 NC | 2.2062 1.7551 0.0000 | 1.5729 1.7292 3.9899**+03 | 1.5087**+04 2.7800**+02 4.8914**+02 | 1.4325**+04 1.5896**+02 2.6562**+02 | |

PROFIL 0201 = PROFIL 0102
TAUW FROM CF (TAB.2, INTERPOLATED)

CAT 78025 KUSSOY/HORSTMAN BOUNDARY CONDITIONS AND EVALUATED DATA. SI UNITS

| RUN | MO * | TW/TR | RED2W | CF | H12 | H12K | PW | PD |
|-------------------------|------------------------|------------------------|------------------------|------------------------|--------|------------------------|------------------------|------------------------|
| X * | POO* | PW/PD | RED2D | CQ * | H32 | H32K | TW* | TD |
| RZ * | TOD* | TAUW * | DZ | PIZ | H42 | D2K | UD | TR |
| 780250211 | 1.8520 | 1.0442 | 2.3275 ⁺ 04 | 9.5445 ⁻ 04 | 3.5246 | 1.5195 | 1.4875 ⁺ 04 | 1.6283 ⁺ 04 |
| 3.4400 ⁻ 01 | 1.0132 ⁺ 05 | 0.9135 | 3.5944 ⁺ 04 | 0.0000 ⁺ 00 | 1.7543 | 1.7374 | 2.7800 ⁺ 02 | 1.6489 ⁺ 02 |
| -1.2385 ⁻ 01 | 2.7800 ⁺ 02 | 3.7314 ⁺ 01 | 2.4774 ⁻ 03 | NC | 0.0000 | 3.4166 ⁻ 03 | 4.7681 ⁺ 02 | 2.6624 ⁺ 02 |
| 780250212 | 1.8700 | 1.0447 | 2.2567 ⁺ 04 | 1.1627 ⁻ 03 | 3.2261 | 1.4884 | 1.5406 ⁺ 04 | 1.5838 ⁺ 04 |
| 3.8400 ⁻ 01 | 1.0132 ⁺ 05 | 0.9727 | 3.5094 ⁺ 04 | 0.0000 ⁺ 00 | 1.7595 | 1.7460 | 2.7800 ⁺ 02 | 1.6359 ⁺ 02 |
| -1.2385 ⁻ 01 | 2.7800 ⁺ 02 | 4.5077 ⁺ 01 | 2.4361 ⁻ 03 | NC | 0.0000 | 3.2255 ⁻ 03 | 4.7954 ⁺ 02 | 2.6610 ⁺ 02 |
| 780250213 | 1.9790 | 1.0479 | 2.1440 ⁺ 04 | 1.3897 ⁻ 03 | 2.9536 | 1.4062 | 1.4235 ⁺ 04 | 1.3380 ⁺ 04 |
| 3.8400 ⁻ 01 | 1.0132 ⁺ 05 | 1.0639 | 3.4796 ⁺ 04 | 0.0000 ⁺ 00 | 1.7908 | 1.7809 | 2.7800 ⁺ 02 | 1.5589 ⁺ 02 |
| -1.2385 ⁻ 01 | 2.7800 ⁺ 02 | 5.0975 ⁺ 01 | 2.5272 ⁻ 03 | NC | 0.0000 | 3.2202 ⁻ 03 | 4.9541 ⁺ 02 | 2.6530 ⁺ 02 |
| 780250214 | 2.0390 | 1.0496 | 1.7885 ⁺ 04 | 1.5238 ⁻ 03 | 3.3638 | 1.3279 | 1.2300 ⁺ 04 | 1.2187 ⁺ 04 |
| 4.0400 ⁻ 01 | 1.0132 ⁺ 05 | 1.0093 | 2.9727 ⁺ 04 | 0.0000 ⁺ 00 | 1.8231 | 1.8178 | 2.7800 ⁺ 02 | 1.5179 ⁺ 02 |
| -1.2385 ⁻ 01 | 2.7800 ⁺ 02 | 5.4045 ⁺ 01 | 2.2167 ⁻ 03 | NC | 0.0000 | 2.9115 ⁻ 03 | 5.0367 ⁺ 02 | 2.6487 ⁺ 02 |

PROFIL 0201 = PROFIL 0102
TAUM FROM CF (TAB.2, INTERPOLATED)

780250207 KUSSOY/HORSTMAN PROFILE TABULATION 55 POINTS, DELTA AT POINT 43

| I | Y | PT2/P | P/PD | TO/TOD | M/MD | U/UD | T/TD | R/RD*U/UD |
|------|------------------------|------------------------|---------|---------|---------|---------|---------|-----------|
| 1 | 0.0000 ⁺ 00 | 1.0000 ⁺ 00 | 0.79001 | 1.00000 | 0.00000 | 0.00000 | 1.82906 | 0.00000 |
| 2 | 5.0000 ⁻ 04 | 1.5568 ⁺ 00 | 0.79001 | 1.00000 | 0.40324 | 0.51194 | 1.61178 | 0.25093 |
| 3 | 7.5000 ⁻ 04 | 1.5922 ⁺ 00 | 0.79001 | 1.00000 | 0.41405 | 0.52397 | 1.60145 | 0.25848 |
| 4 | 1.0000 ⁻ 03 | 1.7596 ⁺ 00 | 0.79001 | 1.00000 | 0.45972 | 0.57353 | 1.55636 | 0.29112 |
| 5 | 1.5000 ⁻ 03 | 1.9175 ⁺ 00 | 0.79001 | 1.00000 | 0.49656 | 0.61192 | 1.51862 | 0.31833 |
| 6 | 2.0000 ⁻ 03 | 2.1931 ⁺ 00 | 0.79001 | 1.00000 | 0.55157 | 0.66661 | 1.46065 | 0.36055 |
| 7 | 2.5000 ⁻ 03 | 2.3959 ⁺ 00 | 0.79001 | 1.00000 | 0.58743 | 0.70054 | 1.42219 | 0.38914 |
| 8 | 3.0000 ⁻ 03 | 2.5752 ⁺ 00 | 0.79001 | 1.00000 | 0.61690 | 0.72741 | 1.39038 | 0.41331 |
| 9 | 3.5000 ⁻ 03 | 2.7297 ⁺ 00 | 0.79001 | 1.00000 | 0.64096 | 0.74868 | 1.36435 | 0.43351 |
| 10 | 4.0000 ⁻ 03 | 2.8744 ⁺ 00 | 0.79001 | 1.00000 | 0.66257 | 0.76727 | 1.34099 | 0.45201 |
| 11 | 4.5000 ⁻ 03 | 2.9833 ⁺ 00 | 0.79001 | 1.00000 | 0.67829 | 0.78049 | 1.32403 | 0.46569 |
| 12 | 5.0000 ⁻ 03 | 3.0914 ⁺ 00 | 0.79001 | 1.00000 | 0.69352 | 0.79305 | 1.30764 | 0.47912 |
| 13 | 6.0000 ⁻ 03 | 3.2827 ⁺ 00 | 0.79001 | 1.00000 | 0.71955 | 0.81399 | 1.27974 | 0.50249 |
| 14 | 7.0000 ⁻ 03 | 3.4474 ⁺ 00 | 0.79001 | 1.00000 | 0.74116 | 0.83087 | 1.25673 | 0.52230 |
| 15 | 8.0000 ⁻ 03 | 3.5940 ⁺ 00 | 0.79001 | 1.00000 | 0.75982 | 0.84507 | 1.23699 | 0.53971 |
| 16 | 9.0000 ⁻ 03 | 3.7005 ⁺ 00 | 0.79469 | 1.00000 | 0.77308 | 0.85496 | 1.22305 | 0.55553 |
| 17 | 1.0000 ⁻ 02 | 3.8090 ⁺ 00 | 0.79938 | 1.00000 | 0.78635 | 0.86469 | 1.20918 | 0.57163 |
| 18 | 1.1000 ⁻ 02 | 3.9154 ⁺ 00 | 0.80406 | 1.00000 | 0.79912 | 0.87390 | 1.19591 | 0.58755 |
| 19 | 1.2000 ⁻ 02 | 4.0362 ⁺ 00 | 0.80874 | 1.00000 | 0.81336 | 0.88399 | 1.18121 | 0.60524 |
| 20 | 1.3000 ⁻ 02 | 4.1379 ⁺ 00 | 0.81343 | 1.00000 | 0.82515 | 0.89220 | 1.16912 | 0.62076 |
| 21 | 1.4000 ⁻ 02 | 4.2672 ⁺ 00 | 0.81811 | 1.00000 | 0.83988 | 0.90228 | 1.15411 | 0.63960 |
| 22 | 1.5000 ⁻ 02 | 4.3856 ⁺ 00 | 0.82436 | 1.00000 | 0.85314 | 0.91119 | 1.14071 | 0.65849 |
| 23 | 1.6000 ⁻ 02 | 4.4880 ⁺ 00 | 0.83060 | 1.00000 | 0.86444 | 0.91866 | 1.12938 | 0.67563 |
| 24 | 1.7000 ⁻ 02 | 4.6010 ⁺ 00 | 0.83763 | 1.00000 | 0.87672 | 0.92665 | 1.11716 | 0.69479 |
| 25 | 1.8000 ⁻ 02 | 4.6925 ⁺ 00 | 0.84699 | 1.00000 | 0.88654 | 0.93295 | 1.10744 | 0.71354 |
| 26 | 1.9000 ⁻ 02 | 4.7991 ⁺ 00 | 0.85558 | 1.00000 | 0.89784 | 0.94010 | 1.09635 | 0.73364 |
| 27 | 2.0000 ⁻ 02 | 4.8882 ⁺ 00 | 0.86495 | 1.00000 | 0.90717 | 0.94592 | 1.08725 | 0.75252 |
| 28 | 2.1000 ⁻ 02 | 4.9830 ⁺ 00 | 0.87354 | 1.00000 | 0.91699 | 0.95197 | 1.07773 | 0.77160 |
| 29 | 2.2000 ⁻ 02 | 5.0934 ⁺ 00 | 0.88290 | 1.00000 | 0.92829 | 0.95882 | 1.06687 | 0.79349 |
| 30 | 2.3000 ⁻ 02 | 5.1661 ⁺ 00 | 0.89383 | 1.00000 | 0.93566 | 0.96324 | 1.05983 | 0.81237 |
| 31 | 2.4000 ⁻ 02 | 5.2443 ⁺ 00 | 0.90398 | 1.00000 | 0.94352 | 0.96790 | 1.05236 | 0.83143 |
| 32 | 2.5000 ⁻ 02 | 5.3331 ⁺ 00 | 0.91179 | 1.00000 | 0.95236 | 0.97309 | 1.04402 | 0.84985 |
| 33 | 2.6000 ⁻ 02 | 5.4128 ⁺ 00 | 0.92194 | 1.00000 | 0.96022 | 0.97765 | 1.03664 | 0.86947 |
| 34 | 2.7000 ⁻ 02 | 5.4830 ⁺ 00 | 0.93052 | 1.00000 | 0.96709 | 0.98160 | 1.03023 | 0.88660 |
| 35 | 2.8000 ⁻ 02 | 5.5538 ⁺ 00 | 0.93833 | 1.00000 | 0.97397 | 0.98551 | 1.02385 | 0.90320 |
| 36 | 2.9000 ⁻ 02 | 5.6149 ⁺ 00 | 0.94692 | 1.00000 | 0.97986 | 0.98884 | 1.01840 | 0.91943 |
| 37 | 3.0000 ⁻ 02 | 5.6815 ⁺ 00 | 0.95550 | 1.00000 | 0.98625 | 0.99241 | 1.01254 | 0.93651 |
| 38 | 3.1000 ⁻ 02 | 5.7175 ⁺ 00 | 0.96487 | 1.00000 | 0.98969 | 0.99432 | 1.00939 | 0.95047 |
| 39 | 3.2000 ⁻ 02 | 5.7537 ⁺ 00 | 0.97190 | 1.00000 | 0.99312 | 0.99622 | 1.00625 | 0.96221 |
| 40 | 3.3000 ⁻ 02 | 5.7848 ⁺ 00 | 0.97970 | 1.00000 | 0.99607 | 0.99785 | 1.00357 | 0.97412 |
| 41 | 3.4000 ⁻ 02 | 5.8004 ⁺ 00 | 0.98673 | 1.00000 | 0.99754 | 0.99866 | 1.00223 | 0.98321 |
| 42 | 3.5000 ⁻ 02 | 5.8108 ⁺ 00 | 0.99454 | 1.00000 | 0.99853 | 0.99919 | 1.00134 | 0.99241 |
| D 43 | 3.6000 ⁻ 02 | 5.8264 ⁺ 00 | 1.00000 | 1.00000 | 1.00000 | 1.00000 | 1.00000 | 1.00000 |
| 44 | 3.7000 ⁻ 02 | 5.8420 ⁺ 00 | 1.00781 | 1.00000 | 1.00147 | 1.00080 | 0.99867 | 1.00997 |
| 45 | 3.8000 ⁻ 02 | 5.8629 ⁺ 00 | 1.01249 | 1.00000 | 1.00344 | 1.00188 | 0.99689 | 1.01756 |
| 46 | 3.9000 ⁻ 02 | 5.8629 ⁺ 00 | 1.01795 | 1.00000 | 1.00344 | 1.00188 | 0.99689 | 1.02305 |
| 47 | 4.0000 ⁻ 02 | 5.8734 ⁺ 00 | 1.02264 | 1.00000 | 1.00442 | 1.00241 | 0.99600 | 1.02922 |
| 48 | 4.2500 ⁻ 02 | 5.8891 ⁺ 00 | 1.03357 | 1.00000 | 1.00589 | 1.00321 | 0.99467 | 1.04244 |
| 49 | 4.5000 ⁻ 02 | 5.7744 ⁺ 00 | 1.06479 | 1.00000 | 0.99509 | 0.99731 | 1.00446 | 1.05721 |
| 50 | 4.7500 ⁻ 02 | 5.7020 ⁺ 00 | 1.08821 | 1.00000 | 0.98821 | 0.99350 | 1.01074 | 1.06966 |
| 51 | 5.0000 ⁻ 02 | 5.5843 ⁺ 00 | 1.12334 | 1.00000 | 0.97692 | 0.98718 | 1.02112 | 1.08600 |
| 52 | 5.2500 ⁻ 02 | 5.4881 ⁺ 00 | 1.15925 | 1.00000 | 0.96758 | 0.98188 | 1.02977 | 1.10534 |
| 53 | 5.5000 ⁻ 02 | 5.4881 ⁺ 00 | 1.15925 | 1.00000 | 0.96758 | 0.98188 | 1.02977 | 1.10534 |
| 54 | 5.7500 ⁻ 02 | 5.4679 ⁺ 00 | 1.15925 | 1.00000 | 0.96562 | 0.98076 | 1.03160 | 1.10212 |
| 55 | 6.0000 ⁻ 02 | 5.4529 ⁺ 00 | 1.15925 | 1.00000 | 0.96415 | 0.97991 | 1.03297 | 1.09970 |

INPUT VARIABLES Y,M,P/PD,TO=TOD

| 7802S0209 | | KUSSOY/HORSTMAN | | PROFILE TABULATION | | 55 POINTS, DELTA AT POINT 41 | | |
|-----------|------------------------|------------------------|---------|--------------------|---------|------------------------------|---------|-----------|
| I | Y | PTZ/P | P/PD | TO/TOD | M/MD | U/UD | T/TD | R/RD*U/UD |
| 1 | 0.0000 ⁺ 00 | 1.0000 ⁺ 00 | 0.92981 | 1.00000 | 0.00000 | 0.00000 | 1.80963 | 0.00000 |
| 2 | 5.0000 ⁻ 04 | 1.3488 ⁺ 00 | 0.92981 | 1.00000 | 0.33201 | 0.42794 | 1.66136 | 0.23950 |
| 3 | 7.5000 ⁻ 04 | 1.3712 ⁺ 00 | 0.93415 | 1.00000 | 0.34145 | 0.43907 | 1.65354 | 0.24805 |
| 4 | 1.0000 ⁻ 03 | 1.4047 ⁺ 00 | 0.93705 | 1.00000 | 0.35487 | 0.45476 | 1.64219 | 0.25949 |
| 5 | 1.5000 ⁻ 03 | 1.4482 ⁺ 00 | 0.94428 | 1.00000 | 0.37127 | 0.47371 | 1.62795 | 0.27477 |
| 6 | 2.0000 ⁻ 03 | 1.5108 ⁺ 00 | 0.95224 | 1.00000 | 0.39314 | 0.49859 | 1.60836 | 0.29519 |
| 7 | 2.5000 ⁻ 03 | 1.5889 ⁺ 00 | 0.96020 | 1.00000 | 0.41799 | 0.52630 | 1.58537 | 0.31876 |
| 8 | 3.0000 ⁻ 03 | 1.6840 ⁺ 00 | 0.96889 | 1.00000 | 0.44533 | 0.55608 | 1.55927 | 0.34554 |
| 9 | 3.5000 ⁻ 03 | 1.7935 ⁺ 00 | 0.97829 | 1.00000 | 0.47366 | 0.58616 | 1.53145 | 0.37444 |
| 10 | 4.0000 ⁻ 03 | 1.8885 ⁺ 00 | 0.98915 | 1.00000 | 0.49602 | 0.60933 | 1.50903 | 0.39941 |
| 11 | 4.5000 ⁻ 03 | 1.9821 ⁺ 00 | 1.00000 | 1.00000 | 0.51640 | 0.62999 | 1.48830 | 0.42329 |
| 12 | 5.0000 ⁻ 03 | 2.0694 ⁺ 00 | 1.01302 | 1.00000 | 0.53429 | 0.64777 | 1.46990 | 0.44643 |
| 13 | 6.0000 ⁻ 03 | 2.2198 ⁺ 00 | 1.03835 | 1.00000 | 0.56312 | 0.67573 | 1.43994 | 0.48727 |
| 14 | 7.0000 ⁻ 03 | 2.3671 ⁺ 00 | 1.06295 | 1.00000 | 0.58946 | 0.70052 | 1.41232 | 0.52724 |
| 15 | 8.0000 ⁻ 03 | 2.4991 ⁺ 00 | 1.08755 | 1.00000 | 0.61183 | 0.72101 | 1.38874 | 0.56464 |
| 16 | 9.0000 ⁻ 03 | 2.6155 ⁺ 00 | 1.11071 | 1.00000 | 0.63072 | 0.73791 | 1.36878 | 0.59878 |
| 17 | 1.0000 ⁻ 02 | 2.7297 ⁺ 00 | 1.13169 | 1.00000 | 0.64861 | 0.75358 | 1.34986 | 0.63178 |
| 18 | 1.1000 ⁻ 02 | 2.8278 ⁺ 00 | 1.15340 | 1.00000 | 0.66352 | 0.76638 | 1.33410 | 0.66258 |
| 19 | 1.2000 ⁻ 02 | 2.9251 ⁺ 00 | 1.17511 | 1.00000 | 0.67793 | 0.77855 | 1.31888 | 0.69369 |
| 20 | 1.3000 ⁻ 02 | 3.0144 ⁺ 00 | 1.19247 | 1.00000 | 0.69085 | 0.78929 | 1.30525 | 0.72109 |
| 21 | 1.4000 ⁻ 02 | 3.0773 ⁺ 00 | 1.21491 | 1.00000 | 0.69980 | 0.79662 | 1.29584 | 0.74686 |
| 22 | 1.5000 ⁻ 02 | 3.1448 ⁺ 00 | 1.23227 | 1.00000 | 0.70924 | 0.80427 | 1.28592 | 0.77072 |
| 23 | 1.6000 ⁻ 02 | 3.2060 ⁺ 00 | 1.24964 | 1.00000 | 0.71769 | 0.81104 | 1.27706 | 0.79363 |
| 24 | 1.7000 ⁻ 02 | 3.2680 ⁺ 00 | 1.26773 | 1.00000 | 0.72614 | 0.81775 | 1.26822 | 0.81743 |
| 25 | 1.8000 ⁻ 02 | 3.3345 ⁺ 00 | 1.28075 | 1.00000 | 0.73509 | 0.82477 | 1.25888 | 0.83910 |
| 26 | 1.9000 ⁻ 02 | 3.4019 ⁺ 00 | 1.29378 | 1.00000 | 0.74404 | 0.83171 | 1.24957 | 0.86114 |
| 27 | 2.0000 ⁻ 02 | 3.5048 ⁺ 00 | 1.29378 | 1.00000 | 0.75746 | 0.84199 | 1.23565 | 0.88159 |
| 28 | 2.1000 ⁻ 02 | 3.6135 ⁺ 00 | 1.29378 | 1.00000 | 0.77137 | 0.85246 | 1.22129 | 0.90306 |
| 29 | 2.2000 ⁻ 02 | 3.7165 ⁺ 00 | 1.29378 | 1.00000 | 0.78429 | 0.86202 | 1.20802 | 0.92321 |
| 30 | 2.3000 ⁻ 02 | 3.8620 ⁺ 00 | 1.27641 | 1.00000 | 0.80219 | 0.87500 | 1.18976 | 0.93872 |
| 31 | 2.4000 ⁻ 02 | 4.0404 ⁺ 00 | 1.24964 | 1.00000 | 0.82356 | 0.89011 | 1.16816 | 0.95220 |
| 32 | 2.5000 ⁻ 02 | 4.2933 ⁺ 00 | 1.20188 | 1.00000 | 0.85288 | 0.91019 | 1.13890 | 0.96053 |
| 33 | 2.6000 ⁻ 02 | 4.6512 ⁺ 00 | 1.13169 | 1.00000 | 0.89264 | 0.93621 | 1.10000 | 0.96319 |
| 34 | 2.7000 ⁻ 02 | 5.0837 ⁺ 00 | 1.05282 | 1.00000 | 0.93837 | 0.96450 | 1.05647 | 0.96117 |
| 35 | 2.8000 ⁻ 02 | 5.2002 ⁺ 00 | 1.04342 | 1.00000 | 0.95030 | 0.97160 | 1.04533 | 0.96982 |
| 36 | 2.9000 ⁻ 02 | 5.3133 ⁺ 00 | 1.03473 | 1.00000 | 0.96173 | 0.97830 | 1.03476 | 0.97828 |
| 37 | 3.0000 ⁻ 02 | 5.4178 ⁺ 00 | 1.02605 | 1.00000 | 0.97217 | 0.98433 | 1.02518 | 0.98517 |
| 38 | 3.1000 ⁻ 02 | 5.5083 ⁺ 00 | 1.01737 | 1.00000 | 0.98111 | 0.98943 | 1.01703 | 0.98976 |
| 39 | 3.2000 ⁻ 02 | 5.5945 ⁺ 00 | 1.00868 | 1.00000 | 0.98956 | 0.99419 | 1.00938 | 0.99351 |
| 40 | 3.3000 ⁻ 02 | 5.6507 ⁺ 00 | 1.00434 | 1.00000 | 0.99503 | 0.99724 | 1.00446 | 0.99713 |
| D 41 | 3.4000 ⁻ 02 | 5.7020 ⁺ 00 | 1.00000 | 1.00000 | 1.00000 | 1.00000 | 1.00000 | 1.00000 |
| 42 | 3.5000 ⁻ 02 | 5.7537 ⁺ 00 | 0.99566 | 1.00000 | 1.00497 | 1.00274 | 0.99556 | 1.00284 |
| 43 | 3.6000 ⁻ 02 | 5.7952 ⁺ 00 | 0.99132 | 1.00000 | 1.00895 | 1.00491 | 0.99202 | 1.00420 |
| 44 | 3.7000 ⁻ 02 | 5.7640 ⁺ 00 | 1.00000 | 1.00000 | 1.00596 | 1.00328 | 0.99468 | 1.00865 |
| 45 | 3.8000 ⁻ 02 | 5.7227 ⁺ 00 | 1.00868 | 1.00000 | 1.00199 | 1.00110 | 0.99822 | 1.01159 |
| 46 | 3.9000 ⁻ 02 | 5.7330 ⁺ 00 | 1.00868 | 1.00000 | 1.00298 | 1.00164 | 0.99733 | 1.01304 |
| 47 | 4.0000 ⁻ 02 | 5.7382 ⁺ 00 | 1.00868 | 1.00000 | 1.00348 | 1.00192 | 0.99689 | 1.01377 |
| 48 | 4.2500 ⁻ 02 | 5.7485 ⁺ 00 | 1.00868 | 1.00000 | 1.00447 | 1.00246 | 0.99600 | 1.01523 |
| 49 | 4.5000 ⁻ 02 | 5.7382 ⁺ 00 | 1.00868 | 1.00000 | 1.00348 | 1.00192 | 0.99689 | 1.01377 |
| 50 | 4.7500 ⁻ 02 | 5.7330 ⁺ 00 | 1.00868 | 1.00000 | 1.00298 | 1.00164 | 0.99733 | 1.01304 |
| 51 | 5.0000 ⁻ 02 | 5.7124 ⁺ 00 | 1.00868 | 1.00000 | 1.00099 | 1.00055 | 0.99911 | 1.01013 |
| 52 | 5.2500 ⁻ 02 | 5.6969 ⁺ 00 | 1.00868 | 1.00000 | 0.99950 | 0.99973 | 1.00044 | 1.00796 |
| 53 | 5.5000 ⁻ 02 | 5.5741 ⁺ 00 | 1.02605 | 1.00000 | 0.98757 | 0.99308 | 1.01117 | 1.00769 |
| 54 | 5.7500 ⁻ 02 | 5.7175 ⁺ 00 | 0.98698 | 1.00000 | 1.00149 | 1.00082 | 0.99867 | 0.98911 |
| 55 | 6.0000 ⁻ 02 | 5.6815 ⁺ 00 | 0.96454 | 1.00000 | 0.99801 | 0.99890 | 1.00178 | 0.96177 |

INPUT VARIABLES Y,M,P/PD,TO=TOD

| 7802S0214 | | KUSSOY/HORSTMAN | | PROFILE TABULATION | | 55 POINTS, DELTA AT POINT 37 | | |
|-----------|-----------------------|-----------------------|---------|--------------------|---------|------------------------------|---------|-----------|
| I | Y | PT2/P | P/PD | TO/TOD | M/MD | U/UD | T/TD | R/RD*U/UD |
| 1 | 0.0000 ⁺⁰⁰ | 1.0000 ⁺⁰⁰ | 1.00930 | 1.00000 | 0.00000 | 0.00000 | 1.83150 | 0.00000 |
| 2 | 5.0000 ⁻⁰⁴ | 1.8222 ⁺⁰⁰ | 1.00465 | 1.00000 | 0.47425 | 0.58909 | 1.54295 | 0.38357 |
| 3 | 7.5000 ⁻⁰⁴ | 1.9220 ⁺⁰⁰ | 1.00155 | 1.00000 | 0.49681 | 0.61244 | 1.51963 | 0.40364 |
| 4 | 1.0000 ⁻⁰³ | 2.0325 ⁺⁰⁰ | 0.99768 | 1.00000 | 0.51986 | 0.63573 | 1.49545 | 0.42412 |
| 5 | 1.5000 ⁻⁰³ | 2.1904 ⁺⁰⁰ | 0.99070 | 1.00000 | 0.55027 | 0.66560 | 1.46312 | 0.45069 |
| 6 | 2.0000 ⁻⁰³ | 2.3189 ⁺⁰⁰ | 0.97986 | 1.00000 | 0.57332 | 0.68760 | 1.43838 | 0.46841 |
| 7 | 2.5000 ⁻⁰³ | 2.4192 ⁺⁰⁰ | 0.96979 | 1.00000 | 0.59049 | 0.70361 | 1.41986 | 0.48058 |
| 8 | 3.0000 ⁻⁰³ | 2.5082 ⁺⁰⁰ | 0.95740 | 1.00000 | 0.60520 | 0.71709 | 1.40393 | 0.48901 |
| 9 | 3.5000 ⁻⁰³ | 2.5937 ⁺⁰⁰ | 0.94810 | 1.00000 | 0.61893 | 0.72946 | 1.38905 | 0.49790 |
| 10 | 4.0000 ⁻⁰³ | 2.6880 ⁺⁰⁰ | 0.93571 | 1.00000 | 0.63364 | 0.74250 | 1.37309 | 0.50598 |
| 11 | 4.5000 ⁻⁰³ | 2.7882 ⁺⁰⁰ | 0.92564 | 1.00000 | 0.64885 | 0.75573 | 1.35660 | 0.51565 |
| 12 | 5.0000 ⁻⁰³ | 2.8778 ⁺⁰⁰ | 0.92022 | 1.00000 | 0.66209 | 0.76707 | 1.34225 | 0.52588 |
| 13 | 6.0000 ⁻⁰³ | 3.0248 ⁺⁰⁰ | 0.91557 | 1.00000 | 0.68318 | 0.78475 | 1.31944 | 0.54454 |
| 14 | 7.0000 ⁻⁰³ | 3.1807 ⁺⁰⁰ | 0.91557 | 1.00000 | 0.70476 | 0.80237 | 1.29619 | 0.56676 |
| 15 | 8.0000 ⁻⁰³ | 3.2974 ⁺⁰⁰ | 0.92486 | 1.00000 | 0.72045 | 0.81489 | 1.27935 | 0.58910 |
| 16 | 9.0000 ⁻⁰³ | 3.4171 ⁺⁰⁰ | 0.93726 | 1.00000 | 0.73615 | 0.82717 | 1.26258 | 0.61403 |
| 17 | 1.0000 ⁻⁰² | 3.5318 ⁺⁰⁰ | 0.95198 | 1.00000 | 0.75086 | 0.83846 | 1.24695 | 0.64012 |
| 18 | 1.1000 ⁻⁰² | 3.6450 ⁺⁰⁰ | 0.96592 | 1.00000 | 0.76508 | 0.84917 | 1.23191 | 0.66582 |
| 19 | 1.2000 ⁻⁰² | 3.7767 ⁺⁰⁰ | 0.97754 | 1.00000 | 0.78127 | 0.86113 | 1.21490 | 0.69288 |
| 20 | 1.3000 ⁻⁰² | 3.8784 ⁺⁰⁰ | 0.98761 | 1.00000 | 0.79353 | 0.87003 | 1.20210 | 0.71478 |
| 21 | 1.4000 ⁻⁰² | 3.9943 ⁺⁰⁰ | 0.99923 | 1.00000 | 0.80726 | 0.87982 | 1.18785 | 0.74011 |
| 22 | 1.5000 ⁻⁰² | 4.0784 ⁺⁰⁰ | 1.01007 | 1.00000 | 0.81707 | 0.88671 | 1.17773 | 0.76048 |
| 23 | 1.6000 ⁻⁰² | 4.1721 ⁺⁰⁰ | 1.02169 | 1.00000 | 0.82786 | 0.89419 | 1.16666 | 0.78307 |
| 24 | 1.7000 ⁻⁰² | 4.2672 ⁺⁰⁰ | 1.03021 | 1.00000 | 0.83865 | 0.90156 | 1.15565 | 0.80369 |
| 25 | 1.8000 ⁻⁰² | 4.3635 ⁺⁰⁰ | 1.03718 | 1.00000 | 0.84944 | 0.90882 | 1.14472 | 0.82345 |
| 26 | 1.9000 ⁻⁰² | 4.4612 ⁺⁰⁰ | 1.04183 | 1.00000 | 0.86023 | 0.91599 | 1.13385 | 0.84165 |
| 27 | 2.0000 ⁻⁰² | 4.5556 ⁺⁰⁰ | 1.04725 | 1.00000 | 0.87052 | 0.92273 | 1.12354 | 0.86008 |
| 28 | 2.1000 ⁻⁰² | 4.6833 ⁺⁰⁰ | 1.04725 | 1.00000 | 0.88426 | 0.93158 | 1.10989 | 0.87900 |
| 29 | 2.2000 ⁻⁰² | 4.7991 ⁺⁰⁰ | 1.04725 | 1.00000 | 0.89652 | 0.93934 | 1.09782 | 0.89608 |
| 30 | 2.3000 ⁻⁰² | 4.9544 ⁺⁰⁰ | 1.04183 | 1.00000 | 0.91270 | 0.94940 | 1.08202 | 0.91413 |
| 31 | 2.4000 ⁻⁰² | 5.1127 ⁺⁰⁰ | 1.03718 | 1.00000 | 0.92889 | 0.95923 | 1.06641 | 0.93294 |
| 32 | 2.5000 ⁻⁰² | 5.2837 ⁺⁰⁰ | 1.03253 | 1.00000 | 0.94605 | 0.96944 | 1.05005 | 0.95327 |
| 33 | 2.6000 ⁻⁰² | 5.4629 ⁺⁰⁰ | 1.02789 | 1.00000 | 0.96371 | 0.97969 | 1.03344 | 0.97442 |
| 34 | 2.7000 ⁻⁰² | 5.6353 ⁺⁰⁰ | 1.01782 | 1.00000 | 0.98038 | 0.98914 | 1.01795 | 0.98901 |
| 35 | 2.8000 ⁻⁰² | 5.7433 ⁺⁰⁰ | 1.01007 | 1.00000 | 0.99068 | 0.99488 | 1.00849 | 0.99644 |
| 36 | 2.9000 ⁻⁰² | 5.7952 ⁺⁰⁰ | 1.00465 | 1.00000 | 0.99559 | 0.99758 | 1.00402 | 0.99821 |
| 0 37 | 3.0000 ⁻⁰² | 5.8420 ⁺⁰⁰ | 1.00000 | 1.00000 | 1.00000 | 1.00000 | 1.00000 | 1.00000 |
| 38 | 3.1000 ⁻⁰² | 5.8839 ⁺⁰⁰ | 0.99613 | 1.00000 | 1.00392 | 1.00214 | 0.99644 | 1.00162 |
| 39 | 3.2000 ⁻⁰² | 5.9049 ⁺⁰⁰ | 0.99303 | 1.00000 | 1.00589 | 1.00320 | 0.99467 | 1.00155 |
| 40 | 3.3000 ⁻⁰² | 5.9417 ⁺⁰⁰ | 0.99070 | 1.00000 | 1.00932 | 1.00506 | 0.99157 | 1.00418 |
| 41 | 3.4000 ⁻⁰² | 5.9681 ⁺⁰⁰ | 0.98761 | 1.00000 | 1.01177 | 1.00638 | 0.98936 | 1.00459 |
| 42 | 3.5000 ⁻⁰² | 5.9998 ⁺⁰⁰ | 0.98606 | 1.00000 | 1.01471 | 1.00795 | 0.98672 | 1.00728 |
| 43 | 3.6000 ⁻⁰² | 6.0211 ⁺⁰⁰ | 0.98606 | 1.00000 | 1.01667 | 1.00900 | 0.98496 | 1.01012 |
| 44 | 3.7000 ⁻⁰² | 6.0317 ⁺⁰⁰ | 0.98606 | 1.00000 | 1.01766 | 1.00952 | 0.98408 | 1.01155 |
| 45 | 3.8000 ⁻⁰² | 6.0317 ⁺⁰⁰ | 0.98683 | 1.00000 | 1.01766 | 1.00952 | 0.98408 | 1.01234 |
| 46 | 3.9000 ⁻⁰² | 6.0317 ⁺⁰⁰ | 0.98838 | 1.00000 | 1.01766 | 1.00952 | 0.98408 | 1.01393 |
| 47 | 4.0000 ⁻⁰² | 6.0317 ⁺⁰⁰ | 0.99070 | 1.00000 | 1.01766 | 1.00952 | 0.98408 | 1.01632 |
| 48 | 4.2500 ⁻⁰² | 6.0317 ⁺⁰⁰ | 0.99535 | 1.00000 | 1.01766 | 1.00952 | 0.98408 | 1.02108 |
| 49 | 4.5000 ⁻⁰² | 5.9628 ⁺⁰⁰ | 1.01394 | 1.00000 | 1.01128 | 1.00611 | 0.98980 | 1.03065 |
| 50 | 4.7500 ⁻⁰² | 5.9364 ⁺⁰⁰ | 1.02324 | 1.00000 | 1.00883 | 1.00479 | 0.99201 | 1.03642 |
| 51 | 5.0000 ⁻⁰² | 5.8839 ⁺⁰⁰ | 1.03253 | 1.00000 | 1.00392 | 1.00214 | 0.99644 | 1.03843 |
| 52 | 5.2500 ⁻⁰² | 5.7744 ⁺⁰⁰ | 1.05190 | 1.00000 | 0.99362 | 0.99650 | 1.00580 | 1.04217 |
| 53 | 5.5000 ⁻⁰² | 5.4028 ⁺⁰⁰ | 1.16421 | 1.00000 | 0.95782 | 0.97630 | 1.03895 | 1.09401 |
| 54 | 5.7500 ⁻⁰² | 5.3978 ⁺⁰⁰ | 1.17351 | 1.00000 | 0.95733 | 0.97601 | 1.03941 | 1.10193 |
| 55 | 6.0000 ⁻⁰² | 5.3978 ⁺⁰⁰ | 1.17351 | 1.00000 | 0.95733 | 0.97601 | 1.03941 | 1.10193 |

INPUT VARIABLES Y,M,P/PD,TO=TOD

7802S KUSSOY/H/A TURBULENCE DATA
 7802S0102 UT= 2.0444E+01 RHDW= 1.0656E-01 TW= 2.7800E+02 D** 1.5557E-01

| I | Y [M] | U' UT | V' UT | W' UT | RHD*U'V' RHDW*UT2 | (RHD U)' RHDW*UT | RHD' RHDW |
|----|-----------|-----------|-----------|-----------|----------------------|---------------------|--------------|
| 1 | 2.0000E-3 | 1.7602E+0 | 8.8011E-1 | 8.2834E-1 | NM | 3.4977E+0 | 6.6552E-2 |
| 2 | 2.5000E-3 | 1.4496E+0 | 6.4714E-1 | 9.3189E-1 | NM | 2.9235E+0 | 5.6468E-2 |
| 3 | 3.1000E-3 | 1.4237E+0 | 5.9537E-1 | 8.5423E-1 | NM | 2.9757E+0 | 5.6468E-2 |
| 4 | 3.6000E-3 | 1.4237E+0 | 5.9537E-1 | 7.7657E-1 | -4.7703E-1 | 3.0279E+0 | 5.6468E-2 |
| 5 | 4.2000E-3 | 1.3202E+0 | 5.9537E-1 | 6.9891E-1 | -5.3378E-1 | 2.8712E+0 | 5.4452E-2 |
| 6 | 4.7000E-3 | 1.2943E+0 | 5.9537E-1 | 6.7303E-1 | -6.4459E-1 | 2.8712E+0 | 5.4452E-2 |
| 7 | 5.7000E-3 | 1.2425E+0 | 6.4714E-1 | 6.4714E-1 | -7.5541E-1 | 2.8712E+0 | 5.2435E-2 |
| 8 | 6.8000E-3 | 1.2166E+0 | 6.4714E-1 | 6.4714E-1 | -7.4054E-1 | 2.8712E+0 | 5.2435E-2 |
| 9 | 7.8000E-3 | 1.1907E+0 | 6.4714E-1 | 6.4714E-1 | -7.1486E-1 | 2.8712E+0 | 5.2435E-2 |
| 10 | 8.9000E-3 | 1.1649E+0 | 6.2126E-1 | 6.2126E-1 | -7.1892E-1 | 2.8712E+0 | 5.2435E-2 |
| 11 | 1.0000E-2 | 1.1131E+0 | 6.4714E-1 | 6.4714E-1 | -6.6081E-1 | 2.7668E+0 | 5.2435E-2 |
| 12 | 1.2100E-2 | 1.0872E+0 | 6.2126E-1 | 6.2126E-1 | -6.2838E-1 | 2.8712E+0 | 5.2435E-2 |
| 13 | 1.4300E-2 | 1.0613E+0 | 6.2126E-1 | 5.9537E-1 | -6.0270E-1 | 2.9235E+0 | 5.4452E-2 |
| 14 | 1.6400E-2 | 1.0613E+0 | 6.2126E-1 | 5.9537E-1 | -6.2297E-1 | 3.0279E+0 | 5.6468E-2 |
| 15 | 1.8500E-2 | 1.0872E+0 | 6.4714E-1 | 6.2126E-1 | -6.2297E-1 | 3.1845E+0 | 5.8485E-2 |
| 16 | 2.0600E-2 | 1.0613E+0 | 5.9537E-1 | 5.6949E-1 | -5.5000E-1 | 3.2367E+0 | 5.8485E-2 |
| 17 | 2.2800E-2 | 1.0613E+0 | 5.6949E-1 | 5.4360E-1 | -5.5135E-1 | 3.4459E+0 | 6.2519E-2 |
| 18 | 2.4900E-2 | 1.0354E+0 | 5.6949E-1 | 5.1771E-1 | -5.0946E-1 | 3.4977E+0 | 6.4535E-2 |
| 19 | 2.7000E-2 | 1.0354E+0 | 5.4360E-1 | 4.9183E-1 | -4.9865E-1 | 3.6021E+0 | 6.4535E-2 |
| 20 | 2.9100E-2 | 9.8366E-1 | 5.1771E-1 | 4.4006E-1 | -4.1892E-1 | 3.5409E+0 | 6.4535E-2 |
| 21 | 3.1200E-2 | 8.2834E-1 | 4.6594E-1 | 3.6240E-1 | -3.0000E-1 | 3.0801E+0 | 5.6468E-2 |
| 22 | 3.3400E-2 | 6.7303E-1 | 4.1417E-1 | 3.3651E-1 | -1.9865E-1 | 2.6102E+0 | 4.6385E-2 |
| 23 | 3.5500E-2 | 4.9183E-1 | 3.1063E-1 | 2.5886E-1 | -1.0270E-1 | 1.8794E+0 | 3.4284E-2 |
| 24 | 3.7600E-2 | 4.9183E-1 | 3.3651E-1 | 2.5886E-1 | -9.1892E-2 | 1.8794E+0 | 3.4284E-2 |
| 25 | 3.9800E-2 | 3.1063E-1 | 3.3651E-1 | 2.0709E-1 | -5.9459E-2 | 1.2007E+0 | 2.2184E-2 |
| 26 | 4.1900E-2 | 2.3297E-1 | 2.5886E-1 | 1.2943E-1 | -2.7027E-2 | 8.8748E-1 | 1.6134E-2 |
| 27 | 4.4000E-2 | 1.5531E-1 | 2.3297E-1 | 7.7657E-2 | -2.5676E-2 | 6.7866E-1 | 1.2100E-2 |
| 28 | 4.6100E-2 | 1.8120E-1 | 3.1063E-1 | 7.7657E-2 | -4.5946E-2 | 6.7866E-1 | 1.2100E-2 |
| 29 | 4.8200E-2 | 1.2943E-1 | 2.3297E-1 | 5.1771E-2 | -1.8919E-2 | 5.2204E-1 | 1.0084E-2 |
| 30 | 5.0400E-2 | 1.2943E-1 | 2.0709E-1 | 5.1771E-2 | -9.4595E-3 | 4.6984E-1 | 8.0669E-3 |
| 31 | 5.2500E-2 | 1.2943E-1 | 2.0709E-1 | 5.1771E-2 | -8.1081E-3 | 4.6984E-1 | 8.0669E-3 |
| 32 | 5.4600E-2 | 1.0354E-1 | 1.5531E-1 | 5.1771E-2 | -6.7568E-3 | 4.1764E-1 | 8.0669E-3 |

7802S KUSSOY/H/A TURBULENCE DATA
 7802S0109 UT= 1.5433E+01 RHDW= 1.5287E-01 TW= 2.7800E+02 D** 2.1309E-01

| I | Y [M] | U' UT | V' UT | W' UT | RHD*U'V' RHDW*UT2 | (RHD U)' RHDW*UT | RHD' RHDW |
|----|-----------|-----------|-----------|-----------|----------------------|---------------------|--------------|
| 1 | 1.9000E-3 | 2.6746E+0 | NM | 1.6459E+0 | NM | 4.3865E+0 | 6.7476E-2 |
| 2 | 2.4000E-3 | 2.7432E+0 | 1.3373E+0 | 1.6802E+0 | NM | 4.5793E+0 | 7.0287E-2 |
| 3 | 3.0000E-3 | 2.7432E+0 | 1.3716E+0 | 1.6459E+0 | NM | 4.8203E+0 | 7.3099E-2 |
| 4 | 3.5000E-3 | 2.7089E+0 | 1.3373E+0 | 1.6116E+0 | NM | 4.9167E+0 | 7.3099E-2 |
| 5 | 4.0000E-3 | 2.6403E+0 | 1.2002E+0 | 1.5431E+0 | NM | 4.8203E+0 | 7.0287E-2 |
| 6 | 5.0000E-3 | 2.5718E+0 | 1.1316E+0 | 1.4745E+0 | NM | 5.0131E+0 | 7.1693E-2 |
| 7 | 6.1000E-3 | 2.5032E+0 | 1.1316E+0 | 1.4402E+0 | -1.6793E+0 | 5.2059E+0 | 7.3099E-2 |
| 8 | 7.2000E-3 | 2.4003E+0 | 1.0973E+0 | 1.3716E+0 | -1.6612E+0 | 5.2541E+0 | 7.4504E-2 |
| 9 | 8.3000E-3 | 2.3660E+0 | 1.0973E+0 | 1.2344E+0 | -1.6711E+0 | 5.2541E+0 | 7.4504E-2 |
| 10 | 9.3000E-3 | 2.2631E+0 | 1.0287E+0 | 1.1316E+0 | -1.6744E+0 | 5.2059E+0 | 7.3099E-2 |
| 11 | 1.0400E-2 | 2.1260E+0 | 1.0630E+0 | 1.0630E+0 | -1.8612E+0 | 5.0131E+0 | 7.1693E-2 |
| 12 | 1.2500E-2 | 1.9202E+0 | 1.0630E+0 | 9.9441E-1 | -1.8727E+0 | 4.7721E+0 | 6.7476E-2 |
| 13 | 1.4700E-2 | 1.7488E+0 | 1.1659E+0 | 9.2583E-1 | -1.6000E+0 | 4.5793E+0 | 6.3258E-2 |
| 14 | 1.6800E-2 | 1.6116E+0 | 1.2344E+0 | 9.2583E-1 | -1.6760E+0 | 4.4829E+0 | 6.1853E-2 |
| 15 | 1.8900E-2 | 1.5431E+0 | 1.2687E+0 | 8.9154E-1 | -1.4512E+0 | 4.3865E+0 | 6.0447E-2 |
| 16 | 2.1000E-2 | 1.4745E+0 | 1.0287E+0 | 8.2296E-1 | -1.1306E+0 | 4.2901E+0 | 5.9041E-2 |
| 17 | 2.3100E-2 | 1.4402E+0 | 9.2583E-1 | 7.5438E-1 | -9.8182E-1 | 4.1937E+0 | 5.6230E-2 |
| 18 | 2.5300E-2 | 1.3716E+0 | 7.8867E-1 | 6.8580E-1 | -7.2562E-1 | 4.0009E+0 | 5.2013E-2 |
| 19 | 2.7400E-2 | 1.2687E+0 | 7.8867E-1 | 6.1722E-1 | -5.4876E-1 | 3.7116E+0 | 5.0607E-2 |
| 20 | 2.9600E-2 | 1.1659E+0 | 8.5725E-1 | 5.1435E-1 | -4.6116E-1 | 3.3742E+0 | 4.6390E-2 |
| 21 | 3.1700E-2 | 7.5438E-1 | 6.5151E-1 | 3.7719E-1 | -1.9669E-1 | 2.1209E+0 | 2.9521E-2 |
| 22 | 3.3800E-2 | 5.4864E-1 | 7.2009E-1 | 3.0861E-1 | -7.1074E-2 | 1.5907E+0 | 2.1086E-2 |
| 23 | 3.5900E-2 | 4.1148E-1 | 5.1435E-1 | 2.7432E-1 | -2.8099E-2 | 1.1569E+0 | 1.6869E-2 |
| 24 | 3.8000E-2 | 3.0861E-1 | 5.8293E-1 | 2.0861E-1 | -2.6446E-2 | 9.6406E-1 | 1.2652E-2 |
| 25 | 4.0200E-2 | 2.4003E-1 | 4.1148E-1 | 3.0861E-1 | -1.3223E-2 | 6.7484E-1 | 9.8402E-3 |
| 26 | 4.1500E-2 | 2.0574E-1 | NM | 2.7432E-1 | NM | 5.7844E-1 | 8.4345E-3 |

7802S

KUSSOY/H/A

TURBULENCE DATA

7802S0209

UT= 1.4370E+01 RHDW= 1.4805E-01 TW= 2.7800E+02 D*= 2.9842E-01

| I | Y [M] | U' UT | V' UT | W' UT | RHO*U'V' RHDW*UT2 | (RHO U)' RHDW*UT | RHO' RHDW |
|----|-----------|-----------|-----------|-----------|----------------------|---------------------|--------------|
| 1 | 1.3000E-3 | 2.2464E+0 | NM | NM | NM | 3.1538E+0 | 4.4998E-2 |
| 2 | 1.6000E-3 | 2.4305E+0 | 1.1784E+0 | 1.7308E+0 | NM | 3.5280E+0 | 5.0804E-2 |
| 3 | 2.1000E-3 | 2.7619E+0 | 1.2153E+0 | 1.8045E+0 | NM | 4.1160E+0 | 5.9513E-2 |
| 4 | 2.7000E-3 | 3.0934E+0 | 1.2521E+0 | 1.8045E+0 | NM | 4.8109E+0 | 6.8222E-2 |
| 5 | 3.2000E-3 | 3.2775E+0 | 1.2889E+0 | 1.7676E+0 | NM | 5.2385E+0 | 7.4029E-2 |
| 6 | 3.7000E-3 | 3.4616E+0 | 1.2889E+0 | 1.8045E+0 | NM | 5.7196E+0 | 8.1286E-2 |
| 7 | 4.2000E-3 | 3.3880E+0 | 1.2153E+0 | 1.7676E+0 | NM | 5.8265E+0 | 8.2738E-2 |
| 8 | 5.3000E-3 | 3.2039E+0 | 1.1416E+0 | 1.6572E+0 | NM | 5.8800E+0 | 8.2738E-2 |
| 9 | 6.4000E-3 | 2.8356E+0 | 1.0680E+0 | 1.4730E+0 | NM | 5.6127E+0 | 7.5480E-2 |
| 10 | 7.4000E-3 | 2.6146E+0 | 1.0680E+0 | 1.2889E+0 | NM | 5.4523E+0 | 7.4029E-2 |
| 11 | 8.5000E-3 | 2.5042E+0 | 1.0311E+0 | 1.2521E+0 | NM | 5.3989E+0 | 7.2577E-2 |
| 12 | 9.5000E-3 | 2.3569E+0 | 9.5747E-1 | 1.1784E+0 | -1.0551E+0 | 5.2920E+0 | 6.9674E-2 |
| 13 | 1.1700E-2 | 2.1359E+0 | 9.9430E-1 | 1.1048E+0 | -1.4705E+0 | 5.2385E+0 | 6.9674E-2 |
| 14 | 1.3800E-2 | 1.9886E+0 | 1.1048E+0 | 1.0311E+0 | -1.6811E+0 | 5.1316E+0 | 6.8222E-2 |
| 15 | 1.6000E-2 | 1.7308E+0 | 1.2889E+0 | 9.5747E-1 | -1.6575E+0 | 4.8109E+0 | 6.2416E-2 |
| 16 | 1.8100E-2 | 1.5467E+0 | 1.3626E+0 | 8.8382E-1 | -1.4291E+0 | 4.3833E+0 | 5.6610E-2 |
| 17 | 2.0200E-2 | 1.3994E+0 | 1.1784E+0 | 7.7334E-1 | -1.1181E+0 | 4.1694E+0 | 5.3707E-2 |
| 18 | 2.2300E-2 | 1.2889E+0 | 8.8382E-1 | 6.6287E-1 | -9.0945E-1 | 4.0091E+0 | 5.2255E-2 |
| 19 | 2.4400E-2 | 1.2521E+0 | 6.6287E-1 | 5.1556E-1 | -6.5945E-1 | 4.0091E+0 | 5.2255E-2 |
| 20 | 2.6600E-2 | 1.2153E+0 | 5.5239E-1 | 5.1556E-1 | -5.6496E-1 | 3.9022E+0 | 5.0804E-2 |
| 21 | 2.8700E-2 | 1.1416E+0 | 5.5239E-1 | 4.7874E-1 | -3.7008E-1 | 3.6883E+0 | 4.7901E-2 |
| 22 | 3.0800E-2 | 9.5747E-1 | 6.6287E-1 | 4.7874E-1 | -1.9488E-1 | 3.1003E+0 | 4.0643E-2 |
| 23 | 3.3000E-2 | 6.6287E-1 | 8.4700E-1 | 4.4191E-1 | -1.8307E-1 | 2.1382E+0 | 2.7579E-2 |
| 24 | 3.5100E-2 | 5.1556E-1 | 7.3652E-1 | 4.0509E-1 | -6.2992E-2 | 1.6571E+0 | 2.1773E-2 |
| 25 | 3.7200E-2 | 3.3143E-1 | 5.5239E-1 | 4.4191E-1 | -5.1181E-2 | 1.0691E+0 | 1.4515E-2 |
| 26 | 3.9300E-2 | 2.2096E-1 | 5.5239E-1 | 4.4191E-1 | -4.1339E-2 | 6.9491E-1 | 8.7092E-3 |
| 27 | 4.0100E-2 | 1.8413E-1 | NM | NM | NM | 6.4145E-1 | 8.7092E-3 |

7802S

KUSSOY/H/A

TURBULENCE DATA

7802S0214

UT= 1.8728E+01 RHDW= 1.5409E-01 TW= 2.7800E+02 D*= 1.3784E-01

| I | Y [M] | U' UT | V' UT | W' UT | RHO*U'V' RHDW*UT2 | (RHO U)' RHDW*UT | RHO' RHDW |
|----|-----------|-----------|-----------|-----------|----------------------|---------------------|--------------|
| 1 | 1.3000E-3 | 1.0455E+0 | 5.0863E-1 | 9.3249E-1 | NM | 1.6946E+0 | 3.0682E-2 |
| 2 | 1.6000E-3 | 1.1020E+0 | 5.6514E-1 | 9.3249E-1 | NM | 1.8128E+0 | 3.2077E-2 |
| 3 | 1.9000E-3 | 1.1585E+0 | 5.9340E-1 | 9.3249E-1 | NM | 1.8916E+0 | 3.3472E-2 |
| 4 | 2.4000E-3 | 1.1585E+0 | 5.9340E-1 | 8.7597E-1 | NM | 1.9310E+0 | 3.4866E-2 |
| 5 | 2.9000E-3 | 1.1868E+0 | 6.2166E-1 | 8.7597E-1 | NM | 2.0099E+0 | 3.4866E-2 |
| 6 | 3.5000E-3 | 1.2716E+0 | 6.7817E-1 | 8.7597E-1 | NM | 2.1675E+0 | 3.7656E-2 |
| 7 | 4.0000E-3 | 1.3281E+0 | 7.0643E-1 | 8.4771E-1 | -6.1359E-1 | 2.2857E+0 | 3.9050E-2 |
| 8 | 5.1000E-3 | 1.4411E+0 | 7.6294E-1 | 8.4771E-1 | -7.1269E-1 | 2.5222E+0 | 4.3234E-2 |
| 9 | 6.1000E-3 | 1.4976E+0 | 7.9120E-1 | 8.1946E-1 | -7.7506E-1 | 2.6404E+0 | 4.4629E-2 |
| 10 | 7.2000E-3 | 1.5259E+0 | 7.9120E-1 | 8.1946E-1 | -7.8731E-1 | 2.7980E+0 | 4.7418E-2 |
| 11 | 8.3000E-3 | 1.4976E+0 | 7.6294E-1 | 7.9120E-1 | -7.6281E-1 | 2.8375E+0 | 4.8813E-2 |
| 12 | 9.3000E-3 | 1.4694E+0 | 7.6294E-1 | 7.6294E-1 | -7.3274E-1 | 2.8769E+0 | 4.8813E-2 |
| 13 | 1.1500E-2 | 1.4129E+0 | 7.3469E-1 | 7.3469E-1 | -7.0935E-1 | 2.9951E+0 | 5.0208E-2 |
| 14 | 1.3600E-2 | 1.3846E+0 | 7.0643E-1 | 7.0643E-1 | -7.3051E-1 | 3.1133E+0 | 5.1602E-2 |
| 15 | 1.5700E-2 | 1.3281E+0 | 6.7817E-1 | 6.7817E-1 | -7.0156E-1 | 3.1527E+0 | 5.2997E-2 |
| 16 | 1.7800E-2 | 1.2433E+0 | 6.4991E-1 | 5.9340E-1 | -6.4922E-1 | 3.1921E+0 | 5.4392E-2 |
| 17 | 2.0000E-2 | 1.2151E+0 | 5.9340E-1 | 5.6514E-1 | -5.7906E-1 | 3.2709E+0 | 5.4392E-2 |
| 18 | 2.2100E-2 | 1.1868E+0 | 5.9340E-1 | 5.3689E-1 | -5.0668E-1 | 3.2709E+0 | 5.4392E-2 |
| 19 | 2.4200E-2 | 1.1585E+0 | 5.3689E-1 | 4.5211E-1 | -4.4432E-1 | 3.2315E+0 | 5.4392E-2 |
| 20 | 2.6400E-2 | 1.0738E+0 | 4.8037E-1 | 4.8037E-1 | -3.4633E-1 | 3.1133E+0 | 5.1602E-2 |
| 21 | 2.8500E-2 | 9.8900E-1 | 5.0863E-1 | 4.2386E-1 | -2.4276E-1 | 2.8769E+0 | 4.7418E-2 |
| 22 | 3.0600E-2 | 9.0423E-1 | 5.0863E-1 | 3.9560E-1 | -1.6815E-1 | 2.5222E+0 | 4.1840E-2 |
| 23 | 3.2700E-2 | 7.0643E-1 | 4.8037E-1 | 3.9560E-1 | -1.1804E-1 | 1.9310E+0 | 3.2077E-2 |
| 24 | 3.4800E-2 | 5.3689E-1 | 4.5211E-1 | 3.6734E-1 | -8.9087E-2 | 1.4581E+0 | 2.3709E-2 |
| 25 | 3.7000E-2 | 3.9560E-1 | 4.8037E-1 | 3.6734E-1 | -6.9042E-2 | 1.0640E+0 | 1.8131E-2 |
| 26 | 3.9100E-2 | 2.8257E-1 | 4.2386E-1 | 3.3909E-1 | -4.4543E-2 | 7.4877E-1 | 1.2552E-2 |
| 27 | 4.0100E-2 | 2.2606E-1 | NM | NM | NM | 6.3054E-1 | 1.1157E-2 |

| | | |
|--|--|--------|
|  | M: 3.0 falling to 2.6 or 2.3 R THETA x 10 ⁻³ : 2.7 - 5.4 TW/TR: 1.0 | 7803 |
| | | APG-AW |
| Continuous wind tunnel with fixed symmetrical nozzle. W = 0.079, H = 0.086 m. PO: 0.097 MN/m ² TO: 317K. Air, dew-point 236K. RE/m x 10 ⁻⁶ : 6.6. | | |
| LADERMAN A.J., 1978b. Pressure gradient effects on supersonic boundary layer turbulence. Ford Aerospace & Communications Corp., Aeronutronic Division. Rep. No. U-6467. Newport Beach, Calif. And Laderman (1979), A.J. Laderman, private communications. | | |

- 1 The tests took place on ramps which replaced the tunnel floor block to form a smooth continuation of the nozzle. Two were used. "Ramp 1" (series 01) had a profile in which the start of the curvature ($X = 0$) occurred immediately at the nozzle exit plane. "Ramp 3" (series 02) had an initial straight portion 25.4 mm long before curvature started ($X = 0$). Dimensions are given in Table 1. The ramps were designed to give, without allowance for boundary layer effects, constant pressure gradients corresponding to nominal $\frac{\tau_w}{\rho K} = \frac{1}{K_0} = \left[\left(\frac{\rho}{\rho_w} \right) \left(\frac{dp}{dx} \right) \right]$ of 0.4 and 1.85 for series 01 and 02 respectively.
- 2 Flow uniformity and two-dimensionality were assessed by Pitot surveys in the volume over the ramp.
- 5 These included continuous Pitot surveys in the cross flow direction (Z) for $-10 < Z < 10$ mm at seven axial stations for about 12 constant Y -values and continuous surveys in the vertical direction were made at the same X stations for, approximately, $Z = 0, \pm 4, \pm 10$ mm. Sample results from these surveys are given graphically and show the flow to be generally free of significant disturbances. The continuous lateral Pitot surveys given show that for "ramp 1" cross-flow variations in the free stream are negligible, but that in the boundary layer there may be variations of up to 10% of the free stream value over this central 20 mm of the 79 mm wide test section. The samples for "ramp 3" show much less variation, one case showing virtually none while the other varies by about 8%. We wonder (E) therefore whether it is entirely proper to say that there are "only marginal cross flow effects." Disturbances originate from the $X = 0$ region in each case, of negligible strength for "ramp 3" but fairly marked for "ramp 1". With the exception of profiles near $X = 0$ which intersect this shock, it should have no significant effect. The "leading edge" disturbances and the running together of the ramp-induced
- 4 compression wave are the only waves shown in schlieren photographs. The test boundary layer developed
- 5 in the favourable pressure gradient on the nozzle wall. Turbulence is fully developed at the start of the test zone.
- 6 Each ramp was provided with static tapings ($d = 0.84$ mm) at 12.7 mm intervals. Preston tubes 1, 1.63 and 2.36 mm in diameter were used, the results from all three agreeing within 5%. For the main investigation all data were obtained using the 1 mm tube and the Bradshaw & Unsworth(1974) correlation.
- 7 Pitot, static pressure and T_0 profiles were obtained separately, the probe being able to move in both X and the Y directions. Traverses were however made vertically rather than normal to the ramp surface. The Pitot probe was constructed of circular tubing ($d_1 = 0.152, d_2 = 0.076$ mm) which was etched so that the outer surface gradually tapered to an orifice with negligible wall thickness ($d_1 = d_2 = 0.076$ mm). The streamwise length of the probe was 6.3 mm, with the taper extending over the first 3.1 mm. The static pressure probe was an ogive-cylinder probe ($d = 0.51$ mm) with four orifices equally spaced round the circumference 6.3 mm from the tip. The probes were mounted parallel to the ramp surface at the profile station. The T_0 probe consisted of an unshielded thermocouple junction mounted 1.4 mm ahead of a ceramic insulating support ($d = 2.4, l = 25.4$ mm). The chromel-alumel wires ($d = 0.038$ mm) were welded together to form a disc 0.13 mm in diameter.

8 For "ramp 1" the profile stations, excepting 0101 which was in the nozzle ($X = -12.7$ mm), were approximately midway between the static pressure tapings. For "ramp 3" profiles 0201-0203 are in a nominally zero pressure gradient region, again starting in the nozzle. Profiles 0204 ($X = 0$) 0208/10/12/14/ were approximately over static tapings, the remainder about midway between them. The
 9 author has interpolated data where necessary, and also incorporated in the data reduction procedure a programme which interpolates the reduced profile data to give values along the local normals to the ramp surface. It is this interpolated data which is presented. The wall temperature was assumed
 10 to be 300K. No corrections were made to Pitot data, rarefaction and viscous effects being negligible. Wall interference effects were observed very near the wall but not corrected for. Wall interference affected the SPP readings for $Y < 1.2$ mm, and in this region near the wall, the static pressure was interpolated to match the wall static pressure.

12 The editors have accepted the data as presented by the author except for moving the D-state point out, for both series, to a position chosen on the basis of the P0 profile. The profiles constitute two
 13 series, one for each ramp, at 10 and 14 successive stations for "ramp 1" and "ramp 3" respectively.
 14 The wall shear stress values given in the tables are those obtained by the author in a fit to the Coles wall-and-wake law, which were used for consistency with the value of δ used in subsequent data reduction aimed at giving shear stress profiles. The Preston tube values are generally lower than the profile derived values, the maximum difference being 9% at the rear of "ramp 3".

§ DATA: 78030101-0214. Pitot, static pressure and T0 profiles obtained separately. $NX = 10$ and 14 . (Supporting Preston tube CF values).

15 Editors' comments. Experiments on curved walls, giving rise to a 'simple wave' structure, are very few in number. These data must be welcomed therefore as providing information at very close intervals in a flow field of a type only really effectively studied by Sturek & Danberg (CAT 7101). In non-dimensional terms (as described by the value of β_1) the pressure gradients are of order one half (02) and one eighth (01) of the flow in CAT 7101. The dimensionless pressure gradient for (02) is about the same as for the straight wall case studied by Lewis et al. (CAT 7201).

A principal aim of the study, as for the ZPG case, CAT 7702, was to document the flow field in preparation for measurements of the turbulence quantities in the flow field. If the accuracy and resolution are sufficiently great, mean flow measurements can also provide an estimate of the shear stress distribution through the boundary layer, and much of the original report is devoted to this aspect.

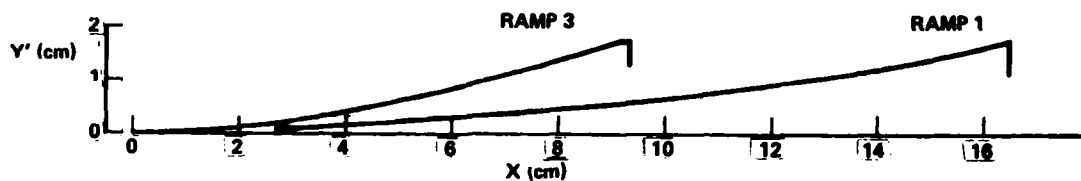
For a comparison with "standard" - AG 253 - semi-empirical relationships and other measurements we have chosen series 02 which describes the flow with the stronger pressure-gradient distribution. Figure 1 shows 4 velocity profiles, 0203 in the ZPG region and 0206, 0211, 0214 at various stations in the APG region. This experimental data falls below the logarithmic law as given by eqn.(3.3.9) of AG 253, shown as a solid line. This is probably not a true physical effect but rather caused by CF values which are too high by about 20%^{*)}. The measurements extend further into the viscous sublayer than those of Sturek & Danberg (1971), cf. Figs.(5.3.15) to (5.3.17) of AG 253. We cannot understand the behaviour of the profiles in the outer region of the boundary layer (Fig. 2) which apparently show no influence of the pressure gradient since all of them agree well with eqn.(3.3.17) of AG 253, as represented by the solid line, derived for zero-pressure gradient flows. Further

^{*)}This may be a result of the determination of the skin friction via the transformed Coles' velocity profile, a procedure which needs a value for the boundary layer thickness δ . As we have shown in section 7, AG 253, δ is particularly ill defined in compressible boundary layers with normal pressure gradients and therefore afflicted with a large uncertainty.

it is interesting to note that τ_w increases and δ_2 remains almost constant downstream from profiles 0105 and 0207, respectively. In this respect we again see the effect of bulk compression overcoming the fall in τ_w and rise in δ_2 observed in APG incompressible flows. The trend here is suppressed rather than reversed as in the more extreme case as studied by Sturek & Danberg (CAT 7101). However, we would again point out that conventional integral thicknesses in these flows do not have a proper physical meaning (AG 253, §7). Agreement between the temperature-velocity relationship according to van Driest (see AG 253) and the measured data is very good (deviations are below 2%).

Table 1: Model coordinates

Facsimile from source paper. Author's symbols and units.



| RAMP CONTOUR | | | |
|--------------|---------|--------|---------|
| RAMP 1 | | RAMP 3 | |
| X (cm) | Y' (cm) | X (cm) | Y' (cm) |
| 2.736 | 0.076 | 1.27 | 0.0475 |
| 4.006 | 0.142 | 2.54 | 0.176 |
| 5.276 | 0.225 | 3.81 | 0.372 |
| 6.439 | 0.316 | 5.08 | 0.626 |
| 7.709 | 0.430 | 6.35 | 0.933 |
| 8.979 | 0.559 | 7.62 | 1.289 |
| 10.249 | 0.703 | 8.89 | 1.689 |
| 11.519 | 0.861 | 9.144 | 1.774 |
| 12.789 | 1.033 | | |
| 14.059 | 1.219 | | |
| 15.329 | 1.409 | | |

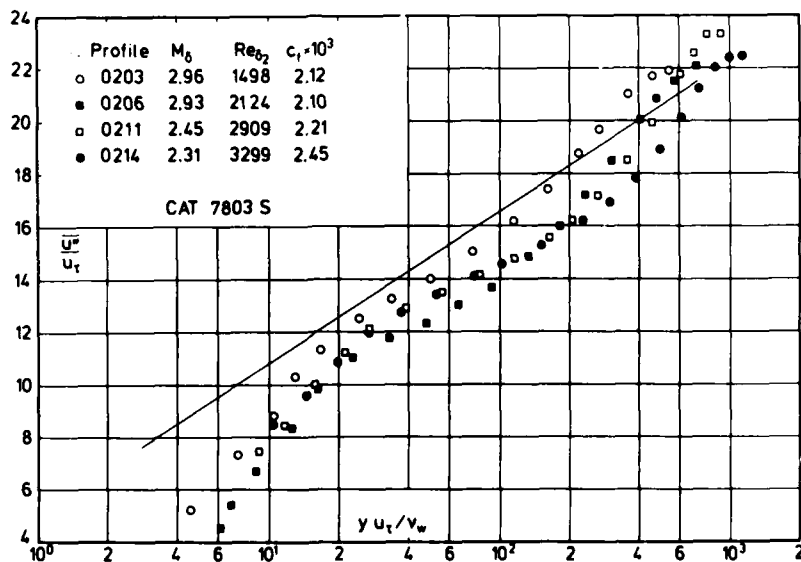
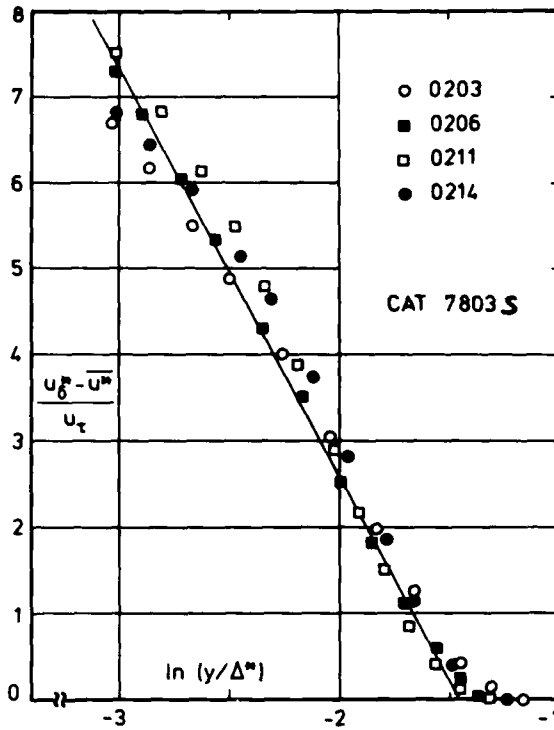


Fig. 1 Law of the wall for a compressible boundary layer in an adverse pressure gradient (adiabatic wall, origin not defined). Laderman (1978).



Outer law for a compressible boundary layer in an adverse pressure gradient (adiabatic wall, origin not defined). Laderman (1978).

| CAT 7803S | | LADERMAN BOUNDARY CONDITIONS AND EVALUATED DATA. SI UNITS | | | | | | | |
|------------------------|-----------------------|---|-----------------------|-----------------------|--------|-----------------------|-----------------------|-----------------------|--|
| PUN | MD * | TW/TR | RED2W | CF | H12 | H12K | PW | PD* | |
| X * | POD | PW/PD | RED2D | CO | H32 | H32K | TW* | TD | |
| RZ | TOD* | TAUW * | OZ | PI2 | H42 | D2K | UD | TR | |
| 7803S0101 | 3.0360 | 1.0137 | 1.1904 ⁺⁰³ | 2.1469 ⁻⁰³ | 5.3391 | 1.4592 | 2.5728 ⁺⁰³ | 2.5051 ⁺⁰³ | |
| -1.2700 ⁻⁰² | 9.7111 ⁺⁰⁴ | 1.0271 | 2.7862 ⁺⁰³ | NM | 1.8003 | 1.7731 | 3.0000 ⁺⁰² | 1.1161 ⁺⁰² | |
| INFINITE | 3.1735 ⁺⁰² | 3.4700 ⁺⁰¹ | 4.3855 ⁻⁰⁴ | NC | 0.0608 | 6.8024 ⁻⁰⁴ | 6.4307 ⁺⁰² | 2.9595 ⁺⁰² | |
| 7803S0102 | 2.8571 | 1.0114 | 1.4975 ⁺⁰³ | 2.2001 ⁻⁰³ | 4.1663 | 1.4469 | 3.3805 ⁺⁰³ | 3.0545 ⁺⁰³ | |
| 2.7356 ⁻⁰² | 9.0428 ⁺⁰⁴ | 1.1067 | 3.2631 ⁺⁰³ | NM | 1.7842 | 1.7594 | 3.0000 ⁺⁰² | 1.2044 ⁺⁰² | |
| INFINITE | 3.1706 ⁺⁰² | 3.8400 ⁺⁰¹ | 4.9945 ⁻⁰⁴ | NC | 0.0583 | 7.1472 ⁻⁰⁴ | 6.2866 ⁺⁰² | 2.9661 ⁺⁰² | |
| 7803S0103 | 2.8300 | 1.0144 | 1.6900 ⁺⁰³ | 2.1573 ⁻⁰³ | 4.1305 | 1.4007 | 3.5557 ⁺⁰³ | 3.2496 ⁺⁰³ | |
| 4.0056 ⁻⁰² | 9.2310 ⁺⁰⁴ | 1.0942 | 3.6540 ⁺⁰³ | NM | 1.7693 | 1.7676 | 3.0000 ⁺⁰² | 1.2144 ⁺⁰² | |
| INFINITE | 3.1596 ⁺⁰² | 3.9300 ⁺⁰¹ | 5.3711 ⁻⁰⁴ | NC | 0.0397 | 7.6759 ⁻⁰⁴ | 6.2528 ⁺⁰² | 2.9573 ⁺⁰² | |
| 7803S0104 | 2.7724 | 1.0095 | 1.7077 ⁺⁰³ | 2.1942 ⁻⁰³ | 4.3626 | 1.3597 | 3.6238 ⁺⁰³ | 3.4899 ⁺⁰³ | |
| 5.2756 ⁻⁰² | 9.0801 ⁺⁰⁴ | 1.0384 | 3.5944 ⁺⁰³ | NM | 1.7991 | 1.7807 | 3.0000 ⁺⁰² | 1.2500 ⁺⁰² | |
| INFINITE | 3.1717 ⁺⁰² | 4.1200 ⁺⁰¹ | 5.2338 ⁻⁰⁴ | NC | 0.0677 | 7.5655 ⁻⁰⁴ | 6.2148 ⁺⁰² | 2.9718 ⁺⁰² | |
| 7803S0105 | 2.8311 | 1.0096 | 1.8632 ⁺⁰³ | 2.2188 ⁻⁰³ | 4.1557 | 1.3930 | 3.7307 ⁺⁰³ | 3.3898 ⁺⁰³ | |
| 6.4389 ⁻⁰² | 9.6467 ⁺⁰⁴ | 1.1006 | 4.0124 ⁺⁰³ | NM | 1.7965 | 1.7752 | 3.0000 ⁺⁰² | 1.2197 ⁺⁰² | |
| INFINITE | 3.1749 ⁺⁰² | 4.2200 ⁺⁰¹ | 5.6866 ⁻⁰⁴ | NC | 0.0699 | 8.0457 ⁻⁰⁴ | 6.2689 ⁺⁰² | 2.9715 ⁺⁰² | |
| 7803S0106 | 2.7711 | 1.0100 | 2.0243 ⁺⁰³ | 2.2428 ⁻⁰³ | 3.7170 | 1.3453 | 4.0015 ⁺⁰³ | 3.6165 ⁺⁰³ | |
| 7.7089 ⁻⁰² | 9.3906 ⁺⁰⁴ | 1.1064 | 4.2606 ⁺⁰³ | NM | 1.8012 | 1.7842 | 3.0000 ⁺⁰² | 1.2501 ⁺⁰² | |
| INFINITE | 3.1701 ⁺⁰² | 4.3600 ⁺⁰¹ | 5.9900 ⁻⁰⁴ | NC | 0.0557 | 8.2187 ⁻⁰⁴ | 6.2121 ⁺⁰² | 2.9704 ⁺⁰² | |
| 7803S0107 | 2.7156 | 1.0079 | 2.0706 ⁺⁰³ | 2.2277 ⁻⁰³ | 4.0441 | 1.3849 | 4.1979 ⁺⁰³ | 3.9217 ⁺⁰³ | |
| 8.9789 ⁻⁰² | 9.3531 ⁺⁰⁴ | 1.0704 | 4.2572 ⁺⁰³ | NM | 1.7968 | 1.7768 | 3.0000 ⁺⁰² | 1.2821 ⁺⁰² | |
| INFINITE | 3.1732 ⁺⁰² | 4.5100 ⁺⁰¹ | 5.8388 ⁻⁰⁴ | NC | 0.0623 | 8.1708 ⁻⁰⁴ | 6.1652 ⁺⁰² | 2.9765 ⁺⁰² | |
| 7803S0108 | 2.6230 | 1.0090 | 2.0949 ⁺⁰³ | 2.2769 ⁻⁰³ | 3.9736 | 1.3811 | 4.5190 ⁺⁰³ | 4.2770 ⁺⁰³ | |
| 1.0249 ⁻⁰¹ | 8.8431 ⁺⁰⁴ | 1.0566 | 4.1596 ⁺⁰³ | NM | 1.7994 | 1.7803 | 3.0000 ⁺⁰² | 1.3316 ⁺⁰² | |
| INFINITE | 3.1639 ⁺⁰² | 4.6900 ⁺⁰¹ | 5.7151 ⁻⁰⁴ | NC | 0.0523 | 7.8927 ⁻⁰⁴ | 6.0686 ⁺⁰² | 2.9733 ⁺⁰² | |
| 7803S0109 | 2.5769 | 1.0058 | 2.1930 ⁺⁰³ | 2.3306 ⁻⁰³ | 3.8427 | 1.3690 | 4.7429 ⁺⁰³ | 4.5506 ⁺⁰³ | |
| 1.1519 ⁻⁰¹ | 8.7619 ⁺⁰⁴ | 1.0427 | 4.2655 ⁺⁰³ | NM | 1.8039 | 1.7844 | 3.0000 ⁺⁰² | 1.3619 ⁺⁰² | |
| INFINITE | 3.1707 ⁺⁰² | 4.9300 ⁺⁰¹ | 5.7881 ⁻⁰⁴ | NC | 0.0597 | 7.9030 ⁻⁰⁴ | 6.0296 ⁺⁰² | 2.9826 ⁺⁰² | |
| 7803S0110 | 2.5781 | 1.0060 | 2.3248 ⁺⁰³ | 2.3901 ⁻⁰³ | 3.5126 | 1.3270 | 4.9860 ⁺⁰³ | 4.5952 ⁺⁰³ | |
| 1.2789 ⁻⁰¹ | 8.8633 ⁺⁰⁴ | 1.0851 | 4.5245 ⁺⁰³ | NM | 1.8104 | 1.7953 | 3.0000 ⁺⁰² | 1.3611 ⁺⁰² | |
| INFINITE | 3.1703 ⁺⁰² | 5.1100 ⁺⁰¹ | 6.0719 ⁻⁰⁴ | NC | 0.0579 | 8.0228 ⁻⁰⁴ | 6.0304 ⁺⁰² | 2.9821 ⁺⁰² | |

| CAT 78035 LADERMAN BOUNDARY CONDITIONS AND EVALUATED DATA, SI UNITS | | | | | | | | | |
|---|------------------------|------------------------|------------------------|------------------------|--------|------------------------|------------------------|------------------------|--|
| RUN | MD * | TW/TR | REDZW | CF | H12 | H12K | PH | PD* | |
| X * | POD | PW/PD | REDZD | CO | H32 | H32K | T* | TD | |
| RZ | TOD* | TAUW * | DZ | PIZ | H42 | D2K | UD | TR | |
| 7803S0201 | 2.9480 | 1.0104 | 1.4666 ⁺ 03 | 2.0850 ⁻ 03 | 4.7259 | 1.4231 | 2.9050 ⁺ 03 | 2.7672 ⁺ 03 | |
| -3.1750 ⁻ 02 | 9.4007 ⁺ 04 | 1.0498 | 3.3074 ⁺ 03 | NM | 1.7936 | 1.7677 | 3.0000 ⁺ 02 | 1.1610 ⁺ 02 | |
| INFINITE | 3.1790 ⁺ 02 | 3.5100 ⁺ 01 | 5.1376 ⁻ 04 | NC | 0.0708 | 7.6738 ⁻ 04 | 6.3688 ⁺ 02 | 2.9692 ⁺ 02 | |
| 7803S0202 | 2.9613 | 1.0096 | 1.5320 ⁺ 03 | 2.1526 ⁻ 03 | 4.3434 | 1.3994 | 2.9884 ⁺ 03 | 2.7404 ⁺ 03 | |
| -1.9050 ⁻ 02 | 9.4970 ⁺ 04 | 1.0905 | 3.4703 ⁺ 03 | NM | 1.7914 | 1.7671 | 3.0000 ⁺ 02 | 1.1556 ⁺ 02 | |
| INFINITE | 3.1822 ⁺ 02 | 3.6200 ⁺ 01 | 5.3825 ⁻ 04 | NC | 0.0814 | 7.8384 ⁻ 04 | 6.3824 ⁺ 02 | 2.9714 ⁺ 02 | |
| 7803S0203 | 2.9571 | 1.0104 | 1.4835 ⁺ 03 | 2.1268 ⁻ 03 | 4.8350 | 1.4088 | 2.8949 ⁺ 03 | 2.7653 ⁺ 03 | |
| -6.3500 ⁻ 03 | 9.5233 ⁺ 04 | 1.0469 | 3.3575 ⁺ 03 | NM | 1.7986 | 1.7752 | 3.0000 ⁺ 02 | 1.1566 ⁺ 02 | |
| INFINITE | 3.1795 ⁺ 02 | 3.6000 ⁺ 01 | 5.1747 ⁻ 04 | NC | 0.0688 | 7.7477 ⁻ 04 | 6.3764 ⁺ 02 | 2.9691 ⁺ 02 | |
| 7803S0204 | 2.9229 | 1.0095 | 1.5040 ⁺ 03 | 2.1403 ⁻ 03 | 4.7930 | 1.4204 | 2.9056 ⁺ 03 | 2.7969 ⁺ 03 | |
| 0.0000 ⁺ 00 | 9.1482 ⁺ 04 | 1.0389 | 3.3560 ⁺ 03 | NM | 1.8041 | 1.7832 | 3.0000 ⁺ 02 | 1.1742 ⁺ 02 | |
| INFINITE | 3.1805 ⁺ 02 | 3.5800 ⁺ 01 | 5.2871 ⁻ 04 | NC | 0.0869 | 7.8367 ⁻ 04 | 6.3503 ⁺ 02 | 2.9718 ⁺ 02 | |
| 7803S0205 | 2.9194 | 1.0118 | 1.5546 ⁺ 03 | 2.2925 ⁻ 03 | 4.5490 | 1.4759 | 3.1255 ⁺ 03 | 2.7637 ⁺ 03 | |
| 6.3500 ⁻ 03 | 8.9922 ⁺ 04 | 1.1309 | 3.4719 ⁺ 03 | NM | 1.7807 | 1.7551 | 3.0000 ⁺ 02 | 1.1731 ⁺ 02 | |
| INFINITE | 3.1729 ⁺ 02 | 3.7800 ⁺ 01 | 5.5351 ⁻ 04 | NC | 0.0727 | 8.0345 ⁻ 04 | 6.3399 ⁺ 02 | 2.9649 ⁺ 02 | |
| 7803S0206 | 2.9347 | 1.0103 | 2.1378 ⁺ 03 | 2.0977 ⁻ 03 | 1.9081 | 1.4467 | 3.8924 ⁺ 03 | 2.6570 ⁺ 03 | |
| 1.9050 ⁻ 02 | 8.8461 ⁺ 04 | 1.4649 | 4.7955 ⁺ 03 | NM | 1.7773 | 1.7592 | 3.0000 ⁺ 02 | 1.1676 ⁺ 02 | |
| INFINITE | 3.1787 ⁺ 02 | 3.3600 ⁺ 01 | 7.8571 ⁻ 04 | NC | 0.0669 | 8.9842 ⁻ 04 | 6.3579 ⁺ 02 | 2.9695 ⁺ 02 | |
| 7803S0207 | 2.7166 | 1.0067 | 2.2074 ⁺ 03 | 2.1997 ⁻ 03 | 2.9378 | 1.4783 | 4.6046 ⁺ 03 | 3.6783 ⁺ 03 | |
| 3.1750 ⁻ 02 | 8.7858 ⁺ 04 | 1.2518 | 4.5353 ⁺ 03 | NM | 1.7635 | 1.7431 | 3.0000 ⁺ 02 | 1.2831 ⁺ 02 | |
| INFINITE | 3.1770 ⁺ 02 | 4.1800 ⁺ 01 | 6.6366 ⁻ 04 | NC | 0.0634 | 8.5395 ⁻ 04 | 6.1698 ⁺ 02 | 2.9800 ⁺ 02 | |
| 7803S0208 | 2.6319 | 1.0058 | 2.3978 ⁺ 03 | 2.2052 ⁻ 03 | 2.9267 | 1.4205 | 5.2167 ⁺ 03 | 4.1617 ⁺ 03 | |
| 3.8100 ⁻ 02 | 8.7247 ⁺ 04 | 1.2535 | 4.7639 ⁺ 03 | NM | 1.7557 | 1.7405 | 3.0000 ⁺ 02 | 1.3307 ⁺ 02 | |
| INFINITE | 3.1744 ⁺ 02 | 4.4500 ⁺ 01 | 6.6977 ⁻ 04 | NC | 0.0665 | 8.5719 ⁻ 04 | 6.0874 ⁺ 02 | 2.9826 ⁺ 02 | |
| 7803S0209 | 2.6099 | 1.0055 | 2.6902 ⁺ 03 | 2.3032 ⁻ 03 | 2.2019 | 1.4947 | 5.7947 ⁺ 03 | 4.3069 ⁺ 03 | |
| 4.4450 ⁻ 02 | 8.7273 ⁺ 04 | 1.3454 | 5.2983 ⁺ 03 | NM | 1.7534 | 1.7362 | 3.0000 ⁺ 02 | 1.3435 ⁺ 02 | |
| INFINITE | 3.1738 ⁺ 02 | 4.7300 ⁺ 01 | 7.3573 ⁻ 04 | NC | 0.0590 | 8.6606 ⁻ 04 | 6.0654 ⁺ 02 | 2.9835 ⁺ 02 | |
| 7803S0210 | 2.5793 | 1.0052 | 3.0627 ⁺ 03 | 2.3320 ⁻ 03 | 1.9910 | 1.4382 | 6.3290 ⁺ 03 | 4.7237 ⁺ 03 | |
| 5.0800 ⁻ 02 | 9.1286 ⁺ 04 | 1.3398 | 5.9591 ⁺ 03 | NM | 1.7558 | 1.7389 | 3.0000 ⁺ 02 | 1.3614 ⁺ 02 | |
| INFINITE | 3.1729 ⁺ 02 | 5.1300 ⁺ 01 | 7.7790 ⁻ 04 | NC | 0.0536 | 9.0701 ⁻ 04 | 6.0341 ⁺ 02 | 2.9845 ⁺ 02 | |
| 7803S0211 | 2.4447 | 1.0029 | 2.8971 ⁺ 03 | 2.2048 ⁻ 03 | 2.9192 | 1.3687 | 6.7134 ⁺ 03 | 5.8113 ⁺ 03 | |
| 5.7150 ⁻ 02 | 9.1091 ⁺ 04 | 1.1552 | 5.3417 ⁺ 03 | NM | 1.7713 | 1.7594 | 3.0000 ⁺ 02 | 1.4445 ⁺ 02 | |
| INFINITE | 3.1710 ⁺ 02 | 5.3600 ⁺ 01 | 6.5004 ⁻ 04 | NC | 0.0650 | 8.3321 ⁻ 04 | 5.8909 ⁺ 02 | 2.9915 ⁺ 02 | |
| 7803S0212 | 2.3761 | 1.0013 | 2.7860 ⁺ 03 | 2.3409 ⁻ 03 | 3.2335 | 1.3935 | 7.0130 ⁺ 03 | 6.2692 ⁺ 03 | |
| 6.3500 ⁻ 02 | 8.8298 ⁺ 04 | 1.1186 | 4.9974 ⁺ 03 | NM | 1.7688 | 1.7557 | 3.0000 ⁺ 02 | 1.4893 ⁺ 02 | |
| INFINITE | 3.1709 ⁺ 02 | 5.8000 ⁺ 01 | 6.0533 ⁻ 04 | NC | 0.0679 | 7.9030 ⁻ 04 | 5.8138 ⁺ 02 | 2.9960 ⁺ 02 | |
| 7803S0213 | 2.3544 | 1.0003 | 3.0826 ⁺ 03 | 2.3982 ⁻ 03 | 2.7648 | 1.3982 | 7.6700 ⁺ 03 | 6.5227 ⁺ 03 | |
| 6.9850 ⁻ 02 | 8.8810 ⁺ 04 | 1.1759 | 5.4789 ⁺ 03 | NM | 1.7695 | 1.7574 | 3.0000 ⁺ 02 | 1.5046 ⁺ 02 | |
| INFINITE | 3.1727 ⁺ 02 | 6.0700 ⁺ 01 | 6.5302 ⁻ 04 | NC | 0.0741 | 8.0801 ⁻ 04 | 5.7904 ⁺ 02 | 2.9992 ⁺ 02 | |
| 7803S0214 | 2.2889 | 0.9986 | 3.2010 ⁺ 03 | 2.380 ⁻ 03 | 2.8936 | 1.3568 | 8.0542 ⁺ 03 | 7.2365 ⁺ 03 | |
| 7.6200 ⁻ 02 | 8.8924 ⁺ 04 | 1.1130 | 5.5419 ⁺ 03 | NM | 1.7820 | 1.7712 | 3.0000 ⁺ 02 | 1.5495 ⁺ 02 | |
| INFINITE | 3.1730 ⁺ 02 | 6.4700 ⁺ 01 | 6.3803 ⁻ 04 | NC | 0.0737 | 8.0250 ⁻ 04 | 5.7125 ⁺ 02 | 3.0042 ⁺ 02 | |

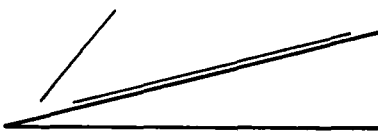
| 7803S0214 LADERMAN PROFILE TABULATION 101 POINTS, DELTA AT POINT 87 | | | | | | | | |
|---|------------------------|------------------------|---------|---------|---------|---------|---------|-----------|
| I | Y | PTZ/P | P/PD | TO/TOD | M/MD | U/UD | T/TD | R/RD*U/UD |
| 1 | 0.0000 ⁺ 00 | 1.0000 ⁺ 00 | 1.11300 | 0.94547 | 0.00000 | 0.00000 | 1.93611 | 0.00000 |
| 2 | 7.3040 ⁻ 05 | 1.3984 ⁺ 00 | 1.11153 | 0.95082 | 0.30977 | 0.41202 | 1.76919 | 0.25886 |
| 3 | 8.2969 ⁻ 05 | 1.4313 ⁺ 00 | 1.11133 | 0.95377 | 0.32088 | 0.42604 | 1.76292 | 0.26857 |
| 4 | 1.0283 ⁻ 04 | 1.5308 ⁺ 00 | 1.11093 | 0.95570 | 0.35138 | 0.46256 | 1.73288 | 0.29654 |
| 5 | 1.0226 ⁻ 04 | 1.6213 ⁺ 00 | 1.11053 | 0.95742 | 0.37591 | 0.49124 | 1.70774 | 0.31945 |
| 6 | 1.4056 ⁻ 04 | 1.7286 ⁺ 00 | 1.11016 | 0.95920 | 0.40193 | 0.52094 | 1.67988 | 0.34427 |
| 7 | 1.5049 ⁻ 04 | 1.7930 ⁺ 00 | 1.10996 | 0.96008 | 0.41626 | 0.53695 | 1.66394 | 0.35818 |
| 8 | 1.6042 ⁻ 04 | 1.8360 ⁺ 00 | 1.10976 | 0.96055 | 0.42536 | 0.54696 | 1.65354 | 0.36709 |
| 9 | 1.7034 ⁻ 04 | 1.8765 ⁺ 00 | 1.10956 | 0.96098 | 0.43362 | 0.55598 | 1.64399 | 0.37524 |
| 10 | 1.7829 ⁻ 04 | 1.9167 ⁺ 00 | 1.10940 | 0.96139 | 0.44156 | 0.56457 | 1.63476 | 0.38313 |
| 11 | 1.9219 ⁻ 04 | 1.9461 ⁺ 00 | 1.10912 | 0.96169 | 0.44719 | 0.57062 | 1.62817 | 0.38871 |
| 12 | 2.0410 ⁻ 04 | 1.9889 ⁺ 00 | 1.10888 | 0.96211 | 0.45519 | 0.57915 | 1.61875 | 0.39673 |
| 13 | 2.1602 ⁻ 04 | 2.0236 ⁺ 00 | 1.10864 | 0.96245 | 0.46153 | 0.58584 | 1.61127 | 0.40309 |
| 14 | 2.4183 ⁻ 04 | 2.0814 ⁺ 00 | 1.10812 | 0.96299 | 0.47175 | 0.59656 | 1.59911 | 0.41339 |
| 15 | 2.6566 ⁻ 04 | 2.1385 ⁺ 00 | 1.10763 | 0.96352 | 0.48154 | 0.60670 | 1.58740 | 0.42333 |
| 16 | 2.9148 ⁻ 04 | 2.1879 ⁺ 00 | 1.10711 | 0.96396 | 0.48978 | 0.61516 | 1.57748 | 0.43173 |
| 17 | 3.1531 ⁻ 04 | 2.2367 ⁺ 00 | 1.10663 | 0.96439 | 0.49774 | 0.62324 | 1.56786 | 0.43989 |
| 18 | 3.4113 ⁻ 04 | 2.2708 ⁺ 00 | 1.10611 | 0.96470 | 0.50319 | 0.62874 | 1.56129 | 0.44544 |
| 19 | 3.7489 ⁻ 04 | 2.3124 ⁺ 00 | 1.10542 | 0.96526 | 0.50973 | 0.63536 | 1.55366 | 0.45206 |
| 20 | 3.9872 ⁻ 04 | 2.3574 ⁺ 00 | 1.10494 | 0.96579 | 0.51668 | 0.64232 | 1.54544 | 0.45923 |
| 21 | 4.1460 ⁻ 04 | 2.3754 ⁺ 00 | 1.10462 | 0.96603 | 0.51942 | 0.64506 | 1.54225 | 0.46201 |
| 22 | 4.4042 ⁻ 04 | 2.4082 ⁺ 00 | 1.10410 | 0.96647 | 0.52438 | 0.64998 | 1.53645 | 0.46708 |
| 23 | 4.9602 ⁻ 04 | 2.4684 ⁺ 00 | 1.10297 | 0.96731 | 0.53333 | 0.65884 | 1.52604 | 0.47619 |
| 24 | 5.4368 ⁻ 04 | 2.5172 ⁺ 00 | 1.10201 | 0.96801 | 0.54043 | 0.66581 | 1.51779 | 0.48342 |
| 25 | 5.9531 ⁻ 04 | 2.5648 ⁺ 00 | 1.10097 | 0.96872 | 0.54726 | 0.67247 | 1.50991 | 0.49034 |

(continued)

(continued)

| 7803S0214 | | LADERMAN | | PROFILE TABULATION | | | 101 POINTS, DELTA AT POINT 87 | | |
|-----------|-------------------------|-------------------------|---------|--------------------|---------|---------|-------------------------------|-----------|--|
| I | Y | PT2/P | P/PD | TO/TOD | M/MD | U/UD | T/TD | R/RD*U/UD | |
| 26 | 6.5091 ^m -04 | 2.6110 ^m +00 | 1.09984 | 0.96944 | 0.55379 | 0.67880 | 1.50242 | 0.49691 | |
| 27 | 7.2042 ^m -04 | 2.6610 ^m +00 | 1.09844 | 0.97019 | 0.56075 | 0.68549 | 1.49439 | 0.50387 | |
| 28 | 7.9389 ^m -04 | 2.7250 ^m +00 | 1.09695 | 0.97071 | 0.56952 | 0.69369 | 1.48359 | 0.51291 | |
| 29 | 8.6936 ^m -04 | 2.7784 ^m +00 | 1.09543 | 0.97165 | 0.57670 | 0.70052 | 1.47553 | 0.52007 | |
| 30 | 9.4085 ^m -04 | 2.8104 ^m +00 | 1.09398 | 0.97277 | 0.58097 | 0.70476 | 1.47159 | 0.52392 | |
| 31 | 1.0084 ^m -03 | 2.8662 ^m +00 | 1.09262 | 0.97330 | 0.58830 | 0.71150 | 1.46268 | 0.53149 | |
| 32 | 1.0719 ^m -03 | 2.9059 ^m +00 | 1.09133 | 0.97362 | 0.59346 | 0.71618 | 1.45634 | 0.53668 | |
| 33 | 1.1533 ^m -03 | 2.9629 ^m +00 | 1.08969 | 0.97403 | 0.60077 | 0.72274 | 1.44729 | 0.54416 | |
| 34 | 1.2189 ^m -03 | 3.0000 ^m +00 | 1.08836 | 0.97431 | 0.60548 | 0.72694 | 1.44148 | 0.54887 | |
| 35 | 1.2904 ^m -03 | 3.0345 ^m +00 | 1.08692 | 0.97455 | 0.60982 | 0.73079 | 1.43610 | 0.55310 | |
| 36 | 1.4075 ^m -03 | 3.1035 ^m +00 | 1.08456 | 0.97564 | 0.61839 | 0.73855 | 1.42637 | 0.56156 | |
| 37 | 1.5287 ^m -03 | 3.1756 ^m +00 | 1.08211 | 0.97626 | 0.62721 | 0.74626 | 1.41565 | 0.57043 | |
| 38 | 1.6498 ^m -03 | 3.2608 ^m +00 | 1.07966 | 0.97744 | 0.63746 | 0.75529 | 1.40386 | 0.58087 | |
| 39 | 1.7709 ^m -03 | 3.3311 ^m +00 | 1.07722 | 0.97743 | 0.64577 | 0.76215 | 1.39294 | 0.58940 | |
| 40 | 1.8841 ^m -03 | 3.4109 ^m +00 | 1.07493 | 0.97788 | 0.65508 | 0.76992 | 1.38138 | 0.59912 | |
| 41 | 2.0033 ^m -03 | 3.4804 ^m +00 | 1.07252 | 0.97832 | 0.66305 | 0.77653 | 1.37158 | 0.60722 | |
| 42 | 2.1264 ^m -03 | 3.5620 ^m +00 | 1.06983 | 0.97892 | 0.67230 | 0.78413 | 1.36036 | 0.61667 | |
| 43 | 2.2475 ^m -03 | 3.6447 ^m +00 | 1.06729 | 0.97940 | 0.68153 | 0.79159 | 1.34905 | 0.62626 | |
| 44 | 2.3726 ^m -03 | 3.7360 ^m +00 | 1.06522 | 0.97995 | 0.69156 | 0.79959 | 1.33682 | 0.63714 | |
| 45 | 2.4958 ^m -03 | 3.8277 ^m +00 | 1.06389 | 0.98119 | 0.70148 | 0.80769 | 1.32573 | 0.64817 | |
| 46 | 2.6169 ^m -03 | 3.9136 ^m +00 | 1.06323 | 0.98181 | 0.71065 | 0.81486 | 1.31481 | 0.65895 | |
| 47 | 2.7400 ^m -03 | 3.9939 ^m +00 | 1.06263 | 0.98237 | 0.71909 | 0.82139 | 1.30476 | 0.66896 | |
| 48 | 2.8611 ^m -03 | 4.0809 ^m +00 | 1.06257 | 0.98290 | 0.72813 | 0.82827 | 1.29396 | 0.68015 | |
| 49 | 2.9862 ^m -03 | 4.1789 ^m +00 | 1.06063 | 0.98416 | 0.73817 | 0.83609 | 1.28290 | 0.69123 | |
| 50 | 3.1094 ^m -03 | 4.2674 ^m +00 | 1.05911 | 0.98539 | 0.74711 | 0.84302 | 1.27322 | 0.70126 | |
| 51 | 3.2325 ^m -03 | 4.3696 ^m +00 | 1.05767 | 0.98612 | 0.75731 | 0.85054 | 1.26138 | 0.71318 | |
| 52 | 3.3556 ^m -03 | 4.4621 ^m +00 | 1.05824 | 0.98740 | 0.76641 | 0.85744 | 1.25165 | 0.72494 | |
| 53 | 3.4748 ^m -03 | 4.5685 ^m +00 | 1.05768 | 0.98814 | 0.77674 | 0.86486 | 1.23978 | 0.73783 | |
| 54 | 3.5959 ^m -03 | 4.6709 ^m +00 | 1.05570 | 0.98934 | 0.78655 | 0.87203 | 1.22918 | 0.74896 | |
| 55 | 3.7170 ^m -03 | 4.7820 ^m +00 | 1.05399 | 0.98997 | 0.79705 | 0.87932 | 1.21710 | 0.76148 | |
| 56 | 3.8362 ^m -03 | 4.8894 ^m +00 | 1.05354 | 0.99136 | 0.80707 | 0.88653 | 1.20660 | 0.77407 | |
| 57 | 3.9573 ^m -03 | 4.9831 ^m +00 | 1.05395 | 0.99196 | 0.81570 | 0.89240 | 1.19689 | 0.78581 | |
| 58 | 4.0785 ^m -03 | 5.0955 ^m +00 | 1.05219 | 0.99326 | 0.82593 | 0.89953 | 1.18617 | 0.79793 | |
| 59 | 4.2016 ^m -03 | 5.2028 ^m +00 | 1.05152 | 0.99446 | 0.83558 | 0.90616 | 1.17608 | 0.81019 | |
| 60 | 4.3207 ^m -03 | 5.3064 ^m +00 | 1.05019 | 0.99501 | 0.84478 | 0.91214 | 1.16582 | 0.82167 | |
| 61 | 4.4419 ^m -03 | 5.4159 ^m +00 | 1.04898 | 0.99571 | 0.85441 | 0.91836 | 1.15530 | 0.83384 | |
| 62 | 4.5610 ^m -03 | 5.5108 ^m +00 | 1.04856 | 0.99743 | 0.86266 | 0.92415 | 1.14765 | 0.84436 | |
| 63 | 4.6821 ^m -03 | 5.6118 ^m +00 | 1.04816 | 0.99752 | 0.87135 | 0.92939 | 1.13767 | 0.85627 | |
| 64 | 4.8053 ^m -03 | 5.7259 ^m +00 | 1.04656 | 0.99865 | 0.88106 | 0.93565 | 1.12775 | 0.86829 | |
| 65 | 4.9264 ^m -03 | 5.8346 ^m +00 | 1.04450 | 0.99926 | 0.89021 | 0.94126 | 1.11797 | 0.87940 | |
| 66 | 5.0535 ^m -03 | 5.9451 ^m +00 | 1.04302 | 1.00032 | 0.89942 | 0.94704 | 1.10870 | 0.89094 | |
| 67 | 5.1726 ^m -03 | 6.0538 ^m +00 | 1.04171 | 1.00087 | 0.90838 | 0.95237 | 1.09921 | 0.90255 | |
| 68 | 5.2938 ^m -03 | 6.1387 ^m +00 | 1.04192 | 1.00175 | 0.91532 | 0.95667 | 1.09241 | 0.91247 | |
| 69 | 5.4169 ^m -03 | 6.2344 ^m +00 | 1.04079 | 1.00242 | 0.92307 | 0.96129 | 1.08451 | 0.92253 | |
| 70 | 5.5420 ^m -03 | 6.3205 ^m +00 | 1.03951 | 1.00266 | 0.92999 | 0.96519 | 1.07712 | 0.93149 | |
| 71 | 5.6612 ^m -03 | 6.4030 ^m +00 | 1.03831 | 1.00297 | 0.93658 | 0.96890 | 1.07023 | 0.94001 | |
| 72 | 5.7803 ^m -03 | 6.4979 ^m +00 | 1.03646 | 1.00336 | 0.94409 | 0.97312 | 1.06244 | 0.94932 | |
| 73 | 5.9014 ^m -03 | 6.5853 ^m +00 | 1.03389 | 1.00320 | 0.95096 | 0.97669 | 1.05484 | 0.95729 | |
| 74 | 6.0226 ^m -03 | 6.6554 ^m +00 | 1.03230 | 1.00322 | 0.95643 | 0.97957 | 1.04897 | 0.96400 | |
| 75 | 6.1417 ^m -03 | 6.7178 ^m +00 | 1.03140 | 1.00343 | 0.96128 | 0.98220 | 1.04400 | 0.97034 | |
| 76 | 6.2629 ^m -03 | 6.7764 ^m +00 | 1.02977 | 1.00317 | 0.96580 | 0.98441 | 1.03890 | 0.97576 | |
| 77 | 6.3840 ^m -03 | 6.8455 ^m +00 | 1.02655 | 1.00268 | 0.97111 | 0.98690 | 1.03277 | 0.98095 | |
| 78 | 6.5071 ^m -03 | 6.9056 ^m +00 | 1.02368 | 1.00308 | 0.97571 | 0.98943 | 1.02833 | 0.98495 | |
| 79 | 6.6263 ^m -03 | 6.9581 ^m +00 | 1.02151 | 1.00264 | 0.97971 | 0.99124 | 1.02369 | 0.98914 | |
| 80 | 6.7454 ^m -03 | 7.0071 ^m +00 | 1.01921 | 1.00223 | 0.98342 | 0.99290 | 1.01938 | 0.99274 | |
| 81 | 6.8666 ^m -03 | 7.0472 ^m +00 | 1.01680 | 1.00224 | 0.98645 | 0.99443 | 1.01624 | 0.99497 | |
| 82 | 6.9857 ^m -03 | 7.0794 ^m +00 | 1.01519 | 1.00176 | 0.98888 | 0.99540 | 1.01323 | 0.99732 | |
| 83 | 7.1068 ^m -03 | 7.1111 ^m +00 | 1.01304 | 1.00109 | 0.99126 | 0.99624 | 1.01009 | 0.99916 | |
| 84 | 7.2280 ^m -03 | 7.1450 ^m +00 | 1.01015 | 1.00098 | 0.99380 | 0.99745 | 1.00735 | 1.00022 | |
| 85 | 7.3531 ^m -03 | 7.1736 ^m +00 | 1.00671 | 1.00046 | 0.99594 | 0.99824 | 1.00463 | 1.00030 | |
| 86 | 7.4782 ^m -03 | 7.2033 ^m +00 | 1.00350 | 1.00035 | 0.99816 | 0.99927 | 1.00224 | 1.00053 | |
| D 87 | 7.6033 ^m -03 | 7.2281 ^m +00 | 1.00000 | 1.00000 | 1.00000 | 1.00000 | 1.00000 | 1.00000 | |
| 88 | 7.7224 ^m -03 | 7.2477 ^m +00 | 0.99678 | 1.00032 | 1.00145 | 1.00087 | 0.99883 | 0.99882 | |
| 89 | 7.8436 ^m -03 | 7.2656 ^m +00 | 0.99425 | 0.99951 | 1.00278 | 1.00111 | 0.99667 | 0.99869 | |
| 90 | 7.9667 ^m -03 | 7.2871 ^m +00 | 0.99070 | 0.99927 | 1.00438 | 1.00176 | 0.99480 | 0.99763 | |
| 91 | 8.0878 ^m -03 | 7.3063 ^m +00 | 0.98689 | 0.99930 | 1.00580 | 1.00247 | 0.99338 | 0.99591 | |
| 92 | 8.2090 ^m -03 | 7.3241 ^m +00 | 0.98317 | 0.99934 | 1.00711 | 1.00313 | 0.99209 | 0.99410 | |
| 93 | 8.3321 ^m -03 | 7.3391 ^m +00 | 0.97931 | 0.99916 | 1.00822 | 1.00357 | 0.99079 | 0.99195 | |
| 94 | 8.4512 ^m -03 | 7.3517 ^m +00 | 0.97524 | 0.99828 | 1.00915 | 1.00357 | 0.98897 | 0.98964 | |
| 95 | 8.5724 ^m -03 | 7.3688 ^m +00 | 0.97190 | 0.99878 | 1.01041 | 1.00443 | 0.98820 | 0.98786 | |
| 96 | 8.6935 ^m -03 | 7.3725 ^m +00 | 0.96925 | 0.99895 | 1.01068 | 1.00464 | 0.98808 | 0.98549 | |
| 97 | 8.8166 ^m -03 | 7.3828 ^m +00 | 0.96622 | 0.99877 | 1.01144 | 1.00492 | 0.98715 | 0.98362 | |
| 98 | 8.9358 ^m -03 | 7.3956 ^m +00 | 0.96228 | 0.99870 | 1.01238 | 1.00533 | 0.98613 | 0.98102 | |
| 99 | 9.0549 ^m -03 | 7.4143 ^m +00 | 0.95764 | 0.99858 | 1.01375 | 1.00593 | 0.98463 | 0.97836 | |
| 100 | 9.1761 ^m -03 | 7.4287 ^m +00 | 0.95417 | 0.99862 | 1.01481 | 1.00646 | 0.98361 | 0.97633 | |
| 101 | 9.2952 ^m -03 | 7.4373 ^m +00 | 0.95092 | 0.99877 | 1.01544 | 1.00683 | 0.98312 | 0.97386 | |

INPUT VARIABLES Y,M,TO/TOD,P/PD - P/PD[1],P/PD[2] LINEAR EXTRAPOLATED
TO/TOD[1]=300/TOD

| | | |
|---|---|-----------------|
|  | M: 10.0 - 11.6 R THETA x 10 ⁻³ : 2.9 - 19 TW/TR: 0.42 - 1.05 | 7804 |
| | | ZPG AW - SHT |
| Axially symmetric blow-down tunnel. Running time 5s. D = 1.52 m. M = 18 (Free-stream). 2<P0<14 MN/m ² (Reservoir). T0: 305K. Helium, 9<RE/m x 10 ⁻⁶ <46 (Free-stream). | | |
| WATSON R.D., 1978. Characteristics of Mach 10 transitional and turbulent boundary layers. NASA TP 1243 And: Watson R.D., private communications, Watson et al., CAT 7305. | | |

- The report cited above includes the data for Watson et al., CAT 7305, obtained on "model 1". The details below apply to tests with "model 2" only. The test boundary layer was formed on a flat surface (L = 2.29, W = 0.61 m) inclined at 4° to the free stream. The leading edge (X = 0) had a maximum thickness of 0.1 mm, and was positioned 0.102 m below the tunnel centreline and 0.171 m from the final nozzle plane. The surface was cooled by liquid nitrogen in three streamwise sections, X = 0-0.23, 0.23-1.59, 1.59-2.29 m. Before each run the coolant was cut off, and 5 sec. allowed for the model temperature to stabilise. On the centreline, two chambers for instrumentation with interchangeable
- 2 sections of surface were provided running from X = 0.38-1.41, 1.49-2.29 m. The tunnel test core is
 - 3 about 0.4 m in diameter, with a free-stream Mach number gradient of about 0.125/m. On the basis
 - 5 of the peak in local heat transfer measurements, transition occurred in the range of 0.8<X<1.1 m.
- for the results presented here. End plates were mounted on the model extending up to the position calculated for the shock, assuming inviscid flow. Oil flow studies showed that the flow was effectively two-dimensional over the central instrumented strip. Small corner effects were observed at the junction of the end plates and the test surface.
- 6 Static pressure was measured at 20 stations from X = 0.416 to 2.159 m with tapings of diameter 3.18 mm. Iron-constantan thermocouples were used at about 70 X-stations from X = 0.423 to 2.237 m to give the wall temperature. They were also used to give the local heat-flux with the thin wall transient technique. The skin thickness was approximately 0.51 mm, thermocouple conduction errors were calculated to be insignificant, while errors due to local nonuniformity of thin skin temperature were estimated to be less than 1%. This calculation was not made for every case, and for some cooled wall cases relatively large variations in TW/T0 were observed. Skin friction was measured with an FEB (Kistler model 322) for which the floating element diameter was 9.4 mm, with a gap of 0.064 mm. The balances were matched to the interchangeable instrumentation plates so that the elements were no more than 0.03 mm below the surface. Errors due to protrusion and gap size are estimated as less than 5%, following Allen (1976). The operation and calibration of several balances were checked in a vacuum chamber at near liquid nitrogen temperatures. Two were found suitable for use under these conditions. The precooling process took 1-2 hrs, during which time the balance temperature became very close to that of the surrounding surface. A haze formed on the model surface at the very low temperatures used (about 77K). The surface near the balance was kept clear by a jet of pure helium, retracted immediately before a run.
 - 7 Pitot, static pressure and T0 profiles were measured. Different Pitot probes were used. Initial work using the same probe as for CAT 7305 had shown rather large probe-wall interference effects. The probe finally used was a CPP (d₁ = 0.51 mm), which tapered to a diameter of 2.3 mm at a point about 12.7 mm downstream of the tip. The static pressure probe used was a CCP (half angle of nose 42.5°, d₁ = 3.2 mm, four orifices of 0.8 mm diameter, 12.2 mm downstream of the tip) which gave rise to large interference effects so that measurements with it were abandoned. The STP was a form of semishielded fine wire probe. The sensor was a coil of tungsten wire, wire diameter 10 μm, coil diameter 100 μm, mounted in a peripheral shield (h₁ = 0.61, b₁ = 2.0 mm) on the end of two prongs (d = 0.4, l = 5.6 mm). The l/d ratio of the wire itself was about 800. The probe and calibration procedures are described by Weinstein (1973).

- 9 The use of interchangeable sections of model skin, each instrumented for a part of the investigation requires a great deal of interpolation and normalisation. The profile data given here are as interpolated and processed by the author (private communication). Pitot profile data were normalised to a constant tunnel reservoir pressure of 13.79 MN/m² (which does not imply a constant POD value). Pitot and T0 profiles in general were taken at slightly different TW/TOD values. The TW values are interpolated to correspond to the TOD values prevailing during the T0 profile measurements. C_f values, measured at the profile X-stations, were found to be weak functions of TW/TOD and Re_x so
- 12 that no adjustment was made. Heat transfer data have been interpolated by the editors, firstly, as functions of X, to the profile stations for each experimental temperature condition, and secondly, as functions of interpolated TW/TOD, for each profile station to the authors' TW/TOD value as
- 9 stated for the temperature profile. The static pressure measurements showed unacceptable interference effects, so that the static pressure was assumed constant through the boundary layer at the wall value as interpolated for X. Variation of PW with TW/TOD was found to be small, and PW/P(free stream) was
- 10 assumed to be a function of X only. Probe-wall interference was found to a significant factor with all probes, if assessed by the static pressure change induced at the wall. It was sufficient to eliminate the P-profile data from further consideration. At a given level of induced static pressure, however, Pitot and T0 probes are not so directly affected. No wall proximity correction was applied. Rarefaction corrections were calculated for the Pitot probes and not found significant for the cases presented here (Weinstein, Appendix B of source paper). Real gas correction factors (Erikson, 1960) and ideal gas correction factors (Muehler, 1957) were used in data reduction, while the low temperature viscosity of Helium (Maddalon and Jackson, 1970) was approximated by

$$\mu \text{Ns/m}^2 = 5.023 \left(\frac{T^{1.647}}{T+0.83} \right) \times 10^{-7}$$

at low temperatures (below T = 8K), and the power relation

$$\mu \text{Ns/m}^2 = 5.0277 \times 10^{-7} T^{0.647}$$

- 12 at higher temperatures. The editors present fully interpolated and reduced data as received from the
- 13 author (private communication). These consist of three series of 7 profiles at nominal constant tunnel
- 14 reservoir conditions, each set for a given nominal value of TW/TR (01 - 1.05; 02 - 0.44; 03 - 0.56).
- 12 The PW and CF values attached to the profile are as presented by the author, the CQ values as interpolated by the editors. The authors' viscosity law has been replaced by that of Neubert (1974). The source paper additionally contains raw data (Pitot and T0 profiles) corresponding to CAT 7305, and a restricted amount of data from an additional upstream station (X = 0.356 m) corresponding to the general conditions of the data given here. Wall data are also tabulated there for a range of other Reynolds numbers.

§ DATA: 78050101-0307. Pitot and T0 profiles measured separately. CF from FEB. CQ from thin wall transient technique. NX = 7.

- 15 Editors' comments. These results further extend the useful coverage of the transitional range treated by Watson et al. (CAT 7305) from the adiabatic wall case to flows with strong heat transfer. Series 01 should be strictly comparable to CAT 7305 (Fig. 4.4.4 to 4.4.6 of AG 352), at slightly higher Reynolds numbers. The heat transfer cases are not strictly isothermal wall flows. This is a consequence of the fact that the temperature is not maintained constant by the cooling system, the heat transfer loading on the strongly precooled surface building up rapidly at the start of the 5 sec. run. Thus the wall temperature, once flow is fully established, is noticeably higher in the region of greatest heat flux near completion of transition (X = 0.76 m). (Compare with source, Fig. 11).

At these Mach numbers, there is a strong viscous interaction between the boundary layer and the resulting curved bow shock near the leading edge. In consequence the flow outside the boundary layer is rotational, and the exterior flow states can only be determined if both Pitot and static pressure (or another functionally equivalent pair) are measured (see also Varner & Adams, 1980). It is a pity, therefore, that despite the wall interference problems experienced with the static probe,

values are not available in the outer part of the layer and the exterior flow. Any static pressure variation following on the bow shock curvature will be small, away from the leading edge, but static pressure gradients which result from the changes in rate of displacement thickness growth near transition will be approximately MD times the associated longitudinal variation. This implies a 10% static pressure change in a Y-distance of about 40 mm, about the boundary layer thickness. Corresponding errors in the determination of a local P_0 value from the PT2 value are 15% (eqn. 7.1.3 of AGARDograph 253), so that it is difficult if not impossible to select a δ -value and so D-state on any sensible basis in a flow of this nature. The integral values presented here should not therefore be expected to be very accurate.

The measured longitudinal static pressure variation here is a good example of the type of pressure distribution discussed in § 6.4.2 of AG 253 in connection with the earlier results of CAT 7305. The authors calculated the exterior flow field produced by the experimental displacement surface, as evaluated assuming no normal pressure gradient (source, figure 9) and were then able to calculate back to the longitudinal static pressure variations which are remarkably similar in shape to the experimental values given here. (Source, Figs. 13, 14).

Series 01 (Fig. 1) is a good example of a boundary layer which begins laminar (profile 0101) and, moving through transition (profile 0102), gradually develops the equilibrium wake strength of the "developed" turbulent velocity profile (0106). This is confirmed by the behaviour of the profiles as shown in the outer law plot (Fig. 2a). For a further discussion of the adiabatic compressible boundary layer at high Mach numbers the reader is referred to § 4.4 of AG 253. Series 02 provides the interesting extension of the study to the isothermal case although this last condition is not completely fulfilled. A comparison between the outer law plots of series 01 and 02 - Figs. 2a and 2b - shows little difference. This means that the outer region of the boundary layer is little affected by wall cooling which we would expect to stabilize the laminar boundary layer and delay transition. Such transitional behaviour could be deduced from the plots of profiles 0203 to 0206 in fig. 3 if we assume that the parallel shift of these profiles is not caused by a systematic error in the skin friction measurements (approximately -10%). The low value of τ_w indicates that the mean skin friction has not reached the value appropriate to the turbulent velocity profile (see also Fig. 4.4.5 of AG 253). The rather high data points at the lower end of the log-law region are probably due to aerodynamic interference effects as discussed at length by the author. Agreement between the measured temperature profiles and the "standard" theoretical relationship, eqn.(2.5.37) of AG 253, is good except for profiles 0203 and 0301. Some disagreement is found for most profiles in the near wall region, probably again due to aerodynamic interference effects of the probe.

Further tests on a porous surface (without overall mass-transfer) are reported in Watson (1979). No change in wall shear or boundary layer growth was observed, so that a possible transmission of energy by the fluctuating pressure field into the cavity behind the porous surface was found to have negligible effect.

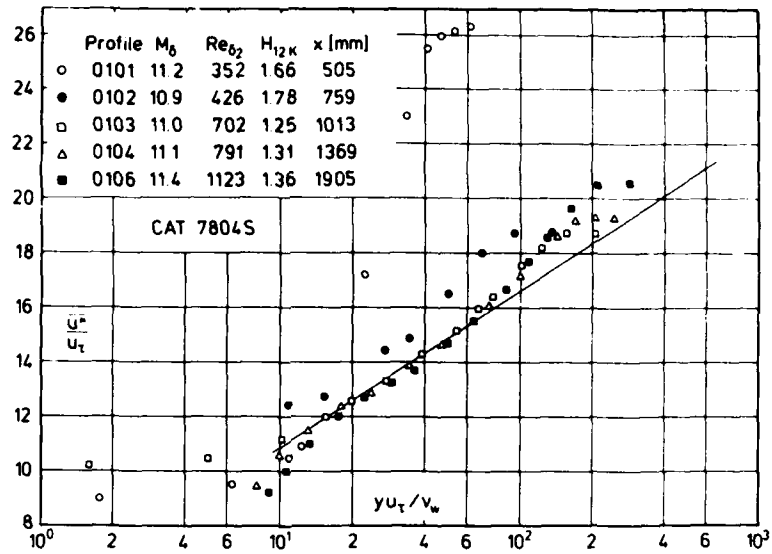


Fig. 1 Law of the wall for a laminar / transitional / turbulent compressible boundary layer (defined origin, adiabatic wall, ZPG, c_f from FEB). Watson (1978).

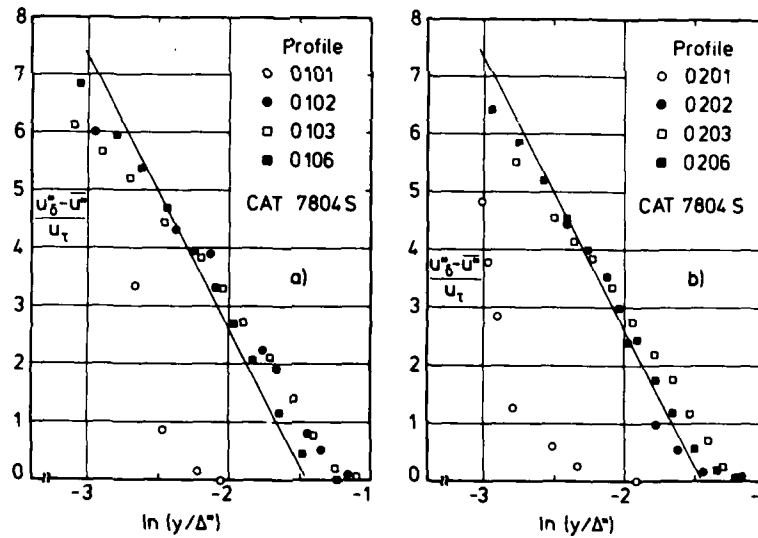


Fig. 2 Outer law for a compressible boundary layer - laminar / transitional / turbulent - (defined origin, isothermal wall, ZPG). Watson (1978).

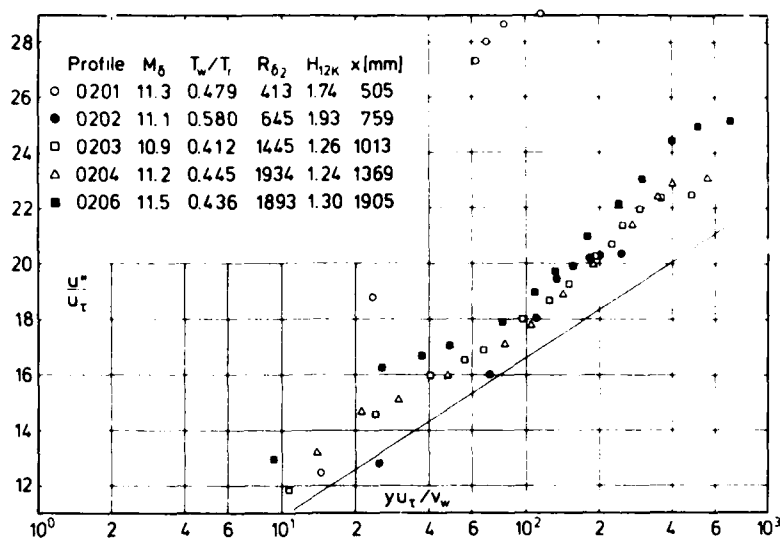


Fig. 3 Law of the wall for a laminar / transitional / turbulent compressible boundary layer (defined origin, isothermal wall, ZPG, c_f from FEB). Watson (1978).

| CAT 7804S | | WATSON BOUNDARY CONDITIONS AND EVALUATED DATA, SI UNITS | | | | | | | |
|-----------------------|-----------------------|---|-----------------------|------------------------|---------|-----------------------|-----------------------|-----------------------|--|
| RUN | MD * | TW/TR | RED2W | CF | H12 | H12K | PW | PD* | |
| X * | POD | PW/PD* | RED2D | CO * | H32 | H32K | TW* | TD | |
| RZ | T00* | TAUW * | DZ | PI2 | H42 | D2K | UD | TR | |
| 7804S0101 | 11.1750 | 1.0561 | 3.5213 ⁺⁰² | 1.4817 ⁻⁰⁴ | 94.1550 | 1.6603 | 6.3570 ⁺⁰² | 6.3570 ⁺⁰² | |
| 5.0500 ⁻⁰¹ | 7.5295 ⁺⁰⁶ | 1.0000 | 3.9813 ⁺⁰³ | -4.2425 ⁻⁰⁶ | 1.7809 | 1.6834 | 2.9667 ⁺⁰² | 7.3310 ⁺⁰⁰ | |
| INFINITE | 3.1265 ⁺⁰² | 9.8040 ⁺⁰⁰ | 9.4675 ⁻⁰⁵ | NC | 0.1276 | 1.4499 ⁻⁰³ | 1.7811 ⁺⁰³ | 2.8090 ⁺⁰² | |
| 7804S0102 | 10.9380 | 1.0527 | 4.2557 ⁺⁰² | 3.0388 ⁻⁰⁴ | 64.5007 | 1.7852 | 7.2809 ⁺⁰² | 7.2809 ⁺⁰² | |
| 7.5900 ⁻⁰¹ | 7.7675 ⁺⁰⁶ | 1.0000 | 4.6392 ⁺⁰³ | -1.5992 ⁻⁰⁵ | 1.9164 | 1.8739 | 2.9944 ⁺⁰² | 7.7403 ⁺⁰⁰ | |
| INFINITE | 3.1658 ⁺⁰² | 2.2063 ⁺⁰¹ | 1.0551 ⁻⁰⁴ | NC | 0.5492 | 6.2047 ⁻⁰⁴ | 1.7913 ⁺⁰³ | 2.8446 ⁺⁰² | |
| 7804S0103 | 11.0380 | 1.0382 | 7.0193 ⁺⁰² | 3.0142 ⁻⁰⁴ | 72.9073 | 1.2538 | 7.5704 ⁺⁰² | 7.5704 ⁺⁰² | |
| 1.0130 ⁺⁰⁰ | 8.4430 ⁺⁰⁶ | 1.0000 | 7.6972 ⁺⁰³ | -8.3043 ⁻⁰⁶ | 1.9044 | 1.8497 | 2.9278 ⁺⁰² | 7.5388 ⁺⁰⁰ | |
| INFINITE | 3.1386 ⁺⁰² | 2.3173 ⁺⁰¹ | 1.6131 ⁻⁰⁴ | NC | 0.3119 | 1.0948 ⁻⁰³ | 1.7840 ⁺⁰³ | 2.8200 ⁺⁰² | |
| 7804S0104 | 11.1020 | 1.0418 | 7.9140 ⁺⁰² | 2.8258 ⁻⁰⁴ | 82.5595 | 1.3126 | 7.5360 ⁺⁰² | 7.5360 ⁺⁰² | |
| 1.3690 ⁺⁰⁰ | 8.6450 ⁺⁰⁶ | 1.0000 | 8.7745 ⁺⁰³ | -9.2777 ⁻⁰⁶ | 1.8916 | 1.8092 | 2.9389 ⁺⁰² | 7.4568 ⁺⁰⁰ | |
| INFINITE | 3.1397 ⁺⁰² | 2.1877 ⁺⁰¹ | 1.8111 ⁻⁰⁴ | NC | 0.1295 | 1.4150 ⁻⁰³ | 1.7846 ⁺⁰³ | 2.8209 ⁺⁰² | |
| 7804S0105 | 11.2250 | 1.0298 | 9.6193 ⁺⁰² | 2.5784 ⁻⁰⁴ | 80.2262 | 1.5731 | 7.3153 ⁺⁰² | 7.3153 ⁺⁰² | |
| 1.6510 ⁺⁰⁰ | 8.8556 ⁺⁰⁶ | 1.0000 | 1.0737 ⁺⁰⁴ | -7.9363 ⁻⁰⁶ | 1.8840 | 1.7577 | 2.9611 ⁺⁰² | 7.4391 ⁺⁰⁰ | |
| INFINITE | 3.2004 ⁺⁰² | 1.9809 ⁺⁰¹ | 2.2511 ⁻⁰⁴ | NC | 0.2699 | 1.8131 ⁻⁰³ | 1.8022 ⁺⁰³ | 2.8753 ⁺⁰² | |
| 7804S0106 | 11.3980 | 1.0658 | 1.1233 ⁺⁰³ | 2.3109 ⁻⁰⁴ | 85.1802 | 1.3642 | 7.1636 ⁺⁰² | 7.1636 ⁺⁰² | |
| 1.9050 ⁺⁰⁰ | 9.3445 ⁺⁰⁶ | 1.0000 | 1.3193 ⁺⁰⁴ | -6.2096 ⁻⁰⁶ | 1.8933 | 1.8209 | 2.9722 ⁺⁰² | 7.0031 ⁺⁰⁰ | |
| INFINITE | 3.1042 ⁺⁰² | 1.7926 ⁺⁰¹ | 2.5713 ⁻⁰⁴ | NC | 0.1835 | 2.1272 ⁻⁰³ | 1.7756 ⁺⁰³ | 2.7887 ⁺⁰² | |
| 7804S0107 | 11.5100 | 1.0570 | 1.6871 ⁺⁰³ | 2.1477 ⁻⁰⁴ | 95.0760 | 1.2376 | 7.1085 ⁺⁰² | 7.1085 ⁺⁰² | |
| 2.1590 ⁺⁰⁰ | 9.7264 ⁺⁰⁶ | 1.0000 | 2.0015 ⁺⁰⁴ | -5.2588 ⁻⁰⁶ | 1.9059 | 1.8908 | 2.9500 ⁺⁰² | 6.8765 ⁺⁰⁰ | |
| INFINITE | 3.1069 ⁺⁰² | 1.6858 ⁺⁰¹ | 3.8005 ⁻⁰⁴ | NC | 0.0017 | 3.3613 ⁻⁰³ | 1.7767 ⁺⁰³ | 2.7910 ⁺⁰² | |
| 7804S0201 | 11.2930 | 0.4790 | 4.1258 ⁺⁰² | 1.8100 ⁻⁰⁴ | 93.6376 | 1.7421 | 6.3570 ⁺⁰² | 6.3570 ⁺⁰² | |
| 5.0500 ⁻⁰¹ | 7.9257 ⁺⁰⁶ | 1.0000 | 2.8468 ⁺⁰³ | 4.1577 ⁻⁰⁵ | 1.7693 | 1.7437 | 1.3333 ⁺⁰² | 7.1182 ⁺⁰⁰ | |
| INFINITE | 3.0987 ⁺⁰² | 1.2231 ⁺⁰¹ | 6.4470 ⁻⁰⁵ | NC | 0.1918 | 9.8941 ⁻⁰⁴ | 1.7736 ⁺⁰³ | 2.7838 ⁺⁰² | |
| 7804S0202 | 11.1340 | 0.5800 | 6.4487 ⁺⁰² | 3.4598 ⁻⁰⁴ | 74.6694 | 1.9271 | 7.2809 ⁺⁰² | 7.2809 ⁺⁰² | |
| 7.5900 ⁻⁰¹ | 8.4705 ⁺⁰⁶ | 1.0000 | 4.9224 ⁺⁰³ | 4.9661 ⁻⁰⁵ | 1.8913 | 1.8391 | 1.6222 ⁺⁰² | 7.3522 ⁺⁰⁰ | |
| INFINITE | 3.1131 ⁺⁰² | 2.6028 ⁺⁰¹ | 1.0296 ⁻⁰⁴ | NC | 0.4107 | 7.4115 ⁻⁰⁴ | 1.7771 ⁺⁰³ | 2.7970 ⁺⁰² | |
| 7804S0203 | 10.9270 | 0.4124 | 1.4454 ⁺⁰³ | 3.4583 ⁻⁰⁴ | 46.0738 | 1.2598 | 7.5704 ⁺⁰² | 7.5704 ⁺⁰² | |
| 1.0130 ⁺⁰⁰ | 8.0369 ⁺⁰⁶ | 1.0000 | 8.6016 ⁺⁰³ | 8.1766 ⁻⁰⁵ | 1.8712 | 1.8388 | 1.1500 ⁺⁰² | 7.6027 ⁺⁰⁰ | |
| INFINITE | 3.1034 ⁺⁰² | 2.6055 ⁺⁰¹ | 1.8408 ⁻⁰⁴ | NC | 0.8413 | 8.6287 ⁻⁰⁴ | 1.7736 ⁺⁰³ | 2.7885 ⁺⁰² | |
| 7804S0204 | 11.1740 | 0.4455 | 1.9341 ⁺⁰³ | 3.0365 ⁻⁰⁴ | 45.2493 | 1.2380 | 7.5360 ⁺⁰² | 7.5360 ⁺⁰² | |
| 1.3690 ⁺⁰⁰ | 8.9221 ⁺⁰⁶ | 1.0000 | 1.2486 ⁺⁰⁴ | 6.3234 ⁻⁰⁵ | 1.8956 | 1.8447 | 1.2667 ⁺⁰² | 7.4217 ⁺⁰⁰ | |
| INFINITE | 3.1646 ⁺⁰² | 2.3814 ⁺⁰¹ | 2.5451 ⁻⁰⁴ | NC | 0.9307 | 1.2343 ⁻⁰³ | 1.7919 ⁺⁰³ | 2.8432 ⁺⁰² | |
| 7804S0205 | 11.0030 | 0.4319 | 1.8215 ⁺⁰³ | 2.8805 ⁻⁰⁴ | 52.7118 | 1.3308 | 7.3153 ⁺⁰² | 7.3153 ⁺⁰² | |
| 1.6510 ⁺⁰⁰ | 8.0330 ⁺⁰⁶ | 1.0000 | 1.1286 ⁺⁰⁴ | 6.4061 ⁻⁰⁵ | 1.8892 | 1.8257 | 1.2056 ⁺⁰² | 7.5075 ⁺⁰⁰ | |
| INFINITE | 3.1063 ⁺⁰² | 2.1263 ⁺⁰¹ | 2.4425 ⁻⁰⁴ | NC | 0.7677 | 1.5052 ⁻⁰³ | 1.7747 ⁺⁰³ | 2.7910 ⁺⁰² | |
| 7804S0206 | 11.4680 | 0.4364 | 1.8926 ⁺⁰³ | 2.4787 ⁻⁰⁴ | 67.7031 | 1.2980 | 7.1636 ⁺⁰² | 7.1636 ⁺⁰² | |
| 1.9050 ⁺⁰⁰ | 9.6283 ⁺⁰⁶ | 1.0000 | 1.2539 ⁺⁰⁴ | 5.4304 ⁻⁰⁵ | 1.8990 | 1.8529 | 1.2500 ⁺⁰² | 7.1082 ⁺⁰⁰ | |
| INFINITE | 3.1888 ⁺⁰² | 1.9464 ⁺⁰¹ | 2.4769 ⁻⁰⁴ | NC | 0.5259 | 1.5275 ⁻⁰³ | 1.7998 ⁺⁰³ | 2.8645 ⁺⁰² | |
| 7804S0207 | 11.4230 | 0.3808 | 2.2044 ⁺⁰³ | 2.4980 ⁻⁰⁴ | 65.7860 | 1.4985 | 7.1085 ⁺⁰² | 7.1085 ⁺⁰² | |
| 2.1590 ⁺⁰⁰ | 9.3724 ⁺⁰⁶ | 1.0000 | 1.3264 ⁺⁰⁴ | 5.8627 ⁻⁰⁵ | 1.9060 | 1.8666 | 1.1056 ⁺⁰² | 7.2988 ⁺⁰⁰ | |
| INFINITE | 3.2314 ⁺⁰² | 1.9312 ⁺⁰¹ | 2.7243 ⁻⁰⁴ | NC | 0.5894 | 1.6510 ⁻⁰³ | 1.8116 ⁺⁰³ | 2.9029 ⁺⁰² | |

| CAT 7804S | | WATSON BOUNDARY CONDITIONS AND EVALUATED DATA. SI UNITS | | | | | | | |
|-------------|-------------|---|-------------|-------------|---------|-------------|-------------|-------------|--|
| RUM | MD * | TW/TR | RE02W | CF | H12 | H12K | PW | PD* | |
| X * | POD | PW/PD* | RE02D | CO * | H32 | H32K | TW* | TD | |
| PZ | TOO* | TAUM * | D2 | P12 | H42 | D2K | UD | TR | |
| 7804S0301 | 11.2850 | 0.6205 | 4.1001**+02 | 1.5848**-04 | 81.6429 | 2.0756 | 6.3570**+02 | 6.3570**+02 | |
| 5.0500**-01 | 7.8983**+06 | 1.0000 | 3.3516**+03 | 2.9673**-05 | 1.8060 | 1.6328 | 1.6944**+02 | 6.9926**+00 | |
| INFINITE | 3.0398**+02 | 1.0694**+01 | 7.4204**+05 | NC | 0.4343 | 8.5148**-04 | 1.7566**+03 | 2.7309**+02 | |
| 7804S0302 | 11.2460 | 0.6542 | 6.4960**+02 | 4.5249**-04 | 74.6272 | 1.9813 | 7.2809**+02 | 7.2809**+02 | |
| 7.5900**-01 | 8.8946**+06 | 1.0000 | 5.4533**+03 | 3.8144**-05 | 1.9017 | 1.8446 | 1.8111**+02 | 7.1361**+00 | |
| INFINITE | 3.0813**+02 | 3.4729**+01 | 1.0864**+04 | NC | 0.4436 | 7.4404**-04 | 1.7684**+03 | 2.7682**+02 | |
| 7804S0303 | 10.9250 | 0.5206 | 1.0227**+03 | 3.6565**-04 | 64.0603 | 1.2730 | 7.5704**+02 | 7.5704**+02 | |
| 1.0130**+00 | 8.0297**+06 | 1.0000 | 7.0830**+03 | 6.0152**-05 | 1.9060 | 1.8626 | 1.4389**+02 | 7.5383**+00 | |
| INFINITE | 3.0760**+02 | 2.7538**+01 | 1.4996**+04 | NC | 0.4675 | 8.5659**-04 | 1.7657**+03 | 2.7639**+02 | |
| 7804S0304 | 11.1520 | 0.5660 | 1.2279**+03 | 3.0176**-04 | 70.4212 | 1.2805 | 7.5360**+02 | 7.5360**+02 | |
| 1.3690**+00 | 8.8367**+06 | 1.0000 | 9.2390**+03 | 4.1698**-05 | 1.8984 | 1.8539 | 1.5944**+02 | 7.3821**+00 | |
| INFINITE | 3.1357**+02 | 2.3573**+01 | 1.8739**+04 | NC | 0.3853 | 1.1780**-03 | 1.7836**+03 | 2.8172**+02 | |
| 7804S0305 | 11.6470 | 0.5458 | 1.6447**+03 | 2.5632**-04 | 60.4650 | 1.3015 | 7.3153**+02 | 7.3153**+02 | |
| 1.6510**+00 | 1.0606**+07 | 1.0000 | 1.2961**+04 | 4.1868**-05 | 1.9104 | 1.9118 | 1.5278**+02 | 6.7397**+00 | |
| INFINITE | 3.1164**+02 | 2.1201**+01 | 2.3012**+04 | NC | 0.7139 | 1.2465**-03 | 1.7799**+03 | 2.7993**+02 | |
| 7804S0306 | 11.4490 | 0.5252 | 1.7854**+03 | 2.7882**-04 | 74.2033 | 1.4315 | 7.1636**+02 | 7.1636**+02 | |
| 1.9050**+00 | 9.5506**+06 | 1.0000 | 1.3307**+04 | 4.3096**-05 | 1.9068 | 1.8517 | 1.5000**+02 | 7.1097**+00 | |
| INFINITE | 3.1791**+02 | 2.1822**+01 | 2.6338**+04 | NC | 0.4195 | 1.7669**-03 | 1.7970**+03 | 2.8559**+02 | |
| 7804S0307 | 11.8330 | 0.5149 | 2.1329**+03 | 2.3761**-04 | 75.5826 | 1.3254 | 7.1085**+02 | 7.1085**+02 | |
| 2.1590**+00 | 1.1136**+07 | 1.0000 | 1.6520**+04 | 3.7567**-05 | 1.8834 | 1.8481 | 1.4833**+02 | 6.7246**+00 | |
| INFINITE | 3.2074**+02 | 1.9712**+01 | 2.9622**+04 | NC | 0.4796 | 2.3490**-03 | 1.8063**+03 | 2.8808**+02 | |

TRAPEZOIDAL RULE FOR 0207

| 7804S0201 | | WATSON PROFILE TABULATION 18 POINTS, DELTA AT POINT 14 | | | | | | | |
|-----------|-------------|--|------|---------|---------|---------|----------|-----------|--|
| I | Y | PT2/P | P/PD | TO/TOD | M/MD | U/UD | T/TD | R/RD*U/UD | |
| 1 | 0.0000**+00 | 1.0000**+00 | NM | 0.43026 | 0.00000 | 0.00000 | 18.72988 | 0.00000 | |
| 2 | 1.0312**-03 | 2.6364**+00 | NM | 0.86885 | 0.10597 | 0.53614 | 25.59703 | 0.02095 | |
| 3 | 1.6764**-03 | 8.7571**+00 | NM | 0.89316 | 0.21043 | 0.77273 | 13.48486 | 0.05730 | |
| 4 | 3.5712**-03 | 2.8268**+01 | NM | 0.96931 | 0.38535 | 0.92547 | 5.76767 | 0.16046 | |
| 5 | 3.7084**-03 | 3.9983**+01 | NM | 0.97273 | 0.45938 | 0.94647 | 4.24483 | 0.22297 | |
| 6 | 3.9675**-03 | 5.5418**+01 | NM | 0.97791 | 0.54169 | 0.96263 | 3.15808 | 0.30481 | |
| 7 | 4.3637**-03 | 7.9463**+01 | NM | 0.98478 | 0.64944 | 0.97709 | 2.26360 | 0.43165 | |
| 8 | 4.9047**-03 | 1.0652**+02 | NM | 0.98962 | 0.75247 | 0.98616 | 1.71757 | 0.57416 | |
| 9 | 5.4077**-03 | 1.2727**+02 | NM | 0.99349 | 0.82276 | 0.99132 | 1.45172 | 0.68286 | |
| 10 | 5.8674**-03 | 1.3882**+02 | NM | 0.99575 | 0.85942 | 0.99384 | 1.33729 | 0.74318 | |
| 11 | 6.9723**-03 | 1.6263**+02 | NM | 0.99862 | 0.93042 | 0.99753 | 1.14494 | 0.86782 | |
| 12 | 8.3464**-03 | 1.7871**+02 | NM | 0.99892 | 0.97544 | 0.99888 | 1.04863 | 0.95256 | |
| 13 | 9.6545**-03 | 1.8570**+02 | NM | 1.00050 | 0.99439 | 1.00012 | 1.01155 | 0.98870 | |
| D 14 | 1.0638**-02 | 1.8780**+02 | NM | 1.00000 | 1.00000 | 1.00000 | 1.00000 | 1.00000 | |
| 15 | 1.3396**-02 | 1.9541**+02 | NM | 1.00222 | 1.02011 | 1.00156 | 0.96397 | 1.03900 | |
| 16 | 1.5641**-02 | 1.9776**+02 | NM | 1.00222 | 1.02625 | 1.00169 | 0.95272 | 1.05141 | |
| 17 | 1.8329**-02 | 2.0320**+02 | NM | 1.00222 | 1.04031 | 1.00199 | 0.92769 | 1.08009 | |
| 18 | 2.0579**-02 | 2.0665**+02 | NM | 1.00222 | 1.04911 | 1.00216 | 0.91250 | 1.09826 | |

INPUT VARIABLES Y,M,TO ASSUME P=PD

| 7804S0202 | | WATSON PROFILE TABULATION 13 POINTS, DELTA AT POINT 12 | | | | | | | |
|-----------|-------------|--|------|---------|---------|---------|----------|-----------|--|
| I | Y | PT2/P | P/PD | TO/TOD | M/MD | U/UD | T/TD | R/RD*U/UD | |
| 1 | 0.0000**+00 | 1.0000**+00 | NM | 0.52106 | 0.00000 | 0.00000 | 22.06297 | 0.00000 | |
| 2 | 1.4630**-03 | 7.9999**+00 | NM | 0.89942 | 0.20343 | 0.76248 | 14.04828 | 0.05428 | |
| 3 | 4.0513**-03 | 2.0495**+01 | NM | 0.94991 | 0.33178 | 0.89309 | 7.24606 | 0.12325 | |
| 4 | 6.2967**-03 | 4.3681**+01 | NM | 0.97992 | 0.48725 | 0.95437 | 3.83653 | 0.24876 | |
| 5 | 7.6657**-03 | 8.6372**+01 | NM | 0.99549 | 0.68690 | 0.98481 | 2.05546 | 0.47912 | |
| 6 | 8.9662**-03 | 1.0581**+02 | NM | 1.00070 | 0.76064 | 0.99185 | 1.70033 | 0.58333 | |
| 7 | 1.0683**-02 | 1.5455**+02 | NM | 1.00014 | 0.91989 | 0.99793 | 1.17689 | 0.84794 | |
| 8 | 1.1471**-02 | 1.6327**+02 | NM | 0.99946 | 0.94557 | 0.99834 | 1.11472 | 0.89560 | |
| 9 | 1.1671**-02 | 1.6660**+02 | NM | 0.99945 | 0.95518 | 0.99859 | 1.09296 | 0.91366 | |
| 10 | 1.3970**-02 | 1.7759**+02 | NM | 0.99850 | 0.98626 | 0.99892 | 1.02584 | 0.97376 | |
| 11 | 1.6457**-02 | 1.8102**+02 | NM | 0.99991 | 0.99578 | 0.99986 | 1.00820 | 0.99172 | |
| D 12 | 1.6652**-02 | 1.8236**+02 | NM | 1.00000 | 1.00000 | 1.00000 | 1.00000 | 1.00000 | |
| 13 | 1.8854**-02 | 1.8269**+02 | NM | 0.99936 | 1.00036 | 0.99969 | 0.99866 | 1.00103 | |

INPUT VARIABLES Y,M,TO ASSUME P=PD

7804S0203

WATSON

PROFILE TABULATION

97 POINTS, DELTA AT POINT 55

| I | Y | PTZ/P | P/PO | TO/TOD | M/MD | U/UD | T/TD | R/RD*U/UD |
|------|-------------------------|-------------------------|------|---------|---------|---------|----------|-----------|
| 1 | 0.0000 ⁺ +00 | 1.0000 ⁺ +00 | NM | 0.37056 | 0.00000 | 0.00000 | 15.12625 | 0.00000 |
| 2 | 8.3820 ⁻ -05 | 1.2521 ⁺ +01 | NM | 0.40706 | 0.26229 | 0.55290 | 4.44361 | 0.12442 |
| 3 | 4.0132 ⁻ -04 | 1.2767 ⁺ +01 | NM | 0.54788 | 0.26494 | 0.64315 | 5.89296 | 0.10914 |
| 4 | 9.1440 ⁻ -04 | 1.3491 ⁺ +01 | NM | 0.77442 | 0.27263 | 0.77031 | 7.98350 | 0.09644 |
| 5 | 1.5469 ⁻ -03 | 1.4946 ⁺ +01 | NM | 0.87111 | 0.28745 | 0.82755 | 8.28814 | 0.09985 |
| 6 | 2.1285 ⁻ -03 | 1.6957 ⁺ +01 | NM | 0.88819 | 0.30676 | 0.84776 | 7.63728 | 0.11100 |
| 7 | 2.5248 ⁻ -03 | 1.8528 ⁺ +01 | NM | 0.89819 | 0.32104 | 0.86044 | 7.18328 | 0.11978 |
| 8 | 2.7610 ⁻ -03 | 1.8953 ⁺ +01 | NM | 0.90353 | 0.32479 | 0.86494 | 7.09187 | 0.12196 |
| 9 | 2.8575 ⁻ -03 | 1.9499 ⁺ +01 | NM | 0.90573 | 0.32955 | 0.86839 | 6.94360 | 0.12506 |
| 10 | 2.9134 ⁻ -03 | 2.0225 ⁺ +01 | NM | 0.90698 | 0.33577 | 0.87200 | 6.74437 | 0.12929 |
| 11 | 3.0175 ⁻ -03 | 2.1317 ⁺ +01 | NM | 0.90933 | 0.34493 | 0.87732 | 6.46947 | 0.13561 |
| 12 | 3.2385 ⁻ -03 | 2.3023 ⁺ +01 | NM | 0.91434 | 0.35874 | 0.88559 | 6.09387 | 0.14532 |
| 13 | 3.6195 ⁻ -03 | 2.5505 ⁺ +01 | NM | 0.92288 | 0.37796 | 0.89700 | 5.63232 | 0.15926 |
| 14 | 4.1478 ⁻ -03 | 2.8849 ⁺ +01 | NM | 0.93174 | 0.40240 | 0.90934 | 5.10669 | 0.17807 |
| 15 | 4.7041 ⁻ -03 | 3.2362 ⁺ +01 | NM | 0.93598 | 0.42656 | 0.91822 | 4.63376 | 0.19816 |
| 16 | 5.1613 ⁻ -03 | 3.4973 ⁺ +01 | NM | 0.94723 | 0.44367 | 0.92798 | 4.37477 | 0.21212 |
| 17 | 5.4305 ⁻ -03 | 3.6675 ⁺ +01 | NM | 0.95039 | 0.45447 | 0.93201 | 4.20563 | 0.22161 |
| 18 | 5.5626 ⁻ -03 | 3.7703 ⁺ +01 | NM | 0.95149 | 0.46088 | 0.93395 | 4.10651 | 0.22743 |
| 19 | 5.6337 ⁻ -03 | 3.8551 ⁺ +01 | NM | 0.95206 | 0.46609 | 0.93533 | 4.02700 | 0.23226 |
| 20 | 5.7302 ⁻ -03 | 4.0184 ⁺ +01 | NM | 0.95285 | 0.47598 | 0.93771 | 3.88122 | 0.24160 |
| 21 | 5.9233 ⁻ -03 | 4.3045 ⁺ +01 | NM | 0.95498 | 0.49282 | 0.94192 | 3.65310 | 0.25784 |
| 22 | 6.2636 ⁻ -03 | 4.7225 ⁺ +01 | NM | 0.95883 | 0.51643 | 0.94780 | 3.36830 | 0.28139 |
| 23 | 6.7564 ⁻ -03 | 5.2803 ⁺ +01 | NM | 0.96391 | 0.54635 | 0.95469 | 3.05337 | 0.31267 |
| 24 | 7.3609 ⁻ -03 | 5.9122 ⁺ +01 | NM | 0.96880 | 0.57838 | 0.96113 | 2.76144 | 0.34806 |
| 25 | 7.8791 ⁻ -03 | 6.4282 ⁺ +01 | NM | 0.97220 | 0.60328 | 0.96555 | 2.56162 | 0.37693 |
| 26 | 8.2474 ⁻ -03 | 6.7418 ⁺ +01 | NM | 0.97379 | 0.61792 | 0.96780 | 2.45308 | 0.39453 |
| 27 | 8.4430 ⁻ -03 | 6.9618 ⁺ +01 | NM | 0.97664 | 0.62799 | 0.97017 | 2.38669 | 0.40649 |
| 28 | 8.5395 ⁻ -03 | 7.1915 ⁺ +01 | NM | 0.97680 | 0.63833 | 0.97118 | 2.31481 | 0.41955 |
| 29 | 8.6081 ⁻ -03 | 7.4458 ⁺ +01 | NM | 0.97692 | 0.64958 | 0.97222 | 2.24004 | 0.43402 |
| 30 | 8.7605 ⁻ -03 | 7.7853 ⁺ +01 | NM | 0.97861 | 0.66432 | 0.97425 | 2.15076 | 0.45298 |
| 31 | 9.0399 ⁻ -03 | 8.3321 ⁺ +01 | NM | 0.98156 | 0.68738 | 0.97746 | 2.02211 | 0.48339 |
| 32 | 9.4894 ⁻ -03 | 9.2849 ⁺ +01 | NM | 0.98428 | 0.72582 | 0.98137 | 1.82815 | 0.53681 |
| 33 | 1.0071 ⁻ -02 | 1.0420 ⁺ +02 | NM | 0.98856 | 0.76910 | 0.98596 | 1.64342 | 0.59994 |
| 34 | 1.0683 ⁻ -02 | 1.1444 ⁺ +02 | NM | 0.99243 | 0.80617 | 0.98970 | 1.50714 | 0.65667 |
| 35 | 1.1156 ⁻ -02 | 1.2215 ⁺ +02 | NM | 0.99590 | 0.83298 | 0.99260 | 1.41996 | 0.69903 |
| 36 | 1.1445 ⁻ -02 | 1.2658 ⁺ +02 | NM | 0.99846 | 0.84799 | 0.99448 | 1.37535 | 0.72308 |
| 37 | 1.1577 ⁻ -02 | 1.2791 ⁺ +02 | NM | 0.99953 | 0.85248 | 0.99519 | 1.36286 | 0.73022 |
| 38 | 1.1646 ⁻ -02 | 1.2978 ⁺ +02 | NM | 0.99884 | 0.85870 | 0.99509 | 1.34289 | 0.74100 |
| 39 | 1.1758 ⁻ -02 | 1.3331 ⁺ +02 | NM | 0.99928 | 0.87032 | 0.99574 | 1.30899 | 0.76070 |
| 40 | 1.1994 ⁻ -02 | 1.3847 ⁺ +02 | NM | 0.99961 | 0.88707 | 0.99650 | 1.26195 | 0.78965 |
| 41 | 1.2382 ⁻ -02 | 1.4489 ⁺ +02 | NM | 0.99955 | 0.90748 | 0.99716 | 1.20743 | 0.82586 |
| 42 | 1.2951 ⁻ -02 | 1.5206 ⁺ +02 | NM | 1.00000 | 0.92972 | 0.99808 | 1.15248 | 0.86603 |
| 43 | 1.3597 ⁻ -02 | 1.5873 ⁺ +02 | NM | 0.99921 | 0.94994 | 0.99828 | 1.10437 | 0.90394 |
| 44 | 1.4150 ⁻ -02 | 1.6383 ⁺ +02 | NM | 0.99916 | 0.96513 | 0.99868 | 1.07073 | 0.93271 |
| 45 | 1.4506 ⁻ -02 | 1.6644 ⁺ +02 | NM | 0.99987 | 0.97282 | 0.99924 | 1.05506 | 0.94709 |
| 46 | 1.4699 ⁻ -02 | 1.6766 ⁺ +02 | NM | 1.00000 | 0.97639 | 0.99940 | 1.04769 | 0.95391 |
| 47 | 1.4783 ⁻ -02 | 1.6826 ⁺ +02 | NM | 1.00005 | 0.97813 | 0.99947 | 1.04412 | 0.95724 |
| 48 | 1.4872 ⁻ -02 | 1.6924 ⁺ +02 | NM | 1.00013 | 0.98096 | 0.99958 | 1.03832 | 0.96269 |
| 49 | 1.5067 ⁻ -02 | 1.7024 ⁺ +02 | NM | 0.99984 | 0.98389 | 0.99952 | 1.03201 | 0.96852 |
| 50 | 1.5420 ⁻ -02 | 1.7161 ⁺ +02 | NM | 0.99936 | 0.98783 | 0.99937 | 1.02351 | 0.97642 |
| 51 | 1.5961 ⁻ -02 | 1.7297 ⁺ +02 | NM | 0.99939 | 0.99176 | 0.99949 | 1.01564 | 0.98410 |
| 52 | 1.6622 ⁻ -02 | 1.7364 ⁺ +02 | NM | 0.99962 | 0.99369 | 0.99966 | 1.01205 | 0.98775 |
| 53 | 1.7170 ⁻ -02 | 1.7402 ⁺ +02 | NM | 1.00032 | 0.99478 | 1.00003 | 1.01058 | 0.98956 |
| 54 | 1.7640 ⁻ -02 | 1.7486 ⁺ +02 | NM | 0.99995 | 0.99716 | 0.99990 | 1.00550 | 0.99443 |
| D 55 | 1.7892 ⁻ -02 | 1.7585 ⁺ +02 | NM | 1.00000 | 1.00000 | 1.00000 | 1.00000 | 1.00000 |
| 56 | 1.8016 ⁻ -02 | 1.7640 ⁺ +02 | NM | 1.00070 | 1.00156 | 1.00039 | 0.99767 | 1.00273 |
| 57 | 1.8097 ⁻ -02 | 1.7675 ⁺ +02 | NM | 1.00070 | 1.00256 | 1.00041 | 0.99571 | 1.00472 |
| 58 | 1.8273 ⁻ -02 | 1.7704 ⁺ +02 | NM | 1.00070 | 1.00339 | 1.00043 | 0.99412 | 1.00635 |
| 59 | 1.8585 ⁻ -02 | 1.7749 ⁺ +02 | NM | 1.00070 | 1.00467 | 1.00046 | 0.99165 | 1.00889 |
| 60 | 1.9070 ⁻ -02 | 1.7846 ⁺ +02 | NM | 1.00070 | 1.00741 | 1.00053 | 0.98638 | 1.01434 |
| 61 | 1.9688 ⁻ -02 | 1.7898 ⁺ +02 | NM | 1.00070 | 1.00888 | 1.00056 | 0.98359 | 1.01726 |
| 62 | 2.0340 ⁻ -02 | 1.7937 ⁺ +02 | NM | 1.00070 | 1.00998 | 1.00059 | 0.98150 | 1.01945 |
| 63 | 2.0846 ⁻ -02 | 1.7937 ⁺ +02 | NM | 1.00070 | 1.00998 | 1.00059 | 0.98150 | 1.01945 |
| 64 | 2.1171 ⁻ -02 | 1.7953 ⁺ +02 | NM | 1.00070 | 1.01043 | 1.00060 | 0.98063 | 1.02036 |
| 65 | 2.1331 ⁻ -02 | 1.7972 ⁺ +02 | NM | 1.00070 | 1.01098 | 1.00061 | 0.97959 | 1.02146 |
| 66 | 2.1435 ⁻ -02 | 1.7995 ⁺ +02 | NM | 1.00070 | 1.01162 | 1.00063 | 0.97838 | 1.02274 |
| 88 | 2.9337 ⁻ -02 | 1.8239 ⁺ +02 | NM | 1.00070 | 1.01849 | 1.00079 | 0.96555 | 1.03650 |
| 89 | 2.9990 ⁻ -02 | 1.8190 ⁺ +02 | NM | 1.00070 | 1.01711 | 1.00076 | 0.96810 | 1.03374 |
| 90 | 3.0668 ⁻ -02 | 1.8161 ⁺ +02 | NM | 1.00070 | 1.01629 | 1.00074 | 0.96963 | 1.03208 |
| 91 | 3.1209 ⁻ -02 | 1.8119 ⁺ +02 | NM | 1.00070 | 1.01510 | 1.00071 | 0.97185 | 1.02970 |
| 92 | 3.1509 ⁻ -02 | 1.8135 ⁺ +02 | NM | 1.00070 | 1.01556 | 1.00072 | 0.97100 | 1.03061 |
| 93 | 3.1725 ⁻ -02 | 1.8135 ⁺ +02 | NM | 1.00070 | 1.01556 | 1.00072 | 0.97100 | 1.03061 |
| 94 | 3.1801 ⁻ -02 | 1.8125 ⁺ +02 | NM | 1.00070 | 1.01528 | 1.00072 | 0.97151 | 1.03006 |
| 95 | 3.1910 ⁻ -02 | 1.8083 ⁺ +02 | NM | 1.00070 | 1.01409 | 1.00069 | 0.97374 | 1.02768 |
| 96 | 3.2106 ⁻ -02 | 1.8099 ⁺ +02 | NM | 1.00070 | 1.01455 | 1.00070 | 0.97288 | 1.02860 |
| 97 | 3.2438 ⁻ -02 | 1.8063 ⁺ +02 | NM | 1.00070 | 1.01354 | 1.00067 | 0.97477 | 1.02658 |

INPUT VARIABLES Y,M,TO ASSUME P=PD

7804S0206

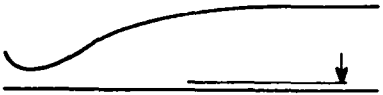
WATSON

PROFILE TABULATION

125 POINTS, DELTA AT POINT 85

| I | Y | PTZ/P | P/PD | TO/TOD | M/MD | U/UD | T/TD | R/RD*U/UD |
|------|------------|------------|------|---------|---------|---------|----------|-----------|
| 1 | 0.0000*+00 | 1.0000*+00 | NM | 0.39202 | 0.00000 | 0.00000 | 17.58599 | 0.00000 |
| 2 | 4.5720*-04 | 8.5676*+00 | NM | 0.61594 | 0.20483 | 0.63889 | 9.72874 | 0.06567 |
| 3 | 1.2548*-03 | 9.1420*+00 | NM | 0.88237 | 0.21198 | 0.77376 | 13.32359 | 0.05807 |
| 4 | 1.8440*-03 | 1.0093*+01 | NM | 0.88872 | 0.22332 | 0.78981 | 12.50839 | 0.06314 |
| 5 | 2.2047*-03 | 1.0735*+01 | NM | 0.89278 | 0.23064 | 0.79949 | 12.01573 | 0.06654 |
| 6 | 2.4003*-03 | 1.1047*+01 | NM | 0.89522 | 0.23413 | 0.80416 | 11.79691 | 0.06817 |
| 7 | 2.5121*-03 | 1.1174*+01 | NM | 0.89839 | 0.23552 | 0.80698 | 11.73958 | 0.06874 |
| 8 | 2.6492*-03 | 1.1493*+01 | NM | 0.90022 | 0.23901 | 0.81123 | 11.51988 | 0.07042 |
| 9 | 2.9261*-03 | 1.2122*+01 | NM | 0.90364 | 0.24581 | 0.81917 | 11.10540 | 0.07376 |
| 10 | 3.3985*-03 | 1.3342*+01 | NM | 0.90913 | 0.25828 | 0.83247 | 10.38823 | 0.08014 |
| 11 | 4.0589*-03 | 1.4872*+01 | NM | 0.91632 | 0.27319 | 0.84729 | 9.61884 | 0.08809 |
| 12 | 4.7523*-03 | 1.6459*+01 | NM | 0.92348 | 0.28784 | 0.86065 | 8.93990 | 0.09627 |
| 13 | 5.3823*-03 | 1.7794*+01 | NM | 0.92949 | 0.29962 | 0.87071 | 8.44530 | 0.10310 |
| 14 | 5.7912*-03 | 1.8943*+01 | NM | 0.93310 | 0.30938 | 0.87794 | 8.05261 | 0.10903 |
| 15 | 6.0503*-03 | 1.9267*+01 | NM | 0.93583 | 0.31209 | 0.88069 | 7.96333 | 0.11059 |
| 16 | 6.1798*-03 | 1.9648*+01 | NM | 0.93714 | 0.31522 | 0.88296 | 7.84591 | 0.11254 |
| 17 | 6.2992*-03 | 2.0214*+01 | NM | 0.93834 | 0.31985 | 0.88590 | 7.67167 | 0.11548 |
| 18 | 6.5126*-03 | 2.1042*+01 | NM | 0.94054 | 0.32647 | 0.89021 | 7.43505 | 0.11973 |
| 19 | 6.9240*-03 | 2.2314*+01 | NM | 0.94451 | 0.33641 | 0.89669 | 7.10461 | 0.12621 |
| 20 | 7.5260*-03 | 2.4165*+01 | NM | 0.95031 | 0.35037 | 0.90539 | 6.67769 | 0.13558 |
| 21 | 8.2550*-03 | 2.6646*+01 | NM | 0.95601 | 0.36824 | 0.91491 | 6.17294 | 0.14821 |
| 22 | 8.9002*-03 | 2.9329*+01 | NM | 0.96021 | 0.38664 | 0.92311 | 5.70024 | 0.16194 |
| 23 | 9.4005*-03 | 3.1424*+01 | NM | 0.96265 | 0.40042 | 0.92845 | 5.37634 | 0.17269 |
| 24 | 9.7333*-03 | 3.2760*+01 | NM | 0.96446 | 0.40896 | 0.93172 | 5.19043 | 0.17951 |
| 25 | 9.9263*-03 | 3.3078*+01 | NM | 0.96549 | 0.41097 | 0.93276 | 5.15139 | 0.18107 |
| 26 | 1.0046*-02 | 3.3522*+01 | NM | 0.96620 | 0.41376 | 0.93386 | 5.09405 | 0.18332 |
| 27 | 1.0239*-02 | 3.4350*+01 | NM | 0.96737 | 0.41890 | 0.93576 | 4.99001 | 0.18753 |
| 28 | 1.0579*-02 | 3.6079*+01 | NM | 0.96941 | 0.42946 | 0.93937 | 4.78453 | 0.19634 |
| 29 | 1.1120*-02 | 3.9137*+01 | NM | 0.97185 | 0.44751 | 0.94467 | 4.45619 | 0.21199 |
| 30 | 1.1814*-02 | 4.3458*+01 | NM | 0.97481 | 0.47183 | 0.95101 | 4.06243 | 0.23410 |
| 31 | 1.2515*-02 | 4.7724*+01 | NM | 0.97754 | 0.49468 | 0.95636 | 3.73756 | 0.25588 |
| 32 | 1.3063*-02 | 5.1219*+01 | NM | 0.97970 | 0.51264 | 0.96023 | 3.50850 | 0.27369 |
| 33 | 1.3457*-02 | 5.3454*+01 | NM | 0.98103 | 0.52381 | 0.96250 | 3.37648 | 0.28506 |
| 34 | 1.3660*-02 | 5.4786*+01 | NM | 0.98169 | 0.53035 | 0.96373 | 3.30215 | 0.29185 |
| 35 | 1.3792*-02 | 5.5810*+01 | NM | 0.98209 | 0.53532 | 0.96460 | 3.24694 | 0.29708 |
| 36 | 1.3937*-02 | 5.6897*+01 | NM | 0.98253 | 0.54055 | 0.96550 | 3.19033 | 0.30263 |
| 37 | 1.4234*-02 | 5.9569*+01 | NM | 0.98341 | 0.55319 | 0.96752 | 3.05892 | 0.31629 |
| 38 | 1.4707*-02 | 6.4534*+01 | NM | 0.98483 | 0.57595 | 0.97082 | 2.84126 | 0.34169 |
| 39 | 1.5392*-02 | 7.1036*+01 | NM | 0.98760 | 0.60446 | 0.97508 | 2.60219 | 0.37471 |
| 40 | 1.6101*-02 | 7.7960*+01 | NM | 0.99049 | 0.63341 | 0.97908 | 2.38924 | 0.40979 |
| 41 | 1.6711*-02 | 8.3697*+01 | NM | 0.99192 | 0.65644 | 0.98161 | 2.23609 | 0.43898 |
| 42 | 1.7163*-02 | 8.7590*+01 | NM | 0.99275 | 0.67161 | 0.98312 | 2.14281 | 0.45880 |
| 43 | 1.7447*-02 | 9.0833*+01 | NM | 0.99329 | 0.68399 | 0.98424 | 2.07063 | 0.47533 |
| 44 | 1.7572*-02 | 9.2035*+01 | NM | 0.99352 | 0.68852 | 0.98465 | 2.04516 | 0.48145 |
| 45 | 1.7716*-02 | 9.2989*+01 | NM | 0.99378 | 0.69210 | 0.98502 | 2.02558 | 0.48629 |
| 46 | 1.7953*-02 | 9.6306*+01 | NM | 0.99413 | 0.70439 | 0.98596 | 1.95925 | 0.50324 |
| 47 | 1.8369*-02 | 1.0097*+02 | NM | 0.99477 | 0.72131 | 0.98729 | 1.87345 | 0.52699 |
| 48 | 1.8979*-02 | 1.0771*+02 | NM | 0.99571 | 0.74512 | 0.98906 | 1.76197 | 0.56134 |
| 49 | 1.9703*-02 | 1.1618*+02 | NM | 0.99702 | 0.77398 | 0.99114 | 1.63988 | 0.60440 |
| 50 | 2.0361*-02 | 1.2400*+02 | NM | 0.99812 | 0.79970 | 0.99284 | 1.54135 | 0.64414 |
| 51 | 2.0881*-02 | 1.2986*+02 | NM | 0.99869 | 0.81845 | 0.99390 | 1.47469 | 0.67397 |
| 52 | 2.1199*-02 | 1.3401*+02 | NM | 0.99890 | 0.83144 | 0.99491 | 1.43072 | 0.69511 |
| 53 | 2.1387*-02 | 1.3643*+02 | NM | 0.99904 | 0.83894 | 0.99487 | 1.40625 | 0.70746 |
| 54 | 2.1526*-02 | 1.3878*+02 | NM | 0.99913 | 0.84618 | 0.99517 | 1.38316 | 0.71949 |
| 55 | 2.1714*-02 | 1.4145*+02 | NM | 0.99925 | 0.85429 | 0.99553 | 1.35798 | 0.73309 |
| 56 | 2.2080*-02 | 1.4483*+02 | NM | 0.99927 | 0.86449 | 0.99589 | 1.32709 | 0.75043 |
| 57 | 2.2636*-02 | 1.5164*+02 | NM | 0.99929 | 0.88464 | 0.99656 | 1.26905 | 0.78528 |
| 58 | 2.3343*-02 | 1.5833*+02 | NM | 0.99932 | 0.90399 | 0.99718 | 1.21679 | 0.81952 |
| 59 | 2.4072*-02 | 1.6451*+02 | NM | 0.99932 | 0.92152 | 0.99769 | 1.17214 | 0.85117 |
| 60 | 2.4628*-02 | 1.6952*+02 | NM | 0.99909 | 0.93547 | 0.99796 | 1.13806 | 0.87690 |
| 61 | 2.5029*-02 | 1.7240*+02 | NM | 0.99901 | 0.94341 | 0.99813 | 1.11937 | 0.89169 |
| 62 | 2.5245*-02 | 1.7355*+02 | NM | 0.99901 | 0.94655 | 0.99821 | 1.11214 | 0.89756 |
| 63 | 2.5397*-02 | 1.7393*+02 | NM | 0.99899 | 0.94759 | 0.99823 | 1.10973 | 0.89952 |
| 64 | 2.5578*-02 | 1.7476*+02 | NM | 0.99899 | 0.94986 | 0.99829 | 1.10457 | 0.90378 |
| 65 | 2.5903*-02 | 1.7659*+02 | NM | 0.99897 | 0.95483 | 0.99841 | 1.09336 | 0.91315 |
| 66 | 2.6396*-02 | 1.7875*+02 | NM | 0.99904 | 0.96067 | 0.99859 | 1.08050 | 0.92419 |
| 67 | 2.7069*-02 | 1.8132*+02 | NM | 0.99918 | 0.96756 | 0.99883 | 1.06568 | 0.93727 |
| 68 | 2.7783*-02 | 1.8403*+02 | NM | 0.99857 | 0.97480 | 0.99870 | 1.04964 | 0.95147 |
| 69 | 2.8407*-02 | 1.8608*+02 | NM | 0.99988 | 0.98021 | 0.99948 | 1.03972 | 0.96130 |
| 70 | 2.8852*-02 | 1.8737*+02 | NM | 0.99937 | 0.98361 | 0.99931 | 1.03219 | 0.96815 |
| 71 | 2.9149*-02 | 1.8780*+02 | NM | 0.99944 | 0.98474 | 0.99937 | 1.02994 | 0.97032 |
| 72 | 2.9329*-02 | 1.8793*+02 | NM | 0.99960 | 0.98509 | 0.99946 | 1.02939 | 0.97092 |
| 73 | 2.9489*-02 | 1.8800*+02 | NM | 0.99972 | 0.98526 | 0.99952 | 1.02916 | 0.97121 |
| 74 | 2.9746*-02 | 1.8843*+02 | NM | 0.99995 | 0.98640 | 0.99966 | 1.02708 | 0.97331 |
| 75 | 3.0183*-02 | 1.8913*+02 | NM | 1.00031 | 0.98823 | 0.99989 | 1.02374 | 0.97670 |
| 76 | 3.0767*-02 | 1.8966*+02 | NM | 0.99979 | 0.98962 | 0.99966 | 1.02039 | 0.97969 |
| 77 | 3.1501*-02 | 1.9073*+02 | NM | 0.99916 | 0.99241 | 0.99941 | 1.01415 | 0.98547 |
| 78 | 3.2154*-02 | 1.9200*+02 | NM | 0.99990 | 0.99573 | 0.99985 | 1.00830 | 0.99162 |
| 79 | 3.2675*-02 | 1.9298*+02 | NM | 0.99997 | 0.99826 | 0.99994 | 1.00338 | 0.99657 |
| 80 | 3.3007*-02 | 1.9399*+02 | NM | 1.00002 | 1.00087 | 1.00003 | 0.99831 | 1.00172 |
| 81 | 3.3216*-02 | 1.9405*+02 | NM | 1.00003 | 1.00105 | 1.00004 | 0.99799 | 1.00205 |
| 82 | 3.3360*-02 | 1.9361*+02 | NM | 1.00005 | 0.99991 | 1.00002 | 1.00022 | 0.99980 |
| 83 | 3.3604*-02 | 1.9314*+02 | NM | 1.00009 | 0.99869 | 1.00001 | 1.00265 | 0.99737 |
| 84 | 3.3972*-02 | 1.9308*+02 | NM | 1.00012 | 0.99852 | 1.00003 | 1.00303 | 0.99701 |
| D 85 | 3.4519*-02 | 1.9365*+02 | NM | 1.00000 | 1.00000 | 1.00000 | 1.00000 | 1.00000 |
| 86 | 3.5212*-02 | 1.9449*+02 | NM | 1.00003 | 1.00218 | 1.00007 | 0.99579 | 1.00430 |
| 124 | 5.0101*-02 | 1.9314*+02 | NM | 1.00003 | 0.99869 | 0.99999 | 1.00260 | 0.99740 |
| 125 | 5.0615*-02 | 1.9234*+02 | NM | 1.00003 | 0.99660 | 0.99994 | 1.00672 | 0.99327 |

INPUT VARIABLES Y,M,TD ASSUME P=PD

| | | |
|--|---|-------------|
| <p>rough</p>  | <p>M: 2.9 RE THETA $\times 10^{-3}$: 2.7-58 TW/TR: 1</p> | <p>7901</p> |
| <p>Boundary layer channel. Effectively continuous. $W = 0.33$ m. $0.015 < PO < 0.42$ MN/m². $TO: 320K$. Air, dew point 215 - 233K. $1 < RE/m \times 10^{-6} < 30$.</p> | | |
| <p>VOISINET R.L.P., 1979a. Influence of roughness and blowing on compressible turbulent boundary layer flow. NSWC TR 79-153. <u>And:</u> Voisinnet (1979b); Voisinnet R.L.P., private communications; CAT 7202, CAT 7304</p> | | |

- 1 The test boundary layer was formed on the straight test wall which faces a flexible half-nozzle ($X = 0$ at the throat). The test wall was 2.50 m long, and from $X = 1.22$ the normal smooth surface was replaced by one of a number of interchangeable rough and porous test plate inserts ($W = 0.305$, $L = 1.0$ m). The construction of these surfaces is shown in Fig. 1, details of the roughness screens being given in Table 1. The woven square mesh material was attached so that the mesh grid was at 45° to the flow direction. The layers below the roughness grid were designed to ensure an even
- 2 distribution of the air supply for boundary layer mass addition. Axial Pitot surveys showed that
- 4 the flow in the test region was free of pressure gradients and disturbances. The Mach number distribution for $0 < X < X_T$ was designed to be

$$M = 2.9 - 1.9 \left(1 + 0.55972 \frac{X}{X_T}\right) \left(1 - \frac{X}{X_T}\right)^2$$

where $X_T = 1.143$ m was the nominal start of the test rhombus, just upstream of the start of the porous plate surface. In practice the test section Mach number was slightly higher than 2.9 by an amount depending on the boundary layer growth in the test section. In the test area the wall was at room temperature, while the throat area was slightly heated, so that the tunnel total temperature could be adjusted to give adiabatic wall conditions throughout the boundary layer growth.

- 6 Static pressure tapings were mounted on all test plates. A thermocouple was also attached to each plate to give a value for TW. A floating element balance was used with a rectangular element ($W = 0.127$, $L = 0.254$ m), centred on $X = 1.88$ m. The blowing arrangements and the rough surface were as for the rest of the insert, the roughness screen being cut from and aligned with the piece of wire mesh surrounding it. The surrounding edge gap was less than 0.25 mm with no load applied. The balance was a positive displacement device, the restoring force being supplied by interchangeable leaf springs to give a full deflection (0.25 mm) load range from 50 to 1000 mg.
- 7 Pitot and T_0 profile measurements were made in the same general way as for CAT 7202, CAT 7304. The Pitot probe was an FPP ($h_2 = 0.076$, $b_2 = 2.54$ mm). The TTP was a FWP for which the sensing element was a chromel-alumel thermocouple junction at the centre of a traverse fine wire ($d = 0.0254$, $L = 3.56$ mm). The two probes were mounted side by side in a common holder.
- 8 The centre of the balance element was at $X = 1.88$ m, while profiles were measured at $X = 1.98$ m. "The differences in measurement location were accounted for in combining skin friction and boundary layer profile parameters." Static pressure was assumed constant through the layers and evaluated from Pitot measurements in the free stream. At the higher unit Reynolds numbers the FWP proved too fragile and the temperature was deduced from the Crocco/Van Driest temperature-velocity correlation.
- 10 No corrections were applied to the Pitot data and (E) Sutherland's viscosity law was used. The
- 12 editors present the profile data for the case of no mass transfer as provided by the author,
- 13 incorporating his assumptions and data reduction procedures. There are four sets of single station profiles. The first set were taken with a smooth wall surface (0101-0112) for $2.7 < Re_\theta \times 10^{-3} < 39$. In

sets 02-04, four profiles are given for each of the three roughness meshes covering a range
 14 $7 < Re_{\theta} \times 10^{-3} < 58$. Skin friction values are given for all profiles. The original report also includes profiles for three blowing rates for each roughness mesh, over the same unit Reynolds number range, and a great deal of fine detail of the skin friction measurements, for all cases whether presented here or not.

§ DATA: 79010101-0404. Pitot and TO profiles measured simultaneously. CF from FEB. NX = 1.

15 Editors comments. The experiment provides a usefully wide range of coverage for one type of roughness ($0 \leq k u_{\tau} / \nu_w \leq 276$) at $M_{\theta} = 3$, supplemented in the original report by results for three rates of blowing. The balance element is relatively large, so that many of the usual measurement difficulties associated with these instruments are avoided. One selected profile from the smooth wall results is shown in Fig. 2 as a basis for comparison. Except for profiles^{*)} 0109 and 0110 which show discrepancies, the general pattern of the profiles is typical of a fully developed ZPG boundary layer, but as for other NOL/NSWC adiabatic wall data (CAT 7202) the profile lies relatively high in relation to the "standard" wall law. The wake component also is higher than usual (see Figs. 3.3.13, 4.2.19 and the discussion of the wake strength in § 3.3.3 of AGARDograph 253). Agreement with the standard outer law is on the whole better than for the earlier data (AG 253 - Fig. 4.2.20), and examples for the smooth wall and each roughness height are presented in Fig. 3. The slight S-shape of the outer law profile is however characteristic of this experiment and different from the behaviour of the profiles obtained by Shutts & Fenter (1955) or Young (1965) (AG 253 - Fig. 4.6.5).

When the Reynolds number Re_{δ_2} is increased for a given Mach number and roughness height, the dimensionless roughness height $k u_{\tau} / \nu_w$ increases and the profile as a whole is shifted progressively downwards in relation to the wall law (Fig. 4) while the outer law is unaffected (Fig. 3, profile 0304). For the lowest dimensionless roughness heights (profiles 0201, 0202 and 0301) the surface is aerodynamically smooth, and the profiles are as for the formally smooth surface of series 01. In Fig. 5 we show profiles 0204, 0304 and 0404 which have the highest values $k u_{\tau} / \nu_w$ of each series, plotted versus $\log y/k$ and compare them with a "standard" log law $\bar{u}^+ = 2.50 \ln(y/k) + 8.50$ (eqn. 4.6.4 of AGARDograph 253). Agreement is satisfactory though this relationship strictly should only hold for velocity profiles with $(k u_{\tau} / \nu_w) > 70$. The rough-to-smooth skin friction coefficient ratios of the profiles shown in the above figures fall within the band presented by Reda (1974) and reproduced as Fig. (4.6.1) in AG 253. The author states that the transformed velocity profiles agree with low speed behaviour if k_s/k equals 1.2 where k_s is the equivalent sand grain height.

The velocity profiles extend well into the viscous sublayer, and agreement between the measured temperature profiles and the temperature relation, eqn.(2.5.37, AG 253) is good. The author's published values of Re_{θ} are in error being out by a factor of 2.54.

Comparisons may be made with the experiments by Young (CAT 6506) and Shutts & Fenter (CAT 5502) who all used floating element balances, as did Reda (1974), though tabulated information is not available for this last study. The data given in the legends of figures 2, 4 and 5 were calculated with a D-state at PO max and differ slightly from the "Kopfdaten" printed in the tables below.

*) Not shown here

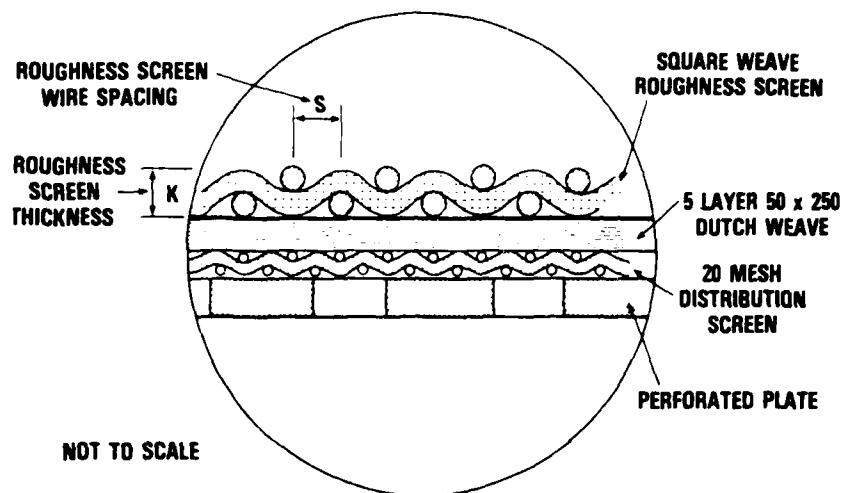


Fig. 1 Test Panel, Cross Section (from Voisinet).

| MULTILAYER COMPOSITE | TYPICAL ALL PANELS | | |
|------------------------|--|------------|------------|
| PERFORATED PLATE | 22-GAGE 1.58 mm DIA HOLES ON 4.76 mm CENTERS 60° STAGGERED PATTERN 0.782 mm THICKNESS | | |
| DISTRIBUTION MESH | 20 MESH, 0.406 mm DIA WIRES 0.584 mm THICKNESS | | |
| FIVE-LAYER DUTCH WEAVE | 5 LAYERS 50 x 250 MESH DUTCH WEAVE 0.864 mm THICKNESS | | |
| ROUGHNESS SCREENS | 1 | 2 | 3 |
| K-(mm/MCH) | 0.1/0.004 | 0.33/0.013 | 1.25/0.049 |
| d_w -WIRE DIA (mm) | 0.05842 | 0.1905 | 0.7112 |
| MESH (WIRES PER INCH) | 200 | 60 | 14 |
| S- MESH SPACING (mm) | 0.127 | 0.4233 | 1.8143 |
| S/d_w | 2.174 | 2.22 | 2.551 |
| S/K | 1.25 | 1.28 | 1.48 |
| % CALENDAR | 13.0 | 13.3 | 12.5 |

Table 1 Porous roughened test samples (from Voisinet).

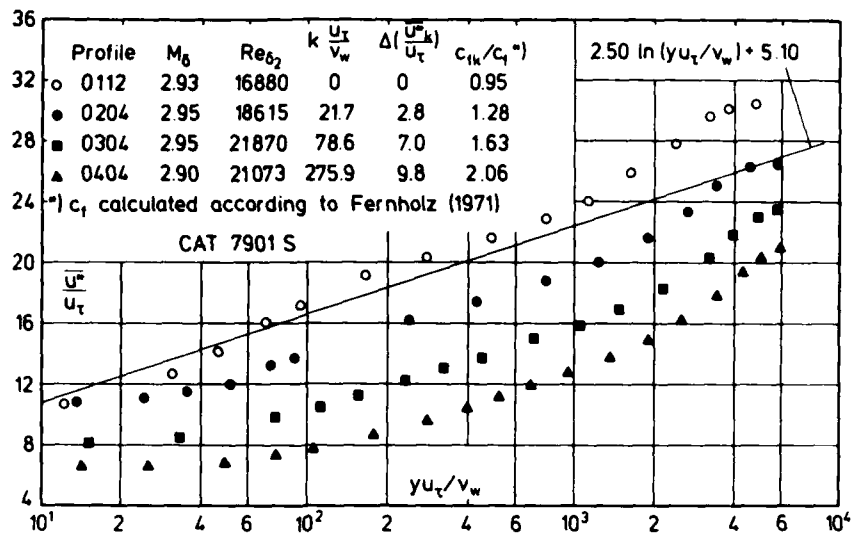


Fig. 2 Law of the wall for compressible turbulent boundary layers over rough walls (adiabatic wall, zero pressure gradient, origin not defined.) Voisinet (1979).

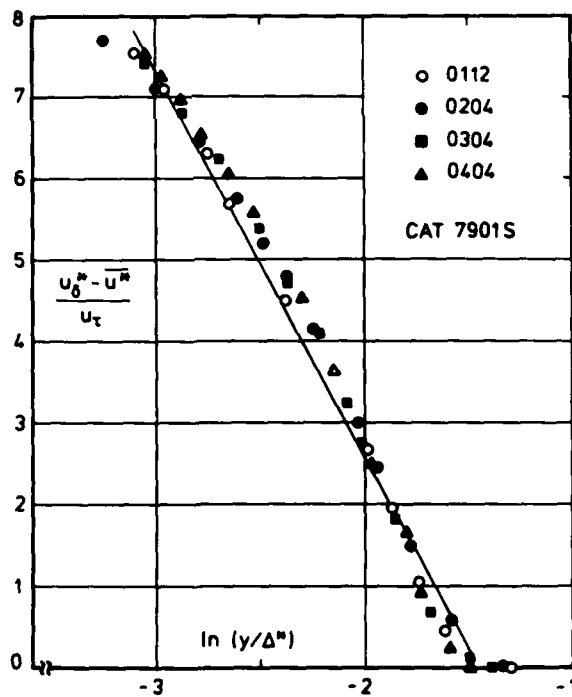


Fig. 3 Outer law for compressible turbulent boundary layers over rough walls (adiabatic wall, zero pressure gradient, origin not defined). Voisinet (1979).

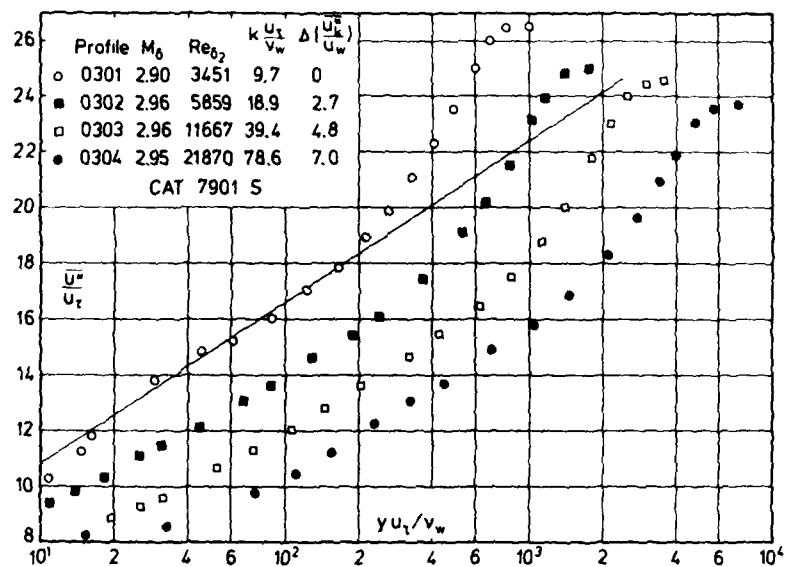


Fig. 4 Law of the wall for compressible turbulent boundary layers over rough walls (adiabatic wall, zero pressure gradient, origin not defined). Voisinet (1979).

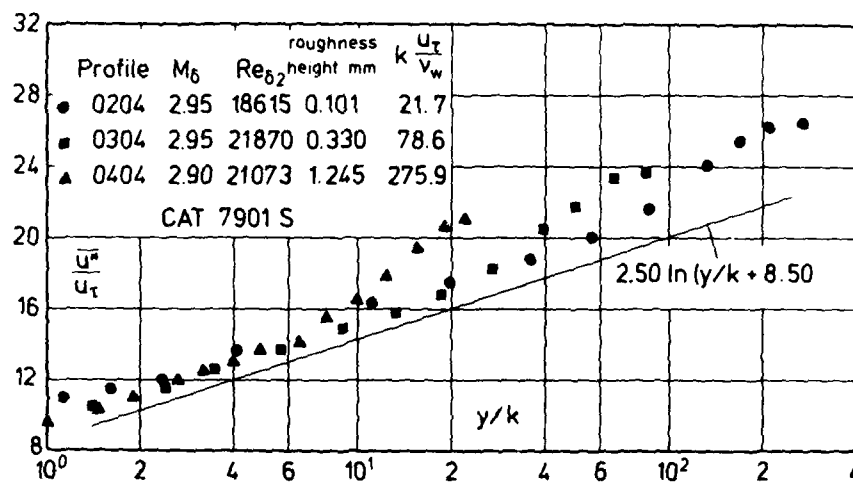


Fig. 5 Law of the wall for compressible turbulent boundary layers over rough walls (adiabatic wall, zero pressure gradient, origin not defined). Voisinet (1979).

| CAT 79015 | | BOUNDARY CONDITIONS AND EVALUATED DATA. SI UNITS | | | | | | | |
|-------------------------------------|------------------------------------|--|--|--------------------------------|----------------------------|--------------------------------|--|--|--|
| RUN X * RZ | MD # POD* TOD* | TW/TR PW/PD* TAUM * | RED2W REO2D DZ | CF CQ PI2* | H12 H32 H42 | H12K H32K D2K | PW TW* UD | PD TD TR | |
| 7901S0101 1.9810**00 INFINITE | 2.8704 1.5440**04 3.2120**02 | 0.9880 1.0000 5.0550**00 | 1.2566**03 2.6974**03 2.4813**03 | 1.7148**03 NM 0.0000**00 | 4.7971 1.7854 0.1312 | 1.4407 1.7600 3.7933**03 | 5.1112**02 2.9680**02 6.3386**02 | 5.1112**02 1.2131**02 3.0041**02 | |
| 7901S0102 1.9810**00 INFINITE | 2.9282 5.2950**04 3.2080**02 | 0.9906 1.0000 1.4130**01 | 3.1374**03 6.9038**03 1.9081**03 | 1.4659**03 NM 0.0000**00 | 4.8942 1.7927 0.1086 | 1.3643 1.7708 2.9577**03 | 1.6060**03 2.9690**02 6.3819**02 | 1.6060**03 1.1816**02 2.9973**02 | |
| 7901S0103 1.9810**00 INFINITE | 2.9131 5.1990**04 3.1510**02 | 0.9923 1.0000 1.4000**01 | 3.2946**03 7.2378**03 1.9691**03 | 1.4609**03 NM 0.0000**00 | 4.9212 1.7738 0.1026 | 1.4014 1.7535 3.0738**03 | 1.6133**03 2.9220**02 6.3129**02 | 1.6133**03 1.1682**02 2.9448**02 | |
| 7901S0104 1.9810**00 INFINITE | 2.9053 1.0560**05 3.2530**02 | 0.9784 1.0000 2.5390**01 | 5.7106**03 1.2309**04 1.7185**03 | 1.2960**03 NM 0.0000**00 | 4.6457 1.7996 0.1512 | 1.3354 1.7795 2.5918**03 | 3.3157**03 2.9750**02 6.4079**02 | 3.3157**03 1.2101**02 3.0405**02 | |
| 7901S0105 1.9810**00 INFINITE | 2.9360 1.0380**05 3.2020**02 | 0.9939 1.0000 2.5040**01 | 5.2504**03 1.1622**04 1.6412**03 | 1.3337**03 NM 0.0000**00 | 4.9013 1.8025 0.0940 | 1.3328 1.7821 2.5242**03 | 3.1114**03 2.9730**02 6.3822**02 | 3.1114**03 1.1755**02 2.9912**02 | |
| 7901S0106 1.9810**00 INFINITE | 2.9345 1.0370**05 3.1590**02 | 0.9955 1.0000 2.4660**01 | 5.5936**03 1.2418**04 1.7201**03 | 1.3131**03 NM 0.0000**00 | 4.9943 1.7893 0.0789 | 1.3623 1.7685 2.6862**03 | 3.1155**03 2.9380**02 6.3380**02 | 3.1155**03 1.1604**02 2.9511**02 | |
| 7901S0107 1.9810**00 INFINITE | 2.9221 2.0480**05 3.1890**02 | 1.0027 1.0000 4.4250**01 | 9.7016**03 2.1520**04 1.5196**03 | 1.1809**03 NM 0.0000**00 | 4.9922 1.8075 0.0432 | 1.3173 1.7883 2.3334**03 | 6.2692**03 2.9880**02 6.3581**02 | 6.2692**03 1.1777**02 2.9798**02 | |
| 7901S0108 1.9810**00 INFINITE | 2.9252 2.0730**05 3.1920**02 | 0.9811 1.0000 4.4680**01 | 1.0322**04 2.2537**04 1.5770**03 | 1.1810**03 NM 0.0000**00 | 4.5409 1.8130 0.1773 | 1.2980 1.7958 2.3317**03 | 6.3160**03 2.9260**02 6.3636**02 | 6.3160**03 1.1773**02 2.9825**02 | |
| 7901S0109 1.9810**00 INFINITE | 2.9206 2.1110**05 3.2000**02 | 0.9728 1.0000 4.5580**01 | 1.0401**04 2.2511**04 1.5485**03 | 1.1786**03 NM 0.0000**00 | 4.5157 1.8144 0.1820 | 1.2973 1.7958 2.2832**03 | 6.4767**03 2.9090**02 6.3679**02 | 6.4767**03 1.1826**02 2.9902**02 | |
| 7901S0110 1.9810**00 INFINITE | 2.9142 3.0920**05 3.1980**02 | 0.9784 1.0000 6.3350**01 | 1.3726**04 2.9768**04 1.3919**03 | 1.1125**03 NM 0.0000**00 | 4.6106 1.8161 0.1399 | 1.2960 1.7993 2.0443**03 | 9.5786**03 2.9240**02 6.3607**02 | 9.5786**03 1.1851**02 2.9887**02 | |
| 7901S0111 1.9810**00 INFINITE | 2.9390 4.1220**05 3.1850**02 | 1.0093 1.0000 8.3030**01 | 1.6332**04 3.6661**04 1.2958**03 | 1.1164**03 NM 0.0000**00 | 4.8447 1.8278 0.0772 | 1.2755 1.8102 1.9279**03 | 1.2300**04 3.0030**02 6.3676**02 | 1.2300**04 1.1677**02 2.9752**02 | |
| 7901S0112 1.9810**00 INFINITE | 2.9334 4.1710**05 3.0980**02 | 1.0276 1.0000 8.3350**01 | 1.6880**04 3.8513**04 1.2887**03 | 1.1024**03 NM 0.0000**00 | 4.8927 1.8295 0.0584 | 1.2797 1.8111 1.9165**03 | 1.2552**04 2.9740**02 6.2757**02 | 1.2552**04 1.1386**02 2.8942**02 | |
| 7901S0201 1.9810**00 INFINITE | 2.9642 5.2060**04 3.1490**02 | 1.0019 1.0000 1.4190**01 | 3.1578**03 7.1316**03 1.9908**03 | 1.5426**03 NM 0.0000**00 | 5.1293 1.7827 0.0689 | 1.3773 1.7601 3.1607**03 | 1.4956**03 2.9460**02 6.3513**02 | 1.4956**03 1.1421**02 2.9403**02 | |
| 7901S0202 1.9810**00 INFINITE | 2.9438 1.0400**05 3.1370**02 | 1.0006 1.0000 2.5440**01 | 5.6706**03 1.2700**04 1.7453**03 | 1.3612**03 NM 0.0000**00 | 5.0614 1.7873 0.0672 | 1.3630 1.7659 2.7494**03 | 3.0810**03 2.9320**02 6.3233**02 | 3.0810**03 1.1477**02 2.9301**02 | |
| 7901S0203 1.9810**00 INFINITE | 2.9628 2.0490**05 3.1580**02 | 0.9964 1.0000 5.0540**01 | 9.9644**03 2.2383**04 1.5929**03 | 1.3943**03 NM 0.0000**00 | 5.1580 1.8008 0.0302 | 1.3261 1.7801 2.4980**03 | 5.8988**03 2.9380**02 6.3593**02 | 5.8988**03 1.1460**02 2.9488**02 | |
| 7901S0204 1.9810**00 INFINITE | 2.9521 4.1340**05 3.1540**02 | 1.0073 1.0000 1.0810**02 | 1.8615**04 4.2001**04 1.4701**03 | 1.4651**03 NM 0.0000**00 | 4.9568 1.8148 0.0652 | 1.2948 1.7960 2.2393**03 | 1.2095**04 2.9670**02 6.3469**02 | 1.2095**04 1.1498**02 2.9456**02 | |
| 7901S0301 1.9810**00 INFINITE | 2.8870 5.1920**04 3.1880**02 | 0.9846 1.0000 1.4520**01 | 3.4151**03 7.3680**03 2.0122**03 | 1.4849**03 NM 0.0000**00 | 4.9980 1.7717 0.0595 | 1.3919 1.7509 3.1851**03 | 1.6760**03 2.9350**02 6.3286**02 | 1.6760**03 1.1954**02 2.9808**02 | |
| 7901S0302 1.9810**00 INFINITE | 2.9506 1.0400**05 3.1710**02 | 0.9975 1.0000 3.0510**01 | 5.7981**03 1.2965**04 1.8163**03 | 1.6417**03 NM 0.0000**00 | 5.2496 1.7706 0.0289 | 1.3879 1.7497 2.9392**03 | 3.0496**03 2.9540**02 6.3628**02 | 3.0496**03 1.1568**02 2.9615**02 | |
| 7901S0303 1.9810**00 INFINITE | 2.9316 2.0900**05 3.1860**02 | 1.0012 1.0000 6.5490**01 | 1.1298**04 2.5129**04 1.7455**03 | 1.7261**03 NM 0.0000**00 | 5.2817 1.7686 0.0093 | 1.3938 1.7474 2.8388**03 | 6.3066**03 2.9800**02 6.3627**02 | 6.3066**03 1.1718**02 2.9765**02 | |
| 7901S0304 1.9810**00 INFINITE | 2.9371 4.1320**05 3.1380**02 | 1.0261 1.0000 1.3620**02 | 2.1668**04 4.9348**04 1.7014**03 | 1.8241**03 NM 0.0000**00 | 5.0687 1.7828 0.0727 | 1.3702 1.7594 2.7209**03 | 1.2365**04 3.0080**02 6.3190**02 | 1.2365**04 1.1514**02 2.9314**02 | |

| CAT 7901S | | VOISINET | | BOUNDARY CONDITIONS AND EVALUATED DATA. SI UNITS | | | | | |
|-----------------------|-----------------------|-----------------------|-----------------------|--|--------|-----------------------|-----------------------|-----------------------|--|
| RUN | MD * | TW/TR | RED2W | CF | H12 | H12K | PW | PD | |
| X * | POD* | PW/PD* | RED2D | CQ | H32 | H32K | TW* | TD | |
| RZ | TOD* | TAUW * | D2 | PT2* | H42 | D2K | UD | TR | |
| 7901S0401 | 2.8652 | 0.9905 | 4.2412 ⁺⁰³ | 2.0709 ⁻⁰³ | 5.1613 | 1.5301 | 1.7621 ⁺⁰³ | 1.7621 ⁺⁰³ | |
| 1.9810 ⁺⁰⁰ | 5.2810 ⁺⁰⁴ | 1.0000 | 9.1171 ⁺⁰³ | NM | 1.7245 | 1.6975 | 2.9480 ⁺⁰² | 1.2044 ⁺⁰² | |
| INFINITE | 3.1820 ⁺⁰² | 2.0970 ⁺⁰¹ | 2.4124 ⁻⁰³ | 0.0000 ⁺⁰⁰ | 0.0784 | 4.0002 ⁻⁰³ | 6.3046 ⁺⁰² | 2.9763 ⁺⁰² | |
| 7901S0402 | 2.8903 | 0.9917 | 7.6375 ⁺⁰³ | 2.2284 ⁻⁰³ | 5.2681 | 1.5422 | 3.3051 ⁺⁰³ | 3.3051 ⁺⁰³ | |
| 1.9810 ⁺⁰⁰ | 1.0290 ⁺⁰⁵ | 1.0000 | 1.6593 ⁺⁰⁴ | NM | 1.7219 | 1.6939 | 2.9530 ⁺⁰² | 1.1925 ⁺⁰² | |
| INFINITE | 3.1850 ⁺⁰² | 4.3070 ⁺⁰¹ | 2.2875 ⁻⁰³ | 0.0000 ⁺⁰⁰ | 0.0757 | 3.8468 ⁻⁰³ | 6.3283 ⁺⁰² | 2.9778 ⁺⁰² | |
| 7901S0403 | 2.9121 | 0.9886 | 1.3450 ⁺⁰⁴ | 2.3705 ⁻⁰³ | 5.3703 | 1.5047 | 6.2465 ⁺⁰³ | 6.2465 ⁺⁰³ | |
| 1.9810 ⁺⁰⁰ | 2.0100 ⁺⁰⁵ | 1.0000 | 2.9347 ⁺⁰⁴ | NM | 1.7332 | 1.7062 | 2.9740 ⁺⁰² | 1.1940 ⁺⁰² | |
| INFINITE | 3.2190 ⁺⁰² | 6.7900 ⁺⁰¹ | 2.1284 ⁻⁰³ | 0.0000 ⁺⁰⁰ | 0.0395 | 3.5890 ⁻⁰³ | 6.3799 ⁺⁰² | 3.0084 ⁺⁰² | |
| 7901S0404 | 2.8833 | 0.9935 | 2.0821 ⁺⁰⁴ | 2.3792 ⁻⁰³ | 5.0307 | 1.4607 | 1.0054 ⁺⁰⁴ | 1.0054 ⁺⁰⁴ | |
| 1.9810 ⁺⁰⁰ | 3.0970 ⁺⁰⁵ | 1.0000 | 4.5180 ⁺⁰⁴ | NM | 1.7471 | 1.7219 | 2.9580 ⁺⁰² | 1.1958 ⁺⁰² | |
| INFINITE | 3.1840 ⁺⁰² | 1.3920 ⁺⁰² | 2.0607 ⁻⁰³ | 0.0000 ⁺⁰⁰ | 0.0954 | 3.3573 ⁻⁰³ | 6.3216 ⁺⁰² | 2.9772 ⁺⁰² | |
| 7901S0405 | 2.9096 | 0.9926 | 2.6720 ⁺⁰⁴ | 2.5041 ⁻⁰³ | 5.0431 | 1.4545 | 1.2831 ⁺⁰⁴ | 1.2831 ⁺⁰⁴ | |
| 1.9810 ⁺⁰⁰ | 4.1130 ⁺⁰⁵ | 1.0000 | 5.8380 ⁺⁰⁴ | NM | 1.7514 | 1.7250 | 3.0020 ⁺⁰² | 1.2016 ⁺⁰² | |
| INFINITE | 3.2360 ⁺⁰² | 1.9040 ⁺⁰² | 2.0819 ⁻⁰³ | 0.0000 ⁺⁰⁰ | 0.1095 | 3.3961 ⁻⁰³ | 6.3947 ⁺⁰² | 3.0244 ⁺⁰² | |

TRAPEZOIDAL RULE FOR 0112
 ROUGHNESS SCREEN THICKNESS 01: 0.00000 CM 02: 0.01016 CM
 03: 0.03302 CM 04: 0.12450 CM

| 7901S0204 | | VOISINET | | PROFILE TABULATION | | 42 POINTS, DELTA AT POINT 30 | | |
|-----------|-----------------------|-----------------------|------|--------------------|---------|------------------------------|---------|-----------|
| I | Y | PT2/P | P/PD | TO/TOD | M/MD | U/UD | T/TD | R/RD*U/UD |
| 1 | 0.0000 ⁺⁰⁰ | 1.0000 ⁺⁰⁰ | NM | 0.94100 | 0.00000 | 0.00000 | 2.58114 | 0.00000 |
| 2 | 6.4000 ⁻⁰⁵ | 1.7018 ⁺⁰⁰ | NM | 0.95830 | 0.30680 | 0.46103 | 2.25813 | 0.20416 |
| 3 | 1.1400 ⁻⁰⁴ | 1.7367 ⁺⁰⁰ | NM | 0.95880 | 0.31307 | 0.46921 | 2.24624 | 0.20888 |
| 4 | 1.6500 ⁻⁰⁴ | 1.8179 ⁺⁰⁰ | NM | 0.95830 | 0.32685 | 0.48656 | 2.21597 | 0.21957 |
| 5 | 2.4100 ⁻⁰⁴ | 1.9354 ⁺⁰⁰ | NM | 0.95940 | 0.34514 | 0.50950 | 2.17915 | 0.23381 |
| 6 | 2.6700 ⁻⁰⁴ | 2.0447 ⁺⁰⁰ | NM | 0.96090 | 0.36076 | 0.52878 | 2.14838 | 0.24613 |
| 7 | 3.1800 ⁻⁰⁴ | 2.1614 ⁺⁰⁰ | NM | 0.96250 | 0.37634 | 0.54763 | 2.11741 | 0.25863 |
| 8 | 3.4300 ⁻⁰⁴ | 2.1998 ⁺⁰⁰ | NM | 0.96295 | 0.38125 | 0.55347 | 2.10743 | 0.26263 |
| 9 | 4.1900 ⁻⁰⁴ | 2.3471 ⁺⁰⁰ | NM | 0.96410 | 0.39938 | 0.57450 | 2.06924 | 0.27764 |
| 10 | 1.1300 ⁻⁰³ | 3.2187 ⁺⁰⁰ | NM | 0.97130 | 0.49033 | 0.67186 | 1.87749 | 0.35785 |
| 11 | 2.0190 ⁻⁰³ | 3.7256 ⁺⁰⁰ | NM | 0.97520 | 0.53531 | 0.71499 | 1.78393 | 0.40079 |
| 12 | 2.7810 ⁻⁰³ | 4.0434 ⁺⁰⁰ | NM | 0.97770 | 0.56153 | 0.73872 | 1.73065 | 0.42684 |
| 13 | 3.6450 ⁻⁰³ | 4.3666 ⁺⁰⁰ | NM | 0.97950 | 0.58694 | 0.76047 | 1.67875 | 0.45300 |
| 14 | 4.6860 ⁻⁰³ | 4.7031 ⁺⁰⁰ | NM | 0.98070 | 0.61221 | 0.78092 | 1.62711 | 0.47994 |
| 15 | 5.7790 ⁻⁰³ | 5.0977 ⁺⁰⁰ | NM | 0.98330 | 0.64053 | 0.80324 | 1.57260 | 0.51077 |
| 16 | 6.9220 ⁻⁰³ | 5.5467 ⁺⁰⁰ | NM | 0.98540 | 0.67125 | 0.82593 | 1.51395 | 0.54554 |
| 17 | 7.8610 ⁻⁰³ | 5.9380 ⁺⁰⁰ | NM | 0.98700 | 0.69689 | 0.84384 | 1.46619 | 0.57553 |
| 18 | 8.7760 ⁻⁰³ | 6.2670 ⁺⁰⁰ | NM | 0.98810 | 0.71773 | 0.85771 | 1.42810 | 0.60059 |
| 19 | 1.0020 ⁻⁰² | 6.8003 ⁺⁰⁰ | NM | 0.99020 | 0.75025 | 0.87847 | 1.37103 | 0.64074 |
| 20 | 1.0884 ⁻⁰² | 7.1896 ⁺⁰⁰ | NM | 0.99080 | 0.77311 | 0.89195 | 1.33107 | 0.67010 |
| 21 | 1.2383 ⁻⁰² | 7.8520 ⁺⁰⁰ | NM | 0.99360 | 0.81051 | 0.91361 | 1.27059 | 0.71904 |
| 22 | 1.3526 ⁻⁰² | 8.4090 ⁺⁰⁰ | NM | 0.99640 | 0.84066 | 0.93030 | 1.22464 | 0.75965 |
| 23 | 1.4491 ⁻⁰² | 8.8806 ⁺⁰⁰ | NM | 0.99750 | 0.86535 | 0.94277 | 1.18694 | 0.79429 |
| 24 | 1.5939 ⁻⁰² | 9.5459 ⁺⁰⁰ | NM | 0.99800 | 0.89902 | 0.95841 | 1.13648 | 0.84331 |
| 25 | 1.7310 ⁻⁰² | 1.0113 ⁺⁰¹ | NM | 0.99920 | 0.92676 | 0.97095 | 1.09762 | 0.88459 |
| 26 | 1.9317 ⁻⁰² | 1.0749 ⁺⁰¹ | NM | 1.00110 | 0.95691 | 0.98417 | 1.05777 | 0.93041 |
| 27 | 2.1628 ⁻⁰² | 1.1275 ⁺⁰¹ | NM | 1.00250 | 0.98110 | 0.99422 | 1.02694 | 0.96815 |
| 28 | 2.3406 ⁻⁰² | 1.1459 ⁺⁰¹ | NM | 1.00180 | 0.98943 | 0.99700 | 1.01537 | 0.98192 |
| 29 | 2.5870 ⁻⁰² | 1.1615 ⁺⁰¹ | NM | 1.00160 | 0.99644 | 0.99950 | 1.00614 | 0.99340 |
| D 30 | 2.7394 ⁻⁰² | 1.1694 ⁺⁰¹ | NM | 1.00000 | 1.00000 | 1.00000 | 1.00000 | 1.00000 |
| 31 | 2.9731 ⁻⁰² | 1.1693 ⁺⁰¹ | NM | 0.99940 | 0.99993 | 0.99968 | 0.99949 | 1.00019 |
| 32 | 3.2271 ⁻⁰² | 1.1490 ⁺⁰¹ | NM | 0.99950 | 0.99085 | 0.99639 | 1.01120 | 0.98535 |
| 33 | 3.5319 ⁻⁰² | 1.1505 ⁺⁰¹ | NM | 0.99950 | 0.99153 | 0.99664 | 1.01033 | 0.98645 |
| 34 | 3.8799 ⁻⁰² | 1.1564 ⁺⁰¹ | NM | 0.99850 | 0.99417 | 0.99712 | 1.00593 | 0.99124 |
| 35 | 4.2939 ⁻⁰² | 1.1536 ⁺⁰¹ | NM | 0.99720 | 0.99292 | 0.99600 | 1.00622 | 0.98985 |
| 36 | 4.5555 ⁻⁰² | 1.1452 ⁺⁰¹ | NM | 0.99640 | 0.98913 | 0.99420 | 1.01029 | 0.98408 |
| 37 | 4.8628 ⁻⁰² | 1.1420 ⁺⁰¹ | NM | 0.99510 | 0.98770 | 0.99302 | 1.01080 | 0.98241 |
| 38 | 5.0381 ⁻⁰² | 1.1408 ⁺⁰¹ | NM | 0.99510 | 0.98716 | 0.99282 | 1.01150 | 0.98154 |
| 39 | 5.3353 ⁻⁰² | 1.1490 ⁺⁰¹ | NM | 0.99410 | 0.99085 | 0.99369 | 1.00574 | 0.98802 |
| 40 | 5.5817 ⁻⁰² | 1.1581 ⁺⁰¹ | NM | 0.99430 | 0.99492 | 0.99529 | 1.00075 | 0.99455 |
| 41 | 5.7341 ⁻⁰² | 1.1605 ⁺⁰¹ | NM | 0.99370 | 0.99600 | 0.99539 | 0.99876 | 0.99662 |
| 42 | 5.8661 ⁻⁰² | 1.1588 ⁺⁰¹ | NM | 0.99310 | 0.99522 | 0.99480 | 0.99915 | 0.99565 |

INPUT VARIABLES Y,M,TO/TOD (MODIFIED CROCCO) ASSUME P=PD
 MEASURED: PO-PROFILE
 AT I= 8 VALUES OF INPUT PROFILES WERE AVERAGED BECAUSE OF SAME Y

| 7901S0404 | | VOISINET | PROFILE TABULATION | 80 POINTS, DELTA AT POINT 59 | | | | |
|-----------|-----------------------|-----------------------|--------------------|------------------------------|---------|---------|---------|-----------|
| I | Y | PTZ/P | P/PD | TO/TOD | M/MD | U/UD | T/TD | R/RD*U/UD |
| 1 | 0.0000 ⁺⁰⁰ | 1.0000 ⁺⁰⁰ | NM | 0.92910 | 0.00000 | 0.00000 | 2.47390 | 0.00000 |
| 2 | 6.4000 ⁻⁰⁵ | 1.3468 ⁺⁰⁰ | NM | 0.93730 | 0.23109 | 0.34987 | 2.29221 | 0.15263 |
| 3 | 1.1400 ⁻⁰⁴ | 1.3535 ⁺⁰⁰ | NM | 0.93520 | 0.23310 | 0.35227 | 2.28381 | 0.15425 |
| 4 | 2.1600 ⁻⁰⁴ | 1.3857 ⁺⁰⁰ | NM | 0.93640 | 0.24240 | 0.36532 | 2.27144 | 0.16083 |
| 5 | 2.9200 ⁻⁰⁴ | 1.4249 ⁺⁰⁰ | NM | 0.93880 | 0.25304 | 0.38034 | 2.25921 | 0.16835 |
| 6 | 3.4300 ⁻⁰⁴ | 1.4571 ⁺⁰⁰ | NM | 0.94000 | 0.26133 | 0.39180 | 2.24769 | 0.17431 |
| 7 | 4.1900 ⁻⁰⁴ | 1.4835 ⁺⁰⁰ | NM | 0.93930 | 0.26785 | 0.40039 | 2.23451 | 0.17919 |
| 8 | 4.7000 ⁻⁰⁴ | 1.5224 ⁺⁰⁰ | NM | 0.94000 | 0.27701 | 0.41271 | 2.21972 | 0.18593 |
| 9 | 5.4600 ⁻⁰⁴ | 1.5589 ⁺⁰⁰ | NM | 0.94035 | 0.28521 | 0.42357 | 2.20555 | 0.19205 |
| 10 | 8.0000 ⁻⁰⁴ | 1.6926 ⁺⁰⁰ | NM | 0.94220 | 0.31239 | 0.45896 | 2.15855 | 0.21262 |
| 11 | 1.0290 ⁻⁰³ | 1.8125 ⁺⁰⁰ | NM | 0.94450 | 0.33375 | 0.48617 | 2.12192 | 0.22912 |
| 12 | 1.2570 ⁻⁰³ | 1.9184 ⁺⁰⁰ | NM | 0.94540 | 0.35078 | 0.50709 | 2.08976 | 0.24265 |
| 13 | 1.5370 ⁻⁰³ | 2.0496 ⁺⁰⁰ | NM | 0.94650 | 0.37006 | 0.53021 | 2.05281 | 0.25829 |
| 14 | 1.7910 ⁻⁰³ | 2.1643 ⁺⁰⁰ | NM | 0.94780 | 0.38570 | 0.54863 | 2.02324 | 0.27116 |
| 15 | 2.1210 ⁻⁰³ | 2.2865 ⁺⁰⁰ | NM | 0.94920 | 0.40142 | 0.56674 | 1.99337 | 0.28432 |
| 16 | 2.3750 ⁻⁰³ | 2.4162 ⁺⁰⁰ | NM | 0.95000 | 0.41723 | 0.58438 | 1.96174 | 0.29789 |
| 17 | 2.6290 ⁻⁰³ | 2.4895 ⁺⁰⁰ | NM | 0.95020 | 0.42583 | 0.59372 | 1.94398 | 0.30542 |
| 18 | 2.8830 ⁻⁰³ | 2.5934 ⁺⁰⁰ | NM | 0.95290 | 0.43766 | 0.60713 | 1.92439 | 0.31549 |
| 19 | 3.0610 ⁻⁰³ | 2.6654 ⁺⁰⁰ | NM | 0.95360 | 0.44564 | 0.61569 | 1.90885 | 0.32255 |
| 20 | 3.2890 ⁻⁰³ | 2.7165 ⁺⁰⁰ | NM | 0.95360 | 0.45118 | 0.62143 | 1.89705 | 0.32758 |
| 21 | 3.5430 ⁻⁰³ | 2.8070 ⁺⁰⁰ | NM | 0.95450 | 0.46083 | 0.63157 | 1.87832 | 0.33624 |
| 22 | 3.7210 ⁻⁰³ | 2.8691 ⁺⁰⁰ | NM | 0.95450 | 0.46731 | 0.63810 | 1.86453 | 0.34223 |
| 23 | 3.9750 ⁻⁰³ | 2.9554 ⁺⁰⁰ | NM | 0.95470 | 0.47616 | 0.64696 | 1.84613 | 0.35044 |
| 24 | 4.2290 ⁻⁰³ | 3.0335 ⁺⁰⁰ | NM | 0.95490 | 0.48399 | 0.65471 | 1.82989 | 0.35779 |
| 25 | 4.5090 ⁻⁰³ | 3.0918 ⁺⁰⁰ | NM | 0.95480 | 0.48975 | 0.66026 | 1.81750 | 0.36328 |
| 26 | 4.7120 ⁻⁰³ | 3.1641 ⁺⁰⁰ | NM | 0.95540 | 0.49679 | 0.66721 | 1.80375 | 0.36990 |
| 27 | 4.9660 ⁻⁰³ | 3.2241 ⁺⁰⁰ | NM | 0.95600 | 0.50255 | 0.67288 | 1.79272 | 0.37534 |
| 28 | 5.4990 ⁻⁰³ | 3.3876 ⁺⁰⁰ | NM | 0.95900 | 0.51788 | 0.68821 | 1.76600 | 0.38970 |
| 29 | 5.8040 ⁻⁰³ | 3.4783 ⁺⁰⁰ | NM | 0.96210 | 0.52617 | 0.69690 | 1.75425 | 0.39726 |
| 30 | 6.0580 ⁻⁰³ | 3.5504 ⁺⁰⁰ | NM | 0.96440 | 0.53265 | 0.70359 | 1.74480 | 0.40325 |
| 31 | 6.3120 ⁻⁰³ | 3.6163 ⁺⁰⁰ | NM | 0.96600 | 0.53851 | 0.70941 | 1.73539 | 0.40879 |
| 32 | 6.6420 ⁻⁰³ | 3.7077 ⁺⁰⁰ | NM | 0.96790 | 0.54693 | 0.71718 | 1.72201 | 0.41648 |
| 33 | 6.9220 ⁻⁰³ | 3.7775 ⁺⁰⁰ | NM | 0.96960 | 0.55256 | 0.72308 | 1.71242 | 0.42226 |
| 34 | 7.2520 ⁻⁰³ | 3.8624 ⁺⁰⁰ | NM | 0.97200 | 0.55981 | 0.73023 | 1.70153 | 0.42916 |
| 35 | 7.6070 ⁻⁰³ | 3.9989 ⁺⁰⁰ | NM | 0.97590 | 0.57126 | 0.74143 | 1.68452 | 0.44014 |
| 36 | 7.9880 ⁻⁰³ | 4.0992 ⁺⁰⁰ | NM | 0.97900 | 0.57951 | 0.74951 | 1.67274 | 0.44807 |
| 37 | 8.4460 ⁻⁰³ | 4.2113 ⁺⁰⁰ | NM | 0.98160 | 0.58860 | 0.75799 | 1.65840 | 0.45706 |
| 38 | 8.6740 ⁻⁰³ | 4.2890 ⁺⁰⁰ | NM | 0.98210 | 0.59480 | 0.76323 | 1.64649 | 0.46355 |
| 39 | 9.0550 ⁻⁰³ | 4.3985 ⁺⁰⁰ | NM | 0.98170 | 0.60344 | 0.76999 | 1.62818 | 0.47292 |
| 40 | 9.3090 ⁻⁰³ | 4.4894 ⁺⁰⁰ | NM | 0.98050 | 0.61052 | 0.77510 | 1.61185 | 0.48088 |
| 41 | 9.5380 ⁻⁰³ | 4.5633 ⁺⁰⁰ | NM | 0.98100 | 0.61620 | 0.77974 | 1.60120 | 0.48697 |
| 42 | 9.8170 ⁻⁰³ | 4.6274 ⁺⁰⁰ | NM | 0.98260 | 0.62109 | 0.78415 | 1.59398 | 0.49194 |
| 43 | 1.0528 ⁻⁰² | 4.8849 ⁺⁰⁰ | NM | 0.98130 | 0.64034 | 0.79816 | 1.55366 | 0.51373 |
| 44 | 1.1443 ⁻⁰² | 5.1978 ⁺⁰⁰ | NM | 0.98260 | 0.66296 | 0.81510 | 1.51167 | 0.53921 |
| 45 | 1.2306 ⁻⁰² | 5.4664 ⁺⁰⁰ | NM | 0.98480 | 0.68175 | 0.82915 | 1.47914 | 0.56056 |
| 46 | 1.3322 ⁻⁰² | 5.8598 ⁺⁰⁰ | NM | 0.98630 | 0.70836 | 0.84758 | 1.43174 | 0.59200 |
| 47 | 1.4338 ⁻⁰² | 6.2735 ⁺⁰⁰ | NM | 0.98840 | 0.73527 | 0.86561 | 1.38597 | 0.62455 |
| 48 | 1.5354 ⁻⁰² | 6.6305 ⁺⁰⁰ | NM | 0.99070 | 0.75771 | 0.88025 | 1.34961 | 0.65223 |
| 49 | 1.6345 ⁻⁰² | 7.0765 ⁺⁰⁰ | NM | 0.99220 | 0.78483 | 0.89663 | 1.30520 | 0.68697 |
| 50 | 1.7234 ⁻⁰² | 7.5007 ⁺⁰⁰ | NM | 0.99280 | 0.80977 | 0.91065 | 1.26468 | 0.72006 |
| 51 | 1.8148 ⁻⁰² | 7.9173 ⁺⁰⁰ | NM | 0.99500 | 0.83352 | 0.92416 | 1.22931 | 0.75177 |
| 52 | 1.9418 ⁻⁰² | 8.5750 ⁺⁰⁰ | NM | 0.99620 | 0.86970 | 0.94271 | 1.17494 | 0.80234 |
| 53 | 2.0790 ⁻⁰² | 9.2107 ⁺⁰⁰ | NM | 0.99780 | 0.90327 | 0.95909 | 1.12741 | 0.85070 |
| 54 | 2.1704 ⁻⁰² | 9.6554 ⁺⁰⁰ | NM | 0.99870 | 0.92602 | 0.96956 | 1.09623 | 0.88444 |
| 55 | 2.2492 ⁻⁰² | 9.9801 ⁺⁰⁰ | NM | 0.99970 | 0.94229 | 0.97696 | 1.07494 | 0.90885 |
| 56 | 2.3863 ⁻⁰² | 1.0528 ⁺⁰¹ | NM | 1.00060 | 0.96913 | 0.98836 | 1.04008 | 0.95028 |
| 57 | 2.4829 ⁻⁰² | 1.0819 ⁺⁰¹ | NM | 1.00020 | 0.98304 | 0.99363 | 1.02166 | 0.97257 |
| 58 | 2.5743 ⁻⁰² | 1.1030 ⁺⁰¹ | NM | 1.00020 | 0.99306 | 0.99748 | 1.00891 | 0.98867 |
| 59 | 2.6556 ⁻⁰² | 1.1178 ⁺⁰¹ | NM | 1.00000 | 1.00000 | 1.00000 | 1.00000 | 1.00000 |
| 60 | 2.7648 ⁻⁰² | 1.1259 ⁺⁰¹ | NM | 1.00020 | 1.00378 | 1.00151 | 0.99549 | 1.00605 |
| 61 | 2.8740 ⁻⁰² | 1.1292 ⁺⁰¹ | NM | 1.00090 | 1.00531 | 1.00243 | 0.99429 | 1.00819 |
| 62 | 2.9807 ⁻⁰² | 1.1302 ⁺⁰¹ | NM | 0.99910 | 1.00579 | 1.00171 | 0.99190 | 1.00989 |
| 63 | 3.1179 ⁻⁰² | 1.1299 ⁺⁰¹ | NM | 1.00090 | 1.00565 | 1.00256 | 0.99386 | 1.00875 |
| 64 | 3.4938 ⁻⁰² | 1.1255 ⁺⁰¹ | NM | 1.00440 | 1.00361 | 1.00355 | 0.99989 | 1.00366 |
| 65 | 3.7503 ⁻⁰² | 1.1263 ⁺⁰¹ | NM | 1.00560 | 1.00395 | 1.00428 | 1.00065 | 1.00363 |
| 66 | 4.0729 ⁻⁰² | 1.1266 ⁺⁰¹ | NM | 1.00560 | 1.00413 | 1.00434 | 1.00043 | 1.00391 |
| 67 | 4.3752 ⁻⁰² | 1.1298 ⁺⁰¹ | NM | 1.00510 | 1.00558 | 1.00464 | 0.99812 | 1.00653 |
| 68 | 4.5250 ⁻⁰² | 1.1318 ⁺⁰¹ | NM | 1.00580 | 1.00652 | 1.00534 | 0.99765 | 1.00771 |
| 69 | 4.7079 ⁻⁰² | 1.1330 ⁺⁰¹ | NM | 1.00580 | 1.00708 | 1.00554 | 0.99696 | 1.00861 |
| 70 | 4.9975 ⁻⁰² | 1.1337 ⁺⁰¹ | NM | 1.00520 | 1.00739 | 1.00536 | 0.99598 | 1.00942 |
| 71 | 5.2794 ⁻⁰² | 1.1315 ⁺⁰¹ | NM | 1.00330 | 1.00638 | 1.00403 | 0.99534 | 1.00873 |
| 72 | 5.5258 ⁻⁰² | 1.1317 ⁺⁰¹ | NM | 1.00220 | 1.00649 | 1.00352 | 0.99412 | 1.00946 |
| 73 | 5.8890 ⁻⁰² | 1.1273 ⁺⁰¹ | NM | 1.00140 | 1.00444 | 1.00236 | 0.99587 | 1.00652 |
| 74 | 6.3157 ⁻⁰² | 1.1233 ⁺⁰¹ | NM | 1.00070 | 1.00257 | 1.00131 | 0.99750 | 1.00382 |
| 75 | 6.6485 ⁻⁰² | 1.1246 ⁺⁰¹ | NM | 0.99960 | 1.00316 | 1.00098 | 0.99567 | 1.00534 |
| 76 | 7.0803 ⁻⁰² | 1.1216 ⁺⁰¹ | NM | 0.99890 | 1.00177 | 1.00011 | 0.99670 | 1.00343 |
| 77 | 7.5070 ⁻⁰² | 1.1220 ⁺⁰¹ | NM | 0.99890 | 1.00194 | 1.00018 | 0.99648 | 1.00371 |
| 78 | 7.9108 ⁻⁰² | 1.1229 ⁺⁰¹ | NM | 0.99840 | 1.00239 | 1.00010 | 0.99542 | 1.00470 |
| 79 | 8.3782 ⁻⁰² | 1.1177 ⁺⁰¹ | NM | 0.99820 | 0.99997 | 0.99909 | 0.99824 | 1.00084 |
| 80 | 8.6170 ⁻⁰² | 1.1092 ⁺⁰¹ | NM | 0.99740 | 0.99598 | 0.99718 | 1.00243 | 0.99477 |

INPUT VARIABLES Y,M,TO/TOD (MODIFIED CROCCO) ASSUME P=PD
 MEASURED: PO=PROFILE
 AT I= 9 VALUES OF INPUT PROFILES WERE AVERAGED BECAUSE OF SAME Y

| | | |
|--|---|------------------|
|  | M: 2.5 (upstream) R THETA $\times 10^{-3}$: 24 (upstream) TW/TR: 1 | 7902 |
| | | RELAXATION AW |
| Blowdown tunnel with axisymmetric fixed nozzle. Running time: 60s. W = 0.114 m, H = 0.082 m. PO: 0.5 MN/m ² . TO: 295K. Air.RE/m $\times 10^{-6}$: 50. | | |
| CHEW Y.T., SQUIRE L.C., 1979. The boundary layer development downstream of a shock interaction at an expansion corner. ARC R&M 3839. And: Squire L.C., private communications. Also: Chew Y.T., 1979 | | |

- 1 The test boundary layer was formed on the lower nozzle block of the tunnel 0.114 m wide, facing a fixed contoured upper block. The general arrangement is as for Jeromin, CAT 6602 and Thomas, CAT 7401. The block was straight from a point upstream of the throat to a point ($X = 0$) at which the surface turned down to give a 6° expansion corner. The inclined surface was about (E) 0.15 m long. The block could be traversed so as to move the expansion corner in relation to the throat, which was typically about 0.54 m upstream. A plane shock generator could be mounted in the free stream, and was used to give flow deflections of 4° , 6° and 8° . The relative position of the lower plate was adjusted so that, for the runs with 6° shock deflection, the shock wave impinged on the boundary layer at $X = -20$, 0, or $+20$ mm. For the other shock deflections, the shock met the boundary layer at the corner ($X = 0$).
- 3 The profile data for the flow upstream of the corner (series 01) indicate that the flow is effectively
- 5 a fully developed equilibrium turbulent layer. Three-dimensional effects were assessed by a momentum balance, the greatest discrepancy in a value for D2 being 6% just downstream of the corner. Differences between wall pressure measured on the centreline and at $Z = \pm 19$ mm ranged up to about 16% just downstream of the nominal shock position, as a result of curvature produced in the incident shock by the tunnel side walls, which cause the shock to curve forward off the centreline (Chew, 1979).
- 6 Wall pressure was measured at 186 tappings ($d = 0.3$ mm) drilled normal to the surface in three rows at $Z = -19$, 0, $+19$ mm, (E) except for tappings actually at the corner which were drilled along the bisector of the angle. Wall temperature was measured by 4 thermocouples distributed along the test surface. A Preston tube ($d_1 = 0.419$, $d_2 = 0.21$ mm) was used with the calibration of Allen (1973). Values obtained using the Hopkins and Keener (1966) calibration were about 3% lower, while a change to Allen's revised (1977b) calibration gives changes of at most 2%.

- Static pressure profiles were measured with a CCP ($\alpha = 2.5^\circ$, $d_1 = 1$ mm. Two static holes, $d = 0.4$ mm in the top and bottom 14 mm downstream from the base of the conical tip). For profiles upstream and more than 50 mm downstream of the shock, the maximum variation was 1%. Variations up to 4% were found
- 9 near the shock but in many cases where this maximum was found the tip of the probe intersected the shock so it is not clear whether the variation is genuine. The authors assumed the static pressure for a profile to be constant at the local wall value. No profile extends out so far as to intersect the reflected wave. Initial total temperature measurements using a ECP were not pursued. The temperature profile was deduced from the Crocco/van Driest temperature-velocity correlation, using instantaneous values of stagnation and wall temperature for each Pitot reading. The recovery factor used was 0.89. For the calculation of integral values and for a determination of the local shear stress from a momentum balance, the profile data were interpolated to a fixed Y-grid. Two complete sets of data were obtained at each station since it was only possible to measure 25 profile points

- in a single run, with the data logger used. These were reduced separately, the differences between sets, as shown by the authors' D2 values being at most 2% for the runs without shocks. Differences at the 2%-3% level are common in the flows with shocks, with an untypical peak (E) of about 10%. No profile corrections were applied.
- 12 The editors have presented one of the two complete sets of data incorporating the authors' assumptions and data reduction procedures. This was originally received as a private communication and is the
 13 alternative to that published in the source paper. The seven series consist of: surveys upstream (01) and downstream (02) of the corner, with no shock; series (03, 04, 05) with shocks giving deflections of 4°, 6° and 8° respectively; and series (06, 07) with a 6° shock displaced to hit the test surface
 14 at $X = -20$ mm, $+20$ mm respectively. The CF values are those given by the authors using the Allen (1973) calibration.

§ DATA: 7902 0101-0107. Pitot profiles and CF from Preston tubes. $NX = 7$.

- 15 Editors' comments. This entry describes one of a series of experiments made in the same facility with predominantly the same instrumentation. In addition to Jeromin (CAT 6602) and Thomas (CAT 7401), much work has been done on compressible boundary layers with mass addition (for a brief survey see Squire et al., 1977). The present study investigates the influence of an abrupt disturbance on a boundary layer and its recovery downstream. In the constant pressure cases (series 01 and 02) the velocity profiles show the typical scatter ($\pm 5\%$) above and below the logarithmic law (Fig. 1) with wake strength values of $3.30 < \Delta(\bar{u}^*/u_\tau) < 4.20$ which are on the high side compared with other experiments in the same Reynolds number range (cf. Fig. 3.3.6 of AG 253). The expansion causes the Mach number for the second set to rise from 2.57 to 2.84 at the corner which should, if anything, decrease the wake strength (cf. Fig. 5.2.3) but this is not observed (0202). The outer law plot for series 01 shows some similarity with the adverse pressure-gradient profiles of Thomas (cf. Fig. 5.2.4 of AG 253) while the profiles of series 02 behave as if they were in a zero pressure gradient (Fig. 2).

From among the boundary layers (series 03 to 07) recovering from a strong disturbance, series 05 is the most illuminating one. Fig. 3 shows the log-law plot in which there is an astonishing long log-law region with a wake component characteristic of severe adverse pressure gradients. The profiles relax in downstream direction recovering to a wake with about the same wake strength as the profiles in series 01 and 02. This "unfinished" recovery to the zero pressure-gradient case can be readily observed in Fig. 4a. A proper ZPG "equilibrium" profile should fall on the full line which represents eqn. (3.3.17) of AG 253. Fig. 5 shows velocity profiles downstream of the expansion corner when a 6° shock strikes the surface 20 mm upstream of the corner (series 06). These profiles are distinguished by being self-similar. They have nearly constant Mach number, and skin friction, Reynolds number and shape parameter. This is certainly a unique case the relevance of which the authors overlooked in their discussion of the results, and which was, it seems, unplanned. The profiles in the outer law plot (Fig. 4b) are very similar to those of Thomas (CAT 7401) in a moderate adverse pressure gradient (Fig. 5.2.4, AG 253).

The velocity profiles do not extend into the viscous sublayer ($Y^+_{min} \approx 30$) and they are relatively short (18 data points). Since pressure gradients were weak in the flow regions investigated measurements of skin friction by means of a FEB would have been possible and would have given an even firmer basis for the general validity of the log-law as claimed by the authors. By the same token Preston tube values here should be reasonably reliable.

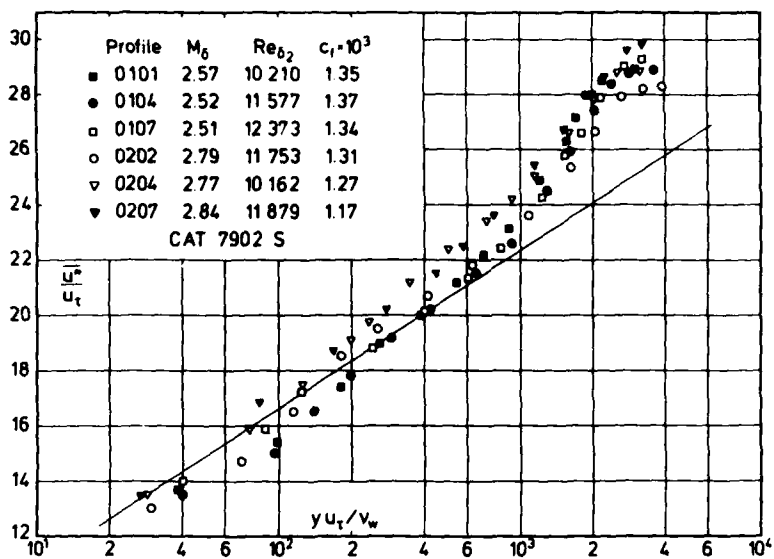


Fig. 1 Law of the wall for a compressible boundary layer (adiabatic wall, origin not defined). Chew & Squire (1979).

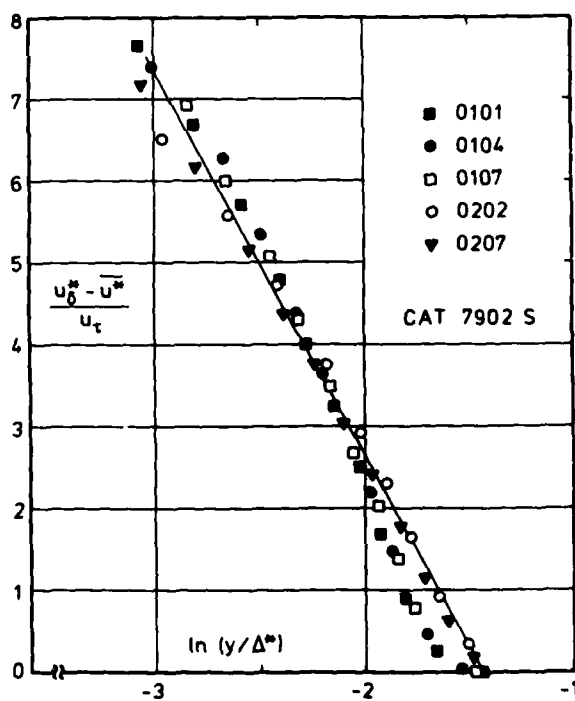


Fig. 2 Outer law for a compressible boundary layer (adiabatic wall, origin not defined). Chew & Squire (1979).

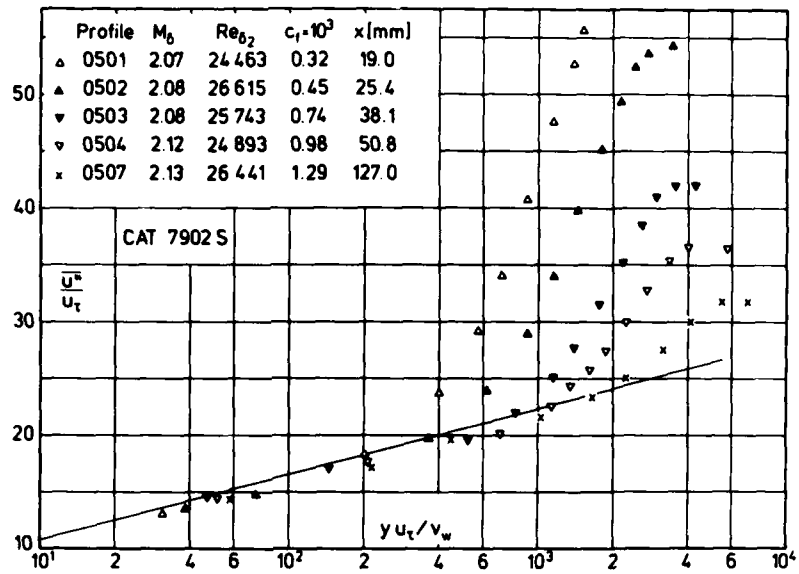


Fig. 3 Law of the wall for a compressible boundary layer (adiabatic wall, origin not defined, strong shock interaction). Chew & Squire (1979).

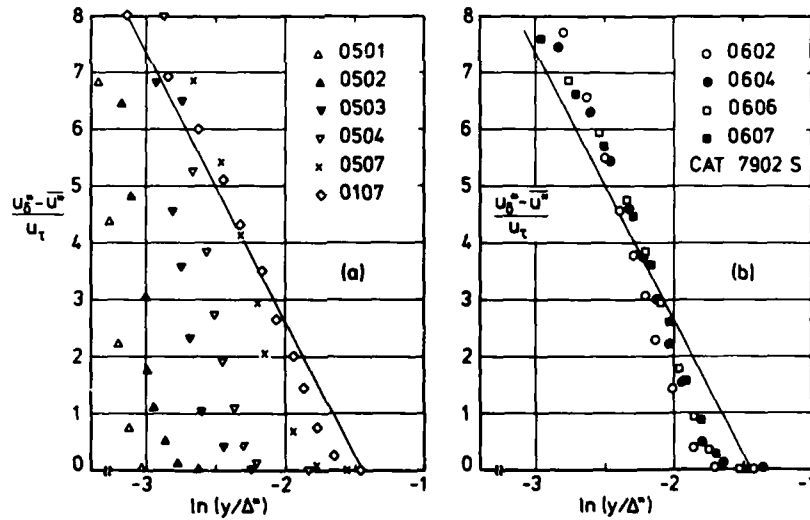


Fig. 4 Outer law for a compressible boundary layer (adiabatic wall, origin not defined; (a) strong shock interaction). Chew & Squire (1979).

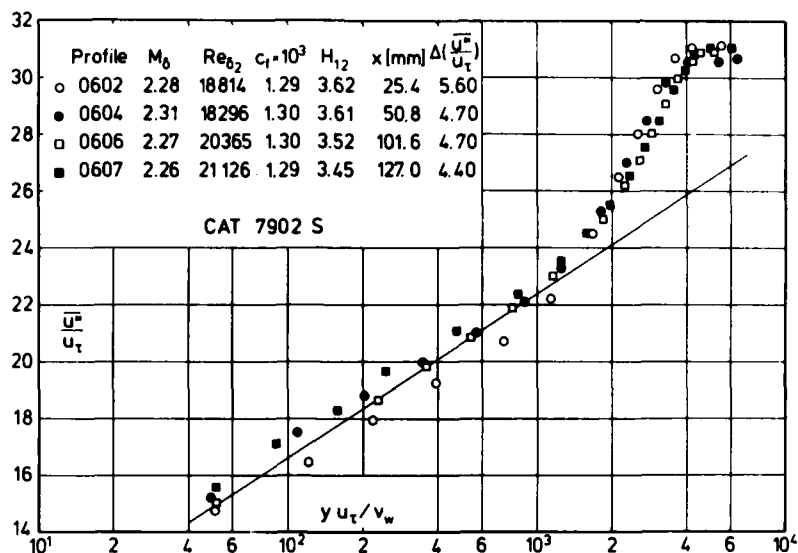


Fig. 5 Law of the wall for a compressible boundary layer (adiabatic wall, origin not defined). Chew & Squire (1979).

| CAT 7902S | | CHEW / SQUIRE | | BOUNDARY CONDITIONS AND EVALUATED DA | | | | SI UNITS | |
|------------------------|-----------------------|-----------------------|-----------------------|--------------------------------------|--------|-----------------------|-----------------------|-----------------------|--|
| RUN | MD * | TW/TR | RED2W | CF * | H12 | H12K | PW* | PD* | |
| X * | POD | PW/PD* | RED2D | CO * | H32 | H32K | TU* | TD | |
| RZ | TOD* | TAUW | DZ | PI2* | H42 | D2K | UD | TR | |
| 7902S0101 | 2.5610 | 1.0482 | 1.0051 ⁺⁰⁴ | 1.3600 ⁻⁰³ | 4.1830 | 1.3709 | 2.8062 ⁺⁰⁴ | 2.8062 ⁺⁰⁴ | |
| -1.0160 ⁻⁰¹ | 5.2711 ⁺⁰⁵ | 1.0000 | 2.0282 ⁺⁰⁴ | 0.0000 ⁺⁰⁰ | 1.7973 | 1.7799 | 2.8976 ⁺⁰² | 1.2708 ⁺⁰² | |
| INFINITE | 2.9378 ⁺⁰² | 1.7521 ⁺⁰² | 4.0705 ⁻⁰⁴ | 0.0000 ⁺⁰⁰ | 0.0607 | 5.8366 ⁻⁰⁴ | 5.7884 ⁺⁰² | 2.7644 ⁺⁰² | |
| 7902S0102 | 2.5340 | 1.0381 | 1.0339 ⁺⁰⁴ | 1.3400 ⁻⁰³ | 4.0576 | 1.3504 | 2.8544 ⁺⁰⁴ | 2.8544 ⁺⁰⁴ | |
| -7.6200 ⁻⁰² | 5.1417 ⁺⁰⁵ | 1.0000 | 2.0464 ⁺⁰⁴ | 0.0000 ⁺⁰⁰ | 1.8055 | 1.7888 | 2.8967 ⁺⁰² | 1.2975 ⁺⁰² | |
| INFINITE | 2.9637 ⁺⁰² | 1.7192 ⁺⁰² | 4.2030 ⁻⁰⁴ | 0.0000 ⁺⁰⁰ | 0.0697 | 5.9079 ⁻⁰⁴ | 5.7872 ⁺⁰² | 2.7904 ⁺⁰² | |
| 7902S0103 | 2.5340 | 1.0430 | 1.0859 ⁺⁰⁴ | 1.3800 ⁻⁰³ | 4.0811 | 1.3547 | 2.8751 ⁺⁰⁴ | 2.8751 ⁺⁰⁴ | |
| -5.0800 ⁻⁰² | 5.1790 ⁺⁰⁵ | 1.0000 | 2.1583 ⁺⁰⁴ | 0.0000 ⁺⁰⁰ | 1.8028 | 1.7865 | 2.8992 ⁺⁰² | 1.2925 ⁺⁰² | |
| INFINITE | 2.9523 ⁺⁰² | 1.7834 ⁺⁰² | 4.3769 ⁻⁰⁴ | 0.0000 ⁺⁰⁰ | 0.0649 | 6.1844 ⁻⁰⁴ | 5.7760 ⁺⁰² | 2.7797 ⁺⁰² | |
| 7902S0104 | 2.5200 | 1.0431 | 1.1441 ⁺⁰⁴ | 1.3800 ⁻⁰³ | 4.0653 | 1.3602 | 2.9096 ⁺⁰⁴ | 2.9096 ⁺⁰⁴ | |
| -3.8100 ⁻⁰² | 5.1283 ⁺⁰⁵ | 1.0000 | 2.2625 ⁺⁰⁴ | 0.0000 ⁺⁰⁰ | 1.7986 | 1.7822 | 2.8937 ⁺⁰² | 1.2975 ⁺⁰² | |
| INFINITE | 2.9455 ⁺⁰² | 1.7849 ⁺⁰² | 4.5845 ⁻⁰⁴ | 0.0000 ⁺⁰⁰ | 0.0641 | 6.4927 ⁻⁰⁴ | 5.7553 ⁺⁰² | 2.7741 ⁺⁰² | |
| 7902S0105 | 2.5310 | 1.0420 | 1.1905 ⁺⁰⁴ | 1.3600 ⁻⁰³ | 4.0806 | 1.3579 | 2.9234 ⁺⁰⁴ | 2.9234 ⁺⁰⁴ | |
| -2.5400 ⁻⁰² | 5.2414 ⁺⁰⁵ | 1.0000 | 2.3613 ⁺⁰⁴ | 0.0000 ⁺⁰⁰ | 1.7997 | 1.7830 | 2.8989 ⁺⁰² | 1.2953 ⁺⁰² | |
| INFINITE | 2.9547 ⁺⁰² | 1.7828 ⁺⁰² | 4.7295 ⁻⁰⁴ | 0.0000 ⁺⁰⁰ | 0.0656 | 6.7025 ⁻⁰⁴ | 5.7754 ⁺⁰² | 2.7821 ⁺⁰² | |
| 7902S0106 | 2.4970 | 1.0546 | 1.1751 ⁺⁰⁴ | 1.3700 ⁻⁰³ | 4.0230 | 1.3467 | 2.9785 ⁺⁰⁴ | 2.9785 ⁺⁰⁴ | |
| -1.2700 ⁻⁰² | 5.0654 ⁺⁰⁵ | 1.0000 | 2.3250 ⁺⁰⁴ | 0.0000 ⁺⁰⁰ | 1.8037 | 1.7880 | 2.9062 ⁺⁰² | 1.3015 ⁺⁰² | |
| INFINITE | 2.9245 ⁺⁰² | 1.7810 ⁺⁰² | 4.6646 ⁻⁰⁴ | 0.0000 ⁺⁰⁰ | 0.0527 | 6.5538 ⁻⁰⁴ | 5.7116 ⁺⁰² | 2.7557 ⁺⁰² | |
| 7902S0107 | 2.5100 | 1.0427 | 1.2344 ⁺⁰⁴ | 1.3400 ⁻⁰³ | 4.0158 | 1.3439 | 2.9923 ⁺⁰⁴ | 2.9923 ⁺⁰⁴ | |
| -6.3500 ⁻⁰³ | 5.1928 ⁺⁰⁵ | 1.0000 | 2.4300 ⁺⁰⁴ | 0.0000 ⁺⁰⁰ | 1.8027 | 1.7873 | 2.8986 ⁺⁰² | 1.3058 ⁺⁰² | |
| INFINITE | 2.9511 ⁺⁰² | 1.7683 ⁺⁰² | 4.8502 ⁻⁰⁴ | 0.0000 ⁺⁰⁰ | 0.0643 | 6.6200 ⁻⁰⁴ | 5.7507 ⁺⁰² | 2.7800 ⁺⁰² | |

| CAT 79025 | | CHEM / SQUIRE | | BOUNDARY CONDITIONS AND EVALUATED DATA, SI UNITS | | | | | | |
|---|--|--|--|--|----------------------------|--|--|--|--|--|
| RUN X * RZ | MO * POD TOD* | TW/TR PW/PD* TAUW | REDZW REDZD DZ | CF * CQ * PIZ* | H12 H32 H42 | H12K H32K D2K | PW T4* UD | PD* TD TR | | |
| 790250201 1.9050 ^{m-02} INFINITE | 2.7630 5.3223 ^{m+05} 2.8976 ^{m+02} | 1.0650 1.0000 1.4750 ^{m+02} | 1.0939 ^{m+04} 2.4260 ^{m+04} 5.2667 ^{m-04} | 1.3300 ^{m-03} 0.0000 ^{m+00} 0.0000 ^{m+00} | 4.5013 1.8341 0.0543 | 1.2863 1.8190 7.5258 ^{m-04} | 2.0753 ^{m+04} 2.8921 ^{m+02} 5.9322 ^{m+02} | 2.0753 ^{m+04} 1.1467 ^{m+02} 2.7155 ^{m+02} | | |
| 790250202 2.5400 ^{m-02} INFINITE | 2.7940 5.4880 ^{m+05} 2.9192 ^{m+02} | 1.0531 1.0000 1.4609 ^{m+02} | 1.1753 ^{m+04} 2.6130 ^{m+04} 5.6433 ^{m-04} | 1.3100 ^{m-03} 0.0000 ^{m+00} 0.0000 ^{m+00} | 4.5526 1.8314 0.0664 | 1.2960 1.8136 8.1137 ^{m-04} | 2.0408 ^{m+04} 2.8753 ^{m+02} 5.9764 ^{m+02} | 2.0408 ^{m+04} 1.1382 ^{m+02} 2.7304 ^{m+02} | | |
| 790250203 3.8100 ^{m-02} INFINITE | 2.7860 5.3298 ^{m+05} 2.9226 ^{m+02} | 1.0531 1.0000 1.3953 ^{m+02} | 1.1379 ^{m+04} 2.5210 ^{m+04} 5.6024 ^{m-04} | 1.2800 ^{m-03} 0.0000 ^{m+00} 0.0000 ^{m+00} | 4.5392 1.8306 0.0660 | 1.2982 1.8130 8.0526 ^{m-04} | 2.0064 ^{m+04} 2.8832 ^{m+02} 5.9773 ^{m+02} | 2.0064 ^{m+04} 1.1451 ^{m+02} 2.7377 ^{m+02} | | |
| 790250204 5.0800 ^{m-02} INFINITE | 2.7710 5.1194 ^{m+05} 2.9321 ^{m+02} | 1.0480 1.0000 1.3460 ^{m+02} | 1.0153 ^{m+04} 2.2263 ^{m+04} 5.1335 ^{m-04} | 1.2700 ^{m-03} 0.0000 ^{m+00} 0.0000 ^{m+00} | 4.4946 1.8318 0.0704 | 1.3033 1.8135 7.3260 ^{m-04} | 1.9719 ^{m+04} 2.8794 ^{m+02} 5.9744 ^{m+02} | 1.9719 ^{m+04} 1.1564 ^{m+02} 2.7475 ^{m+02} | | |
| 790250205 7.6200 ^{m-02} INFINITE | 2.8680 5.5200 ^{m+05} 2.9223 ^{m+02} | 1.0526 1.0000 1.2989 ^{m+02} | 1.0881 ^{m+04} 2.4894 ^{m+04} 5.5831 ^{m-04} | 1.2300 ^{m-03} 0.0000 ^{m+00} 0.0000 ^{m+00} | 4.7035 1.8373 0.0697 | 1.2903 1.8187 8.0711 ^{m-04} | 1.8340 ^{m+04} 2.8770 ^{m+02} 6.0441 ^{m+02} | 1.8340 ^{m+04} 1.1048 ^{m+02} 2.7333 ^{m+02} | | |
| 790250206 1.0160 ^{m-01} INFINITE | 2.7270 4.8191 ^{m+05} 2.9311 ^{m+02} | 1.0471 1.0000 1.2404 ^{m+02} | 1.0931 ^{m+04} 2.3541 ^{m+04} 5.6284 ^{m-04} | 1.2000 ^{m-03} 0.0000 ^{m+00} 0.0000 ^{m+00} | 4.4199 1.8237 0.0692 | 1.3129 1.8053 8.0582 ^{m-04} | 1.9857 ^{m+04} 2.8783 ^{m+02} 5.9353 ^{m+02} | 1.9857 ^{m+04} 1.1784 ^{m+02} 2.7488 ^{m+02} | | |
| 790250207 1.2700 ^{m-01} INFINITE | 2.8430 5.4541 ^{m+05} 2.9383 ^{m+02} | 1.0470 1.0000 1.2460 ^{m+02} | 1.1879 ^{m+04} 2.6773 ^{m+04} 6.0426 ^{m-04} | 1.1700 ^{m-03} 0.0000 ^{m+00} 0.0000 ^{m+00} | 4.6584 1.8287 0.0736 | 1.3005 1.8099 8.8038 ^{m-04} | 1.8823 ^{m+04} 2.8786 ^{m+02} 6.0405 ^{m+02} | 1.8823 ^{m+04} 1.1230 ^{m+02} 2.7495 ^{m+02} | | |
| 790250301 1.9050 ^{m-02} INFINITE | 2.3510 5.0514 ^{m+05} 2.9300 ^{m+02} | 1.0287 1.0000 1.6019 ^{m+02} | 1.5092 ^{m+04} 2.7658 ^{m+04} 5.1740 ^{m-04} | 1.1100 ^{m-03} 0.0000 ^{m+00} 0.0000 ^{m+00} | 3.7254 1.7886 0.0705 | 1.3837 1.7704 7.0925 ^{m-04} | 3.7301 ^{m+04} 2.8495 ^{m+02} 5.5606 ^{m+02} | 3.7301 ^{m+04} 1.3916 ^{m+02} 2.7700 ^{m+02} | | |
| 790250302 2.5400 ^{m-02} INFINITE | 2.4250 5.7961 ^{m+05} 2.9287 ^{m+02} | 1.0307 1.0000 1.6009 ^{m+02} | 1.6745 ^{m+04} 3.1633 ^{m+04} 5.3534 ^{m-04} | 1.0200 ^{m-03} 0.0000 ^{m+00} 0.0000 ^{m+00} | 3.9270 1.7734 0.0707 | 1.4042 1.7550 7.6059 ^{m-04} | 3.8128 ^{m+04} 2.8489 ^{m+02} 5.6405 ^{m+02} | 3.8128 ^{m+04} 1.3458 ^{m+02} 2.7641 ^{m+02} | | |
| 790250303 3.8100 ^{m-02} INFINITE | 2.4060 5.3215 ^{m+05} 2.9291 ^{m+02} | 1.0302 1.0000 1.7242 ^{m+02} | 1.5603 ^{m+04} 2.9248 ^{m+04} 5.3397 ^{m-04} | 1.1800 ^{m-03} 0.0000 ^{m+00} 0.0000 ^{m+00} | 3.8166 1.7897 0.0713 | 1.3671 1.7730 7.4147 ^{m-04} | 3.6060 ^{m+04} 2.8493 ^{m+02} 5.6204 ^{m+02} | 3.6060 ^{m+04} 1.3575 ^{m+02} 2.7657 ^{m+02} | | |
| 790250304 5.0800 ^{m-02} INFINITE | 2.4560 5.3571 ^{m+05} 2.9218 ^{m+02} | 1.0327 1.0000 1.7155 ^{m+02} | 1.5300 ^{m+04} 2.9310 ^{m+04} 5.4356 ^{m-04} | 1.2100 ^{m-03} 0.0000 ^{m+00} 0.0000 ^{m+00} | 3.8607 1.8070 0.0719 | 1.3351 1.7922 7.4888 ^{m-04} | 3.3577 ^{m+04} 2.8457 ^{m+02} 5.6666 ^{m+02} | 3.3577 ^{m+04} 1.3243 ^{m+02} 2.7557 ^{m+02} | | |
| 790250305 7.6200 ^{m-02} INFINITE | 2.4570 5.0790 ^{m+05} 2.8986 ^{m+02} | 1.0413 1.0000 1.6924 ^{m+02} | 1.3973 ^{m+04} 2.6983 ^{m+04} 5.2215 ^{m-04} | 1.2600 ^{m-03} 0.0000 ^{m+00} 0.0000 ^{m+00} | 3.8092 1.8238 0.0647 | 1.2927 1.8124 7.0694 ^{m-04} | 3.1785 ^{m+04} 2.8468 ^{m+02} 5.4511 ^{m+02} | 3.1785 ^{m+04} 1.3132 ^{m+02} 2.7338 ^{m+02} | | |
| 790250306 1.0160 ^{m-01} INFINITE | 2.4910 5.2331 ^{m+05} 2.8817 ^{m+02} | 1.0480 1.0000 1.6208 ^{m+02} | 1.4204 ^{m+04} 2.7959 ^{m+04} 5.2945 ^{m-04} | 1.2000 ^{m-03} 0.0000 ^{m+00} 0.0000 ^{m+00} | 3.8844 1.8237 0.0598 | 1.2846 1.8123 7.2337 ^{m-04} | 3.1095 ^{m+04} 2.8461 ^{m+02} 5.6636 ^{m+02} | 3.1095 ^{m+04} 1.2859 ^{m+02} 2.7158 ^{m+02} | | |
| 790250307 1.2700 ^{m-01} INFINITE | 2.4920 5.3287 ^{m+05} 2.9119 ^{m+02} | 1.0355 1.0000 1.6472 ^{m+02} | 1.5917 ^{m+04} 3.1006 ^{m+04} 5.8620 ^{m-04} | 1.2000 ^{m-03} 0.0000 ^{m+00} 0.0000 ^{m+00} | 3.8454 1.8181 0.0713 | 1.2715 1.8081 8.0550 ^{m-04} | 3.1578 ^{m+04} 2.8416 ^{m+02} 5.6941 ^{m+02} | 3.1578 ^{m+04} 1.2988 ^{m+02} 2.7441 ^{m+02} | | |
| 790250401 1.9050 ^{m-02} INFINITE | 2.2030 5.3034 ^{m+05} 2.8731 ^{m+02} | 1.0458 1.0000 1.3920 ^{m+02} | 2.0326 ^{m+04} 3.5723 ^{m+04} 5.7531 ^{m-04} | 8.3000 ^{m-04} 0.0000 ^{m+00} 0.0000 ^{m+00} | 3.8143 1.7137 0.0443 | 1.5640 1.6927 8.2333 ^{m-04} | 4.9366 ^{m+04} 2.8508 ^{m+02} 5.3333 ^{m+02} | 4.9366 ^{m+04} 1.4580 ^{m+02} 2.7259 ^{m+02} | | |
| 790250402 2.5400 ^{m-02} INFINITE | 2.2660 5.8040 ^{m+05} 2.9042 ^{m+02} | 1.0337 1.0000 1.5308 ^{m+02} | 2.3047 ^{m+04} 4.1069 ^{m+04} 6.3281 ^{m-04} | 8.7000 ^{m-04} 0.0000 ^{m+00} 0.0000 ^{m+00} | 3.8523 1.7213 0.0588 | 1.5313 1.7002 9.1064 ^{m-04} | 4.8953 ^{m+04} 2.8439 ^{m+02} 5.4383 ^{m+02} | 4.8953 ^{m+04} 1.4328 ^{m+02} 2.7512 ^{m+02} | | |
| 790250403 3.8100 ^{m-02} INFINITE | 2.2590 5.3284 ^{m+05} 2.8867 ^{m+02} | 1.0425 1.0000 1.7691 ^{m+02} | 2.0715 ^{m+04} 3.7086 ^{m+04} 6.1505 ^{m-04} | 1.0900 ^{m-03} 0.0000 ^{m+00} 0.0000 ^{m+00} | 3.7434 1.7451 0.0514 | 1.4641 1.7269 8.6801 ^{m-04} | 4.5436 ^{m+04} 2.8513 ^{m+02} 5.4136 ^{m+02} | 4.5436 ^{m+04} 1.4286 ^{m+02} 2.7351 ^{m+02} | | |
| 790250404 5.0800 ^{m-02} INFINITE | 2.2700 5.1166 ^{m+05} 2.9452 ^{m+02} | 1.0311 1.0000 1.8563 ^{m+02} | 1.8207 ^{m+04} 3.2376 ^{m+04} 5.7827 ^{m-04} | 1.2000 ^{m-03} 0.0000 ^{m+00} 0.0000 ^{m+00} | 3.6235 1.7664 0.0637 | 1.3979 1.7521 7.9938 ^{m-04} | 4.2885 ^{m+04} 2.8766 ^{m+02} 5.4813 ^{m+02} | 4.2885 ^{m+04} 1.4504 ^{m+02} 2.7897 ^{m+02} | | |
| 790250405 7.6200 ^{m-02} INFINITE | 2.3210 5.0961 ^{m+05} 2.9365 ^{m+02} | 1.0339 1.0000 1.8292 ^{m+02} | 1.7108 ^{m+04} 3.1103 ^{m+04} 5.6983 ^{m-04} | 1.2300 ^{m-03} 0.0000 ^{m+00} 0.0000 ^{m+00} | 3.6544 1.7864 0.0643 | 1.3599 1.7720 7.8071 ^{m-04} | 3.9438 ^{m+04} 2.8723 ^{m+02} 5.5327 ^{m+02} | 3.9438 ^{m+04} 1.4135 ^{m+02} 2.7781 ^{m+02} | | |
| 790250406 1.0160 ^{m-01} INFINITE | 2.3080 5.0372 ^{m+05} 2.9233 ^{m+02} | 1.0357 1.0000 1.8988 ^{m+02} | 1.8066 ^{m+04} 3.2741 ^{m+04} 5.9910 ^{m-04} | 1.2800 ^{m-03} 0.0000 ^{m+00} 0.0000 ^{m+00} | 3.6092 1.7926 0.0624 | 1.3460 1.7795 8.1378 ^{m-04} | 3.9783 ^{m+04} 2.8652 ^{m+02} 5.5054 ^{m+02} | 3.9783 ^{m+04} 1.4154 ^{m+02} 2.7665 ^{m+02} | | |
| 790250407 1.2700 ^{m-01} INFINITE | 2.2930 5.0483 ^{m+05} 2.9403 ^{m+02} | 1.0318 1.0000 1.9529 ^{m+02} | 1.9313 ^{m+04} 3.4672 ^{m+04} 6.3343 ^{m-04} | 1.3000 ^{m-03} 0.0000 ^{m+00} 0.0000 ^{m+00} | 3.5728 1.7920 0.0654 | 1.3468 1.7791 8.5724 ^{m-04} | 4.0817 ^{m+04} 2.8721 ^{m+02} 5.5038 ^{m+02} | 4.0817 ^{m+04} 1.4332 ^{m+02} 2.7835 ^{m+02} | | |

| 7902S0602 | | CHEW / SQUIRE | | PROFILE TABULATION | | | 20 POINTS, DELTA AT POINT 20 | | |
|-----------|------------------------|------------------------|------|--------------------|---------|---------|------------------------------|-----------|--|
| I | Y | PT2/P | P/PO | TO/TOD | M/MD | U/UD | T/TD | R/RD*U/UD | |
| 1 | 0.0000 ⁺ 00 | 1.0000 ⁺ 00 | NM | 0.97292 | 0.00000 | 0.00000 | 1.98445 | 0.00000 | |
| 2 | 9.0000 ⁻ 05 | 1.6876 ⁺ 00 | NM | 0.97363 | 0.39386 | 0.51505 | 1.71008 | 0.30118 | |
| 3 | 2.1000 ⁻ 04 | 1.9220 ⁺ 00 | NM | 0.97539 | 0.44430 | 0.57083 | 1.65071 | 0.34581 | |
| 4 | 3.8000 ⁻ 04 | 2.1772 ⁺ 00 | NM | 0.97717 | 0.48991 | 0.61874 | 1.59508 | 0.38791 | |
| 5 | 6.9000 ⁻ 04 | 2.4456 ⁺ 00 | NM | 0.97893 | 0.53202 | 0.66080 | 1.54273 | 0.42833 | |
| 6 | 1.2800 ⁻ 03 | 2.7849 ⁺ 00 | NM | 0.98104 | 0.57982 | 0.70604 | 1.48273 | 0.47617 | |
| 7 | 1.9800 ⁻ 03 | 3.1915 ⁺ 00 | NM | 0.98340 | 0.63158 | 0.75204 | 1.41782 | 0.53042 | |
| 8 | 2.4700 ⁻ 03 | 3.5511 ⁺ 00 | NM | 0.98536 | 0.67368 | 0.78723 | 1.36550 | 0.57652 | |
| 9 | 2.9100 ⁻ 03 | 3.9361 ⁺ 00 | NM | 0.98733 | 0.71579 | 0.82049 | 1.31393 | 0.62445 | |
| 10 | 3.3200 ⁻ 03 | 4.3327 ⁺ 00 | NM | 0.98924 | 0.75658 | 0.85092 | 1.26493 | 0.67270 | |
| 11 | 3.6900 ⁻ 03 | 4.7202 ⁺ 00 | NM | 0.99099 | 0.79430 | 0.87756 | 1.22063 | 0.71894 | |
| 12 | 4.0700 ⁻ 03 | 5.0789 ⁺ 00 | NM | 0.99252 | 0.82763 | 0.89994 | 1.18238 | 0.76113 | |
| 13 | 4.4300 ⁻ 03 | 5.4128 ⁺ 00 | NM | 0.99387 | 0.85746 | 0.91909 | 1.14893 | 0.79996 | |
| 14 | 4.7300 ⁻ 03 | 5.8056 ⁺ 00 | NM | 0.99537 | 0.89123 | 0.93980 | 1.11197 | 0.84517 | |
| 15 | 5.2800 ⁻ 03 | 6.2898 ⁺ 00 | NM | 0.99711 | 0.93114 | 0.96300 | 1.06961 | 0.90033 | |
| 16 | 5.6700 ⁻ 03 | 6.6321 ⁺ 00 | NM | 0.99827 | 0.95833 | 0.97806 | 1.04159 | 0.93901 | |
| 17 | 6.2300 ⁻ 03 | 6.9557 ⁺ 00 | NM | 0.99931 | 0.98333 | 0.99138 | 1.01644 | 0.97535 | |
| 18 | 7.3000 ⁻ 03 | 7.1528 ⁺ 00 | NM | 0.99993 | 0.99825 | 0.99910 | 1.00172 | 0.99739 | |
| 19 | 8.3200 ⁻ 03 | 7.1645 ⁺ 00 | NM | 0.99996 | 0.99912 | 0.99955 | 1.00086 | 0.99869 | |
| D 20 | 9.6700 ⁻ 03 | 7.1762 ⁺ 00 | NM | 1.00000 | 1.00000 | 1.00000 | 1.00000 | 1.00000 | |

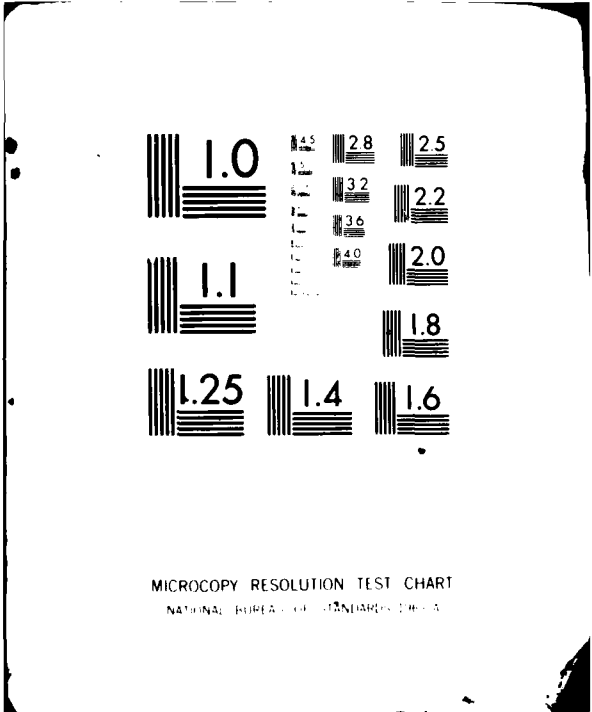
INPUT VARIABLES Y,M ASSUME P=PD AND VAN DRIEST

| 7902S0604 | | CHEW / SQUIRE | | PROFILE TABULATION | | | 21 POINTS, DELTA AT POINT 21 | | |
|-----------|------------------------|------------------------|------|--------------------|---------|---------|------------------------------|-----------|--|
| I | Y | PT2/P | P/PO | TO/TOD | M/MD | U/UD | T/TD | R/RD*U/UD | |
| 1 | 0.0000 ⁺ 00 | 1.0000 ⁺ 00 | NM | 0.98664 | 0.00000 | 0.00000 | 2.03688 | 0.00000 | |
| 2 | 9.0000 ⁻ 05 | 1.7814 ⁺ 00 | NM | 0.98050 | 0.41049 | 0.53778 | 1.71634 | 0.31333 | |
| 3 | 2.0000 ⁻ 04 | 2.1693 ⁺ 00 | NM | 0.98217 | 0.48288 | 0.61545 | 1.62446 | 0.37886 | |
| 4 | 3.7000 ⁻ 04 | 2.4221 ⁺ 00 | NM | 0.98328 | 0.52232 | 0.65511 | 1.57309 | 0.41645 | |
| 5 | 6.4000 ⁻ 04 | 2.7104 ⁺ 00 | NM | 0.98453 | 0.56307 | 0.69412 | 1.51966 | 0.45676 | |
| 6 | 1.0400 ⁻ 03 | 2.9661 ⁺ 00 | NM | 0.98562 | 0.59645 | 0.72460 | 1.47588 | 0.49096 | |
| 7 | 1.6300 ⁻ 03 | 3.2753 ⁺ 00 | NM | 0.98691 | 0.63416 | 0.75746 | 1.42669 | 0.53092 | |
| 8 | 2.2900 ⁻ 03 | 3.6569 ⁺ 00 | NM | 0.98844 | 0.67750 | 0.79323 | 1.37082 | 0.57866 | |
| 9 | 2.8800 ⁻ 03 | 4.0699 ⁺ 00 | NM | 0.99003 | 0.72128 | 0.82725 | 1.31542 | 0.62889 | |
| 10 | 3.3000 ⁻ 03 | 4.4078 ⁺ 00 | NM | 0.99127 | 0.75509 | 0.85212 | 1.27351 | 0.66911 | |
| 11 | 3.7500 ⁻ 03 | 4.7618 ⁺ 00 | NM | 0.99251 | 0.78890 | 0.87582 | 1.23249 | 0.71061 | |
| 12 | 4.1900 ⁻ 03 | 5.1612 ⁺ 00 | NM | 0.99384 | 0.82531 | 0.90008 | 1.18938 | 0.75676 | |
| 13 | 4.5900 ⁻ 03 | 5.5234 ⁺ 00 | NM | 0.99499 | 0.85696 | 0.92014 | 1.15289 | 0.79811 | |
| 14 | 5.0100 ⁻ 03 | 5.9470 ⁺ 00 | NM | 0.99627 | 0.89250 | 0.94159 | 1.11302 | 0.84597 | |
| 15 | 5.4600 ⁻ 03 | 6.3444 ⁺ 00 | NM | 0.99741 | 0.92458 | 0.96000 | 1.07810 | 0.89046 | |
| 16 | 6.0000 ⁻ 03 | 6.7674 ⁺ 00 | NM | 0.99855 | 0.95752 | 0.97802 | 1.04328 | 0.93745 | |
| 17 | 6.4200 ⁻ 03 | 7.0076 ⁺ 00 | NM | 0.99918 | 0.97573 | 0.98761 | 1.02451 | 0.96398 | |
| 18 | 7.3800 ⁻ 03 | 7.2465 ⁺ 00 | NM | 0.99978 | 0.99350 | 0.99673 | 1.00651 | 0.99028 | |
| 19 | 8.6600 ⁻ 03 | 7.2819 ⁺ 00 | NM | 0.99987 | 0.99610 | 0.99804 | 1.00390 | 0.99416 | |
| 20 | 9.9300 ⁻ 03 | 7.3055 ⁺ 00 | NM | 0.99993 | 0.99783 | 0.99891 | 1.00216 | 0.99675 | |
| D 21 | 1.1740 ⁻ 02 | 7.3351 ⁺ 00 | NM | 1.00000 | 1.00000 | 1.00000 | 1.00000 | 1.00000 | |

INPUT VARIABLES Y,M ASSUME P=PD AND VAN DRIEST

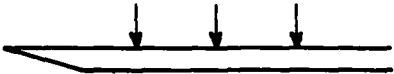
| 7902S0606 | | CHEW / SQUIRE | | PROFILE TABULATION | | | 19 POINTS, DELTA AT POINT 19 | | |
|-----------|------------------------|------------------------|------|--------------------|---------|---------|------------------------------|-----------|--|
| I | Y | PT2/P | P/PO | TO/TOD | M/MD | U/UG | T/TD | R/RD*U/UD | |
| 1 | 0.0000 ⁺ 00 | 1.0000 ⁺ 00 | NM | 0.97267 | 0.00000 | 0.00000 | 1.97420 | 0.00000 | |
| 2 | 9.0000 ⁻ 05 | 1.7268 ⁺ 00 | NM | 0.97391 | 0.40502 | 0.52670 | 1.69108 | 0.31146 | |
| 3 | 4.1000 ⁻ 04 | 2.3273 ⁺ 00 | NM | 0.97820 | 0.51653 | 0.64463 | 1.55755 | 0.41388 | |
| 4 | 6.3000 ⁻ 04 | 2.5906 ⁺ 00 | NM | 0.97990 | 0.55575 | 0.68269 | 1.50898 | 0.45242 | |
| 5 | 9.7000 ⁻ 04 | 2.8510 ⁺ 00 | NM | 0.98150 | 0.59145 | 0.71577 | 1.46459 | 0.48872 | |
| 6 | 1.4200 ⁻ 03 | 3.1198 ⁺ 00 | NM | 0.98307 | 0.62583 | 0.74626 | 1.42190 | 0.52483 | |
| 7 | 2.0700 ⁻ 03 | 3.4665 ⁺ 00 | NM | 0.98500 | 0.66725 | 0.78123 | 1.37080 | 0.56991 | |
| 8 | 2.6500 ⁻ 03 | 3.8050 ⁺ 00 | NM | 0.98678 | 0.70516 | 0.81158 | 1.32463 | 0.61269 | |
| 9 | 3.2900 ⁻ 03 | 4.1336 ⁺ 00 | NM | 0.98842 | 0.73997 | 0.83812 | 1.28287 | 0.65332 | |
| 10 | 4.0100 ⁻ 03 | 4.6192 ⁺ 00 | NM | 0.99068 | 0.78845 | 0.87301 | 1.22599 | 0.71208 | |
| 11 | 4.6100 ⁻ 03 | 5.0117 ⁺ 00 | NM | 0.99239 | 0.82547 | 0.89810 | 1.18370 | 0.75872 | |
| 12 | 5.1600 ⁻ 03 | 5.4478 ⁺ 00 | NM | 0.99417 | 0.86470 | 0.92328 | 1.14009 | 0.80983 | |
| 13 | 5.9100 ⁻ 03 | 6.0583 ⁺ 00 | NM | 0.99647 | 0.91670 | 0.95456 | 1.08429 | 0.88035 | |
| 14 | 6.5800 ⁻ 03 | 6.5484 ⁺ 00 | NM | 0.99818 | 0.95637 | 0.97688 | 1.04336 | 0.93629 | |
| 15 | 7.3500 ⁻ 03 | 6.9155 ⁺ 00 | NM | 0.99938 | 0.98502 | 0.99222 | 1.01469 | 0.97786 | |
| 16 | 8.2000 ⁻ 03 | 7.0945 ⁺ 00 | NM | 0.99995 | 0.99868 | 0.99932 | 1.00129 | 0.98804 | |
| 17 | 9.1700 ⁻ 03 | 7.1411 ⁺ 00 | NM | 1.00009 | 1.00220 | 1.00113 | 0.99786 | 1.00328 | |
| 18 | 1.0150 ⁻ 02 | 7.1353 ⁺ 00 | NM | 1.00007 | 1.00176 | 1.00090 | 0.99829 | 1.00262 | |
| D 19 | 1.1160 ⁻ 02 | 7.1120 ⁺ 00 | NM | 1.00000 | 1.00000 | 1.00000 | 1.00000 | 1.00000 | |

INPUT VARIABLES Y,M ASSUME P=PD AND VAN DRIEST



MICROCOPY RESOLUTION TEST CHART
NATIONAL BUREAU OF STANDARDS-1963-A

| CAT 7902S | | CHEW / SQUIRE | | BOUNDARY CONDITIONS AND EVALUATED DATA. SI UNITS | | | | |
|------------------|---------------------|-------------------------|----------------------|--|-------------------|---------------------|-----------------|-----------------|
| RUN X * RZ | MD * POD T00* | TW/TR PW/PD* TAUW | RED2W RED2D D2 | CF * CQ * PI2* | H12 H32 H42 | H12K H32K D2K | PW T#* UD | PD* TD TR |
| 7902S0501 | 2.0670 | 1.0259 | 2.4463**+04 | 3.2000**+04 | 4.2367 | 2.0264 | 5.7571**+04 | 5.7571**+04 |
| 1.9050**+02 | 5.0003**+05 | 1.0000 | 4.0126**+04 | 0.0000**+00 | 1.6173 | 1.5875 | 2.8667**+02 | 1.5826**+02 |
| INFINITE | 2.9349**+02 | 5.5098**+01 | 6.6218**+04 | 0.0000**+00 | 0.0528 | 9.6488**+04 | 5.2136**+02 | 2.7943**+02 |
| 7902S0502 | 2.0800 | 1.0302 | 2.6386**+04 | 4.5000**+04 | 4.1071 | 1.9091 | 5.8467**+04 | 5.8467**+04 |
| 2.5400**+02 | 5.1823**+05 | 1.0000 | 4.3653**+04 | 0.0000**+00 | 1.6238 | 1.5967 | 2.8663**+02 | 1.5672**+02 |
| INFINITE | 2.9232**+02 | 7.9680**+01 | 6.9539**+04 | 0.0000**+00 | 0.0496 | 1.0179**+03 | 5.2208**+02 | 2.7822**+02 |
| 7902S0503 | 2.0710 | 1.0397 | 2.5217**+04 | 7.5000**+04 | 3.7821 | 1.6939 | 5.6399**+04 | 5.6399**+04 |
| 3.8100**+02 | 4.9292**+05 | 1.0000 | 4.1931**+04 | 0.0000**+00 | 1.6597 | 1.6400 | 2.8586**+02 | 1.5546**+02 |
| INFINITE | 2.8882**+02 | 1.2700**+02 | 6.8774**+04 | 0.0000**+00 | 0.0419 | 9.8913**+04 | 5.1773**+02 | 2.7495**+02 |
| 7902S0504 | 2.1170 | 1.0343 | 2.4513**+04 | 9.8000**+04 | 3.6327 | 1.5609 | 5.3572**+04 | 5.3572**+04 |
| 5.0800**+02 | 5.0309**+05 | 1.0000 | 4.1262**+04 | 0.0000**+00 | 1.6994 | 1.6830 | 2.8673**+02 | 1.5375**+02 |
| INFINITE | 2.9156**+02 | 1.6470**+02 | 6.8632**+04 | 0.0000**+00 | 0.0509 | 9.6998**+04 | 5.2630**+02 | 2.7223**+02 |
| 7902S0505 | 2.1810 | 1.0411 | 2.3195**+04 | 1.1900**+03 | 3.5422 | 1.4291 | 4.9229**+04 | 4.9229**+04 |
| 7.6200**+02 | 5.1097**+05 | 1.0000 | 4.0251**+04 | 0.0000**+00 | 1.7483 | 1.7349 | 2.8564**+02 | 1.4812**+02 |
| INFINITE | 2.8903**+02 | 1.9506**+02 | 6.7131**+04 | 0.0000**+00 | 0.0497 | 9.2811**+04 | 5.3219**+02 | 2.7437**+02 |
| 7902S0506 | 2.1640 | 1.0261 | 2.4587**+04 | 1.2600**+03 | 3.4086 | 1.3948 | 5.0401**+04 | 5.0401**+04 |
| 1.0160**+01 | 5.0940**+05 | 1.0000 | 4.1839**+04 | 0.0000**+00 | 1.7658 | 1.7527 | 2.8613**+02 | 1.5162**+02 |
| INFINITE | 2.9362**+02 | 2.0817**+02 | 7.0970**+04 | 0.0000**+00 | 0.0640 | 9.5599**+04 | 5.3425**+02 | 2.7885**+02 |
| 7902S0507 | 2.1250 | 1.0290 | 2.6352**+04 | 1.2900**+03 | 3.3302 | 1.3867 | 5.2055**+04 | 5.2055**+04 |
| 1.2700**+01 | 4.9500**+05 | 1.0000 | 4.4304**+04 | 0.0000**+00 | 1.7706 | 1.7583 | 2.8597**+02 | 1.5360**+02 |
| INFINITE | 2.9233**+02 | 2.1226**+02 | 7.5454**+04 | 0.0000**+00 | 0.0598 | 1.0039**+03 | 5.2804**+02 | 2.7790**+02 |
| 7902S0601 | 2.2520 | 1.0277 | 1.8899**+04 | 1.2500**+03 | 3.5629 | 1.3826 | 4.3851**+04 | 4.3851**+04 |
| 1.9050**+02 | 5.0864**+05 | 1.0000 | 3.3333**+04 | 0.0000**+00 | 1.7647 | 1.7517 | 2.8378**+02 | 1.4466**+02 |
| INFINITE | 2.9138**+02 | 1.9459**+02 | 5.8473**+04 | 0.0000**+00 | 0.0661 | 8.0613**+04 | 5.4306**+02 | 2.7612**+02 |
| 7902S0602 | 2.2800 | 1.0274 | 1.8814**+04 | 1.2900**+03 | 3.6257 | 1.3938 | 4.2541**+04 | 4.2541**+04 |
| 2.5400**+02 | 5.1553**+05 | 1.0000 | 3.3526**+04 | 0.0000**+00 | 1.7689 | 1.7552 | 2.8401**+02 | 1.4315**+02 |
| INFINITE | 2.9191**+02 | 1.9969**+02 | 5.8985**+04 | 0.0000**+00 | 0.0678 | 8.1466**+04 | 5.4688**+02 | 2.7644**+02 |
| 7902S0603 | 2.2800 | 1.0286 | 1.7629**+04 | 1.3100**+03 | 3.5745 | 1.3635 | 4.1024**+04 | 4.1024**+04 |
| 3.8100**+02 | 4.9717**+05 | 1.0000 | 3.1450**+04 | 0.0000**+00 | 1.7810 | 1.7680 | 2.8392**+02 | 1.4290**+02 |
| INFINITE | 2.9147**+02 | 1.9556**+02 | 5.7258**+04 | 0.0000**+00 | 0.0673 | 7.8115**+04 | 5.4647**+02 | 2.7602**+02 |
| 7902S0604 | 2.3070 | 1.0425 | 1.8296**+04 | 1.3000**+03 | 3.6127 | 1.3388 | 3.9852**+04 | 3.9852**+04 |
| 5.0800**+02 | 5.0380**+05 | 1.0000 | 3.3387**+04 | 0.0000**+00 | 1.7954 | 1.7831 | 2.8382**+02 | 1.3934**+02 |
| INFINITE | 2.8766**+02 | 1.9301**+02 | 5.9681**+04 | 0.0000**+00 | 0.0560 | 8.1007**+04 | 5.4600**+02 | 2.7224**+02 |
| 7902S0605 | 2.3070 | 1.0247 | 1.8784**+04 | 1.2400**+03 | 3.5527 | 1.3298 | 3.9990**+04 | 3.9990**+04 |
| 7.6200**+02 | 5.0553**+05 | 1.0000 | 3.3763**+04 | 0.0000**+00 | 1.7995 | 1.7883 | 2.8262**+02 | 1.4116**+02 |
| INFINITE | 2.9142**+02 | 1.8474**+02 | 6.1256**+04 | 0.0000**+00 | 0.0731 | 8.2366**+04 | 5.4956**+02 | 2.7579**+02 |
| 7902S0606 | 2.2690 | 1.0268 | 2.0093**+04 | 1.3100**+03 | 3.5111 | 1.3452 | 4.1368**+04 | 4.1368**+04 |
| 1.0160**+01 | 4.9279**+05 | 1.0000 | 3.5645**+04 | 0.0000**+00 | 1.7945 | 1.7828 | 2.8359**+02 | 1.4365**+02 |
| INFINITE | 2.9156**+02 | 1.9530**+02 | 6.5142**+04 | 0.0000**+00 | 0.0692 | 8.7353**+04 | 5.4525**+02 | 2.7618**+02 |
| 7902S0607 | 2.2640 | 1.0255 | 2.1126**+04 | 1.2900**+03 | 3.4530 | 1.3176 | 4.2058**+04 | 4.2058**+04 |
| 1.2700**+01 | 4.9710**+05 | 1.0000 | 3.7359**+04 | 0.0000**+00 | 1.8031 | 1.7918 | 2.8381**+02 | 1.4425**+02 |
| INFINITE | 2.9213**+02 | 1.9467**+02 | 6.7698**+04 | 0.0000**+00 | 0.0707 | 8.9803**+04 | 5.4519**+02 | 2.7675**+02 |
| 7902S0701 | 2.2390 | 1.0362 | 1.9378**+04 | 3.8000**+04 | 4.1844 | 1.7846 | 4.4609**+04 | 4.4609**+04 |
| 3.1750**+02 | 5.0702**+05 | 1.0000 | 3.4227**+04 | 0.0000**+00 | 1.6905 | 1.6574 | 2.8601**+02 | 1.4540**+02 |
| INFINITE | 2.9119**+02 | 5.9486**+01 | 5.9794**+04 | 0.0000**+00 | 0.0537 | 8.7016**+04 | 5.4132**+02 | 2.7603**+02 |
| 7902S0702 | 2.2110 | 1.0301 | 2.0023**+04 | 5.2000**+04 | 4.0933 | 1.7382 | 4.6953**+04 | 4.6953**+04 |
| 3.8100**+02 | 5.1078**+05 | 1.0000 | 3.4818**+04 | 0.0000**+00 | 1.6782 | 1.6490 | 2.8525**+02 | 1.4761**+02 |
| INFINITE | 2.9192**+02 | 8.3550**+01 | 5.9767**+04 | 0.0000**+00 | 0.0577 | 8.7250**+04 | 5.3858**+02 | 2.7691**+02 |
| 7902S0703 | 2.1870 | 1.0293 | 2.1315**+04 | 8.2000**+04 | 3.8442 | 1.6240 | 4.7298**+04 | 4.7298**+04 |
| 5.0800**+02 | 4.9556**+05 | 1.0000 | 3.6703**+04 | 0.0000**+00 | 1.6927 | 1.6703 | 2.8516**+02 | 1.4918**+02 |
| INFINITE | 2.9189**+02 | 1.2985**+02 | 6.4176**+04 | 0.0000**+00 | 0.0583 | 9.2429**+04 | 5.3557**+02 | 2.7705**+02 |
| 7902S0704 | 2.2440 | 1.0293 | 2.0948**+04 | 1.0200**+03 | 3.7434 | 1.4969 | 4.4609**+04 | 4.4609**+04 |
| 6.3500**+02 | 5.1100**+05 | 1.0000 | 3.6869**+04 | 0.0000**+00 | 1.7296 | 1.7121 | 2.8481**+02 | 1.4545**+02 |
| INFINITE | 2.9193**+02 | 1.6039**+02 | 6.4294**+04 | 0.0000**+00 | 0.0625 | 9.1351**+04 | 5.4261**+02 | 2.7670**+02 |
| 7902S0705 | 2.2780 | 1.0287 | 1.9738**+04 | 1.1300**+03 | 3.7067 | 1.4383 | 4.2196**+04 | 4.2196**+04 |
| 7.6200**+02 | 5.0977**+05 | 1.0000 | 3.5170**+04 | 0.0000**+00 | 1.7487 | 1.7325 | 2.8508**+02 | 1.4359**+02 |
| INFINITE | 2.9262**+02 | 1.7320**+02 | 6.2730**+04 | 0.0000**+00 | 0.0654 | 8.8319**+04 | 5.4731**+02 | 2.7712**+02 |
| 7902S0706 | 2.3230 | 1.0295 | 1.9477**+04 | 1.2400**+03 | 3.7007 | 1.3874 | 3.9369**+04 | 3.9369**+04 |
| 1.0160**+01 | 5.1032**+05 | 1.0000 | 3.5353**+04 | 0.0000**+00 | 1.7732 | 1.7590 | 2.8389**+02 | 1.4019**+02 |
| INFINITE | 2.9148**+02 | 1.8441**+02 | 6.4075**+04 | 0.0000**+00 | 0.0678 | 8.9035**+04 | 5.5146**+02 | 2.7575**+02 |
| 7902S0707 | 2.3080 | 1.0346 | 1.9357**+04 | 1.2400**+03 | 3.6481 | 1.3652 | 3.9921**+04 | 3.9921**+04 |
| 1.2700**+01 | 5.0547**+05 | 1.0000 | 3.5054**+04 | 0.0000**+00 | 1.7795 | 1.7668 | 2.8603**+02 | 1.4145**+02 |
| INFINITE | 2.9215**+02 | 1.8458**+02 | 6.3864**+04 | 0.0000**+00 | 0.0628 | 8.8035**+04 | 5.5036**+02 | 2.7648**+02 |

| | | |
|--|--|------|
|  | M: 9.3 R THETA x 10 ⁻³ : 3-12 TW/TR: 0.32 | 7903 |
| Gun tunnel with contoured axisymmetric nozzle. Running time 5 ms. D = 0.4 m. PO: 15, 67 MN/m ² . TO: 995, 1025K. Nitrogen. 14 < RE/m 10 ⁻⁶ < 55. | | |
| BARTLETT R.P., EDWARDS A.J., HARVEY J.K., HILLIER R., 1979a. Pitot pressure and total temperature profile measurements in a hypersonic, turbulent boundary layer at M = 9. Aero Rep. 79-01. Imperial College London. And Bartlett R.P. (1981), Edwards A.J. (1981), Bartlett et al. (1979b), private communications. | | |

- 1 The test boundary layer was formed on a flat plate 0.18 m wide and 0.76 m long with leading edge thickness 10 μ m. The model was mounted with the test surface facing upwards 10 mm below the tunnel centre line so as to avoid focused effects of upstream disturbances on the axis. Hanging sideplates were used to suppress the effect of disturbances generated on the underside of the model. A slot was machined in the model surface to receive a range of interchangeable instrumented test surface modules. The slot was 0.10 m wide and extended from X = 0.11 m to 0.76 m, where X = 0 at the leading edge. "A high order of surface finish and fit between the modules was maintained; the surface roughness being better than 15 microns." Measurements of surface pressure showed a systematic fall of about 3-6% along the instrumented section, a consequence of a residual nozzle expansion field, with scatter of less than 10%. For the low Reynolds number tests
- 3 (series 01) a transition trip consisting of a single row of vortex generators 1 mm high and 3 mm apart at X=10 mm was used. The delta-shaped generators were inclined at about 30° to the flow direction. Transition was natural for the high Reynolds number series (02). Transition position was deduced from both surface heat flux measurements and surface Pitot (Preston tube) pressures. The peak heat flux and wall shear values occurred at or upstream of X = 0.16 m. Pressure and heat flux measurements across the width of the instrumented area at 3-4 and 7-9 X-stations showed that these quantities were "uniform to within $\pm 5\%$ over the central third of the model."
- 6 Static pressure tapings (D = 1.37 mm) were positioned at about 30 streamwise stations. Surface temperature and heat transfer rates were measured with thin film gauges at up to 50 X-stations. These gauges were formed by either painting or evaporation through a machined mask onto 3 mm diameter quartz substrates. Special care was taken to ensure that these were mounted accurately level with the model surface, earlier work having shown that this was vital if a consistent result was to be obtained. Surface Pitot readings were taken at 7-11 stations using circular Preston tubes (d = 1.25, 2.07, 2.96 mm).
- 7 Pitot and TO profiles were taken. The Pitot probes were FPP (typically $b_1 = 2.0$, $h_1 = 0.5$, $h_2 = 0.35$ mm). Four tubes were mounted on a rake, and the profiles built up by the superposition of many sets of normalised data. A 'kink' was observed in the inner part of some profiles measured with the original probes similar to that reported by Allen (1972). The tube length was increased by 90%, and this anomaly disappeared. The TO probes were miniature STP using a fine chromel-alumel thermocouple bead. The junction was mounted at the rearward apex of a V formed in the 12.5 μ m diameter wire. This was attached at the forward end to two support prongs (d = 100 μ m) which were splayed outwards within the shield (d_1 appr. 2 mm). The ceramic central support (d = 0.9 mm) was chamfered to minimise blockage, and much attention paid to a proper control of the flow within the shield. The probe was calibrated over a range of Reynolds number in the tunnel, using different total pressures and the expansion field of a flat plate at incidence. The uncorrected reading was low by about 2% at test free stream conditions and by 12% at the lowest Reynolds
- 8 number used. (The design and development is described in detail by Bartlett et al., 1979b.) Pitot traverses were made at X = 0.36, 0.41, 0.46, 0.51 and 0.56 m, while TO profiles were measured for X = 0.36, 0.46, 0.56.

- 7 Mean and fluctuating density values were obtained for a single profile at $X = 0.56$ m at the LP (series 01) running condition, using the electron beam fluorescence technique. The 1 mm diameter 30 kV electron beam was projected through the boundary layer from beneath the model surface. The density of the flow was deduced from the resulting fluorescence in the [0,0] band of the $N_2(2+)$ system, which in the absence of oxygen and the pressure levels used shows a linear relationship between density and light intensity. Two optical detectors were used, one focused at the measuring point within the layer, the other on the beam outside the layer to monitor beam current. Corrections for secondary electron excitation were made. Measurements up to 100 kHz were possible using digital processing.
- 9 All profile data were normalised for run to run variations in tunnel stagnation conditions, assuming that for each nominal condition, $(T_0 - T_w)/(T_{0D} - T_w)$, PT_2/POD and PW/POD were functions of position only and that $P = PW$. PT_2 data were interpolated to the Y values of T_0 measurements. No corrections for shear or wall proximity were applied. Viscosity was calculated from the Sutherland relationship.
- 12 The editors have presented the data as received from the authors, incorporating their data reduction and interpolation procedures. The D-state is that selected by the authors. The profiles given here are the two sets of three for which both Pitot and T_0 measurements were made. The wall data given with the profiles are the values selected by the authors. The very large amount of heat flux and wall shear data from which these values were derived are tabulated in Edwards (1981).
- § DATA: 79030101-0203. Pitot and T_0 profiles obtained piecemeal, separately, in a great number of runs. $NX = 3$. CF from Preston tubes. Heat transfer from thin film gauges. Electron beam studies.
- 15 Editors' comments. This experiment is potentially of great interest as it bridges the gap between wall measurements made in short run (here 5 ms) facilities and profile measurements, usually obtained in tunnels with running times of at least some seconds. (AG 253; §1.1, §1.3). There is an obvious comparison here with the case studied by Watson (CAT 7804S), where, even with a running time of only 5 seconds, substantial local wall temperature changes occurred. The Reynolds number, Mach number and, for 78040201-07, the wall temperature ratio T_w/TR are fairly close.

The mean temperature/velocity relationship agrees fairly well with the van Driest correlation (AG 253, eqn. 2.5.37). Agreement with the log-law is reasonable (Fig. 1), implying an error range of about $\pm 10\%$ in $TAUW$. The wake component is however small though well within the range shown in AG 253 Fig.(3.3.7) except for profile 0201. In the outer law plots (Fig. 2) there is a corresponding tendency for the data to fall below the 'incompressible norm'. We suggest that the profiles, especially in the outer region, have yet to complete transition. The comparable profiles by Watson (see section 4.4 in AG 223 and 0202,3 for series 1; 0204/6/7 for series 2 in section 6) are generally similar except for a more pronounced wake component, which also shows as a much better agreement with the outer law. The Watson CF values seem to be about 20% low, perhaps a result of using an uncooled balance element in a cooled wall.

The electron beam technique and results are discussed in detail in § 4.5.16 of Bartlett (1981). The principal feature is the extension of the technique to high number densities ($n > 10^{24} \text{ m}^{-3}$) in a range more typical of high Reynolds number flow in wind tunnels than the rarified flows in which it was developed and has been extensively used. Here the only comparisons are with McDonald (1975 - see Laderman and Demetriades, CAT 7403) and Wallace (1968), both at lower densities, and both using air as the working fluid so that quenching by the oxygen present would cause significant difficulty. The mean densities deduced from the fluorescence measurements were in good agreement with values deduced from probe measurements in the outer part of the layer, but were increasingly low as the wall was approached. Reflections from the wall are suggested as a possible cause for the discrepancy. Fluctuation measurements were also made and presented both as r.m.s profiles and as spectral distributions at six y -values. Although this work was performed as a feasibility study it would seem to be the most serious attempt to date at applying the technique in turbulent boundary layers but many questions of interpretation must be answered before it may be considered as established.

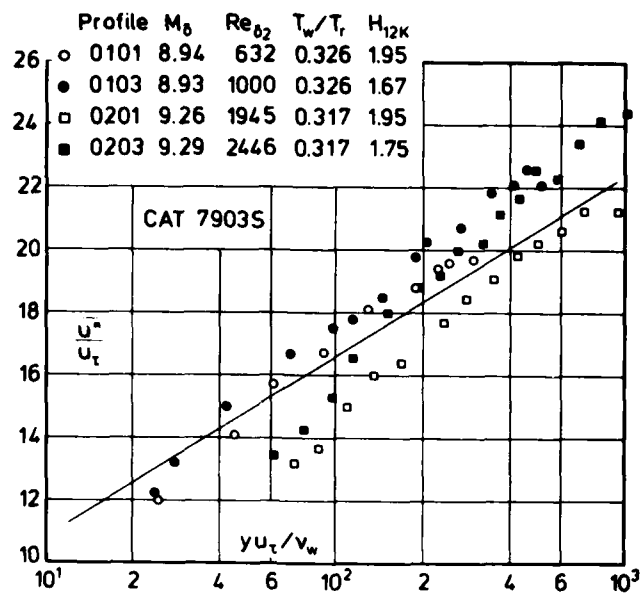


Fig. 1 Law of the wall for a compressible boundary layer with zero pressure gradient (isothermal wall, origin not defined). Bartlett et al. (1979).

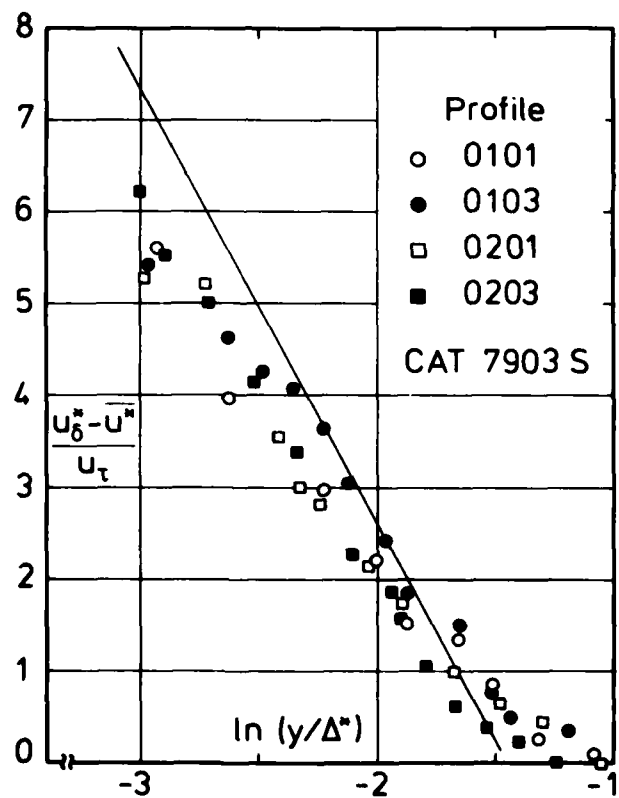


Fig. 2 Outer law for a compressible boundary layer with a zero pressure gradient (isothermal wall, origin not defined). Bartlett et al. (1979).

| CAT 79035 | | BARTLETT/E/H/H | | BOUNDARY CONDITIONS AND EVALUATED DATA. SI UNITS | | | | | |
|-----------------------|-----------------------|-----------------------|-----------------------|--|---------|-----------------------|-----------------------|-----------------------|--|
| RUN | MD * | TW/TR | RED2W | CF | H12 | H12K | PW | PD | |
| X * | POD* | PW/PD* | RED2D | CO * | H32 | H32K | TW* | TD | |
| RZ | TOD* | TAUW * | D2 | PI2* | H42 | D2K | UD | TR | |
| 7903S0101 | 8.9380 | 0.3258 | 6.3202 ⁺⁰² | 1.0757 ⁻⁰³ | 17.3669 | 1.9534 | 7.5384 ⁺⁰² | 7.5384 ⁺⁰² | |
| 2.6000 ⁻⁰¹ | 1.5200 ⁺⁰⁷ | 1.0000 | 2.7304 ⁺⁰³ | 3.1391 ⁻⁰⁴ | 1.8853 | 1.8360 | 2.9300 ⁺⁰² | 5.8725 ⁺⁰¹ | |
| INFINITE | 9.9700 ⁺⁰² | 4.5347 ⁺⁰¹ | 1.8720 ⁻⁰⁴ | 0.0000 ⁺⁰⁰ | 1.0425 | 4.7383 ⁻⁰⁴ | 1.3733 ⁺⁰³ | 8.9942 ⁺⁰² | |
| 7903S0102 | 8.9300 | 0.3258 | 8.4210 ⁺⁰² | 9.8626 ⁻⁰⁴ | 16.7021 | 1.8100 | 7.5830 ⁺⁰² | 7.5830 ⁺⁰² | |
| 3.6000 ⁻⁰¹ | 1.5200 ⁺⁰⁷ | 1.0000 | 3.6319 ⁺⁰³ | 2.8443 ⁻⁰⁴ | 1.8892 | 1.8405 | 2.9300 ⁺⁰² | 5.8824 ⁺⁰¹ | |
| INFINITE | 9.9700 ⁺⁰² | 4.1748 ⁺⁰¹ | 2.4839 ⁻⁰⁴ | 0.0000 ⁺⁰⁰ | 1.0536 | 6.0774 ⁻⁰⁴ | 1.3732 ⁺⁰³ | 8.9943 ⁺⁰² | |
| 7903S0103 | 8.9300 | 0.3262 | 9.9994 ⁺⁰² | 8.5122 ⁻⁰⁴ | 20.5341 | 1.6759 | 7.5830 ⁺⁰² | 7.5830 ⁺⁰² | |
| 5.6000 ⁻⁰¹ | 1.5200 ⁺⁰⁷ | 1.0000 | 4.3187 ⁺⁰³ | 2.5353 ⁻⁰⁴ | 1.8732 | 1.8310 | 2.9300 ⁺⁰² | 5.8741 ⁺⁰¹ | |
| INFINITE | 9.9560 ⁺⁰² | 3.6032 ⁺⁰¹ | 2.9474 ⁻⁰⁴ | 0.0000 ⁺⁰⁰ | 0.8373 | 8.5294 ⁻⁰⁴ | 1.3722 ⁺⁰³ | 8.9817 ⁺⁰² | |
| 7903S0201 | 9.2591 | 0.3173 | 1.9450 ⁺⁰³ | 8.7631 ⁻⁰⁴ | 19.1743 | 1.9513 | 2.6193 ⁺⁰³ | 2.6193 ⁺⁰³ | |
| 3.6000 ⁻⁰¹ | 6.6670 ⁺⁰⁷ | 1.0000 | 8.7454 ⁺⁰³ | 2.6257 ⁻⁰⁴ | 1.8869 | 1.8421 | 2.9300 ⁺⁰² | 5.6442 ⁺⁰¹ | |
| INFINITE | 1.0242 ⁺⁰³ | 1.3778 ⁺⁰² | 1.5691 ⁻⁰⁴ | 0.0000 ⁺⁰⁰ | 1.0148 | 4.2114 ⁻⁰⁴ | 1.3947 ⁺⁰³ | 9.2356 ⁺⁰² | |
| 7903S0202 | 9.3211 | 0.3173 | 2.0616 ⁺⁰³ | 7.6769 ⁻⁰⁴ | 21.1024 | 1.8636 | 2.5061 ⁺⁰³ | 2.5061 ⁺⁰³ | |
| 4.6000 ⁻⁰¹ | 6.6670 ⁺⁰⁷ | 1.0000 | 9.3883 ⁺⁰³ | 2.3918 ⁻⁰⁴ | 1.8814 | 1.8394 | 2.9300 ⁺⁰² | 5.5734 ⁺⁰¹ | |
| INFINITE | 1.0242 ⁺⁰³ | 1.1701 ⁺⁰² | 1.7159 ⁻⁰⁴ | 0.0000 ⁺⁰⁰ | 0.9161 | 4.8302 ⁻⁰⁴ | 1.3952 ⁺⁰³ | 9.2348 ⁺⁰² | |
| 7903S0203 | 9.2850 | 0.3174 | 2.4459 ⁺⁰³ | 6.6558 ⁻⁰⁴ | 22.7713 | 1.7528 | 2.5713 ⁺⁰³ | 2.5713 ⁺⁰³ | |
| 5.6000 ⁻⁰¹ | 6.6670 ⁺⁰⁷ | 1.0000 | 1.1060 ⁺⁰⁴ | 2.1640 ⁻⁰⁴ | 1.8708 | 1.8215 | 2.9300 ⁺⁰² | 5.6128 ⁺⁰¹ | |
| INFINITE | 1.0239 ⁺⁰³ | 1.0328 ⁺⁰² | 1.9988 ⁻⁰⁴ | 0.0000 ⁺⁰⁰ | 0.8177 | 6.1933 ⁻⁰⁴ | 1.3947 ⁺⁰³ | 9.2325 ⁺⁰² | |

TRAPEZOIDAL RULE FOR ALL INTEGRATIONS

| 7903S0101 | BARTLETT/E/H/H | | PROFILE TABULATION | | | 19 POINTS, DELTA AT POINT 15 | | |
|-----------|-----------------------|-----------------------|--------------------|---------|---------|------------------------------|---------|-----------|
| I | Y | PT2/P | P/PO | TO/TOD | M/MD | U/UD | T/TD | R/RD*U/UD |
| 1 | 0.0000 ⁺⁰⁰ | 1.0000 ⁺⁰⁰ | NH | 0.29388 | 0.00000 | 0.00000 | 4.98940 | 0.00000 |
| 2 | 6.9983 ⁻⁰⁴ | 9.4789 ⁺⁰⁰ | NH | 0.78140 | 0.29583 | 0.69577 | 5.53149 | 0.12578 |
| 3 | 7.9903 ⁻⁰⁴ | 1.0502 ⁺⁰¹ | NH | 0.78680 | 0.31222 | 0.71354 | 5.22304 | 0.13661 |
| 4 | 1.2818 ⁻⁰³ | 1.8796 ⁺⁰¹ | NH | 0.81220 | 0.42212 | 0.79918 | 3.58443 | 0.22296 |
| 5 | 1.7499 ⁻⁰³ | 3.0405 ⁺⁰¹ | NH | 0.86780 | 0.53951 | 0.87116 | 2.60732 | 0.33412 |
| 6 | 2.5908 ⁻⁰³ | 4.2074 ⁺⁰¹ | NH | 0.90050 | 0.63603 | 0.91030 | 2.04843 | 0.44439 |
| 7 | 3.2108 ⁻⁰³ | 5.0058 ⁺⁰¹ | NH | 0.93500 | 0.69438 | 0.93775 | 1.82383 | 0.51416 |
| 8 | 3.7006 ⁻⁰³ | 5.5494 ⁺⁰¹ | NH | 0.96510 | 0.73144 | 0.95818 | 1.71605 | 0.55836 |
| 9 | 4.5996 ⁻⁰³ | 7.0838 ⁺⁰¹ | NH | 0.95470 | 0.82716 | 0.96407 | 1.35845 | 0.70969 |
| 10 | 5.3382 ⁻⁰³ | 8.0154 ⁺⁰¹ | NH | 0.97310 | 0.88021 | 0.97812 | 1.23485 | 0.79210 |
| 11 | 5.4684 ⁻⁰³ | 8.0245 ⁺⁰¹ | NH | 0.96390 | 0.88071 | 0.97353 | 1.22189 | 0.79674 |
| 12 | 6.4503 ⁻⁰³ | 9.5146 ⁺⁰¹ | NH | 0.99310 | 0.95944 | 0.99402 | 1.07339 | 0.92606 |
| 13 | 7.0083 ⁻⁰³ | 1.0160 ⁺⁰² | NH | 0.99750 | 0.99161 | 0.99825 | 1.01344 | 0.98501 |
| 14 | 6.2011 ⁻⁰³ | 1.0271 ⁺⁰² | NH | 0.99450 | 0.99700 | 0.99707 | 1.00013 | 0.99694 |
| D 15 | 8.4165 ⁻⁰³ | 1.0332 ⁺⁰² | NH | 1.00000 | 1.00000 | 1.00000 | 1.00000 | 1.00000 |
| 16 | 9.5100 ⁻⁰³ | 1.0458 ⁺⁰² | NH | 0.99110 | 1.00609 | 0.99589 | 0.97983 | 1.01640 |
| 17 | 1.0050 ⁻⁰² | 1.0460 ⁺⁰² | NH | 0.98760 | 1.00619 | 0.99414 | 0.97618 | 1.01839 |
| 18 | 1.1200 ⁻⁰² | 1.0417 ⁺⁰² | NH | 0.99700 | 1.00410 | 0.99874 | 0.98936 | 1.00948 |
| 19 | 1.2955 ⁻⁰² | 1.0334 ⁺⁰² | NH | 0.99510 | 1.00010 | 0.99755 | 0.99491 | 1.00265 |

INPUT VARIABLES Y,H/MD,TO/TOD ASSUME P=PD

| 7903S0102 | BARTLETT/E/H/H | | PROFILE TABULATION | | | 20 POINTS, DELTA AT POINT 19 | | |
|-----------|-----------------------|-----------------------|--------------------|---------|---------|------------------------------|---------|-----------|
| I | Y | PT2/P | P/PO | TO/TOD | M/MD | U/UD | T/TD | R/RD*U/UD |
| 1 | 0.0000 ⁺⁰⁰ | 1.0000 ⁺⁰⁰ | NH | 0.29388 | 0.00000 | 0.00000 | 4.98099 | 0.00000 |
| 2 | 7.2540 ⁻⁰⁴ | 7.7647 ⁺⁰⁰ | NH | 0.73604 | 0.26634 | 0.64436 | 5.85297 | 0.11009 |
| 3 | 8.4045 ⁻⁰⁴ | 1.1083 ⁺⁰¹ | NH | 0.76033 | 0.32143 | 0.70912 | 4.86695 | 0.14570 |
| 4 | 1.1300 ⁻⁰³ | 1.6499 ⁺⁰¹ | NH | 0.80404 | 0.39511 | 0.78078 | 3.90492 | 0.19995 |
| 5 | 1.4011 ⁻⁰³ | 2.3974 ⁺⁰¹ | NH | 0.80902 | 0.47849 | 0.82153 | 2.94786 | 0.27869 |
| 6 | 1.8496 ⁻⁰³ | 2.7176 ⁺⁰¹ | NH | 0.84616 | 0.51004 | 0.85122 | 2.78534 | 0.30561 |
| 7 | 2.4911 ⁻⁰³ | 3.1434 ⁺⁰¹ | NH | 0.87882 | 0.54920 | 0.87932 | 2.56344 | 0.34302 |
| 8 | 2.8938 ⁻⁰³ | 3.5485 ⁺⁰¹ | NH | 0.90361 | 0.58402 | 0.90064 | 2.37823 | 0.37870 |
| 9 | 3.3501 ⁻⁰³ | 3.9683 ⁺⁰¹ | NH | 0.92881 | 0.61804 | 0.92080 | 2.21970 | 0.41483 |
| 10 | 3.9409 ⁻⁰³ | 4.7727 ⁺⁰¹ | NH | 0.92662 | 0.67847 | 0.93095 | 1.88275 | 0.49446 |
| 11 | 4.5757 ⁻⁰³ | 5.3984 ⁺⁰¹ | NH | 0.94703 | 0.72199 | 0.94781 | 1.72341 | 0.54996 |
| 12 | 5.1499 ⁻⁰³ | 5.6071 ⁺⁰¹ | NH | 0.95798 | 0.73593 | 0.95520 | 1.68468 | 0.56699 |
| 13 | 5.7496 ⁻⁰³ | 5.9886 ⁺⁰¹ | NH | 0.97013 | 0.76076 | 0.96446 | 1.60723 | 0.60008 |
| 14 | 6.4223 ⁻⁰³ | 7.7357 ⁺⁰¹ | NH | 0.98078 | 0.86539 | 0.98069 | 1.28421 | 0.76365 |
| 15 | 7.1000 ⁻⁰³ | 8.2647 ⁺⁰¹ | NH | 0.98676 | 0.89467 | 0.98613 | 1.21491 | 0.81169 |
| 16 | 8.2310 ⁻⁰³ | 9.7787 ⁺⁰¹ | NH | 0.99134 | 0.97359 | 0.99405 | 1.04246 | 0.95356 |
| 17 | 9.2099 ⁻⁰³ | 1.0251 ⁺⁰² | NH | 0.98218 | 0.99693 | 0.99087 | 0.98787 | 1.00304 |
| 18 | 1.1300 ⁻⁰² | 1.0293 ⁺⁰² | NH | 0.98994 | 0.99901 | 0.99490 | 0.99179 | 1.00314 |
| D 19 | 1.1749 ⁻⁰² | 1.0314 ⁺⁰² | NH | 1.00000 | 1.00000 | 1.00000 | 1.00000 | 1.00000 |
| 20 | 1.3806 ⁻⁰² | 1.0130 ⁺⁰² | NH | 0.98616 | 0.99100 | 0.99252 | 1.00307 | 0.98948 |

INPUT VARIABLES Y,H/MD,TO/TOD ASSUME P=PD

| 7903S0103 | | BARTLETT/E/H/H | | PROFILE TABULATION | | 30 POINTS, DELTA AT POINT 29 | | |
|-----------|------------------------|------------------------|------|--------------------|---------|------------------------------|---------|-----------|
| I | Y | PT2/P | P/PD | TO/TOD | M/MD | U/UD | T/TD | R/RD*U/UD |
| 1 | 0.0000 ⁺ 00 | 1.0000 ⁺ 00 | NM | 0.29429 | 0.00000 | 0.00000 | 4.98798 | 0.00000 |
| 2 | 7.6960 ⁻ 04 | 6.6732 ⁺ 00 | NM | 0.77599 | 0.24330 | 0.63575 | 6.70602 | 0.09480 |
| 3 | 8.9960 ⁻ 04 | 8.5632 ⁺ 00 | NM | 0.78540 | 0.28060 | 0.68164 | 5.90120 | 0.11551 |
| 4 | 1.3429 ⁻ 03 | 1.4300 ⁺ 01 | NM | 0.81023 | 0.36700 | 0.76651 | 4.36213 | 0.17572 |
| 5 | 1.8499 ⁻ 03 | 1.9171 ⁺ 01 | NM | 0.82075 | 0.42680 | 0.80552 | 3.56210 | 0.22614 |
| 6 | 2.2503 ⁻ 03 | 2.1500 ⁺ 01 | NM | 0.85670 | 0.45260 | 0.83490 | 3.40282 | 0.24535 |
| 7 | 2.6702 ⁻ 03 | 2.5624 ⁺ 01 | NM | 0.86631 | 0.49500 | 0.85618 | 2.99173 | 0.28618 |
| 8 | 3.1161 ⁻ 03 | 2.7172 ⁺ 01 | NM | 0.87482 | 0.51000 | 0.86550 | 2.88004 | 0.30052 |
| 9 | 3.6504 ⁻ 03 | 2.7413 ⁺ 01 | NM | 0.90106 | 0.51230 | 0.87915 | 2.94496 | 0.29853 |
| 10 | 4.1002 ⁻ 03 | 3.0283 ⁺ 01 | NM | 0.89575 | 0.53890 | 0.88481 | 2.69579 | 0.32822 |
| 11 | 4.6501 ⁻ 03 | 3.1524 ⁺ 01 | NM | 0.92019 | 0.55000 | 0.90000 | 2.67767 | 0.33611 |
| 12 | 5.2000 ⁻ 03 | 3.7699 ⁺ 01 | NM | 0.93241 | 0.60220 | 0.91913 | 2.32956 | 0.39455 |
| 13 | 6.0502 ⁻ 03 | 4.5910 ⁺ 01 | NM | 0.94663 | 0.66530 | 0.93870 | 1.99076 | 0.47153 |
| 14 | 6.6001 ⁻ 03 | 5.0803 ⁺ 01 | NM | 0.97026 | 0.70020 | 0.95613 | 1.86461 | 0.51278 |
| 15 | 7.8000 ⁻ 03 | 6.0897 ⁺ 01 | NM | 0.97126 | 0.76720 | 0.96581 | 1.58478 | 0.60943 |
| 16 | 8.2498 ⁻ 03 | 6.5830 ⁺ 01 | NM | 0.96145 | 0.79790 | 0.96443 | 1.46098 | 0.66013 |
| 17 | 8.5995 ⁻ 03 | 6.8311 ⁺ 01 | NM | 0.96465 | 0.81290 | 0.96762 | 1.41690 | 0.68292 |
| 18 | 9.6005 ⁻ 03 | 8.2121 ⁺ 01 | NM | 0.98117 | 0.89180 | 0.98311 | 1.21525 | 0.80897 |
| 19 | 1.0250 ⁻ 02 | 8.8181 ⁺ 01 | NM | 0.98828 | 0.92430 | 0.98916 | 1.14527 | 0.86369 |
| 20 | 1.1099 ⁻ 02 | 9.6473 ⁺ 01 | NM | 0.99269 | 0.96700 | 0.99430 | 1.05727 | 0.94045 |
| 21 | 1.1350 ⁻ 02 | 9.5700 ⁺ 01 | NM | 0.98768 | 0.96310 | 0.99154 | 1.05993 | 0.93548 |
| 22 | 1.2178 ⁻ 02 | 9.9172 ⁺ 01 | NM | 0.99740 | 0.98050 | 0.99752 | 1.03501 | 0.96377 |
| 23 | 1.2350 ⁻ 02 | 1.0437 ⁺ 02 | NM | 0.98568 | 1.00600 | 0.99316 | 0.97464 | 1.01900 |
| 24 | 1.3104 ⁻ 02 | 1.0116 ⁺ 02 | NM | 1.00100 | 0.99030 | 0.99992 | 1.01952 | 0.98077 |
| 25 | 1.4300 ⁻ 02 | 1.0314 ⁺ 02 | NM | 1.00681 | 1.00000 | 1.00340 | 1.00681 | 0.99661 |
| 26 | 1.4352 ⁻ 02 | 1.0314 ⁺ 02 | NM | 0.99429 | 1.00000 | 0.99714 | 0.99429 | 1.00287 |
| 27 | 1.4599 ⁻ 02 | 1.0310 ⁺ 02 | NM | 1.01833 | 0.99980 | 1.00911 | 1.01871 | 0.99058 |
| 28 | 1.5405 ⁻ 02 | 1.0375 ⁺ 02 | NM | 1.01682 | 1.00300 | 1.00855 | 1.01111 | 0.99748 |
| D 29 | 1.6354 ⁻ 02 | 1.0314 ⁺ 02 | NM | 1.00000 | 1.00000 | 1.00000 | 1.00000 | 1.00000 |
| 30 | 1.8096 ⁻ 02 | 1.0318 ⁺ 02 | NM | 1.01943 | 1.00020 | 1.00968 | 1.01904 | 0.99081 |

INPUT VARIABLES Y,M/MD,TO/TOD ASSUME P=PD

| 7903S0201 | | BARTLETT/E/H/H | | PROFILE TABULATION | | 30 POINTS, DELTA AT POINT 29 | | |
|-----------|------------------------|------------------------|------|--------------------|---------|------------------------------|---------|-----------|
| I | Y | PT2/P | P/PD | TO/TOD | M/MD | U/UD | T/TD | R/RD*U/UD |
| 1 | 0.0000 ⁺ 00 | 1.0000 ⁺ 00 | NM | 0.28608 | 0.00000 | 0.00000 | 5.19118 | 0.00000 |
| 2 | 6.3000 ⁻ 04 | 1.0538 ⁺ 01 | NM | 0.77285 | 0.30193 | 0.70626 | 5.47162 | 0.12908 |
| 3 | 7.6968 ⁻ 04 | 1.3235 ⁺ 01 | NM | 0.76135 | 0.34003 | 0.73184 | 4.63221 | 0.15799 |
| 4 | 9.5976 ⁻ 04 | 1.7668 ⁺ 01 | NM | 0.81184 | 0.39474 | 0.79069 | 4.01224 | 0.19707 |
| 5 | 1.1801 ⁻ 03 | 2.1851 ⁺ 01 | NM | 0.85473 | 0.44014 | 0.83383 | 3.58890 | 0.23233 |
| 6 | 1.3097 ⁻ 03 | 2.2863 ⁺ 01 | NM | 0.80064 | 0.45045 | 0.81127 | 3.24373 | 0.25010 |
| 7 | 1.4702 ⁻ 03 | 2.4001 ⁺ 01 | NM | 0.86973 | 0.46175 | 0.85015 | 3.38985 | 0.25079 |
| 8 | 1.5300 ⁻ 03 | 2.4782 ⁺ 01 | NM | 0.83583 | 0.46935 | 0.83631 | 3.17499 | 0.26340 |
| 9 | 2.0700 ⁻ 03 | 3.2468 ⁺ 01 | NM | 0.91862 | 0.53845 | 0.89966 | 2.79161 | 0.32227 |
| 10 | 2.2702 ⁻ 03 | 3.6171 ⁺ 01 | NM | 0.93871 | 0.56876 | 0.91745 | 2.60200 | 0.35259 |
| 11 | 2.4502 ⁻ 03 | 3.7361 ⁺ 01 | NM | 0.92671 | 0.57816 | 0.91382 | 2.49819 | 0.36579 |
| 12 | 2.4797 ⁻ 03 | 3.8273 ⁺ 01 | NM | 0.94251 | 0.58526 | 0.92323 | 2.48842 | 0.37101 |
| 13 | 2.5200 ⁻ 03 | 3.9484 ⁺ 01 | NM | 0.94181 | 0.59456 | 0.92498 | 2.42031 | 0.38217 |
| 14 | 2.5798 ⁻ 03 | 4.1156 ⁺ 01 | NM | 0.92701 | 0.60716 | 0.92036 | 2.29779 | 0.40054 |
| 15 | 2.7698 ⁻ 03 | 4.2671 ⁺ 01 | NM | 0.94691 | 0.61836 | 0.93248 | 2.27400 | 0.41006 |
| 16 | 3.0499 ⁻ 03 | 4.9552 ⁺ 01 | NM | 0.95321 | 0.66687 | 0.94437 | 2.00544 | 0.47091 |
| 17 | 3.1997 ⁻ 03 | 5.3271 ⁺ 01 | NM | 0.96071 | 0.69167 | 0.95198 | 1.89433 | 0.50254 |
| 18 | 3.2897 ⁻ 03 | 5.5758 ⁺ 01 | NM | 0.97540 | 0.70777 | 0.96158 | 1.84581 | 0.52095 |
| 19 | 3.5201 ⁻ 03 | 5.9653 ⁺ 01 | NM | 0.95891 | 0.73227 | 0.95670 | 1.70690 | 0.56049 |
| 20 | 3.7001 ⁻ 03 | 6.3363 ⁺ 01 | NM | 0.97161 | 0.75488 | 0.96582 | 1.63696 | 0.59001 |
| 21 | 3.9902 ⁻ 03 | 7.1741 ⁺ 01 | NM | 0.96431 | 0.80358 | 0.96748 | 1.44951 | 0.66745 |
| 22 | 4.1998 ⁻ 03 | 7.8921 ⁺ 01 | NM | 0.95611 | 0.84308 | 0.96703 | 1.31563 | 0.73503 |
| 23 | 4.3603 ⁻ 03 | 8.2213 ⁺ 01 | NM | 0.97261 | 0.86059 | 0.97683 | 1.28838 | 0.75818 |
| 24 | 5.2798 ⁻ 03 | 1.0042 ⁺ 02 | NM | 0.97560 | 0.95160 | 0.98490 | 1.07122 | 0.91942 |
| 25 | 6.1200 ⁻ 03 | 1.0706 ⁺ 02 | NM | 0.97431 | 0.98270 | 0.98610 | 1.00694 | 0.97930 |
| 26 | 6.3598 ⁻ 03 | 1.0660 ⁺ 02 | NM | 1.00230 | 0.98060 | 1.00005 | 1.04006 | 0.96153 |
| 27 | 7.0502 ⁻ 03 | 1.1029 ⁺ 02 | NM | 0.99650 | 0.99750 | 0.99811 | 1.00123 | 0.99689 |
| 28 | 7.3699 ⁻ 03 | 1.1049 ⁺ 02 | NM | 0.99630 | 0.99840 | 0.99806 | 0.99932 | 0.99874 |
| D 29 | 8.2202 ⁻ 03 | 1.1084 ⁺ 02 | NM | 1.00000 | 1.00000 | 1.00000 | 1.00000 | 1.00000 |
| 30 | 1.0020 ⁻ 02 | 1.1191 ⁺ 02 | NM | 0.99950 | 1.00480 | 1.00001 | 0.99049 | 1.00961 |

INPUT VARIABLES Y,M/MD,TO/TOD ASSUME P=PD

| 7903S0203 | | BARTLETT/E/H/H | | PROFILE TABULATION | | 63 POINTS, DELTA AT POINT 61 | | |
|-----------|-----------------------|-----------------------|------|--------------------|---------|------------------------------|---------|-----------|
| I | Y | PT2/P | P/PD | TO/TOD | M/MD | U/UD | T/TD | R/RD*U/UD |
| 1 | 0.0000 ⁺⁰⁰ | 1.0000 ⁺⁰⁰ | NM | 0.28616 | 0.00000 | 0.00000 | 5.22023 | 0.00000 |
| 2 | 6.2992 ⁻⁰⁴ | 8.6468 ⁺⁰⁰ | NM | 0.67987 | 0.27127 | 0.63424 | 5.46649 | 0.11602 |
| 3 | 6.5028 ⁻⁰⁴ | 8.5989 ⁺⁰⁰ | NM | 0.62886 | 0.27047 | 0.60919 | 5.07305 | 0.12008 |
| 4 | 7.2982 ⁻⁰⁴ | 8.4089 ⁺⁰⁰ | NM | 0.70667 | 0.26728 | 0.64238 | 5.77631 | 0.11121 |
| 5 | 8.0013 ⁻⁰⁴ | 8.8094 ⁺⁰⁰ | NM | 0.75338 | 0.27396 | 0.67054 | 5.99069 | 0.11193 |
| 6 | 9.8975 ⁻⁰⁴ | 1.1249 ⁺⁰¹ | NM | 0.77098 | 0.31156 | 0.71457 | 5.26029 | 0.13584 |
| 7 | 1.1701 ⁻⁰³ | 1.4267 ⁺⁰¹ | NM | 0.81558 | 0.35255 | 0.76704 | 4.73364 | 0.16204 |
| 8 | 1.3496 ⁻⁰³ | 1.7348 ⁺⁰¹ | NM | 0.83088 | 0.38995 | 0.79772 | 4.18494 | 0.19062 |
| 9 | 1.5503 ⁻⁰³ | 1.8515 ⁺⁰¹ | NM | 0.86229 | 0.40321 | 0.82001 | 4.13596 | 0.19826 |
| 10 | 1.5697 ⁻⁰³ | 1.8631 ⁺⁰¹ | NM | 0.89169 | 0.40451 | 0.83458 | 4.25679 | 0.19606 |
| 11 | 1.7704 ⁻⁰³ | 2.0306 ⁺⁰¹ | NM | 0.85699 | 0.42276 | 0.82737 | 3.83018 | 0.21601 |
| 12 | 1.8204 ⁻⁰³ | 2.0344 ⁺⁰¹ | NM | 0.86519 | 0.42316 | 0.83152 | 3.86133 | 0.21534 |
| 13 | 1.8500 ⁻⁰³ | 2.0362 ⁺⁰¹ | NM | 0.85769 | 0.42336 | 0.82800 | 3.82513 | 0.21646 |
| 14 | 1.9804 ⁻⁰³ | 2.1110 ⁺⁰¹ | NM | 0.90149 | 0.43124 | 0.85266 | 3.90953 | 0.21810 |
| 15 | 2.0396 ⁻⁰³ | 2.1676 ⁺⁰¹ | NM | 0.88969 | 0.43712 | 0.84977 | 3.77920 | 0.22485 |
| 16 | 2.1599 ⁻⁰³ | 2.2635 ⁺⁰¹ | NM | 0.87399 | 0.44689 | 0.84651 | 3.58804 | 0.23593 |
| 17 | 2.3199 ⁻⁰³ | 2.3727 ⁺⁰¹ | NM | 0.89499 | 0.45776 | 0.86118 | 3.53920 | 0.24333 |
| 18 | 2.3402 ⁻⁰³ | 2.3960 ⁺⁰¹ | NM | 0.91179 | 0.46006 | 0.87017 | 3.57749 | 0.24323 |
| 19 | 2.3597 ⁻⁰³ | 2.4195 ⁺⁰¹ | NM | 0.89179 | 0.46235 | 0.86149 | 3.47177 | 0.24814 |
| 20 | 2.3902 ⁻⁰³ | 2.4555 ⁺⁰¹ | NM | 0.90589 | 0.46584 | 0.86966 | 3.48512 | 0.24953 |
| 21 | 2.4697 ⁻⁰³ | 2.5428 ⁺⁰¹ | NM | 0.92809 | 0.47422 | 0.88352 | 3.47114 | 0.25453 |
| 22 | 2.6797 ⁻⁰³ | 2.7256 ⁺⁰¹ | NM | 0.93969 | 0.49127 | 0.89531 | 3.32121 | 0.26957 |
| 23 | 2.7001 ⁻⁰³ | 2.7430 ⁺⁰¹ | NM | 0.92639 | 0.49287 | 0.88950 | 3.25711 | 0.27310 |
| 24 | 2.7102 ⁻⁰³ | 2.7528 ⁺⁰¹ | NM | 0.91729 | 0.49377 | 0.88543 | 3.21565 | 0.27535 |
| 25 | 2.8601 ⁻⁰³ | 2.9396 ⁺⁰¹ | NM | 0.95830 | 0.51052 | 0.91067 | 3.18199 | 0.28620 |
| 26 | 2.8999 ⁻⁰³ | 2.9634 ⁺⁰¹ | NM | 0.92939 | 0.51262 | 0.89750 | 3.06540 | 0.29278 |
| 27 | 3.0497 ⁻⁰³ | 3.0548 ⁺⁰¹ | NM | 0.92479 | 0.52059 | 0.89775 | 2.97380 | 0.30189 |
| 28 | 3.0997 ⁻⁰³ | 3.0849 ⁺⁰¹ | NM | 0.92279 | 0.52319 | 0.89756 | 2.94316 | 0.30497 |
| 29 | 3.2310 ⁻⁰³ | 3.1971 ⁺⁰¹ | NM | 0.93819 | 0.53276 | 0.90785 | 2.90378 | 0.31264 |
| 30 | 3.3096 ⁻⁰³ | 3.2243 ⁺⁰¹ | NM | 0.91589 | 0.53506 | 0.89765 | 2.81459 | 0.31893 |
| 31 | 3.4502 ⁻⁰³ | 3.3728 ⁺⁰¹ | NM | 0.93409 | 0.54742 | 0.90995 | 2.76309 | 0.32933 |
| 32 | 3.4697 ⁻⁰³ | 3.4044 ⁺⁰¹ | NM | 0.95310 | 0.55001 | 0.91987 | 2.79704 | 0.32887 |
| 33 | 3.4798 ⁻⁰³ | 3.4203 ⁺⁰¹ | NM | 0.91489 | 0.55131 | 0.90158 | 2.67433 | 0.33712 |
| 34 | 3.4900 ⁻⁰³ | 3.4362 ⁺⁰¹ | NM | 0.94299 | 0.55261 | 0.91567 | 2.74563 | 0.33350 |
| 35 | 3.5104 ⁻⁰³ | 3.4570 ⁺⁰¹ | NM | 0.90309 | 0.55430 | 0.89652 | 2.61593 | 0.34272 |
| 36 | 3.7703 ⁻⁰³ | 3.6840 ⁺⁰¹ | NM | 0.95420 | 0.57245 | 0.92614 | 2.61740 | 0.35384 |
| 37 | 3.9497 ⁻⁰³ | 3.9078 ⁺⁰¹ | NM | 0.94419 | 0.58981 | 0.92532 | 2.46127 | 0.37595 |
| 38 | 4.1098 ⁻⁰³ | 3.9945 ⁺⁰¹ | NM | 0.94799 | 0.59639 | 0.92863 | 2.42453 | 0.38102 |
| 39 | 4.3697 ⁻⁰³ | 4.4102 ⁺⁰¹ | NM | 0.97920 | 0.62701 | 0.95016 | 2.29640 | 0.41376 |
| 40 | 4.4400 ⁻⁰³ | 4.5926 ⁺⁰¹ | NM | 0.95480 | 0.63997 | 0.94067 | 2.16051 | 0.43539 |
| 41 | 4.4696 ⁻⁰³ | 4.6894 ⁺⁰¹ | NM | 0.96175 | 0.64675 | 0.94532 | 2.13637 | 0.44249 |
| 42 | 4.6999 ⁻⁰³ | 4.9243 ⁺⁰¹ | NM | 0.97450 | 0.66291 | 0.95436 | 2.07261 | 0.46046 |
| 43 | 4.9996 ⁻⁰³ | 5.5166 ⁺⁰¹ | NM | 0.98140 | 0.70200 | 0.96384 | 1.88508 | 0.51130 |
| 44 | 5.1902 ⁻⁰³ | 5.7951 ⁺⁰¹ | NM | 0.96860 | 0.71966 | 0.95999 | 1.77942 | 0.53949 |
| 45 | 5.2300 ⁻⁰³ | 5.8638 ⁺⁰¹ | NM | 0.98140 | 0.72395 | 0.96688 | 1.78376 | 0.54205 |
| 46 | 5.4001 ⁻⁰³ | 6.0366 ⁺⁰¹ | NM | 0.97910 | 0.73462 | 0.96714 | 1.73324 | 0.55800 |
| 47 | 5.6897 ⁻⁰³ | 6.5429 ⁺⁰¹ | NM | 0.97650 | 0.76503 | 0.96953 | 1.60605 | 0.60367 |
| 48 | 5.7600 ⁻⁰³ | 6.5633 ⁺⁰¹ | NM | 0.97320 | 0.76623 | 0.96802 | 1.59608 | 0.60650 |
| 49 | 5.9598 ⁻⁰³ | 6.8861 ⁺⁰¹ | NM | 0.99010 | 0.78498 | 0.97847 | 1.55375 | 0.62975 |
| 50 | 6.6803 ⁻⁰³ | 8.3203 ⁺⁰¹ | NM | 0.99250 | 0.86337 | 0.98705 | 1.30702 | 0.75519 |
| 51 | 6.7904 ⁻⁰³ | 8.1397 ⁺⁰¹ | NM | 0.99530 | 0.85389 | 0.98764 | 1.33780 | 0.73826 |
| 52 | 6.9199 ⁻⁰³ | 8.8859 ⁺⁰¹ | NM | 0.99120 | 0.89239 | 0.98868 | 1.22745 | 0.80548 |
| 53 | 7.0596 ⁻⁰³ | 8.8978 ⁺⁰¹ | NM | 0.97410 | 0.89299 | 0.98016 | 1.20477 | 0.81357 |
| 54 | 7.4398 ⁻⁰³ | 9.8722 ⁺⁰¹ | NM | 0.99540 | 0.94086 | 0.99417 | 1.11653 | 0.89041 |
| 55 | 7.7302 ⁻⁰³ | 9.9327 ⁺⁰¹ | NM | 0.97880 | 0.94375 | 0.98603 | 1.09160 | 0.90329 |
| 56 | 7.7496 ⁻⁰³ | 1.0027 ⁺⁰² | NM | 0.99140 | 0.94824 | 0.99264 | 1.09585 | 0.90582 |
| 57 | 8.4203 ⁻⁰³ | 1.0849 ⁺⁰² | NM | 0.99230 | 0.98654 | 0.99539 | 1.01804 | 0.97776 |
| 58 | 8.8754 ⁻⁰³ | 1.0741 ⁺⁰² | NM | 0.99290 | 0.98155 | 0.99541 | 1.02844 | 0.96788 |
| 59 | 9.2796 ⁻⁰³ | 1.1164 ⁺⁰² | NM | 0.98380 | 1.00080 | 0.99191 | 0.98232 | 1.00977 |
| 60 | 1.0080 ⁻⁰² | 1.1087 ⁺⁰² | NM | 0.99010 | 0.99731 | 0.99489 | 0.99516 | 0.99973 |
| D 61 | 1.0420 ⁻⁰² | 1.1146 ⁺⁰² | NM | 1.00000 | 1.00000 | 1.00000 | 1.00000 | 1.00000 |
| 62 | 1.0990 ⁻⁰² | 1.1087 ⁺⁰² | NM | 0.99110 | 0.99731 | 0.99539 | 0.99616 | 0.99923 |
| 63 | 1.1390 ⁻⁰² | 1.1157 ⁺⁰² | NM | 1.01380 | 1.00050 | 1.00690 | 1.01285 | 0.99413 |

INPUT VARIABLES Y,M/MD,TO/TOD ASSUME P=PD
 AT I= 41 VALUES OF INPUT PROFILES WERE AVERAGED BECAUSE OF SAME Y

| | | |
|--|--|----------------|
| <p>axisymmetric</p>  | <p>M: 1.45 (upstream) R THETA x 10⁻³: 40-110 TW/TR: 1.0</p> | 8001 |
| | | SBLI-APG AW |
| <p>Axisymmetric blowdown tunnel. Running time up to one hour. D = 0.25, L = 2.7 m.</p> <p>PO: 0.14 (0.034-0.54) MN/m². TO: 283K. Air. RE/m x 10⁶: 21, (4-25) (upstream).</p> | | |
| <p>MATEER G.G., VIEGAS J.R., 1979. Effect of Mach and Reynolds numbers on a normal shock-wave/turbulent boundary-layer interaction. AIAA P-79-1052. And Mateer et al. (1976); private communications, Mateer G.G., Horstman C.C.</p> | | |

- 1 The test boundary layer was formed on the inner surface of a cylindrical duct of constant (0.248 m) diameter and 2.69 m long. The surface was honed to give a roughness less than 1.6 μm and plated. At the rear end of the duct a hollow cylindrical choke of varying cross-section was inserted and its position adjusted to give a suitable position for a normal shock in the test section. This was more than 1 m upstream of the choke and, by implication, greater than 1.6 m for the case studied here. The duct is essentially the test section used by Kussoy et al. (CAT 7802S) fitted with a nozzle designed to give a Mach number of about 1.5 at entry to the duct. X = 0 is defined as the start of the initial pressure rise through the shock. The first profile measured extends well into the core flow and shows Mach number variations of about 1%. An axial Mach number gradient of $-0.074/\text{m}$ existed in the tube. No information on trips is given, but RE THETA at the first station is 40×10^3 so that the flow may be presumed to be fully turbulent. The test layer has passed through the expansion field of the nozzle but on the evidence of the first profile has not relaxed to equilibrium characteristics in the outer region.
- 2
- 3
- 4
- 6 Static pressure was measured by tappings 0.5 mm in diameter (E) "at intervals of 25.4 mm in the upstream portions and 50.8 mm in the downstream portions." Measurements were also made on the opposite diameter at a number of stations to check flow symmetry. "Instrumentation ports were located on a line at seven positions along the tube and at 45° from the static tap line. Buried wire surface-shear gauges were used to measure the wall shear stress. These appear (E) to be the same as, or at least similar to, those used by Kussoy et al. (CAT 7802S). Preston tube measurements were also made. A surface flow direction indicator was used to detect separation. This consisted of three thin films mounted on the surface, across the flow, one after the other in the mean flow direction. The central film was heated, and the local flow direction shown by a rise in temperature of the, unheated, film which is locally downstream of the hot film. This was calibrated in a step flow. The number of CF values and of flow direction readings is very much greater than the number of ports. These readings were obtained as a function of X by altering the position of the shock, using fixed instrumentation. The profiles were measured at the seven ports with a fixed shock position (E).
- 5
- 7 Pitot, total temperature static pressure and turbulence profiles were measured. The probe in use was supported on the downstream side by a slotted strut extending 100 mm into the flow, with the probe tip 50 mm ahead of the strut. The FPP used was constructed of 1.6 mm tube flattened to give a rectangular tip for which $h_2 = 0.076$, $b_2 = 1.0$ mm. The temperature probe was a FWP as proposed by Vas (1972). Static pressures were measured with a wedge probe made by flattening 1.6 mm tube to give a wedge tip of total included angle 12.5°. Static tappings (d = 0.25 mm) were drilled in each face of the wedge 1.6 mm back from the tip. The probe was calibrated in the undisturbed boundary layer upstream of the shock. Turbulence measurements were made using a supported X-probe of the type described by Mikulla & Horstman (1976).
- 9 Mean flow data are the average of 10 to 15 measurements for each Y position. (This is probably true for the Pitot measurements only - E). "Additional surveys indicate that the static pressure was equal to the wall pressure and that the total temperature was constant throughout the flow." These results may have been assumed in the original data reduction, but see §15 below.

- 12 The editors have presented the data as received from the authors with the exception of a further profile at $X = 1.60$ m, for which we received no wall data. We have set the wall temperature at the recovery temperature with $r = 0.896$. We have moved the D-state out to higher Y values on the basis of the total pressure profiles (see §15 below).
- 13 The profiles form a single set, profile 0101 being upstream of the shock which lies ahead of profile 0102. The complete wall data for this case are given in Table 1, Sect. D. Data for various other cases, at constant shock Mach number for a range of free stream unit Reynolds numbers, and at constant free stream Reynolds number for a range of shock Mach numbers may be found presented graphically in the source paper. These data are also presented in tabular form as cases A-G in the working papers for the 1981 Stanford meeting on calculation of turbulent flows.
- § DATA 8001 0101-0107. Pitot, (T_0), (static pressure) and cross-wire Reynolds shear stress profiles. $NX = 7$. CF from embedded wire gauges (and Preston tubes).
- 15 Editors' comments. The principal value of this study lies in the provision of seven successive Reynolds shear-stress profiles measured with a device analogous to a pair crossed hot wires. These are coupled to mean flow profiles which present certain difficulties of interpretation.

Firstly, there is the question of whether there is a separation bubble or not. Although one is sketched in a paper discussing these data by Coakley, Viegas & Horstman (1977), Mateer and Viegas (1979) consider that it did not occur. It is difficult to match the cases discussed in that paper to the data here, but if their opinion, based on the flow direction indicator results is accepted, while separation is incipient, it has not happened. G.G. Mateer (private communication) considers that the separation gauge results in Mateer et al. (1976) should be disregarded.

The development of some principal flow parameters is shown in Fig. 1. Profile 01 is nominally upstream of the interaction and represents the undisturbed flow. The shock occurs somewhere between 01 and 02. The changes in POD and PW that would be predicted for one-dimensional flow are shown by arrows labelled NS. The POD values will be discussed further below, but the general level of change is consistent with that expected in a one-dimensional normal shock. The PW value, however, as is usual in shock-boundary layer interactions, rises relatively slowly and does not reach, or tend to, the one-dimensional value. This is the consequence of the marked growth in boundary layer thickness, shown also by the curve for D1, which causes a constriction of the subsonic flow behind the shock. The Mach number is therefore higher, and the pressure lower, than for an isentropic one-dimensional flow. The changes in direction, and position, of the displacement surface also cause the shock, a single near-plane surface on the axis, to split into two or more branches near the wall. In this region the total pressure loss is not so great as in the normal shock.

The total pressure profiles for $Y > 30$ mm are shown in Fig. 2. Profile 01, in nominally undisturbed flow, shows little scatter, but in the free stream, shows a systematic variation which suggests the presence of a residual nozzle wave structure. In preparing the figure, the static pressure was assumed constant, but it seems likely that the variation seen here is due to static pressure changes rather than non-uniform total pressure. The downstream profiles show much more scatter (the authors remark on a $\pm 5\%$ variation in Pitot readings in the boundary layer), and all show a total pressure maximum in the range $50 < Y < 60$, with a marked fall as Y increases to the highest values measured at approximately $Y = 100$ mm. The profiles do not, in the range of measurement, show any tendency to a constant value for high Y , but do reach or fall below values characteristic of those behind a normal shock. This is shown more clearly in Fig. 3, presenting the POD curve of Fig. 1 to a much enlarged scale. There is an error band for profile 01, corresponding to the free stream variation, and this results in an error band for the value behind a normal shock, shown hatched. The point values shown downstream represent the highest values recorded and are in all cases significantly above the value for a normal shock. They are probably uncharacteristically high because of the scatter in the data (see Fig. 2), but even with this taken into account confirm the presence of a wall-jet-like flow, with a high total pressure region which has passed through a number of oblique shocks merging on one side with the boundary layer and on the other with the low total

pressure flow which has traversed the normal shock. The gradient observed at high Y is probably more due to time averaging as the shocks move than to any strong mixing at a slip surface springing from the shock intersection.

The data for profile 02 do not extend out into this region, so that in Fig. 3 no arrow showing the extent of the fall in total pressure is shown. For the other profiles, the trend seen in Fig. 2 suggests that they have not reached a final P_0 minimum by $Y = 100$ mm, but if there is a change in the trend at or near this Y value it could easily be obscured by the scatter in the data. If large fluctuations of the normal shock are present, then a low P_0 value might well result. The total pressure loss in a shock is a nonlinear function of shock Mach number, so that an oscillating shock may cause a greater mean total pressure loss than a stationary shock with the same mean Mach number.

The wall shear stress variation shown in Fig. 1 has very little scatter and probably represents a fit of some kind. The earlier results, using Preston tubes (Mateer et al. 1976, Fig. 9) show a marked spread in values. The general picture of a flow with an embedded high total pressure region is further born out by the shear stress profiles, which are presented in §4.5 of the main text. The shear stress reverses sign in all the profiles, including the first (at low levels in the outer region, where this may be an instrumental effect). The sign reversal in profiles 03-07 is not precisely positioned, as there are very large gaps in all profiles except 07. The P_0 maximum lies between the readings for which the sign change occurs, except for 07 where the gap is smaller and the sign change occurs near the maximum in terms of P_0 but substantially closer to the wall in terms of Y . The fairly constant maximum value for P_0 in profiles 04-07 suggests that outwards diffusing shear from the wall has not yet met inwards diffusing shear from the slip surface and that this is therefore an appropriate D-state for the 'boundary layer'.

We assume a flow of wall-jet character in discussing the profiles. Profile 01 is nominally upstream of the interaction, and fits the wall law (Fig. 4) very well for a full decade. The wake component is uncharacteristically weak. This may be a history effect as (E) the profile is probably quite close to the nozzle exit plane. If there are oscillations, this profile should not be affected as it is in a supersonic region. The profiles downstream (we have not plotted 02 as the CF value is our own estimate) do not initially appear to relate to the wall very well. If their position is ignored, however, they all appear to have well defined inner, semilog-law, regions with large wake components leaving at about $y/\delta = 0.1$. It would be easy to obtain a convincing Coles wall-and-wake fit with a CF value about 30% lower than the reported measured value. The buried wire skin-friction gauges used in the experiment are sublayer devices and so should not be strongly affected by pressure gradients, which are in any case quite modest for profiles 03-07. The gauges are however heat transfer devices and so likely to be much affected by oscillating flow. We consider the high apparent shear stress a further indicator of oscillation, and suspect that, particularly with the very high Reynolds number in this case, a wall-and-wake value might well be more representative. The very large wake components are then a result of, firstly, a low $TAUW$ value associated with the adverse pressure gradient, and secondly high U values in consequence of the P_0 values in the "jet".

The data as received by the editors were in the form of profiles of velocity and density. When processed, the resulting total temperature profiles generally show departures of about 1% from the author's implied assumption of constant T_0 , with higher excursions of 3% in profile 05 and 8% in 02. It is not clear whether these represent scattered measurements or some as yet unexplained interaction in the data reduction procedure. In particular, for profile 02, the assumption of constant static pressure may be doubtful and cause these differences to appear.

We feel that the data presented here describe a very interesting case, but that it would be unwise to base any argument on results which need to be known at the 5% level or better. The overall pattern seems clear, but many minor discrepancies remain. More generally, it seems probable that there is a high level of unsteadiness which is related to shock wave fluctuation rather than to turbulence as such. Our feeling is that calculations using this flow as a test case should not commence before profile 03, as there are insufficient data to fix the details of the shock interaction and no CF value for 02. We feel also that

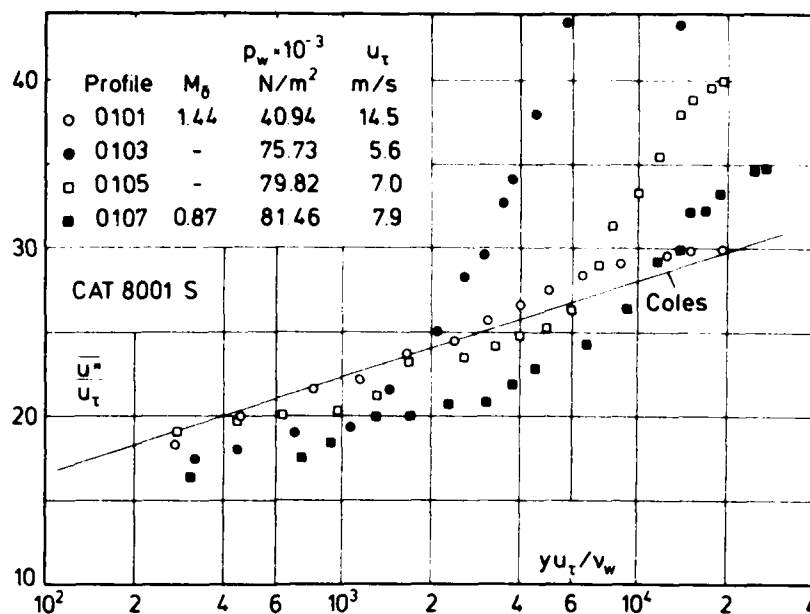


Fig. 4 Law of the wall for a transonic turbulent boundary layer with shock interaction (adiabatic wall, origin not defined $0.9 < M_0 < 1.44$). (Mateer & Viegas 1980).

| CAT 8001S | | MATEER | | BOUNDARY CONDITIONS AND EVALUATED DATA. SI UNITS | | | | | |
|--------------|-------------|-------------|-------------|--|---------|-------------|-------------|-------------|--|
| RUN | MD | TW/TR* | RED2W | CF | H12 | H12K | PW* | PD | |
| X * | POD | PW/PD* | RED2D | CO | H32 | H32K | TW | ID* | |
| RZ * | TOD | TAUW * | DZ | PI2 | H42 | D2K | UD* | TR | |
| 8001S0101 | 1.4378 | 1.0000 | 3.0484**+04 | 1.8060**-03 | 1.6099 | 1.3788 | 4.0935**+04 | 4.0935**+04 | |
| 0.0000**+00 | 1.3743**+05 | 1.0000 | 3.9369**+04 | NM | 1.8593 | 1.8545 | 2.7990**+02 | 2.0424**+02 | |
| -1.2385**-01 | 2.8868**+02 | 1.0698**+02 | 1.8601**-03 | NM | 0.4370 | 1.9754**-03 | 4.1197**+02 | 2.7990**+02 | |
| 8001S0102 | 1.0574 | 1.0000 | 6.0742**+04 | NM | 3.2004 | 2.0631 | 6.5496**+04 | 6.5496**+04 | |
| 1.0160**-01 | 1.3273**+05 | 1.0000 | 7.0423**+04 | NM | 1.6239 | 1.6155 | 2.6466**+02 | 2.2048**+02 | |
| -1.2385**-01 | 2.6978**+02 | NM | 3.1316**-03 | NM | -0.2833 | 3.7078**-03 | 3.1480**+02 | 2.6466**+02 | |
| 8001S0103 | 0.9561 | 1.0000 | 8.6861**+04 | 6.1002**-04 | 2.4572 | 1.9370 | 7.5730**+04 | 7.5730**+04 | |
| 2.0320**-01 | 1.3630**+05 | 1.0000 | 9.8004**+04 | NM | 1.6549 | 1.6457 | 2.8137**+02 | 2.4177**+02 | |
| -1.2385**-01 | 2.8597**+02 | 2.9560**+01 | 4.7070**-03 | NM | 0.0143 | 5.2357**-03 | 2.9806**+02 | 2.8137**+02 | |
| 8001S0104 | 0.9053 | 1.0000 | 9.4118**+04 | 9.6795**-04 | 2.1907 | 1.7065 | 7.8596**+04 | 7.8596**+04 | |
| 3.0480**-01 | 1.3370**+05 | 1.0000 | 1.0498**+05 | NM | 1.6782 | 1.6747 | 2.7708**+02 | 2.4160**+02 | |
| -1.2385**-01 | 2.8120**+02 | 4.3647**+01 | 5.1261**-03 | NM | -0.0174 | 5.6431**-03 | 2.8214**+02 | 2.7708**+02 | |
| 8001S0105 | 0.8898 | 1.0000 | 9.8308**+04 | 1.1411**-03 | 2.0434 | 1.6092 | 7.9824**+04 | 7.9824**+04 | |
| 3.5560**-01 | 1.3353**+05 | 1.0000 | 1.0931**+05 | NM | 1.7095 | 1.7078 | 2.7331**+02 | 2.3935**+02 | |
| -1.2385**-01 | 2.7725**+02 | 5.0484**+01 | 5.2815**-03 | NM | -0.0061 | 5.7495**-03 | 2.7601**+02 | 2.7331**+02 | |
| 8001S0106 | 0.8733 | 1.0000 | 9.8696**+04 | 1.3331**-03 | 1.9257 | 1.5665 | 8.0643**+04 | 8.0643**+04 | |
| 4.0640**-01 | 1.3254**+05 | 1.0000 | 1.0932**+05 | NM | 1.7238 | 1.7227 | 2.7417**+02 | 2.4121**+02 | |
| -1.2385**-01 | 2.7800**+02 | 5.7386**+01 | 5.3821**-03 | NM | 0.0233 | 5.7732**-03 | 2.7193**+02 | 2.7417**+02 | |
| 8001S0107 | 0.8705 | 1.0000 | 9.9778**+04 | 1.5037**-03 | 1.9515 | 1.5275 | 8.1461**+04 | 8.1461**+04 | |
| 4.5720**-01 | 1.3349**+05 | 1.0000 | 1.1047**+05 | NM | 1.7435 | 1.7420 | 2.7241**+02 | 2.3984**+02 | |
| -1.2385**-01 | 2.7619**+02 | 6.4974**+01 | 5.3609**-03 | NM | -0.0207 | 5.7900**-03 | 2.7029**+02 | 2.7241**+02 | |

TRAPEZOIDAL RULE FOR ALL INTEGRATIONS

| I | Y | PT2/P | P/PD | TO/TOD | M/MD | U/UD | T/TD | R/RD*U/UD |
|------|------------------------|------------------------|------|---------|---------|---------|---------|-----------|
| 1 | 0.0000 ⁺ 00 | 1.0000 ⁺ 00 | NM | 0.98393 | 0.00000 | 0.00000 | 1.16380 | 0.00000 |
| 2 | 1.0700 ⁻ 03 | 1.0600 ⁺ 00 | NM | 1.01172 | 0.30305 | 0.32877 | 1.17692 | 0.27934 |
| 3 | 1.4800 ⁻ 03 | 1.0632 ⁺ 00 | NM | 1.01180 | 0.31075 | 0.33699 | 1.17602 | 0.28655 |
| 4 | 1.9200 ⁻ 03 | 1.0722 ⁺ 00 | NM | 1.01661 | 0.33184 | 0.36027 | 1.17874 | 0.30564 |
| 5 | 2.3300 ⁻ 03 | 1.0709 ⁺ 00 | NM | 1.01939 | 0.32881 | 0.35753 | 1.18238 | 0.30239 |
| 6 | 2.7500 ⁻ 03 | 1.0740 ⁺ 00 | NM | 1.02380 | 0.33578 | 0.36575 | 1.18651 | 0.30826 |
| 7 | 3.1700 ⁻ 03 | 1.0725 ⁺ 00 | NM | 1.02139 | 0.33233 | 0.36164 | 1.18421 | 0.30539 |
| 8 | 3.5900 ⁻ 03 | 1.0734 ⁺ 00 | NM | 1.01692 | 0.33436 | 0.36301 | 1.17874 | 0.30797 |
| 9 | 4.0000 ⁻ 03 | 1.0803 ⁺ 00 | NM | 1.01957 | 0.34937 | 0.37945 | 1.17965 | 0.32167 |
| 10 | 4.4300 ⁻ 03 | 1.0774 ⁺ 00 | NM | 1.02590 | 0.34312 | 0.37397 | 1.18789 | 0.31482 |
| 11 | 4.7700 ⁻ 03 | 1.0840 ⁺ 00 | NM | 1.03412 | 0.35709 | 0.39041 | 1.19531 | 0.32662 |
| 12 | 4.8600 ⁻ 03 | 1.0923 ⁺ 00 | NM | 1.02043 | 0.37376 | 0.40548 | 1.17692 | 0.34453 |
| 13 | 5.2700 ⁻ 03 | 1.1055 ⁺ 00 | NM | 1.02551 | 0.39871 | 0.43288 | 1.17874 | 0.36724 |
| 14 | 5.7100 ⁻ 03 | 1.1083 ⁺ 00 | NM | 1.02548 | 0.40391 | 0.43836 | 1.17783 | 0.37217 |
| 15 | 6.1100 ⁻ 03 | 1.1288 ⁺ 00 | NM | 1.01446 | 0.43897 | 0.47260 | 1.15909 | 0.40774 |
| 16 | 6.5400 ⁻ 03 | 1.1011 ⁺ 00 | NM | 1.02042 | 0.39063 | 0.42329 | 1.17421 | 0.36049 |
| 17 | 6.9700 ⁻ 03 | 1.1255 ⁺ 00 | NM | 1.02135 | 0.43350 | 0.46849 | 1.16794 | 0.40113 |
| 18 | 7.3900 ⁻ 03 | 1.1316 ⁺ 00 | NM | 1.02371 | 0.44348 | 0.47945 | 1.16883 | 0.41020 |
| 19 | 7.8200 ⁻ 03 | 1.1275 ⁺ 00 | NM | 1.02421 | 0.43681 | 0.47260 | 1.17062 | 0.40372 |
| 20 | 8.2300 ⁻ 03 | 1.1407 ⁺ 00 | NM | 1.01289 | 0.45782 | 0.49178 | 1.15385 | 0.42621 |
| 21 | 8.6500 ⁻ 03 | 1.1647 ⁺ 00 | NM | 1.01360 | 0.49355 | 0.52877 | 1.14779 | 0.46068 |
| 22 | 9.0800 ⁻ 03 | 1.1731 ⁺ 00 | NM | 1.02025 | 0.50520 | 0.54247 | 1.15298 | 0.47049 |
| 23 | 9.5000 ⁻ 03 | 1.1645 ⁺ 00 | NM | 1.02042 | 0.49316 | 0.53014 | 1.15559 | 0.45876 |
| 24 | 9.9200 ⁻ 03 | 1.1811 ⁺ 00 | NM | 1.01918 | 0.51618 | 0.55342 | 1.14951 | 0.48144 |
| 25 | 1.0340 ⁻ 02 | 1.2002 ⁺ 00 | NM | 1.01170 | 0.54112 | 0.57671 | 1.13586 | 0.50773 |
| 26 | 1.0770 ⁻ 02 | 1.2125 ⁺ 00 | NM | 1.01994 | 0.55638 | 0.59452 | 1.14179 | 0.52069 |
| 27 | 1.1190 ⁻ 02 | 1.2022 ⁺ 00 | NM | 1.01746 | 0.54356 | 0.58082 | 1.14179 | 0.50869 |
| 28 | 1.1620 ⁻ 02 | 1.2269 ⁺ 00 | NM | 1.01206 | 0.57367 | 0.60959 | 1.12915 | 0.53986 |
| 29 | 1.2030 ⁻ 02 | 1.2458 ⁺ 00 | NM | 1.00831 | 0.59541 | 0.63014 | 1.12006 | 0.56259 |
| 30 | 1.2450 ⁻ 02 | 1.2518 ⁺ 00 | NM | 1.00456 | 0.60212 | 0.63562 | 1.11435 | 0.57039 |
| 31 | 1.2890 ⁻ 02 | 1.2855 ⁺ 00 | NM | 1.00562 | 0.63794 | 0.67123 | 1.10709 | 0.60630 |
| 32 | 1.3930 ⁻ 02 | 1.2476 ⁺ 00 | NM | 1.00211 | 0.59737 | 0.63014 | 1.11273 | 0.56630 |
| 33 | 1.4980 ⁻ 02 | 1.3234 ⁺ 00 | NM | 0.99597 | 0.67521 | 0.70411 | 1.08742 | 0.64750 |
| 34 | 1.6020 ⁻ 02 | 1.3305 ⁺ 00 | NM | 0.99327 | 0.68192 | 0.70959 | 1.08280 | 0.65533 |
| 35 | 1.7080 ⁻ 02 | 1.3857 ⁺ 00 | NM | 0.98946 | 0.73099 | 0.75479 | 1.06620 | 0.70793 |
| 36 | 1.8130 ⁻ 02 | 1.3754 ⁺ 00 | NM | 0.99707 | 0.72213 | 0.74932 | 1.07671 | 0.69593 |
| 37 | 1.9190 ⁻ 02 | 1.4497 ⁺ 00 | NM | 0.99952 | 0.78249 | 0.80685 | 1.06324 | 0.75886 |
| 38 | 2.0250 ⁻ 02 | 1.4721 ⁺ 00 | NM | 0.99492 | 0.79936 | 0.82055 | 1.05372 | 0.77872 |
| 39 | 2.1310 ⁻ 02 | 1.5248 ⁺ 00 | NM | 0.99132 | 0.83709 | 0.85342 | 1.03940 | 0.82107 |
| 40 | 2.2370 ⁻ 02 | 1.5578 ⁺ 00 | NM | 0.98008 | 0.85936 | 0.86849 | 1.02136 | 0.85033 |
| 41 | 2.3430 ⁻ 02 | 1.5427 ⁺ 00 | NM | 0.99126 | 0.84928 | 0.86438 | 1.03588 | 0.83444 |
| 42 | 2.4480 ⁻ 02 | 1.6000 ⁺ 00 | NM | 0.99024 | 0.88664 | 0.89726 | 1.02410 | 0.87615 |
| 43 | 2.5540 ⁻ 02 | 1.6120 ⁺ 00 | NM | 0.99370 | 0.89416 | 0.90548 | 1.02547 | 0.88299 |
| 44 | 2.6580 ⁻ 02 | 1.6262 ⁺ 00 | NM | 0.99485 | 0.90289 | 0.91370 | 1.02410 | 0.89220 |
| 45 | 2.7630 ⁻ 02 | 1.6348 ⁺ 00 | NM | 0.99969 | 0.90813 | 0.92055 | 1.02754 | 0.89588 |
| 46 | 2.8690 ⁻ 02 | 1.6735 ⁺ 00 | NM | 0.99769 | 0.93109 | 0.93973 | 1.01864 | 0.92253 |
| 47 | 2.9730 ⁻ 02 | 1.6811 ⁺ 00 | NM | 0.99831 | 0.93547 | 0.94384 | 1.01796 | 0.92718 |
| 48 | 3.0790 ⁻ 02 | 1.6899 ⁺ 00 | NM | 0.99190 | 0.94056 | 0.94521 | 1.00990 | 0.93594 |
| 49 | 3.4290 ⁻ 02 | 1.7426 ⁺ 00 | NM | 0.99082 | 0.96986 | 0.96986 | 1.00000 | 0.96986 |
| 50 | 3.6400 ⁻ 02 | 1.7279 ⁺ 00 | NM | 0.99363 | 0.96186 | 0.96438 | 1.00526 | 0.95934 |
| 51 | 3.8510 ⁻ 02 | 1.7635 ⁺ 00 | NM | 0.99096 | 0.98105 | 0.97945 | 0.99674 | 0.98265 |
| 52 | 4.0600 ⁻ 02 | 1.7642 ⁺ 00 | NM | 0.99302 | 0.98146 | 0.98082 | 0.99869 | 0.98210 |
| 53 | 4.2710 ⁻ 02 | 1.7668 ⁺ 00 | NM | 0.99344 | 0.98283 | 0.98219 | 0.99869 | 0.98348 |
| 54 | 4.4820 ⁻ 02 | 1.7650 ⁺ 00 | NM | 0.99510 | 0.98187 | 0.98219 | 1.00065 | 0.98155 |
| 55 | 4.6940 ⁻ 02 | 1.7688 ⁺ 00 | NM | 0.99441 | 0.98388 | 0.98356 | 0.99935 | 0.98420 |
| 56 | 4.9060 ⁻ 02 | 1.7591 ⁺ 00 | NM | 0.99220 | 0.97872 | 0.97808 | 0.99869 | 0.97936 |
| 57 | 5.1140 ⁻ 02 | 1.7794 ⁺ 00 | NM | 0.99871 | 0.98944 | 0.99041 | 1.00196 | 0.98847 |
| 58 | 5.3250 ⁻ 02 | 1.8021 ⁺ 00 | NM | 1.00894 | 1.00120 | 1.00548 | 1.00857 | 0.99694 |
| D 59 | 5.5350 ⁻ 02 | 1.7997 ⁺ 00 | NM | 1.00000 | 1.00000 | 1.00000 | 1.00000 | 1.00000 |
| 60 | 5.7460 ⁻ 02 | 1.7927 ⁺ 00 | NM | 1.00346 | 0.99634 | 0.99863 | 1.00460 | 0.99406 |
| 61 | 5.9570 ⁻ 02 | 1.7882 ⁺ 00 | NM | 1.00738 | 0.99405 | 0.99863 | 1.00923 | 0.98949 |
| 62 | 6.1690 ⁻ 02 | 1.7909 ⁺ 00 | NM | 1.01049 | 0.99546 | 1.00137 | 1.01190 | 0.98959 |
| 63 | 6.3790 ⁻ 02 | 1.7824 ⁺ 00 | NM | 1.00710 | 0.99100 | 0.99589 | 1.00990 | 0.98613 |
| 64 | 6.5890 ⁻ 02 | 1.7623 ⁺ 00 | NM | 1.00318 | 0.98041 | 0.98493 | 1.00923 | 0.97592 |
| 65 | 6.8000 ⁻ 02 | 1.7779 ⁺ 00 | NM | 1.00838 | 0.98865 | 0.99452 | 1.01190 | 0.98282 |
| 66 | 7.0100 ⁻ 02 | 1.7694 ⁺ 00 | NM | 1.00500 | 0.98418 | 0.98904 | 1.00990 | 0.97934 |
| 67 | 7.2230 ⁻ 02 | 1.7673 ⁺ 00 | NM | 1.00136 | 0.98307 | 0.98630 | 1.00658 | 0.97985 |
| 68 | 7.4340 ⁻ 02 | 1.7664 ⁺ 00 | NM | 0.99662 | 0.98260 | 0.98356 | 1.00196 | 0.98163 |
| 69 | 7.6430 ⁻ 02 | 1.7351 ⁺ 00 | NM | 0.98959 | 0.96575 | 0.96575 | 1.00000 | 0.96575 |
| 70 | 7.8540 ⁻ 02 | 1.7415 ⁺ 00 | NM | 1.01724 | 0.96927 | 0.98219 | 1.02685 | 0.95651 |
| 71 | 8.0650 ⁻ 02 | 1.7340 ⁺ 00 | NM | 1.01326 | 0.96515 | 0.97671 | 1.02410 | 0.95373 |
| 72 | 8.2760 ⁻ 02 | 1.7355 ⁺ 00 | NM | 1.00610 | 0.96598 | 0.97397 | 1.01661 | 0.95806 |
| 73 | 8.4870 ⁻ 02 | 1.7431 ⁺ 00 | NM | 0.99874 | 0.97015 | 0.97397 | 1.00791 | 0.96633 |
| 74 | 8.6980 ⁻ 02 | 1.7028 ⁺ 00 | NM | 0.97600 | 0.94784 | 0.94384 | 0.99157 | 0.95186 |
| 75 | 8.9080 ⁻ 02 | 1.6850 ⁺ 00 | NM | 0.97689 | 0.93775 | 0.93562 | 0.99545 | 0.93990 |

INPUT VARIABLES Y,U/UD,RHO/RHOD ASSUME P=PD
 AT I= 6 VALUES OF INPUT PROFILES WERE AVERAGED BECAUSE OF SAME Y

| 8001S0104 | | MATEER | PROFILE TABULATION | | | 81 POINTS, DELTA AT POINT 63 | | | |
|-----------|------------------------|------------------------|--------------------|---------|---------|------------------------------|---------|-----------|--|
| I | Y | PT2/P | P/PD | T0/TOD | M/MD | U/UD | T/TD | R/RD*U/UD | |
| 1 | 0.0000 ⁺ 00 | 1.0000 ⁺ 00 | NM | 0.98535 | 0.00000 | 0.00000 | 1.14687 | 0.00000 | |
| 2 | 5.3000 ⁻ 04 | 1.1268 ⁺ 00 | NM | 1.12736 | 0.46006 | 0.51809 | 1.26816 | 0.40854 | |
| 3 | 9.0000 ⁻ 04 | 1.0990 ⁺ 00 | NM | 1.00467 | 0.40829 | 0.43560 | 1.13825 | 0.38269 | |
| 4 | 1.3100 ⁻ 03 | 1.1055 ⁺ 00 | NM | 1.00350 | 0.42110 | 0.44863 | 1.13500 | 0.39526 | |
| 5 | 1.7200 ⁻ 03 | 1.1091 ⁺ 00 | NM | 1.01021 | 0.42802 | 0.45731 | 1.14152 | 0.40061 | |
| 6 | 2.1400 ⁻ 03 | 1.1080 ⁺ 00 | NM | 1.01356 | 0.42590 | 0.45586 | 1.14564 | 0.39791 | |
| 7 | 2.5700 ⁻ 03 | 1.1125 ⁺ 00 | NM | 1.01327 | 0.43433 | 0.46454 | 1.14399 | 0.40607 | |
| 8 | 2.9900 ⁻ 03 | 1.1123 ⁺ 00 | NM | 1.01469 | 0.43401 | 0.46454 | 1.14564 | 0.40549 | |
| 9 | 3.4000 ⁻ 03 | 1.1191 ⁺ 00 | NM | 1.00272 | 0.44651 | 0.47467 | 1.13016 | 0.42001 | |
| 10 | 3.8300 ⁻ 03 | 1.1267 ⁺ 00 | NM | 1.00538 | 0.45995 | 0.48915 | 1.13096 | 0.43250 | |
| 11 | 4.2300 ⁻ 03 | 1.1220 ⁺ 00 | NM | 1.01065 | 0.45170 | 0.48191 | 1.13825 | 0.42338 | |
| 12 | 4.6700 ⁻ 03 | 1.1279 ⁺ 00 | NM | 1.00855 | 0.46202 | 0.49204 | 1.13419 | 0.43383 | |
| 13 | 5.0900 ⁻ 03 | 1.1147 ⁺ 00 | NM | 1.00732 | 0.43845 | 0.46744 | 1.13662 | 0.41125 | |
| 14 | 5.5100 ⁻ 03 | 1.1263 ⁺ 00 | NM | 1.00885 | 0.45914 | 0.48915 | 1.13500 | 0.43097 | |
| 15 | 5.9400 ⁻ 03 | 1.1278 ⁺ 00 | NM | 1.01509 | 0.46189 | 0.49349 | 1.14152 | 0.43231 | |
| 16 | 6.3600 ⁻ 03 | 1.1264 ⁺ 00 | NM | 1.01981 | 0.45937 | 0.49204 | 1.14729 | 0.42887 | |
| 17 | 6.7800 ⁻ 03 | 1.1543 ⁺ 00 | NM | 1.01090 | 0.50522 | 0.53690 | 1.12935 | 0.47541 | |
| 18 | 7.2000 ⁻ 03 | 1.1425 ⁺ 00 | NM | 1.01226 | 0.48648 | 0.51809 | 1.13419 | 0.45679 | |
| 19 | 7.6300 ⁻ 03 | 1.1496 ⁺ 00 | NM | 1.00050 | 0.49797 | 0.52677 | 1.11901 | 0.47075 | |
| 20 | 8.0500 ⁻ 03 | 1.1594 ⁺ 00 | NM | 1.00788 | 0.51312 | 0.54414 | 1.12455 | 0.48387 | |
| 21 | 8.4700 ⁻ 03 | 1.1698 ⁺ 00 | NM | 1.00266 | 0.52881 | 0.55861 | 1.11587 | 0.50061 | |
| 22 | 8.8900 ⁻ 03 | 1.1719 ⁺ 00 | NM | 0.99687 | 0.53186 | 0.56006 | 1.10886 | 0.50507 | |
| 23 | 9.3100 ⁻ 03 | 1.1656 ⁺ 00 | NM | 0.99952 | 0.52251 | 0.55137 | 1.11352 | 0.49516 | |
| 24 | 9.7400 ⁻ 03 | 1.1854 ⁺ 00 | NM | 1.00504 | 0.55112 | 0.58177 | 1.11431 | 0.52209 | |
| 25 | 1.0160 ⁻ 02 | 1.1704 ⁺ 00 | NM | 1.00990 | 0.52968 | 0.56151 | 1.12376 | 0.49967 | |
| 26 | 1.0590 ⁻ 02 | 1.1955 ⁺ 00 | NM | 1.00677 | 0.56503 | 0.59624 | 1.11352 | 0.53545 | |
| 27 | 1.1000 ⁻ 02 | 1.2050 ⁺ 00 | NM | 1.00764 | 0.57777 | 0.60926 | 1.11197 | 0.54791 | |
| 28 | 1.1430 ⁻ 02 | 1.1969 ⁺ 00 | NM | 1.00501 | 0.56699 | 0.59768 | 1.11119 | 0.53788 | |
| 29 | 1.1850 ⁻ 02 | 1.2302 ⁺ 00 | NM | 1.00241 | 0.60998 | 0.63965 | 1.09965 | 0.58169 | |
| 30 | 1.2270 ⁻ 02 | 1.2261 ⁺ 00 | NM | 1.00491 | 0.60479 | 0.63531 | 1.10347 | 0.57574 | |
| 31 | 1.2690 ⁻ 02 | 1.2149 ⁺ 00 | NM | 1.00790 | 0.59074 | 0.62229 | 1.10964 | 0.56080 | |
| 32 | 1.3110 ⁻ 02 | 1.2312 ⁺ 00 | NM | 1.01244 | 0.61114 | 0.64399 | 1.11041 | 0.57996 | |
| 33 | 1.4160 ⁻ 02 | 1.2392 ⁺ 00 | NM | 1.00034 | 0.62093 | 0.64978 | 1.09511 | 0.59335 | |
| 34 | 1.5220 ⁻ 02 | 1.2727 ⁺ 00 | NM | 1.00799 | 0.65965 | 0.69030 | 1.09511 | 0.63035 | |
| 35 | 1.6270 ⁻ 02 | 1.3063 ⁺ 00 | NM | 1.01133 | 0.69565 | 0.72648 | 1.09060 | 0.66613 | |
| 36 | 1.7320 ⁻ 02 | 1.3049 ⁺ 00 | NM | 1.01521 | 0.69422 | 0.72648 | 1.09511 | 0.66339 | |
| 37 | 1.8380 ⁻ 02 | 1.3593 ⁺ 00 | NM | 1.00905 | 0.74785 | 0.77569 | 1.07583 | 0.72101 | |
| 38 | 1.9430 ⁻ 02 | 1.3548 ⁺ 00 | NM | 0.99329 | 0.74356 | 0.76556 | 1.06004 | 0.72220 | |
| 39 | 2.0490 ⁻ 02 | 1.3703 ⁺ 00 | NM | 0.99189 | 0.75797 | 0.77858 | 1.05511 | 0.73791 | |
| 40 | 2.1540 ⁻ 02 | 1.4137 ⁺ 00 | NM | 0.99615 | 0.79645 | 0.81621 | 1.05023 | 0.77717 | |
| 41 | 2.2600 ⁻ 02 | 1.4177 ⁺ 00 | NM | 0.99562 | 0.79980 | 0.81910 | 1.04884 | 0.78096 | |
| 42 | 2.3650 ⁻ 02 | 1.4245 ⁺ 00 | NM | 1.00362 | 0.80561 | 0.82779 | 1.05581 | 0.78403 | |
| 43 | 2.4710 ⁻ 02 | 1.4841 ⁺ 00 | NM | 1.00211 | 0.85348 | 0.87120 | 1.04197 | 0.83611 | |
| 44 | 2.5770 ⁻ 02 | 1.4674 ⁺ 00 | NM | 1.00615 | 0.84050 | 0.86107 | 1.04954 | 0.82043 | |
| 45 | 2.6830 ⁻ 02 | 1.4918 ⁺ 00 | NM | 0.99967 | 0.85942 | 0.87554 | 1.03788 | 0.84358 | |
| 46 | 2.7870 ⁻ 02 | 1.4937 ⁺ 00 | NM | 1.00003 | 0.86084 | 0.87699 | 1.03788 | 0.84498 | |
| 47 | 2.8930 ⁻ 02 | 1.5262 ⁺ 00 | NM | 0.99967 | 0.88502 | 0.89870 | 1.03115 | 0.87155 | |
| 48 | 2.9970 ⁻ 02 | 1.5396 ⁺ 00 | NM | 1.00609 | 0.89467 | 0.91027 | 1.03518 | 0.87934 | |
| 49 | 3.1030 ⁻ 02 | 1.5689 ⁺ 00 | NM | 1.00368 | 0.91530 | 0.92764 | 1.02715 | 0.90312 | |
| 50 | 3.2080 ⁻ 02 | 1.6157 ⁺ 00 | NM | 1.00306 | 0.94668 | 0.95514 | 1.01794 | 0.93831 | |
| 51 | 3.3140 ⁻ 02 | 1.5996 ⁺ 00 | NM | 0.99828 | 0.93611 | 0.94356 | 1.01598 | 0.92871 | |
| 52 | 3.4200 ⁻ 02 | 1.6205 ⁺ 00 | NM | 1.00328 | 0.94986 | 0.95803 | 1.01729 | 0.94175 | |
| 53 | 3.5250 ⁻ 02 | 1.6382 ⁺ 00 | NM | 1.00062 | 0.96122 | 0.96671 | 1.01146 | 0.95576 | |
| 54 | 3.6310 ⁻ 02 | 1.6489 ⁺ 00 | NM | 1.00633 | 0.96800 | 0.97540 | 1.01534 | 0.96067 | |
| 55 | 3.7360 ⁻ 02 | 1.6432 ⁺ 00 | NM | 1.00086 | 0.96441 | 0.96961 | 1.01081 | 0.95924 | |
| 56 | 3.8420 ⁻ 02 | 1.6754 ⁺ 00 | NM | 1.00070 | 0.98449 | 0.98698 | 1.00506 | 0.98201 | |
| 57 | 4.0920 ⁻ 02 | 1.6809 ⁺ 00 | NM | 0.99784 | 0.98780 | 0.98842 | 1.00126 | 0.98718 | |
| 58 | 4.2620 ⁻ 02 | 1.6846 ⁺ 00 | NM | 0.99098 | 0.99008 | 0.98698 | 0.99375 | 0.99319 | |
| 59 | 4.4720 ⁻ 02 | 1.6854 ⁺ 00 | NM | 1.00177 | 0.99057 | 0.99276 | 1.00442 | 0.98839 | |
| 60 | 4.6850 ⁻ 02 | 1.6904 ⁺ 00 | NM | 0.99946 | 0.99359 | 0.99421 | 1.00126 | 0.99296 | |
| 61 | 4.8950 ⁻ 02 | 1.6952 ⁺ 00 | NM | 1.00027 | 0.99648 | 0.99711 | 1.00126 | 0.99585 | |
| 62 | 5.1050 ⁻ 02 | 1.7046 ⁺ 00 | NM | 0.99933 | 1.00208 | 1.00145 | 0.99874 | 1.00271 | |
| 63 | 5.3160 ⁻ 02 | 1.7011 ⁺ 00 | NM | 1.00000 | 1.00000 | 1.00000 | 1.00000 | 1.00000 | |
| 64 | 5.5250 ⁻ 02 | 1.6928 ⁺ 00 | NM | 0.99986 | 0.99503 | 0.99566 | 1.00126 | 0.99441 | |
| 65 | 5.7360 ⁻ 02 | 1.6866 ⁺ 00 | NM | 0.99756 | 0.99132 | 0.99132 | 1.00000 | 0.99132 | |
| 66 | 5.9480 ⁻ 02 | 1.7124 ⁺ 00 | NM | 0.99438 | 1.00667 | 1.00289 | 0.99250 | 1.01047 | |
| 67 | 6.1600 ⁻ 02 | 1.7043 ⁺ 00 | NM | 0.98810 | 1.00190 | 0.99566 | 0.98757 | 1.00819 | |
| 68 | 6.3710 ⁻ 02 | 1.6921 ⁺ 00 | NM | 0.98608 | 0.99462 | 0.98842 | 0.98757 | 1.00086 | |
| 69 | 6.5790 ⁻ 02 | 1.6775 ⁺ 00 | NM | 0.99852 | 0.98573 | 0.98698 | 1.00252 | 0.98449 | |
| 70 | 6.7910 ⁻ 02 | 1.6739 ⁺ 00 | NM | 1.00234 | 0.98355 | 0.98698 | 1.00697 | 0.98014 | |
| 71 | 7.0020 ⁻ 02 | 1.6819 ⁺ 00 | NM | 1.01140 | 0.98843 | 0.99566 | 1.01469 | 0.98125 | |
| 72 | 7.2120 ⁻ 02 | 1.6816 ⁺ 00 | NM | 1.00877 | 0.98825 | 0.99421 | 1.01210 | 0.98232 | |
| 73 | 7.4240 ⁻ 02 | 1.6757 ⁺ 00 | NM | 1.00330 | 0.98468 | 0.98842 | 1.00761 | 0.98096 | |
| 74 | 7.6340 ⁻ 02 | 1.6851 ⁺ 00 | NM | 0.99919 | 0.99038 | 0.99132 | 1.00189 | 0.98945 | |
| 75 | 7.8450 ⁻ 02 | 1.6574 ⁺ 00 | NM | 0.99384 | 0.97334 | 0.97395 | 1.00126 | 0.97272 | |
| 76 | 8.0560 ⁻ 02 | 1.6448 ⁺ 00 | NM | 0.99607 | 0.96542 | 0.96816 | 1.00570 | 0.96268 | |
| 77 | 8.2680 ⁻ 02 | 1.6625 ⁺ 00 | NM | 1.01781 | 0.97653 | 0.98842 | 1.02450 | 0.96479 | |
| 78 | 8.4790 ⁻ 02 | 1.6630 ⁺ 00 | NM | 1.01136 | 0.97681 | 0.98553 | 1.01794 | 0.96816 | |
| 79 | 8.6890 ⁻ 02 | 1.6544 ⁺ 00 | NM | 0.99711 | 0.97150 | 0.97395 | 1.00506 | 0.96905 | |
| 80 | 8.9000 ⁻ 02 | 1.6328 ⁺ 00 | NM | 0.98588 | 0.95779 | 0.95658 | 0.99749 | 0.95899 | |
| 81 | 9.1110 ⁻ 02 | 1.6350 ⁺ 00 | NM | 0.98936 | 0.95918 | 0.95948 | 1.00063 | 0.95888 | |

INPUT VARIABLES Y,U/UD,RHD/RHDD ASSUME P=PD
 AT I= 41 VALUES OF INPUT PROFILES WERE AVERAGED BECAUSE OF SAME Y

| 8001S01G5 | | MATEER | | PROFILE TABULATION | | 83 POINTS, DELTA AT POINT 64 | | |
|-----------|------------------------|------------------------|------|--------------------|---------|------------------------------|---------|-----------|
| I | Y | PT2/P | P/PD | TO/TOD | M/MD | U/UD | T/TD | R/RD*U/UD |
| 1 | 0.0000 ⁺ 00 | 1.0000 ⁺ 00 | NM | 0.98578 | 0.00000 | 0.00000 | 1.14189 | 0.00000 |
| 2 | 6.7000 ⁻ 04 | 1.1183 ⁺ 00 | NM | 1.01749 | 0.45274 | 0.48373 | 1.14156 | 0.42374 |
| 3 | 1.0600 ⁻ 03 | 1.1290 ⁺ 00 | NM | 1.01527 | 0.47190 | 0.50296 | 1.13598 | 0.44275 |
| 4 | 1.5000 ⁻ 03 | 1.1338 ⁺ 00 | NM | 1.00460 | 0.48027 | 0.50888 | 1.12267 | 0.45327 |
| 5 | 1.9200 ⁻ 03 | 1.1544 ⁺ 00 | NM | 0.99674 | 0.51432 | 0.54142 | 1.10816 | 0.48857 |
| 6 | 2.3000 ⁻ 03 | 1.1379 ⁺ 00 | NM | 0.99945 | 0.48736 | 0.51479 | 1.11575 | 0.46139 |
| 7 | 2.7300 ⁻ 03 | 1.1586 ⁺ 00 | NM | 0.99980 | 0.52081 | 0.54882 | 1.11043 | 0.49424 |
| 8 | 3.1600 ⁻ 03 | 1.1522 ⁺ 00 | NM | 1.00440 | 0.51082 | 0.53994 | 1.11728 | 0.48326 |
| 9 | 3.5900 ⁻ 03 | 1.1517 ⁺ 00 | NM | 1.00772 | 0.50994 | 0.53994 | 1.12113 | 0.48160 |
| 10 | 4.0000 ⁻ 03 | 1.1844 ⁺ 00 | NM | 1.00887 | 0.55936 | 0.59024 | 1.11347 | 0.53009 |
| 11 | 4.4400 ⁻ 03 | 1.1528 ⁺ 00 | NM | 1.01217 | 0.51167 | 0.54290 | 1.12578 | 0.48224 |
| 12 | 4.8500 ⁻ 03 | 1.1670 ⁺ 00 | NM | 1.00599 | 0.53376 | 0.56361 | 1.11499 | 0.50548 |
| 13 | 5.2700 ⁻ 03 | 1.1691 ⁺ 00 | NM | 0.99967 | 0.53699 | 0.56509 | 1.10741 | 0.51028 |
| 14 | 5.7100 ⁻ 03 | 1.1504 ⁺ 00 | NM | 0.99371 | 0.50781 | 0.53402 | 1.10591 | 0.48288 |
| 15 | 6.1300 ⁻ 03 | 1.1902 ⁺ 00 | NM | 0.99130 | 0.56751 | 0.59320 | 1.09256 | 0.54294 |
| 16 | 6.5400 ⁻ 03 | 1.1787 ⁺ 00 | NM | 0.99658 | 0.55113 | 0.57840 | 1.10142 | 0.52514 |
| 17 | 6.9500 ⁻ 03 | 1.1659 ⁺ 00 | NM | 1.00160 | 0.53204 | 0.56065 | 1.11043 | 0.50490 |
| 18 | 7.3800 ⁻ 03 | 1.1692 ⁺ 00 | NM | 1.00447 | 0.53711 | 0.56657 | 1.11270 | 0.50918 |
| 19 | 7.8100 ⁻ 03 | 1.1995 ⁺ 00 | NM | 1.00770 | 0.58037 | 0.61095 | 1.10816 | 0.55131 |
| 20 | 8.2300 ⁻ 03 | 1.1961 ⁺ 00 | NM | 1.01310 | 0.57578 | 0.60799 | 1.11499 | 0.54529 |
| 21 | 8.6400 ⁻ 03 | 1.1980 ⁺ 00 | NM | 1.01914 | 0.57840 | 0.61243 | 1.12113 | 0.54626 |
| 22 | 9.0600 ⁻ 03 | 1.1859 ⁺ 00 | NM | 1.02181 | 0.56148 | 0.59615 | 1.12734 | 0.52882 |
| 23 | 9.5000 ⁻ 03 | 1.2079 ⁺ 00 | NM | 1.01873 | 0.59178 | 0.62574 | 1.11805 | 0.55967 |
| 24 | 9.9100 ⁻ 03 | 1.2092 ⁺ 00 | NM | 1.00864 | 0.59342 | 0.62426 | 1.10666 | 0.56410 |
| 25 | 1.0340 ⁻ 02 | 1.1948 ⁺ 00 | NM | 1.00452 | 0.57392 | 0.60355 | 1.10591 | 0.54575 |
| 26 | 1.0760 ⁻ 02 | 1.1854 ⁺ 00 | NM | 1.00430 | 0.56069 | 0.59024 | 1.10816 | 0.53263 |
| 27 | 1.1190 ⁻ 02 | 1.2087 ⁺ 00 | NM | 1.00580 | 0.59281 | 0.62278 | 1.10366 | 0.56429 |
| 28 | 1.1620 ⁻ 02 | 1.2206 ⁺ 00 | NM | 1.00861 | 0.60830 | 0.63905 | 1.10366 | 0.57903 |
| 29 | 1.2030 ⁻ 02 | 1.2262 ⁺ 00 | NM | 1.00927 | 0.61555 | 0.64645 | 1.10291 | 0.58613 |
| 30 | 1.2450 ⁻ 02 | 1.2203 ⁺ 00 | NM | 1.00514 | 0.60792 | 0.63757 | 1.09993 | 0.57965 |
| 31 | 1.2870 ⁻ 02 | 1.2252 ⁺ 00 | NM | 0.99488 | 0.61424 | 0.64053 | 1.08745 | 0.58902 |
| 32 | 1.3290 ⁻ 02 | 1.2242 ⁺ 00 | NM | 0.98937 | 0.61303 | 0.63757 | 1.08167 | 0.58943 |
| 33 | 1.4340 ⁻ 02 | 1.2445 ⁺ 00 | NM | 0.99535 | 0.63821 | 0.66420 | 1.08311 | 0.61323 |
| 34 | 1.5390 ⁻ 02 | 1.2620 ⁺ 00 | NM | 1.00132 | 0.65887 | 0.68639 | 1.08528 | 0.63246 |
| 35 | 1.6440 ⁻ 02 | 1.2635 ⁺ 00 | NM | 1.00501 | 0.66061 | 0.68935 | 1.08890 | 0.63307 |
| 36 | 1.7500 ⁻ 02 | 1.3021 ⁺ 00 | NM | 1.00897 | 0.70336 | 0.73225 | 1.08383 | 0.67561 |
| 37 | 1.8530 ⁻ 02 | 1.3032 ⁺ 00 | NM | 1.01394 | 0.70456 | 0.73521 | 1.08890 | 0.67518 |
| 38 | 1.9600 ⁻ 02 | 1.3596 ⁺ 00 | NM | 1.01141 | 0.76112 | 0.78846 | 1.07312 | 0.73474 |
| 39 | 2.0660 ⁻ 02 | 1.3620 ⁺ 00 | NM | 1.00595 | 0.76338 | 0.78846 | 1.06680 | 0.73909 |
| 40 | 2.1720 ⁻ 02 | 1.3588 ⁺ 00 | NM | 0.99809 | 0.76037 | 0.78254 | 1.05917 | 0.73883 |
| 41 | 2.2770 ⁻ 02 | 1.4053 ⁺ 00 | NM | 0.99478 | 0.80291 | 0.82101 | 1.04557 | 0.78522 |
| 42 | 2.3820 ⁻ 02 | 1.4245 ⁺ 00 | NM | 0.99674 | 0.81962 | 0.83728 | 1.04356 | 0.80233 |
| 43 | 2.4850 ⁻ 02 | 1.4440 ⁺ 00 | NM | 0.99934 | 0.83608 | 0.85355 | 1.04223 | 0.81897 |
| 44 | 2.5890 ⁻ 02 | 1.4515 ⁺ 00 | NM | 1.00339 | 0.84225 | 0.86095 | 1.04490 | 0.82395 |
| 45 | 2.6950 ⁻ 02 | 1.4499 ⁺ 00 | NM | 1.00629 | 0.84089 | 0.86095 | 1.04826 | 0.82131 |
| 46 | 2.7980 ⁻ 02 | 1.4910 ⁺ 00 | NM | 1.00852 | 0.87375 | 0.89201 | 1.04223 | 0.85587 |
| 47 | 2.9040 ⁻ 02 | 1.5083 ⁺ 00 | NM | 1.00799 | 0.88704 | 0.90385 | 1.03824 | 0.87056 |
| 48 | 3.0070 ⁻ 02 | 1.5420 ⁺ 00 | NM | 1.00730 | 0.91200 | 0.92604 | 1.03101 | 0.89818 |
| 49 | 3.1140 ⁻ 02 | 1.5187 ⁺ 00 | NM | 1.00547 | 0.89484 | 0.90976 | 1.03363 | 0.88016 |
| 50 | 3.2180 ⁻ 02 | 1.5288 ⁺ 00 | NM | 1.00357 | 0.90237 | 0.91568 | 1.02971 | 0.88926 |
| 51 | 3.3260 ⁻ 02 | 1.5815 ⁺ 00 | NM | 1.00131 | 0.94004 | 0.94822 | 1.01749 | 0.97193 |
| 52 | 3.4310 ⁻ 02 | 1.5905 ⁺ 00 | NM | 0.99918 | 0.94621 | 0.95266 | 1.01369 | 0.93980 |
| 53 | 3.5380 ⁻ 02 | 1.5693 ⁺ 00 | NM | 0.99847 | 0.93153 | 0.93935 | 1.01685 | 0.92378 |
| 54 | 3.6410 ⁻ 02 | 1.6162 ⁺ 00 | NM | 1.00128 | 0.96357 | 0.96893 | 1.01117 | 0.95823 |
| 55 | 3.7480 ⁻ 02 | 1.5961 ⁺ 00 | NM | 1.00143 | 0.95002 | 0.95710 | 1.01495 | 0.94300 |
| 56 | 3.8520 ⁻ 02 | 1.6167 ⁺ 00 | NM | 1.00074 | 0.96387 | 0.96893 | 1.01055 | 0.95882 |
| 57 | 3.9590 ⁻ 02 | 1.6384 ⁺ 00 | NM | 0.99652 | 0.97809 | 0.97929 | 1.00245 | 0.97689 |
| 58 | 4.1660 ⁻ 02 | 1.6579 ⁺ 00 | NM | 0.98955 | 0.99062 | 0.98669 | 0.99208 | 0.99456 |
| 59 | 4.3790 ⁻ 02 | 1.6375 ⁺ 00 | NM | 0.99149 | 0.97753 | 0.97633 | 0.99755 | 0.97873 |
| 60 | 4.5910 ⁻ 02 | 1.6721 ⁺ 00 | NM | 0.99195 | 0.99953 | 0.99556 | 0.99208 | 1.00351 |
| 61 | 4.7990 ⁻ 02 | 1.6682 ⁺ 00 | NM | 0.99615 | 0.99709 | 0.99556 | 0.99694 | 0.99862 |
| 62 | 5.0110 ⁻ 02 | 1.6705 ⁺ 00 | NM | 0.99655 | 0.99857 | 0.99704 | 0.99694 | 1.00010 |
| 63 | 5.2210 ⁻ 02 | 1.6691 ⁺ 00 | NM | 0.99813 | 0.99765 | 0.99704 | 0.99877 | 0.99827 |
| D 64 | 5.4320 ⁻ 02 | 1.6728 ⁺ 00 | NM | 1.00000 | 1.00000 | 1.00000 | 1.00000 | 1.00000 |
| 65 | 5.6430 ⁻ 02 | 1.6733 ⁺ 00 | NM | 0.99947 | 1.00031 | 1.00000 | 0.99939 | 1.00061 |
| 66 | 5.8530 ⁻ 02 | 1.6748 ⁺ 00 | NM | 0.99789 | 1.00123 | 1.00000 | 0.99755 | 1.00246 |
| 67 | 6.0660 ⁻ 02 | 1.6762 ⁺ 00 | NM | 0.99935 | 1.00209 | 1.00148 | 0.99877 | 1.00271 |
| 68 | 6.2730 ⁻ 02 | 1.6568 ⁺ 00 | NM | 0.99971 | 0.98991 | 0.99112 | 1.00246 | 0.98869 |
| 69 | 6.4870 ⁻ 02 | 1.6661 ⁺ 00 | NM | 1.00132 | 0.99582 | 0.99704 | 1.00246 | 0.99459 |
| 70 | 6.6940 ⁻ 02 | 1.6747 ⁺ 00 | NM | 1.00094 | 1.00117 | 1.00148 | 1.00061 | 1.00086 |
| 71 | 6.9070 ⁻ 02 | 1.6762 ⁺ 00 | NM | 0.99935 | 1.00209 | 1.00148 | 0.99877 | 1.00271 |
| 72 | 7.1190 ⁻ 02 | 1.6606 ⁺ 00 | NM | 0.99852 | 0.99230 | 0.99260 | 1.00061 | 0.99199 |
| 73 | 7.3290 ⁻ 02 | 1.6494 ⁺ 00 | NM | 0.99904 | 0.98517 | 0.98669 | 1.00308 | 0.98366 |
| 74 | 7.5420 ⁻ 02 | 1.6420 ⁺ 00 | NM | 0.99838 | 0.98044 | 0.98225 | 1.00370 | 0.97863 |
| 75 | 7.7510 ⁻ 02 | 1.6475 ⁺ 00 | NM | 1.00118 | 0.98396 | 0.98669 | 1.00556 | 0.98124 |
| 76 | 7.9620 ⁻ 02 | 1.6347 ⁺ 00 | NM | 1.00080 | 0.97568 | 0.97929 | 1.00742 | 0.97208 |
| 77 | 8.1730 ⁻ 02 | 1.6315 ⁺ 00 | NM | 1.00148 | 0.97360 | 0.97781 | 1.00867 | 0.96941 |
| 78 | 8.3840 ⁻ 02 | 1.6283 ⁺ 00 | NM | 0.99908 | 0.97156 | 0.97485 | 1.00680 | 0.96827 |
| 79 | 8.5950 ⁻ 02 | 1.6338 ⁺ 00 | NM | 0.99880 | 0.97511 | 0.97781 | 1.00556 | 0.97241 |
| 80 | 8.8060 ⁻ 02 | 1.6270 ⁺ 00 | NM | 0.99761 | 0.97068 | 0.97337 | 1.00556 | 0.96800 |
| 81 | 9.0160 ⁻ 02 | 1.6230 ⁺ 00 | NM | 0.99937 | 0.96801 | 0.97189 | 1.00804 | 0.96414 |
| 82 | 9.2270 ⁻ 02 | 1.6198 ⁺ 00 | NM | 1.00005 | 0.96594 | 0.97041 | 1.00929 | 0.96148 |
| 83 | 9.4380 ⁻ 02 | 1.6189 ⁺ 00 | NM | 1.00424 | 0.96531 | 0.97189 | 1.01369 | 0.95877 |

INPUT VARIABLES Y,U/UD,RHO/RHOD ASSUME P=PD

| 8001S | MATEER | TURBULENCE DATA | | | |
|-----------|----------------|------------------|----------------|----------------|--|
| 8001S0101 | UT= 1.4493E+01 | RHOW= 5.0933E-01 | TW= 2.7990E+02 | D*= 9.1879E-02 | |
| 8001S0103 | UT= 5.6157E+00 | RHOW= 9.3735E-01 | TW= 2.8137E+02 | D*= 5.9400E-01 | |
| 8001S0104 | UT= 6.6470E+00 | RHOW= 9.8788E-01 | TW= 2.7708E+02 | D*= 4.5489E-01 | |

| | 8001S0101 | | 8001S0103 | | 8001S0104 | |
|----|-----------|----------------------|-----------|----------------------|-----------|----------------------|
| I | Y [M] | RHO*U'V' RHOW*UT2 | Y [M] | RHO*U'V' RHOW*UT2 | Y [M] | RHO*U'V' RHOW*UT2 |
| 1 | 1.5900E-3 | 6.7165E-3 | 2.0300E-3 | -6.5984E-1 | 4.0600E-3 | -6.7987E+0 |
| 2 | 2.0300E-3 | -4.8309E-2 | 2.5400E-3 | -9.1927E-1 | 4.5700E-3 | -6.3785E+0 |
| 3 | 2.5400E-3 | -5.3608E-2 | 2.7900E-3 | -8.4031E+0 | 4.8300E-3 | -1.6386E+1 |
| 4 | 2.7900E-3 | -6.4516E-2 | 3.3000E-3 | -1.0321E+1 | 5.8400E-3 | -8.3647E+0 |
| 5 | 3.3000E-3 | -4.8777E-2 | 4.0600E-3 | -1.1731E+1 | 6.6000E-3 | -1.0236E+1 |
| 6 | 3.8100E-3 | -5.1582E-2 | 5.0800E-3 | -1.6299E+1 | 7.3700E-3 | -1.2108E+1 |
| 7 | 4.0600E-3 | 1.4321E-2 | 6.3500E-3 | -1.7032E+1 | 8.6400E-3 | -1.2337E+1 |
| 8 | 4.5700E-3 | -2.9609E-2 | 7.1100E-3 | -1.9626E+1 | 9.9100E-3 | -1.5507E+1 |
| 9 | 5.0800E-3 | -6.3269E-2 | 8.6400E-3 | -2.5773E+1 | 9.9100E-3 | -1.4629E+1 |
| 10 | 5.3300E-3 | -6.3581E-2 | 1.0160E-2 | -2.4363E+1 | 1.1180E-2 | -1.4896E+1 |
| 11 | 5.8400E-3 | -1.1173E-1 | 1.0920E-2 | -2.2672E+1 | 1.2450E-2 | -1.5125E+1 |
| 12 | 6.3500E-3 | -2.2596E-1 | 1.2700E-2 | -2.1544E+1 | 1.3720E-2 | -1.4017E+1 |
| 13 | 6.6000E-3 | -2.0570E-1 | 1.4220E-2 | -1.5171E+1 | 1.5240E-2 | -1.4476E+1 |
| 14 | 7.1100E-3 | -3.7245E-1 | 1.5240E-2 | -1.3986E+1 | 1.7270E-2 | -1.3559E+1 |
| 15 | 7.6200E-3 | -3.0856E-1 | 1.7530E-2 | -7.3316E+0 | 1.9560E-2 | -1.1267E+1 |
| 16 | 7.8700E-3 | -3.7401E-1 | 5.2070E-2 | 2.3517E+0 | 2.0570E-2 | -8.2119E+0 |
| 17 | 8.3800E-3 | -4.3478E-1 | 6.0710E-2 | 3.6827E+0 | 2.1590E-2 | -1.1802E+1 |
| 18 | 8.8900E-3 | -4.6439E-1 | 6.9090E-2 | 3.7899E+0 | 2.3620E-2 | -8.4029E+0 |
| 19 | 9.1400E-3 | -4.8153E-1 | 7.1120E-2 | 4.0549E+0 | 2.5910E-2 | -7.7154E+0 |
| 20 | 9.6500E-3 | -5.7192E-1 | 7.7470E-2 | 3.2033E+0 | 2.8960E-2 | -6.6459E+0 |
| 21 | 1.0160E-2 | -5.6101E-1 | 8.7880E-2 | NM | 3.2000E-2 | -5.4619E-1 |
| 22 | 1.0410E-2 | -5.2673E-1 | 9.8550E-2 | NM | 5.0040E-2 | 3.5903E+0 |
| 23 | 1.0920E-2 | -5.3452E-1 | 1.0185E-1 | NM | 5.6390E-2 | 3.8042E+0 |
| 24 | 1.1430E-2 | -5.6257E-1 | | | 6.2480E-2 | 2.9868E+0 |
| 25 | 1.1680E-2 | -5.6101E-1 | | | 6.8830E-2 | 2.5476E+0 |
| 26 | 1.2190E-2 | -5.0647E-1 | | | 7.1120E-2 | 3.1854E+0 |
| 27 | 1.2950E-2 | -4.7998E-1 | | | 7.5180E-2 | 2.5285E+0 |
| 28 | 1.3460E-2 | -4.7218E-1 | | | 8.1530E-2 | 2.9601E+0 |
| 29 | 1.3970E-2 | -4.9088E-1 | | | 8.7880E-2 | 1.4705E+0 |
| 30 | 1.4220E-2 | -4.4881E-1 | | | 9.3980E-2 | NM |
| 31 | 1.4730E-2 | -5.2673E-1 | | | 9.6270E-2 | NM |
| 32 | 1.5750E-2 | -4.2543E-1 | | | 9.8550E-2 | NM |
| 33 | 1.6760E-2 | -3.8492E-1 | | | 1.0160E-1 | NM |
| 34 | 1.8800E-2 | -2.6180E-1 | | | | |
| 35 | 1.9810E-2 | -2.9609E-1 | | | | |
| 36 | 2.1080E-2 | -1.7609E-1 | | | | |
| 37 | 2.2100E-2 | -2.0103E-1 | | | | |
| 38 | 2.3110E-2 | -1.8233E-1 | | | | |
| 39 | 2.4130E-2 | -1.1002E-1 | | | | |
| 40 | 2.5150E-2 | -1.0114E-1 | | | | |
| 41 | 2.7430E-2 | -6.2802E-2 | | | | |
| 42 | 2.8450E-2 | -4.7218E-2 | | | | |
| 43 | 3.1240E-2 | -4.6283E-2 | | | | |
| 44 | 3.1750E-2 | -2.5245E-2 | | | | |
| 45 | 3.4800E-2 | 3.6621E-2 | | | | |
| 46 | 3.8100E-2 | 0. | | | | |
| 47 | 4.2160E-2 | 5.8439E-2 | | | | |
| 48 | 4.8510E-2 | 7.9476E-2 | | | | |
| 49 | 5.2580E-2 | 8.6489E-2 | | | | |
| 50 | 5.8930E-2 | 1.2451E-1 | | | | |
| 51 | 6.3250E-2 | 1.3386E-1 | | | | |
| 52 | 6.7560E-2 | 1.2950E-1 | | | | |
| 53 | 7.1630E-2 | 1.2062E-1 | | | | |
| 54 | 7.5690E-2 | 1.0722E-1 | | | | |
| 55 | 8.0010E-2 | 8.3372E-2 | | | | |
| 56 | 8.6360E-2 | 1.0799E-1 | | | | |
| 57 | 8.8390E-2 | 8.8671E-2 | | | | |
| 58 | 9.2710E-2 | 6.3425E-2 | | | | |
| 59 | 9.7030E-2 | NM | | | | |
| 60 | 9.9060E-2 | NM | | | | |

8001S

MATEER

TURBULENCE DATA

8001S0105 UT= 7.0451E+00 RHDW= 1.0172E+00 TW= 2.7331E+02 D*= 4.0743E-01
 8001S0106 UT= 7.4847E+00 RHDW= 1.0244E+00 TW= 2.7417E+02 D*= 3.7059E-01
 8001S0107 UT= 7.8986E+00 RHDW= 1.0414E+00 TW= 2.7241E+02 D*= 3.4393E-01

| 8001S0105 | | | 8001S0106 | | 8001S0107 | |
|-----------|-----------|----------------------|-----------|----------------------|-----------|----------------------|
| I | Y [M] | RHD*U*V' RHDW*UTZ | Y [M] | RHD*U*V' RHDW*UTZ | Y [M] | RHD*U*V' RHDW*UTZ |
| 1 | 7.1100E-3 | -7.4960E+0 | 2.0300E-3 | -1.1039E+0 | 2.0300E-3 | -1.0802E+0 |
| 2 | 7.8700E-3 | -8.2886E+0 | 2.5400E-3 | -1.2521E-1 | 2.5400E-3 | -1.6601E+0 |
| 3 | 8.8900E-3 | -7.4960E+0 | 2.7900E-3 | -1.7430E+0 | 2.7900E-3 | -1.9038E+0 |
| 4 | 1.0160E-2 | -9.5434E+0 | 3.3000E-3 | -3.0793E+0 | 3.3000E-3 | -2.3451E+0 |
| 5 | 1.1430E-2 | -9.6425E+0 | 4.0600E-3 | -3.6313E+0 | 4.0600E-3 | -2.3785E+0 |
| 6 | 1.2700E-2 | -1.0930E+1 | 5.0800E-3 | -3.8056E+0 | 5.0800E-3 | -3.4125E+0 |
| 7 | 1.3970E-2 | -1.1591E+1 | 5.8400E-3 | -4.5028E+0 | 5.8400E-3 | -4.6697E+0 |
| 8 | 1.5240E-2 | -1.1690E+1 | 6.6000E-3 | -4.8514E+0 | 7.1100E-3 | -4.8750E+0 |
| 9 | 1.7530E-2 | -9.8406E+0 | 7.8700E-3 | -6.5364E+0 | 8.6400E-3 | -6.2348E+0 |
| 10 | 2.0570E-2 | -9.6094E+0 | 9.1400E-3 | -6.0719E+0 | 1.0410E-2 | -7.3638E+0 |
| 11 | 2.3620E-2 | -7.1328E+0 | 1.0410E-2 | -7.8146E+0 | 1.1680E-2 | -7.4408E+0 |
| 12 | 2.6920E-2 | -3.7975E+0 | 1.2190E-2 | -7.1755E+0 | 1.2950E-2 | -8.0822E+0 |
| 13 | 2.9970E-2 | -3.3352E+0 | 1.3460E-2 | -8.6861E+0 | 1.4220E-2 | -7.2868E+0 |
| 14 | 3.3270E-2 | -8.1565E-1 | 1.4730E-2 | -8.6280E+0 | 1.6260E-2 | -8.5697E+0 |
| 15 | 6.2740E-2 | 3.3683E+0 | 1.6760E-2 | -9.5866E+0 | 1.9560E-2 | -9.2625E+0 |
| 16 | 6.6040E-2 | 3.5334E+0 | 2.0070E-2 | -8.0760E+0 | 2.2610E-2 | -8.1079E+0 |
| 17 | 6.9090E-2 | 3.3022E+0 | 2.3110E-2 | -5.8972E+0 | 2.5910E-2 | -6.5684E+0 |
| 18 | 7.5440E-2 | 2.4469E+0 | 2.7430E-2 | -7.2336E+0 | 2.9970E-2 | -6.7737E+0 |
| 19 | 8.1790E-2 | 2.3710E+0 | 3.1750E-2 | -3.7185E+0 | 3.4290E-2 | -4.6184E+0 |
| 20 | 8.8140E-2 | 2.2323E+0 | 3.4540E-2 | -2.9631E+0 | 3.7590E-2 | -3.7460E+0 |
| 21 | 9.4490E-2 | NM | 3.7850E-2 | -1.8069E+0 | 4.0640E-2 | 4.5414E+0 |
| 22 | 9.8550E-2 | NM | 5.5880E-2 | 3.8056E+0 | 4.3690E-2 | 5.0546E+0 |
| 23 | 1.0185E-1 | NM | 6.2230E-2 | 3.1084E+0 | 4.8010E-2 | 4.0796E+0 |
| 24 | | | 6.8580E-2 | 3.1374E+0 | 5.6130E-2 | 3.2072E+0 |
| 25 | | | 7.4930E-2 | 4.2704E+0 | 6.2990E-2 | 2.6684E+0 |
| 26 | | | 8.3060E-2 | 5.2291E+0 | 6.9090E-2 | 2.6941E+0 |
| 27 | | | 9.1440E-2 | 4.6771E+0 | 7.5440E-2 | 3.5664E+0 |
| 28 | | | 9.7790E-2 | NM | 8.1790E-2 | 3.4381E+0 |
| 29 | | | | | 8.8140E-2 | 3.1302E+0 |
| 30 | | | | | 9.4490E-2 | 2.8224E+0 |
| 31 | | | | | 9.8550E-2 | 2.5658E+0 |
| 32 | | | | | 1.0185E-1 | 2.2117E+0 |

7. REFERENCES

- Acharya M. 1977 Effects of compressibility on boundary layer turbulence. AIAA J. 15, 303-305 and AIAA P-76-334 (1976).
- Acharya, M., Kussoy M.I., Horstman C.C. 1978 Reynolds number and pressure gradient effects on compressible turbulent boundary layers. AIAA Paper 78-199. See also Kussoy, Horstman, Acharya. Finally AIAA J. 16, 1217-1218.
- Adcock J.B., Peterson J.B., Mc Ree D.J. 1965 Experimental investigation of a turbulent boundary layer at Mach 6, high Reynolds numbers and zero heat transfer. NASA TN D - 2907, (CAT 6501).
- Allen J.M. 1972 Pitot probe displacement in a supersonic turbulent boundary layer. NASA TN D - 6759, (CAT 7303).
- Allen J.M. 1973a Evaluation of compressible flow - Preston tube evaluations. NASA TN D - 7190, (CAT 7303).
- Allen J.M. 1973b Evaluation of Preston tube calibration equations in supersonic flow. AIAA J. 11, 1461-1463.
- Allen J.M. 1976 Systematic study of error sources in supersonic skin friction balance measurements. NASA TN D-8291.
- Allen J.M. 1977a Experimental study of error sources in skin friction balance measurements. Trans ASME Ser. I 99, 197-204.
- Allen J.M. 1977b Re-evaluation of compressible flow Preston tube calibrations. NASA TM X-3488.
- Allen J.M. 1977c Re-evaluation of compressible flow Preston tube calibrations. J. Fluid Engrg. 99, 197.
- Ardonceau P., Lee D.H., Alziary de Roquefort T., Goethals R. 1979 Turbulence behaviour in a shock wave/boundary layer interaction. AGARD CP 271.
- Bartlett R.P. 1981 A study of the mean and fluctuating properties of a turbulent hypersonic boundary layer. Ph.D. thesis, Imperial College.
- Bartlett R.P., Edwards A.J., Hillier R. 1979a Development and calibration of a total temperature probe for the Imperial College Aeronautics Dept. gun tunnel. I.C. Aero Rep. 79-02.
- Bartlett R.P., Edwards A.J., Harvey J.K., Hillier R. 1979b Pitot pressure and total temperature profile measurements in a hypersonic turbulent boundary layer at M=9. I.C. Aero Rep. 79-01, (CAT 7903 S).
- Beckwith I.E., Harvey W.D., Clark F.L. 1971 Comparison of turbulent boundary layer measurements at Mach number 19.5 with theory and an assessment of probe errors. NASA TN D-6192, (CAT 7105).
- Behrens W. 1963 Viscous interaction effects on a static pressure probe at M = 6, AIAA J. 1, 2864-2866.
- Behrens W. 1971 Total temperature thermocouple probe based on recovery temperature of circular cylinder. Int. J. Heat Mass Transfer 14, 1621-1630.
- Bellhouse B.J., Schultz D.L. 1967 The determination of fluctuating velocity in air with heated thin film gauges. J. Fluid Mech. 29, 289-295.
- Berg D.E. 1977 Surface roughness effects on the hypersonic turbulent boundary layer. CALTECH Pasadena Ph.D. thesis Univ. Microfilm 77-17260. CAT 7703 S. See also Kubota & Berg.
- Berg D.E. 1978 Surface roughness effects on a Mach 6 turbulent boundary layer. AIAA P-78-1159.
- Berg D.E. 1979 Surface roughness effects on a Mach 6 turbulent boundary layer. AIAA J. 17, 929-930.
- Bonnet J.P., Alziary de Roquefort T. 1980 Determination and optimization of frequency response of constant temperature hot-wire anemometers in supersonic flows. Rev. Sci. Instruments, Vol. 51.
- Boudreau 1969 AEDC TR-69-268.
- Bradshaw P. 1977a Compressible turbulent shear layers. Ann. Rev. Fluid Mech. 9, 33-54.
- Bradshaw P. 1977b An improved van Driest skin-friction formula for compressible turbulent boundary layers. AIAA J. 15, 212-214.
- Bradshaw P., Ferris D.H. 1971 Calculation of boundary layer development using the turbulent energy equation: compressible flow on adiabatic walls. J.F.M. 46, 83-110.

- Bradshaw P., Unsworth K. 1973 A note on Preston tube calibrations in compressible flow. IC Aero Rep. 73-07.
- Bradshaw P., Unsworth K. 1974 Comment on "Evaluation of Preston tube calibration equations in supersonic flow. AIAA J. 12, 1293-1295.
- Bütefisch K.A., Vennemann D. 1974 The electron beam technique in hypersonic rarefied gas dynamics. Progr. in Aeronaut. Sci. 15, 217-255.
- Bushnell D.M., Morris D.J. 1971a Shear stress, eddy-viscosity, and mixing-length distributions in hypersonic turbulent boundary layers. NASA TM-X-2310.
- Bushnell D.M., Morris D.J. 1971b Eddy viscosity distribution in a Mach 20 turbulent boundary layer. AIAA J. 9, 764-766.
- Chew Y.T. 1979 Shock wave and boundary layer interaction in the presence of an expansion corner. Aero Quart. XXX, 506-527.
- Chew Y.T., Squire L.C. 1979 The boundary layer development downstream of a shock interaction at an expansion corner. ARC R & M 3839. CAT 7902 S.
- Coakley T.J., Viegas J.R., Horstman C.C. 1977 Evaluation of turbulence models for three primary types of shock separated boundary layers. AIAA Paper 77-692.
- Coles D. 1953 Measurements in the boundary layer on a smooth flat plate in supersonic flow.
 I. The problem of the turbulent boundary layer.
 II. Instrumentation and experimental techniques at the Jet-Propulsion Laboratory.
 III. Measurements in a flat plate boundary layer at the Jet Propulsion Laboratory.
 J.P.L. Cal. Inst. Tech. Rep. Nos. 20-69, 20-70, 20-71 (from Ph. D. thesis CALTECH Pasadena 1953), CAT 5301
- Coles D. 1955 The law of the wall in turbulent shear flow. 50 Jahre Grenzschichtforschung (ed. by H. Görtler und W. Tollmien). F. Vieweg und Sohn Braunschweig p. 153 ff.
- Coles D. 1956 The law of the wake in the turbulent boundary layer. J. Fluid Mech. 1, 191-226.
- Coles D.E., Hirst E.A. 1969 Proceedings Computation of Turbulent Boundary Layers - 1968 AFOSR-IFP Stanford Conference. Volume II Compiled Data. Stanford University, Stanford U.S.A.
- Collins D.J., Coles D.E., Hicks J.W. 1978 Measurements in the turbulent boundary layer at constant pressure in subsonic and supersonic flow. Pt. 1 Mean flow. AEDC-TR-78-21, CAT 7801 S.
- Danberg J.E. 1960 Measurements of the characteristics of the compressible turbulent boundary layer with air injection. NAVORD Rep. 6683. CAT 6002 S.
- Danberg J.E. 1961 The equilibrium temperature probe, a device for measuring temperatures in a hypersonic layer. NOLTR 61-2.
- Danberg J.E. 1967 Characteristics of the turbulent boundary layer with heat and mass transfer: Data tabulation. NOLTR 67-6, CAT 6702.
- Demetriades A., Laderman A.J. 1973a Reynolds stress measurements in a hypersonic boundary layer, AIAA J. 11, 1594-1597.
- Demetriades A., Laderman A.J. 1973b Final progress report: Advanced penetration problems project (hot wires in compressible flow). SAMSO Rep. 73-129. Philco Ford Corp. Newport Beach Calif.
- Dimotakis P.E., Collins D.J., Lang D.B. 1979 Measurements in the turbulent boundary layer at constant pressure in subsonic and supersonic flow. AEDC-TR-79-49.
- van Driest E.R. 1951 Turbulent boundary layer in compressible fluids. J. Aeronaut. Sci. 18, 145-160.
- Durst F., Melling A., Whitelaw J.H. 1976 Principles and practice of laser-doppler-velocimetry. New York, Academic Press.
- Edwards A.J. 1981 Boundary layer studies at hypersonic speeds. Ph.D. thesis Imperial College London. Also as RNEC TR 81001.
- Erickson W.D. 1960 Real-gas correction factors for hypersonic flow parameters in helium. NASA TN D - 462.
- Fernholz H.H. 1969 Geschwindigkeitsprofile, Temperaturprofile und halbempirische Gesetze in kompressiblen turbulenten Grenzschichten bei konstantem Druck. Ing. Arch. 38, 311-328
- Fernholz H.H. 1971 Ein halbempirisches Gesetz für die Wandreibung in kompressiblen turbulenten Grenzschichten bei isothermer und adiabater Wand. ZAMM 51, T 148-149.

- Fernholz H.H. 1972 Departures from a fully developed turbulent velocity profile on a flat plate in compressible boundary layers. Fluid Dynamics Transactions Vol. 6 Pt. II.
- Fernholz H.H., Finley P.J. 1976 A critical compilation of compressible turbulent boundary layer data. Von Karman Institute for Fluid Dynamics Lecture Series 86.
- Fernholz H.H., Finley P.J. 1977 A critical compilation of compressible turbulent boundary layer data. AGARD AG-223.
- Fernholz H.H., Finley P.J. 1980 A critical commentary on mean flow data for two-dimensional compressible turbulent boundary layers. AGARD-AG-253.
- Finley P.J. 1977 Static pressure in hypersonic nozzle boundary layers. AIAA J. 15, 878 - 881.
- Fischer M.C., Maddalon D.V., Weinstein L.M., Wagner R.D. 1970 Boundary layer surveys on a nozzle wall at $M \approx 20$, including hot-wire fluctuation measurements. AIAA Paper 70-746, (CAT 7001).
- Gates D.F. 1973a Measurements of upstream history effects in compressible turbulent boundary layers. NOL TR 73-152, (CAT 7301).
- Gates D.F. 1973b An experimental investigation of the effect of upstream conditions on the downstream characteristics of compressible turbulent boundary layers - using supersonic half nozzle and conventional flat plate. Ph.D. thesis University Maryland, Univ. Microfilms 73-23731.
- Gates D.F., Allen R.W. 1974 Experimental measurements of upstream history effects in supersonic turbulent flow. Proc. 1974 Heat Transfer and Fluid Mechanics Institute, 330-347.
- Gootzait E. 1976 An experimental investigation of turbulent supersonic boundary layer flow in an adverse pressure gradient. Ph. D. thesis Univ. of Washington.
- Gootzait E., Childs M.E. 1974 Mean and fluctuating flow measurements in axisymmetric supersonic boundary layer flow subjected to distributed adverse pressure gradients. NASA - CR - 139435.
- Gootzait E., Childs M.E. 1977 Turbulence measurements in axisymmetric supersonic boundary layer flow in adverse pressure gradients. AIAA Paper 77-129 and NASA CR-148807
- Hastings R.C., Sawyer W.G. 1970 Turbulent boundary layers on a large flat plate at $M = 4$. RAE. Technical Report 70040 and R + M 3678, (CAT 7006).
- Hill F.K. 1956 Boundary layer measurements in hypersonic flow. J. Aeron. Sci. 23, 35-42.
- Hill F.K. 1959 Turbulent boundary layer measurements at Mach numbers from 8 to 10. Phys. Fluids 2, 668-680, (CAT 5901).
- Hinze J.O. 1959 Turbulence. Mc Graw Hill, New York.
- Hopkins E.J., Keener E.R. 1966 Study of surface Pitots for measuring turbulent skin friction at supersonic Mach numbers - adiabatic wall. NASA TN D 3478, (CAT 6601).
- Hopkins E.J., Inouye M. 1971 An evaluation of theories for predicting turbulent skin friction and heat transfer on flat plates at supersonic and hypersonic Mach numbers. AIAA J. 9, 993-1003.
- Horstman C.C., Owen F.K. 1972 Turbulent properties of a compressible boundary layer. AIAA J. 10, 1418-1424, (CAT 7205).
- Horstman C.C., Owen F.K. 1974 New diagnostic technique for the study of turbulent boundary layer separation. AIAA J. 12, 1436-1438.
- Horstman C.C., Rose W.C. 1977 Hot-wire anemometry in transonic flow. AIAA J. 15, 395-402.
- Horstman C.C., Kussoy M.I., Lanfranco M.J. 1978 An evaluation of several compressible turbulent boundary layer models: Effect of pressure gradient and Reynolds number. AIAA Paper 78-1160.
- Jeromin L.O.F. 1966 Compressible turbulent boundary layer with fluid injection. Ph.D. thesis Cambridge, (CAT 6602).
- Johnson D.A. 1974 Turbulence measurements in a Mach 2.9 boundary layer using laser velocimeter. AIAA J. 12, 711-714.

- Johnson D.A., Rose W.C. 1973 Measurements of turbulence transport properties in a supersonic boundary layer flow using laser velocimeter and hot-wire anemometer techniques. AIAA Paper 73-1045.
- Johnson D.A., Rose W.C. 1975 Laser velocimeter and hot wire anemometer comparisons in a supersonic boundary layer. AIAA J. 13, 512-515.
- Johnson D.A., Rose, W.C. 1976 Turbulence measurements in a transonic boundary layer and free-shear layer using laser velocimetry and hot-wire anemometry techniques. AIAA Paper 76-399.
- Jones R.A., Feller W.V. 1970 Preliminary surveys of the wall boundary layer in a Mach 6 axisymmetric tunnel. NASA TN D-5620, (CAT 7002).
- Kemp J.H., Owen F.K. 1972 Experimental study of nozzle wall boundary layers at Mach numbers 20 to 47, NASA TN D - 6965, (CAT 7206).
- Kestin J. 1979 A course in thermodynamics Vol. II (revised printing) Hemisphere/Mc Graw Hill.
- Keyes F.G. 1952 The heat conductivity, viscosity, specific heat and Prandtl numbers for thirteen gases. Project Squid T.R. no. 37, M.I.T. Cambridge Mass.
- Kistler A.L. 1958 Fluctuation measurements in supersonic turbulent boundary layers. Ballistic Research Laboratories, Rep. 1052 and Phys. Fluids 2 1959, (CAT 5803).
- Ktebanoff P.S. 1955 Characteristics of turbulence in a boundary layer with zero pressure gradient. NACA R 1247.
- Kovaszny L.S.G. 1950 The hot-wire velocimeter in supersonic flow. J. Aeronaut. Sci. 17, 565-572.
- Kovaszny L.S.G. 1953a Development of turbulence measuring equipment. NACA TN 2839 and NACA TR 1209 (1954).
- Kovaszny L.S.G. 1953b Turbulence in supersonic flow. J. Aeronaut. Sci. 20, 657-674, 682.
- Kubota T., Berg D.E. 1977 Surface roughness effects on the hypersonic turbulent boundary layer. CALTECH AD A 042141. See also Berg (1977).
- Kussoy M.I., Horstman C.C. 1975 An experimental documentation of a hypersonic shock-wave turbulent boundary layer interaction flow with and without separation. NASA TM 62-412, (CAT 75015).
- Kussoy M.I., Horstman C.C., Acharya M. 1978 An experimental documentation of pressure gradient and Reynolds number effects on compressible turbulent boundary layers. NASA TM 78 488, (CAT 78025).
- Laderman A.J. 1976 New measurements of turbulent shear stresses in hypersonic boundary layers. AIAA J. 14, 1286-1292.
- Laderman A.J. 1978a Effect of wall temperature on a supersonic turbulent boundary layer. AIAA J. 16, 723-730.
- Laderman A.J. 1978b Pressure gradient effects on supersonic boundary layer turbulence. Ford Aerospace & Communications Corp. Aeronutronics Div. Rep. No. U-6467. Newport Beach, Calif. (CAT 7803 S).
- Laderman A.J. 1978c Effects of Mach number and heat transfer on Reynolds shear stresses in compressible boundary layers. Aeronutronic Publication No. U-6412.
- Laderman A.J. 1979 Adverse pressure gradient effects on supersonic boundary layer turbulence. AIAA Paper 79-1563 and AIAA J. 18, 1186-1195 (1980).
- Laderman A.J., Demetriades A. 1971 Mean flow measurements in a hypersonic turbulent boundary layer. Philco Ford U 4950.
- Laderman A.J., Demetriades A. 1973 Hot-wire measurements of hypersonic boundary layer turbulence. Phys. Fluids 16, 179-181.
- Laderman A.J., Demetriades A. 1974 Mean and fluctuating flow measurements in the hypersonic boundary layer over a cooled wall. J. Fluid Mech. 63, 121-144, (CAT 7403).
- Laderman A.J., Demetriades A. 1976 Turbulent fluctuations in the hypersonic boundary layer over an adiabatic slender cone. Phys. Fluids 19, 359-361.
- Laderman A.J., Demetriades A. 1977 Investigation of the structure of a cooled wall turbulent supersonic boundary layer. Aeronutronics Publ. No. U-6370, (CAT 7702 S).

- Laderman A.J., Demetriades A. 1979 Turbulent shear stresses in compressible boundary layers. AIAA J. 17, 736-744.
- Laurence J.C., Sandborn V.A. 1962 Heat transfer from cylinders. Symposium On Measurements In Unsteady Flow, Worcester. Amer. Soc. Mech. Eng. Publ.
- Lee D.H. 1979 Etude de l'évolution de la turbulence dans une interaction onde de choc - couche limite. Thèse Université de Poitiers.
- Lee R.E., Yanta W.J., Leonas A.C. 1969 Velocity profile, skin friction balance and heat transfer measurements of the turbulent boundary layer at Mach 5 and zero pressure gradient. NOLTR - 69 - 106.
- Lee R.E., Smith R.A. 1974 Evaluation of the turbulent transport terms for a two-dimensional nozzle wall boundary layer flow at Mach 5 with pressure gradient, heat transfer and upstream effects. AIAA Paper 74-96.
- Lewis J.E., Gran R.L., Kubota T. 1972 An experiment on the adiabatic compressible turbulent boundary layer in adverse and favourable pressure gradient. J. Fluid Mech. 51, 657-672 (CAT 7201).
- Mabey D.G. 1977 Some observations on the wake component of the velocity profiles of turbulent boundary layers at subsonic and supersonic speeds. RAE TR 77-004(CAT 7701 S).
- Mabey D.G., Meier H.U., Sawyer W.G. 1974 Experimental and theoretical studies of the boundary layer on a flat plate at Mach numbers from 2.5 to 4.5. RAE TR 74127,(CAT 7402).
- Mabey D.G., Sawyer W.G. 1976 Experimental studies of the boundary layer on a flat plate at Mach numbers from 2.5 to 4.5. ARC R+M 3784.
- Mc Ronald A.D. 1975 Measurements of density and temperature in a hypersonic turbulent boundary layer using the electron beam fluorescence technique. Ph.D. thesis Univ. Southern California.
- Maddalon D.V., Jackson W.E. 1970 A survey of the transport properties of helium at high mach number wind-tunnel conditions. NASA TM X-2020.
- Maise G., McDonald H. 1968 Mixing length and kinematic eddy viscosity in a compressible boundary layer. AIAA J. 6, 73-80.
- Marvin J.G. 1977 Turbulence modelling for compressible flows. NASA TM X-73.188.
- Marvin J.G., Rubesin M.H., Coakley T.J., Kussoy M.I. 1975 An experimental and numerical investigation of shock-wave induced boundary layer separation at hypersonic speeds. AGARD CPP 168, 25.1-25.13.
- Mateer G.G., Brosh A., Viegas J.R. 1976 A normal shock wave turbulent boundary-layer interaction at transonic speeds. AIAA Paper 76-161.
- Mateer G.G., Viegas J.R. 1979 Effect of Mach and Reynolds numbers on a normal shock-wave/turbulent boundary-layer interaction. AIAA Paper 79-1502,(CAT 8001 S).
- Meier H.U. 1967 Messungen von turbulenten Grenzschichten ohne Wärmeübergang bei Überschallgeschwindigkeit an einer ebenen Wand. Aerodynamische Versuchsanstalt Göttingen. 67 A 09.
- Meier H.U. 1970 Experimentelle und theoretische Untersuchungen von turbulenten Grenzschichten bei Überschallströmung. M.P.I. Mitteilungen Nr. 49 (CAT 7003).
- Meier H.U., Rotta J.C. 1970 Experimental and theoretical investigations of temperature distributions in supersonic boundary layers. AIAA Paper 70-744.
- Meier H.U., Rotta J.C. 1971 Temperature distributions in supersonic turbulent boundary layers. AIAA J. 9, 2149-2156.
- Mikulla V., Horstman C.C. 1975a The measurement of shear stress and total heat flux in a nonadiabatic turbulent hypersonic boundary layer. AIAA J. 13, 1607-1613 and AIAA Paper 75-119.
- Mikulla V., Horstman C.C. 1975b Turbulence stress measurements in a non-adiabatic hypersonic boundary layer. AIAA J. 13, 1607 - 1613.
- Mikulla V., Horstman C.C. 1976 Turbulence measurements in hypersonic shock-wave boundary layer interaction flows. AIAA J. 14, 568 - 575.
- Millikan C.B. 1938 A critical discussion of turbulent flows in channels and circular tubes. Proc. 5. Int. Congr. Appl. Mech.

- Morkovin M.V. 1956 Fluctuations and hot-wire anemometry in compressible flows. AGARDograph No. 24.
- Morkovin M.V., 1960 The structure of supersonic turbulent boundary layers. AGARD WIND TUNNEL and MODEL TESTING PANEL.
- Morkovin M.V. 1962 Effects of compressibility on turbulent flows. In: Méchanique de la Turbulence. Editions du Centre Nat. de la Rech. Sci. and The Mechanics of Turbulence, Favre A. (ed.). New York: Gordon & Breach 1964.
- Morkovin M.V., Phinney R.E. 1958 Extended applications of hot-wire anemometry to high speed turbulent boundary layers. Dept. Aeronaut. The Johns Hopkins Univ. ASTIA AD-158-279,(CAT 5806 S).
- Mueller J.N. 1957 Equations, tables and figures for use in the analysis of helium flow at supersonic and hypersonic speeds. NACA TN 4063.
- Neubert W. 1974 Zähigkeit und Recovery-Faktor von Helium für Temperaturen von $0,4^{\circ}$ bis 400° K. Studienarbeit Hermann-Föttinger-Institut für Thermo- und Fluidodynamik, Technische Universität Berlin.
- Newman B. 1951 Some contributions to the study of the turbulent boundary layer near separation. Australian Dept. Supply Rep. No. ACA-53.
- Owen F.K., Horstman C.C. 1974 Turbulence measurements in an equilibrium hypersonic boundary layer. AIAA Paper 74-93.
- Owen F.K., Horstman C.C., Kussoy M.I. 1975 Mean and fluctuating flow measurements of a fully-developed, non-adiabatic hypersonic boundary layer. J. Fluid Mech. 70, 393-413.
- Patel V.C. 1965 Calibration of the Preston tube and limitations on its use in pressure gradients. J. Fluid Mech. 23, 185-208.
- Patel V.C. 1973 A unified view of the law of the wall using mixing length theory. Aero.Quart. 24, 55-70.
- Peake D.J., Brakmann G., Romeskie J.M. 1971 Comparisons between some high Reynolds number turbulent boundary layer experiments of Mach 4 and various recent calculation procedures. Nat. Res. Council of Canada and AGARD-CP-93-71 Paper 11, (CAT 7102).
- Perry A.E., Schofield W.H., Joubert P.N. 1969 Rough wall turbulent boundary layers. J. Fluid Mech. 37, 383-413.
- Perry J.H. 1968 An experimental study of the turbulent boundary layer at high Mach number and high wall heat transfer. Ph.D. thesis Univ. Southampton.
- Perry J.H., East R.A. 1968 Experimental measurements of cold wall turbulent hypersonic boundary layers. AGARD CP NO 30, (CAT 6801).
- Peterson C.W. 1974 Pressure and temperature measurements in a cold wall hypersonic turbulent boundary layer. Proc. 1974 Heat Transfer and Fluid Mech. Inst., 105-121,(CAT 7405 S).
- Peterson C.W., George O.L. 1974 Wind tunnel pressure probes: New calibrations for new geometries and flow environments. AIAA Paper 74-635 and AIAA J. 13, 1263-1264 (1975) and SAND 75-0337 Sandia Labs. Albuquerque N.M (1975).
- Pinckney S.Z. 1974 An improved static probe design. AIAA J. 12, 562-564.
- Pinckney S. 1975 A short static-pressure probe design for supersonic flow. NASA TN-D 7978.
- Ramaswamy M.A. 1971 Experimental investigation of the effect of cooling on the near wake of circular cylinders at Mach number six. Ph.D. thesis, CALTECH, Pasadena Calif.
- Rao G.N .V. 1967 The law of the wall in a thick axisymmetric turbulent boundary layer. Trans. ASME J. Appl. Mech. 34, 237-238.
- Reda D.C. 1974 Compressible turbulent skin friction on rough and rough/wavy walls in adiabatic flow. NOL TR 74-34.
- Reda D.C., Murphy J.D. 1973 Shock wave turbulent boundary layer interactions in rectangular channels. AIAA J. 11, 139-140 and AIAA Paper 72-715.
- Reda D.C., Ketter F.C., Fan C. 1975 Compressible turbulent skin friction on rough and rough/wavy walls in adiabatic flow. AIAA J. 13, 553-555 and AIAA Paper 74-574.

- Richmond R.L. 1957 Experimental investigation of thick, axially symmetric boundary layers on cylinders at subsonic and hypersonic speeds. Guggenheim Aeronaut. Lab. CALTECH Pasadena. Hypersonic Research Project Memo 39, (CAT 5701 S).
- Rose W.C. 1970 A method for analyzing the interaction of an oblique shock wave with a boundary layer. NASA TN 6083.
- Rose W.C. 1973 The behaviour of a compressible turbulent boundary layer in a shock-wave-induced adverse pressure gradient. NASA TN D-7092 (and Ph.D. thesis Univ. Washington 1972)(CAT 7306 S).
- Rose W.C. 1974 Turbulence measurements in a compressible boundary layer. AIAA J. 12, 1060-1064 and AIAA Paper 73-167.
- Rose W.C., Murphy J.D. 1973 Ratio of Reynolds shear stress to turbulent kinetic energy in a boundary layer. The Physics of Fluids 16, 935-937.
- Rose W.C., Johnson D.A. 1974 A study of shock wave turbulent boundary layer interaction using Laser velocimeter and hot-wire anemometer techniques. AIAA Paper 74-95.
- Rose W.C., Johnson D.A. 1975 Turbulence in a shock-wave boundary layer interaction. AIAA J. 13, 884-889.
- Rose W.C., Mc Daid E.P. 1977 Turbulence measurements in transonic flow. AIAA J. 15, 1368-1370, also Proc. AIAA 9th Aerodyn. Testing Conf. Arlington Texas 1976.
- Rotta J.C. 1962 Turbulent boundary layers in incompressible flow. Progress In Aeronautical Sciences, Vol. 2 Pergamon Press.
- Rotta J.C. 1964a Temperaturverteilungen in der turbulenten Grenzschicht an der ebenen Platte. Int. J. Heat Mass Transfer 7, 215-228.
- Rotta J.C. 1964b A review of experimental temperature distribution in supersonic and hypersonic turbulent boundary layers with heat transfer. AVA 64 A 10 Göttingen.
- Rotta J.C. 1965 Heat transfer and temperature distribution in turbulent boundary layers at supersonic and hypersonic flow. AGARDograph 97, 35-63.
- Rubesin M.W., Murphy J.D., Rose W.C. 1974 Wall shear in strongly retarded and separated compressible turbulent boundary layers. AIAA J. 12, 1442-1445.
- Rubesin M.W., Crisalli A.J., Horstman C.C., Acharya M. 1977 A critique of some recent second order closure models for compressible boundary layers. AIAA Paper 77-128.
- Samuels R.D., Peterson J.B., Adcock J.B. 1967 Experimental investigation of the turbulent boundary layer at a Mach number of 6 with heat transfer at high Reynolds numbers. NASA TN D - 3858, (CAT 6701).
- Sandborn V.A. 1974 A review of turbulence measurements in compressible flow. NASA TM X-62 337.
- Schairer E.T. 1980 Turbulence measurements in the boundary layer of a low speed wind tunnel using laser velocimetry. NASA TM 81165.
- Shutts W.H., Hartwig W.H., Weiler J.E. 1955 Final report on turbulent boundary layer and skin friction measurements on a smooth thermally insulated flat plate at supersonic speeds. Report No DRL - 364, CM - 823, (CAT 5501).
- Shutts W.H., Fenter F.W. 1955 Turbulent boundary layer and skin friction measurements on an artificially roughened thermally insulated flat plate at supersonic speeds. Report No DRL-366, CM - 837, (CAT 5502).
- Squire L.C. 1971 Eddy viscosity distributions in compressible turbulent boundary layers with injection. Aeronaut. Quart. XXIII, 169-182.
- Squire L.C., Thomas G.D., Mariott P.G. 1977 Compressible turbulent boundary layers with injection. AIAA J. 15, 425-427.
- Stalmach C.J. 1958 Experimental investigation of the surface impact probe method of measuring local skin friction at supersonic speeds. Univ. of Texas, DRL-410, CF 2675, (CAT 5802).
- Sturek W.B. 1970 An experimental investigation of the supersonic turbulent boundary layer in a moderate adverse pressure gradient Pt. 1. A detailed description of the experiment and tabulation. Ballistic Research Labs. Aberdeen Proving Grounds, Md. BRL Report 1543.

- Sturek W.B. 1971 Ph.D. thesis Univ. of Delaware, Newark, Del.
- Sturek W.B. 1973a Calculations of turbulent shear stress in supersonic turbulent boundary layer zero and adverse pressure gradient flow. AIAA Paper 73-166.
- Sturek W.B. 1973b Wall heat transfer effects on supersonic nozzle wall boundary layer temperature profiles. Ballistic Res. Lab. Memorandum Rep. No. 2328.
- Sturek W.B. 1974 Turbulent boundary layer shear stress distribution for compressible adverse pressure gradient flow. AIAA J. 12, 375-376.
- Sturek W.B., Danberg J.E. 1971a Experimental measurements of the supersonic turbulent boundary layer in a region of moderate adverse pressure gradient. AIAA Paper 71-162.
- Sturek W.B., Danberg J.E. 1971b Supersonic turbulent boundary layer in an adverse pressure gradient. Univ. Delaware T. R. No 141, (CAT 7101).
- Sturek W.B., Danberg J.E. 1971c The supersonic turbulent boundary layer in an adverse pressure gradient experiment and data analysis. AGARD CCP-93-71.
- Sturek W.B., Danberg J.E. 1972a Supersonic turbulent boundary layer in adverse pressure gradient. Pt. I: The experiment. AIAA J. 10, 475-480.
- Sturek W.B., Danberg J.E. 1972b Supersonic turbulent boundary layer in adverse pressure gradient. Pt. II: Data analysis. AIAA J. 10, 630-636.
- Sun C.C., Childs M.E. 1975 Calculations of turbulent shear stress in supersonic boundary layer flows. AIAA J. 13, 224-227.
- Sun C.C., Childs M.E. 1977 An experimental investigation of shock wave turbulent boundary layer interactions with and without boundary layer suction - a data summary report. NASA CR 2872.
- Thomann H. 1968 Effect of streamwise wall curvature on heat transfer in a turbulent boundary layer. J. Fluid Mech., 33, 282-292, (CAT 6800).
- Thomas G.D. 1974 Compressible turbulent boundary layers with combined air injection and pressure gradient. A.R.C. R + M 3779 and Ph.D. thesis Cambridge 1973, (CAT 7401).
- Varner M.O., Adams J.C. 1980 Variable edge entropy and low Reynolds number effects on hypersonic turbulent boundary layers. AIAA Paper 80-0131.
- Vas I.E. 1972 Flow field measurements using a total temperature probe at hypersonic speeds. AIAA J. 10, 317-323 and AIAA Paper 71-273.
- Viegas J.R., Horstman C.C. 1979 Comparison of multiequation turbulence models for several shock boundary-layer interaction flows. AIAA J. 17, 811-820.
- Voisinet R.L.P. 1977 Temperature-step effects on direct measurement of skin-friction drag. NSWC NOL TR 77-7.
- Voisinet R.L.P. 1979a Influence of roughness and blowing on compressible turbulent boundary layer flow. NSWC TR 79-153, (CAT 79015).
- Voisinet R.L.P. 1979b Combined influence of roughness and mass transfer on turbulent skin friction at Mach 2.9. AIAA Paper 79-0003.
- Voisinet R.L.P., Lee R.E. 1972 Measurements of a Mach 4.9 zero pressure gradient turbulent boundary layer with heat transfer NOL TR 72-232, (CAT 7202).
- Voisinet R.L.P., Lee R.E. 1973 Measurements of a supersonic favourable-pressure-gradient turbulent boundary layer with heat transfer - Part 1 - Data compilation. NOL TR 73 - 224, (CAT 7304).
- Voisinet R.L.P., Lee R.E., Meier H.U. 1974 Comparative measurements of total temperature in a supersonic turbulent boundary layer using a conical equilibrium and combined temperature-pressure probe. NOL TR 74-10, (CAT 7404 S).
- Wallace J.E. 1967 Hypersonic turbulent boundary layer studies at cold wall conditions. Proc. 1967 Heat Transfer and Fluid Mech. Inst., 427-451.

- Wallace J.E. 1968 Hypersonic turbulent boundary layer measurements using an electron beam. Cornell Aeronautical Lab. CAL No AN 2112-Y-1 and NASA CR-96612.
- Wallace J.E. 1969 Hypersonic turbulent boundary layer measurements using an electron beam. AIAA J. 7, 757-759.
- Waltrup P.J., Schetz J.A. 1971 An experimental investigation of a compressible turbulent boundary layer subjected to a systematic variation of adverse pressure gradients. Virginia Polytechnic Institute PI - E - 71 - 18, (CAT 7104).
- Waltrup P.J., Schetz J.A. 1973 Supersonic turbulent boundary layer subjected to adverse pressure gradients. AIAA J. 11, 50-58.
- Walz A. 1966 Strömungs- und Temperaturgrenzschichten. Verlag G. Braun Karlsruhe.
- Watson R.D. 1978 Characteristics of Mach 10 transitional and turbulent boundary layers. NASA TP-1243 (CAT 7804 S).
- Watson R.D. 1979 Exploratory investigation of the effect of porous surfaces on hypersonic turbulent boundary layers. NASA TM 78-791.
- Watson R.D., Harris J.E., Anders J.B. 1973 Measurements in a transitional/turbulent Mach 10 boundary layer at high Reynolds numbers. AIAA Paper 73-165, (CAT 7305).
- Weinstein L.M. 1973 Hot wire coil probe for high-speed flows. AIAA J. 11, 1772-1773.
- Wilcox D.C., Traci R.M. 1976 A complete model of turbulence. AIAA Paper 76-351.
- Wilcox D.C., Rubesin M.W. 1980 Progress in turbulence modelling for complex flow fields including effects of compressibility. NASA TP 1517.
- Willmarth W.W., Yang C.S. 1970 Wall pressure fluctuations beneath turbulent boundary layers on a flat plate and a cylinder. J. Fluid Mech. 41, 47 - 80.
- Willmarth W.W., Winkel R.E., Sharma L.K., Bogar T.J. 1976 Axially symmetric turbulent boundary layers on cylinders: Mean velocity profiles and wall pressure fluctuations. J. Fluid Mech. 76, 35-64.
- Winkler E.M. 1954 Stagnation temperature probes for use at high supersonic speeds and elevated temperatures. NAVORD Rep. 3834.
- Winkler E.M., Cha M.H. 1959 Investigation of flat plate hypersonic turbulent boundary layers with heat transfer at a Mach number of 5.2. NOL NAVORD Rep. 6631, (CAT 5902).
- Winter K.G., Rotta J.C., Smith K.G. 1970 Studies of the turbulent boundary layer on a waisted body of revolution in subsonic and supersonic flow. ARC R + M 3633 (supersedes RAE TR 68215), (CAT 7004).
- Winter K.G., Gaudet L. 1973 Turbulent boundary-layer studies at high Reynolds numbers at Mach numbers between 0.2 and 2.8. ARC R + M 3712, (CAT 7302). Supersedes RAE Rep. 70251
- Yanta W.J. 1974 Laser doppler velocimeter measurements of turbulence properties of a Mach 3 turbulent boundary layer. Int. Short Course on Laser Velocimetry Purdue Univ. (Eds. Thompson H.D., Stevenson W.H.).
- Yanta W.J., Smith R.A. 1973 Measurements of turbulence transport properties with a laser-doppler velocimeter. AIAA Paper 73-169.
- Yanta W.J., Lee R.E. 1974 Determination of turbulence transport properties with the Laser-Doppler-velocimeter and conventional time-averaged mean-flow measurements at Mach 3. AIAA Paper 74-575.
- Yanta W.J., Lee R.E. 1976 Measurements of Mach 3 turbulence transport properties on a nozzle wall. AIAA J. 14, 725-729.
- Yanta W.J., Crapo B.J. 1976 Applications of the laser doppler velocimeter to measure subsonic and supersonic flows. AGARD CPP-193, 2.1-2.8.
- Young F.L. 1965 Experimental investigation of the effects of surface roughness on compressible turbulent boundary layer skin friction and heat transfer. Univ. Texas Report DRL - 532, AD 621 085, (CAT 6506).
- Zwarts F. 1970 Compressible turbulent boundary layers. Ph.D. thesis, Mc Gill Univ. Dept. Mech. Eng., (CAT 7007).

REPORT DOCUMENTATION PAGE

| | | | | | | | | | | | | | |
|--------------------------------------|---|-----------------------------|---|--------------------------|-------------------------|---------------------|-------------------|-------------------|-------------|----------------------|-----------------------------------|----------------|--|
| 1. Recipient's Reference | 2. Originator's Reference | 3. Further Reference | 4. Security Classification of Document | | | | | | | | | | |
| | AGARD-AG-263 | ISBN 92-835-1404-1 | UNCLASSIFIED | | | | | | | | | | |
| 5. Originator | Advisory Group for Aerospace Research and Development North Atlantic Treaty Organization 7 rue Ancelle, 92200 Neuilly sur Seine, France | | | | | | | | | | | | |
| 6. Title | A FURTHER COMPILATION OF COMPRESSIBLE BOUNDARY LAYER DATA WITH A SURVEY OF TURBULENCE DATA | | | | | | | | | | | | |
| 7. Presented at | | | | | | | | | | | | | |
| 8. Author(s)/Editor(s) | Professor Dr Ing. H.H.Fernholz, P.J.Finley, M.A., Ph.D. and Dr V.Mikulla | | 9. Date November 1981 | | | | | | | | | | |
| 10. Author's/Editor's Address | See Flyleaf | | 11. Pages 222 | | | | | | | | | | |
| 12. Distribution Statement | This document is distributed in accordance with AGARD policies and regulations, which are outlined on the Outside Back Covers of all AGARD publications. | | | | | | | | | | | | |
| 13. Keywords/Descriptors | <table border="0"> <tr> <td>Turbulent boundary layer</td> <td>Turbulence measurements</td> </tr> <tr> <td>Boundary layer flow</td> <td>Experimental data</td> </tr> <tr> <td>Compressible flow</td> <td>Data tables</td> </tr> <tr> <td>Two dimensional flow</td> <td>Shock boundary layer interactions</td> </tr> <tr> <td>Turbulent flow</td> <td></td> </tr> </table> | | | Turbulent boundary layer | Turbulence measurements | Boundary layer flow | Experimental data | Compressible flow | Data tables | Two dimensional flow | Shock boundary layer interactions | Turbulent flow | |
| Turbulent boundary layer | Turbulence measurements | | | | | | | | | | | | |
| Boundary layer flow | Experimental data | | | | | | | | | | | | |
| Compressible flow | Data tables | | | | | | | | | | | | |
| Two dimensional flow | Shock boundary layer interactions | | | | | | | | | | | | |
| Turbulent flow | | | | | | | | | | | | | |
| 14. Abstract | <p>This volume is a continuation of AGARDographs 223, 253 (Fernholz and Finley 1977, 1980). The data compilation for 59 nominally two dimensional compressible shock-free flows presented in AGARDograph 223 is supplemented by a further 18 cases, including some shock-boundary-layer-interactions. The data are also available on magnetic tape from AGARD centres as for AGARDograph 223.</p> <p>The text preceding the compilation gives a review of the available turbulence measurements. The measurements are compared on the basis of inner and outer region similarity relationships. There is little evidence of any quantitative correlation between different experiments.</p> <p>There is also an examination of the breakdown conditions for the Van-Driest/Crocco mean-flow temperature-velocity correlation and the associated transformation procedures. The effects of extreme transverse curvature on the mean flow are briefly considered.</p> <p>This AGARDograph was prepared at the request of the Fluid Dynamics Panel of AGARD.</p> | | | | | | | | | | | | |

| | | | |
|---|--|---|--|
| <p>AGARDograph No.263 Advisory Group for Aerospace Research and Development, NATO A FURTHER COMPILATION OF COMPRESSIBLE BOUNDARY LAYER DATA WITH A SURVEY OF TURBULENCE DATA by Professor Dr Ing. H.H.Fernholz, P.J.Finley, M.A., Ph.D. and Dr V.Mikulla Published November 1981 222 Pages</p> <p>This volume is a continuation of AGARDographs 223, 253 (Fernholz and Finley 1977, 1980). The data compilation for 59 nominally two dimensional compressible shock-free flows presented in AGARDograph 223 is supplemented by a further 18 cases, including some</p> <p>P.T.O.</p> | <p>AGARD-AG-263</p> <p>Turbulent boundary layer Boundary layer flow Compressible flow Two dimensional flow Turbulent flow Turbulence measurements Experimental data Data tables Shock boundary layer interaction</p> | <p>AGARDograph No.263 Advisory Group for Aerospace Research and Development, NATO A FURTHER COMPILATION OF COMPRESSIBLE BOUNDARY LAYER DATA WITH A SURVEY OF TURBULENCE DATA by Professor Dr Ing. H.H.Fernholz, P.J.Finley, M.A., Ph.D. and Dr V.Mikulla Published November 1981 222 Pages</p> <p>This volume is a continuation of AGARDographs 223, 253 (Fernholz and Finley 1977, 1980). The data compilation for 59 nominally two dimensional compressible shock-free flows presented in AGARDograph 223 is supplemented by a further 18 cases, including some</p> <p>P.T.O.</p> | <p>AGARD-AG-263</p> <p>Turbulent boundary layer Boundary layer flow Compressible flow Two dimensional flow Turbulent flow Turbulence measurements Experimental data Data tables Shock boundary layer interaction</p> |
| <p>AGARDograph No.263 Advisory Group for Aerospace Research and Development, NATO A FURTHER COMPILATION OF COMPRESSIBLE BOUNDARY LAYER DATA WITH A SURVEY OF TURBULENCE DATA by Professor Dr Ing. H.H.Fernholz, P.J.Finley, M.A., Ph.D. and Dr V.Mikulla Published November 1981 222 Pages</p> <p>This volume is a continuation of AGARDographs 223, 253 (Fernholz and Finley 1977, 1980). The data compilation for 59 nominally two dimensional compressible shock-free flows presented in AGARDograph 223 is supplemented by a further 18 cases, including some</p> <p>P.T.O.</p> | <p>AGARD-AG-263</p> <p>Turbulent boundary layer Boundary layer flow Compressible flow Two dimensional flow Turbulent flow Turbulence measurements Experimental data Data tables Shock boundary layer interaction</p> | <p>AGARDograph No.263 Advisory Group for Aerospace Research and Development, NATO A FURTHER COMPILATION OF COMPRESSIBLE BOUNDARY LAYER DATA WITH A SURVEY OF TURBULENCE DATA by Professor Dr Ing. H.H.Fernholz, P.J.Finley, M.A., Ph.D. and Dr V.Mikulla Published November 1981 222 Pages</p> <p>This volume is a continuation of AGARDographs 223, 253 (Fernholz and Finley 1977, 1980). The data compilation for 59 nominally two dimensional compressible shock-free flows presented in AGARDograph 223 is supplemented by a further 18 cases, including some</p> <p>P.T.O.</p> | <p>AGARD-AG-263</p> <p>Turbulent boundary layer Boundary layer flow Compressible flow Two dimensional flow Turbulent flow Turbulence measurements Experimental data Data tables Shock boundary layer interaction</p> |

| | |
|--|--|
| <p>shock-boundary-layer interactions. The data are also available on magnetic tape from AGARD centres as for AGARDograph 223.</p> <p>The text preceding the compilation gives a review of the available turbulence measurements. The measurements are compared on the basis of inner and outer region similarity relationships. There is little evidence of any quantitative correlation between different experiments.</p> <p>There is also an examination of the breakdown conditions for the Van-Driest/Croccon mean-flow temperature-velocity correlation and the associated transformation procedures. The effects of extreme transverse curvature on the mean flow are briefly considered.</p> <p>This AGARDograph was prepared at the request of the Fluid Dynamics Panel of AGARD.</p> <p>ISBN 92-835-1404-1</p> | <p>shock-boundary-layer interactions. The data are also available on magnetic tape from AGARD centres as for AGARDograph 223.</p> <p>The text preceding the compilation gives a review of the available turbulence measurements. The measurements are compared on the basis of inner and outer region similarity relationships. There is little evidence of any quantitative correlation between different experiments.</p> <p>There is also an examination of the breakdown conditions for the Van-Driest/Croccon mean-flow temperature-velocity correlation and the associated transformation procedures. The effects of extreme transverse curvature on the mean flow are briefly considered.</p> <p>This AGARDograph was prepared at the request of the Fluid Dynamics Panel of AGARD.</p> <p>ISBN 92-835-1404-1</p> |
| <p>shock-boundary-layer interactions. The data are also available on magnetic tape from AGARD centres as for AGARDograph 223.</p> <p>The text preceding the compilation gives a review of the available turbulence measurements. The measurements are compared on the basis of inner and outer region similarity relationships. There is little evidence of any quantitative correlation between different experiments.</p> <p>There is also an examination of the breakdown conditions for the Van-Driest/Croccon mean-flow temperature-velocity correlation and the associated transformation procedures. The effects of extreme transverse curvature on the mean flow are briefly considered.</p> <p>This AGARDograph was prepared at the request of the Fluid Dynamics Panel of AGARD.</p> <p>ISBN 92-835-1404-1</p> | <p>shock-boundary-layer interactions. The data are also available on magnetic tape from AGARD centres as for AGARDograph 223.</p> <p>The text preceding the compilation gives a review of the available turbulence measurements. The measurements are compared on the basis of inner and outer region similarity relationships. There is little evidence of any quantitative correlation between different experiments.</p> <p>There is also an examination of the breakdown conditions for the Van-Driest/Croccon mean-flow temperature-velocity correlation and the associated transformation procedures. The effects of extreme transverse curvature on the mean flow are briefly considered.</p> <p>This AGARDograph was prepared at the request of the Fluid Dynamics Panel of AGARD.</p> <p>ISBN 92-835-1404-1</p> |

**DAT
ILM**